Dieter Weichert
Alan Ponter

Editors

Limit States of Materials and Structures

Direct Methods

Springer

Limit States of Materials and Structures

Dieter Weichert · Alan Ponter
Editors

Limit States of Materials and Structures

Direct Methods

Springer

Editors

Dieter Weichert
RWTH Aachen
Inst. Allgemeine Mechanik
Templergraben 64
52062 Aachen
Germany
weichert@iam.rwth-aachen.de

Alan Ponter
University of Leicester
Dept. Engineering
University Road
Leicester
United Kingdom LE1 7RH
asp@le.ac.uk

Preface

To predict loading limits for structures and structural elements is one of the oldest and most important tasks of engineers. Among the theoretical and numerical methods available for this purpose, so-called "Direct Methods", embracing Limit- and Shakedown Analysis, play an eminent role due to the fact that they allow rapid access to the requested information in mathematically constructive manners.

The collection of papers in this book is the outcome of a workshop held at Aachen University of Technology in November 2007. The individual contributions stem in particular from the areas of new numerical developments rendering the methods more attractive for industrial design, extensions of the general methodology to new horizons of application, probabilistic approaches and concrete technological applications.

The papers are arranged according to the order of the presentations in the workshop and give an excellent insight into state-of-the-art developments in this broad and growing field of research.

The editors warmly thank all the scientists, who have contributed by their outstanding papers to the quality of this edition. Special thanks go to Jaan Simon for his great help in putting together the manuscript to its final shape. We hope you may enjoy reading it!

Aachen and Leicester,   *Dieter Weichert*
September 2008   *Alan Ponter*

Contents

Contributors

Barrera, Olga
Department DASTEC, University 'Mediterranea' of Reggio Calabria, via
Melissari I-89124, Reggio Calabria, Italy, e-mail: olga.barrera@unirc.it

Bouby, Céline
LEMTA, Nancy-Université, CNRS, 2, rue Jean Lamour, Vandoeuvre Les
Nancy Cedex, F-54519, France, e-mail: celine.bouby@esstin.uhp-nancy.fr

Bourgeois, Stéphane
Laboratoire de Mécanique et d'Acoustique (UPR 7051) & Ecole Centrale de
Marseille, Technopole de Chateau-Gombert, 38 rue de Joliot Curie, 13451
Marseille cedex 20, France, e-mail: stephane.bourgeois@ec-marseille.fr

Caron, Isabelle
Laboratoire d'Ingénierie des Systèmes Mécaniques et des Matériaux, EA2336,
Institut Supérieur de Mécanique de Paris (SUPMECA), 3 rue Fernand Hainaut,
93407 Saint-Ouen cedex, France, e-mail: genevieve.inglebert@supmeca.fr

Da Silva Botelho, Tony
Laboratoire d'Ingénierie des Systèmes Mécaniques et des Matériaux, EA2336,
Institut Supérieur de Mécanique de Paris (SUPMECA), 3 rue Fernand Hainaut,
93407 Saint-Ouen cedex, France, e-mail: genevieve.inglebert@supmeca.fr

Débordes, Olivier
Laboratoire de Mécanique et d'Acoustique (UPR 7051) & Ecole Centrale de
Marseille, Technopole de Chateau-Gombert, 38 rue de Joliot Curie, 13451
Marseille cedex 20, France, e-mail: olivier.debordes@ec-marseille.fr

De Saxcé, Géry
Laboratoire de Mécanique de Lille, UMR CNRS 8107, Université des
Sciences et Technologies de Lille, Cité Scientifique, F-59655 Villeneuve
d'Ascq cedex, France, e-mail: gery.desaxce@univ-lille1.fr

Fuschi, Paolo
Department DASTEC, University 'Mediterranea' of Reggio Calabria, via
Melissari I-89124, Reggio Calabria, Italy, e-mail: paolo.fuschi@unirc.it

Hachemi, Abdelkader
RWTH Aachen, Institut für Allgemeine Mechanik, Templergraben 64, 52062
Aachen, Germany, e-mail: hachemi@iam.rwth-aachen.de

Inglebert, Geneviève
Laboratoire d'Ingénierie des Systèmes Mécaniques et des Matériaux, EA2336,
Institut Supérieur de Mécanique de Paris (SUPMECA), 3 rue Fernand Hainaut,
93407 Saint-Ouen cedex, France, e-mail: genevieve.inglebert@supmeca.fr

Kammoun, Zied
Ecole Polytech. de Tunisie, Laboratoire de Systèmes et de Mécanique
Appliquée, e-mail: kammounzied@yahoo.fr

Loute, Etienne
Facultés universitaires Saint-Louis, Bld. Jardin Botanique 43, 1000 Brussels,
Belgium, e-mail: loute@fusl.ac.be

Li, Hua-Xiang
Department of Engineering Science, University of Oxford, Oxford OX1 3PJ,
UK, e-mail: huaxiang.li@eng.ox.ac.uk

Magoariec, Hélène
Laboratoire de Tribologie et Dynamique des Systèmes (UMR 5513) & Ecole
Centrale de Lyon, Bâtiment G8, 36 avenue Guy de Collongue, 69134 Ecully
cedex, France, e-mail: helene.magoariec@ec-Lyon.fr

Marti, Kurt
Universität der Bundeswehr München (UniBwM), Institut für Mathe-
matik und Rechneranwendung, Werner-Heisenberg-Weg 39, 85577
Neubiberg/München, Germany, e-mail: kurt.marti@unibw-muenchen.de

Mouhtamid, Said
RWTH Aachen, Institut für Allgemeine Mechanik, Templergraben 64, 52062
Aachen, Germany, e-mail: mouhtami@iam.rwth-aachen.de

Nguyen, An Danh
RWTH Aachen, Institut für Allgemeine Mechanik, Templergraben 64, 52062
Aachen, Germany, e-mail: andanh@iam.rwth-aachen.de

Oueslati, Abdelbacet
Laboratoire de Mécanique de Lille, UMR CNRS 8107, Université des
Sciences et Technologies de Lille, Cité Scientifique, F-59655 Villeneuve
dŠAscq cedex, France, e-mail: abdelbacet.oueslati@univ-lille1.fr

Pastor, Franck
Université Catholique de Louvain, Laboratoire CESAME, Avenue
Georges Lemaître 4, B1348 Louvain-La-Neuve, Belgium, e-mail:
franck.pastor@uclouvain.be

Pastor, Joseph
Université de Savoie, Laboratoire LOCIE, Campus de Savoie-Technolac,
73376 Le Bourget du Lac cedex, France, e-mail: joseph.pastor@univ-savoie.fr

Phạm, Phú Tình
Fachhochschule Aachen (Campus Jülich), Labor Biomechanik, Ginsterweg
1, 52428 Jülich, Germany, e-mail: pham@fh-aachen.de

Pisano, Aurora A.
Department DASTEC, University 'Mediterranea' of Reggio Calabria, via
Melissari I-89124, Reggio Calabria, Italy, e-mail: aurora.pisano@unirc.it

Ponter, Alan R.S.
University of Leicester, Department of Engineering, University Road,
Leicester LE1 7RH, UK, e-mail: asp@leicester.ac.uk

Quillien, Muriel
Laboratoire d'Ingénierie des Systèmes Mécaniques et des Matériaux, EA2336,
Institut Supérieur de Mécanique de Paris (SUPMECA), 3 rue Fernand Hainaut,
93407 Saint-Ouen cedex, France, e-mail: genevieve.inglebert@supmeca.fr

Smaoui, Hichem
Ecole Nationale d'Ingénieurs de Tunis (ENIT), BP 37, Le Belvedere Tunis
1002, Tunisie, e-mail: hichem.smaoui@enit.rnu.tn

Spiliopoulos, Konstantinos V.
National Technical University of Athens, School of Civil Engineering, Heroon
Polytechniou 9, Zografou 15780 Athens, Greece,
e-mail: kvspilio@central.ntua.gr

Staat, Manfred
Fachhochschule Aachen (Campus Jülich), Labor Biomechanik, Ginsterweg
1, 52428 Jülich, Germany, e-mail: m.staat@fh-aachen.de

Thoré, Philippe
Université de Savoie, Laboratoire LOCIE, Campus de Savoie-Technolac, 73376
Le Bourget du Lac cedex, France, e-mail: philippe.thore@univ-savoie.fr

Trần, Thanh Ngọc
Fachhochschule Aachen (Campus Jülich), Labor Biomechanik, Ginsterweg
1, 52428 Jülich, Germany, e-mail: tran@fh-aachen.de

Tritsch, Jean-Bernard
Laboratoire de Mécanique de Lille, UMR CNRS 8107, Université des
Sciences et Technologies de Lille, Cité Scientifique, F-59655 Villeneuve
d'Ascq cedex, France, e-mail: jeanbernard.tritsch@univ-lille1.fr

Vũ, Dúc Khôi
University of Erlangen-Nuremberg, Institute of Applied Mechanics,
Egerlandstrasse 5, 91058 Erlangen, Germany, e-mail: Vu@ltm.uni-
erlangen.de

Weichert, Dieter
RWTH Aachen, Institut für Allgemeine Mechanik, Templergraben 64, 52062
Aachen, Germany, e-mail: weichert@iam.rwth-aachen.de

Yu, Hai-Sui
University of Nottingham, School of Civil Engineering, University Park,
Coates Building, Room B65, NG 7 2RD Nottingham, UK, e-mail: hai-
sui.yu@nottingham.ac.uk

Zier, Simone
Universität der Bundeswehr München (UniBwM), Institut für Mathe-
matik und Rechneranwendung, Werner-Heisenberg-Weg 39, 85577
Neubiberg/München, Germany, e-mail: simone.zier@unibw-muenchen.de

The Linear Matching Method for Limit Loads, Shakedown Limits and Ratchet Limits

A.R.S. Ponter

Abstract The paper describes the application of the Linear Matching Method to the direct evaluation of limits associated with an elastic-perfectly plastic body subjected to cyclic loading. Methods for limit load and shakedown limit are followed by ratchet limits. The method is distinguished from other programming methods by ensuring that equilibrium and compatibility are satisfied at each stage. The method has been extended beyond the range of most other direct methods by including ratchet limits and high temperature material behaviour. Implementation is possible within the user routines of commercial finite element codes. The paper emphasise the theoretical characteristics of the method and discusses significant aspects of convergence, both theoretical and numerical. The application of the method to industrial Life Assessment problems and to geotechnical problems is summarized.

1 Introduction

Classically, numerical methods for Direct Method have relied upon the application of mathematical programming methods to limit load and shakedown limit theorems of plasticity and this is strongly reflected in other papers in this volume. Either upper or lower bound methods are possible depending on whether the approximating continuum descriptions correspond to equilibrium stress fields or compatible strain fields. The objective function, a load parameter, is then either maximized or minimized according the upper and lower bounds of classical plasticity.

This approach has both advantages and disadvantages. Mathematical programming procedures have progressed significantly in recent years and highly

Alan R.S. Ponter
Department of Engineering, University of Leicester, Leicester, UK
e-mail: asp@le.ac.uk

efficient solution methods are widely available producing fast and reliable solution methods. However, the general methodology relies upon the classical theorems of plasticity and extensions do not exist to behaviour outside shakedown or to other material behaviour, time dependent creep behaviour in particular. For this reason, alternative approaches have been considered that provide a more flexible approach to the formulation of direct methods. A number of methods discussed within the design community [6, 13, 21] have proved to have a common theme, the representation of stress and strain fields through linear problems with spatially varying moduli. This first occurred through Marriot's [21] observation that very good lower bound limit loads could be found by systematically decreasing the Young's modulus in regions of high stress in a standard linear elastic solution. This has the effect of reducing the maximum stress and hence increasing the load at which all stresses lie within yield. This simple procedure can be very successful in computing safe lower bounds but, to the present time, has not been developed into a method for evaluation the maximum lower bound, i.e. the limit load.

The Linear Matching Method [8, 23, 25, 26, 28] adopts the basic assumption that limit state solutions may be developed from linear solutions with spatially varying moduli and builds it into a programming method. In this paper, the method is described for an elastic-perfectly plastic body for the evaluation of all the possible limits; limit load, shakedown limit and ratchet limit. It is shown for shakedown that the method becomes a convergent upper bound method. Each iteration provides both a kinematically admissible strain rate history and an equilibrium distribution of residual stress (in the Galerkin sense), both upper and lower bounds are generated that become equal to the minimum upper bound at convergence. This lower bound generally does not monotonically increase. A dual method, based upon equilibrium stresses and the lower bound theorem also exists but appears not to converge for perfect plasticity [23].

The extension of the method to the ratchet limit is then discussed, based upon a general minimum theorem for perfect plasticity [14, 25]. This is followed by a summary of various applications to industrial problems.

2 Definition of the Problem

2.1 External Loads

We consider the problem of a body with volume V subjected to a cyclic history of load $\lambda P_i(x_i, t)$ over part, namely S_T, of the surface S, and a cyclic history of temperature $\lambda \theta(x_i, t)$ within V. On the remainder of S, namely S_U, the displacement rate $\dot{u}_i = 0$. Both load and temperature history have the same cycle time Δt and, in the following, we are concerned with the behaviour of the body in a typical cycle $0 \leq t \leq \Delta t$ in a cyclic state. The (positive) load parameter λ allows us to consider a class of loading histories.

2.2 Material Behaviour

Consider such a body composed of a solid under conditions of small strains where the total strain is the sum of a linearly elastic and perfectly plastic component,

$$\dot{\varepsilon}_{ij} = \dot{\varepsilon}_{ij}^e + \dot{\varepsilon}_{ij}^p, \tag{1}$$

where the plastic strains are associated with a strictly convex yield condition $f(\sigma_{ij}) = 0$

$$\dot{\varepsilon}_{ij}^p = 0, \quad f < 0,$$
$$\dot{\varepsilon}_{ij}^p = \dot{\alpha}\frac{\partial f}{\partial \sigma_{ij}}, \quad f = 0. \tag{2}$$

The elastic moduli are assumed to be independent of temperature.

2.3 Structure of the Asymptotic Cyclic Solution

For the problem defined above the stresses and strain rates will asymptote to a cyclic state, where

$$\sigma_{ij}(t) = \sigma_{ij}(t + \Delta t), \; \dot{\varepsilon}_{ij}(t) = \dot{\varepsilon}_{ij}(t + \Delta t). \tag{3}$$

In the following we are concerned with the properties of this asymptotic solution.

Consider a typical cycle, $0 \leq t \leq \Delta t$. The cyclic solution may be expressed in terms of three components, the elastic solution, a transient solution accumulated up to the beginning of the cycle and a residual solution that represents the remaining changes within the cycle. The linear elastic solution (i.e. $\dot{\varepsilon}_{ij}^p = 0$) is denoted by $\lambda\hat{\sigma}_{ij}$ and $\lambda\hat{\varepsilon}_{ij}$. The general form of the stress solution is given by

$$\sigma_{ij}(x_i, t) = \lambda\hat{\sigma}_{ij}(x_i, t) + \bar{\rho}_{ij}(x_i) + \rho_{ij}^r(x_i, t), \tag{4}$$

where $\bar{\rho}_{ij}$ denotes a constant residual stress field in equilibrium with zero surface traction on S_T and corresponds to the residual state of stress at the beginning and end of the cycle. The history ρ_{ij}^r is the change in the residual stress during the cycle and satisfies

$$\rho_{ij}^r(x_i, 0) = \rho_{ij}^r(x_i, \Delta t) = 0. \tag{5}$$

The total plastic strain is similarly subdivided into two parts

$$\varepsilon_{ij}^p = \varepsilon_{ij}^{pT}(x_i) + \varepsilon_{ij}^{pr}(x_i, t), \tag{6}$$

where ε_{ij}^{pT} denotes the accumulation of plastic strain at the beginning of the cycle and ε_{ij}^{pr} denotes the additional plastic strain during the cycle.

The relationship between the transient and residual quantities is given by

$$\varepsilon_{ij}^{T} = C_{ijkl}\bar{\rho}_{ij} + \varepsilon_{ij}^{pT}, \tag{7}$$

$$\varepsilon_{ij}^{r} = C_{ijkl}\rho_{ij}^{r} + \varepsilon_{ij}^{pr}, \tag{8}$$

where both ε_{ij}^{T} and ε_{ij}^{r} are compatible strain fields. C_{ijkl} denotes the linear elastic compliance tensor. The cyclic solution is always non-unique to the extent that the transient plastic strain ε_{ij}^{pT} may contain an arbitrary additional compatible component. Note that

$$\varepsilon_{ij}^{pr}(x_i, \Delta t) - \varepsilon_{ij}^{pr}(x_i, 0) = \Delta\varepsilon_{ij}^{pr} = \int_{0}^{\Delta t} \dot{\varepsilon}_{ij}^{pr}\,\mathrm{d}t \tag{9}$$

the accumulated plastic strain during a cycle which, for consistency may be added to ε_{ij}^{T}. Hence as both ε_{ij}^{T} and $\varepsilon_{ij}^{T}+\Delta\varepsilon_{ij}^{pr}$ are compatible then $\Delta\varepsilon_{ij}^{pr}$ is also compatible with a displacement field Δu_i, the accumulation of displacement per cycle.

This argument emphasises the crucial role of the residual plastic strain rate history $\dot{\varepsilon}_{ij}^{pr}$ in defining the cyclic state. If $\dot{\varepsilon}_{ij}^{pr}$ were known for $0 \leq t \leq \Delta t$ then $\rho_{ij}^{r}(x_i, t)$ is uniquely defined by the solution of the initial strain rate problem defined by the time derivative of (8),

$$\dot{\varepsilon}_{ij}^{r} = C_{ijkl}\dot{\rho}_{ij}^{r} + \dot{\varepsilon}_{ij}^{pr} \tag{10}$$

and the initial condition (5). The cyclic stress history (4) is then known except for $\bar{\rho}_{ij}$. However the additional requirement of the compatibility of $\Delta\varepsilon_{ij}^{pr}$ is sufficient to define $\bar{\rho}_{ij}$ and hence the entire history of stress in the cycle is known and the final condition of (5) is always satisfied. It is natural, therefore, to concentrate on a class of inelastic strain rate histories that have the same properties as the solution $\dot{\varepsilon}_{ij}^{pr}$. We will refer to all strain rate histories as $\dot{\varepsilon}_{ij}^{c}$ that accumulate over a cycle to a compatible strain increment $\Delta\varepsilon_{ij}^{c}$ as kinematically admissible (KA).

3 Shakedown Theorems

In this section we consider the case of shakedown. The shakedown limit can be seen to be that range of load multiplier $\lambda \leq \lambda_s$ for which the changing residual stress ρ_{ij}^{r} is zero, where λ_s is the shakedown limit. In the following we state the shakedown theorems and then convert the upper bound theorem into a form naturally aligned to the subsequent discussion of the Linear Matching Method.

3.1 Lower Bound Theorem (Melan's Theorem) [10]

If a time constant residual stress field $\bar{\rho}$ exists such that superposition with induced elastic stresses $\lambda_{LB}\hat{\sigma}_{ij}(x,t)$ forms a safe state of stress everywhere in the structure, i.e.

$$f\left(\lambda_{LB}\hat{\sigma}_{ij} + \bar{\rho}_{ij}\right) \leq 0, \quad \text{then } \lambda_{LB} \leq \lambda_s. \tag{11}$$

3.2 Upper Bound Theorem (Koiter's Theorem) [10]

For all kinematically admissible (KA) strain rate histories $\dot{\varepsilon}_{ij}^c$, $\int_0^{\Delta t} \dot{\varepsilon}_{ij}^c \mathrm{d} = \Delta\varepsilon_{ij}^c$, consider the load parameter $\lambda_{UB} > 1$ from the work balance,

$$\lambda_{UB} \int_0^T \int_V \hat{\sigma}_{ij}(x,t)\,\dot{\varepsilon}_{ij}^c(x,t)\mathrm{d}V\mathrm{d}t = \int_0^T \int_V D(\dot{\varepsilon}_{ij}^c)\mathrm{d}V\mathrm{d}t = \int_0^T \int_V \sigma_{ij}^c \dot{\varepsilon}_{ij}^c \mathrm{d}V\mathrm{d}t, \tag{12}$$

where σ_{ij}^c denotes a state of associated with $\dot{\varepsilon}_{ij}^c$ at yield. Then $\lambda_{UB} \geq \lambda_s$.

3.3 An Alternative Form of the Upper Bound Theorem

The following form of the upper bound theorem allows the Linear Matching Method to be displayed as a programming method and paves the way for extensions to other material models and loads in excess of shakedown. Consider the functional

$$I(\dot{\varepsilon}_{ij}^c, \lambda) = \int_V \int_0^{\Delta t} (\sigma_{ij}^c \dot{\varepsilon}_{ij}^c - \lambda\hat{\sigma}_{ij}\dot{\varepsilon}_{ij}^c)\mathrm{d}t\mathrm{d}V. \tag{13}$$

Then the upper bound theorem (12) may be expressed in the form;

$$I(\dot{\varepsilon}_{ij}^c, \lambda_{UB}^c) = 0 \quad \text{and} \quad I(\dot{\varepsilon}_{ij}^c, \lambda_s) \geq 0. \tag{14}$$

More significantly, for two kinematically admissible strain rate histories, $\dot{\varepsilon}_{ij}^i$ and $\dot{\varepsilon}_{ij}^f$ such that

$$I(\dot{\varepsilon}_{ij}^f, \lambda_{UB}^i) \leq I(\dot{\varepsilon}_{ij}^i, \lambda_{UB}^i) \quad \text{then } \lambda_{UB}^f \leq \lambda_{UB}^i. \tag{15}$$

Hence a process that reduces the value of $I(\dot{\varepsilon}_{ij}^{c}, \lambda_{UB}^{c})$ for constant λ, also reduces λ_{UB} and forms the basis for methods of obtaining the minimum λ_{UB} within a class of kinematically admissible strain rate histories.

4 The Linear Matching Method

The method for shakedown may be expressed in general terms, independent of the (convex) yield condition. Consider a class of linear viscous materials $\sigma_{ij}^{L} = \frac{\partial U(\dot{\varepsilon}_{ij}^{i})}{\partial \dot{\varepsilon}_{ij}^{i}} = L_{ijkl}\dot{\varepsilon}_{kl}$ expressed in terms of the compliance tensor $L_{ijkl}(x_i)$, which may vary spatially over the volume of the body, and associated flow potential $U(\dot{\varepsilon}_{ij})$. Consider now an initial KA $\dot{\varepsilon}_{ij}^{i}$ with associated stress at yield σ_{ij}^{pi}. The linear material is now matched to these yield values so that

$$\text{Matching condition:} \quad \sigma_{ij}^{Li} = \frac{\partial U(\dot{\varepsilon}_{ij}^{i})}{\partial \dot{\varepsilon}_{ij}^{i}} = \sigma_{ij}^{pi}. \tag{16}$$

Hence the yield condition and the linear material provide the same stress for this strain rate history. Equation (16) places restrictions on the compliance tensor $L_{ijkl}(x_i)$ but, generally, will not uniquely define it. The objective is now to define a linear problem with a solution that defines a new KA strain rate history $\dot{\varepsilon}_{ij}^{f}$ that reduces $I(\dot{\varepsilon}_{ij}^{i}, \lambda_{UB}^{i})$ and hence, from (15), reduces λ_{UB}. Before such a process can be constructed it is necessary to place restrictions on $L_{ijkl}(x_i)$ in the form of a sufficient condition for convergence.

4.1 Sufficient Condition for Convergence

Consider the following path integral in strain rate space. For arbitrary strain rate $\dot{\varepsilon}_{ij}^{f}$ the following inequality is required

$$\int\limits_{\dot{\varepsilon}_{ij}^{i}}^{\varepsilon_{ij}^{f}} (\sigma_{ij}^{L} - \sigma_{ij}^{p})\mathrm{d}\dot{\varepsilon}_{ij} \geq 0. \tag{17}$$

Or, equivalently

$$U(\dot{\varepsilon}_{ij}^{f}) - U(\dot{\varepsilon}_{ij}^{i}) - \frac{\partial U}{\partial \dot{\varepsilon}_{ij}^{i}}(\dot{\varepsilon}_{ij}^{f} - \dot{\varepsilon}_{ij}^{i}) \geq (\sigma_{ij}^{pf} - \sigma_{ij}^{pi})\dot{\varepsilon}_{ij}^{f} \geq 0. \tag{18}$$

In simple terms we require that the linear material is 'more convex' than the yield condition. A simple geometric interpretation of this condition
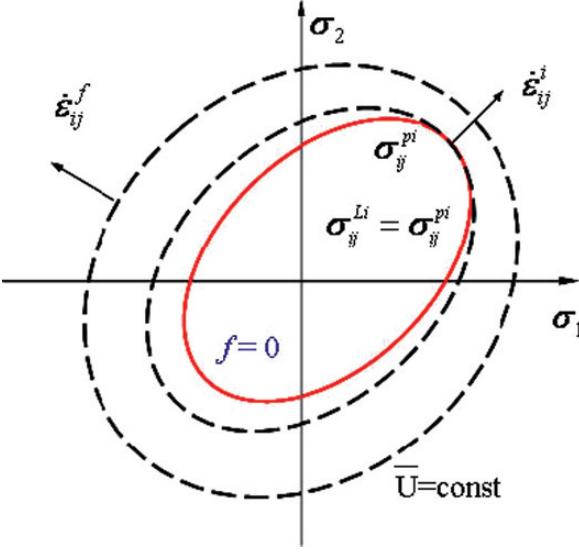
Fig. 1 The sufficient condition for convergence (18) requires that the surface of constant $\overline{U}$ which is tangent to the yield surface at the matching point, otherwise lies outside the yield surface [28]

exists in stress space [26], as shown in Fig. 1. The surface of constant $\overline{U}$, the complementary energy function of the linear material, that passes through the matching point, otherwise surrounds or coincides with the yield surface, as shown. For the von Mises yield condition contours of constant $\overline{U}$ coincide with the yield surface for an incompressible linear material defined by a spatially varying shear modulus μ, $U(\bar{\dot{\varepsilon}}) = \frac{3\mu}{4}\bar{\dot{\varepsilon}}^2$, where $\bar{\dot{\varepsilon}}$ denotes the von Mises effective strain rate. Returning to the general argument, considering the following quadratic version of I

$$K(\dot{\varepsilon}_{ij}^c, \lambda) = \int_V \int_0^{\Delta t} (U(\dot{\varepsilon}_{ij}^c) - \lambda \hat{\sigma}_{ij}\dot{\varepsilon}_{ij}^c)\mathrm{d}t\mathrm{d}V. \tag{19}$$

If we minimize $K(\dot{\varepsilon}_{ij}^c, \lambda_{UB}^i)$ for all KA strain rate histories so that

$$K(\dot{\varepsilon}_{ij}^f, \lambda_{UB}^i) \le K(\dot{\varepsilon}_{ij}^i, \lambda_{UB}^i). \tag{20}$$

Then, from (18), it is easily shown that $I(\dot{\varepsilon}_{ij}^f, \lambda_{UB}^i) \le I(\dot{\varepsilon}_{ij}^i, \lambda_{UB}^i)$ and hence $\lambda_{UB}^f \le \lambda_{UB}^i$ and the solution of the associated linear problem yields a reduced value of λ.

4.2 The Minimising Linear Problem

As K is quadratic and U convex, Eq. (18), it is a simple matter to define
the strain rate history that defines the minimum of K. This is given by the
constitutive equation

$$\frac{\partial U}{\partial \dot{\varepsilon}_{ij}^f} = \lambda \hat{\sigma}_{ij} + \bar{\rho}_{ij}^f \quad \text{or equivalently } \dot{\varepsilon}_{ij}^f = \bar{L}_{ijkl}(\lambda_{UB}^i \hat{\sigma}_{kl} + \bar{\rho}_{ij}^f), \qquad (21)$$

where $\bar{\rho}_{ij}^f$ defines, as before, a time constant residual stress field and $\bar{L}_{ijkl}(x_i)$
is the dual tensor corresponding to $L_{ijkl}(x_i)$. The solution of this problem
follows when the condition is imposed that $\dot{\varepsilon}_{ij}^f$ is KA, i.e.

$$\Delta \varepsilon_{ij}^f = \int_0^{\Delta t} \dot{\varepsilon}_{ij}^f \mathrm{d}t = \lambda_{UB}^i \left[\int_0^{\Delta t} \bar{L}_{ijkl} \hat{\sigma}_{kl} \mathrm{d}t \right] + \left[\int_0^{\Delta t} \bar{L}_{ijkl} \mathrm{d}t \right] \bar{\rho}_{ij}^f. \qquad (22)$$

This defines a linear initial stress problem for equilibrium residual stress $\bar{\rho}_{ij}^f$
and compatible strain increment $\Delta \varepsilon_{ij}^f$. The strain rate history is then given
by Eq. (21).

For the von Mises yield condition, $U(\bar{\dot{\varepsilon}}) = \frac{3\mu}{4}\bar{\dot{\varepsilon}}^2$, and the matching condi-
tion (16) becomes

$$\mu = \frac{2\sigma_y}{3\bar{\dot{\varepsilon}}^i}. \qquad (23)$$

The linear problem (21) becomes

$$\dot{\varepsilon}_{ij}^f = \frac{3}{2\mu}(\lambda_{UB}^i \hat{\sigma}_{ij}' + \bar{\rho}_{ij}'^f), \; \dot{\varepsilon}_{kk}^f = 0, \qquad (24)$$

i.e.

$$\Delta \varepsilon_{ij}^f = \int_0^{\Delta t} \dot{\varepsilon}_{ij}^f \mathrm{d}t = \frac{3}{2\bar{\mu}}(\sigma_{ij}^{init} + \bar{\rho}_{ij}'^f), \Delta \varepsilon_{kk}^f = 0 \qquad (25)$$

where

$$\frac{1}{\bar{\mu}} = \int_0^{\Delta t} \frac{1}{\mu} \mathrm{d}t \text{ and } \sigma_{ij}^{init} = \bar{\mu} \int_0^{\Delta t} \frac{1}{\mu}\lambda \hat{\sigma}_{ij}' \mathrm{d}t. \qquad (26)$$

an upper "dash" refers to the deviatoric components.

4.3 Further Convergence Considerations

The process is begun by assuming an arbitrary distribution of linear moduli, usually constant, and repeating the process to convergence. In summary, for a particular body geometry, history of loading and associated linear elastic solution history $\hat{\sigma}_{ij}$, the process of computing an acceptable minimum upper bound load parameter $\lambda_{UB}^{\min}$ requires the following conditions to be satisfied

(1) For the chosen yield condition, the convexity inequality (18) is always satisfied.
(2) The class of strain rates and associated strain increments are such that the minimum upper bound is contained within this class. For example, if the class of linear material chosen assumes incompressibility whereas the associated flow rule allows the possibility of compressibility, the process may not identify the minimum upper bound.
(3) The class of compatible strain distributions chosen for the solution of the linear problem is sufficiently wide to include the strain distribution corresponding to an acceptable minimum upper bound.

Conditions (1) and (2) are satisfied by an appropriate choice of a class of linear materials. Condition (3) is central to the implementation of the method within a finite element scheme. Equilibrium of the residual stress field $\bar{\rho}_{ij}$ relies upon the class of displacement field Δu_i from which $\Delta \varepsilon_{ij}$ is derived. $\bar{\rho}_{ij}$ is in equilibrium if and only if

$$\int_V \bar{\rho}_{ij} \Delta \varepsilon_{ij} \mathrm{d}V = 0 \tag{27}$$

for all members of the class of Δu_i under consideration. Hence the process will converge to the least upper bound associated within this class of displacement fields. Hence, for a given finite element mesh the process will converge to the least upper bound associated with the mesh geometry. However, in the implementation in a commercial code, such as ABAQUS used for the solutions here, the volume integration is not exact but usually relies upon Gaussian integration that would give an exact integral if the linear material constants were constant throughout an element. Hence the equilibrium condition (26) is replaced by the finite condition;

$$\sum_{el} \sum_{k} w_k \bar{\rho}_{ij}^k \Delta \varepsilon_{ij}^k = 0, \tag{28}$$

where w_k are the Gaussian weighting factors at the Gauss integration point. In this case the process converges to the least upper bound associated with (28) as the equilibrium condition.

4.4 An Associated Lower Bound

Each iterative solution generates an equilibrium residual stress field $\bar{\rho}_{ij}$ and hence, for some range of values of $\lambda = \lambda_{LB}$, $f(\lambda_{LB}\hat{\sigma}_{ij} + \bar{\rho}_{ij}) \leq 0$ for $0 \leq t \leq \Delta t$. The maximum lower bound $\lambda_{LB}^{\max}$ will be less than the least upper bound but it is not possible, at the present time, to make any certain statement about the variation of $\lambda_{LB}^{\max}$ with iterations. Upon convergence when consecutive solutions are identical for a von Mises yield condition, from the matching condition $\bar{\sigma}^f = \sigma_y$ within the plastic mechanism region and $\bar{\sigma}^f \leq \sigma_y$ in the rigid region. Hence

$$\lambda_{LB}^{\max} = \lambda_{UB}^{Min} \tag{29}$$

for equilibrium defined by either (27), where the matching condition is applied everywhere, or by (28) where the matching condition is applied at Gauss points. However, this is a point-wise condition, whereas the upper bound is a volume integral where deviation from convergence at a few Gauss points has little effect on the upper bound. Hence convergence of the upper bound in terms of a particular number of significant figures may allow some deviation from convergence locally. Hence generally the upper bound converges (monotonically) more quickly than the lower bound and their relative rate of convergence becomes greater with increasing degrees of freedom. This phenomenon is demonstrated in the following example. When the method is applied to large scale industrial problem where the number of degrees of freedom becomes very high, convergence is usually judged entirely in terms of the upper bound. There is clearly an opportunity for error analysis in defining this process and this awaits future developments. Entirely empirical experiments on the example problem discussed below indicates that the relative error in the upper bound for six nodded triangular nodes is proportional to approximately h/a where h is a characteristic element size and a is a characteristic body dimension [19].

4.5 An Example [11]

Consider the limit load problem shown in Fig. 2 where a tube with a part through thickness crack is subjected to an axial uniform distributed load P. In Fig. 3 the variation of both the upper and lower bound with iteration number is shown for a uniform finite element mesh of six nodded axisymmetric finite elements. It can be seen that both the upper and lower bound converge to a common value that is greater than the known analytic solution. The convergence of the upper bound is monotonic whereas the lower bound does not change monotonically and shows sequences of both increase and reduction. This type of behaviour is commonly observed, particularly for triangular fi-
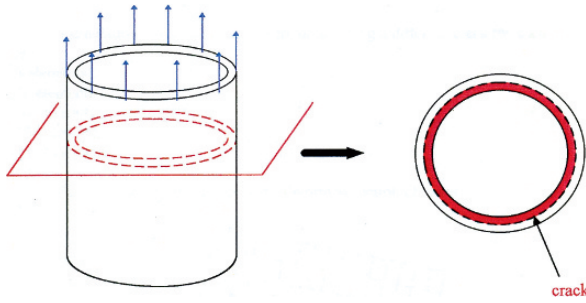
Fig. 2 Axially loaded cylinder subjected to axial load and a part through- thickness circumferential crack
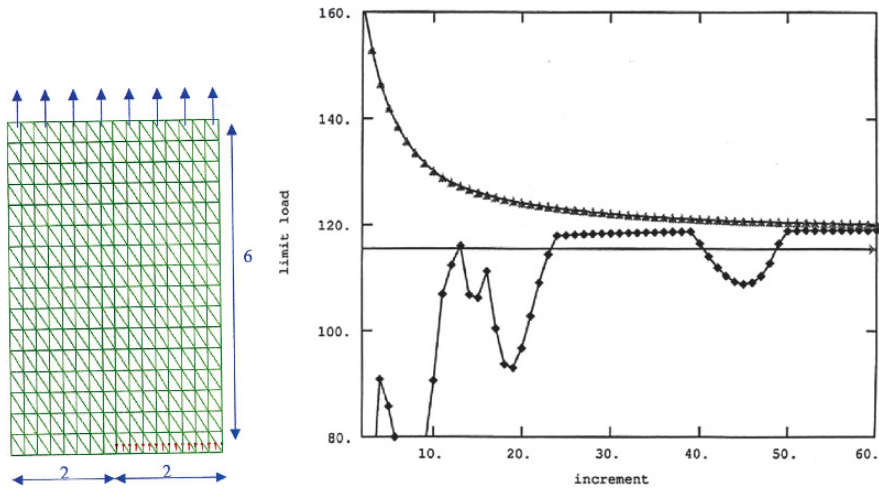
Fig. 3 Convergence of limit load of crack problem of Fig. 2, a uniform mesh

nite elements. In Fig. 4 the solution is shown for a finite element mesh that has been refined in the vicinity of the crack tip and the region of the volume where the strains are concentrated in the converged solution. In this case the upper bound converges to a solution within 0.4% of the analytic solution.

The lower bound has not completely converged within 30 iterations. This behaviour is typical of both limit load and shakedown solutions. When used for the solution of practical problems, convergence is generally assumed to have taken place when the upper bound ceases to change by a small quantity, usually less than one in the sixth significant figure. With such a convergence criterion convergence usually occurs within, at most, sixty iterations and usually a significantly smaller number.

The rate of converge depends upon the nature of the problem and is less dependent on the number of degrees of freedom. In the example above the upper bound for the more refined mesh, Fig. 4 converges more rapidly than for the courser mesh, Fig. 3. A more significant factor is the extent of the volume
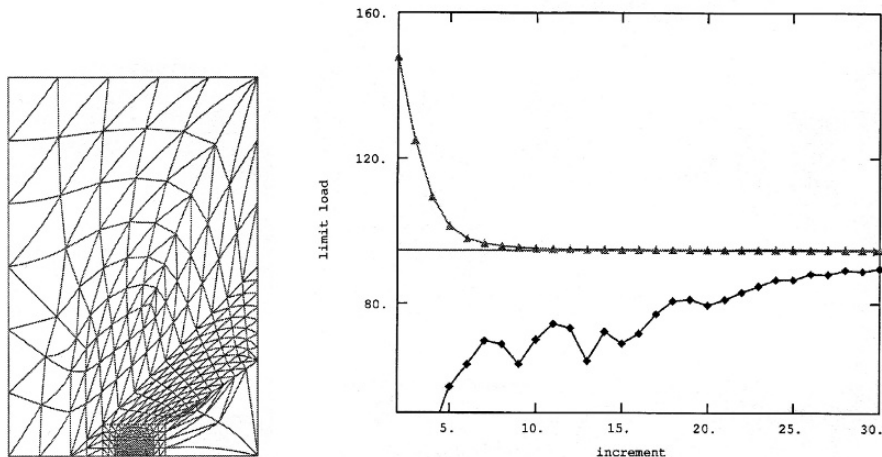
Fig. 4 Solution of the problem of Fig. 2 for a finite element refined at the crack tip and in regions of plastic flow

occupied by material where the plastic strains are near zero in the converged solution, rigid regions. As can be seen from the matching condition for the von Mises yield condition, Eq. (23) in regions where the stress and strain rate are low, the shear modulus μ becomes large. As the iterations progress, μ converges to constant values within the plastic mechanism, but continues to increase, iteration by iteration, in the rigid regions. If allowed to continue, this can sometime cause numerical instabilities. It is normal practice to allow μ to increase to such a value that the contribution of the strain rates to the upper bound are negligible in terms of the convergence criterion and then to keep it at that value for subsequent iterations.

There are many published limit load and shakedown solutions in the literature [9–12, 26–28].

5 The Ratchet Limit

In the following we discuss the evaluation of the ratchet limit, the value of λ where the cyclic solution changes from one where local plastic strains occur that do not increase cyclically, to a cyclic state when there is an increase of displacement per cycle. To achieve this, the minimum theorem, (14) for shakedown is extended to an arbitrary cyclic state.

5.1 A General Minimum Theorem

The methods discussed below are based on a general minimum theorem for cyclic loading [14,25]. For a typical cycle $0 \leq t \leq \Delta t$ consider the functional,

$$I(\dot{\varepsilon}_{ij}^c, \lambda) = \int\limits_0^{\Delta t} \int\limits_V (\sigma_{ij}^c - (\lambda \hat{\sigma}_{ij} + \rho_{ij}^c)) \dot{\varepsilon}_{ij}^c \mathrm{dtd}V, \tag{30}$$

where $\dot{\varepsilon}_{ij}^c$ is kinematically admissible and the stress state σ_{ij}^c is associated with $\dot{\varepsilon}_{ij}^c$ at yield. We now apply two additional conditions which place a restriction on the magnitude of $\dot{\varepsilon}_{ij}^c$.

(1) Corresponding to $\dot{\varepsilon}_{ij}^c$ we define a cyclic history of residual stress $\rho_{ij}^c(x_i, t)$ which satisfies the relationship

$$\dot{\varepsilon}_{ij}^{cc} = C_{ijkl} \dot{\rho}_{ij}^c + \dot{\varepsilon}_{ij}^c, \tag{31}$$

where $\dot{\varepsilon}_{ij}^{cc}$ is a compatible strain rate. Note that $\rho_{ij}^c(0) = \rho_{ij}^c(\Delta t) = 0$.
(2) Corresponding to $\rho_{ij}^c(x_i, t)$ we place a restriction on the absolute magnitude of $\dot{\varepsilon}_{ij}^c$ by requiring that there exists a *constant* residual stress field $\bar{\rho}_{ij}$ so that the composite stress history

$$\sigma_{ij}^* = \lambda \hat{\sigma}_{ij} + \bar{\rho}_{ij} + \rho_{ij}^c \tag{32}$$

satisfies the yield condition $f(\sigma_{ij}^*) \leq 0$ for $0 \leq t \leq \Delta t$.

For any kinematically admissible $\dot{\varepsilon}_{ij}^c$ and prescribed λ

$$I(\dot{\varepsilon}_{ij}^c, \lambda) \geq 0 \tag{33}$$

and $I(\dot{\varepsilon}_{ij}^c, \lambda) = 0$ when $\dot{\varepsilon}_{ij}^c = \dot{\varepsilon}_{ij}^{pr}$ the exact cyclic solution.

The upper bound shakedown theorem is recovered when $\dot{\varepsilon}_{ij}^c$ is so small that ρ_{ij}^c is negligible compared with $\lambda \hat{\sigma}_{ij}$. The largest value of λ for which this condition is satisfied is the shakedown limit λ_s and hence, we recover the result (13) and (14). In the following arguments will be confined to the von Mises yield condition, although they may be generalized to a general yield condition.

5.2 Evaluation of the Ratchet Limit

This limit corresponds to the load where the exact solution, in the steady states, changes from one where no accumulated strain occurs over a cycle to one where the accumulation corresponds to a displacement on which the loads do work. The direct evaluation of the ratchet limit falls outside the range of

methods that rely upon the application of mathematical programming methods as no bounding theorems exist. However, it is possible to, numerically, evaluate the limit in some cases. These methods rely upon the evaluation of the changing residual stress $\rho_{ij}^c(x_i, t)$ by the minimization of increments of the functional I, Eq. (30), for an increment of strain $d\varepsilon_{ij}^c$ occurring during the time interval $(t, t + dt)$, assuming $\rho_{ij}^c(x_i, t)$ is known

$$dI(d\varepsilon_{ij}^c, \lambda) = \int_V (\sigma_{ij}^c - (\lambda\hat{\sigma}_{ij} + \rho_{ij}^c(t) + d\rho_{ij}^c))d\varepsilon_{ij}^c dV. \tag{34}$$

In this case we define a linear relationship between $d\varepsilon_{ij}^c$ and a corresponding increment of stress $d\rho_{ij}^c$. Matching this linear material with shear modulus $\bar{\mu}$ to the yield condition yield;

$$\bar{\mu} = \sigma_y/\bar{\varepsilon}(d\varepsilon_{ij}^i), \tag{35}$$

where, as before, $d\varepsilon_{ij}^i$ is a previously evaluated estimate. Taking into account that the increment of total strain is made up of both an elastic and plastic component, we arrive at the following equation for an improved estimate of $d\varepsilon_{ij}^c$,

$$d\varepsilon_{ij}^{fT} = \frac{3}{2\mu^e}d\rho_{ij}^{f'} + \frac{3}{2\bar{\mu}}(\lambda\hat{\sigma}_{ij} + \rho_{ij}^c + d\rho_{ij}^f)' \quad \text{and} \quad d\varepsilon_{kk}^f = 0, \tag{36}$$

where μ^e denotes the shear modulus for the elastic strain increment and $d\varepsilon_{ij}^{Tf}$ denotes the compatible total strain increment. An upper 'dash' refers to deviatoric components.

The approach here exactly matches that of the shakedown method and is a simple matter to demonstrate that

$$dI(d\varepsilon_{ij}^f) \leq d(d\varepsilon_{ij}^i). \tag{37}$$

However the application of this algorithm through the entire cycle requires prior knowledge of the initial residual stress $\bar{\rho}_{ij}$. There exist, therefore, two interconnecting numerical strategies;

(a) If we possess an estimate of ρ_{ij}^c throughout the cycle from estimates of $d\rho_{ij}^c$, it is possible to evaluate estimates of $\bar{\rho}_{ij}$ by applying the shakedown algorithm, described in Sect. 4, where the elastic solution is augmented by ρ_{ij}^c.

(b) If we possess an estimate of $\bar{\rho}_{ij}$, then we are able to generate estimates of $d\rho_{ij}^c$ by the method described above.

Process (a) reduces I assuming ρ_{ij}^c is known whereas process (b) reduces increments d assuming $\bar{\rho}_{ij}$ is known. In the particular case discussed in the next section, these two processes can be decoupled.

5.3 A Simplified Method

In one particular case, a strictly convergent method may be derived from these results. The method was derived for problems where the variable loading is dominated by a change of temperature between two extremes [8]. In this case it is permissible to make two assumptions; the plastic strains are produced at only two instants, $t = t_1$ and $t = t_2$ in the cycle and; for values of λ near to but greater than the shakedown limit, the load state will be in the reverse plasticity regime within the ratchet limit. In this case corresponding increments of residual stress, $d\rho_{ij}^1$ and $d\rho_{ij}^2$, and plastic strain, $d\varepsilon_{ij}^1$ and $d\varepsilon_{ij}^2$ are related by

$$d\varepsilon_{ij}^1 + d\varepsilon_{ij}^2 = 0 \quad \text{and} \quad d\rho_{ij}^1 + d\rho_{ij}^2 = 0. \tag{38}$$

This results in the following two equations from (36);

$$d\varepsilon_{ij}^{1Tf} = \frac{3}{2\mu^e}d\rho_{ij}^{1f\prime} + \frac{3}{2\bar{\mu}}(\lambda\hat{\sigma}_{ij}(t_1) + \bar{\rho} + d\rho_{ij}^{1f})^\prime, \tag{39a}$$

$$-d\varepsilon_{ij}^{1fT} = -\frac{3}{2\mu^e}d\rho_{ij}^{1f\prime} + \frac{3}{2\bar{\mu}}(\lambda\hat{\sigma}_{ij}(t_2) + (\bar{\rho}_{ij} + d\rho_{ij}^{1f}) - d\rho_{ij}^{1f})^\prime. \tag{39b}$$

Hence it is possible to eliminate $\bar{\rho}_{ij}$, the residual stress at the beginning of the cycle between Eqs. (39a) and (39b),

$$d\varepsilon_{ij}^{1Tf} = \frac{3}{2\mu^e}d\rho_{ij}^{1f\prime} + \frac{3}{4\bar{\mu}}(\lambda(\hat{\sigma}_{ij}(t_1) - \hat{\sigma}_{ij}(t_2)) + d\rho_{ij}^{1f})^\prime. \tag{40}$$

For fixed λ it can be shown that this is a strictly convergent process [8]. The proximity of the load point to the ratchet limit may then be evaluated by applying an additional constant load with its own load parameter. This involves the application of the shakedown method where the elastic solution is augmented by the evaluated values of $d\rho_{ij}^c$. This yields the ratchet boundary [8]. This limited application corresponds to the method normally applied in the Life Assessment method R5 [15]. Based on this simple assumption, a set of methods have been devised for the R5 methods [11, 12] where examples of both shakedown and ratchet solutions are given as well as extensions to time dependent behaviour.

5.4 A Direct Method

The following describes a first attempt to provide a direct evaluation of the ratchet limit, making use of the algorithms described above in Sect. 5.2.

The additional ingredient that makes this possible is a reinterpretation of the general minimum theorem (30) to (33).

We look for a value of λ where the exact solution satisfies a certain finite strain constraint. For example, we may require that the accumulated effective plastic strain at a particular point in a structure has a specific small positive value. In this case we seek a value of λ that exceeds the ratchet limit λ_R by a small amount. There exists a subclass of kinematically admissible strain rate histories that satisfy this constraint which we denote by $\dot{\varepsilon}_{ij}^{cc}$ (or increments $d\varepsilon_{ij}^{cc}$ for numerical solutions). The minimum theorem may be applied to this subclass of histories where $\lambda = \lambda^{cc}$ now only applies to those values where the exact solution satisfies this condition. Hence the following upper bound may be derived from (30) to (33)

$$\lambda^{cc} \leq \frac{\displaystyle\int_0^{\Delta t} \int_V (\sigma_{ij}^c - \rho_{ij}^{cc})\dot{\varepsilon}_{ij}^{cc}\,dV\,dt}{\displaystyle\int_0^{\Delta t} \int_V \hat{\sigma}_{ij}\dot{\varepsilon}_{ij}^{cc}\,dV\,dt} = \lambda_{UB}^{cc} \tag{41}$$

with a corresponding form in the incremental case. The member of the class $\dot{\varepsilon}_{ij}^{cc}$ that minimizes the upper bound λ_{UB}^{cc} provides the exact solution λ^{cc}.

The application of this theorem within a numerical scheme poses the particular problem of finding a procedure, of the type discussed above, were we remain within this predefined class $\dot{\varepsilon}_{ij}^{cc}$. By linear scaling, any kinematically admissible strain rate history may be changed to one that satisfies the required condition. However, the resulting solution that generates from such a strain rate history by the application of a matching procedure generally falls outside the class. The following suggested procedure attempts to make the best use of known methods but lacks a strict convergence proof.

The numerical procedure consisting of four stages is proposed based on the procedures (a) and (b) discussed in Sect. 3.1.

(1) A value of $\bar{\rho}_{ij}$ is obtained by applying procedure (a).
(2) Procedure (b) is then applied to produce a sequence of $d\varepsilon_{ij}^c$ throughout the cycle.
(3) The accumulated strain over the cycle is evaluated and a linear scaling factor is found that returns the strain increment history to the defined class, with a simultaneous scaling of $d\rho_{ij}^c$.
(4) The upper bound (41) provides a new estimate of λ_{UB}^{cc}.

The process then reverts to stage 1. The process is begun with an arbitrary constant choice of the shear moduli and assuming the $d\rho_{ij}^c$ are zero for the first application of stage 1.

Fig. 5 Bree problem

$$\sigma_t = P/P_L$$

$$\theta - \theta_0$$

x
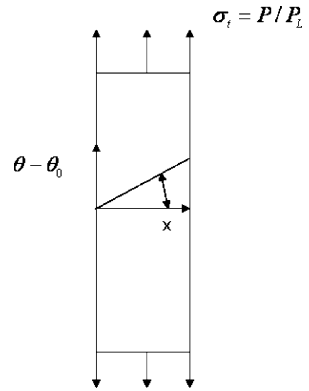
Although each stage corresponds to a numerical process that improves the solution, in the sense of reducing either I or d, no strict convergence proof seems possible at the present time. The primary barrier to a convergence proof is the fact that the sequences of plastic strain increments $d\varepsilon_{ij}^c$ so generated are not necessarily kinematically admissible. However, the method has been applied to simple problems and consistently converges although not necessarily monotonically as the following example demonstrates.

Consider the plane stress problem shown in Fig. 5, the simplest form of the Bree problem [7]. A plate is subjected to an axial stress σ_p and a varying linear through thickness temperature gradient, characterized by a maximum thermo elastic stress σ_t, the variation being between this value and zero temperature gradient. The plate is restrained against in-plane bending. Hence compatibility implies constant axial strain and equilibrium that axial stress integrates to the total applied stress. Figure 7 shows contours in the Bree

λ
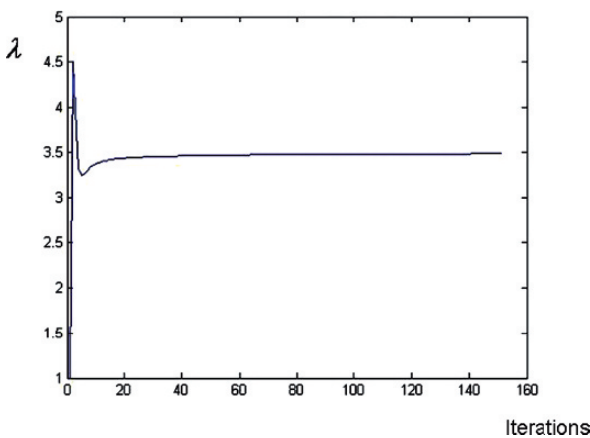
Iterations

Fig. 6 Variation of λ_{UB}^{cc} with number of iterations for $\Delta\bar{\varepsilon}_p = \sigma_y/E$ and $\sigma_p/\sigma_t = 4$
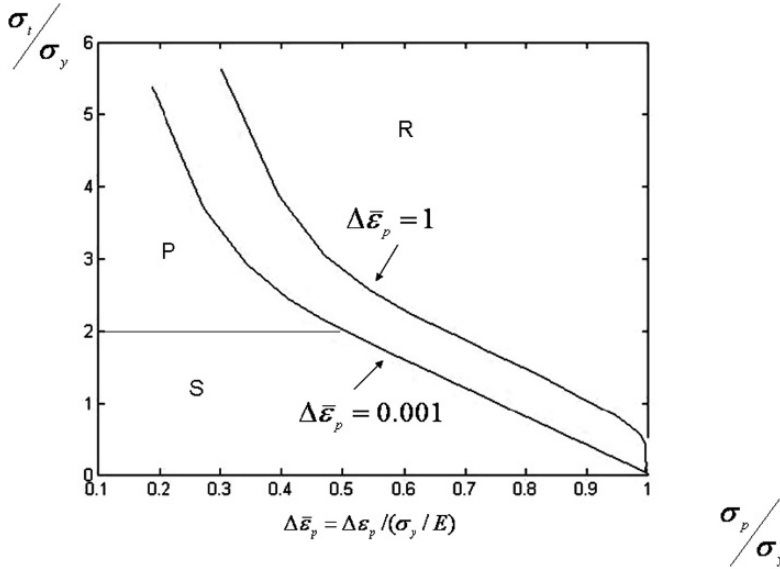
Fig. 7 A sequence of converged solutions for $E\Delta\bar{\varepsilon}_p/\sigma_y = 0.001$ and 1

diagram of a set of converged solutions for various ratios of σ_p/σ_t and for $\Delta\bar{\varepsilon}_p = 0.001\sigma_y/E$ a very small ratchet rate and $\Delta\bar{\varepsilon}_p = \sigma_y/E$. Convergence occurred for all solutions. A convergence sequence is shown in Fig. 6 for the more severe case where $\Delta\bar{\varepsilon}_p = \sigma_y/E$. Convergence is smooth but does not monotonically reduce. All solutions converged to the analytic solution of Bree [7], taking into account integration errors.

6 Further Applications

The shakedown method and the simplified ratchet boundary method have been extensively adapted for the material range involved in the High Temperature Life Assessment Method R5 [11,12]. Formal extension of the shakedown procedure to Norton creep has been given [22] as well as the extension of the ratchet boundary method to include creep relaxation during high temperature dwell times [12]. A method for bodies entirely within the creep range have been discussed [1, 16]. These methods have been applied to a number of industrial problems, including the characterisation of the behaviour of welds subjected to creep/fatigue conditions [10]. The characterisation of crack tip fields and residual strength of cracked structures subjected to cyclic thermal load has been discussed by [16–18]. The evaluation of the shakedown limit of a half space subjected to repeated rolling Hertzian contact forces over an elliptic contact region has been discussed by Ponter et al. [27].

The convergence condition of Sect. 4 is generally not satisfied by yield conditions that characterise the behaviour of soils and granular materials. Further, the flow rule at the limit state is non-associated if the yield condition is taken as the failure envelope. For the Drucker-Prager yield condition the method thus has been adapted by using both the hydrostatic pressure and the effective strain as the matching quantities [2–5]. In this way methods may be devised for both an associated and a non-associated flow rule. For this adapted method, a strict convergence proof is not available, but the conditions for the limit or shakedown state are satisfied if the process does converge. Converged solutions have been discussed for a number of problems, including rolling contact problems [2, 5].

7 Conclusions

The Linear Matching Method is an effective and convenient method for the evaluation of limit and shakedown limits in perfect plasticity. Extensions to problems have been achieved that lie outside the range of methods that rely upon the application of mathematical programming methods to the theorems of plasticity. For this reason the method has been developed into a set of direct methods for high temperature life assessment issues and applied to geotechnical problems. Implementation within the user routines of commercial finite element codes allows the method to be introduced into industrial practice.

References

1. Boulbibane M. and Ponter A.R.S. (2003), "A Finite Element Method for the Evaluation of Design Limits for Creep Fatigue Interaction", International Journal for Numerical Methods in Engineering, 58, 2065–2082
2. Boulbibane M. and Ponter A.R.S. (2005), "Extension of the Linear Matching Method Applicability to Geotechnical Problems", Computer Methods in Applied Mechanics and Engineering, 194, 4633–4650
3. Boulbibane M. and Ponter A.R.S. (2005), "Limit Loads for Multilayered Half-Space Using the Linear Matching Method", Computers and Geotechnics, 32, 535–544

4. Boulbibane M. and Ponter A.R.S (2005), "The Linear Matching Method for Geomechanics Problems Using the Linear Matching Method", Geomechnique, 55, 10, 731–739

5. Boulbibane M. and Ponter A.R.S. (2006), "The Linear Matching Method for Limit Loads and Shakedown Analysis of Geotechnical Problems", Journal of Numerical and Analytic Methods in Geomechanics, 30, 157–179

6. Boyle J.T., Hamilton R., Shi J., and Mackenzie D. (1997), "Simple Method of Calculating Lower-Bound Limit Loads for Axisymmetric Thin Shells", Journal of Pressure Vessel Technology, 119, 236–242

7. Bree J. (1987), "Elasto-Plastic Behaviour of Thin Tubes Subjected to Internal Pressure and Intermittent High Heat Fluxes with Application to Fast-Nuclear-Reactor Fuel Elements", Journal of Strain Analysis, 2, 226–238

8. Chen H.F. and Ponter A.R.S. (2001), "A Method for the Evaluation of a Ratchet Limit and the Amplitude of Plastic Strain for Bodies Subjected to Cyclic Loading", European Journal of Mechanics A/Solids, 20, 555–572

9. Chen H.F. and Ponter A.R.S. (2005), "On the Behaviour of a Particulate Metal Matrix Composite Subjected to Cyclic Temperature and Constant Stress", Computational Material Science, 34, 425–441

10. Chen H.F. and Ponter A.R.S. (2007), "'Modeling of the Behaviour of a Welded Joint Subjected to Reverse Bending Moment at High Temperature', Transactions on ASME", Journal of Pressure Vessel Technology, 129, 254

11. Chen H.F., Ponter A.R.S., and Ainsworth R.A. (2006), "The Linear Matching Method Applied to the High Temperature Life Assessment of Structures. Part 1. Assessments Involving Constant Residual Stress Fields", International Journal of Pressure Vessels and Piping, 83, 123–135

12. Chen H.F., Ponter A.R.S. and Ainsworth R.A. (2006), "The Linear Matching Method Applied to the High Temperature Life Assessment of Structures. Part 2. Assessments Beyond Shakedown Involving Changing Residual Stress Fields", International Journal of Pressure Vessels and Piping, 83, 136–147

13. Fernando C.P.D. and Seshadri R. (1993), "Limit Loads of Framed Structures and Arches Using the Gloss R-Node Method", Transactions of the ASME, 17, 2, 197–214

14. Gokhfeld D.A. and Cherniavsky D.F. (1980), "Limit Analysis of Structures at Thermal Cycling", Sijthoff & Noordhoff. Alphen an Der Rijn, The Netherlands

15. Goodall I.W., Goodman A.M., Chell G.C., Ainsworth R.A., and Williams J.A. (1991), "R5: An Assessment Procedure for the High Temperature Response of Structures", Nuclear Electric Ltd., Report, Barnwood, Gloucester

16. Habibullah M.S. and Ponter A.R.S. (2005), "Ratchetting Limits for Cracked Bodies subjected to cyclic loads and temperature", Engineering Fracture Mechanics, 2005, 72, 1702–1716

17. Habibullah M.S. and Ponter A.R.S. (2006), "A Crack Tip Field Estimation Technique for the High Temperature Cyclic Loading of Structures Submitted for Publication," Fatigue and Fracture of Engineering Materials and Structures, 29, 373–387

18. Habibullah M.S. and Ponter A.R.S. (2006), "Representation of the High Temperature Crack Tip Fields Using Reference Stress Concepts", Fatigue and Fracture of Engineering Materials and Structures, 29, 389–399

19. Hentz S. (1998) "Finite Element State Solutions, Accuracy of an Iterative Method", Report, Department of Engineering, University of Leicester and Department de Genie Mecanique, ENS de Cachan, Paris

20. Koiter W.T. (1960), "General Theorems of Elastic-Plastic Solids", in Progress in Solid Mechanics, eds. J.N. Sneddon, R. Hill, Vol 1, 167–221

21. Marriot D.L., "Evaluation of Deformation or Load Control of Stresses Under Inelastic Conditions Using Elastic Finite Element Stress Analysis", Proc. ASME PVP Conf., 136, Pittsburgh, 1988

22. Ponter A.R.S. (2001), "A Minimum Theorem for the Cyclic Behaviour of Creeping Bodies", Meccanica, 36, 37–47

23. Ponter A.R.S. (2007), "The Linear Matching Method for the Evaluation of Limit Loads, Shakedown Limits and Related Problems", Variational Formulations in Mechanics in Theory and Applications, Ed Taroco E., de Souza Neto and Novotny, CIMNE, Barcelona, Spain, 243–262

24. Ponter A.R.S. and Boulbibane M. (2003), "Minimum Theorems and the Linear Matching Method for Bodies in a Cyclic State of Creep", European Journal of Mechanics, A/Solids, 21, 2003, 915–925

25. Ponter A.R.S. and Chen H.F. (2001), "A Minimum Theorem for Cyclic Loading in Excess of Shakedown, with Applications to the Evaluation of a Ratchet Limit", European Journal of Mechanics A/Solids, 20, 539–554

26. Ponter A.R.S. and Engelhardt M. (2000), "Shakedown Limits for a General Yield Condition: Implementation and Examples for a Von Mises Yield Condition", European Journal of Mechanics, A/Solids, 19, 3, 423–446

27. Ponter A.R.S., Chen H.F., Ciavarella M., and Specchia G. (2006), "Shakedown Analyses for Rolling and Sliding Contact Problems", International Journal of Solids and Structures, 43, 4201–4219

28. Ponter A.R.S, Fuschi P., and Engelhardt M. (2000), "Limit Analysis for a General Class of Yield Conditions", European Journal of Mechanics, A/Solids, 19, 3, 401–422

Large Problems in Numerical Limit Analysis: A Decomposition Approach

F. Pastor, Z. Kammoun, E. Loute, J. Pastor, and H. Smaoui

Abstract A decomposition approach of the kinematical method of limit analysis is first presented. It is based on a mixed variational approach and on a convex interior point solver, using linear or quadratic discontinuous velocity fields. Exposed in plane strain, this method appears rapidly convergent, as verified in the Tresca compressed bar problem. Then the method is applied to the classical problem of the stability factor of a Tresca vertical slope: the upper bound is lowered from 3.882 to 3.7778. This value is to be compared to the lower bound just increased from 3.772 to 3.7752 by using the same solver in the extension of the method to the statical decomposition problem with infinite elements.

Franck Pastor

Université catholique de Louvain, Laboratoire CESAME, 1348 Louvain la Neuve, Belgium, e-mail: franck.pastor@uclouvain.be

Zied Kammoun

Ecole Polytechnique de Tunisie, Laboratoire de Systèmes et de Mécanique Appliquée, B. P. 743, 2078 La Marsa, Tunisie, e-mail: kammounzied@yahoo.fr

Etienne Loute

Facultés universitaires Saint-Louis and Louvain School of Management, Bld. Jardin Botanique 43, 1000 Brussels, Belgium, e-mail: loute@fusl.ac.be

Joseph Pastor

Université de Savoie, Polytech' Savoie, Laboratoire LOCIE, 73376 Le Bourget du Lac, France, e-mail: joseph.pastor@univ-savoie.fr

Hichem Smaoui

Ecole Nationale d'Ingénieurs de Tunis, B. P. 37, Le Belvédère, 1002 Tunis, Tunisie, e-mail: hichem.smaoui@enit.rnu.tn

1 Introduction

The paper of Lysmer [12] is the first which numerically deals with the static method of limit analysis (LA) in geotechnics using a finite element method (FEM). Based on this work, an improved static approach, also restricted to a bounded mechanical system, was proposed in [25]; this drawback was eliminated in [22] with the definition of infinite extension zones allowing the stress fields to remain admissible everywhere beyond the finite element mesh. All these works used a linearized approximation of the plasticity criterion.

Built upon the work in paper [5], powerful non-linear algorithms have recently been proposed, as in [10,11] for Tresca and Coulomb materials in the 2D and 3D cases, using also the previous extension elements in the static case. Another non-linear interior point formulation was proposed in [8], essentially valid for von Mises statical plane problems. On the other hand, an interior point optimization solver, which was presented in [14] was improved in [16,17] for solving the static problems for Gurson materials—where conic programming does not apply—and von Mises materials as a special case. Henceforth, this optimization solver will be called IP-OPT.

To our knowledge, the first mixed approaches were proposed in [1] and [2] for continuous velocity fields and piecewise linear criteria, and for the general case in [3] and in [26]. In [4] the mixed approach was extended to discontinuous linear velocities in plane strain. In [9], for 2D and 3D cases, thin finite elements were used to simulate the discontinuity segment, also for linear velocity fields, in a rather complicated way. In any case, these mixed formulations cannot be extended, as they are, to the quadratic velocity case without loosing the kinematical character.

Another mixed formulation, based on various convexity properties, was proposed in [20], and extended to the discontinuous quadratic velocity case in [21], providing rigorous kinematical solutions. Based on the previously mentioned IP-OPT code, these formulations appear to be very efficient and robust on a variety of mechanical problems [15,18,19].

In the following, after a short summary of the optimization solver, we briefly recall the mixed method used as a rigorous kinematical approach. Then we present the proposed decomposition approach in plane strain, and its detailed application to the problem of the compressed bar between rough dies and to the classical—still not exactly solved—problem of the stability of a vertical slope in a Tresca (or von Mises) material.

As regards the vertical slope problem, we give the very recent results of the decomposition method extended to the statical case in [7], using discontinuous linear stress triangles with extension elements, and IP-OPT. Both statical and kinematical decomposition approaches result in the best bracketing of the stability factor for this celebrated problem in geotechnics.

2 Interior Point Method and Convex Optimization

In [16], a general interior point algorithm for solving the statical problem of LA, hereafter named IP-OPT, is detailed. This paper focused on solving the plane strain LA problems for both von Mises and Gurson materials. The resulting optimization problems present a linear objective function and a mix of linear and non-linear convex constraints. For problems where the plasticity criterion is the von Mises or Drucker-Prager criterion, the non-linear constraints are convex quadratic inequalities, generating SOCP problems for which efficient algorithms and codes exist. Unfortunately these codes give not enough accuracy when post-analyzing the solutions, in the kinematical as well as in the statical present problems, resulting in non-admissible solutions for large scale problems. The IP-OPT code has allowed to overcome this drawback, being limited only by the RAM amount of the Mac Book Pro 3 GHz used for the calculations.

The general form of the optimization problems to be solved here is as follows:

$$\begin{aligned} \max \ & \boldsymbol{c}^T\boldsymbol{x} \\ \text{s. t. } & \boldsymbol{Ax} = \boldsymbol{b}\,, \\ & \mathbf{g}(\boldsymbol{x}) + \boldsymbol{s} = \boldsymbol{0}\,,\ \boldsymbol{s} \geqslant \boldsymbol{0}\,, \end{aligned} \tag{1}$$

where $\boldsymbol{c}, \boldsymbol{x} \in \mathbb{R}^n$, $\boldsymbol{b} \in \mathbb{R}^m$, $\boldsymbol{A} \in \mathbb{R}^{m \times n}$ is the matrix of the linear constraints, $\mathbf{g} = (g_1, \ldots, g_p)$ is a vector-valued function of p convex numerical functions g_i, and $\boldsymbol{s} \in \mathbb{R}_+^p$ is the vector of slack variables associated with these convex constraints.

The "primal-dual interior point method" consists in solving, instead of the previous problem, the following one, parametrized by $\mu > 0$, the "barrier parameter":

$$\begin{aligned} \min \ & \left(-\boldsymbol{c}^T\boldsymbol{x} - \mu \sum_{i=1}^p \ln(s_i) \right) \\ \text{s. t. } & \boldsymbol{Ax} = \boldsymbol{b}\,, \\ & \mathbf{g}(\boldsymbol{x}) + \boldsymbol{s} = \boldsymbol{0}\,,\ \boldsymbol{s} > \boldsymbol{0}\,. \end{aligned} \tag{2}$$

Using the "primal-dual interior point method", the problem (1) has a solution if and only if the following conditions are satisfied:

$$\begin{aligned} -\boldsymbol{c} + \boldsymbol{A}^T\boldsymbol{w} + \left(\frac{\partial \mathbf{g}}{\partial \boldsymbol{x}} \right)^T \boldsymbol{y} &= \boldsymbol{0}\,, \\ \boldsymbol{Ax} - \boldsymbol{b} &= \boldsymbol{0}\,, \\ \mathbf{g}(\boldsymbol{x}) + \boldsymbol{s} &= \boldsymbol{0}\,, \\ \boldsymbol{Y}\boldsymbol{S}\boldsymbol{e} &= \mu\boldsymbol{e}\,, \end{aligned} \tag{3}$$

where $\boldsymbol{w} \in \mathbb{R}^m$, $\boldsymbol{y} \in \mathbb{R}^p$, $\boldsymbol{e} = [1 \ldots 1]^T \in \mathbb{R}^p$ and $\boldsymbol{Y}$, $\boldsymbol{S}$ are the diagonal matrices associated with $\boldsymbol{y}$ and $\boldsymbol{s}$, respectively; $\mu > 0$ and $\boldsymbol{s} > \boldsymbol{0}$ imply $\boldsymbol{y} > \boldsymbol{0}$.

For each given μ the non-linear system (3) is approximately solved by one iteration of the Newton method, thereby providing an approximate solution of the parametrized problem (2). Using a sequence of values for μ decreasing to zero, we make the latter converge to the solution of (1). Indeed, as μ approaches 0, Eqs. (3) come close to the KKT conditions for the original problem. The code and its MATLAB implementation are fully detailed in [15].

3 Succinct Presentation of Limit Analysis

According to Salençon [29], a stress tensor field $\boldsymbol{\sigma}$ is said to be admissible if it is both statically admissible (SA, i.e., equilibrium equations, stress vector continuity, and stress boundary conditions are verified) and plastically admissible (PA, i.e., $f(\boldsymbol{\sigma}) \leqslant 0$, where $f(\boldsymbol{\sigma})$ is the (convex) plasticity criterion of the material). Similarly, a strain rate tensor field v is admissible if it is kinematically admissible (KA, i.e., derived from a piecewise continuous velocity vector field $\boldsymbol{u}$, with bounded discontinuities $[\boldsymbol{u}]$, such that the velocity boundary conditions are verified) and plastically admissible (PA, i.e., the associated flow rules (5a), (5b) are verified).

Let us assume, as in [29], that the virtual power rate P_{ext} of the external loads can be written as the scalar product of a loading vector $\boldsymbol{Q}$, whose components are called here loading parameters; and a generalized velocity vector $\mathbf{q} = \mathbf{q}(\boldsymbol{u})$, the components of which are called kinematical parameters. Following [1], let us consider a KA virtual velocity field $\boldsymbol{u}$; the virtual power principle (VPP) states that the stress tensor fields $\boldsymbol{\sigma}$, the stress vector field $\boldsymbol{T}$ (on the velocity discontinuity surfaces), and the vector $\boldsymbol{Q}$ are in equilibrium, if for any KA $\boldsymbol{u}$, the following variational equation is verified:

$$P_{\text{ext}} = \boldsymbol{Q} \cdot \mathbf{q}(\boldsymbol{u}) = \int_V \boldsymbol{\sigma} : \mathsf{v}\, \mathrm{d}V + \int_{S_d} \boldsymbol{T} \cdot [\boldsymbol{u}]\, \mathrm{d}S\,. \tag{4}$$

In (4), V is the volume of the mechanical system, and S_d is the union of the velocity discontinuity surfaces. The results in terms of $\boldsymbol{Q}$ will be interpreted as a kinematic bound if, at the appropriate points of V, the variables verify the following conditions, where $\boldsymbol{u}$ is KA and $\mathbf{q}^d$ is a fixed value of $\mathbf{q}(\boldsymbol{u})$:

$$\mathsf{v} = \lambda \frac{\partial f}{\partial \boldsymbol{\sigma}}\,, \qquad \lambda f(\boldsymbol{\sigma}) = 0\,, \qquad \lambda \geqslant 0\,, \qquad f(\boldsymbol{\sigma}) \leqslant 0\,, \tag{5a}$$

$$[\boldsymbol{u}] = \xi \frac{\partial f_{nt}}{\partial \boldsymbol{T}}\,, \qquad \xi f_{nt}(\boldsymbol{T}) = 0\,, \qquad \xi \geqslant 0\,, \qquad f_{nt}(\boldsymbol{T}) \leqslant 0\,, \tag{5b}$$

$$\mathbf{q}(\boldsymbol{u}) = \mathbf{q}^d\,. \tag{5c}$$

The criterion $f_{nt}(\boldsymbol{T})$ results from the projection of the plasticity criterion $f(\boldsymbol{\sigma})$ on the Mohr plane, where $\boldsymbol{n}$ is the normal to the element of the velocity discontinuity surface and $\boldsymbol{T} = (\sigma_{nn}, \sigma_{nt})$ is the stress vector on this element.

More precisely, $f_{nt}(\boldsymbol{T})$ is the solution of the following system:

$$f(\sigma_{nn}, \sigma_{tt}, \sigma_{nt}) = 0\,, \quad \frac{\partial f}{\partial \sigma_{tt}} = 0\,. \tag{6}$$

It is worth noting that, if (5a) and (5b) are verified, the quantities $\boldsymbol{\sigma} : \mathsf{v}$ and $\boldsymbol{T} \cdot [\boldsymbol{u}]$ become, respectively, the *convex* unit dissipated powers $\pi_V(\mathsf{v})$ and $\pi_d([\boldsymbol{u}])$ of LA, i.e.:

$$\pi_V(\mathsf{v}) = \boldsymbol{\sigma} : \mathsf{v}\,, \quad \pi_d([\boldsymbol{u}]) = \boldsymbol{T} \cdot [\boldsymbol{u}]\,. \tag{7}$$

4 Kinematic Method of LA: A Mixed Finite Element Formulation

The equivalence between the classical kinematical method and the present mixed approach is detailed in [15] and [18]. For the sake of conciseness, we only recall here the main features of this mixed method in the quadratic case, referring the reader to the previously mentioned references for details.

4.1 Case of Continuous Velocity Fields

Starting from [20], the algorithm is presented in the quadratic velocity case, using numerical notations in the resulting final expressions; the mechanical plane strain system is discretized in triangular finite elements, with displacement velocities as virtual variables, and three specific apex stress tensors as real variables. First we examine the continuous velocity case as regards the VPP (4), and the role of the inter-element discontinuity segments in the next subsection.

Located at the three apexes and the three middles of the sides of the triangle, the six-component nodal vectors $\{u_x\}$ and $\{u_y\}$ can be written using interpolation matrices calculated for each element. Thus, from its definition, the external power can be written as:

$$P_{ext} = \mathbf{q}(\boldsymbol{u}) \cdot \boldsymbol{Q} = \{q(u)\}^T\{Q\} = \{u\}^T[\beta]\{Q\}\,, \tag{8}$$

where $[\beta]^T$ is the matrix resulting from the calculation of the generalized velocity $\mathbf{q}(\boldsymbol{u})$.

Inside the triangular element k, the strain rate tensor $\{v\}$ is defined by the classical equation:

$$\{v\} = [B]_k \{u_k\}\,, \tag{9}$$

where the vector $\{u_k\}$ collects the twelve degrees of freedom of the element k, and $[B]_k$ is computed relatively to its twelve nodal displacements.

As detailed in [19], inside the triangle (of area S_k), the strain rate tensor $\{v\}$ is PA and associated to the stress tensor at the apexes of the triangle; therefore the product $\boldsymbol{\sigma} : v$ equals $\pi(v)$ at these apexes. As v is linearly varying, from the convexity of the set of the PA strain rates it is PA everywhere in the triangle (see [13] and [29]). The dissipated power, i.e. the integral of $\pi(v)$, can then be upper bounded by replacing the integral of $\boldsymbol{\sigma} : v$ by its linear interpolation over the triangle. Hence the VPP (4) numerically becomes:

$$\{q(u)\}^T\{Q\} = \sum_k S_k \left[\{v_i\}^T\{\sigma_i\} + \{v_j\}^T\{\sigma_j\} + \{v_m\}^T\{\sigma_m\} \right]/3 \quad \forall \text{ KA } \{u\},$$
(10)

where k is the index of the triangle and (i, j, m) refer to the three apexes of the element. Using (9) at the apexes, and after the assembly of the elements, the relationship (10) gives rise to the final numerical system:

$$\{u\}^T \left[-[\alpha]\{\sigma\} + [\beta]\{Q\} \right] = 0 \quad \forall \text{ KA } \{u\},$$
(11)

where the matrix $[\alpha]$ results from the assembly of the submatrices $[\alpha]_k = S_k[B]_k^T/3$ calculated at the apexes of each triangle k in the numerical VPP (10). Finally the mixed problem to be solved is the following:

$$\max \{q^d\}^T\{Q\}$$
(12a)
$$\text{s. t. } -[\alpha]\{\sigma\} + [\beta]\{Q\} = 0,$$
(12b)
$$f(\sigma) \leqslant 0 \text{ at all apexes}.$$
(12c)

This is the optimization problem (1), with $\boldsymbol{A} = [-[\alpha], [\beta]]$, $\boldsymbol{b} = \boldsymbol{0}$, $\boldsymbol{x}^T = \{\{\sigma\}^T, \{Q\}^T\}$.

Then, the optimal primal-dual solution $(\{w\}, \{y\}, \{\sigma\}, \{Q\})$ of this problem verifies (3) with $\mu_i e_i = 0$, i.e., $y_i \geqslant 0$ if $f(\sigma_i) = 0$, and $y_i = 0$ otherwise, at each apex i of the triangles. After transposition, the first equation in (3) becomes:

$$-\{c\}^T + \{w\}^T \left[-[\alpha], [\beta] \right] + \{y\}^T \left\{ \frac{\partial f}{\partial \sigma} \right\} = 0.$$
(13)

Identifying $\{w\}^T$ as $\{u\}^T$, we shortly recall various items that will be useful to formulate the decomposition approach in the next section, referring to [19] for details:

- The vector $\{c\}$ equals $\mathbf{q}^d$; then Eq. (13) becomes $\{u\}^T[\beta] = \mathbf{q}(\boldsymbol{u})^T = \mathbf{q}^{d^T}$, as the components of $\{Q\}$ do not have to verify any criterion condition: the kinematic loading condition $\mathbf{q}(\boldsymbol{u}) = \mathbf{q}^d$ is verified.
- The KA conditions (null velocity components) will be taken into account by removing the corresponding rows of the final constraint matrix. Nonzero

imposed values define generalized velocities which are imposed as components of the vector $\mathbf{q}^d$ hereafter. This point gives the way to impose the velocity values at the interfaces further.

- The $\{c\}$ functional coefficients are null, except for the components of $\{Q\}$. From the structure of $[\alpha]$ and (13), the normality law (5a) is verified at the apexes with multipliers λ_i proportional to the y_i. Consequently the tensors $\boldsymbol{\sigma}$ and v are PA and associated at each apex, where the product $\boldsymbol{\sigma} : \mathsf{v}$ equals $\pi(\mathsf{v})$, and the value of (10) is confirmed as an upper bound to the dissipated power all over the triangular element.

4.2 Implementing Velocity Discontinuities

According to [23] and [30], a discontinuity surface element (of normal $\boldsymbol{n}$) can be assimilated to a thin zone whose thickness vanishes such that the appropriate static and kinematic variables are respectively the stress vector $\boldsymbol{T} = (T_n, T_t) = (\sigma_{nn}, \sigma_{nt})$ and the velocity jump vector $[\boldsymbol{u}] = ([u_n], [u_t])$ associated by the normality law relative to the $f_{nt}(\boldsymbol{T}) = 0$ criterion.

The velocity jump $[\boldsymbol{u}]$ is defined as the difference between the velocities of two contiguous points along a discontinuity segment named 1–2 in the following. The dissipated power along the segment is written, in plane strain, as:

$$P_{\text{diss}}([\boldsymbol{u}]) = \int_{1-2} \pi_d([\boldsymbol{u}])\, \mathrm{d}l = \int_{1-2} \boldsymbol{T} \cdot [\boldsymbol{u}]\, \mathrm{d}l\,, \tag{14}$$

where $\boldsymbol{T}$ and $\boldsymbol{u}$ are associated through (5b). Relation (14) then requires $[\boldsymbol{u}]$ to be PA anywhere along the segment 1–2. In order to do this we force the velocity jump to vary linearly along the segment as in [19], by imposing that the jump at the middle is half the sum of the end jumps through appropriate row condensations. Now, as in the volume case, let us add a numerical stress vector $\boldsymbol{T}$ at each end of the discontinuity segments. From the convexity of the function $\pi([\boldsymbol{u}])$, we here also upper bound the dissipated power along any segment 1–2 by writing, in numerical notations:

$$P_{\text{diss}}([\boldsymbol{u}]) = L_{1-2}\left(\{[u]\}_1^T \{T\}_1 + \{[u]\}_2^T \{T\}_2\right)\Big/2\,, \tag{15}$$

where L_{1-2} is the length of the segment 1–2.

In fact, as in [20], we add a stress *tensor*—expressed in the (n, t) axes as $\sigma_{nn} = T_n$, σ_{tt}, $\sigma_{nt} = T_t$—at each end of the discontinuity segment. The σ_{tt} component does not appear in the definition (15); the corresponding column of the matrix $\boldsymbol{A}$ remains zero. From (13), at each end of the segment we obtain $0 = y\frac{\partial f}{\partial \sigma_{tt}}$, i.e., the projection condition (6) defining the f_{nt} criterion, whose expression is then not necessary.

When problem (12) is completed and solved, $[\boldsymbol{u}]$ is PA and associated to $\boldsymbol{\sigma}$ at both ends of segment 1–2, through the same reasoning as for the triangles.

Then, owing to its linear variation along 1–2, $[\boldsymbol{u}]$ is PA anywhere because of the convex character of the PA $[\boldsymbol{u}]$ set, and (15) is verified as an upper bound.

5 The Proposed Decomposition Method

The present decomposition is based on a partition of the FEM mesh, however without connection with the so-called domain decomposition methods, fully and readably presented in the reference [27]. Moreover, these methods seem not to be applied to the optimization problems, as it can be seen in the very complete reference [31] about the state of the art on the domain decomposition approach.

As regards the limit analysis problem, up to our knowledge, the domain decomposition approach was only used in [6] for a classical kinematical approach, with non-overlapping sub-domains. However, no detail is given about how the variable values are updated at the interfaces from one iteration to another. *A contrario*, the present method proceeds iteratively with, at each decomposition level, an auxiliary problem for each interface in order to upgrade their interface variables; moreover, a few iterations are necessary in fact. Hereunder we present the method and, afterwards, its application to two standard mechanical problems.

The method was first developed in the continuous velocity case; it is presented on the problem of a bar compressed under rough rigid plates of ratio width versus height equaling 2 (Fig. 1). Due to the symmetries of the problem, only the upper left quarter of the bar is meshed in 4×2 squares or rectangles diagonally subdivided in four triangles. The velocities vary linearly and continuously along each interface. The (half) rigid plate (of width b) goes down with a uniform, vertical velocity U_0 which is created through the action of a central vertical force F to be determined. The isotropic, homogeneous material obeys the von Mises (or Tresca) criterion with cohesion c. The velocities of the bar and the plate at the interface are the same, i.e. no sliding is allowed so that the dissipated power is only volumetric. There is here only one loading parameter $Q = F$ and the generalized associated velocity is $q^d = U_0$; both will be the same for all subproblems because of a
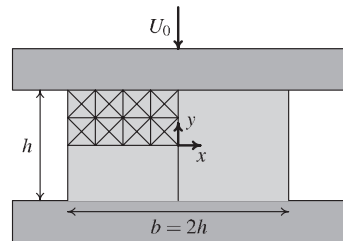
Fig. 1 The compressed bar, $b = 2h$, mesh $2N \times N$, here $N = 2$

vertical partition of the mesh; this is a fair feature, as it will be seen in the second problem where the loading exterior factor is the volumetric weight.

A simple four-block mechanism for the whole problem gives $F/(bc) = 2.5$. The exact solution is due to J. Salençon [28], namely 2.42768 in the present case.

5.1 The Starting Problem

Solving this first reduced problem allows to obtain a good initialization for the velocities at the separating interfaces of the target problem (Fig. 2) by an appropriate interpolation. Another solution should consist in extracting
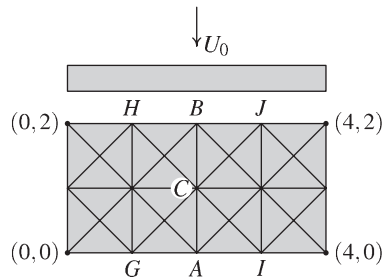
Fig. 2 The target problem

the interface values from an analytical kinematical solution; however this technique, generally less efficient in terms of convergence rate, needs also a preliminary treatment specific to the considered mechanical problem. Hence we begin with solving the 2×1 problem of the same bar problem, Fig. 3.
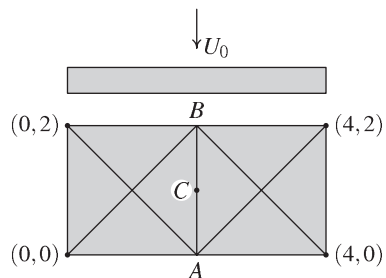
Fig. 3 The starting problem

The solution of this starting problem gives the initial nodal values at the points A, B, C, i.e. $\boldsymbol{u}^A$, $\boldsymbol{u}^B$ and $\boldsymbol{u}^C$ which will be taken as boundary conditions, in fact as new kinematical parameters q_i for the left (II$_\mathrm{l}$) and the right (II$_\mathrm{r}$) subsequent problems II. The velocity in C is calculated by linear interpolation, owing to the assumed linear variation of the velocity inside

the triangles. Note finally that a complete starting solution could also be extrapolated for the two following subproblems, but it is well known that this possibility is much less efficient in the present interior point method than in the linear programming case, hence it has not been tested here.

5.2 The Left Problem
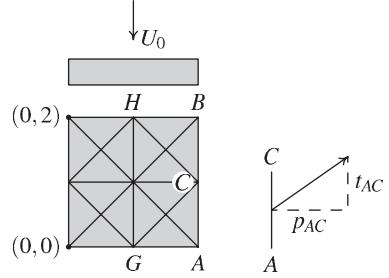
Fig. 4 The left problem
II_g

Figure 4 shows how the "left" problem is meshed. We denote respectively the lengths of the sides AC and BC by l_{AC} and l_{BC}, the values of σ_{xx} and σ_{xy} on the side AC by p_{AC} and t_{AC}, and p_{BC} and t_{BC} their values on the side BC. These stress components are taken as constant on their sides because constant stress tensors in the triangles are needed here to keep the kinematical character.

Let us now express the power of the external forces P_{ext} explicitly:

$$
\begin{aligned}
P_{\text{ext}} &= FU_0 + \int_{AC} pu_x \, \mathrm{d}y + \int_{CB} pu_x \, \mathrm{d}y + \int_{AC} tu_y \, \mathrm{d}y + \int_{CB} tu_y \, \mathrm{d}y \\
&= FU_0 + p_{AC}l_{AC}\frac{u_x^A + u_x^C}{2} + p_{CB}l_{CB}\frac{u_x^C + u_x^B}{2} \qquad (16) \\
&\quad + t_{AC}l_{AC}\frac{u_y^A + u_y^C}{2} + t_{CB}l_{CB}\frac{u_y^C + u_y^B}{2}.
\end{aligned}
$$

By reordering (16) we obtain seven generalized velocities q_i^d which are the six components of the velocities at the points A, B, C, and U_0 as expected.

Finding the loading parameters Q_i will consist in defining a kinematical parameter equal to the displacement velocity component at each nodal point of the interface, and the associated loading parameters through the expression of the external power. Then we define the functional of the left problem (Fig. 4) as:

$$P_{\text{ext}} = FU_0 + Q_1 u_x^A + Q_2 u_y^A + Q_3 u_x^C + Q_4 u_y^C + Q_5 u_x^B + Q_6 u_y^B. \quad (17)$$

As detailed in the second item of Sect. 4.1, the equality between $\mathbf{q}(\mathbf{u})$ and $\mathbf{q}^d$ in the optimal solution will lead to the expected verification of the new boundary conditions. It is worth noting that the previous parameters come in fact from the usual FEM definition of the nodal forces via the equivalence, along an interface element, between the virtual powers of the nodal forces and the stress distribution assumed to vary as the strain rate tensor in the adjacent element, resulting here in a constant one.

In the case of linearized velocity jumps of the second example (discontinuous quadratic velocities), the present mesh would have six nodes on the interface, giving rise to thirteen final loading parameters by assuming an affine distribution of the stress vector. The corresponding value of the dissipated power will be exactly calculated by a Simpson integration using the nodes at the ends and the middle of the interface segment, as the integrand variation will be cubic along the segment.

Relation (17) gives the functional to be maximized for the problem II_l: it will be noted $FU_0 + Q_i q_i$ using the usual Einstein convention with $i = 1, \ldots, 6$. At the optimum, the functional will be equal to the dissipated power in the mesh of this problem, or to its upper bound in the second example as defined in the Sect. 4.

5.3 The Right Problem

This time the velocities $\mathbf{u}^A$, $\mathbf{u}^B$, $\mathbf{u}^C$ are imposed at the left side of the mesh of Fig. 5. This problem is analogous to the preceding one, except the appearance of the symmetry at the right side. As previously we have:

$$P_{\text{ext}} = QU_0 + p'_{AC} l_{AC} \frac{u_x^A + u_x^C}{2} + p'_{CB} l_{CB} \frac{u_x^C + u_x^B}{2}$$
$$+ t'_{AC} l_{AC} \frac{u_y^A + u_y^C}{2} + t'_{CB} l_{CB} \frac{u_y^C + u_y^B}{2}, \quad (18)$$

and, after reordering:

$$P_{\text{ext}} = FU_0 + Q'_1 u_x^A + Q'_2 u_y^A + Q'_3 u_x^C + Q'_4 u_y^C + Q'_5 u_x^B + Q'_6 u_y^B = FU_0 + Q'_i q_i. \quad (19)$$

Here also, the optimal P_{ext} is equal to the dissipated power over the mesh, or to its upper bound in the quadratic case. Joining all interface nodal points of the II_l and II_r optimal solutions gives an admissible solution for the whole problem, i.e. the target problem. The target dissipated power is the sum of the subproblem's ones, giving a target functional value lower (or at least equal) than that of the starting problem.

Fig. 5 The right problem
II$_r$
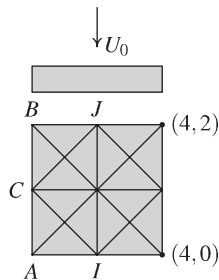
In order to progress by iterating the process, updating the velocities at the interface is obviously needed; hence the idea of the following specific phase III to improve these interface values.

5.4 Phase III
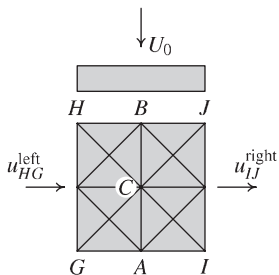
Fig. 6 The central problem

Prior to this phase the optimal values along the GH segment obtained in the II$_l$ problem and the values along IJ in II$_r$ are saved in an external file. The solution of this problem III (Fig. 6) is obtained as in the previous problem, except that the loading parameters are now defined from the lateral sides HG and IJ (here thirteen parameters in total); the updated values at the central interface AB correspond to a lower dissipated power in the $GHJI$ mesh. Note that, at this stage, combining (by post-analysis) the field of the left part of II$_l$ and the field of the right part of II$_r$ with the field of the present phase gives an admissible field for the target problem, with a dissipated power lower than the previous one.

Finally, by going back to phase II with the new values on ACB, the process can be resumed. Each following iteration, namely a global one, consists in solving the problems III, II$_l$ and II$_r$.

6 Kinematical Tests

The proposed decomposition approach was first investigated in the case of the compressed bar for continuous velocities, and afterwards has been extended to the classical problem of the vertical slope in the discontinuous quadratic case. The latter problem is a difficult one, as it leads to very large optimization problems, and also because it needs a high accuracy level—and a meticulous post-analysis of the solution fields—in order to guarantee the numerical final value of the optimal loading parameter.

6.1 The Compressed Bar Problem

6.1.1 First Level Decomposition

The mechanical problem is defined in Fig. 2 with 4×2 squares of 4 triangles each, named a 4×2 problem for the sake of simplicity. Let us consider now a 64×32 target problem, and a 32×16 starting problem. These meshes were selected as a good compromise between efficiency and CPU time in accordance with the number of calculations to be conducted for these validation tests. Moreover, it is worth recalling the absence of locking problems in this mixed approach, unlike the classical approach. For simplicity the cohesion c was initialized to unity in these numerical problems.

Figure 7 gives the evolution of the loading parameter F/c from the starting value 159.01, (i.e. $F/(bc) = 2.4845$, with $b = 64$ and $c = 1$) versus the iteration number to the best value which is 157.339. The three subproblems (II and III) here are 32×32 ones. Solving directly the target problem gives the asymptotic value 157.33, the exact solution giving 155.37.
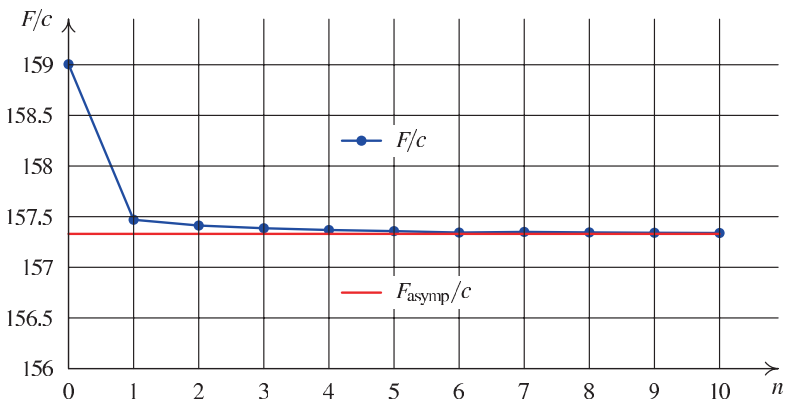
Fig. 7 Variation of F/c related to the iterations number n

6.1.2 Second Level Decomposition

The target problem is again the 64×32 which gives the optimal value $F/c = 157.33$ in 1030 seconds of CPU time. The problems II are themselves subdivided into subproblems.

The problem II_l gives birth to the subproblem II_{ll} and II_{lr} and the problem II_r to the subproblems II_{rl} and II_{rr}. Consequently three problems III are defined: III_l for the problems II_{ll} and II_{lr}, III_r for the problems II_{rl} and II_{rr}, and finally a central III_c to update the central interface. The whole process is illustrated in Fig. 8.
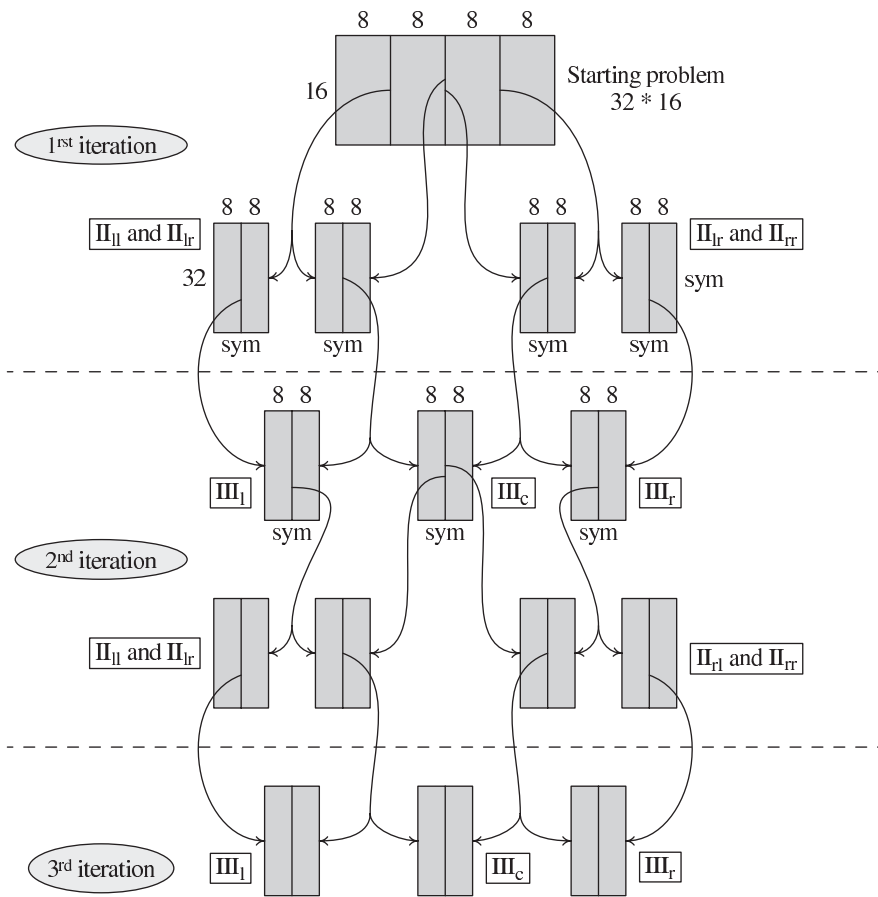
Fig. 8 Second-level decomposition of the 64×32 plate

The final result (157.463) of Table 1 must be compared to the one obtained after the first iteration of the first level decomposition, i.e. 157.469 in 533 s, the target problem giving 157.33 in 1033 s.

Table 1 Compressed bar 64×32: results of the second-level decomposition

Iteration	1	Iteration	2	3	4
		III_l	41.7815	41.7128	41.6814
Starting	159.0051	III_r	36.6723	36.6817	36.6915
		III_c	41.5183	41.5467	41.5486
Time	66 s	Time	343 s	387 s	70 s (start. point)
II_{ll}	33.4242	II_{ll}	42.3162	42.2861	42.2724
II_{lr}	40.1507	II_{lr}	41.6370	41.6215	41.6215
II_{rl}	41.5851	II_{rl}	40.1323	40.1462	40.1462
II_{rr}	42.4637	II_{rr}	33.4320	33.4309	33.4309
F_{tot}	157.6238	F_{tot}	157.5176	157.4847	157.4627
Time	350 s	Time	430 s	357 s	243 s (start. point)

It can be seen that four level-2 iterations are necessary to improve the value obtained at the first level-1 iteration, using the same starting problem in both cases. Also, at the iteration 4 we have used the complete solution of iteration 3—i.e. all the x, s, w, y solutions of (3)—as a starting point for the optimization algorithm, resulting in less CPU time: we can see that this possibility should actually be used right from the first iteration. This efficiency comes from the fact that only the functional changes from one iteration to another in this approach.

6.2 The Vertical Slope Problem

6.2.1 Position of the Problem

This time the decomposition method is applied using the finest model, i.e. the discontinuous quadratic one, to the vertical slope problem in a Tresca material, the height of which being denoted H, the weight γ and cohesion c. The best known upper bound for Q_γ ($=\gamma H/c$) was given as 3.782 in [24], the best lower bound as 3.772 in [10]. The mesh is square with $N \times N$ rectangles of four triangles each.

In a first time, a global, coarser mesh is optimized by a power law acting on the coordinates in order to concentrate the mesh at the bottom of the slope. Then the optimized mesh is divided into horizontal slices of the same number of elements. Indeed a first cut in vertical slices has pointed out that the last right slice had no sufficient possibilities of free plastic flow, inducing a number of convergence problems.

In the present case, the generalized velocity q_γ (here taken as $\int (cu_y/H)\, dS$ where the axis y is vertical) is not the same for all subproblems, contrary to the previous compressed bar where the plate acted on all subproblems with the same velocity. *Via* the (systematic) post-analysis, at each step are

imposed to the subproblem i its quota of q_γ—i.e. $q_{\gamma i}^d$—obtained from the solution fields of the previous step as the interface velocities; indeed the sum of the $q_{\gamma i}^d$ remains equal to the initial q_γ^d. The global mesh is an $N \times N$ square for all tests.
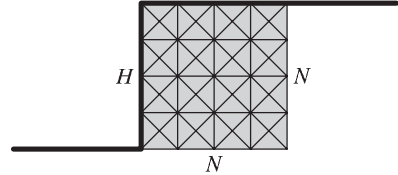
Fig. 9 The vertical slope with a $N = 4$ mesh

6.2.2 Details of the Tests

From $N = 16$ to 96, the problem is solved directly. Beyond this size, the Cholesky subroutine used by IP-OPT needs more RAM memory than the 4 GB available on our Mac Pro Apple 3 GHz. It is worth noting also that only the IP-OPT runs beyond the $N = 70$ case, contrary to commercial codes. Then, from $N = 100$ to $N = 120$ the problem was split into two subproblems in a level-1 decomposition.

For $N = 120$, two iterations were performed (starting-II$_{\text{top}}$-II$_{\text{bottom}}$, then III-II$_{\text{top}}$-II$_{\text{bottom}}$), and the results were the following:

- starting problem ($N \times N = 60 \times 60$) : $\gamma H/c = 3.7813$;
- iteration 1 : $\gamma H/c = 3.7789$;
- iteration 2 : $\gamma H/c = 3.7788$.

Clearly, at least for this problem where the decomposition approach was intensively tested, the first iteration is sufficient if the subproblem meshes are well refined. This should be attributed to the discontinuous character combined to the quadratic variation of the velocities, solved without any problem using the IP-OPT code in all cases.

For $N = 144$, 160, 176 and 200, both subproblems were themselves decomposed in a level-2 decomposition. The final optimal 200×200 value was $\gamma H/c = 3.7778$. In fact, in the post analysis, the dissipated power also was re-calculated using the analytical π functions, lowering the IP-OPT value from 3.77793 to 3.77779, with all verifications better than 10^{-6} in all subproblems: this confirms the previously mentioned efficiency of the method in spite of optimizing an upper bound to the real dissipated power.

Figure 10 shows the variation of the stability factor versus the number of rectangles of the previous mesh: it seems that the result could be still slightly improved by using a higher level of decomposition on a more powerful machine.

Finally, Fig. 11 shows the deformed meshes of the four 200×50 subproblems. This figure can be highly zoomed if viewed on a computer screen as it
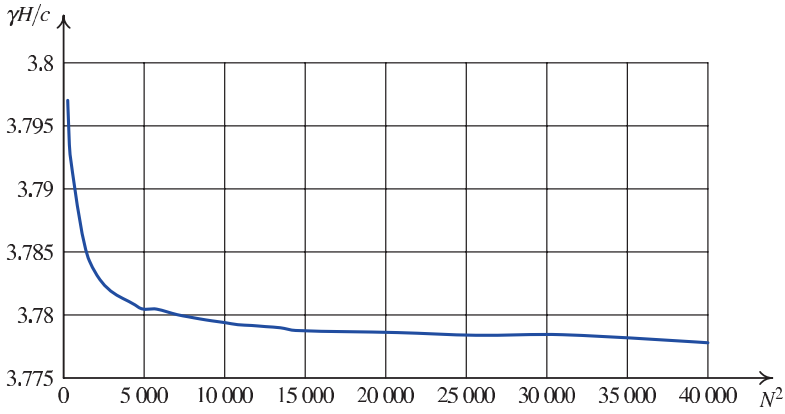
Fig. 10 The vertical slope: $\gamma H/c$ versus the size of the mesh
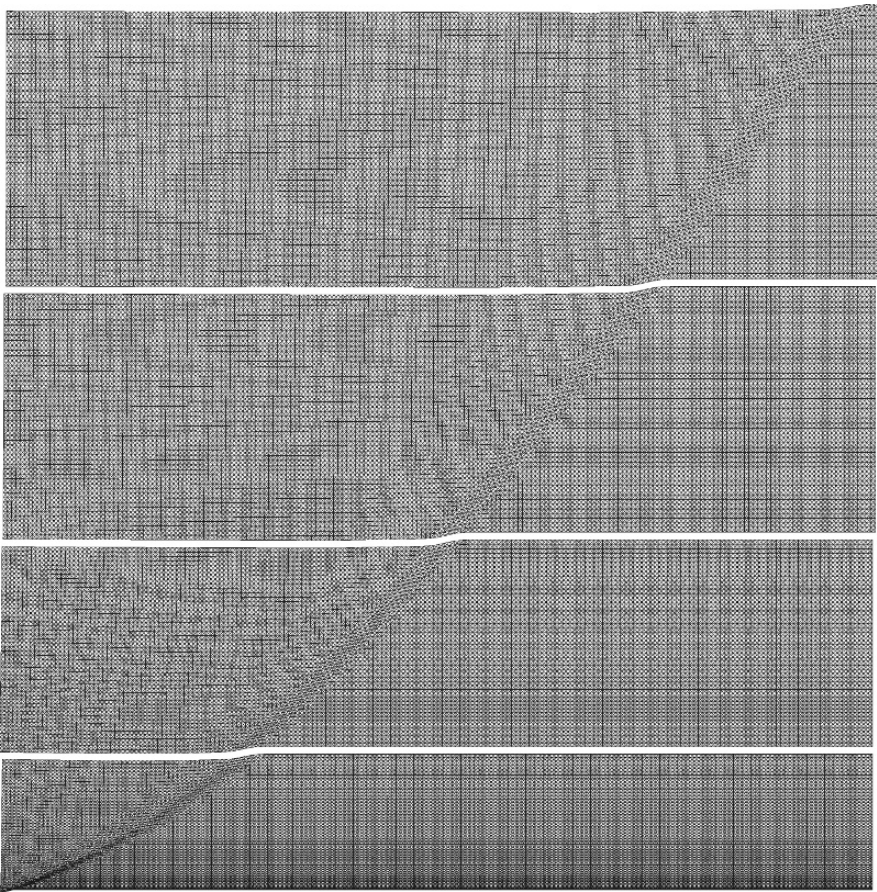
Fig. 11 The Tresca vertical slope, $N = 200$: deformed meshes of the four 200×50 subproblems. Dissipated powers, with as input data $c = 1$ and $H = 200$: $4.56 - 4.95 - 4.66 - 4.72$

is plotted using the Asymptote vectorial drawing tool under LaTeX. In this case, the CPU times vary from one to six hours for the subproblems. To be complete, let us note that the target problem 200×200 ($160,000$ quadratic discontinuous triangles) should give a problem with $2,230,000$ variables and $1,490,000$ linear constraints plus $743,000$ non-linear ones!

7 Extension to the Statical Approach: First Results

The decomposition method presented in the previous section has just been extended to the classical lower bound approach of LA in [7] where a detailed presentation is given. As suggested in Fremond and Salençon (1973) the problem is replaced by an equivalent one, such that the soil is weightless and the boundary conditions are defined by $\sigma_n = \gamma h, \tau_{nt} = 0$ on the surface of the soil, h denoting the depth measured from the upper surface.

In the following, first results for the vertical slope problem described in Sect. 6.2 are reported, presenting improved lower bounds, again made possible by using the code IP-OPT. The domain occupied by the soil is modelled by discontinuous linear stress triangles and infinite extension zones as in [22]; in Fig. 12 an example mesh is depicted showing the subdomain partitions typically used in the decomposition procedure.
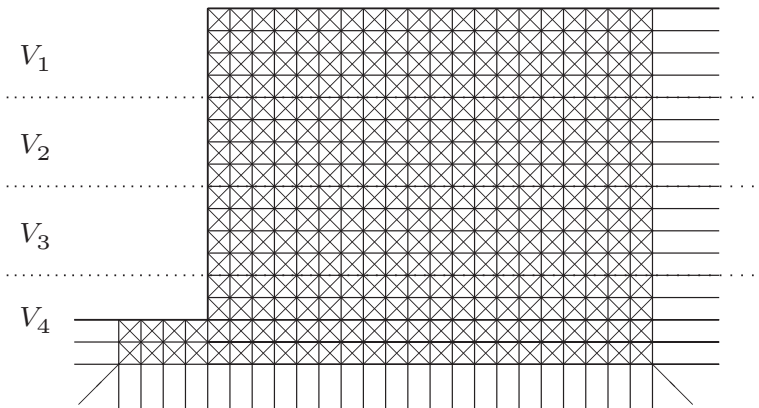
Fig. 12 Vertical slope: a typical 4-block partition ($M \times N = 24 \times 16$)

The lower bound is determined for various mesh sizes as shown in Table 2. The best lower bound is $\gamma H/c = 3.7752$, obtained with 351,824 elements, which is an improved value with respect to the best known value 3.772 in [10]. It is worth noting that a meticulous analysis of the redundancies induced by the extension conditions was necessary to make the final optimization problem full row rank, as required by IP-OPT. This code was again the only one

Table 2 Vertical slope and decomposition level 2: lower bound results after 9 iterations

$M \times N$	Number of FE	Result
260×184	179408	3.77452
270×200	200336	3.77466
300×224	249600	3.77482
316×240	281104	3.77500
344×280	351824	3.77522

able to run these large non-linear problems, with admissibility conditions a posteriori verified better than 10^{-8} in all the tests. Contrary to the kinematical case, up to ten iterations of the decomposition process were needed in this statical approach to get convergence to the final value, as shown in Fig. 13. Finally, with the upper bound reported Sect. 6.2, we obtain for this problem:

$$3.7752 \le \gamma H/c \le 3.7778 \,.$$
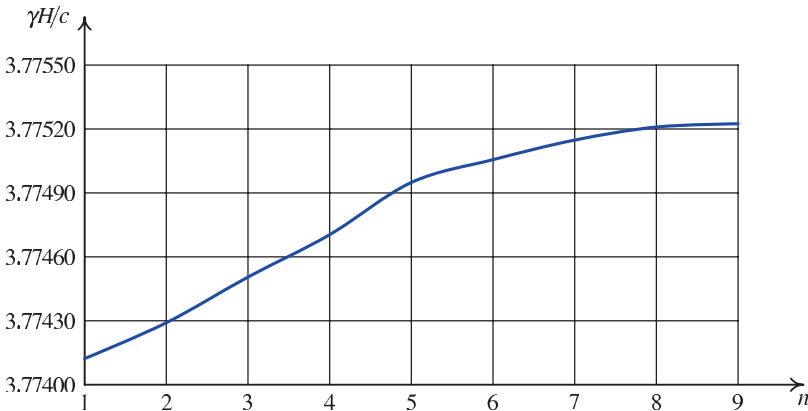
Fig. 13 The vertical slope: $\gamma H/c$ versus the iteration number n, 344×280 mesh

8 Conclusion

The proposed decomposition method fully uses the specific features of the mixed but fully kinematical approach. Its remarkable efficiency lies in fact in the constant robustness and the rapidity of the IP-OPT solver under MATLAB.

In the kinematical case, from the first iteration a good accuracy of the final optimum is obtained, with a regular improvement during the following ones.

Hence, using a refined starting problem, we can iterate the decomposition process, here to the level two, and obtain very good and accurate solutions for meshes out of reach directly, especially for open problems where a fine bracketing of the solution yet exists. For example, in the case of the vertical slope problem, we were able to lower the upper bound from 3.782 to 3.7778, by decomposing an optimization problem which up to now has been intractable directly, at least to our knowledge.

The decomposition method has just been extended to the statical case, using discontinuous linear stress triangles and infinite extension elements. Here also the code IP-OPT was the only one able to solve the very large final non-linear optimization problems. Hence the previous lower bound (3.772, [10]) has been increased to 3.7752 by using also a level-2 decomposition, resulting in the best bracketing to date: $3.7752 \leq \gamma H/c \leq 3.7778$.

References

1. Anderheggen, E., Knopfel, H.: Finite element limit analysis using linear programming. Int. J. Solid. Struct. **8**, 1413–1431 (1972)
2. Capurso, M.: Limit analysis of continuous media with piecewise linear yield conditions. Meccanica **1**, 53–58 (1971)
3. Christiansen, E.: Limit analysis of collapse states. In: Ciarlet, P.G., Lions, J.L. (eds.), Handbook of Numerical Analysis, North-Holland, Amsterdam, pp. 193–312. (1996)
4. Ciria, H., Peraire, J.: Limit analysis and convex optimization: Applications. In: 9th ASCE Specialty Conference on Probabilistic Mechanics and Structural Reliability. Albuquerque (2004)
5. Herskovits, J.: A two-stage feasible directions algorithm for nonlinearly constrained optimization. Math. Program. **36**, 19–38 (1986)
6. Huang, J., Xu, W., Thomson, P., Di, S.: A general rigid-plastic/rigid-viscoplastic FEM for metal-forming processes based on the potential reduction interior point method. Int. J. Mach. Tool Manuf. **43**, 379–389 (2003)
7. Kammoun, Z., Pastor, F., Smaoui, H., Pastor, J.: A decomposition of the static problem in limit analysis. In: Proceedings of the Second Euromediterranean Symposium on Advances in Geomaterials and Structures. Hammamet, Tunisie (2008)
8. Krabbenhoft, K., Damkilde, L.: A general non-linear optimization algorithm for lower bound limit analysis. Int. J. Num. Meth. Engng. **56**, 165–184 (2003)
9. Krabbenhoft, K., Lyamin, A., Hijaj, M., Sloan, S.: A new discontinuous upper bound limit analysis formulation. Int. J. Num. Meth. Engng. **63**, 1069–1088 (2005)
10. Lyamin, A.V., Sloan, S.W.: Lower bound limit analysis using nonlinear programmlng. Int. J. Numer. Meth. Engng. **55**, 573–611 (2002)
11. Lyamin, A.V., Sloan, S.W.: Upper bound limit analysis using linear finite elements and non-linear programming. Int. J. Numer. Anal. Meth. Geomech. **26**, 181–216 (2002)
12. Lysmer, J.: Limit analysis of plane problems in soil mechanics. J. Soil Mech. Found. Div., ASCE **96**, 1311–1334 (1970)
13. Makrodimopoulos, A., Martin, C.: Upper bound limit analysis using simplex strain elements and second-order cone programming. Int. J. Num. Anal. Meth. Geomech. **31**, 835–865 (2007)
14. Pastor, F.: Résolution d'un problème d'optimisation à contraintes linéaires et quadratiques par une méthode de point intérieur : application à l'Analyse Limite. Mémoire de DEA de mathématiques appliquées, Université de Lille 1 (2001)

15. Pastor, F.: Résolution par des méthodes de point intérieur de problèmes de programmation convexe posés par l'analyse limite. Thèse de doctorat, Facultés universitaires Notre-Dame de la Paix, Namur (2007)

16. Pastor, F., Loute, E.: Solving limit analysis problems: An interior-point method. Commun. Numer. Meth. Engng. **21**(11), 631–642 (2005)

17. Pastor, F., Loute, E., Pastor, J.: Limit analysis and convex optimization: Applications. In: 17$^{\text{ème}}$ Congrès Français de Mécanique-CFM 2005. Université de Troyes (2005)

18. Pastor, F., Loute, E., Pastor, J., Trillat, M.: Mixed method and convex optimization for limit analysis of homogeneous gurson materials: A kinematical approach. Eur. J. Mechan. A/ Solid. **28,** 25–35 (2009)

19. Pastor, F., Thoré, Ph., Loute, E., Pastor, J., Trillat, M.: Convex optimization, limit analysis and porous materials: Application to gurson and porous drucker-prager materials. Engng. Frac. Mechan. **75**, 1367–1383 (2008)

20. Pastor, F., Trillat, M., Pastor, J., Loute, E.: Stress-based upper-bound method and convex optimization: Case of the Gurson material. C. R. Mécanique, Acad. Sc. Paris **334**, 213–219 (2006)

21. Pastor, F., Trillat, M., Pastor, J., Loute, E., Thoré, Ph.: Convex optimization and stress-based lower/upper bound methods for limit analysis of porous polymer materials. In: J. Besson, D. Steglish, D. Moinereau (eds.) 9th European Mechanics of Materials Conference, EMMC9. Ecole des Mines de Paris – EDF (May 2006)

22. Pastor, J.: Analyse limite : détermination numérique de solutions statiques complètes. Application au talus vertical. Jl. Méc. Appl. (now Eur. Jl. Mech.-A/Solids) **2**, 167–196 (1978)

23. Pastor, J.: Application de la théorie de l'analyse limite aux milieux isotropes et orthotropes de révolution. Thèse d'Etat, UJF-INPG, Grenoble (1983)

24. Pastor, J., Loute, E., Thai, T.H.: Interior point optimization and limit analysis: an application. Commun. Numer. Meth. Engng. **19**, 779–785 (2003)

25. Pastor, J., Turgeman, S.: Mise en œuvre numérique des méthodes de l'analyse limite pour les matériaux de von mises et de coulomb standards en déformation plane. Mech. Res. Comm. **3**, 469–474 (1976)

26. Radenkovic, D., Nguyen, Q.S.: La dualité des théorèmes limites pour une structure en matériau rigide-plastique standard. Arch. Mechan. **24**(5–6), 991–998 (1972)

27. Saad, Y.: Iterative Methods for Sparse Linear Systems, Second Edition. SIAM, Philadelphia (2003)

28. Salençon, J.: Théorie des charges limites: poinçonnement d'une plaque par deux poinçons symétriques en déformation plane. Comptes Rendus Mécanique, Acad. Sc. Paris **265**, 869–872 (1967)

29. Salençon, J.: Théorie de la plasticité pour les applications à la mécanique des sols. Eyrolles, Paris (1974)

30. Salençon, J.: Calcul à la rupture et analyse limite. presses des Ponts et Chaussées, Paris (1983)

31. Widlund, O., Keyes, D.: Domain Decomposition Methods in Science and Engineering XVI. Lectures Notes in Computational Science and Engineering. Springer, New York (2007)

Gurson Model for Porous Pressure Sensitive Materials

J. Pastor and Ph. Thoré

Abstract The macroscopic criterion of a porous material is investigated using the Gurson spherical model, but with a pressure-dependent matrix. Owing to the isotropy of the resultant macroscopic material, the problem is analyzed under axisymmetry assumption. In both statical and kinematical approaches, specific quadratic formulations were used for the stress and displacement velocity fields in the triangular finite elements. To improve the efficiency, analytical continuous fields, derived from the solution to the problem of a cavity under internal pressure, were superimposed on the FEM fields. The final problems result in conic optimization, or linear programming after linearizing the criterion, so as to determine the "porous Coulomb" criterion. A fine iterative post-analysis strictly restores the admissibility of the statical and kinematical solutions. The comparison with a "translated modified Camclay" criterion shows that this criterion might be considered as a satisfactory approximation for some values of internal friction angle and porosity. Finally, a detailed comparison with the "porous Drucker-Prager" case is presented.

Nomenclature

- c Cohesion (Coulomb material).
- ϕ Internal friction angle (Coulomb material).
- f Porosity rate.
- $f(\boldsymbol{\sigma})$ Yield criterion.
- k Pure shear limit of a von Mises or Drucker-Prager material.
- λ Plastic multiplier.
- ξ Plastic multiplier (discontinuity surface).

Joseph Pastor and Philippe Thoré
Laboratoire LOCIE, Polytech'Savoie, 73376 Le Bourget du Lac, France,
e-mail: joseph.pastor@univ-savoie.fr; philippe.thore@univ-savoie.fr

- $\quad\pi_v(\mathsf{v})$ Volumic dissipated power rate.
- $\quad\pi_d([\boldsymbol{u}])$ Unit dissipated power rate on a discontinuity surface.
- $\quad\boldsymbol{Q}$ Loading parameter vector.
- $\quad\mathbf{q}$ Generalized velocity vector.
- $\quad\Sigma_{ij}$ Macroscopic (average) stress tensor.
- $\quad E_{ij}$ Macroscopic (average) strain tensor.
- $\quad\boldsymbol{u}$ Displacement velocity vector.
- $\quad\mathsf{v}$ Strain rate tensor.

Acronyms
- PWL   Piecewise Linearization.
- LP-IP   Linear Programming—Interior Point.
- KA, SA, PA   Kinematically, Statically or Plastically Admissible.
- SOCP   Second Order Conic Programming.

1 Introduction

As regards the limit state assessment of isotropic porous materials, the Gurson's model still remains the basis of numerous works in its way of modeling the porous material, or as a key reference for comparisons of experimental, analytical or numerical results.

Originally [4, 5], this analytical model concerns porous materials whose matrix obeys the von Mises criterion. The porous material is modeled by a hollow sphere, considered as an "Elementary Volume" (EV), submitted to average strain rates at the boundary. Due to the isotropic character of the resultant material, the loading can be axisymmetrical, without loss of generality.

Hereunder, based on Gurson's *spherical* model and on Limit Analysis (LA), both statical and kinematical specific approaches have been carried out. They are first applied to Coulomb porous materials; the results are also compared with *ad hoc* modified Cam-clay criteria, and with previous results for porous Drucker-Prager materials in order to point out the differences between the resulting macroscopic criteria.

2 Succinct Presentation of Limit Analysis

According to Salençon [9], a stress tensor field $\boldsymbol{\sigma}$ is said to be admissible if it is both statically admissible (SA, i.e., equilibrium equations, stress vector continuity and stress boundary conditions are verified) and plastically admissible (PA, i.e., $f(\boldsymbol{\sigma}) \leqslant 0$, where $f(\boldsymbol{\sigma})$ is the (convex) plasticity criterion of the material).

Similarly, a strain rate tensor field v is admissible if it is kinematically admissible (KA, i.e., derived from a piecewise continuous velocity vector field $\boldsymbol{u}$, with bounded discontinuities $[\boldsymbol{u}]$, such that the velocity boundary conditions are verified) and plastically admissible (PA, i.e., the associated flow rules (2a), (2b) are verified).

Let us assume, as in [9], that the virtual power P_{ext} of the external loads can be written as the scalar product of a loading vector $\boldsymbol{Q}$, whose components are called here loading parameters, and a generalized velocity vector $\mathbf{q} = \mathbf{q}(\boldsymbol{u})$, the components of which are called kinematical parameters. Following [1], let us consider a KA virtual velocity field $\boldsymbol{u}$; the virtual power principle (VPP) states that the stress tensor field $\boldsymbol{\sigma}$, the stress vector field $\boldsymbol{T}$ (on the velocity discontinuity surfaces), and the vector $\boldsymbol{Q}$ are in equilibrium, if for any KA $\boldsymbol{u}$, the following variational equation is verified:

$$P_{\text{ext}} = \boldsymbol{Q} \cdot \mathbf{q}(\boldsymbol{u}) = \int_V \boldsymbol{\sigma} : \mathsf{v}\, dV + \int_{S_d} \boldsymbol{T} \cdot [\boldsymbol{u}]\, dS. \tag{1}$$

where V is the volume of the mechanical system and S_d the union of the velocity discontinuity surfaces.

The results in terms of $\boldsymbol{Q}$ will be interpreted as a kinematic bound if, at the appropriate points of V, the variables verify the following conditions, where $\boldsymbol{u}$ is KA and $\mathbf{q}^d$ is a fixed value of $\mathbf{q}(\boldsymbol{u})$:

$$\mathsf{v} = \lambda \frac{\partial f}{\partial \boldsymbol{\sigma}}, \qquad \lambda f(\boldsymbol{\sigma}) = 0, \qquad \lambda \geqslant 0, \qquad f(\boldsymbol{\sigma}) \leqslant 0, \tag{2a}$$

$$[\boldsymbol{u}] = \xi \frac{\partial f_{nt}}{\partial \boldsymbol{T}}, \qquad \xi f_{nt}(\boldsymbol{T}) = 0, \qquad \xi \geqslant 0, \qquad f_{nt}(\boldsymbol{T}) \leqslant 0, \tag{2b}$$

$$\mathbf{q}(\boldsymbol{u}) = \mathbf{q}^d. \tag{2c}$$

The criterion $f_{nt}(\boldsymbol{T})$ results from the projection of the plasticity criterion $f(\boldsymbol{\sigma})$ on the Mohr plane, where $\boldsymbol{n}$ is the normal to the element of the velocity discontinuity surface and $\boldsymbol{T} = (\sigma_{nn}, \sigma_{nt})$ is the stress vector on this element. More precisely, $f_{nt}(\boldsymbol{T})$ is the solution of the following system:

$$f(\sigma_{nn}, \sigma_{tt}, \sigma_{nt}) = 0, \quad \frac{\partial f}{\partial \sigma_{tt}} = 0. \tag{3}$$

It is worth noting that, if (2a) and (2b) are verified, the quantities $\boldsymbol{\sigma} : \mathsf{v}$ and $\boldsymbol{T} \cdot [\boldsymbol{u}]$ become, respectively, the *convex* unit dissipated powers $\pi_V(\mathsf{v})$ and $\pi_d([\boldsymbol{u}])$ of LA, i.e.:

$$\pi_V(\mathsf{v}) = \boldsymbol{\sigma} : \mathsf{v}, \quad \pi_d([\boldsymbol{u}]) = \boldsymbol{T} \cdot [\boldsymbol{u}]. \tag{4}$$

3 Homogenization Technique—The Gurson's Model

3.1 The Mechanical Model

As said above, the porous material is replaced by an isotropic homogeneous material represented by an "Elementary Volume"; in the present case, this elementary volume is a hollow sphere with a central cavity (see Fig. 1). At the boundary of the sphere are imposed the velocities defined as $u_i = E_{ij}x_j$, where E_{ij} are the fixed components of the axisymmetric average strain rate, in the global *principal* cartesian (x_1, x_2, x_3) frame $(E_{xx} = E_{yy}, E_{zz})$. As usual, the material is assumed zero-weight.
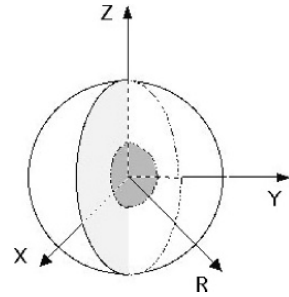
Fig. 1 The "Elementary volume" of the Gurson's spherical model

3.2 The Loading Parameters

The macroscopic stresses Σ_{ij} being related to the microscopic stresses σ_{ij} by the averaging relations:

$$\Sigma_{ij} = \frac{1}{V} \int_V \sigma_{ij}\,\mathrm{d}V, \tag{5}$$

the LA loading parameters are defined as follows, in the present *axisymmetrical* case $(\Sigma_{xx} = \Sigma_{yy})$:

$$\begin{aligned}
\Sigma_m &= (\Sigma_{xx} + \Sigma_{yy} + \Sigma_{zz})/3 = (2\Sigma_{xx} + \Sigma_{zz})/3, \\
\Sigma_{gps} &= (\Sigma_{xx} + \Sigma_{yy})/2 - \Sigma_{zz} = \Sigma_{xx} - \Sigma_{zz}, \\
\Sigma_{ps} &= \sqrt{3}(\Sigma_{xx} - \Sigma_{yy})/2 \quad = 0,
\end{aligned} \tag{6}$$

and the macroscopic equivalent stress expresses as:

$$\Sigma_{eqv}^2 = \Sigma_{ps}^2 + \Sigma_{gps}^2 = \Sigma_{gps}^2 \Rightarrow \Sigma_{eqv} = \Sigma_{xx} - \Sigma_{zz}. \tag{7}$$

Hence, owing to the axisymmetrical assumption and the isotropy of the resulting material, the present problem has only two loading parameters (Σ_m and $\Sigma_{eqv} = \Sigma_{gps}$).

3.3 The Generalized Velocities

The macroscopic strain rates E_{ij} are defined from the chosen boundary conditions. Here, the LA generalized velocities are defined as (with $E_{xx} = E_{yy}$):

$$
\begin{aligned}
E_m &= E_{xx} + E_{yy} + E_{zz} &&= 2\,E_{xx} + E_{zz}, \\
E_{gps} &= 2\left[(E_{xx} + E_{yy})/2 - E_{zz}\right]/3 = 2(E_{xx} - E_{zz})/3, \\
E_{ps} &= (E_{xx} - E_{yy})/\sqrt{3} &&= 0.
\end{aligned}
\tag{8}
$$

3.4 Reminder: The "Porous von Mises" or Gurson Material

The analytical Gurson's criterion reads:

$$
\frac{\Sigma_{eqv}^2}{3k^2} + 2f \cosh\left[\frac{\sqrt{3}\,\Sigma_m}{2k}\right] = 1 + f^2,
\tag{9}
$$

where f is the porosity of the material and k the cohesion (or limit shear stress) of the matrix. This analytical Gurson's formulation gives, as outlined by J.-B. Leblond [6], a rigorous upper bound of the criterion solution from this model, in terms of limit analysis.

4 Finite Element and Optimization Implementation

Due to the axisymmetrical conditions, the simulation domain is a one-quarter of a meridian plane, treated in cylindrical coordinates. This domain is meshed into discontinuous triangular elements. Since linear fields have been proved insufficient, both stress and displacement velocity fields are represented by quadratic functions of the coordinates.

The first runs were performed with the SOCP MOSEK code, but many difficulties arose, in both approaches, regarding the convergence. Hence, after linearization, the optimization was carried out with the "Interior Point Linear Programming" (LP-IP) XA code, in both approaches, as it was the only commercial code robust enough to solve the final, rather badly conditioned problems generated in the present axisymmetrical cases.

5 The Statical Approach for a Porous Coulomb Material

The statical or lower-bound approach, consists in optimizing a functional, e.g., Σ_{gps}, under various imposed values Σ_m^0 of Σ_m, provided that the set of following constraints (equalities and inequalities) is satisfied.

After the optimization, a post-analysis, which is necessary because of the highly non-linear character of the stress field, verifies the admissibility of the solution and, as long as the solution is not strictly admissible all over the domain, restarts the optimization after some adequate readjustments, as will be seen below.

5.1 The Coulomb Criterion (Recall)

The criterion expresses as:

$$f(\boldsymbol{\sigma}) = |\sigma_i - \sigma_j| - 2\,c\,\cos\phi + (\sigma_i + \sigma_j)\sin\phi \le 0, \qquad (10)$$

where c is the cohesion of the material and ϕ its internal friction angle; σ_i and σ_j are the principal stresses ($i, j = 1, 2, 3$, with $i \ne j$).

"Unwieldy" in 3D cases, this criterion gives rise to a system of 3 pairs of inequations such as:

$$\begin{cases} \sigma_i - \sigma_j - 2\,c\,\cos\phi + (\sigma_i + \sigma_j)\sin\phi \le 0, \\ \sigma_j - \sigma_i - 2\,c\,\cos\phi + (\sigma_i + \sigma_j)\sin\phi \le 0. \end{cases} \qquad (11)$$

Actually, this system reduces to 3 *conic* inequations, the other inequations being redundant. But another difficulty stands: the principal stresses and directions are unknown when one expresses the present constraints, which makes it necessary to translate these inequations into a known reference set; using the $\sigma_R, \sigma_\theta, \sigma_Z, \tau_{RZ}$ stress components in cylindrical coordinates, these inequations become, after some transformations (cf. [8]):

$$\begin{cases} \Delta \le - \quad \alpha\sin\phi + 2c\,\cos\phi, \\ \Delta \le \quad \left[\alpha - 2\sigma_\theta \frac{1+\sin\phi}{1-\sin\phi}\right] + 4c\,\frac{\cos\phi}{1-\sin\phi}, \\ \Delta \le - \quad \left[\alpha - 2\sigma_\theta \frac{1-\sin\phi}{1+\sin\phi}\right] + 4c\,\frac{\cos\phi}{1+\sin\phi}, \end{cases} \qquad (12)$$

with $\quad \alpha = \sigma_R + \sigma_Z \quad$ and $\quad \Delta = \sqrt{(\sigma_R - \sigma_Z)^2 + 4\tau_{RZ}^2}.$

5.2 The Stress Field

The affine formulation being too "poor" to give satisfactory results, the FEM discontinuous stress field expresses with *quadratic* functions, as follows:

$$
\begin{cases}
\sigma_R &= A & + B\,R & + C\,Z & + H\,RZ & + I\,R^2 & + J\,Z^2, \\
\sigma_\theta &= A & + B_\theta R & + C\,Z & + H_\theta RZ & + I_\theta R^2 & + J\,Z^2, \\
\sigma_Z &= A_Z & + B_Z R & + C_Z Z & + H_Z RZ & + I_Z R^2 & + J_Z Z^2, \\
\tau_{RZ} &= & B_\tau R & & + H_\tau RZ & + I_\tau R^2.
\end{cases}
\tag{13}
$$

It is worth noting that the formulation has been adjusted so as to eliminate R from the fraction denominators containing R, in the equilibrium equations (15) below.

Despite this improvement, the results were not satisfactory enough, essentially in compression, owing to the average strain rate boundary conditions; hence an analytical continuous field was superposed on the FEM field; this analytical field is an extension of the solution to the problem of a cavity expanded or compressed under internal pressure proposed in [3]; its expression is rather simple in an (r, θ, φ) set of spherical coordinates; the internal radius of the cavity being denoted by a and ε being a coefficient whose value is $+1$ in the traction case and -1 in the compression case, its components are:

$$
\begin{cases}
\sigma_r &= c \cot \phi \left[1 - \left(\frac{a}{r} \right)^{\frac{4\,\varepsilon \sin \phi}{1+\varepsilon \sin \phi}} \right], \\
\sigma_\theta = \sigma_\varphi &= c \cot \phi \left[1 - \frac{1-\varepsilon \sin \phi}{1+\varepsilon \sin \phi} \left(\frac{a}{r} \right)^{\frac{4\,\varepsilon \sin \phi}{1+\varepsilon \sin \phi}} \right].
\end{cases}
\tag{14}
$$

These expressions are translated afterwards into cylindrical coordinates.

5.3 The Equalities

Equalities are imposed in order to:

- define the macroscopic stresses (4 equations),
- express the equilibrium equations (3×2 equations per triangular element):

$$
\begin{cases}
\frac{\partial \sigma_R}{\partial R} + \frac{\partial \tau_{RZ}}{\partial Z} + \frac{\sigma_R - \sigma_\theta}{R} = 0, \\
\frac{\partial \tau_{RZ}}{\partial R} + \frac{\partial \sigma_Z}{\partial Z} + \frac{\tau_{RZ}}{R} = 0,
\end{cases}
\tag{15}
$$

as mentioned in Sect. 5.2, these equations have induced the specific choice of the stress field inside the elements;
- ensure the continuity of the stress vector across the segments separating adjacent elements: at both ends and in the middle of each discontinuity

segment, because of the quadratic character of the FEM field (3×2 equations per discontinuity segment);

- express the boundary conditions: the stress vector is null along the sides bordering the cavity (3×2 equations per boundary segment);
- satisfy the symmetry conditions, since the simulation domain is a one-quarter of a meridian plane: the microscopic tangential stress is null on the horizontal plane (3 equations per segment).

5.4 The PA Condition Inequalities

The 3 inequations (12) of the Coulomb criterion are conic, but they are written in such a way that they have the same left hand member (Δ), which is the sole non-linear term of these inequations.

Hence, by inserting a new unknown Y between the two members, one obtains a new *conic* inequation:

$$\Delta \leq Y, \tag{16}$$

which adds to the 3 inequations of the original system, but where Y replaces Δ, making them *linear*, which is much more convenient.

The conic inequation (16) is linearized, by the so-called "PWL" method, generating a system of *mps* linear inequations; the higher this value *mps* is given, the better is the approximation, depending upon the programmer's decision.

Finally, one has a set of $(3 + mps)$ inequations per point; because of the non-linearity of the global stress field, these conditions are imposed at 7 points per element (each apex, the middle of each side and the center of gravity), which makes an amount of $7 \times (3 + mps)$ inequations per element.

5.5 The Post-analysis Process

After the optimization, a rigorous post-analysis is carried out:

- verification of the stress vector continuity across every boundary between adjacent elements; in fact, the stress vector jump is always smaller than 10^{-5};
- subdivision of each element into a great number of "subtriangles" (more than 200 subtriangles), in order to compensate for the non-linearity of the stress field and improve the accuracy of the next two steps;
- computation of accurate Σ_m and Σ_{gps} values, by integral calculation on each subtriangle, followed by a summation on the whole domain;

- verification of the Coulomb criterion inside each subtriangle of each element; this verification is performed with the three original inequations (10), instead of their modified expression (12), since the principal stresses are computable at this stage (the stress field is known).
  To set an example, in order to verify the following inequation in a subtriangle:

$$\frac{|\sigma_1 - \sigma_2| + (\sigma_1 + \sigma_2)\sin\phi}{2\,c\,\cos\phi} \leq 1, \tag{17}$$

  the successive steps are:

  - calculation of the k ratio: $\quad k = \frac{|\sigma_1 - \sigma_2| + (\sigma_1 + \sigma_2)\sin\phi}{2\,c\,\cos\phi};$
  - if $\quad k \leq 1$: no specific action, since the inequation is satisfied in the current subtriangle; hence, jump to the next inequation or next apex. . .
  - if $\quad k > 1$: storage of the current "faulty" element's number, and of k if it is larger than the value previously stored during the current post-analysis step;

- if at least one element is "faulty", reiteration of the optimization, after modification of the PA conditions in every "faulty" element: the original cohesion c, or its previously modified value c_c, is replaced by a new smaller fictitious value c_c: $c_c = c_c/k$, in order to make more severe the PA conditions in these elements during the next optimization step: thanks to that numerical artifice, the original Coulomb criterion will be more easily satisfied in the next post-analysis.
- because of some "diffusion effect", the next post-analysis often detects new faulty elements, making it necessary to reiterate again the optimization: as long as the solution is not found admissible *all over the domain*, the optimization is reiterated, as many times as necessary.

6 The Kinematical Approach for a Porous Coulomb Material

The kinematical approach, or upper-bound approach, consists in optimizing a functional, related to the dissipated power, for instance under various imposed values Σ_m^0 of Σ_m, provided that the set of following constraints is satisfied. Once again, the optimization itself is carried out with the LP-IP XA code, after linearization.

After the optimization, a post-analysis, which is necessary because of the non-linear character of the superimposed displacement velocity field, verifies the admissibility of the solution and, as long as the solution is not quite admissible all over the domain, reiterates the optimization after some adequate readjustments, as will be seen below.

6.1 The Displacement Velocity Field

The FEM discontinuous displacement velocity field expresses as follows:

$$
\begin{cases}
u_R = R\,(A + B\,R + C\,Z), \\
u_\theta = 0, \\
u_Z = D + E\,R + F\,Z + H\,RZ + I\,R^2 + J\,Z^2.
\end{cases} \tag{18}
$$

Similarly to what was done in the statical approach, and for the same reason, an analytical continuous field was superposed on the FEM field, deduced from the solution to the problem of a cavity expanded or compressed under internal pressure (cf. [3]). In an (r, θ, φ) set of spherical coordinates, this *radial* field expresses as:

$$
u_r = \varepsilon\,\frac{G}{r^{2\alpha}}, \quad \text{with} \quad \alpha = \frac{1 - \varepsilon \sin \phi}{1 + \varepsilon \sin \phi}, \tag{19}
$$

where ε is a coefficient whose value is $+1$ in the traction case and -1 in the compression case. Indeed, the expression of u_r is translated into cylindrical coordinates.

6.2 The Equalities

In the kinematical approach, one has to satisfy the set of following equations:

- the outer boundary conditions: $u_i = E_{ij}x_j$, where the E_{ij} are fixed, (8 equations per boundary segment);
- the definition of the generalized velocities E_m and E_{gps} (2 equations);
- the symmetry conditions, since the simulation domain is a one-quarter of a meridian plane: the vertical u_z component is null on the horizontal plane (3 equations per segment).

6.3 The PA Condition Inequalities

In order to have an exact evaluation of the internal dissipated power, the displacement velocity field u and the strain rate field v must satisfy, prior to the application of the Virtual Power Principle, both of these PA conditions:

- **The volumetric PA condition** (i.e., concerning the power dissipated in the volume):
$$
(|v_1| + |v_2| + |v_3|) \sin \phi \le \text{tr}(v), \tag{20}
$$
where v_1, v_2 and v_3 are the principal strain rates.

Since the principal strain rates and directions are not known, one has to translate the original inequation (20) into the cylindrical coordinate set (R, θ, Z).

Inserting a new unknown Y, in a way similar to what was done in the statical approach, one obtains the following system, after some transformations:

$$\begin{cases} \sqrt{(v_R - v_Z)^2 + 4v_{RZ}^2} \leq Y, \\ \quad |v_R + v_Z| \qquad \leq Y, \\ \qquad\qquad Y \leq \frac{v_R + v_\theta + v_Z}{\sin \phi} - |v_\theta|. \end{cases} \qquad (21)$$

The first inequation of the system is conic; it is linearized, by the "PWL" method, generating a system of mps linear inequations; the two last inequations give rise to 2 inequalities ($3 \times (4+mps)$ inequations per element).

- **The discontinuity PA condition** (i.e., concerning the discontinuity lines):

$$[\boldsymbol{u}] = \xi_i \frac{\partial f_i(\boldsymbol{T})}{\partial \boldsymbol{T}}, \quad \xi_i \geq 0. \qquad (22)$$

These discontinuity conditions express that the velocity jump $[\boldsymbol{u}]$ is a linear combination of the directions orthogonal to the f_i boundary sides of the cone representing the Coulomb's criterion (see Fig. 2); as a consequence, $[\boldsymbol{u}]$'s direction is inside the cone built on these directions.

As $[\boldsymbol{u}]$ is a quadratic function of the coordinates, the discontinuity PA condition is "linearized", i.e., the velocity jump at the middle of the segment is imposed as half the sum of the apex jumps: by imposing (22) at the ends of the segment, $[\boldsymbol{u}]$ is PA everywhere on the segment (3×2 linear equations per discontinuity segment).

Fig. 2 PA condition on a discontinuity line: the direction of the $[\boldsymbol{u}]$ vector is inside the cone defined by the directions orthogonal to the boundary sides of the cone representing Coulomb's criterion in the Mohr diagram
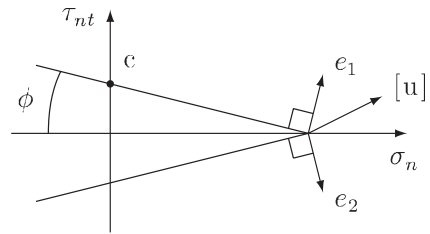
6.4 The Optimization

- **The functional**: from the Virtual Power Principle, expressed in function of the loading parameters:

$$\frac{P_{tot}}{V_{tot}} = E_m \Sigma_m + E_{gps} \Sigma_{gps}, \qquad (23)$$

the functional becomes, for instance:

$$\Sigma_{gps} = \left[\, P_{tot}/V_{tot} - E_m^0 \, \Sigma_m^0 \,\right] / E_{gps}^0, \tag{24}$$

under various fixed values Σ_m^0, with $E_{gps}^0 = 1$.

- **Optimization**: as said above, the optimization is carried out with the LP-IP XA code, and followed by a post-analysis described more precisely in the next section.

- **Penalty**: the post-analysis shows that, for some elements, although satisfied at the apices, the original inequation (20) is not satisfied *inside* the element, because of the non-linearity of the superimposed continuous field. To remedy this situation, the third inequation of the modified system (21) has been added a small term—let it be named p, for "penalty"—which makes the inequation more severe:

$$Y \le \frac{v_R + v_\theta + v_z}{\sin\phi} - |v_\theta| - p. \tag{25}$$

Thanks to that penalty, the two members of the inequation (20) are "distanced" from each other by the penalty p, making it easier to satisfy the original inequation *inside* the element.

6.5 The Post-analysis Process

As announced above, the optimization is followed by a rigorous post-analysis:

- Verification of the discontinuity PA condition across every boundary between adjacent elements; one can observe that:
  - the error is always smaller than 10^{-5};
  - the power dissipated along discontinuities is negligible.

- subdivision of each element into a great number of "subtriangles" (more than 200 subtriangles), in order to compensate for the non-linearity of the superposed continuous displacement field and improve the accuracy of the next two steps;
- computation of accurate values of the power dissipated on the discontinuity lines and inside the elements, by integral calculation on each discretized discontinuity line and inside the subtriangles, followed by a summation on the whole domain;
- verification of the PA condition inside each subtriangle of each element; this verification is performed with the original inequation (20):

$$(|v_1| + |v_2| + |v_3|)\sin\phi \le \mathrm{tr}(\mathbf{v}).$$

In order to verify this inequation in a subtriangle, the successive steps are:

– calculation of the difference δ: $\delta = (|v_1| + |v_2| + |v_3|) \sin \phi - \mathrm{tr}(\mathsf{v})$;

– if $\delta \leq 0$: no specific action, since the inequation is satisfied in the current subtriangle; hence, jump to the next inequation or subtriangle . . .

– if $\delta > 0$: storage of the current "faulty" element's number, and of δ if it is larger than the value previously stored during the current post-analysis step;

• if at least one element is "faulty", the optimization is reiterated, after modification of the penalty in every "faulty" element: the new penalty is added to its original value (zero), or to its previously modified value, so as to make more severe the PA condition in these elements during the next optimization step; this numerical artifice will make it more easy to satisfy the original PA condition in the next post-analysis.

• similarly to the statical approach, because of some "diffusion effect", the next post-analysis often finds other faulty elements, making it necessary to restart again the optimization: the optimization is reiterated, as many times as necessary, as long as the solution is not admissible *everywhere* in the domain.

7 Applications

As regards the "quality" of the results, one would observe the following facts:

• on the one hand, the optimization must be reprocessed many times, especially in the kinematical approach, because of the "diffusion effect", mentioned above;

• on the other hand, the rigorously admissible solutions finally obtained are very close to the "raw" solutions given by the first optimization, thanks to the efficiency of the numerical artifices used in both approaches; this compensates for the just above mentioned drawback;

• as a consequence, the statical and kinematical admissible solutions are very close to each other, which gives the results a high reliability.

Hereunder, we firstly present the behaviour of the "Porous Coulomb" material for various values of the porosity and of the internal friction angle. As the comparison with the Cam-clay criterion appeared to be interesting in the first runs, we carried on the comparison for several more runs. Then, we present a comparison with a "Porous Drucker-Prager" material and recall some previous results obtained with this material.

7.1 Influence of the Internal Friction Angle and of the Porosity for a "Porous Coulomb" Material

The graphs confirm (see Fig. 3) the existence of corners on the mean stress axis; as pointed by Rudnicki and Rice, such corners might be related to a possible initiation of strain localization.
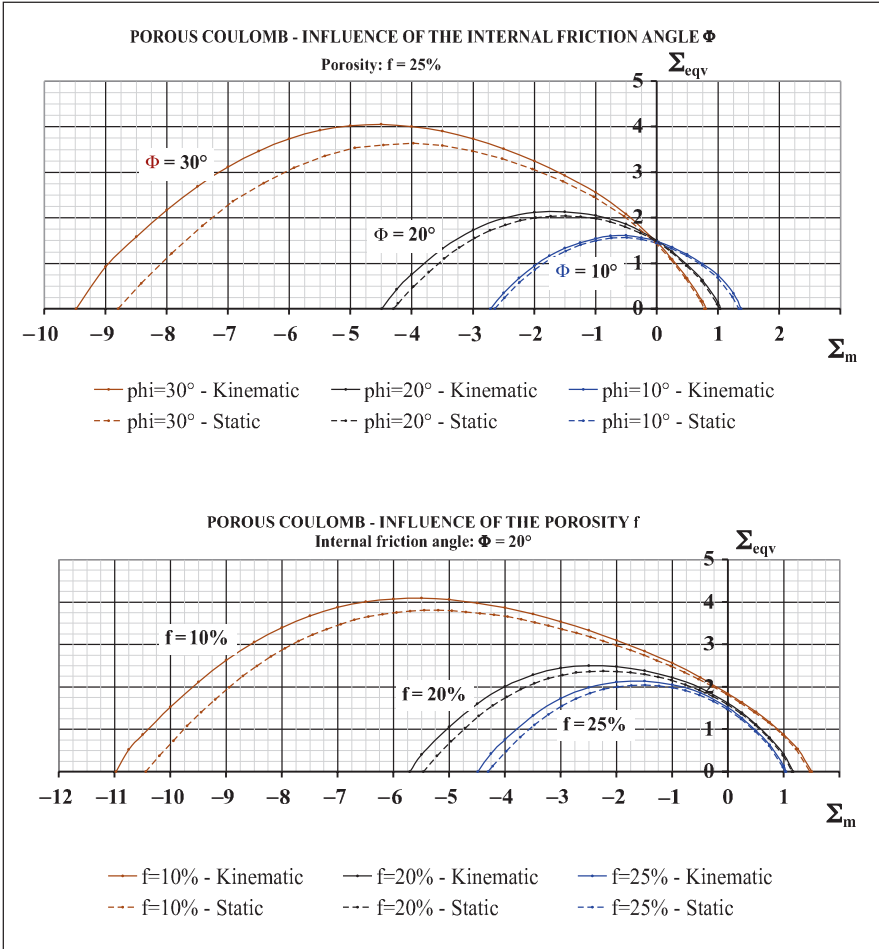
Fig. 3 Porous Coulomb material:
- *top*: influence of the internal friction angle ϕ for a fixed value of the porosity ($f = 25\%$);
- *bottom*: influence of the porosity for a fixed value of the internal friction angle ($\phi = 20°$);
- number of elements: 3120 in the kinematical approach, 640 in the statical approach

Moreover, it is worth noting that, when the internal friction angle varies, without change of the porosity, the graphs confirm the existence of a fixed point for a null value of the mean stress.

7.2 Comparison with an Ad Hoc Modified Cam-Clay Criterion

Some results obtained with the porous Coulomb material, very close to those obtained with the translated modified Cam-clay criterion, suggested to carry on the comparison.

7.2.1 The Cam-Clay Criterion (Recall)

The Cam-clay criterion has undergone several evolutions:

- original Cam-clay: $\Sigma_{eqv} = M \Sigma_m \left[\ln \frac{\Sigma_m}{p_c} - 1 \right]$,   (26)

- modified Cam-clay: $\Sigma_{eqv} = M \sqrt{\Sigma_m \left[2p_c - \Sigma_m \right]}$,   (27)

where p_c is the abscissa of the maximum of Σ_{eqv} and M a parameter:

$$M = \frac{6 \sin \phi}{3 - \sin \phi}.$$ (28)

As the Cam-clay criterion accounts for pulverulent materials, we have defined here the following "translated" formulations, to compare with our results:

- original translated: $\Sigma_{eqv} = M \left(\Sigma_m - p_0 \right) \left[\ln \frac{\Sigma_m - p_0}{p_c - p_0} - 1 \right]$,   (29)

- modified translated: $\Sigma_{eqv} = M \sqrt{\left(p_0 - \Sigma_m \right) \left(\Sigma_m - p_1 \right)}$,   (30)

with: $p_0 = c \cot \phi \left[1 - f^{\frac{4}{3} \frac{\sin \phi}{1 + \sin \phi}} \right]$, $p_1 = c \cot \phi \left[1 - f^{-\frac{4}{3} \frac{\sin \phi}{1 - \sin \phi}} \right]$.   (31)

The parameters p_0 and p_1 are the two exact analytical solutions, for a porous Coulomb material, in the cases of isotropical traction and compression, respectively.

It is worth noting that the "modified translated" criterion is obtained by a micro–macro analysis, without any other hypothesis. Moreover, let us notice that both graphs of "original" formulations are strongly dissymmetrical and present a corner on the mean stress axis, on the compression side, whereas both graphs of "modified" formulations do not present any corner and are symmetrical (see Fig. 4).
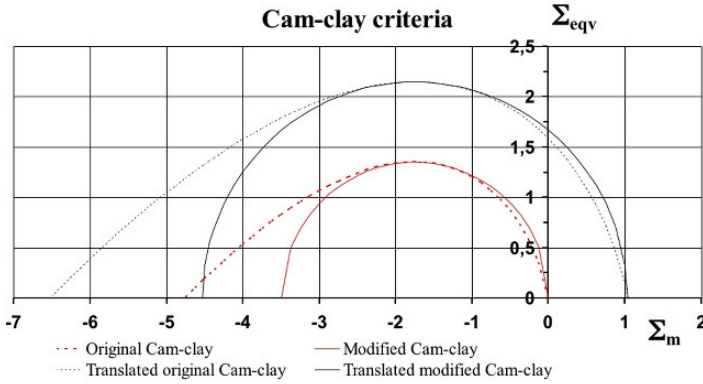
Fig. 4 Cam-clay criteria: both "non-translated" formulations are adapted to pulverulent materials, whereas the "translated" formulations are adapted to non-pulverulent materials

7.2.2 Comparison Between the "Modified Translated" Cam-Clay and "Porous Coulomb" Criteria for Fixed Values of the Porosity or Internal Friction Angle

The comparison between the "modified translated" Cam-clay and "Porous Coulomb" criteria, presented in Fig. 5, shows that the Cam-clay criterion can be a satisfactory approximation to the Porous Coulomb, around $f = 25\%$ and $\phi = 20°$ only, though it does not take into account the corners on the mean stress axis.

7.3 Comparison with the Porous Drucker-Prager Criterion

In addition, we have compared the results obtained with the porous Coulomb criterion with those obtained with the porous Drucker-Prager criterion; for the latter, we have successfully used the SOCP MOSEK code, which made it unnecessary to linearize the PA condition, in the statical approach as well as in the kinematical approach.

7.3.1 The Drucker-Prager Criterion (Recall)

The Drucker-Prager criterion expresses as:

$$f(\boldsymbol{\sigma}) = \sqrt{J_2} + \alpha \operatorname{tr}(\boldsymbol{\sigma}) - k \leq 0, \tag{32}$$

where s is the deviatoric stress tensor and J_2 the second invariant of s:
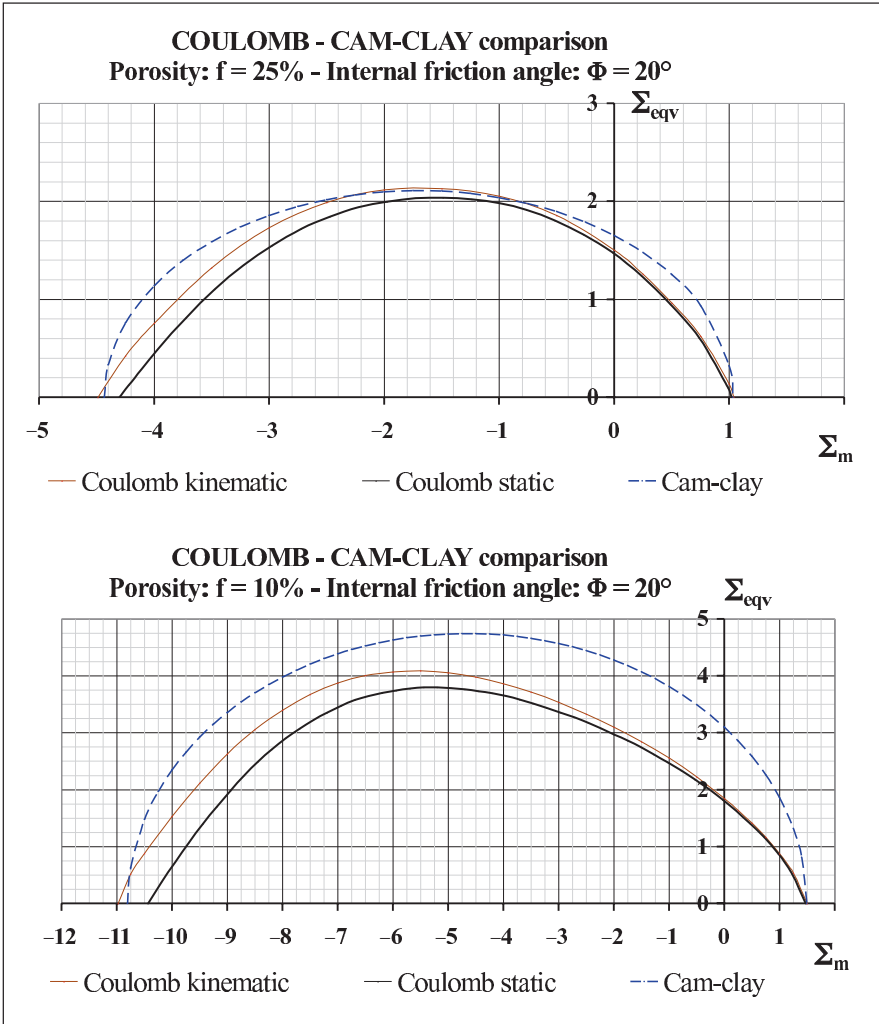
Fig. 5 Comparison between the "modified translated" Cam-clay and "Porous Coulomb" criteria

$$J_2 = \frac{1}{2}\,\mathrm{tr}(\mathsf{s}^2), \quad \text{with} \quad \mathsf{s} = \boldsymbol{\sigma} - \frac{1}{3}\,\mathrm{tr}(\boldsymbol{\sigma})\,\mathbf{1}, \tag{33}$$

α is a coefficient depending on the internal friction angle ϕ, k is the pure shear limit:

$$\alpha = \frac{\sin\phi}{\sqrt{3\,(3+\sin^2\phi)}}, \quad k = 3\,\alpha\,H = 3\,\alpha\,\frac{c}{\tan\phi}, \tag{34}$$

$$\phi \in \left[0; \frac{\pi}{2}\right] \quad \Rightarrow \quad \alpha \in \left[0; \frac{\sqrt{3}}{6}\right].$$

In an (x, y, z) reference frame, the 3D criterion becomes:

$$\sqrt{\left[\frac{2}{\sqrt{3}}\left(\frac{\sigma_x+\sigma_y}{2}-\sigma_z\right)\right]^2 + (\sigma_x-\sigma_y)^2 + (2\tau_{xy})^2 + (2\tau_{xz})^2 + (2\tau_{yz})^2} \leq$$
$$2k - 2\alpha(\sigma_x + \sigma_y + \sigma_z). \tag{35}$$

After an obvious change of variables, (35) can be rewritten as a conic constraint:

$$\sqrt{\sum_{j=1}^{n} x_j^2} \leq x_{n+1}, \tag{36}$$

and used directly by the SOCP MOSEK code, i.e., without linearization.

7.3.2 Comparison Between the Porous Drucker-Prager and Coulomb Criteria

Figure 6 shows a comparison between the two criteria for a fixed value of the porosity: $f = 10\%$, and two values of the internal friction angle: $\phi = 10°$ and $\phi = 20°$.

One can see that, despite the similarity of the two criteria, the Drucker-Prager's graph does not present any obvious corner on the mean stress axis, contrary to the Coulomb's graph; moreover, the Drucker-Prager's convex domain is noticeably smaller than Coulomb's one. We finally note that using Drucker-Prager instead of Coulomb, after a plane strain identification, may give significantly different results.

7.3.3 Previous Results Obtained with the "Porous Drucker-Prager" Criterion

For the sake of completeness, we briefly recall the results first given in [7] and [10], where our numerical results were compared to those of [2] in the pure three-dimensional case.

In [2], the authors suggested a non-linear homogenization technique to determine the stress states on the boundary of the macroscopic admissible stress field, for a "Porous Drucker-Prager" criterion. Their yield criterion was written as:
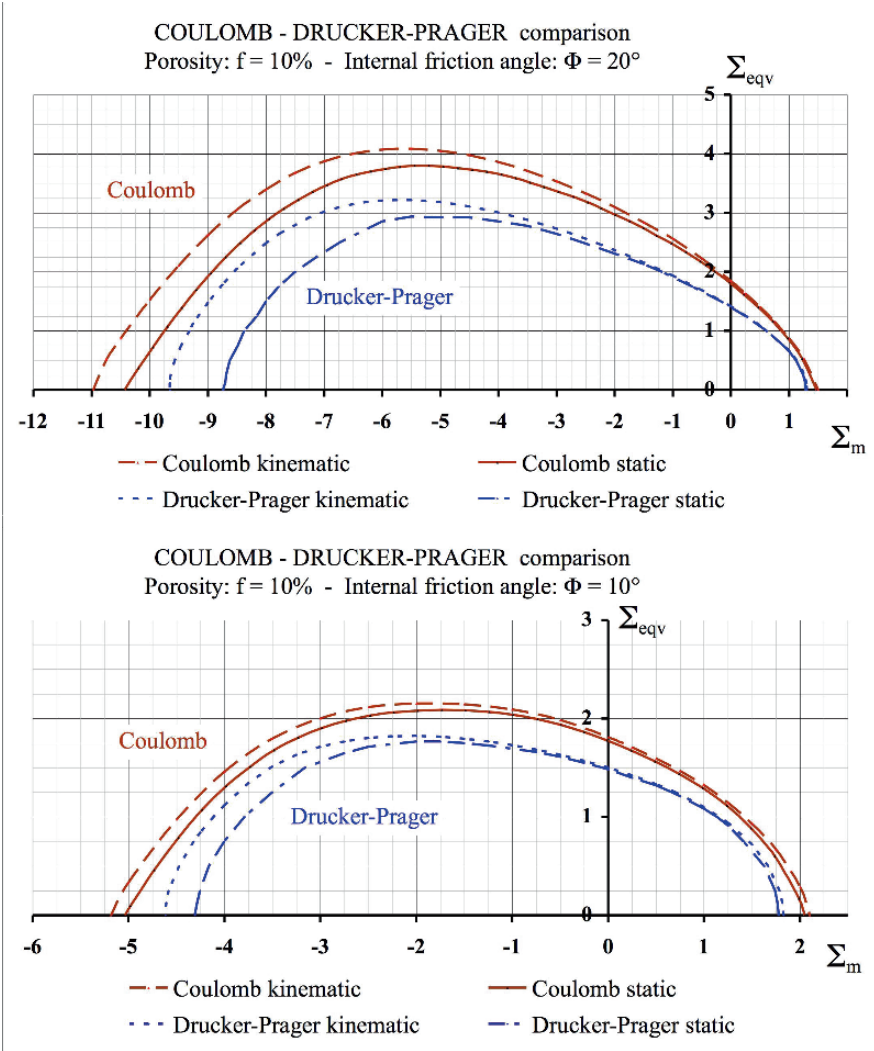
Fig. 6 Comparison between the "Porous Drucker-Prager" and "Porous Coulomb" criteria;
- *top*:   porosity $f = 10\%$, internal friction angle $\phi = 20°$;
- *bottom*: porosity $f = 10\%$, internal friction angle $\phi = 10°$

$$\frac{2 + 4f/3}{3T^2} \Sigma_{eqv}^2 + \left(\frac{3f}{2T^2} - 1\right) \Sigma_m^2 + 2(1-f)H\Sigma_m - (1-f)^2 H^2 = 0, \quad (37)$$

where $T = 3\sqrt{2}\alpha$. Considering Eq. (37) where $\Sigma_{eqv} = 0$ and Σ_m is the unknown, it can be noted that if $f > 2T^2/3$, i.e., when ϕ is smaller than a critical value, the two Σ_m solution values have opposite signs. As a consequence, failure is possible in compression as well as in traction (Fig. 7, bottom). For ϕ

values above this critical value, both Σ_m solution values are positive, which means that failure is impossible in compression.

Figure 7 shows that the criterion given by Eq. (37) is very close to our results on the right side of the curve, i.e., in the expansion case. Nevertheless, our results show that failure is possible in compression as well as in traction, which is not predicted by (37) above the critical friction angle ϕ (Fig. 7, top).
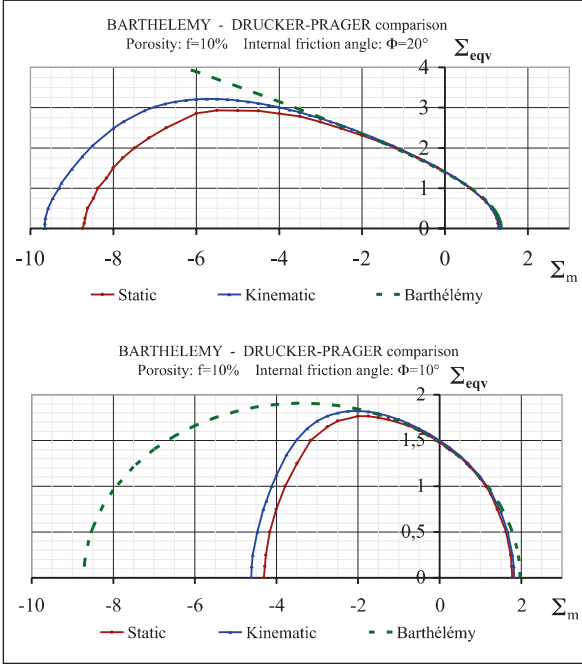
Fig. 7 Comparison between the "Porous Drucker-Prager" criterion and the criterion of [2];
- critical internal friction angle for $f = 10\%$: $\phi \simeq 16°$;
- *top*:   porosity $f = 10\%$, internal friction angle $\phi = 20°$;
- *bottom*: porosity $f = 10\%$, internal friction angle $\phi = 10°$

8 Conclusion

Using the LP-IP XA code to analyze the yield criterion of a "Porous Coulomb" material, on the basis of the Gurson model, and using *up to* quadratic discontinuous FEM fields in both approaches, the results of this micro-macro study show the efficiency and the reliability of the presented methods, since the upper and lower bounds found were very close to each other; they confirm, on the mean pressure axis, the existence of corners, which might be related to a possible initiation of strain localization.

The "modified translated" Cam-clay criterion should be worthwhile, since this criterion is obtained by a micro–macro analytical and numerical analysis, without any other hypothesis; however it does not take into account the corner on the mean pressure axis, and the similarity is limited to a restricted range of porosity and internal friction angle.

Using the SOCP MOSEK code to analyze the yield criterion of a "Porous Drucker-Prager" material on the basis of the Gurson model, our results confirm the fact that failure is possible in compression as well as in traction. Moreover, the results of this micro-macro study show significant differences between the porous Drucker-Prager and Coulomb criteria: the Drucker-Prager's convex domain is noticeably smaller than Coulomb's one and the corresponding criterion does not present corners on the mean pressure axis.

References

1. Anderheggen, E., Knopfel, H.: Finite element limit analysis using linear programming. Int. J. Solid. Struct. **8**, 1413–1431 (1972)
2. Barthélémy, J. F., Dormieux, L.: Détermination du critère de rupture macroscopique d'un milieu poreux par homogénéisation non linéaire. Comptes Rendus Mécanique **331**, 271–276, Acad. Sc., Paris (2003)
3. Chadwick, P.: The quasi-static expansion of a spherical cavity in metals and ideal soils. Quart. J. Mechan. Appl. Math. **12**, 52–71 (1959)
4. Gurson, L. A.: Plastic flow and fracture of ductile materials incorporating void nucleation, growth and interaction. Ph. D. Thesis. Brown University (1975)
5. Gurson, L. A.: Continuum theory of ductile rupture by void nucleation and growth – part 1: yield criteria and flow rules for porous ductile media. ASME J. Engng. Mater. Technol. **99**, 2–15 (1977)
6. Leblond, J.-B.: Mécanique de la rupture fragile et ductile, Etudes en mécanique des matériaux et des structures. In: Hermes science (ed.) (2003)
7. Pastor, F., Trillat, M., Pastor, J., Loute, E., Thoré, Ph.: Convex optimization and stress-based lower/upper bound methods for limit analysis of porous polymer materials. In: Besson, J., Steglish, D., Moinereau, D. (eds,) 9th European mechanics of materials conference, EMMC9, Ecole des Mines de Paris–EDF, May (2006)
8. Pastor, J., Turgeman S.: Limit analysis in axisymmetrical problems: Numerical determination of complete statical solutions. Int. J. Mech. Sci. **24**, 95–117 (1982)
9. Salençon, J.: Théorie de la plasticité pour les applications à la mécanique des sols. Eyrolles, Paris (1974)
10. Trillat, M., Pastor, J., Thoré, Ph.: Limit analysis and conic programming: "Porous Drucker-Prager" material and Gurson's model. Comptes Rendus Mécanique **334**, 599–604, Acad. Sc., Paris (2006)

A Direct Method for the Determination of Effective Strength Domains for Periodic Elastic-Plastic Media

S. Bourgeois, H. Magoariec, and O. Débordes

Abstract This work is devoted to the analysis of the mechanical strength of heterogeneous periodic media submitted to variable loads. The shakedown static approach is coupled with the homogenisation theory to obtain the strength domains: the effective ultimate yield surfaces and shakedown domains. This direct method leads to constrained optimization problems on a three-dimensional unit cell. In order to treat general microstructures, the FEM is used and a specific formulation is introduced to rigorously take into account the specificities of the localisation problems. It eventually leads to discretized constrained optimization problems. Using this method, this work is focused on the case of heterogeneous plates, which exhibit periodic microstructures only in the two in-plane directions. The effective model (Love-Kirchhoff) is obtained by solving problems on a 3D unit cell. Membrane-bending couplings and three dimensional effects are naturally taken into account. The effective strength domains are obtained in terms of in-plane stresses and bending moments. The method is first validated for a homogeneous plate. Two other examples are also proposed : a sandwich plate and a periodically perforated plate.

Stéphane Bourgeois and Olivier Débordes
Laboratoire de Mécanique et d'Acoustique (UPR 7051) & Ecole Centrale de Marseille, 38 rue Joliot Curie, Technopôle de Château-Gombert, 13451 Marseille cedex 20, France, e-mail: stephane.bourgeois@ec-marseille.fr; olivier.debordes@ec-marseille.fr

Hélène Magoariec
Laboratoire de Tribologie et Dynamique des Systèmes (UMR 5513) & Ecole Centrale de Lyon, Bât. G8, 36 avenue Guy de Collongue, 69134 Ecully cedex, France, e-mail: helene.magoariec@ec-lyon.fr

1 Introduction

Limit analysis and shakedown theories are used to study the reliability of structures with respect to failure by unlimited plastic dissipation. Shakedown analysis is devoted to the case of variable loads while the limit analysis theory is relevant to monotonic loading [12]. Limit analysis can be considered as a particular case of shakedown. The shakedown theory provides the safe loading domains, which can be bounded using the static approach proposed by Melan [24] and the kinematic approach due to Koiter [15]. It should be noticed that the static and kinematic theorems have been initially established for elastic perfectly plastic materials and then extended to more sophisticated materials, as mentioned in [9]. Shakedown of structures can be studied through two different methods: incremental analysis following particular loading pathes and direct method requiring the envelope of the considered loading pathes. The direct method leads to a constrained optimization problem which provides the admissible domain for the loading process in a straight forward manner.

A lot of structures exhibit heterogeneities which affect the effective behaviour. Taking into account these heterogeneities may lead to heavy computations. When the size of the heterogeneities is much smaller than the size of the structure, homogenisation theory can be used to substitute the initial heterogeneous problem by an equivalent homogeneous one. In the framework of three-dimensional periodic media, the foundation of the theory for the coupling between homogenisation and limit analysis was laid by Suquet [27], who proposed a definition for the effective ultimate yield surface. The unit cell is then considered as a microstructure submitted to effective stresses. The method was applied among others to perforated sheets [23], fibre-reinforced composites [8,11] and stability of soils [29]. More recently, using the works of Caillerie [3] and Suquet [27], some authors investigated the case of periodic plates (see [2,26]). Starting from a thin three-dimensional structure, periodic in two directions, an effective homogeneous Love-Kirchhoff plate model has been obtained. The definition of the effective ultimate yield surface proposed in [27] has been extended, providing the plastically admissible domain for the generalized effective stresses (in-plane stresses and bending moments). A recent application to layered composite plates can be found in [7].

In the framework of shakedown, the determination of safe loading domains of unidirectional composites under axisymmetric loading by Tarn et al. [28] constituted the pioneer work. The other studies about the coupling of homogenisation and shakedown are more recent. The kinematic approach of Koiter was applied in [25] to study the load-carrying capacity of metal matrix composites submitted to cyclic thermal loading. Additional applications to fibre-reinforced composites and perforated sheets can be found in [4,5,21] and [22]. Shakedown of metal matrix composites has been studied in [30] and [10].

Magoariec et al. [20] have proposed a direct numerical approach to determine the effective strength domains for 3D-periodic heterogeneous media, using the static approach of Melan [24]. The present contribution is an extension of the approach to the case of periodic plates. This is a generalization of the work of Bourgeois et al. [2], dealing with the effective ultimate yield surface for heterogeneous periodic plates. The effective model is a Love-Kirchhoff model, which takes into account the 3D-effects at the scale of the unit cell, treated as a three-dimensional microstructure. All the couplings (membrane-bending) are naturally taken into account within this approach. The effective strength domains are obtained in terms of macroscopic generalized stresses: in-plane stresses and bending moments.

In Sect. 2, the static approach of Melan and the resulting optimization problem are recalled. Some numerical aspects on the use of the finite element method are given. Section 3 is devoted to the extension of the theory to the determination of the effective strength domains of 3D-periodic heterogeneous media. The shakedown theory is coupled with the periodic homogenisation theory. It leads to solve optimization problems on a unit cell. In order to use the finite element method, a specific variational formulation is introduced to rigorously take into account the periodic conditions for the microscopic strains and stresses and the average relation between the microscopic and macroscopic quantities. Section 4 shows the extension to periodic plates. The method is validated for a homogeneous plate by a comparison with results available in literature. Two additional examples are presented: a sandwich plate and a periodically perforated plate.

2 The Static Approach of Shakedown

In this section, the condition for shakedown of an elastic perfectly plastic structure is recalled. The direct approach of shakedown and the associated constrained optimization problem are then presented. Finally, we focus on some technical aspects of the numerical implementation.

2.1 The Classical Static Shakedown Theorem

We consider an elastic perfectly plastic structure V, submitted to body forces $\boldsymbol{f_v}(\boldsymbol{x}, t)$ where $\boldsymbol{x}$ is a point in V and the time $t \in [0, +\infty[$ plays the role of a loading parameter. The boundary ∂V is divided into two parts: surface tractions $\boldsymbol{f_s}(\boldsymbol{x}, t)$ are prescribed on ∂V_f and displacements are fixed on ∂V_u. For the sake of simplicity, the material is considered isotropic. The plasticity domain at each point $\boldsymbol{x}$ is denoted $\mathcal{G}(\boldsymbol{x})$, associated to the yield surface defined by the von Mises criterion:

$$\mathcal{G}(\boldsymbol{x}) = \left\{ \boldsymbol{\sigma}(\boldsymbol{x}) \middle| F(\boldsymbol{\sigma}(\boldsymbol{x}), \sigma_0(\boldsymbol{x})) = \frac{3}{2\,\sigma_0(\boldsymbol{x})^2}\, \boldsymbol{\sigma}^d(\boldsymbol{x}) : \boldsymbol{\sigma}^d(\boldsymbol{x}) - 1 \leq 0 \right\}, \quad (1)$$

where $\sigma_0(\boldsymbol{x})$ and $\boldsymbol{\sigma}^d(\boldsymbol{x})$ are respectively the yield stress and the deviatoric part of $\boldsymbol{\sigma}$ at a given point of coordinates $\boldsymbol{x}$. The loading state at time t is denoted $\mathcal{P}(t)$:

$$\mathcal{P}(t) = \{\boldsymbol{f_v}(\boldsymbol{x}, t), \boldsymbol{x} \in V\} \cup \{\boldsymbol{f_s}(\boldsymbol{x}, t), \boldsymbol{x} \in \partial V_f\}, \quad (2)$$

and it is assumed that the loading path is a linear combination of n independent loading processes $\mathcal{P}_i$:

$$\mathcal{P}(t) = \sum_{i=1}^{n} \mu_i(t)\mathcal{P}_i. \quad (3)$$

Furthermore, the loading is supposed to be bounded and confined in a time-independent loading domain $\mathcal{D}$: conditions are imposed to $\mu_i(t)$ and the domain $\mathcal{D}$ is then a convex polyhedron which can be defined as follows:

$$\mathcal{D} = \left\{ \mathcal{P}(t) \middle| \mathcal{P}(t) = \sum_{i=1}^{n} \mu_i(t)\mathcal{P}_i, \mu_i(t) \in \left[\mu_i^-, \mu_i^+\right] \right\}. \quad (4)$$

The static theorem of Melan states that: if there exists a safety coefficient $\beta > 1$ and a time-independent self-equilibrated residual stress field $\boldsymbol{\rho}(\boldsymbol{x})$, such that:

$$\boldsymbol{\sigma}(\boldsymbol{x}, t) = \beta(\boldsymbol{\sigma}^e(\boldsymbol{x}, P) + \boldsymbol{\rho}(\boldsymbol{x})) \in \mathcal{G}(\boldsymbol{x}) \qquad \forall \boldsymbol{x} \in V, \forall P \in \mathcal{D}, \quad (5)$$

then the structure shakes down for any loading path $\mathcal{P}(t)$ such that $\forall t \in [0, +\infty[,\ \mathcal{P}(t) \in \mathcal{D}$. In Eq. (5), $\boldsymbol{\sigma}^e(\boldsymbol{x}, P)$ is the fictitious elastic stress response of the structure submitted to the loading state P and satisfies the following problem:

$$\begin{cases} \operatorname{div} \boldsymbol{\sigma}^e + \boldsymbol{f_v} = \boldsymbol{0} & \text{in } V, \\ \boldsymbol{\sigma}^e = \mathrm{D} : \boldsymbol{\varepsilon}^e & \text{in } V, \\ \boldsymbol{\varepsilon}^e = \operatorname{grad}_s \boldsymbol{u} & \text{in } V, \\ \boldsymbol{\sigma}^e \cdot \boldsymbol{n} = \boldsymbol{f_s} & \text{on } \partial V_f, \\ \boldsymbol{u} = \boldsymbol{0} & \text{on } \partial V_u, \end{cases} \quad (6)$$

where D is the Hooke tensor and $\boldsymbol{n}$ the outwarding normal on the boundary ∂V_f. The residual stress field $\boldsymbol{\rho}$ satisfies:

$$\begin{cases} \operatorname{div} \boldsymbol{\rho} = \boldsymbol{0} & \text{in } V, \\ \boldsymbol{\rho} \cdot \boldsymbol{n} = \boldsymbol{0} & \text{on } \partial V_f. \end{cases} \quad (7)$$

The direct approach consists in determining the shakedown safety factor α_{sd} such that:

$$\alpha_{sd} = \max_{\boldsymbol{\rho} \in \mathcal{S}^0} \left\{ \alpha \Big| \alpha\, \boldsymbol{\sigma}^e(\boldsymbol{x}, P) + \boldsymbol{\rho}(\boldsymbol{x}) \in \mathcal{G}(\boldsymbol{x}), \forall\, \boldsymbol{x} \in V, \forall\, P \in \mathcal{D} \right\}, \qquad (8)$$

where $\mathcal{S}^0$ is the set of admissible residual stress fields verifying (7). If $\alpha_{sd} > 1$, the structure will shakedown, while it will not if $\alpha_{sd} < 1$. In practice, the coefficient α_{sd} represents the reduction or amplification factor that can be applied to the loading domain $\mathcal{D}$ such that the shakedown occurs in the structure. We recall now that the loading domain is supposed to be a convex polyhedron. Considering the property of convexity of the elastic domain $\mathcal{G}(\boldsymbol{x})$, only the 2^n vertices $P^k = \sum_{i=1}^{n} \mu_i \mathcal{P}_i$, $\mu_i \in \{\mu_i^-, \mu_i^+\}$ of $\mathcal{D}$ can be considered in the optimization problem (8):

$$\alpha_{sd} = \max_{\boldsymbol{\rho} \in \mathcal{S}^0} \left\{ \alpha \Big| \alpha\, \boldsymbol{\sigma}^e(\boldsymbol{x}, P^k) + \boldsymbol{\rho}(\boldsymbol{x}) \in \mathcal{G}(\boldsymbol{x}), \forall\, \boldsymbol{x} \in V, \forall\, P^k, k = 1, 2^n \right\}. \quad (9)$$

It should be noticed that a limit analysis problem leads to the optimization problem (9) with only one loading point P. In addition, if the residual stress is set to zero, the later problem gives the elastic safety factor. In conclusion, the non-linear constrained optimization problem (9) is able to provide three kinds of strength domains: elasticity, limit analysis and shakedown.

2.2 Numerical Aspects

The optimization problem (9) requires numerical methods at two steps: the space dicretization of the stress fields $\boldsymbol{\sigma}^e(\boldsymbol{x}, P)$ and $\boldsymbol{\rho}(\boldsymbol{x})$ and then the resolution of the obtained discretized optimization problem. In the following, the finite element method is used for the first step. In the optimization problem, the stress at each point $\boldsymbol{x}$ of the structure is then replaced by the stress at each integration point of the finite element model. The discretized optimization problem can be written

$$\alpha_{sd} = \max_{\{\rho\}} \left\{ \alpha \left| \begin{array}{l} F(\alpha\, \sigma_{ip}^e(P^k) + \rho_{ip}) \le 0, \forall\, ip, \forall\, P^k, k = 1, 2^n \\ [C]\,\{\rho\} = \{0\} \end{array} \right. \right\}, \qquad (10)$$

where the index ip is referring to integration points and the vector $\{\rho\}$ is composed of the residual stresses at all integration points. As the problem (7) is linear, the condition $\boldsymbol{\rho} \in \mathcal{S}^0$ becomes the equality constraints $[C]\,\{\rho\} = \{0\}$ after discretization where $[C]$ is called the equilibrium matrix. The assembly of this matrix has been implemented in the finite element software SIC [1] which computes also the stresses at each integration point for each loading point. This FEM code generates the data file for the optimization software LANCELOT [6] based on Large and Nonlinear Constraints Extended Lagrangian Optimisation Techniques. This latter freeware is suitable for quite large problems (few thousands of optimization variables and of inequality and equality constraints) and handles quadratic inequality constraints. Typically,

CPU times for shakedown problems presented in Sect. 4.3 vary between few hundreds and few thousands seconds on a Personal Computer.

3 Periodic Heterogeneous Media

We consider heterogeneous media exhibiting a periodic microstructure in three independent directions. The determination of the effective strength domains is based on shakedown analyses on a representative volume element, the unit cell, which generates the whole medium by periodic translations. In the following, the principle exposed in [20] is recalled.

3.1 Cell Problems

The unit cell is considered as a microstructure V submitted to an effective stress Σ such that:

$$\Sigma =< \boldsymbol{\sigma} >_V, \tag{11}$$

where $< \bullet >_V$ is the average operator over the unit cell:

$$< \bullet >_V = \frac{1}{\mathrm{Vol}(V)} \int_V \bullet \, \mathrm{d}V. \tag{12}$$

The effective stress Σ is supposed to be confined in a loading domain $\mathcal{D}$ such that shakedown theory, as presented in Sect. 2, applies. In the optimization problem, the fictitious elastic stress field corresponds to the response of the unit cell satisfying the classical localisation problem:

$$\begin{cases} \mathrm{div}\, \boldsymbol{\sigma}^e = \mathbf{0} & \text{in } V, \\ \boldsymbol{\sigma}^e = \mathsf{D} : \boldsymbol{\varepsilon}^e & \text{in } V, \\ \boldsymbol{\varepsilon}^e = \mathsf{E} + \mathrm{grad}_s \boldsymbol{u}^{\#} & \text{in } V, \\ \boldsymbol{\sigma}^e \cdot \boldsymbol{n} & \text{anti-periodic on } \partial V, \\ \boldsymbol{u}^{\#} & \text{periodic on } \partial V, \\ < \boldsymbol{\sigma}^e >_V = \Sigma, \end{cases} \tag{13}$$

where the effective strain $\mathsf{E} =< \boldsymbol{\varepsilon}^e >_V$ is unknown. The strain field $\boldsymbol{\varepsilon}^e$ is splitted into two parts: the average strain E and a corrective strain derived from the periodic displacement field $\boldsymbol{u}^{\#}$. The condition $\boldsymbol{u}^{\#}$ periodic on ∂V means that the displacement $\boldsymbol{u}^{\#}$ is the same at two opposite points of the boundary. On the contrary, the condition $\boldsymbol{\sigma}^e \cdot \boldsymbol{n}$ anti-periodic on ∂V means that the traction forces are opposite at two opposite points of the boundary. These conditions come from the periodicity of the stress and strain fields.

Associated to the elastic problem (13), the self-equilibrated residual stress field satisfies:

$$\begin{cases} \text{div } \boldsymbol{\rho} = \mathbf{0} & \text{in } V, \\ \boldsymbol{\rho} \cdot \boldsymbol{n} & \text{anti-periodic on } \partial V, \\ < \boldsymbol{\rho} >_V = 0. \end{cases} \qquad (14)$$

In the following, a variational formulation is introduced, taking into account the specificities of the problems (13) and (14):

- periodic and anti-periodic conditions,
- loading in average,
- splitting of the strain field.

3.2 Variational Formulation and Implementation

Let us consider a stress field $\boldsymbol{\sigma}$ satisfying the problems (13) and (14):

$$\begin{cases} \text{div } \boldsymbol{\sigma} = \mathbf{0} & \text{in } V, \\ \boldsymbol{\sigma} \cdot \boldsymbol{n} & \text{anti-periodic on } \partial V, \\ < \boldsymbol{\sigma} >_V = \Sigma. \end{cases} \qquad (15)$$

The variational formulation proposed here is based on a specific test field, consistent with the real kinematics in (13): $\boldsymbol{u}^* = \mathsf{E}^* \cdot \boldsymbol{x} + \boldsymbol{u}^{\#^*}$ with $\boldsymbol{u}^{\#^*}$ periodic on ∂V and E^* uniform in V:

$$\begin{vmatrix} \forall \, \mathsf{E}^* \text{ symmetric and uniform in } V, \\ \forall \, \boldsymbol{u}^{\#^*} \text{ periodic on } \partial V, \\ \int_V \boldsymbol{\sigma} : \left(\mathsf{E}^* + \text{grad}_s \boldsymbol{u}^{\#^*} \right) dV = \text{Vol}(V)\, \Sigma : \mathsf{E}^*. \end{vmatrix} \qquad (16)$$

The problem (13) is equivalent to the formulation (16) with $\boldsymbol{\sigma} = \mathsf{D} : \left(\mathsf{E} + \text{grad}_s \boldsymbol{u}^{\#} \right)$. For the problem (14), $\boldsymbol{\sigma} = \boldsymbol{\rho}$ and the effective stress Σ is set to zero. This formulation has been implemented in the finite element software SIC [1]. The kinematics at the level of each finite element is redefined: the classical degrees of freedom are relative to the periodic displacement $\boldsymbol{u}^{\#}$ and six degrees of freedom (dofs) are added at the level of each element to support the components of the effective strain E. The gradient matrix is modified to take into account these additional dofs. From the variational form (16), we can deduce that the nodal forces associated to the additional dofs are the effective stresses multiplied by the volume of the unit cell. The FEM software eventually provides the inputs of the discretized optimization problem (10): the equilibrium matrix $[C]$ and the elastic stress at each integration point for each loading point $P^k = \Sigma^k$, the vertices of

the loading domain. If only one loading point $P = \Sigma$ is considered, the optimization provides the solution of a limit analysis problem and the effective stress $\alpha_{sd}\Sigma$ is on the ultimate effective yield surface on the boundary of the plastically admissible effective domain $\mathcal{G}^{hom}$ defined in [27] such that:

$$
\mathcal{G}^{hom} = \left\{ \Sigma \left| \begin{array}{l} \operatorname{div} \boldsymbol{\sigma} = \mathbf{0} \quad \text{in } V, \quad \boldsymbol{\sigma} \cdot \boldsymbol{n} \quad \text{anti-periodic on } \partial V \\ < \boldsymbol{\sigma} >_V = \Sigma \\ \boldsymbol{\sigma} \in \mathcal{G}(\boldsymbol{x}), \quad \forall \boldsymbol{x} \in V \end{array} \right. \right\}.
\tag{17}
$$

4 Periodic Heterogeneous Plates

The heterogeneous medium – see Fig. 1 – is assumed to be periodic in only two directions and thin in the third one. When the thickness is much smaller than the in-plane size of the structure, the use of a plate model is relevant. In the framework of linear elasticity, the effective stiffnesses of such a structure have been studied by many authors [3,16–18]. Caillerie [3] has shown that the homogenisation process requires taking into account two small parameters: the ratios $\eta = \frac{t}{L}$ and $\xi = \frac{d}{L}$ where t is the thickness, d the typical size of the period and L the in-plane typical size of the structure (see Fig. 1). Kohn et al. [16] have used two similar parameters for periodic plates with rapidly varying thickness. In the homogenisation process, these small parameters are introduced in the three-dimensional elastic heterogeneous problem and are assumed to tend to zero.
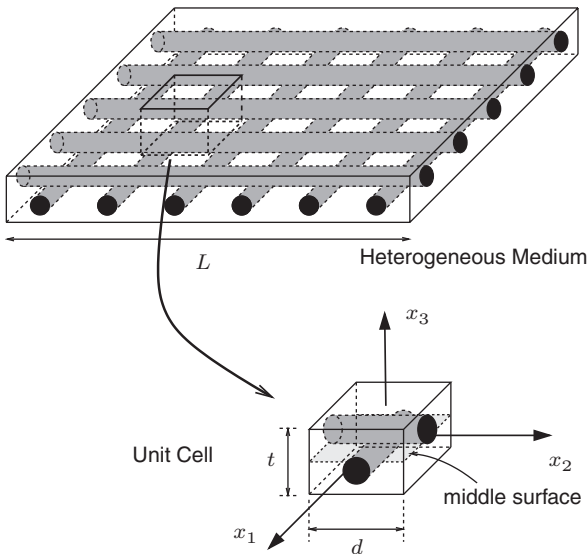
Fig. 1 Homogenisation of periodic plates: heterogeneous medium and unit cell

The effective model is found to be a Love-Kirchhoff plate but the stiffnesses depend on the way the limits are performed: η then ξ tending to zero, ξ then η tending to zero or ξ and η tending to zero together. In the first case, the thickness must be much smaller than the period size. The second one corresponds to the opposite case. The last method is theoretically relevant when the thickness and the period size are of the same order. Nevertheless, the effective model obtained such a way can be used outside its application framework [18]. Contrary to the others, this case leads to consider a three-dimensional unit cell in order to determine the effective stiffnesses: the 3D-effects are naturally taken into account. In the following, the determination of the effective strength domains is based on this model.

4.1 Cell Problems

The boundary ∂V of the unit cell V is composed of the upper surface ∂V_{up}, the lower surface ∂V_{low} and the lateral faces ∂V_{lat}. The axes (O, x_1, x_2, x_3) are chosen such that the middle surface is included in the plane defined by $x_3 = 0$. The in-plane components are denoted by Greek indices which take the values in the set $\{1, 2\}$. The Latin indices run over 1, 2 and 3. Following the idea exposed in the above section, the unit cell is considered as a microstructure submitted to the effective generalized stresses, the in-plane forces $N_{\alpha\beta}$ and the bending moments $M_{\alpha\beta}$, such that

$$N_{\alpha\beta} = <\sigma_{\alpha\beta}>_S, \quad M_{\alpha\beta} = <x_3\,\sigma_{\alpha\beta}>_S, \tag{18}$$

where $< \bullet >_S$ is a new average operator:

$$<\bullet>_S = \frac{1}{\mathrm{Surf}(S)} \int_V \bullet\, dV, \tag{19}$$

where $\mathrm{Surf}(S)$ is the area of the middle surface of the unit cell (see Fig. 1). In the following, the relations (18) are rewritten in the concise form $N =< \boldsymbol{\sigma} >_S$ and $M =< x_3\,\boldsymbol{\sigma} >_S$. The shakedown theory requires the computation of the fictitious elastic stress field, corresponding to a purely elastic unit cell. This stress field satisfies the localisation problem given in [3]:

$$\begin{cases} \mathrm{div}\,\boldsymbol{\sigma}^e = \mathbf{0} & \text{in } V, \\ \boldsymbol{\sigma}^e = \mathsf{D} : \boldsymbol{\varepsilon}^e & \text{in } V, \\ \boldsymbol{\varepsilon}^e = \mathsf{E} + x_3\,\mathsf{K} + \mathrm{grad}_s \boldsymbol{u}^{\#} & \text{in } V, \\ \boldsymbol{\sigma}^e \cdot \boldsymbol{n} & \text{anti-periodic on } \partial V_{lat}, \\ \boldsymbol{\sigma}^e \cdot \boldsymbol{n} = \mathbf{0} & \text{on } \partial V_{low} \text{ and } \partial V_{up}, \\ \boldsymbol{u}^{\#} & \text{periodic on } \partial V_{lat}, \\ <\boldsymbol{\sigma}^e>_S = \mathsf{N}, \\ <x_3\,\boldsymbol{\sigma}>_S = \mathsf{M}, \end{cases} \tag{20}$$

where E and K are the effective generalized strains: the membrane strains $\mathsf{E}_{\alpha\beta}$ and the bending curvatures $\mathsf{K}_{\alpha\beta}$, ($\mathsf{E}_{i3} = \mathsf{E}_{3i} = \mathsf{K}_{i3} = \mathsf{K}_{3i} = 0$). The strain field $\boldsymbol{\varepsilon}^e$ is composed of a Love-Kirchhoff kinematics $\mathsf{E} + x_3\,\mathsf{K}$ and a corrective strain derived from the periodic displacement field $\boldsymbol{u}^{\#}$. Associated to the elastic problem (20), the self-equilibrated residual stress field satisfies:

$$\begin{cases} \operatorname{div}\boldsymbol{\rho} = \boldsymbol{0} & \text{in } V, \\ \boldsymbol{\rho}\cdot\boldsymbol{n} & \text{anti-periodic on } \partial V_{lat}, \\ \boldsymbol{\rho}\cdot\boldsymbol{n} = 0 & \text{on } \partial V_{low} \text{ and } \partial V_{up}, \\ <\boldsymbol{\rho}>_S = 0, \\ <x_3\,\boldsymbol{\rho}>_S = 0. \end{cases} \tag{21}$$

4.2 Numerical Implementation

A stress field $\boldsymbol{\sigma}$ is statically admissible for the problems (20) and (21) if:

$$\begin{cases} \operatorname{div}\boldsymbol{\sigma} = \boldsymbol{0} & \text{in } V, \\ \boldsymbol{\sigma}\cdot\boldsymbol{n} & \text{anti-periodic on } \partial V_{lat}, \\ \boldsymbol{\sigma}\cdot\boldsymbol{n} = 0 & \text{on } \partial V_{low} \text{ and } \partial V_{up}, \\ <\boldsymbol{\sigma}>_S = \mathsf{N}, \\ <x_3\,\boldsymbol{\sigma}>_S = \mathsf{M}. \end{cases} \tag{22}$$

The variational formulation is obtained with the specific test field

$$\boldsymbol{u}^* = \boldsymbol{u}^{LK}(\mathsf{E}^*,\mathsf{K}^*) + \boldsymbol{u}^{\#^*}, \tag{23}$$

such that

$$\begin{cases} \boldsymbol{u}_{\alpha}^{LK}(\mathsf{E}^*,\mathsf{K}^*) = \mathsf{E}_{\alpha\beta}^* \, x_{\beta} + x_3\,\mathsf{K}_{\alpha\beta}^* \, x_{\beta}, \\ \boldsymbol{u}_3^{LK}(\mathsf{E}^*,\mathsf{K}^*) = -\frac{1}{2}\,\mathsf{K}_{11}^* \, (x_1)^2 - \frac{1}{2}\,\mathsf{K}_{22}^* \, (x_2)^2 - \mathsf{K}_{12}^* \, x_1\,x_2, \end{cases} \tag{24}$$

with $\boldsymbol{u}^{\#^*}$ periodic on ∂V_{lat}, E^* and K^* uniform in V satisfying:

$$\mathsf{E}_{i3}^* = \mathsf{E}_{3i}^* = \mathsf{K}_{i3}^* = \mathsf{K}_{3i}^* = 0. \tag{25}$$

The test field is consistent with the Love-Kirchhoff kinematics in (20), *i.e.*:

$$\operatorname{grad}_s \boldsymbol{u}^{LK} = \mathsf{E}^* + x_3\mathsf{K}^*. \tag{26}$$

The Eqs. (22) are then equivalent to the variational formulation

$$\left| \begin{array}{l} \forall\, \mathsf{E}^* \text{ and } \forall\, \mathsf{K}^* \text{ symmetric, uniform in } V \text{ with } \mathsf{E}^*_{i3} = \mathsf{E}^*_{3i} = \mathsf{K}^*_{i3} = \mathsf{K}^*_{3i} = 0, \\ \forall\, \boldsymbol{u}^{\#^*} \text{ periodic on } \partial V_{lat}, \\ \displaystyle\int_V \boldsymbol{\sigma} : \left(\mathsf{E}^* + x_3\, \mathsf{K}^* + \mathrm{grad}_s \boldsymbol{u}^{\#^*} \right) \, dV = \mathrm{Surf}(S) \left(\mathsf{N} : \mathsf{E}^* + \mathsf{M} : \mathsf{K}^* \right). \end{array} \right.$$

(27)

The variational form of the problem (20) is found if we set

$$\boldsymbol{\sigma} = \mathsf{D} : \left(\mathsf{E} + x_3\, \mathsf{K} + \mathrm{grad}_s \boldsymbol{u}^{\#} \right).$$

(28)

For the problem (21), $\boldsymbol{\sigma} = \boldsymbol{\rho}$ and the effective generalized stresses N and M are set to zero.

This formulation has been implemented in the finite element software SIC [1]. The kinematics at the level of each finite element is redefined: the components $\mathsf{E}_{\alpha\beta}$ and $\mathsf{K}_{\alpha\beta}$ of the effective generalized strains are taken into account by introducing six additional degrees of freedom to all elements. The classical dofs are associated to the periodic displacement $\boldsymbol{u}^{\#}$. The gradient matrix is modified to take into account the specific kinematics. The FEM code generates the inputs of the discretized optimization problem (10) to determine the effective strength domains of the effective Love-Kirchhoff model. If we consider only one loading point $P = \{\mathsf{N}, \mathsf{M}\}$, the effective generalized stresses $\alpha\mathsf{N}$ and $\alpha\mathsf{M}$ belong to the ultimate effective yield surface, which is the boundary of the plastically admissible effective domain $\mathcal{G}_{LK}^{hom}$ defined in [2] and [26]:

$$\mathcal{G}_{LK}^{hom} = \left\{ \{\mathsf{N}, \mathsf{M}\} \left| \begin{array}{l} \mathrm{div}\, \boldsymbol{\sigma} = \boldsymbol{0} \quad \text{in } V, \boldsymbol{\sigma} \cdot \boldsymbol{n} \quad \text{anti-periodic on } \partial V, \\ \boldsymbol{\sigma} \cdot \boldsymbol{n} = 0 \quad \text{on } \partial V_{low} \text{ and } \partial V_{up}, \\ < \boldsymbol{\sigma} >_S = \mathsf{N}, \quad < x_3\, \boldsymbol{\sigma} >_S = \mathsf{M}, \\ \boldsymbol{\sigma} \in \mathcal{G}(\boldsymbol{x}), \quad \forall \boldsymbol{x} \in V \end{array} \right. \right\}.$$

(29)

4.3 Applications

This section illustrates the determination of the effective strength domains for some periodic plates according to shakedown, limit analysis and elasticity. In the first example, we consider a homogeneous plate to validate the approach. The results are compared to those available in literature. The second example is a so-called sandwich plate, periodic in one in-plane direction and invariant in the second one. In a last example, we compute the safety domains of a plate periodically perforated in the two in-plane directions.

4.3.1 Loading Domains

In the following, the unit cells are submitted to a prescribed couple of effective generalized stresses. For the sake of simplicity, we only consider 2D domains but the method is general and can be applied up to 6 non-zero generalized stresses.
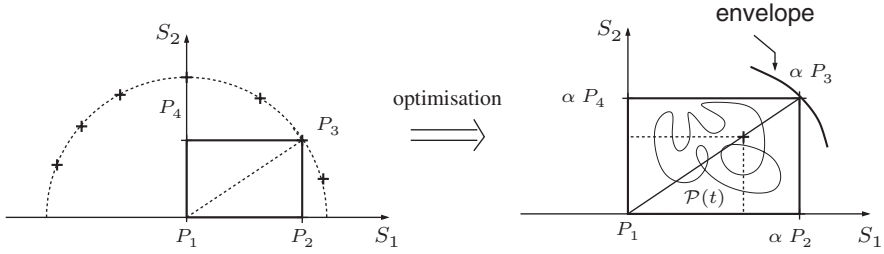
Fig. 2 Principle for obtaining the effective strength domains

The loading domains are rectangular polyhedrons defined by the four vertices (see Fig. 2) $P_1 = (0, 0)$, $P_2 = (S_1, 0)$, $P_3 = (S_1, S_2)$ and $P_4 = (0, S_2)$, where S_1 and S_2 are respectively the first and the second non-zero generalized stresses. The point P_3 of each polyhedron is representative of a point on the initial loading domain. Once the reduction or amplification factor α is computed, we find the homothetic point to P_3 located on the boundary of the strength domain. The elasticity and shakedown curves presented in the graphs are the envelopes of the strength domains and have to be understood as follows:

- elasticity: any loading path confined in a rectangular polyhedron with P_3 on the elasticity envelope and P_1 at the origin is included in the effective initial elastic domain,
- shakedown: any loading path confined in a rectangular polyhedron with P_3 on the shakedown envelope and P_1 at the origin leads to shakedown of the unit cell.

The limit analysis curves presented in the graphs correspond to the intersection of the effective ultimate yield surface with the plane defined by the only two non-zero effective stresses S_1 and S_2.

4.3.2 Validation for a Homogeneous Plate

The effective ultimate yield surface for a homogeneous plate of constant thickness has been widely studied in literature [13,14]. Furthermore, the theoretical elasticity domain can be easily derived. The invariance properties of the plate in the in-plane directions allow us to consider a parallelepipedic unit cell as shown in Fig. 3. The mesh has only one element in the in-plane directions and six in the thickness direction. The mechanical and geometric properties of the considered plate are reported in Table 1.

The unit cell is submitted to combined membrane stress $S_1 = \mathsf{N}_{11}$ and bending moment $S_2 = \mathsf{M}_{11}$. The mesh is finer towards the free surfaces of the plate in order to well capture the elastic limit when bending operates. Each optimization problem is composed of 973 optimization variables, 87 equality constraints and 648 (resp. 162) inequality constraints for shakedown (resp.

Fig. 3 Mesh of the unit cell for the homogeneous plate
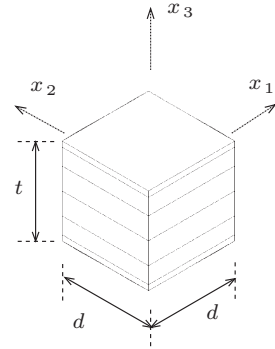
Table 1 Properties of the homogeneous plate

Young's Modulus	Poisson's ratio	Yield Stress	Thickness
$E = 100$ GPa	$\nu = 0.3$	$\sigma_0 = 240$ MPa	$t = 2$ mm

limit analysis). The results are presented in Fig. 4, and are expressed in terms of dimensionless stresses:

$$n_{11} = \frac{N_{11}}{t\,\sigma_0}, \qquad m_{11} = \frac{M_{11}}{(\frac{t}{2})^2\,\sigma_0}. \tag{30}$$

As the von Mises criterion is symmetric with respect to the origin and as the unit cell is symmetric with respect to the middle surface, the strength domains are symmetric with respect to the axes $n_{11} = 0$ and $m_{11} = 0$.
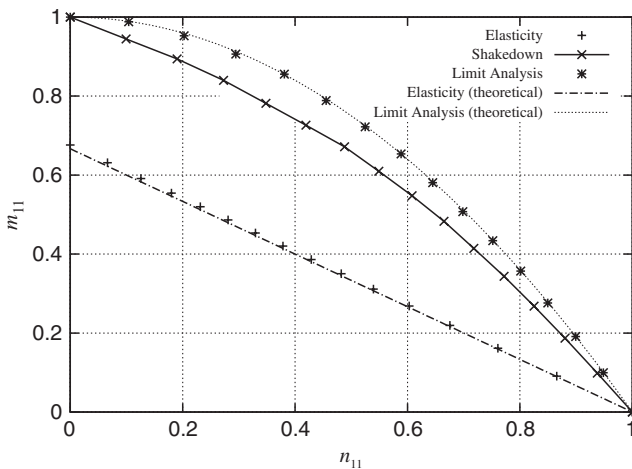
Fig. 4 Results for the homogeneous plate

The results plotted only in the fourth plan $(n_{11} > 0, m_{11} > 0)$ are in good agreement with the available theoretical ones:

- the effective elasticity domain fits well with the theoretical criterion:

$$n_{11} + \frac{3}{2} m_{11} - 1 \leq 0, \tag{31}$$

- the limit analysis curve fits well with the criterion obtained by Ilyushin [14] and Hodge [13] for the effective ultimate yield surface:

$$m_{11} + (n_{11})^2 - 1 = 0. \tag{32}$$

This validates the proposed approach.

4.3.3 Application to a 1D-Periodic Plate

The second example is a metallic sandwich plate consisting of two parallel skins with an unidirectional reinforcement, perpendicular to these skins and periodically arranged in the x_2-direction (see Fig. 5).
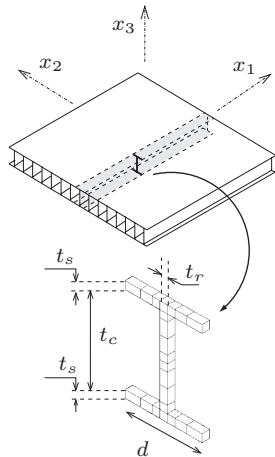
Fig. 5 Sandwich plate and mesh of the unit cell

The geometric properties are reported in Table 2. The mechanical properties are the ones given in Table 1 for the previous example. The unit cell is submitted to combined traction and bending $(S_1 = \mathsf{N}_{11}, S_2 = \mathsf{M}_{11})$. The mesh shown in Fig. 5 is finer in the vicinity of the middle surface in order to capture the yielding across the section. Each optimization problem is composed of 3,565 optimization variables, 453 equality constraints and 2,376 (resp. 594) inequality constraints for shakedown (resp. limit analysis).

Table 2 Geometric properties of the sandwich plate

Skins thickness	Core thickness	Reinforcements thickness	Period size	Total thickness
$t_s = 1$ mm	$t_c = 18$ mm	$t_r = 1$ mm	$d = 15$ mm	$t = 20$ mm
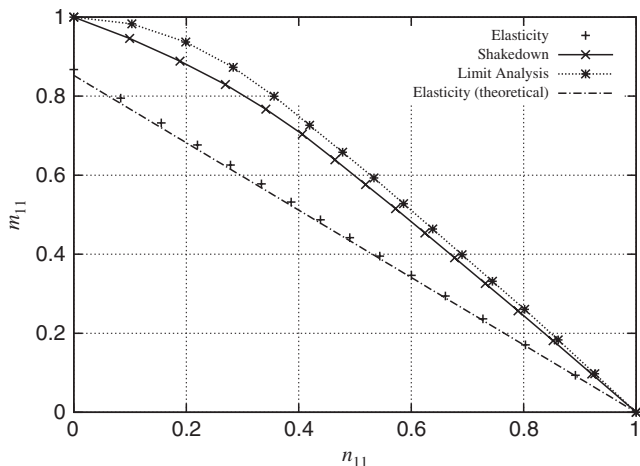
Fig. 6 Results for the sandwich plate

The results presented in Fig. 6 are expressed in terms of dimensionless stresses:

$$n_{11} = \frac{N_{11}}{N_0}, \qquad m_{11} = \frac{M_{11}}{M_0}. \tag{33}$$

N_0 and M_0 are respectively the ultimate yield membrane stress and the ultimate yield bending moment:

$$N_0 = \frac{S_I}{d} \sigma_0, \qquad M_0 = \frac{I_l}{d} \sigma_0, \tag{34}$$

where S_I is the surface area of the cross section of the unit cell in the plane (O, x_2, x_3) and I_l is the linear moment of this cross section with respect to the x_2-axis:

$$S_I = t_r\, t_c + 2\, d\, t_s, \qquad I_l = \frac{1}{4} \left(t_r\, t_c^2 + 2\, d\, t_s\, (t_c + t_s) \right). \tag{35}$$

Only the fourth plan $(n_{11} > 0, m_{11} > 0)$ is considered: the same reasons as in the previous section can be invoked. For this loading process, the criterion for the effective initial elasticity domain can be easily derived:

$$n_{11} + \frac{t}{2} \frac{I_l}{I_q} m_{11} - 1 \leq 0, \tag{36}$$

where I_q is the quadratic moment of the cross section with respect to the x_2-axis:

$$I_q = \frac{1}{12} \left(t_r \, t_c^3 + 2 \, d \, t_s \left(3 \, t_c^2 + 6 \, t_c + 4 \, t_s^2 \right) \right). \tag{37}$$

The numerical results given in Fig. 6 are in good agreement with this theoretical criterion. The small difference is due to the location of the critical integration points when bending operates: they are not exactly located on the upper and lower surfaces of the unit cell. Furthermore, we observe that the theoretical values of the ultimate yield membrane stress N_0 and bending moment M_0 are consistent with the numerical results. It should be noted that the shakedown envelope and the effective ultimate yield surface are very close one to another and the safety margin between shakedown and instantaneous collapse is very low.

4.3.4 Application to a 2D-Periodic Plate

The last example illustrates the ability of the developments to treat general 2D-periodic plates. The considered structure is a periodically perforated plate as shown in Fig. 7.
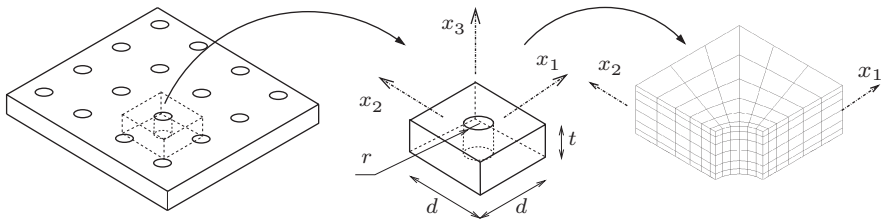
Fig. 7 Perforated plate, unit cell and mesh of the fourth cell

The material and geometric properties are reported in Table 3. Two types of loadings are studied: a bi-axial traction with two non-zero generalized stresses N_{11} and N_{22}, and a combined traction and bending (N_{11}, M_{11}). Taking into account the symmetries of both the unit cell and the loadings, only one fourth of the unit cell is considered. The mesh shown in Fig. 7 is finer in the vicinity of the free surfaces and the hole. Each optimization problem

Table 3 Properties of the perforated plate

Young's modulus	Poisson's ratio	Yield stress	Thickness	Hole radius	Period size
$E = 69550$ MPa	$\nu = 0.337$ mm	$\sigma_0 = 159$ MPa	$t = 2$ mm	$r = 1.15$ mm	$d = 7.69$ mm
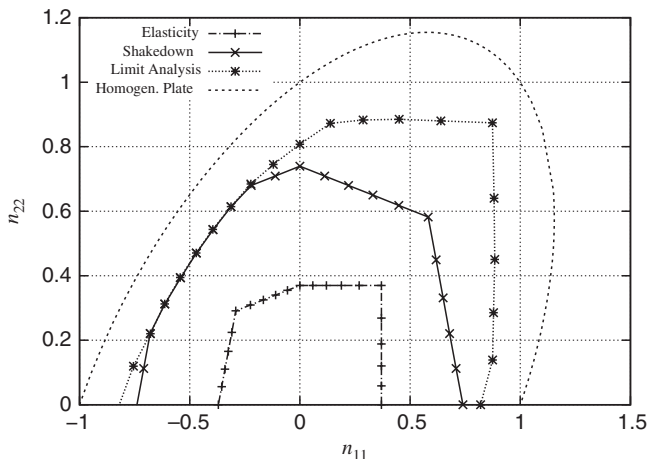
Fig. 8 Results for the perforated plate (bi-axial traction)

is composed of 10,369 optimization variables, 3,267 equality constraints and 6,912 (resp. 1,728) inequality constraints for shakedown (resp. limit analysis).

The results shown in Figs. 8 and 9 are expressed in terms of dimensionless stresses:

$$n_{11} = \frac{N_{11}}{N_0}, \quad n_{22} = \frac{N_{22}}{N_0}, \quad m_{11} = \frac{M_{11}}{M_0}, \tag{38}$$

where $N_0 = t\,\sigma_0$ and $M_0 = (t/2)^2\,\sigma_0$ are the ultimate yield generalized stresses obtained for a homogeneous plate. The comparisons with the safety domains obtained for the no-perforated homogeneous plate studied in Sect. 4.3.2 are made easier.
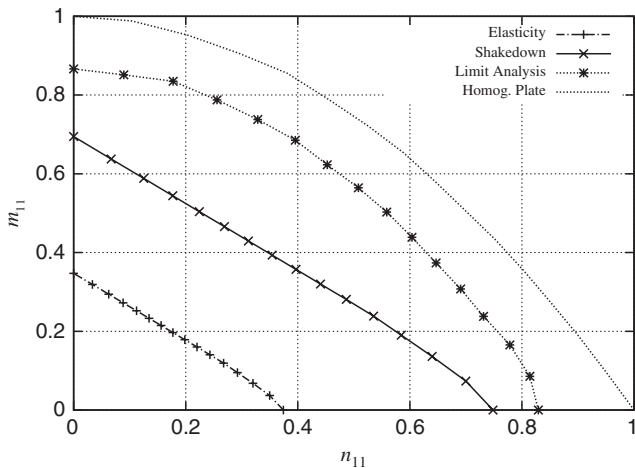
Fig. 9 Results for the perforated plate (bending–traction)

When the plate is submitted to bi-axial traction (see Fig. 8), the results are compared with the ultimate yield surface for a homogeneous plate which coincides in this case with the boundary of the initial elastic domain. The results show the loss of strength due to the presence of the holes. The initial elastic limit for the dimensionless generalized stress in pure traction is close to the theoretical value $\frac{1}{3}$ obtained for a hole in an infinite medium under plane stress assumption. The shakedown envelope and the effective ultimate yield surface have been validated by comparison with results obtained with an incremental approach in [19].

When the plate is submitted to a combined traction and bending, the comparison between the ultimate yield surface for a homogeneous plate and the perforated one emphasises, as expected, a weaker strength (see Fig. 9): the gap is around 15%. The shakedown envelope is quite far from the ultimate yield surface for the perforated plate, while the difference was not so obvious for the homogeneous plate. Finally, it should be noted that the shakedown envelope is twice as large as the initial elasticity domain, which suggests that the shakedown domain and the alternating plasticity domain are identical.

5 Conclusion

In this paper, the direct static approach for shakedown has been coupled with the homogenisation theory to determine the effective strength domains of heterogeneous elastic-plastic media when the microstructure is periodic. The method has been extended to periodic plates and leads to an effective homogeneous Love-Kirchhoff plate. The unit cell is considered as a three-dimensional microstructure submitted to effective generalized stresses including tractions, in-plane shear, bendings and torsion. The numerical tool proposed here allows us to consider general microstructures and any combination of the generalized stresses: all the couplings are naturally taken into account. Three kinds of effective strength domains can be computed: the initial elasticity domain, the shakedown domain and the ultimate yield surface. From the engineering point of view, these domains are useful to establish strength criteria at the macroscopic level, according to elasticity and instantaneous collapse. The shakedown domains may provide some informations about low-cycle fatigue but further theoretical investigations are required.

References

1. Aunay, S.: Architecture de logiciel de modélisation et traitements distribués. PhD thesis, Université Technologique de Compiègne (1990)
2. Bourgeois, S., Débordes, O., Patou, P.: Homogénéisation et plasticité de plaques minces. Rev. Eur. Elts Finis **7**, 39–54 (1998)

3. Caillerie, D.: Thin elastic and periodic plates. Math. Methods Appl. Sci. **6**, 159–191 (1984)
4. Carvelli, V., Maier, G., Taliercio, A.: Shakedown analysis of periodic heterogeneous materials by a kinematic approach, Strojnícky Casopis – Mech. Eng. **50**, 229–240 (1999)
5. Carvelli, V., Maier, G., Taliercio, A.: Kinematic Limit Analysis of Periodic Heterogeneous Media. Comput. Model. Eng. Sci. **1**, 19–30 (2000).
6. Conn, A. R., Gould, N. I. M., Toint, P. L.: LANCELOT: A Fortan Package for Large-Scale Nonlinear Optimization. Springer-Verlag, Berlin (1992).
7. Dallot, J., Sab, K.: Limit analysis of multi-layered plates Part I: The homogenized Love-Kirchhoff model. J. Mech. Phys. Solids **56**, 561–580 (2008)
8. De Buhan, P., Talercio, A.: Critères de résistance macroscopiques pour les composites à fibres. C. R. Acad. Sci. Série II **307**, 227–232 (1988)
9. Duc Chinh, P.: On shakedown theory for elastic-plastic materials and extensions. J. Mech. Phys. Solid. (2007) doi: 10.1016/j.jmps.2007.11.005
10. Dvorak, G.J., Lagoudas, D.C., Huang, C.-M.: Shakedown and fatigue damage in metal matrix composites. In: Weichert, D., Maier, G. (eds.) Inelastic Analysis of Structures Under Variable Repeated Loads, 183–196. Kluwer Academic Publishers, Dordrecht (2000)
11. Francescato, P., Pastor, J.: Lower and upper numerical bounds to the off-axis strength of unidirectional fiber-reinforced composites by limit analysis methods. Eur. J. Mech A/Solid. **16**, 213–234 (1997)
12. Grüning, M.: Die Tragfähigkeit statisch unbestimmer Tragwerke aus Stahl bei beliebig häufig wiederholter Belastung. Springer, Berlin (1926)
13. Hodge, P.G.: The Mathematical Theory of Plasticity. Oxford University Press, London (1959)
14. Ilyushin, A.A.: Plasticité. Eyrolles, Paris (1956)
15. Koiter, W.T.: General theorems for elastic-plastic solids. In: Sneddon, I.N. and Hill, R. (eds.) Progress in Solid Mechanics, 165–221. North Holland, Amsterdam (1960)
16. Kohn, R.V., Vogelius M.: A new model for thin plates with rapidly varying thickness. Int. J. Solid. Struct. **20**, 333–350 (1984)
17. Lewinski, T.: Effective models of composite periodic plates. I Assymptotic solution, II Simplifications due to symetries, III Two-dimensional approaches. Int. J. Solid. Struct. **27**, 1155–1203 (1991)
18. Lewinski, T.: Effective stiffnesses of transversely non-homogeneous plates with unidirectional periodic structure. Int. J. Solid. Struct. **32**, 3261–3287 (1995)
19. Magoariec, H.: Adaptation élastoplastique et homogénéisation périodique. PhD thesis, Université de la Méditerranée (2003)
20. Magoariec, H., Bourgeois, S., Débordes, O.: Elastic plastic shakedown of 3D periodic heterogeneous media: a direct numerical approach. Int. J. Plasticity **20**, 1655–1675 (2004)
21. Maier, G., Carvelli, V., Cocchetti, G.: On direct methods for shakedown and limit analysis. Eur. J. Mech. A/Solid. **19**, S79–S100 (2000)
22. Maier, G., Carvelli, V., Talercio, A.: Limit and Shakedown analysis of periodic heterogeneous media. In: Lemaitre, J. (ed.) Handbook of Materials Behavior Models, 1025–1036. Academic Press, New York (2001)
23. Marigo, J.-J., Mialon, P., Michel J.-C., Suquet, P.: Plasticité et homogénéisation : un exemple de calcul des charges limites d'une structure hétérogène. J. Méc Th. et appl. **6 (1)**, 47–75 (1987)
24. Melan, E.: Theorie statisch unbestimmter Systeme aus ideal-plastischem Baustoff. Sitber. Akad. Wiss Abt. IIa **145**, 195–218 (1936)
25. Ponter, A.R.S., Leckie, F.A.: On the behaviour of metal matrix composites subjected to cyclic thermal loading. J. Mech. Phys. Solid. **46**, 2183–2199 (1998)
26. Sab, K.: Yield design of thin periodic plates by a homogenization technique and an application to masonry walls. C. R. Mécanique. **331**, 641–646 (2003)

27. Suquet, P.: Analyse limite et homogénéisation. C. R. Acad. Sci. Série II **296**, 1355–1358 (1983)
28. Tarn, J.Q., Dvorak, G.J., Rao, M.S.M.: Shakedown of unidirectional composites. Int. J. Solid. Struct. **11**, 751–764 (1983)
29. Turgeman, S., Pastor, J.: Comparaison des charges limites d'une structure hétérogène et homogénéisée. J. Méc. Theor. et Appl. **6 (1)**, 121–143 (1987)
30. Weichert, D., Hachemi, A., Schwabe, F.: Shakedown analysis of composites. Mech. Res. Commun. **26**, 309–318 (1999)

Stochastic Limit Load Analysis of Elasto-Plastic Plane Frames

K. Marti

Abstract Problems from plastic analysis and optimal plastic design are based on the convex, linear or linearized yield/strength condition and the linear equilibrium equation for the stress (state) vector. In practice, one has to take into account stochastic variations of several model parameters, such as material strength parameters, external load factors, cost coefficients, etc.. Hence, in order to get robust maximum load factors, i.e., load factors being insensitive with respect to stochastic parameter variations, the structural analysis problem under stochastic uncertainty must be replaced by an appropriate deterministic substitute problem. Here, a direct approach is proposed based on the primary costs for missing carrying capacity and the recourse costs (e.g. costs for repair, compensation for weakness within the structure, damage, failure, etc.). Based on the mechanical survival conditions of plasticity theory, a quadratic error/loss criterion is developed. The minimum recourse costs can be determined then by solving an optimization problem having a quadratic objective function and linear constraints. For each configuration of the structure, i.e., each vector of model parameters and each design vector, one has then an explicit representation of the "best" internal load distribution. Moreover, also the expected recourse costs can be determined explicitly. Consequently, an explicit stochastic non-linear program results for finding a robust maximum limit load/shakedown factor. The deterministic substitute problems are based on (i) minimizing the expected total costs and (ii) minimizing (e.g.) the weight of the structure subject to an expected recourse cost constraint. Some numerical examples are given.

Kurt Marti
Federal Armed Forces University Munich, Aero-Space Engineering and Technology, 85577 Neubiberg/Munich, Germany, e-mail: kurt.marti@unibw-muenchen.de

1 Introduction

In limit load analysis [2, 3, 10] of plastic mechanical structures the problem is to maximize the load factor μ subject to the survival or safety conditions, consisting of the equilibrium equation and the so-called yield (feasibility) condition of the structure.

Thus, the objective function G_0 to be minimized is defined e.g. by

$$G_0 = G_0(\mu) := -\mu , \quad \mu \geq 0 . \tag{1}$$

In the following, $x_0 = (x_{10}, x_{20}, \ldots, x_{r0})^T$ denotes a fixed design vector, hence, an r-vector x_0 of design variables $x_{10}, \ldots, x_{r0}$, such as sizing variables of the elements of the structure. Moreover, $a = a(\omega)$ is the ν-vector of all random model parameters arising in the underlying mechanical model, such as weight or cost factors $\gamma_{i0} = \gamma_{i0}(\omega)$, yield stresses in compression and tension $\sigma_{yi}^L = \sigma_{yi}^L(\omega), \sigma_{yi}^U = \sigma_{yi}^U(\omega), i = 1, \ldots, B$, load factors contained in the external loading $P = P(a(\omega), \mu)$, etc. Furthermore, $A_i = A_i(x_0), i = 1, \ldots, B$, denote the cross-sectional areas of the elements, bars having length $L_i, i = 1, \ldots, B$. In case of *limit load analysis* [11] the external load is given by

$$P\Big(a(\omega), \mu\Big) := P_0\Big(a(\omega)\Big) + \mu P_1\Big(a(\omega)\Big) , \tag{2a}$$

with certain random vectors $P_0 = P_0\Big(a(\omega)\Big), P_1 = P_1\Big(a(\omega)\Big)$.

As already mentioned above, the optimization of the function $G_0 = G_0(a, \mu)$ is done under the safety or survival conditions of plasticity theory which can be described [13] for plane frames as follows:

(I) *Equilibrium condition*
    After taking into account the boundary conditions, the equilibrium between the m-vector of external loads $P = P\Big(a(\omega), \mu\Big)$ and the $3B$-vector of internal loads $F = (F_1^T, F_2^T, \ldots, F_B^T)^T$ can be described by

$$CF = P\Big(a(\omega), \mu\Big) , \tag{2b}$$

    where C is the $m \times 3B$ equilibrium matrix having rank $C = m$.

(II) *Yield condition (feasibility condition)*
    If no interactions between normal (axial) forces t_i and bending moments m_i^-, m_i^+ at the negative, positive end of the i-th bar of the structures are taken into account, then the feasibility condition for the bar loadings

$$F_i = \begin{pmatrix} t_i \\ m_i^- \\ m_i^+ \end{pmatrix} , \quad i = 1, \ldots, B , \tag{3}$$

reads

$$F_i^L\Big(a(\omega), x_0\Big) \le F_i \le F_i^U\Big(a(\omega, x_0)\Big), \quad i = 1, \ldots, B \,, \qquad (4a)$$

where the bounds F_i^L, F_i^U containing the plastic capacities with respect to axial forces and moments are given by

$$F_i^L\Big(a(\omega), x_0\Big) := \begin{pmatrix} -N_{ipl}^L\Big(a(\omega), x_0\Big) \\ -M_{ipl}\Big(a(\omega), x_0\Big) \\ -M_{ipl}\Big(a(\omega), x_0\Big) \end{pmatrix} = \begin{pmatrix} \sigma_{yi}^L\Big(a(\omega)\Big) A_i(x_0) \\ -\sigma_{yi}^U\Big(a(\omega)\Big) W_{ipl}(x_0) \\ -\sigma_{yi}^U\Big(a(\omega)\Big) W_{ipl}(x_0) \end{pmatrix} (4b)$$

$$F_i^U\Big(a(\omega), x_0\Big) := \begin{pmatrix} N_{ipl}^U\Big(a(\omega), x_0\Big) \\ M_{ipl}\Big(a(\omega), x_0\Big) \\ M_{ipl}(a(\omega), x_0) \end{pmatrix} = \begin{pmatrix} \sigma_{yi}^U\Big(a(\omega)\Big) A_i(x_0) \\ \sigma_{yi}^U\Big(a(\omega)\Big) W_{ipl}(x_0) \\ \sigma_{yi}^U\Big(a(\omega)\Big) W_{ipl}(x_0) \end{pmatrix} . \quad (4c)$$

Here,

$$W_{ipl} = W_{ipl}(x_0) := A_i \bar{y}_{ic} \qquad (4d)$$

denotes the plastic section modulus with the arithmetic mean

$$\bar{y}_{ic} = \frac{1}{2}(y_{i1} + y_{i2}) \qquad (4e)$$

of the centroids y_{i1}, y_{i2} of the two half areas of the cross-sectional areas A_i of the bars $i = 1, \ldots, B$.

Taking into account also interactions between normal forces t_i and moments m_i^-, m_i^+, besides (4a) we have additional feasibility conditions of the type

$$-h_l \eta_i^L\Big(a(\omega), x_0\Big) \le H_l F_i \le h_l \eta_i^U\Big(a(\omega), x_0\Big) \,, \qquad (4f)$$

where $\big(H_l(N_{i0}, M_{i0}), h_l\big)l = 1, \ldots, l_0$, are given row vectors obtained from piecewise linearization of the yield domains of the bars, and η_i^L, η_i^U are defined by

$$\eta_i^L\Big(a(\omega), x_0\Big) = \min \left\{ \frac{N_{ipl}^L\Big(a(\omega), x_0\Big)}{N_{i0}}, \frac{M_{ipl}\Big(a(\omega), x_0\Big)}{M_{i0}} \right\}, \qquad (4g)$$

$$\eta_i^U\Big(a(\omega), x_0\Big) = \min \left\{ \frac{N_{ipl}^U\Big(a(\omega), x_0\Big)}{N_{io}}, \frac{M_{ipl}\Big(a(\omega), x_0\Big)}{M_{i0}} \right\}, \qquad (4h)$$

with certain chosen reference values $N_{i0}, M_{i0}, i = 1, \ldots, B$, for the plastic capacities.

According to (4a,f), the feasibility condition for the vector F of interior loads (member forces and moments) can be represented uniformly by the conditions

$$\widetilde{F}_{il}^L\Big(a(\omega), x_0\Big) \le \widetilde{H}_l F_i \le \widetilde{F}_{il}^U\Big(a(\omega), x_0\Big), \quad i = 1, \ldots, B, \quad l = 1, 2, \ldots, l_0 + 3 \,,$$
(5a)

where the row 3-vectors $\widetilde{H}_l$ and the bounds $\widetilde{F}_{il}^L, \widetilde{F}_{il}^U, \ i = 1, \ldots, B,$ $l = 1, \ldots, l_0 + 3$, are defined by (4a–c) and (4f–h). Let $\boldsymbol{e}_1, \boldsymbol{e}_2, \boldsymbol{e}_3$ denote the unit vectors of $\mathbb{R}^3$.

Defining the $(l_0 + 3) \times 3$ matrix $\widetilde{H}^{(i)}$ by

$$\widetilde{H}^{(i)} := \begin{pmatrix} \boldsymbol{e}_1^T \\ \boldsymbol{e}_2^T \\ \boldsymbol{e}_3^T \\ H_4(N_{i0}, M_{i0}) \\ \vdots \\ H_{l_0+3}(N_{i0}, M_{i0}) \end{pmatrix}$$
(5b)

and the $(l_0 + 3)$-vectors $\widetilde{F}_i^L = \widetilde{F}_i^L\Big(a(\omega), x_0\Big), \widetilde{F}_i^U = \widetilde{F}_i^U\Big(a(\omega), x_0\Big)$ by

$$\widetilde{F}_i^L := \begin{pmatrix} F_i^L \\ -h_1 \eta_i^L \\ \vdots \\ -h_{l_0} \eta_i^L \end{pmatrix}, \quad \widetilde{F}_i^U := \begin{pmatrix} F_i^U \\ h_1 \eta_i^U \\ \vdots \\ h_{l_0} \eta_i^U \end{pmatrix},$$

the feasibility condition can also be represented by

$$\widetilde{F}_i^L\Big(a(\omega), x_0\Big) \le \widetilde{H}^{(i)} F_i \le \widetilde{F}_i^U\Big(a(\omega), x_0\Big), \quad i = 1, \ldots, B \,.$$
(6)

2 State and Cost Functions

Defining the quantities

$$\widetilde{F}_{il}^c = \widetilde{F}_{il}^c\Big(a(\omega), x_0\Big) := \frac{\widetilde{F}_{il}^L + \widetilde{F}_{il}^U}{2} \,,$$
(7a)

$$\widetilde{\varrho}_{il} = \widetilde{\varrho}_{il}\Big(a(\omega), x_0\Big) := \frac{\widetilde{F}_{il}^U - \widetilde{F}_{il}^L}{2} \,,$$
(7b)

with $i = 1, \ldots, B$ and $l = 1, \ldots, l_0 + 3$, the feasibility condition (5a) or (6) can be described by

$$|z_{il}| \leq 1, \quad i = 1, \ldots, B, \quad l = 1, \ldots, l_0 + 3 , \tag{8a}$$

with the quotients

$$z_{il} = z_{il}(F_i; a, x_0) = \frac{\widetilde{H}_l F_i - \widetilde{F}_{il}^c}{\widetilde{\varrho}_{il}}, \quad i = 1, \ldots, B, \quad l = 1, \ldots, l_0 + 3 . \tag{8b}$$

The quotient $z_{il}, i = 1, \ldots, B, l = 1, \ldots, l_0 + 3$, denotes the relative deviation of the load component $\widetilde{H}_l^{(i)} F_i$ from its "ideal" value $\widetilde{F}_{il}^c$ with respect to the radius $\widetilde{\varrho}_{il}$ of the feasible interval $[\widetilde{F}_{il}^L, \widetilde{F}_{il}^U]$. According to (8a,b), the absolute values $|z_{il}|$ of the quotients z_{il} should not exceed the value 1. The absolute value $|z_{il}|$ of the quotient z_{il} denotes the percentage of use of the available plastic capacity by the corresponding load component. Obviously, $|z_{il}| = 1, |z_{il}| > 1$, resp., means maximal use, overcharge of the available resources.

Consider now the $(l_0 + 3)$-vectors

$$z_i := (z_{i1}, z_{i2}, \ldots, z_{il_0+3})^T = \left(\frac{\widetilde{H}_1 F_i - \widetilde{F}_{i1}^c}{\widetilde{\varrho}_{i1}}, \frac{\widetilde{H}_2 F_i - \widetilde{F}_{i2}^c}{\widetilde{\varrho}_{i2}}, \cdots , \right.$$

$$\left. \frac{\widetilde{H}_{l_0+3} F_i - \widetilde{F}_{il_0+3}^c}{\widetilde{\varrho}_{il_0+3}} \right)^T . \tag{8c}$$

With

$$\widetilde{\varrho}_i := \begin{pmatrix} \widetilde{\varrho}_{i1} \\ \widetilde{\varrho}_{i2} \\ \vdots \\ \widetilde{\varrho}_{il_0+3} \end{pmatrix}, \quad \widetilde{\varrho}_{id} := \begin{pmatrix} \widetilde{\varrho}_{i1} & 0 & \ldots & 0 \\ 0 & \widetilde{\varrho}_{i2} & \ldots & 0 \\ \vdots & & \ddots & \vdots \\ 0 & 0 & \ldots & \widetilde{\varrho}_{il_0+3} \end{pmatrix}, \quad \widetilde{F}_i^c := \begin{pmatrix} \widetilde{F}_{i1}^c \\ \widetilde{F}_{i2}^c \\ \vdots \\ \widetilde{F}_{il_0+3}^c \end{pmatrix}, \tag{8d}$$

we get

$$z_i = \widetilde{\varrho}_{id}^{-1} (\widetilde{H}^{(i)} F_i - \widetilde{F}_i^c) . \tag{8e}$$

Using (8b–d), we find

$$\widetilde{F}_i^c = \left(A_i \frac{\sigma_{yi}^L + \sigma_{yi}^U}{2}, 0, 0, h_1 \frac{\eta_i^U - \eta_i^L}{2}, \ldots, h_{l_0} \frac{\eta_i^U - \eta_i^L}{2} \right)^T , \tag{8f}$$

$$\widetilde{\varrho}_i = \left(A_i \frac{\sigma_{yi}^U - \sigma_{yi}^L}{2}, A_i \sigma_{yi}^U \bar{y}_{ic}, A_i \sigma_{yi}^U \bar{y}_{ic}, h_1 \frac{\eta_i^U + \eta_i^L}{2}, \ldots, h_{l_0} \frac{\eta_i^U + \eta_i^L}{2} \right)^T . \tag{8g}$$

The vector z_i can be represented then, cf. (3), by

$$z_i = \left(\frac{t_i - A_i \frac{\sigma_{yi}^L + \sigma_{yi}^U}{2}}{A_i \frac{\sigma_{yi}^U - \sigma_{yi}^L}{2}}, \frac{m_i^-}{A_i \sigma_{yi}^U \bar{y}_{ic}}, \frac{m_i^+}{A_i \sigma_{yi}^U \bar{y}_{ic}}, \frac{H_1 F_i - h_1 \frac{\eta_i^U - \eta_i^L}{2}}{h_1 \frac{\eta_i^U + \eta_i^L}{2}}, \dots, \right.$$

$$\left. \frac{H_{l_0} F_i - h_{l_0} \frac{\eta_i^U - \eta_i^L}{2}}{h_{l_0} \frac{\eta_i^U + \eta_i^L}{2}} \right)^T . \tag{9a}$$

In case of symmetry $\sigma_{yi}^L = -\sigma_{yi}^U$ we get

$$z_i = \left(\frac{t_i}{A_i \sigma_{yi}^U}, \frac{m_i^-}{A_i \sigma_{yi}^U \bar{y}_{ic}}, \frac{m_i^+}{A_i \sigma_{yi}^U \bar{y}_{ic}}, \frac{H_1 F_i}{h_1 \eta_i^U}, \dots, \frac{H_{l_0} F_i}{h_{l_0} \eta_i^U} \right)^T . \tag{9b}$$

According to the methods introduced in [13–15], the fulfillment of the survival condition for elasto-plastic frame structures, hence, the equilibrium condition (2a,b) and the feasibility condition (6) or (8a,b), can be described by means of the *state function* $s^* = s^*\big(a(\omega), \mu\big)$ defined, in the present case, by

$$s^* = s^*\Big(a(\omega), \mu\Big) := \min \Big\{ s : \Big| z_{il}\big(F_i; a(\omega), x_0\big) \Big| - 1 \le s, \ i = 1, \dots, B,$$

$$l = 1, \dots, l_0 + 3, \ CF = P\Big(a(\omega), \mu\Big) \Big\} . \tag{10}$$

Hence, the state function s^* is the minimum value function of the linear program (LP)

$$\min s \tag{11a}$$

s.t.

$$\Big| z_{il}\Big(F_i; a(\omega), x_0\Big) \Big| - 1 \le s, \ \ i = 1, \dots, B, \ \ l = 1, \dots, l_0 + 3 , \tag{11b}$$

$$CF = P\Big(a(\omega), \mu\Big) . \tag{11c}$$

Since the objective function s is bounded from below and a feasible solution (s, F) always exists, LP (11a–c) has an optimal solution $(s^*, F^*) = \left(s^*\Big(a(\omega), \mu\Big), F^*\Big(a(\omega), \mu\Big) \right)$ for each configuration $\Big(a(\omega), x\Big)$ of the structure.

Consequently, for the survival of the structure we have the following criterion, cf. [15]:

Theorem 1. *The elasto-plastic frame structure having configuration (a, x_0) carries the exterior load $P = P(a, \mu)$ safely if and only if*

$$s^*(a, \mu) \le 0 . \tag{12}$$

Obviously, the constraint (11b) in the LP (11a–c) can also be represented by

$$\left\| z\Big(F; a(\omega), x_0\Big) \right\|_\infty - 1 \le s \ , \tag{13a}$$

where $z = z\Big(F; a(\omega), x_0\Big)$ denotes the $B(l_0 + 3)$-vector

$$z\Big(F; a(\omega), x_0\Big) := \left(z_1\Big(F; a(\omega), x_0\Big)^T, \ldots, z_B\Big(F; a(\omega), x_0\Big)^T \right)^T, \tag{13b}$$

and $\|z\|_\infty$ is the maximum norm

$$\|z\|_\infty := \max_{\substack{1 \le i \le B \\ 1 \le l \le l_0+3}} |z_{il}| \ . \tag{13c}$$

If we put

$$\hat{s} = 1 + s \quad \text{or} \quad s = \hat{s} - 1 \ , \tag{14}$$

from (10) we obtain

$$s^*(a, \mu) = \hat{s}^*(a, \mu) - 1 \ , \tag{15a}$$

where the transformed state function $\hat{s}^* = \hat{s}^*(a, x)$ reads

$$\hat{s}^*(a, \mu) := \min \left\{ \left\| z(F; a, x_0) \right\|_\infty : CF = P(a, \mu) \right\} \ . \tag{15b}$$

Hence, $\hat{s}^* = \hat{s}^*(a, \mu)$ is the minimum value function of the LP

$$\min_{CF = P(a, \mu)} \left\| z(F; a, x_0) \right\|_\infty \ . \tag{16}$$

The following inequalities for norms or power/Hölder means $\|z\|$ in $\mathbb{R}^{B(l_0+3)}$ are well known [1, 8]:

$$\frac{1}{B(l_0 + 3)} \|z\|_\infty \le \frac{1}{B(l_0 + 3)} \|z\|_1$$

$$\le \frac{1}{\sqrt{B(l_0 + 3)}} \|z\|_2 \le \|z\|_\infty \le \|z\|_2 \ , \tag{17a}$$

where

$$\|z\|_1 := \sum_{i=1}^{B} \sum_{l=1}^{l_0+3} |z_{il}|, \|z\|_2 := \sqrt{\sum_{i=1}^{B} \sum_{l=1}^{l_0+3} z_{il}^2} \ . \tag{17b}$$

Replacing in (15b) the norm $\| \cdot \|_\infty$ by $\| \cdot \|_2$, from (17a) we get

$$\frac{1}{B(l_0+3)}\hat{s}^*(a,\mu) \leq \frac{1}{\sqrt{B(l_0+3)}}\hat{s}_2^*(a,\mu) \leq \hat{s}^*(a,\mu) \leq \hat{s}_2^*(a,\mu) \,, \qquad (18a)$$

where $\hat{s}_2^* = \hat{s}_2^*(a,\mu)$ is the modified state function function defined by

$$\hat{s}_2^*(a,\mu) := \min\left\{\left\|z(F;a,x_0)\right\|_2 : CF = P(a,\mu)\right\} \,. \qquad (18b)$$

Obviously, we have

$$\hat{s}_2^*(a,\mu) = \sqrt{G_1^*(a,\mu)} \,, \qquad (18c)$$

where $G_1^*(a,\mu)$ is the minimum value function of the quadratic program

$$\min_{CF=P\left(a(\omega),\mu\right)} \sum_{i=1}^{B} \sum_{l=1}^{l_0+3} z_{il}(F_i;a,x_0)^2 \,. \qquad (19)$$

2.1 Cost Functions

The inequalities in (18a) show that for structural analysis and optimal design purposes we may work also with the state function $\hat{s}_2^* = \hat{s}_2^*(a,\mu)$ which can be defined easily by means of the quadratic program (19).

According to the definition (8b) and the corresponding technical interpretation of the quotients z_{il}, the transformed state function $\hat{s}^* = \hat{s}^*(a,\mu)$ represents the maximum degree of use of the plastic capacities *relative* to the available plastic capacities in the members (bars) of the plane frame with configuration (a,x). While the definition (15b) of $\hat{s}^*$ is based on the absolute value function

$$c_1(z_{il}) = |z_{il}| \,, \qquad (20a)$$

in the definition (18b) of $\hat{s}_2^*$ occur quadratic functions

$$c_2(z_{il}) = z_{il}^2 \,, \quad i = 1,\ldots,B \,, \quad l = 1,\ldots,l_0+3 \,. \qquad (20b)$$

If different weights are used in the objective function (19), then for the bars we obtain, cf. (8c), the cost functions

$$q_i(z_i) = \|W_{i0}z_i\|^2 \,, \quad i = 1,\ldots,B \,, \qquad (20c)$$

with an $(l_0+3) \times (l_0+3)$ matrix of weights W_{i0}.

The total weighted quadratic costs resulting from a load distribution F acting on the plastic plane frame having configuration (a,x) are given, cf. (18c), (19), (20c), by

$$G_1 := \sum_{i=1}^{B} \|W_{i0} z_i\|^2 = \sum_{i=1}^{B} z_i^T W_{i0}^T W_{i0} z_i . \tag{21a}$$

Defining

$$W_0 := \begin{pmatrix} W_{10} & 0 & \dots & 0 \\ 0 & W_{20} & \dots & 0 \\ \vdots & \vdots & \ddots & \vdots \\ 0 & 0 & \dots & W_{B0} \end{pmatrix}, \quad z := \begin{pmatrix} z_1 \\ z_2 \\ \vdots \\ z_B \end{pmatrix}, \tag{21b}$$

we also have

$$G_1 = G_1(a, x_0; F) = z^T W_0^T W_0 z$$
$$= \|W_0 z\|_2^2 = \|z\|_{2,W_0}^2 , \tag{21c}$$

where $\| \cdot \|_{2,W_0}$ denotes the *weighted Euclidean norm*

$$\|z\|_{2,W_0} := \|W_0 z\|_2 . \tag{21d}$$

Using the weighted quadratic cost function (20c), the state function $\hat{s}_2^* = \hat{s}_2^*(a, \mu)$ is replaced by

$$\hat{s}_{2,W_0}^*(a, \mu) := \min \left\{ \|z(F; a, x_0)\|_{2,W_0} : CF = P(a, \mu) \right\} . \tag{21e}$$

Since

$$\|z\|_{2,W_0} = \|W_0 z\|_2 \leq \|W_0\| \, \|z\|$$

with the norm $\|W_0\|$ of the matrix W_0, we find

$$\hat{s}_{2,W_0}^*(a, \mu) \leq \|W_0\| \hat{s}_2^*(a, \mu) . \tag{21f}$$

On the other hand, in case

$$\|W_0 z\|_2 \geq \underline{W}_0 \|z\|_2$$

with a positive constant $\underline{W}_0 > 0$, we have

$$\hat{s}_{2,W_0}^*(a, \mu) \geq \underline{W}_0 \hat{s}_2^*(a, \mu) \quad \text{or} \quad \hat{s}_2^*(a, \mu) \leq \frac{1}{\underline{W}_0} \hat{s}_{2,W_0}^*(a, \mu) . \tag{21g}$$

Putting

$$\widetilde{H} := \begin{pmatrix} \widetilde{H}^{(1)} & & & \\ & \widetilde{H}^{(2)} & & \\ & & \ddots & \\ & & & \widetilde{H}^{(B)} \end{pmatrix}, \quad \widetilde{F}^c := \begin{pmatrix} \widetilde{F}_1^c \\ \widetilde{F}_2^c \\ \vdots \\ \widetilde{F}_B^c \end{pmatrix}, \quad \widetilde{\varrho} := \begin{pmatrix} \widetilde{\varrho}_1 \\ \widetilde{\varrho}_2 \\ \vdots \\ \widetilde{\varrho}_B \end{pmatrix}, \tag{21h}$$

with (8e) we find

$$G_1 = G_1(a(\omega), x_0; F) = (F - \widetilde{F}^c)^T \widetilde{H}^T \widetilde{\varrho}_d^{-1} W_0^T W_0 \widetilde{\varrho}_d^{-1} \widetilde{H}(F - \widetilde{F}^c) , \quad (22a)$$

assuming that

$$\widetilde{F}^c = \widetilde{H}\widetilde{F}^c . \tag{22b}$$

The symmetric case $\sigma_{yi}^L = -\sigma_{yi}^U, \quad i = 1, \ldots, B$, yields $\widetilde{F}^c = 0$ and therefore

$$G_1 = G_1(a(\omega), x_0; F) = F^T \widetilde{H}^T \widetilde{\varrho}_d^{-1} W_0^T W_0 \widetilde{\varrho}_d^{-1} \widetilde{H} F . \tag{22c}$$

3 Minimum Expected Quadratic Costs

According to the equilibrium conditions (2a,b), the total vector F of member loads fulfills

$$CF = P(a(\omega), \mu) .$$

Let $\mu \geq 0$ denote a load factor, and let be $a = a(\omega)$ a realization of vector $a(\cdot)$ of model parameters. Based on (22a) and (22c), a cost minimum internal load distribution

$$F^* = F^*(a(\omega), \mu)$$

of the structure can be obtained by solving the following optimization problem with quadratic objective function and linear constraints

$$\min_{CF=P(a(\omega),\mu)} G_1(a(\omega), x_0; F) . \tag{23}$$

Solving the related stochastic optimization problem [14]

$$\min_{CF=P(a(\omega),\mu) \text{ a.s.}} EG_1(a(\omega), x_0; F) , \tag{24}$$

we get the minimum expected (total) quadratic costs

$$\overline{G}_1^* = \overline{G}_1^*(\mu) , \tag{25a}$$

where $\overline{G}_1^*(\mu)$ may be obtained by interchanging expectation and minimization

$$\overline{G}_1^*(\mu) = E \min\{G_1(a(\omega), x_0; F) : CF = P(a(\omega), \mu)\} . \tag{25b}$$

The internal minimization problem (23)

$$\min G_1(a(\omega), x_0; F) \text{s.t.} CF = P(a(\omega), \mu) ,$$

hence,

$$\min_{CF=P(a(\omega),\mu)} (F - \widetilde{F}^c)^T \widetilde{H}^T \widetilde{\varrho}_d^{-1} W_0^T W_0 \widetilde{\varrho}_d^{-1} \widetilde{H}(F - \widetilde{F}^c) , \qquad (26)$$

with quadratic objective function and linear constraints with respect to F can be solved by means of Lagrange techniques.

We put

$$W = W(a, x_0) := \widetilde{H}^T \widetilde{\rho}_d^{-1} W_0^T W_0 \widetilde{\rho}_d^{-1} \widetilde{H} \qquad (27)$$

and define the Lagrangian of (26):

$$L = L(F, \lambda) := (F - \widetilde{F}^c)^T W(F - \widetilde{F}^c) + \lambda^T (CF - P(a(\omega), \mu)) . \qquad (28a)$$

The necessary and sufficient optimality conditions for a minimum point (F^*, λ^*) read:

$$0 = \nabla_F L = 2W(F - \widetilde{F}^c) + C^T \lambda \qquad (28b)$$
$$0 = \nabla_\lambda L = CF - P. \qquad (28c)$$

Supposing that W is regular, we get

$$F = \widetilde{F}^c - \frac{1}{2} W^{-1} C^T \lambda \qquad (28d)$$

and

$$P = CF = C\widetilde{F}^c - \frac{1}{2} CW^{-1} C^T \lambda , \qquad (28e)$$

hence,

$$F^* = \widetilde{F}^c - \frac{1}{2} W^{-1} C^T \lambda^* = \widetilde{F}^c - W^{-1} C^T (CW^{-1} C^T)^{-1} (C\widetilde{F}^c - P). \quad (28f)$$

Inserting (28f) into the objective function $G_1(a(\omega), x_0; F)$, according to (22a) and (27) we find

$$\begin{aligned}
G_1^* &= G_1^*(a(\omega), \mu) \\
&= (F^* - \widetilde{F}^c)^T W(F^* - \widetilde{F}^c) \\
&= \left((C\widetilde{F}^c - P)^T (CW^{-1} C^T)^{-1} CW^{-1} \right) W \\
&\quad \left(W^{-1} C^T (CW^{-1} C^T)^{-1} (C\widetilde{F}^c - P) \right) \\
&= (C\widetilde{F}^c - P)^T (CW^{-1} C^T)^{-1} (C\widetilde{F}^c - P) \\
&= \mathrm{tr}(CW^{-1} C^T)^{-1} (C\widetilde{F}^c - P)(C\widetilde{F}^c - P)^T , \qquad (28g)
\end{aligned}$$

The minimal expected value $\overline{G_1^*}$ is then given by

$$\overline{G_1^*} = EG_1^*\big(a(\omega), \mu\big)$$

$$= E\big(C\widetilde{F}^c(a(\omega), x_0) - P\big(a(\omega), \mu\big)\big)^T \Big(CW\big(a(\omega), x_0\big)^{-1}C^T\Big)^{-1}$$

$$\Big(C\widetilde{F}^c\big(a(\omega), x_0\big) - P\big(a(\omega), \mu\big)\Big)$$

$$= E \operatorname{tr} \Big(CW\big(a(\omega), x_0\big)^{-1}C^T\Big)^{-1}\Big(C\widetilde{F}^c\big(a(\omega), x_0\big) - P\big(a(\omega), \mu\big)\Big)$$

$$\times \Big(C\widetilde{F}^c\big(a(\omega), x_0\big) - P\big(a(\omega), \mu\big)\Big)^T . \tag{29a}$$

If $\sigma_{yi}^L = -\sigma_{yi}^U$, $i = 1, \ldots, B$, then $\widetilde{F}^c = 0$ and

$$\overline{G_1^*}(\mu) = EP(a(\omega), \mu))^T (CW(a(\omega), x_0)^{-1}C^T)^{-1}P(a(\omega), \mu)$$

$$= \operatorname{tr} E\Big(CW\big(a(\omega), x_0\big)^{-1}C^T\Big)^{-1}P\big(a(\omega), \mu\big)P\big(a(\omega), \mu\big)^T . \tag{29b}$$

Since the vector $P = P(a(\omega), \mu)$ of external loads and the vector of yield stresses $\sigma^U = \sigma^U(a(\omega), x)$ are stochastically independent, then in case $\sigma_{yi}^L = -\sigma_{yi}^U$, $i = 1, \ldots, B$, we have

$$\overline{G_1^*}(\mu) = EP(a(\omega), \mu))^T \overline{U}(x_0)P(a(\omega), \mu)$$

$$= \operatorname{tr} \overline{U}(x_0)EP(a(\omega), \mu)P(a(\omega), \mu)^T , \tag{29c}$$

where

$$\overline{U}(x_0) := EK(a, x_0)^{-1} , \tag{29d}$$

with

$$K(a, x_0) := CK_0(a, x_0)C^T \tag{30a}$$

and

$$K_0(a, x_0) := W(a, x_0)^{-1} = (\widetilde{H}^T \widetilde{\varrho}_d^{-1} W_0^T W_0 \widetilde{\varrho}_d^{-1} \widetilde{H})^{-1}. \tag{30b}$$

We compare now, especially in case $\widetilde{F}^c = 0$, formula (28g) for the costs $G_1^* = G_1^*(a, \mu)$ with the formula

$$\Gamma := u^T P$$

for the "*compliance*" of an elastic structure [10], where

$$u := K_{el}^{-1}P$$

is the vector of displacements, and K_{el} denotes the stiffness matrix in case of an elastic structure. Obviously, the cost function $G_1^* = G_1^*(a, \mu)$ may be interpreted as a *generalized compliance function*, and the $m \times m$ matrix $K = K(a, x_0)$ can be interpreted as the "generalized stiffness matrix" of the underlying plastic mechanical structure. If we suppose that

$$W_{i0} := \begin{pmatrix} w_{i1}^0 & & 0 \\ & w_{i2}^0 & \\ 0 & & w_{i3}^0 \end{pmatrix}, i = 1, \ldots, B \tag{30c}$$

are diagonal weight matrices, then, cf. (8g),

$$\widetilde{\varrho}_d^{-1} W_0^T W_0 \widetilde{\varrho}_d^{-1} = \operatorname{diag}\left(\left(\frac{w_{il}^0}{\widetilde{\varrho}_{il}} \right)^2 \right). \tag{30d}$$

4 Deterministic Substitute Problems

4.1 Maximization of the Load Factor Subject to Reliability Constraints

With the expected primary cost function

$$\overline{G_0}(\mu) = \varphi(\mu)$$

e.g. $\varphi^0(\mu) := -\mu$, see (1), and the expected cost function $\overline{G_1^*} = \overline{G_1^*}(\mu)$ representing the expected total quadratic costs resulting from a violation of the feasibility condition (4a,f), we get [5–7] the optimization problem

$$\min \ \overline{G_0}(\mu) \tag{31a}$$
$$\text{s.t.} \ \overline{G_1^*}(\mu) \le G_1^{\max}, \tag{31b}$$
$$\mu \ge 0. \tag{31c}$$

As shown in the following, for $W_0 = I$ (identity matrix) the expected cost constraint (31b) can also be interpreted as a reliability constraint.

According to Theorem 1, (12) and (15a,b), for the probability of survival $p_s = p_s(\mu)$ of the elasto-plastic structure having load factor μ, we have

$$p_s(\mu) := P\left(s^*\big(a(\omega), \mu\big) \le 0 \right)$$
$$= P\left(\hat{s}^*\big(a(\omega), \mu\big) - 1 \le 0 \right) = P\left(\hat{s}^*\big(a(\omega), \mu\big) \le 1 \right). \tag{32}$$

Knowing from (18a,b) that, in case $W_0 = I$,

$$\frac{1}{\sqrt{B(l_0 + 3)}} \hat{s}_2^*(a, \mu) \le \hat{s}^*(a, \mu) \le \hat{s}_2^*(a, \mu),$$

we obtain the probability inequalities

$$P\left(\hat{s}_2^*\big(a(\omega), \mu\big) \le 1 \right) \le p_s(\mu) \le P\left(\hat{s}_2^*(a, \mu) \le \sqrt{B(l_0 + 3)} \right). \tag{33a}$$

Due to the first definition of $G_1^* = G_1^*(a, \mu)$ by (18c) and (19), related to the case $W_0 = I$, we also have

$$P\Big(G_1^*\big(a(\omega), \mu\big) \le 1\Big) \le p_s(\mu) \le P\Big(G_1^*\big(a(\omega), \mu\big) \le B(l_0 + 3)\Big) . \qquad (33b)$$

Using now a non-negative, non-decreasing, measurable function h on $\mathbb{R}_+$, for any $g_1 > 0$ we find [12, 14]

$$P\Big(G_1^*\big(a(\omega), \mu\big) \le g_1\Big) \ge 1 - \frac{Eh\Big(G_1^*\big(a(\omega), \mu\big)\Big)}{h(g_1)} . \qquad (34a)$$

In the case $h(t) = t$ we get the inequality

$$P\Big(G_1^*\big(a(\omega), \mu\big) \le g_1\Big) \ge 1 - \frac{\overline{G_1^*}(\mu)}{g_1} , \qquad (34b)$$

where the expectation $\overline{G_1^*}(\mu) = EG_1^*\big(a(\omega), \mu\big)$ is given by (29a) or (29b). The probabilistic constraint

$$P\Big(G_1^*\big(a(\omega), \mu\big) \le g_1\Big) \ge \alpha_{\min} , \qquad (35a)$$

cf. (33b), can be guaranteed then by the condition

$$\overline{G_1^*}(\mu) \le g_1(1 - \alpha) , \qquad (35b)$$

see (31b).

4.2 Minimum Expected Total Costs

For a load factor $\mu \ge 0$ and a vector F of internal loads fulfilling the equilibrium conditions (2a,b), according to (1) and (22a,b) we have the total costs

$$G(a(\omega), \mu; F) := G_0(a(\omega), \mu) + G_1(a(\omega), x_0; F) . \qquad (36a)$$

Here, the weight or scale matrices W_{i0} and the weight cost factors γ_{i0}, $i = 1, \ldots, B$, must be selected such that the dimensions of G_0 and G_1 coincide.

Minimizing now the expected total costs

$$\begin{aligned}
\overline{G} = \overline{G}(\mu) &= EG(a(\omega), \mu; F(\omega)) \qquad (36b)\\
&= E(G_0(a(\omega), \mu) + G_1(a(\omega), x_0; F(\omega)))\\
&= EG_0(a(\omega), \mu) + EG_1(a(\omega), x_0; F(\omega))\\
&= \overline{G_0}(\mu) + EG_1(a(\omega), x_0; F(\omega))
\end{aligned}$$

subject to the equilibrium conditions (2a,b) and the remaining condition

$$\mu \geq 0 \,, \tag{36c}$$

we obtain the stochastic optimization problem

$$\min \ E(G_0(a(\omega), \mu) + G_1(a(\omega), x_0; F(\omega))) \tag{37a}$$
$$\text{s.t.} \ \ CF(\omega) = P\big(a(\omega), \mu\big) \quad \text{a.s.} \tag{37b}$$
$$\mu \geq 0 \,. \tag{37c}$$

Obviously, (37a–c) has the following two-stage structure:

Step 1: Select $\mu \geq 0$ without knowledge of the actual realization $a = a(\omega)$ of the model parameters, but knowing the probability distribution or certain moments of $a(\cdot)$;

Step 2: Determine $F = F^*(\omega)$ after realization of $a = a(\omega)$.

Therefore, problem (37a–c) is equivalent to

$$\min_{\mu \geq 0} E \left(\overline{G_0}(\mu) + \min_{CF = P(a(\omega), \mu)} G_1(a(\omega), x_0; F) \right) \,. \tag{38}$$

According to definition (25b) of $\overline{G_1^*}(\mu)$, problem (38) can be represented also by

$$\min_{\mu \geq 0} \left(\overline{G_0}(\mu) + \overline{G_1^*}(\mu) \right) \,. \tag{39}$$

5 Limit Load Analysis

In limit load analysis [4, 9], the external load $P = P\big(a(\omega), \mu\big)$ is given by

$$P\big(a(\omega), \mu\big) := P_0\big(a(\omega)\big) + \mu P_1\big(a(\omega)\big) \,, \tag{40}$$

with certain random m-vectors $P_0 = P_0\big(a(\omega)\big), P_1 = P_1\big(a(\omega)\big)$. According to (29a), for the minimum expected cost function $\overline{G_1^*} = \overline{G_1^*}(\mu)$ we have

$$\overline{G_1^*}(\mu) = E \operatorname{tr} K\big(a(\omega), x_0\big)^{-1} \left(C\widetilde{F}^c\big(a(\omega), x_0\big) - P\big(a(\omega), \mu\big) \right)$$
$$\times \left(C\widetilde{F}^c\big(a(\omega), x_0\big) - P\big(a(\omega), \mu\big) \right)^T$$

with

$$K\big(a(\omega), x_0\big) = CK_0\big(a(\omega), x_0\big)C^T = CW\big(a(\omega), x_0\big)^{-1}C^T \,.$$

Because of (40), for $\overline{G_1^*} = \overline{G_1^*}(\mu)$ we find the quadratic function

$$\overline{G_1^*}(\mu) = \overline{g_0^*} - \mu\overline{g_1^*} + \mu^2\overline{g_2^*}, \quad \mu \geq 0, \tag{41a}$$

where

$$\overline{g_0^*} = \overline{G_1^*}(0) = E \operatorname{tr} K\Big(a(\omega), x_0\Big)^{-1} \Big(C\widetilde{F^c}\Big(a(\omega), x_0\Big) - P_0\Big(a(\omega)\Big)\Big)$$
$$\times\Big(C\widetilde{F^c}\Big(a(\omega), x_0\Big) - P_0\Big(a(\omega)\Big)\Big)^T, \tag{41b}$$

$$\overline{g_1^*} = E \operatorname{tr} K\Big(a(\omega), x_0\Big)^{-1} \Big(C\widetilde{F^c}\Big(a(\omega), x_0\Big)\Big) - P_0\Big(a(\omega)\Big)P_1\Big(a(\omega)\Big)^T$$
$$+P_1\Big(a(\omega)\Big)\Big(C\widetilde{F^c}\Big(a(\omega), x_0\Big) - P_0\Big(a(\omega)\Big)^T\Big), \tag{41c}$$

$$\overline{g_2^*} = E \operatorname{tr} K\Big(a(\omega), x_0\Big)^{-1} P_1\Big(a(\omega)\Big)P_1\Big(a(\omega)\Big)^T. \tag{41d}$$

In the case $\sigma_{yi}^L = -\sigma_{yi}^U$, $i = 1, \ldots, B$, and therefore $\widetilde{F^c} = 0$, we have

$$\overline{g_0^*} = \operatorname{tr} EK\Big(a(\omega), x_0\Big)^{-1} EP_0\Big(a(\omega)\Big)P_0\Big(a(\omega)\Big)^T, \tag{41b'}$$

$$\overline{g_1^*} = -\operatorname{tr} EK\Big(a(\omega), x_0\Big)^{-1} E\Big(P_0\Big(a(\omega)\Big)P_1\Big(a(\omega)\Big)^T$$
$$+P_1\Big(a(\omega)\Big)P_0\Big(a(\omega)\Big)^T\Big), \tag{41c'}$$

$$\overline{g_2^*} = \operatorname{tr} EK\Big(a(\omega), x_0\Big)^{-1} EP_1\Big(a(\omega)\Big)P_1\Big(a(\omega)\Big)^T, \tag{41d'}$$

since the random material and load parameters are stochastically independent. Note that

$$g_0^* \geq 0, \quad g_2^* > 0. \tag{42}$$

The substitute problem described in Sects. 4.1 and 4.2 have then the following explicit form:

(A) **Expected cost (reliability) constraints**

$$\min \ \overline{G}_0(\mu) \tag{43a}$$
$$\text{s.t. } g_0^* - \mu g_1^* + \mu^2 g_2^* \leq G_1^{\max}, \tag{43b}$$
$$\mu \geq 0. \tag{43c}$$

(B) **Expected total cost minimization**

$$\min_{\mu \geq 0} \overline{G}_0(\mu) + g_0^* - \mu g_1^* + \mu^2 g_2^*. \tag{44}$$

6 Complete Limit Load Analysis

Up to now the computation of the maximum load factor $\mu^* = \mu^*(x_0)$ has been considered, see Sect. 5, for an elasto-plastic mechanical structure having a given, fixed design $x_0 \in D$. In the following we are looking for a load factor

$$\mu^* = \mu^*(D)$$

being globally maximum with respect to arbitrary designs x varying in a given, fixed admissible domain $D \subset \mathbb{R}^r$.

Hence, for a design vector $x = (x_1, \ldots, x_r)^T \in D$ and a load factor $\mu \geq 0$, we define

$$\hat{x} := \begin{pmatrix} x \\ \mu \end{pmatrix} = (x_1, x_2, \ldots, x_r, \mu)^T .$$

Furthermore, we first suppose that the structure consists of uniform material with a symmetric random yield stress in compression and tension. Hence, we assume next to

$$\sigma_{yi}^U = -\sigma_{yi}^L = \sigma_y^U = \sigma_y^U(\omega), \quad i = 1, \ldots, B , \tag{45}$$

with a random yield stress $\sigma_y^U(\omega)$. Due to (8e) we have

$$\tilde{\varrho}_i\big(a(\omega), x\big) = A_i(\sigma_{yi}^U, \sigma_{yi}^U \overline{y}_{ic}, \sigma_{yi}^U \overline{y}_{ic}, \sigma_{yi}^U h_1 \eta_i, \ldots, \sigma_{yi}^U h_{l_0} \eta_i)^T$$
$$= \sigma_y^U A_i(1, \overline{y}_{ic}, \overline{y}_{ic}, h_1 \eta_i, \ldots, h_{l_0} \eta_i)^T := \sigma_y^U \tilde{\varrho}_i(x) \tag{46a}$$

and therefore, see (8d),

$$\tilde{\varrho}\big(a(\omega), x\big) = \sigma_y^U(\omega) \tilde{\varrho}(x) \tag{46b}$$

with $\tilde{\varrho}_i(x) := A_i(1, \overline{y}_{ic}, \overline{y}_{ic}, h_1 \eta_i, \ldots, h_{l_0} \eta_i)^T, \eta_i := \min\left\{\dfrac{1}{N_{i0}}, \dfrac{\overline{y}_{ic}}{M_{i0}}\right\}$ and

$$\tilde{\varrho}(x) = \begin{pmatrix} \tilde{\varrho}_1(x) \\ \vdots \\ \tilde{\varrho}_B(x) \end{pmatrix} . \tag{46c}$$

According to (30a,b), for *fixed weight matrices* $W_{i0}, i = 1, \ldots, B$, we obtain

$$K\big(a(\omega), x\big) = C K_0\big(a(\omega), x\big) C^T \tag{47a}$$

with

$$K_0\big(a(\omega), x\big) = (\widetilde{H}^T \tilde{\varrho}_d^{-1} W_0^T W_0 \tilde{\varrho}_d^{-1} \widetilde{H})^{-1}$$
$$= \sigma_y^U(\omega)^2 \tilde{K}_0(x) , \tag{47b}$$

where
$$\tilde{K}_0(x) := \left(\tilde{H}^T \tilde{\varrho}(x)_d^{-1} W_0^T W_0 \tilde{\varrho}(x)_d^{-1} \tilde{H} \right)^{-1} . \tag{47c}$$

Now, (29d,e), (30a,b) and (47a–c) yield

$$K\big(a(\omega), x\big) = \sigma_y^U(\omega)^2 C \tilde{K}_0(x) C^T = \sigma_y^U(\omega)^2 \tilde{K}(x) \tag{48a}$$

with the deterministic matrix

$$\tilde{K}(x) := C \tilde{K}_0(x) C^T . \tag{48b}$$

Moreover, we get

$$U\big(a(\omega), x\big) := K\big(a(\omega), x\big)^{-1} = \left(\sigma_y^U(\omega)^2 \tilde{K}(x) \right)^{-1}$$
$$= \frac{1}{\sigma_y^U(\omega)^2} \tilde{K}(x)^{-1} . \tag{48c}$$

Hence, see (29d),

$$\overline{U}(x) = EU\big(a(\omega), x\big) = \left(E \frac{1}{\sigma_y^U(\omega)^2} \right) \tilde{K}(x)^{-1} . \tag{48d}$$

In case of a *random* weight matrix $W_0 = W_0\big(a(\omega)\big)$, for $\overline{U}(x)$ we also obtain a representation of the type (48d), provided that (i) the random variables $W_0\big(a(\omega)\big)$ and $\sigma_y^U(\omega)$ are stochastically independent and (ii) $\widetilde{K}(x)$ is defined by

$$\widetilde{K}(x) := \left(E \left(C \tilde{K}_0 \big(W(a(\omega)), x \big) C^T \right)^{-1} \right)^{-1} . \tag{48e}$$

Corresponding to (29c), with $\hat{x} = \begin{pmatrix} x \\ \mu \end{pmatrix}$ we get

$$\overline{G_1^*}(\hat{x}) = EG_1^*\big(a(\omega), \hat{x}\big)$$
$$= \operatorname{tr} \overline{U}(x) EP\big(a(\omega), \mu\big) P\big(a(\omega), \mu\big)^T$$
$$= \left(E \frac{1}{\sigma_y^U(\omega)^2} \right) \operatorname{tr} \tilde{K}(x)^{-1} EP\big(a(\omega), \mu\big) P\big(a(\omega), \mu\big)^T . \tag{49}$$

Representing the $m \times m$ matrix

$$B(\mu) := EP\big(a(\omega), \mu\big) P\big(a(\omega), \mu\big)^T$$
$$= \overline{P}(\mu) \overline{P}(\mu)^T + \operatorname{cov}\Big(P\big(a(\cdot), \mu\big) \Big)$$
$$= \big(b_1(\mu), b_2(\mu), \ldots, b_m(\mu) \big) \tag{50a}$$

by its columns $b_j(\mu), j = 1, \ldots, m$, where we still set

$$\overline{P}(\mu) := EP\big(a(\omega), \mu\big) , \tag{50b}$$

$$\mathrm{cov}\Big(P\big(a(\cdot), \mu\big)\Big) := E\Big(P\big(a(\omega), \mu\big) - \overline{P}(\mu)\Big)\Big(P\big(a(\omega), \mu\big) - \overline{P}(\mu)\Big)^T \tag{50c}$$

we find

$$Z(\hat{x}) = (z_1, z_2, \ldots, z_m) := E\left(\frac{1}{\sigma_y^U(\omega)^2}\right) \tilde{K}(x)^{-1} B(\mu)$$

$$= E\left(\frac{1}{\sigma_y^U(\omega)^2}\right) \big(\tilde{K}(x)^{-1} b_1(x), \tilde{K}(x)^{-1} b_2(\mu), \ldots, \tilde{K}(x)^{-1} b_m(\mu)\big) \tag{50d}$$

However, (50d) is equivalent to the following equations for the columns z_j, $j = 1, \ldots, B$,

$$\tilde{K}(x) z_j = E\left(\frac{1}{\sigma_y^U(\omega)^2}\right) b_j(\mu), \quad j = 1, \ldots, m . \tag{51}$$

With Eq. (51) for $z_j, j = 1, \ldots, m$, the expected cost function $\overline{G}_1^*(\hat{x})$ can be represented now by

$$\overline{G}_1^*(\hat{x}) = tr(z_1, z_2, \ldots, z_m). \tag{52}$$

Having (51) and (52), the deterministic substitute problems (31a–c) and (39) can be represented as follows:

Theorem 2. Expected cost based optimization (ECBO). *Suppose that $W_{i0}, i = 1, \ldots, B$, are given fixed weight matrices. Then the expected costbased optimization problem (31a–c) can be represented by*

$$\min \ \overline{G}_0(\mu) \tag{53a}$$

$$\text{s.t. } tr(z_1, z_2, \ldots, z_m) \leq G_1^{\max} , \tag{53b}$$

$$\tilde{K}(x) z_j = E\left(\frac{1}{\sigma_y^U(\omega)^2}\right) b_j(\mu), \quad j = 1, \ldots, m , \tag{53c}$$

$$x \in D, \quad \mu \geq 0 , \tag{53d}$$

where the vectors $b_j = b_j(\mu), j = 1, \ldots, m$, are given by (50a).

Obviously, (53a–d) is an ordinary deterministic parameter optimization problem having the additional auxiliary variables $z_j \in \mathbb{R}^m, j = 1, \ldots, m$.

For the second substitute problem we get this result:

Theorem 3. Minimum expected costs. *Suppose that $W_{0i}, i = 1, \ldots, B$, are given fixed weight matrices. Then the minimum expected cost problem (39) can be represented by*

$$\min \ \overline{G}_0(\mu) + \mathrm{tr}(z_1, z_2, \ldots, z_m) \tag{54a}$$

$$\text{s.t. } \tilde{K}(x)z_j = E\left(\frac{1}{\sigma_y^U(\omega)^2}\right) b_j(\mu), \quad j = 1, \ldots, m , \tag{54b}$$

$$x \in D, \quad \mu \geq 0 . \tag{54c}$$

Remark 1. According to (48b) and (47c), the matrix $\tilde{K} = \tilde{K}(x)$ is a simple function of the design vector x.

6.1 The Case of Non-uniform Material

If a representation of

$$\overline{U}(x) = EU\big(a(\omega), x\big) = EK\big(a(\omega), x\big)^{-1} = \beta(\omega)\widetilde{K}(x)^{-1} ,$$

see (29d), (30a,b), of the type (48d) does not hold, then we may apply the approximative procedure described in the following.

First, the probability distribution $P_{a(\cdot)}$ of the random vector $a = a(\omega)$ of model parameters is approximated, as far it concerns the subvector $a_I = a_I(\omega)$ of $a = a(\omega)$ of model parameters arising in the matrix

$$K = K\big(a(\omega), x\big) = K\big(a_I(\omega), x\big) ,$$

by a discrete distribution

$$\hat{P}_{a_I(\cdot)} := \sum_{s=1}^{N} \alpha_s \varepsilon_{a_I^{(s)}} \tag{55}$$

having realizations $a_I^{(s)}$ taken with probabilities $\alpha_s, s = 1, \ldots, N$.

Then, the matrix function $\overline{U} = \overline{U}(x)$ can be approximated by

$$\hat{\overline{U}}(x) := \sum_{s=1}^{N} \alpha_s K^{(s)}(x)^{-1} , \tag{56a}$$

where

$$K^{(s)}(x) := K(a_I^{(s)}, x) = CK_0(a_I^{(s)}, x)C^T , \tag{56b}$$

see (30b). Consequently, the expected cost function $\overline{G_1^*} = \overline{G_1^*}(\hat{x})$ is approximated by

$$\hat{\overline{G_1^*}}(\hat{x}) := \mathrm{tr}\,\hat{\overline{U}}(x)EP\big(a(\omega), \mu\big)P\big(a(\omega), \mu\big)^T$$

$$= \sum_{s=1}^{N} \alpha_s \,\mathrm{tr}\,K^{(s)}(x)^{-1}EP\big(a(\omega), \mu\big)P\big(a(\omega), \mu\big)^T . \tag{57}$$

Corresponding to (50d), we define now the auxiliary matrix variables

$$z^{(s)} = (z_1^{(s)}, z_2^{(s)}, \ldots, z_m^{(s)}) := K^{(s)}(x)^{-1} B(\mu)$$
$$= \left(K^{(s)}(x)^{-1} b_1(\mu), K^{(s)}(x)^{-1} b_2(\mu) \ldots, K^{(s)}(x)^{-1} b_m(\mu) \right) , \quad (58)$$

where $B = B(\mu)$ is defined again by (50a). Thus, for the columns $z_j^{(s)}$, $j = 1, \ldots, m$, we obtain the conditions

$$K^{(s)}(x) z_j^{(s)} = b_j(\mu), \quad j = 1, \ldots, m , \quad (59)$$

for each $s = 1, \ldots, N$. According to (57) and (58), the approximate expected cost function $\widehat{\overline{G_1^*}} = \overline{\widehat{G_1^*}}$ reads

$$\overline{\widehat{G_1^*}}(\hat{x}) = \sum_{s=1}^{N} \alpha_s \, \mathrm{tr} \left(z_1^{(s)}, z_2^{(s)}, \ldots, z_m^{(s)} \right), \quad (60)$$

where $z_j^{(s)}$, $j = 1, \ldots, m$, $s = 1, \ldots, N$, are given by (59).

Because of the close relationship between the representations (60) and (52) for $\widehat{\overline{G_1^*}}, \overline{G_1^*}$, approximate mathematical optimization problems result from (60) which are similar to (53a–d), (54a–c), respectively.

7 Numerical Example

In order to consider the properties of the presented methods, the two-storey frame in Fig. 1 with rectangular cross-sectional area $A = b\,h$, with height h and width b is studied. The numerical results presented in this section for substitute Problem 4.1, i.e. the maximization of the load factor subject to the expected cost (reliability) constraint, were obtained by Simone Zier, Institute for Mathematics and Computer Applications, Federal Armed Forces University Munich.

In the following we study the influence of the normal distributed force component $P_{2x}(\omega)$ on the limit load analysis. In order to determine the probability of failure, we use a discrete approximation of the normal distribution according to Fig. 2. The primary cost function is defined, cf. (1), by $G_0(\mu) = -\gamma\mu$ with a weight factor $\gamma > 0$.

We take $\gamma = 10$, and for the elements w_{ik}^0 of the 3×3 diagonal weight matrices W_{i0} we choose $w_{ik}^0 = w = 100$, $w_{ik}^0 = w = 200$, resp., $i = 1, \ldots, 6$, $k = 1, 2, 3$. Furthermore, the external load vector $P\big(a(\omega), \mu\big)$, cf. (2a), is given by $P_0\big(a(\omega)\big) := 0$ and

$$P_1\big(a(\omega)\big) := \left(P_{11}^T, P_{12}^T, 0^T, 0^T \right)^T .$$

Fig. 1 Two-storey frame

$L = 1.000\,mm, E = 72.000\,\dfrac{\text{N}}{\text{mm}^2}$

$\sigma^U = -\sigma^L = 216\,\dfrac{\text{N}}{\text{mm}^2}$

$P_{11} = \begin{pmatrix} 10.000\,\text{N} \\ 0\,\text{N} \\ 0\,\text{N mm} \end{pmatrix}, \quad P_{12} = \begin{pmatrix} P_{2x}(\omega) \\ -1.000\,\text{N} \\ 0\,\text{N mm} \end{pmatrix}$

$\text{with}\,P_{2x} \sim N(\mu, 100)$
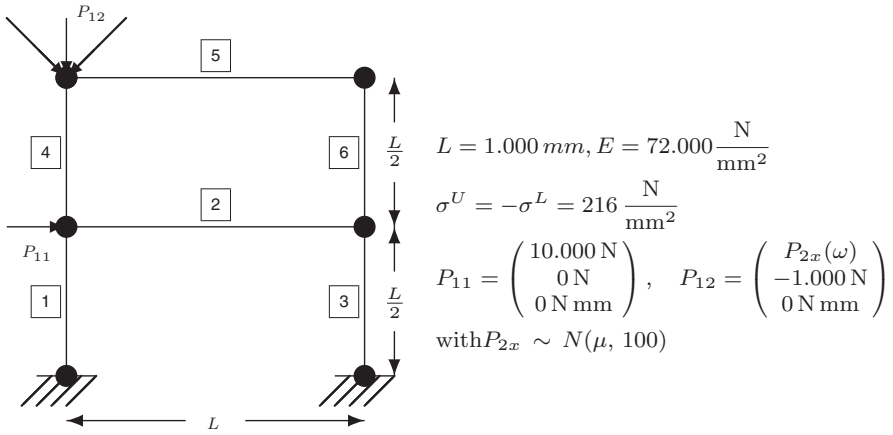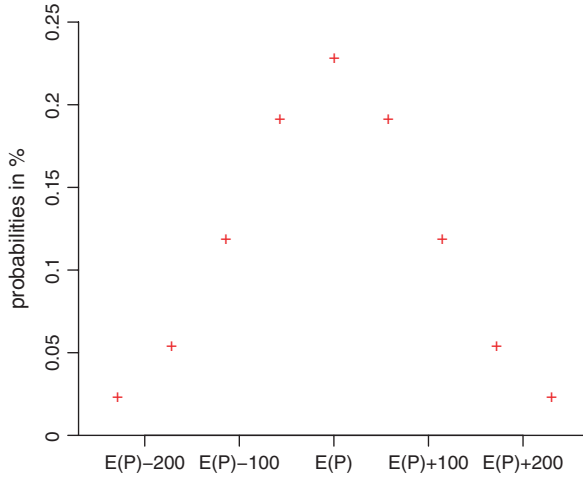
Fig. 2 Discretisation of the normal distribution $N \sim (E(P), 100^2)$ with 9 realisations

Finally, we set $G_1^{\max} := 50000$, and we take the cross-sectional area $600\,\mathrm{mm}^2$, $10\,\mathrm{mm}^2$, resp., for the bars 1–3, 4–6, see [16].

As can be seen by Figs. 3 and 5 for $w = 100, 200$, resp., the maximum load factor μ^* is decreasing, the expected costs are increasing with increasing expected load component $\overline{P}_{2x}$. Moreover, with increasing $\overline{P}_{2x}$, the probability of failure p_f may increase too, see Fig. 4(a). However, in case of a sufficiently high cost factor w, p_f remains at a very low level see Fig. 4(b).

Comparing Figs. 3 and 5, we observe the same behaviour of the maximum load factor and the expected costs for $w = 100$, $w = 200$, resp.; however, the values of the maximum load factor μ^* are smaller in case of the large cost factor $w = 200$.
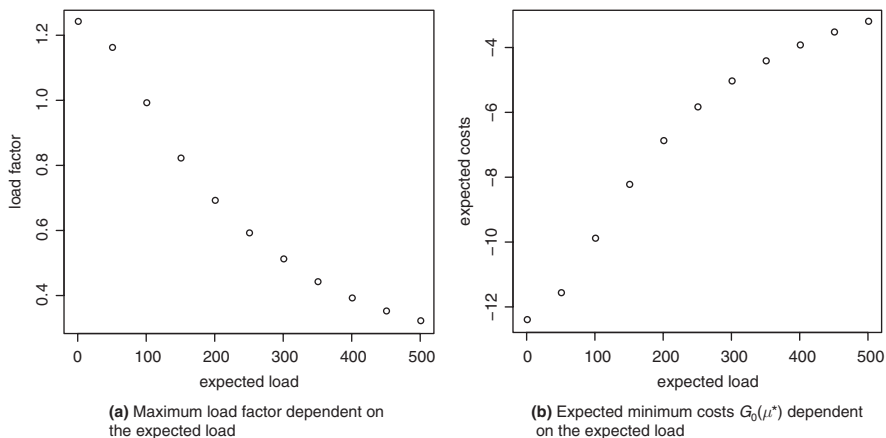
(a) Maximum load factor dependent on the expected load

(b) Expected minimum costs $G_0(\mu^*)$ dependent on the expected load

Fig. 3 Influence of the expected load on the load factor and the expected costs for $w = 100$

(a) Probability of failure dependent on the expected load for $\omega = 100$

(b) Probability of failure dependent on the expected load for $\omega = 200$

Fig. 4 Influence of the height of the cross-sectional area on the load factor and the expected total costs

(a) Maximum load factor dependent on the expected load

(b) Expected minimum costs $G_0(\mu^*)$ dependent on the expected load
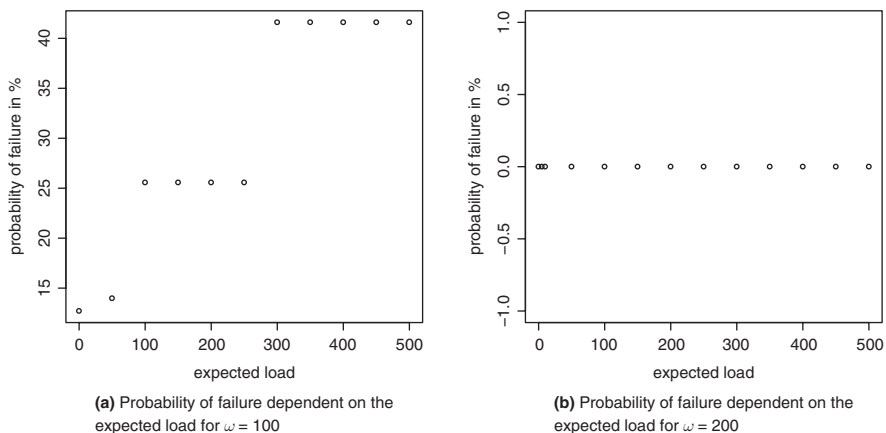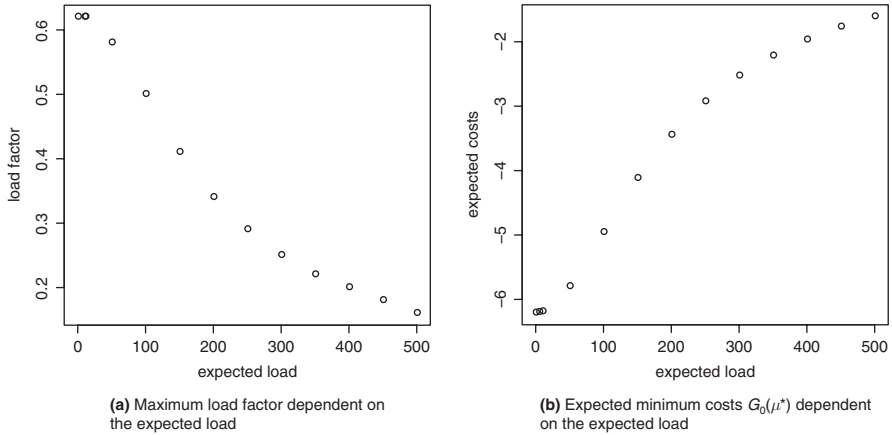
Fig. 5 Influence of the expected load on the load factor and the expected costs for $w = 200$

References

1. Bullen, P.S.: Handbook of Means and Their Inequalities. Kluwer Academic Publ., Dordrecht [etc.] (2003)
2. Cocchetti, G., Maier, G.: Static shakedwon theorems in piecewise linearized plasticity. Arch. Appl. Mech. **68**, 651–661 (1988)
3. Corradi, L., Zavelani, A.: A linear programming approach to shakedown analysis of structures. Comput. Meth. Appl. Mech. Engng. **3**, 37–53 (1974)
4. Damkilde, L., Krenk, S.: Limits – a system for limit state analysis and optimal material layout. Comput. Struct. **64** (1–4), 709–718 (1997)
5. Ditlevsen, O., Madsen, H.O.: Structural Reliability Methods. J. Wiley, New York (1996)
6. Frangopol, D.M.: Reliability-Based optimum structural design. In: Sundarajan, C. (ed.) Probabilistic Structural Mechanics Handbook, pp. 352–387, Chapman and Hall, New York (1995)
7. Gasser, M., Schuëller, G.I.: Some basic principles in reliability-based optimisation(RBO) of structures and mechanical components. In: Marti, K., Kall, P. (eds.) Stochastic Programming Methods and Technical Applications, Lecture Notes in Economics and Mathematical Systems **458**, 80–103, Springer-Verlag, Berlin (1998)
8. Hardy, G.H., Littlewood, J.E., Pólya, G.: Inequalities. Cambridge Univ. Press, London (1973)
9. Kaliszky, S.: Plasticity: Theory and Engineering Applications. Elsevier, Amsterdam (1989)
10. Kamenjarzh, J.A.: Limit Analysis of Solids and Structures. CRC Press, Boca Raton [etc.] (1996)
11. König, J.A.: Shakedown of Elastic-Plastic Structures. Elsevier, Amsterdam etc. (1987)
12. Marti, K. : Approximation and derivatives of probabilities of survival in structural analysis and design. Struct. Opt. **13**, 230–243 (1997)
13. Marti, K.: Stochastic optimisation methods in optimal engineering design under stochastic uncertainty. ZAMM **83** (11), 1–18 (2003)
14. Marti, K.: Stochastic Optimisation Methods. Springer-Verlag, Berlin-Heidelberg-New York (2005)

15. Marti, K.: Reliability Analysis of Technical Systems / Structures by means of Polyhedral Approximation of the Safe / Unsafe Domain. GAMM Mitteilungen **30 (2)**, 211–254 (2007)
16. Zier, S.: Optimal design of frames under stochastic uncertainties. PAMM **7 (1)**, 1061805–106186 (2007)

Limit Load Analysis of Plane Frames Under Stochastic Uncertainty

S. Zier and K. Marti

Abstract Using the first collapse theorem the necessary and sufficient constraints of a structure consist of the yield condition and the equilibrium condition. In the recent field of research stochastic uncertainties have been taken into account. This leads to a stochastic optimization problem which cannot be solved using the traditional methods. Instead of that appropriate (deterministic) substitute problems must be formulated. In the following, the limit load analysis of plane frames is treated where the load is supposed to be stochastic. Here, both forces and moments have to be taken into consideration. The recourse problem will be formulated in general and in the standard form of stochastic linear programming (SLP). After the formulation of the stochastic optimization problem, the expected value problem and the recourse problem with discretisation are introduced as representatives of substitute problems. Subsequently, some numerical results of the application of the presented methods to a two-storey frame are shown.

1 Formulation of the Problem

At the beginning general aspects of plastic analysis are mentioned including the static and the kinematic theorem. Afterwards foundations of plastic theory are given.

Simone Zier and Kurt Marti
Federal Armed Forces University Munich, Aero-Space Engineering and Technology, 85577 Neubiberg/Munich, Germany, e-mail: simone.zier@unibw-muenchen.de; kurt.marti@unibw-muenchen.de

1.1 Plastic Analysis of Structures

Many materials, e.g. most of metals, have distinct, plastic properties, i.e., they are ductile, see e.g. [4, 13]. Even after the stress intensity attains the yield point stress, such materials can deform considerably without breaking. This implies that if the stress intensity at a certain point of a hyperstatic structure reaches the critical (yield) value, the structure does not necessarily fail or deform excessively. Instead, a certain amount of stress redistribution takes place and some further load increments can be supported. Structural failure does not occur before a kinematic mechanism of unconstrained plastic flow develops. Thus, the actual load-carrying capacity of a structure is higher (in some cases quite considerably) than that derived from classical elastic analysis.

A crucial question for the engineer designing structures like buildings, bridges, etc., or structural components is to which extent a plastic deformation is permissible without leading to a failure of the structure, the component, resp., with respect to the expected load and material strength conditions. Applying standard methods, the load carrying capacity is determined using a certain code with general rules for safety evaluations. The use of such general rules may be very expensive in the safety evaluation and design of a structure. On the other hand, safety assessment and design based on stochastic optimization techniques taking into account the available knowledge about random parameter variations reduce the expected total project costs (primary costs, e.g. costs of construction, plus recourse costs, e.g. strengthening costs) considerably. In addition to that, by using analytical methods, it is possible to relate the optimal solution of a stochastic linear problem with certain cost coefficients and the optimal solution of a chance constrained or reliability-based program with a certain bound for the probability of failure [10]. Consequently, this way one obtains more robust (safe) information about the maximum load factors, hence, the carrying capacity. A further big advantage of stochastic optimization methods is the possibility of updates of the maximum load factors based on inspection, sampling and other posterior information about the probability distribution of the random parameters.

For elastic-perfectly plastic materials, the ultimate load condition corresponding to complete collapse of the structure can be obtained through application of a pair of dual theorems [7, 9, 13]:

(ST)   *Static Theorem (lower bound or safe theorem)*
        If any stress distribution throughout the structure can be found which is everywhere in equilibrium internally and balances the external loads, and at the same time does not violate the yield condition, those external loads will be carried safely by the structure.

(KT)   *Kinematic Theorem (upper bound or unsafe theorem)*
        Collapse occurs if a collapse mechanism, fulfilling the compatibility

condition, exists such that the work done by the external loads is larger than the corresponding internal plastic work.

Limit analysis is concerned [2–12, 14–20, 23, 24] with establishing the strength of a structure, i.e., its capacity for the supporting of loads. Hence, using the plastic ductility of structural materials in improving the design of structures, limit analysis is not concerned with deformation: it can not therefore provide the load carrying capacity for a structure with elements that have a limited ductility or deformability, nor for a structure which becomes unstable because of the displacements induced by plastic deformation, see [7, 9, 14, 16].

1.2 Foundations from Plasticity Theory

A frame is a structure consisting of a certain number B of beams or bars which are rigid-jointed among each other and the foundation at a certain number J of nodes [21].

In limit load analysis the aim is to maximize the load factor μ while several constraints have to be fulfilled. For the equilibrium condition the equation

$$CF = \mu P_0 \tag{1a}$$

has to hold, where C represents the equilibrium matrix, F is the vector of the interior forces and moments, and P_0 denotes an external reference load vector.

We suppose that the frame is built of elasto-plastic material. That means that the behaviour under load is at first elastic and can be described linearly by Hooke's Law and then after exceeding a limit – called yield stress – the material starts yielding. This behaviour is described by the yield condition

$$F \in K \tag{1b}$$

with the feasible domain K.

In addition we have the non-negativity condition

$$\mu \geq 0 \tag{1c}$$

for the load factor μ to be maximized.

We suppose that the external reference load is not deterministic, but depends on certain stochastic parameters, describing random external load variations due to e.g. wave, wind, snow loads, etc.

If we denote the stochastic elements as ω we get the external loads $P_0(\omega)$ as functions of ω. Problem (1a–c) can be fomulated therefore as

$$\max \mu \tag{2a}$$

$$\text{s.t.} \quad CF = \mu P_0(\omega) \qquad \text{almost surely (a.s.)} \tag{2b}$$

$$F \in K \qquad \text{a.s.} \tag{2c}$$

$$\mu \geq 0\,. \tag{2d}$$

While the actual realisation of the random element ω is not known, we suppose that its distribution is known.

A basic principle to cope with uncertainty is based on compensation, corrections, hence, recourse. Recourse is the ability to take corrective actions - such as repair, strenghtening, etc. – after a random event has taken place.

We add so called recourse costs $Q(y)$ in the case that the yield condition is violated. Here, y are auxiliary variables introduced to describe whether or not the yield condition is violated.

Before we formulate the recourse problem in a mathematical way, we need to introduce some more notations.

For each beam i the element-load vector

$$F_i = (f_i, m_i^+, m_i^-)^T,$$

built of the normal force f_i, the moment m_i^+ at the positive (right) end of the beam and the moment m_i^- at the negative (left) end is considered. These vectors are summarized in the total vector of the internal loads

$$F = (F_1^T, \ldots, F_B^T)^T.$$

Besides that we need also plastic capacities. The tension capacity N_{ipl}^U can be calculated by

$$N_{ipl}^U = \sigma_{yi}^U A_i, \tag{3a}$$

where σ_{yi}^U is the yield stress in tension. The compression capacity N_{ipl}^L is analogue

$$N_{ipl}^L = |\sigma_{yi}^L| A_i = -\sigma_{yi}^L A_i, \tag{3b}$$

where σ_{yi}^L is the yield stress in compression.

The moment capacity M_{ipl} is given by

$$M_{ipl} = \sigma_{yi}^U W_{ipl}, \tag{3c}$$

where W_{ipl} is the plastic section modulus [9, 18].

The plastic capacity of an element concerning compression F_i^L, concerning tension F_i^U, resp., can then be described by

$$F_i^L = (-N_{ipl}^L, -M_{ipl}, -M_{ipl})^T, \tag{3d}$$

$$F_i^U = (N_{ipl}^U, M_{ipl}, M_{ipl})^T, \tag{3e}$$

respectively.

1.3 Linearization of the Yield Condition

The feasible domain is given by

$$K = \left\{ (N, M)^T \in \mathbb{R}^2 : \left| \frac{N}{N_{pl}} \right|^\alpha + \left| \frac{M}{M_{pl}} \right| \leq 1 \right\}. \tag{4}$$

Here, α is a geometric parameter which depends on the cross-sectional area of the beams. In [9] several values for α for special cross-sectional areas are given. The feasible domain for certain cross-sectional areas can be seen in Fig. 1.

However, this is no linear condition. In order to apply linear optimization methods, being faster and numerically easier to handle, piecewise linear approximations are needed.

The most simple approximation is by a square from outside the admissible domain as seen in Fig. 2(a).

In doing so, the yield condition can simply be written as

$$F^L \leq F \leq F^U. \tag{5}$$
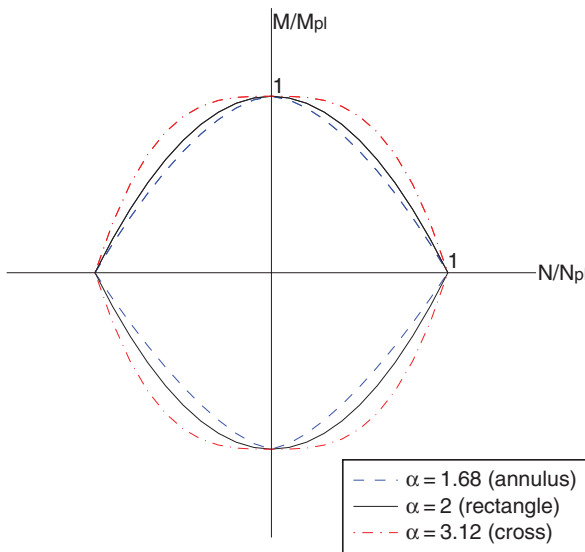
Fig. 1 Feasible domain $K = \left\{ (N, M)^T \in R^2 : \left| \frac{N}{N_{pl}} \right|^\alpha + \left| \frac{M}{M_{pl}} \right| \leq 1 \right\}$

(a) Zero order   (b) First order
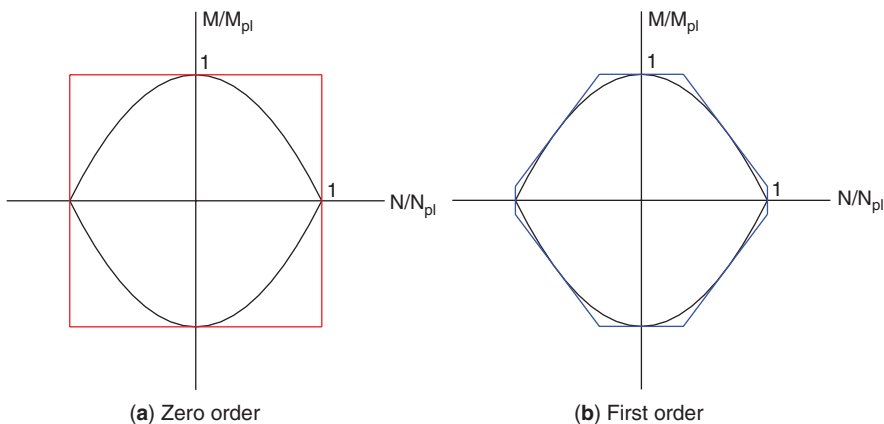
Fig. 2 Piecewise linear approximation of the feasible domain K from outside

Since there is no relationship between the plastic capacities, this approximation is called approximation without M-N-interaction.

A better approximation from outside is achieved by considering certain tangents to the feasible domain.

In Fig. 2(b) an approximation of first order using four additional tangents can be seen.

In the following, the approximation of zero order from outside is considered, that means without M-N-interaction where the yield condition can be written as (5). That means, with (3a–e), for each element-load vector F_i the inequalities

$$\sigma_{yi}^L \, A_i \le f_i \le \sigma_{yi}^U \, A_i, \tag{6a}$$

$$-\sigma_{yi}^U \, W_{ipl} \le m_i^+ \le \sigma_{yi}^U \, W_{ipl}, \tag{6b}$$

$$-\sigma_{yi}^U \, W_{ipl} \le m_i^- \le \sigma_{yi}^U \, W_{ipl} \tag{6c}$$

have to hold. If we introduce

$$\bar{y}_{ic} := \frac{W_{ipl}}{A_i} \tag{7}$$

and the auxiliary variables $z_i^L, z_i^U, z_i^{+L}, z_i^{+U}, z_i^{-L}$ and z_i^{-U}, we get for (6a–c) the equalities

$$\sigma_{yi}^{L} A_i + z_i^{L} = f_i, \tag{8a}$$

$$f_i + z_i^{U} = \sigma_{yi}^{U} A_i, \tag{8b}$$

$$-\sigma_{yi}^{U} A_i \bar{y}_{ic} + z_i^{+L} = m_i^{+}, \tag{8c}$$

$$m_i^{+} + z_i^{+U} = \sigma_{yi}^{U} A_i \bar{y}_{ic}, \tag{8d}$$

$$-\sigma_{yi}^{U} A_i \bar{y}_{ic} + z_i^{-L} = m_i^{-}, \tag{8e}$$

$$m_i^{-} + z_i^{-U} = \sigma_{yi}^{U} A_i \bar{y}_{ic}. \tag{8f}$$

If an auxiliary variable is non-negative, the associated inequality is satisfied. Otherwise it is violated. In order to get a formulation with only non-negative variables, we split the auxiliary variables into their positive and negative part and get the constraints

$$\sigma_{yi}^{L} A_i + y_i^{L+} - y_i^{L-} = f_i, \tag{9a}$$

$$f_i + y_i^{U+} - y_i^{U-} = \sigma_{yi}^{U} A_i, \tag{9b}$$

$$-\sigma_{yi}^{U} A_i \bar{y}_{ic} + y_i^{+L+} - y_i^{+L-} = m_i^{+}, \tag{9c}$$

$$m_i^{+} + y_i^{+U+} - y_i^{+U-} = \sigma_{yi}^{U} A_i \bar{y}_{ic}, \tag{9d}$$

$$-\sigma_{yi}^{U} A_i \bar{y}_{ic} + y_i^{-L+} - y_i^{-L-} = m_i^{-}, \tag{9e}$$

$$m_i^{-} + y_i^{-U+} - y_i^{-U-} = \sigma_{yi}^{U} A_i \bar{y}_{ic}, \tag{9f}$$

$$y_i^{L+}, y_i^{L-}, y_i^{U+}, y_i^{U-}, y_i^{+L+}, y_i^{+L-}, y_i^{+U+}, y_i^{+U-}, y_i^{-L+}, y_i^{-L-}, y_i^{-U+}, y_i^{-U-} \geq 0. \tag{9g}$$

If we eliminate f_i, m_i^{+} and m_i^{-}, by inserting (9a), (9c), (9e), resp., into (9b), (9d), (9f), resp., we can reduce the system of equations for a single beam i to

$$y_i^{L+} - y_i^{L-} + y_i^{U+} - y_i^{U-} = -(\sigma_{yi}^{L} - \sigma_{yi}^{U}) A_i, \tag{10a}$$

$$y_i^{+L+} - y_i^{+L-} + y_i^{+U+} - y_i^{+U-} = 2\sigma_{yi}^{U} A_i \bar{y}_{ic}, \tag{10b}$$

$$y_i^{-L+} - y_i^{-L-} + y_i^{-U+} - y_i^{-U-} = 2\sigma_{yi}^{U} A_i \bar{y}_{ic}, \tag{10c}$$

$$y_i^{L+}, y_i^{L-}, y_i^{U+}, y_i^{U-}, y_i^{+L+}, y_i^{+L-}, y_i^{+U+}, y_i^{+U-}, y_i^{-L+}, y_i^{-L-}, y_i^{-U+}, y_i^{-U-} \geq 0, \tag{10d}$$

which can be formulated for the whole structure by

$$
\begin{pmatrix} I_B - I_B \ I_B - I_B \\ & I_B - I_B \ I_B - I_B \\ & & I_B - I_B \ I_B - I_B \end{pmatrix} \cdot
\begin{pmatrix} y^{L+} \\ y^{L-} \\ y^{U+} \\ y^{U-} \\ y^{+L+} \\ y^{+L-} \\ y^{+U+} \\ y^{+U-} \\ y^{-L+} \\ y^{-L-} \\ y^{-U+} \\ y^{-U-} \end{pmatrix} =
$$

$$
= - \begin{pmatrix} \sigma_{y1}^L - \sigma_{y1}^U \\ & \ddots \\ & & \sigma_{yB}^L - \sigma_{yB}^U \\ -2\sigma_{y1}^U \cdot \bar{y}_{1c} \\ & \ddots \\ & & -2\sigma_{yB}^U \cdot \bar{y}_{Bc} \\ -2\sigma_{y1}^U \cdot \bar{y}_{1c} \\ & \ddots \\ & & -2\sigma_{yB}^U \cdot \bar{y}_{Bc} \end{pmatrix} \cdot
\begin{pmatrix} A_1 \\ \vdots \\ A_B \end{pmatrix}, \quad (11)
$$

with the $B \times B$ identity matrix I_B and the vectors $y^\Gamma = (y_1^\Gamma, \dots, y_B^\Gamma)$ with $\Gamma \in \{L+, L-, U+, U-, +L+, +L-, +U+, +U-, -L+, -L-, -U+, -U-\}$.

1.4 Cost Function

Instead of maximizing the load factor μ, we often minimize a kind of cost function with can be built easily by the negative load factor which is eventually weighted by a factor γ. These are then called costs of first stage or initial costs.

Such an approach, considering the appearing costs, is a standard one in the reliability-based structural optimization. More precisely, the objective function represents the life cycle costs and has to consider, besides the already mentioned initial construction costs, the expected cost consequences related to partial or total system failure [5,6]. Furthermore, the probabilities of failure can always be interpreted by expected costs. Indeed, the corresponding cost function is just the characteristic function of the domain of failure.

The costs which result from violation of the yield condition – also called costs of second stage or penalty or recourse costs – are in many cases described by additive terms. One possible way to build a total costfunction is

$$G_0(\mu) = - \gamma\mu + \sum_{i=1}^{B} \frac{1}{L_i A_i} \left(q_i^L y_i^{L-} + q_i^U y_i^{U-} + q_i^{+L} y_i^{+L-} \right.$$
$$\left. + q_i^{+U} y_i^{+U-} + q_i^{-L} y_i^{-L-} + q_i^{-U} y_i^{-U-} \right) \tag{12}$$

$$\text{with} \quad q_i^L = \gamma_i^L \frac{L_i}{E_i}, \qquad\qquad q_i^U = \gamma_i^U \frac{L_i}{E_i},$$
$$q_i^{+L} = \gamma_i^{+L} \frac{L_i}{E_i} \frac{1}{\bar{y}_{ic}}, \qquad q_i^{+U} = \gamma_i^{+U} \frac{L_i}{E_i} \frac{1}{\bar{y}_{ic}},$$
$$q_i^{-L} = \gamma_i^{-L} \frac{L_i}{E_i} \frac{1}{\bar{y}_{ic}}, \qquad q_i^{-U} = \gamma_i^{-U} \frac{L_i}{E_i} \frac{1}{\bar{y}_{ic}}.$$

Here, q_i are costfactors which consist of a weighting factor γ_i which controls how heavy each violation is punished and quotients $\frac{L_i}{E_i}, \frac{L_i}{E_i} \frac{1}{\bar{y}_{ic}}$, resp., which results in the same dimension for all terms, namely volums [15, 22].

These quotients are used since a change in the volume ΔV can be expressed by
$$\Delta V = A \, \Delta L \tag{13a}$$
which, after including the relationships
$$\Delta L = \frac{L}{E} \Delta\sigma \tag{13b}$$
for the change in length under elastic consideration and
$$\Delta\sigma = \frac{\Delta F}{A} \pm \frac{\Delta M}{W} \tag{13c}$$
in the case where the cross-sectional area is symmetric to the neutral fibre can be written as

$$\Delta V = A \, \Delta L = A \frac{L}{E} \Delta\sigma,$$
$$= A \frac{L}{E} \left(\frac{\Delta F}{A} \pm \frac{\Delta M}{W} \right),$$
$$= \frac{L}{E} \Delta F \pm \frac{L}{E} \frac{A}{W} \Delta M,$$
$$= \frac{L}{E} \Delta F \pm \frac{L}{E} \frac{1}{\bar{y}_c} \Delta M, \tag{14}$$

where "+" is used for the upper fibre and "−" for the lower one.

In order to add these costs to the dimensionless load factor μ we scale them with a reference volume, namely the volume of each beam $L_i A_i$.

1.5 Reformulation of the Equilibrium Condition

In order to have a uniform formulation of all constraints, we also eliminate
the variables f_i, m_i^+ and m_i^- from the equilibrium condition (2b)

$$
CF = C \cdot \begin{pmatrix} F_1 \\ \vdots \\ F_B \end{pmatrix} = C \cdot \begin{pmatrix} f_1 \\ m_1^+ \\ m_1^- \\ \vdots \\ f_B \\ m_B^+ \\ m_B^- \end{pmatrix} = \mu P_0(\omega) \tag{15}
$$

by inserting (9a), (9c) and (9e) which leads to

$$
C \cdot \begin{pmatrix} \sigma_{y1}^L A_1 + y_1^{L+} - y_1^{L-} \\ -\sigma_{y1}^U A_1 \bar{y}_{1c} + y_1^{+L+} - y_1^{+L-} \\ -\sigma_{y1}^U A_1 \bar{y}_{1c} + y_1^{-L+} - y_1^{-L-} \\ \vdots \\ \sigma_{yB}^L A_B + y_B^{L+} - y_B^{L-} \\ -\sigma_{yB}^U A_B \bar{y}_{Bc} + y_B^{-L+} - y_B^{-L-} \end{pmatrix} = C \cdot \begin{pmatrix} \sigma_{y1}^L A_1 \\ -\sigma_{y1}^U A_1 \bar{y}_{1c} \\ -\sigma_{y1}^U A_1 \bar{y}_{1c} \\ \vdots \\ \sigma_{yB}^L A_B \\ -\sigma_{yB}^U A_B \bar{y}_{Bc} \\ -\sigma_{yB}^U A_B \bar{y}_{Bc} \end{pmatrix} + C \cdot \begin{pmatrix} y_1^{L+} - y_1^{L-} \\ y_1^{+L+} - y_1^{+L-} \\ y_1^{-L+} - y_1^{-L-} \\ \vdots \\ y_B^{L+} - y_B^{L-} \\ y_B^{+L+} - y_B^{+L-} \\ y_B^{-L+} - y_B^{-L-} \end{pmatrix}
$$

$$
= \mu P_0(\omega). \tag{16}
$$

Therefore, the equilibrium condition (2b) can be represented in matrix form

$$
\tilde{C} \cdot \begin{pmatrix} I_B & -I_B & & & & \\ & & I_B & -I_B & & \\ & & & & I_B & -I_B \end{pmatrix} \cdot \begin{pmatrix} y^{L+} \\ y^{L-} \\ y^{+L+} \\ y^{+L-} \\ y^{-L+} \\ y^{-L-} \end{pmatrix} - \mu P_0(\omega) =
$$

$$
- \tilde{C} \cdot \begin{pmatrix} \sigma_{y1}^L & & & & & \\ & \ddots & & & & \\ & & \sigma_{yB}^L & & & \\ -\sigma_{y1}^U \bar{y}_{1c} & & & & & \\ & \ddots & & & & \\ & & -\sigma_{yB}^U \bar{y}_{Bc} & & & \\ -\sigma_{y1}^U \bar{y}_{1c} & & & & & \\ & \ddots & & & & \\ & & -\sigma_{yB}^U \bar{y}_{Bc} \end{pmatrix} \cdot \begin{pmatrix} A_1 \\ \vdots \\ A_B \end{pmatrix}; \tag{17}
$$

where the matrix $\tilde{C}$ results from the equilibrium matrix C by a certain permutation of columns.

1.6 Standard Form of a Stochastic Linear Programming with Recourse

By introducing the recourse matrix

$$
W := \begin{pmatrix}
I_B & -I_B & I_B & -I_B & & & & & & & \\
& & & I_B & -I_B & I_B & -I_B & & & & \\
& & & & & & I_B & -I_B & I_B & -I_B & \\
& \tilde{C} \cdot \begin{pmatrix} I_B & -I_B & 0 & 0 & & & & \\ & & I_B & -I_B & 0 & 0 & \\ & & & & I_B & -I_B & 0 & 0 \end{pmatrix}
\end{pmatrix}
\tag{18}
$$

and the matrix

$$
H := \begin{pmatrix} H_1 \\ H_2 \end{pmatrix}
\tag{19}
$$

with

$$
H_1 = \begin{pmatrix}
\sigma_{y1}^L - \sigma_{y1}^U & & & & \\
& \ddots & & & \\
& & \sigma_{yB}^L - \sigma_{yB}^U & & \\
-2\sigma_{y1}^U \cdot \bar{y}_{1c} & & & \ddots & \\
& & & & -2\sigma_{yB}^U \cdot \bar{y}_{Bc} \\
-2\sigma_{y1}^U \cdot \bar{y}_{1c} & & & \ddots & \\
& & & & -2\sigma_{yB}^U \cdot \bar{y}_{Bc}
\end{pmatrix}
\quad \text{and} \quad
H_2 = \tilde{C} \cdot \begin{pmatrix}
\sigma_{y1}^L & & & & \\
& \ddots & & & \\
& & \sigma_{yB}^L & & \\
-\sigma_{y1}^U \bar{y}_{1c} & & & \ddots & \\
& & & & -\sigma_{yB}^U \bar{y}_{Bc} \\
-\sigma_{y1}^U \bar{y}_{1c} & & & \ddots & \\
& & & & -\sigma_{yB}^U \bar{y}_{Bc}
\end{pmatrix},
\tag{20}
$$

problem (2a–d) with the modified objective function (12) and the reformulated constraints (11) and (17) can be formulated in the standard form of a stochastic linear programming with recourse [11]

$$
\min c^T x + q^T y \tag{21a}
$$
$$
T(\omega)x + Wy = h \qquad a.s. \tag{21b}
$$
$$
x, y \geq 0. \tag{21c}
$$

Here, the following notations are used, whereas the superscript "$(\cdot)^T$" indicates a transposition:

$$c := -\gamma, \tag{22a}$$

$$x := \mu, \tag{22b}$$

$$A := \left(A_1, \ldots, A_B \right)^T, \tag{22c}$$

$$h := -HA, \tag{22d}$$

$$y := \left(y^{L+T}, y^{L-T}, y^{U+T}, y^{U-T}, y^{+L+T}, y^{+L-T}, y^{+U+T}, y^{+U-T}, \right.$$
$$\left. y^{-L+T}, y^{-L-T}, y^{-U+T}, y^{-U-T} \right)^T, \tag{22e}$$

$$T(\omega) := \left(0^T, 0^T, 0^T, -P_0^T(\omega) \right)^T, \tag{22f}$$

$$q := \left(0^T, \tilde{q}^{L\,T}, 0, \tilde{q}^{U\,T}, 0^T, \tilde{q}^{+L\,T}, 0^T, \tilde{q}^{+U\,T}, \right.$$
$$\left. 0^T, \tilde{q}^{-L\,T}, 0^T, \tilde{q}^{-U\,T} \right)^T, \tag{22g}$$

If a more accurate linear approximation of the yield domain is used, the same representation with slightly modified technology and recourse matrices can be achieved.

2 Substitute Problems

The problem in programme (21a–c) is that the vector $T(\omega)$ is random because it includes the stochastic external reference load vector $P_0(\omega)$. Thus, appropriate substitute problems must be formulated.

2.1 Expected Value Problem

A first possibility is to consider the expected value problem (EVP). It is characterized by replacing all stochastic variables just by their expectations. Here, the random vector $T(\omega)$ is replaced by its expectation $\overline{T}$. The rest remains unchanged. Problem (21a–c) turns then to

$$\min c^T x + q^T y \tag{23a}$$
$$\overline{T}x + Wy = h \tag{23b}$$
$$x, y \geq 0 \tag{23c}$$

with

$$\overline{T} = \left(0^T, 0^T, 0^T, E\left(-P_0(\omega)^T \right) \right)^T. \tag{23d}$$

This is a simple linear program with the same size as the original one which can be solved by an ordinary LP-solver.

The disadvantage is that with the resulting optimal load factor the survival condition in only fulfilled on average. Therefore, the design is in general not very robust, because a marginal change of the load may lead to a failure of the structure.

2.2 Recourse Problem with Discretisation

Alternatively it is possible to build the recourse problem (RP) with discretisation of the external reference load distribution $P_0(\omega)$.

Each realisation P_{0r} of $P_0 = P_0(\omega)$ is assumed to be taken with probability p_r, $r = 1, \ldots R$, where R is the number of realisations.

The mathematical formulation of the recourse problem reads then

$$\min E(c^T x + q^T y) = c^T x + \sum_{r=1}^{R} p_r q^T y^r \tag{24a}$$

s.t.

$$
\begin{array}{ll}
T^1 x + W y^1 & = h \\
\vdots \qquad \ddots \qquad \vdots & \\
T^R x + \qquad W y^R = h &
\end{array}
\tag{24b}
$$

$$x, \; y^r \geq 0, \; r = 1, \ldots, R \tag{24c}$$

with

$$T^r = \left(0^T, 0^T, 0^T, P_{0r}^T \right)^T, \; r = 1, \ldots, R. \tag{24d}$$

To have r constraints of the form $Tx + Wy = h$, one for each realisation, is a certain disadvantage of this method since the problem size increases with the number of realisations.

3 Numerical Results

In order to consider the properties of the presented method, the two-storey frame in Fig. 3 with rectangular cross-sectional area $A = b\,h$, with height h and width b is studied.

At first we will study the influence of the height on the limit load analysis. We choose the recourse problem, the first order approximation of the feasible domain, an approximation of the normal distribution with 9 realisations as
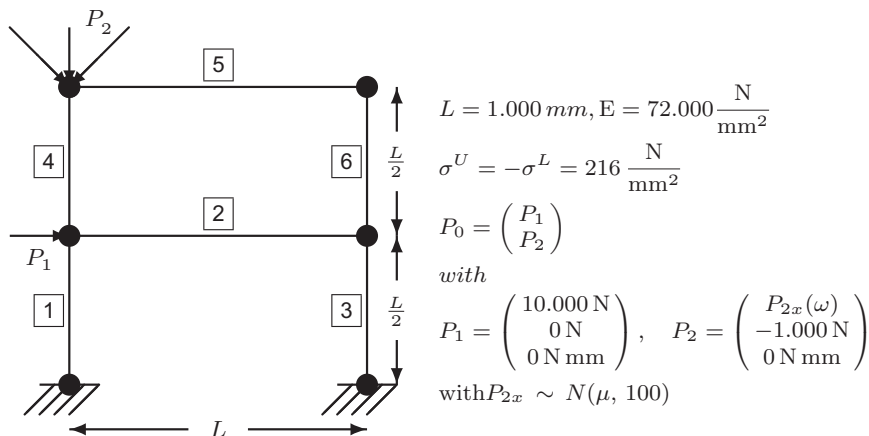
$$L = 1.000\,mm, \mathrm{E} = 72.000\,\frac{\mathrm{N}}{\mathrm{mm}^2}$$

$$\sigma^U = -\sigma^L = 216\,\frac{\mathrm{N}}{\mathrm{mm}^2}$$

$$P_0 = \begin{pmatrix} P_1 \\ P_2 \end{pmatrix}$$

$with$

$$P_1 = \begin{pmatrix} 10.000\,\mathrm{N} \\ 0\,\mathrm{N} \\ 0\,\mathrm{N\,mm} \end{pmatrix}, \quad P_2 = \begin{pmatrix} P_{2x}(\omega) \\ -1.000\,\mathrm{N} \\ 0\,\mathrm{N\,mm} \end{pmatrix}$$

$with P_{2x} \sim N(\mu,\,100)$

Fig. 3 Two-storey frame

shown in Fig. 4, a standard deviation of 100, cost factors of -10, 10,000, resp., and cross-sectional areas of $600\,\mathrm{mm}^2$ for beams 1–3 and $10\,\mathrm{mm}^2$ for beams 4–6 [25].

With increasing height the load factor increases, too, as can be seen in Fig. 5(a).

The reason for this is that with rising height the plastic section modulus increases and therefore the frame can carry bigger forces and moments which leads to a higher load factor. This behaviour is also confirmed regarding to
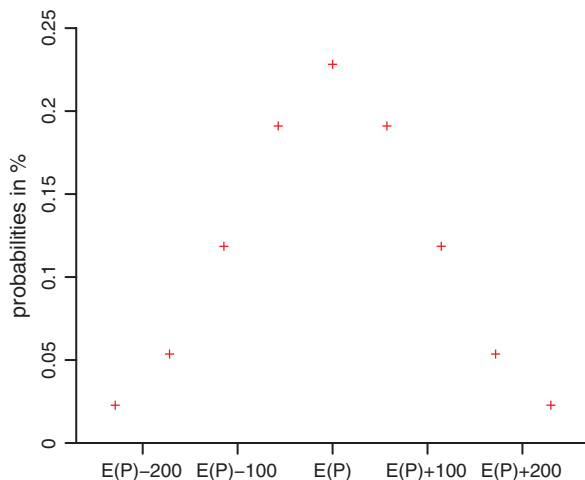

Fig. 4 Discretisation of the normal distribution $N \sim (E(P), 100^2)$ with 9 realisations

(a) Load factor dependent on the height

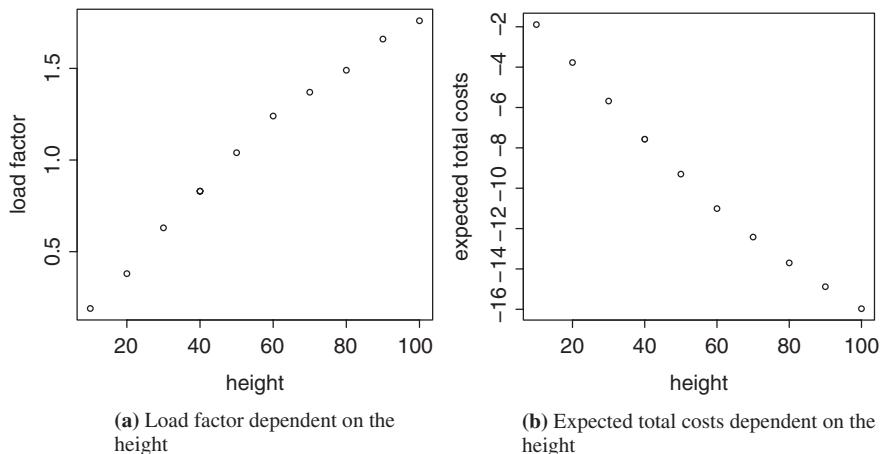**(b)** Expected total costs dependent on the height

Fig. 5 Influence of the height of the cross-sectional area on the load factor and the expected total costs

the expected total costs. They fall in Fig. 5(b) since they depend linearly with negative gradient on the increasing load factor.

With increasing height the cost factors for punishing a failure decrease and therefore a failure is varying very much which can be seen in Fig. 6(a) by regarding the increase of the probability of failure. With it also the penalty costs raise as shown in Fig. 6(b).

(a) Probability of failure dependent on the height

(b) Expected penalty costs dependent on the height
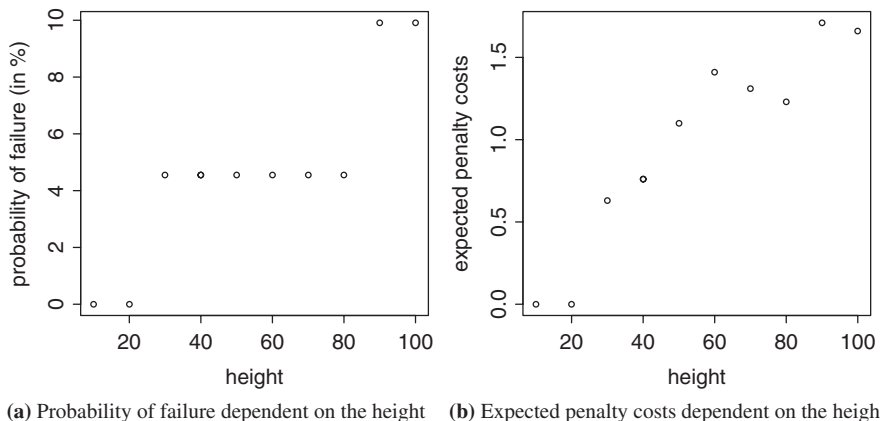
Fig. 6 Influence of the height of the cross-sectional area on the probability of failure and the expected penalty costs

(a) Load factor dependent on the cost factor of first stage

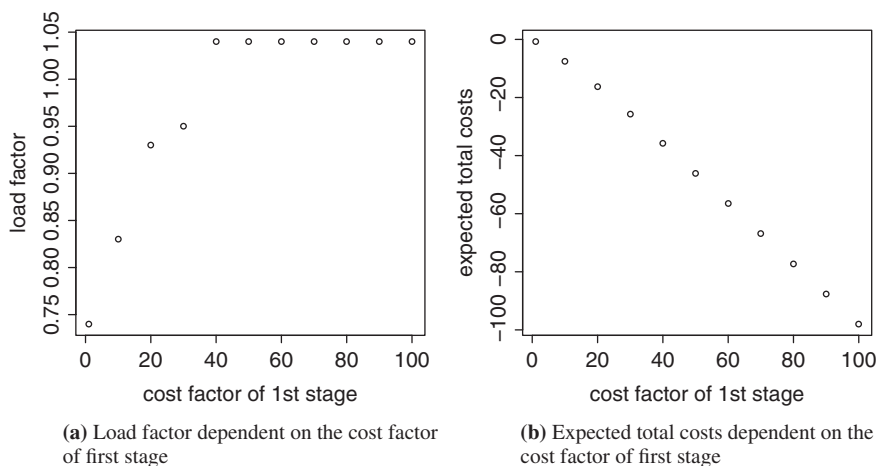**(b)** Expected total costs dependent on the cost factor of first stage

Fig. 7 Influence of the cost factor of first stage on the load factor and the expected total costs

In the following we will study the influence of the cost factors on the limit load analysis. At the beginning, we vary the cost factor of first stage whereas the other quantities are unchanged.

With its increase Figs. 7 and 8 show that nothing happens at the beginning regarding to the load factor, the probability of failure or the expected penalty costs. Only the total costs rise since there is a linear dependence. After the cost factor exceeds a certain limit, the load factor as well as the probability of failure and the expected penalty costs begin falling. That results from the fact that when the cost factor converges to zero, there is hardly any effect
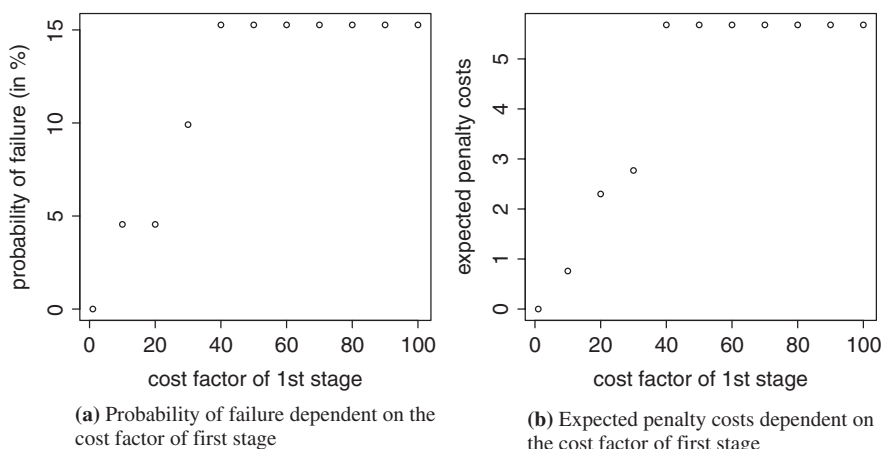

(a) Probability of failure dependent on the cost factor of first stage

(b) Expected penalty costs dependent on the cost factor of first stage

Fig. 8 Influence of the cost factor of first stage on the probability of failure and the exptected penalty costs

of the load factor to the total costs and therefore it is not very important to hold it on a high level. With falling influence of the costs of first stage, the penalty costs get more important and because of that it is tried to reduce them as can be seen in Fig. 8(b). This behaviour is confirmed regarding to the probability of failure and expected penalty costs.

Figure 9(a) shows that with an increase of the penalty cost factor on the other hand the load factor decreases immediately till it reaches a certain limit and with it raise the expected total costs as can be seen in Fig. 9(b).

With an increase of the cost factor of second stage a failure is punished harder. Because of that it is tried to avoid failure which leads to a lower load factor. That is also reflected by considering the probability of failure which, in Fig. 10(a) falls with an increasing penalty cost factor to zero. With it, also the expected penalty costs decrease (see Fig. 10(b)).

In Fig. 11(a) the effects of a modification of the standard deviation on the optimal load factor are presented. It can be seen that it falls with increasing standard deviation. That is not surprising since with rising standard deviation more extreme forces act which lead to a lower load factor. Associated with the decreasing load factor, we notice in Fig. 11(b) that the expected total costs increase since the load factor affects them directly in a negative way.

The probability of failure and therefore also the penalty costs are zero constantly. That shows that increasing uncertainty of the load is compensated completely by a lower load factor so that it has no effect on the failure of the frame.

Now we will study the influence of the cross-sectional areas on the limit load analysis. For that they are scaled equally. For example, the cross-sectional area of the first beam is used for demonstration in Figs. 12 and 13.
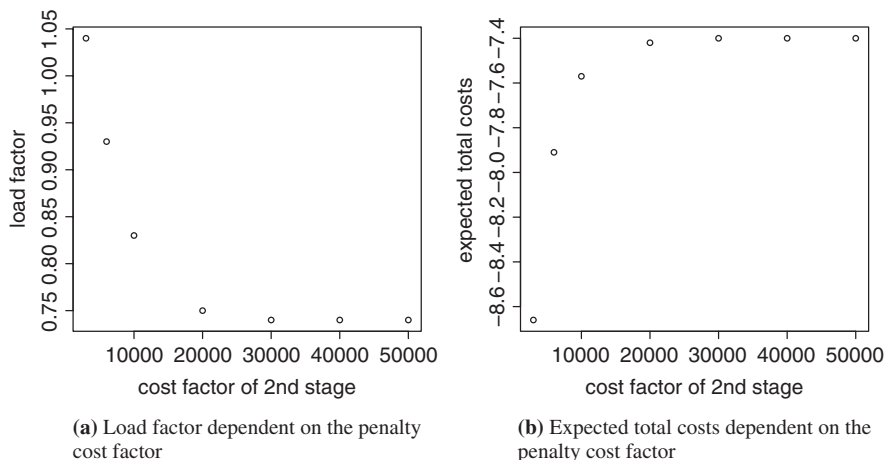

(a) Load factor dependent on the penalty cost factor

(b) Expected total costs dependent on the penalty cost factor

Fig. 9 Influence of the penalty cost factor on the load factor and the exptected total costs

(a) Probability of failure dependent on the penalty cost factor

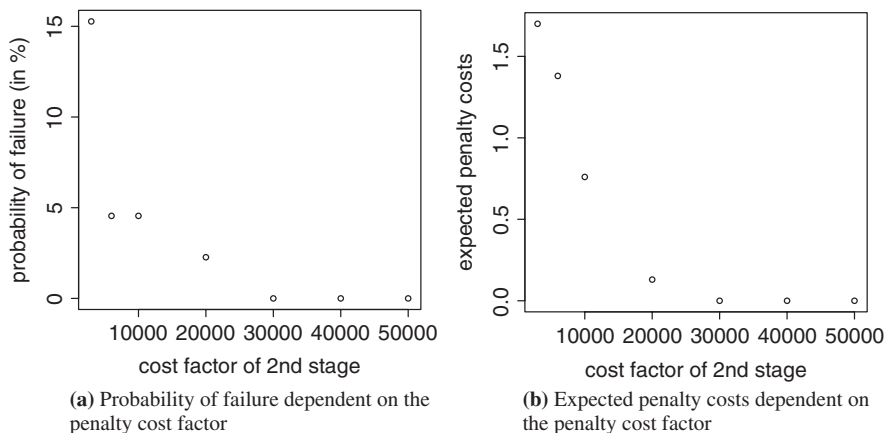**(b)** Expected penalty costs dependent on the penalty cost factor

Fig. 10 Influence of the penalty cost factor on the probability of failure and the expected penalty costs

With its increase the load factor raises in Fig. 12(a), too. That is evident since bigger beams can carry higher forces and moments and therefore the frame can resist higher loads. According to that, the expected total costs decrease in Fig. 12(b) because of the negative influence of the load factor.

The probability of failure and expected penalty costs raise with increasing cross-sectional area till they reach a certain level which is shown in Fig. 13. With increasing cross-sectional area the load factor rises so enormously and that affects the expected total costs so heavily that a failure is accepted. The absolute value of the gradient of the falling costs of first stage has to be therefore greater than the gradient of the increasing penalty costs.
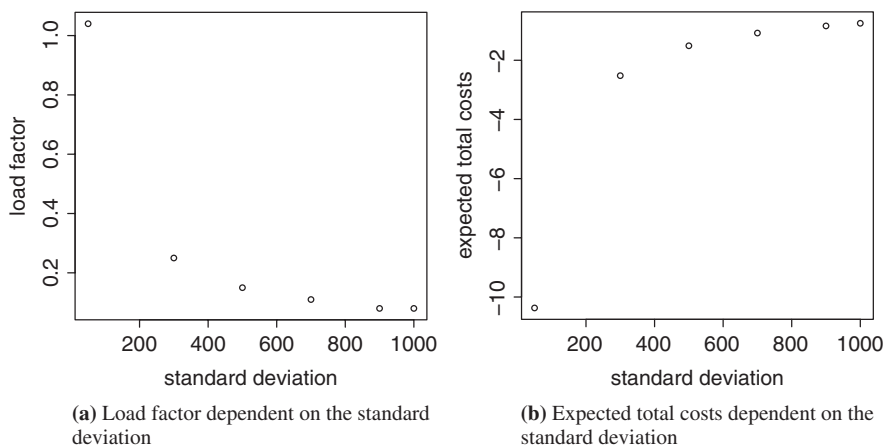

(a) Load factor dependent on the standard deviation

(b) Expected total costs dependent on the standard deviation

Fig. 11 Influence of the standard deviation on the load factor and the expected total costs

(a) Load factor dependent on the cross-sectional areas

(b) Expected total costs dependent on the cross-sectional areas
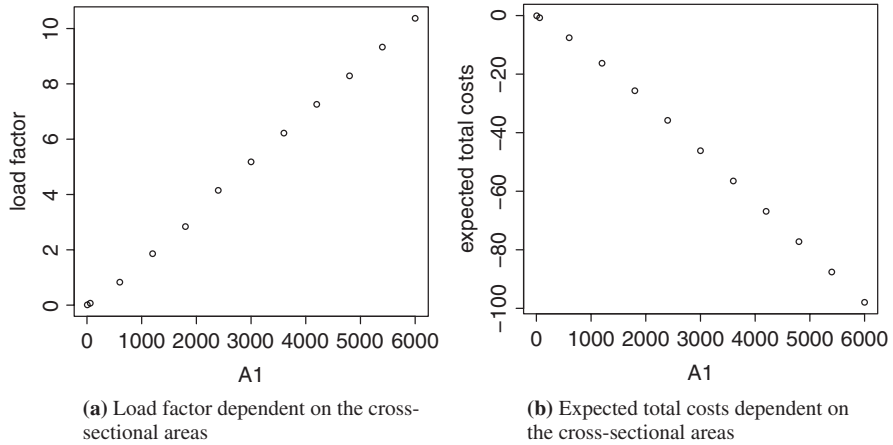
Fig. 12 Influence of the cross-sectional areas on the load factor and the expected total costs with a cost factor ratio 1:1000

If we increase the proportion of the cost factors of second and first stage by changing the cost factor of first stage from -10 to -1 and the one of second stage from 10,000 to 100,000 and carry out the same tests, rising cross-sectional areas lead again to an increase of the load factor and a reduction of the total costs as just described and which is visualised in Fig. 14.

However, the failure is punished so hard that the yield condition is fulfilled in any case and therefore the probability of failure and the penalty costs stay at zero.
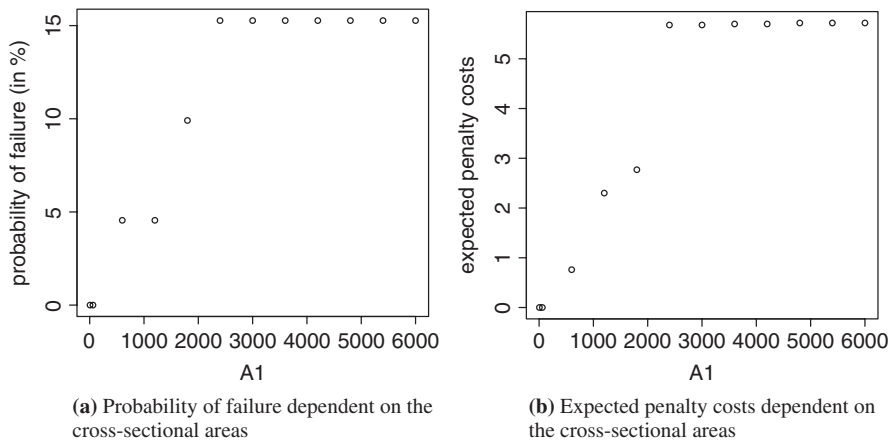

(a) Probability of failure dependent on the cross-sectional areas

(b) Expected penalty costs dependent on the cross-sectional areas

Fig. 13 Influence of the cross-sectional areas on the probability of failure and the expected penalty costs with a cost factor ratio 1:1000

(a) Load factor dependent on the cross-sectional areas

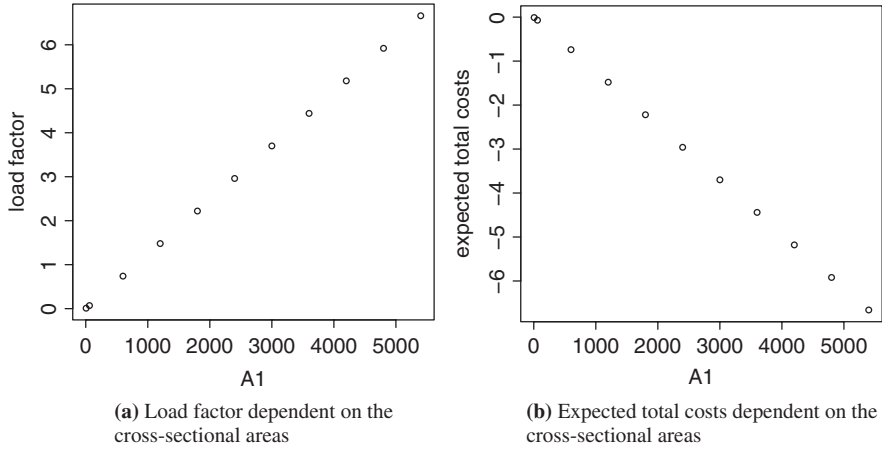**(b)** Expected total costs dependent on the cross-sectional areas

Fig. 14 Influence of the cross-sectional areas on the load factor and the expected total costs with a cost factor ratio 1:100,000

Last but not least we will compare the zero and the first order approximation of the feasible domain. Since the feasible domain corresponding to the first order approximation is a subset of the one of the zero order approximation (see Fig. 2(b)), the conditions are stricter. Therefore the load factor is smaller (see Fig. 15(a)) and the expected total costs are higher which can be confirmed by regarding Fig. 15(b).
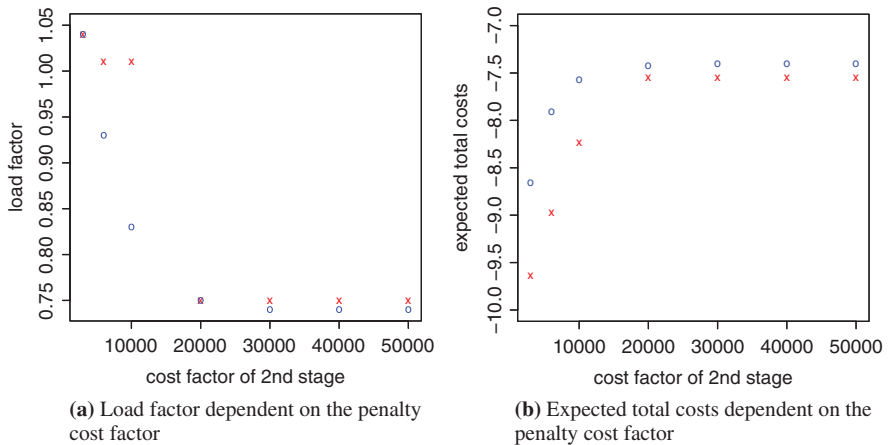

(a) Load factor dependent on the penalty cost factor

(b) Expected total costs dependent on the penalty cost factor

Fig. 15 Comparison of the zero (x) and first (o) order approximation

(a) Load factor dependent on the number of realisations

(b) Probability of failure dependent on the number of realisations
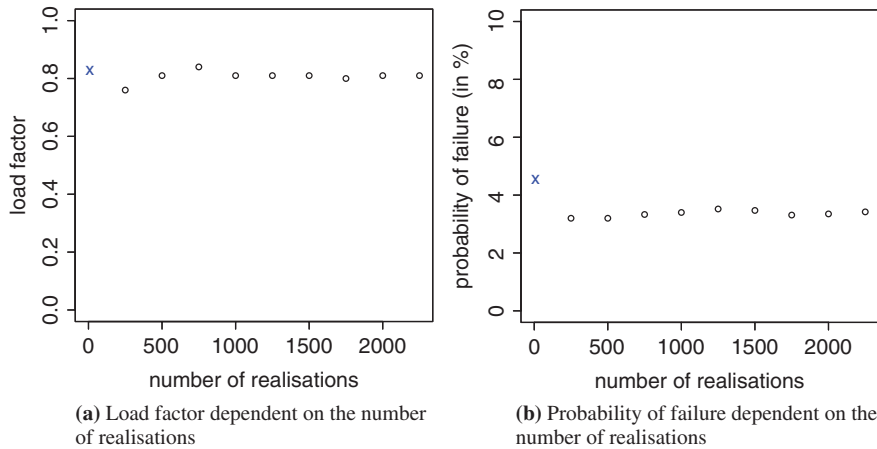
Fig. 16 Influence of the number of realisations on the load factor and the probability of failure – comparison of the results achieved by applying Monte Carlo Method (o) and by approximating the normal distribution (x)

Up to now, the probability of failure has been calculated for the determined nine realisations which have been used to discretise the normal distribution. If one is interested in statements closer to reality, it is a good idea to use the Monte Carlo Method and to increase the number of realisations and not to chose them as a good approximation of the distribution function any longer but to generate them randomly. Here, RANLIB (Library of Fortran Routines for Random Number Generation)[1] has been used to generate normal distributed random variables based on the Forsythe's method [1]. Taking a look at Fig. 16(a), 16(b), resp., we recognize that both the load factor and the probability of failure resulting from Monte Carlo Method (o) hold about the same level as in the case the normal distribution has been approximated (x).

4 Conclusion

Two substitute problems for limit load analysis of plane frames under stochastic uncertainty have been presented, and numerical results of the application of the presented methods to a two-storey frame have been shown. The load factor is positive dependent on the height of the beams, the cost factor of first stage and the cross-sectional areas and negative dependent on the penalty cost factor and the standard deviation. The Monte Carlo Simulation Method has been used as an independent alternative to confirm the results.

---

[1] http://lib.stat.cmu.edu/general/Utexas/ranlib.readme

References

1. Ahrens, J.H., Dieter, U.: Extensions of Forsythe's method for random sampling from the normal distribution. Math. Comput. **27** (124), 927–937 (1973)
2. Charnes, A., Lemke, C.E., Zienkiewicz, O.C.: Virtual work, linear programming and plastic limit analysis. Proc. Roy. Soc. A **25**, 110–116 (1959)
3. Damkilde, L., Kreuk, S.: Limits – A system for limit state analysis and optimal material layout. Comput. Struct. **64** (1–4), 709–718 (1997)
4. Doltsinis, I.: Elements of Plasticity. WIT Press, Ashurst, Southhampton (1999)
5. Gasser, M., Schuëller, G.I.: Some basic principles of reliability-based optimization (RBO) of structures and mechanical components. In: Marti, K., Kall, P. (eds.), Stochastic Programming Methods and Technical Applications, Lecture Notes in Economics and Mathematical Systems (LNEMS) **458**, Springer-Verlag, Berlin/Heidelberg/New York, pp. 80–103 (1998)
6. Gasser, M., Schuëller, G.I.: Reliability-based optimization using approximate methods. In: Marti, K. (ed.), Stochastic Optimization Techniques: Numerical Methods and Technical Applications, Lecture Notes in Economics and Mathematical Systems (LNEMS) **513**, Springer-Verlag, Berlin/Heidelberg/New York, pp. 223–293 (2002)
7. Han, H., Reddy, B.D.: Plasticity – Mathematical Theory and Numerical Analysis. Springer-Verlag, New York (1999)
8. Heitzer, M.: Traglast- und Einspielanalyse zur Bewertung der Sicherheit passiver Komponenten. Dissertation RWTH Aachen (1999)
9. Kaliszky, S.: Plastizitätslehre – Theorie und technische Anwendungen, VDI-Verlag, Düsseldorf (1984)
10. Kall, P.: Stochastic Linear Programming, Springer-Verlag, Berlin/Heidelberg/New York (1976)
11. Kall, P., Wallace, S.W.: Stochastic Programming, John Wiley and Sons Ltd, Chicester (1994)
12. Kirsch, U.: Structural Optimization. Springer-Verlag, Berlin/Heidelberg/New York (1993)
13. König, J.A.: Shakedown of Elastic-Plastic Structures. Elsevier, Amsterdam (1987)
14. Lawo, M.: Optimierung im kunstruktiven Ingenieurbau. Vieweg, Braunschweig/Wiesbaden (1987)
15. Marti, K.: Optimal design of trusses as a stochastic linear programming problem. In: Nowak, A.S. (ed.), Reliability and Optimization of Structural Systems, University of Michigan Press, Ann Arbor, MI, pp. 231–239 (1998)
16. Nielsen, M.P.: Limit Anlaysis and Concrete Plasticity. Prentice Hall, New Jersey (1984)
17. Prager, W. and Shield, R.T.: A general theory of optimal plastic design. J. Appl. Mech. **34** (1), 184–186 (1967)
18. Reckling, K.-A.: Plastizitätstheorie und ihre Anwendung auf Festigkeitsprobleme. Springer-Verlag, Berlin/Heidelberg/New York (1967)
19. Smith, D.L. (ed.): Mathematical Programming Methods in Structural Plasticity. CISM Courses and Lectures **299**, Springer-Verlag, Wien/New York (1990)
20. Smith, D.L., Munro, J.: Plastic analysis and synthesis of frames subject to multiple loadings. Engng. Opt. **2**, 145–157 (1976)
21. Spillers, W.R.: Automated Structural Analysis. Pergamon Press, New York (1972)
22. Stöckl, G.: Optimaler Entwurf elastoplastischer mechanischer Strukturen unter stochastischer Unsicherheit. Fortschritt-Berichte VDI **18 (278)**, VDI-Verlag GbmH, Düsseldorf (2003)
23. Tin-Loi, F.: On the optimal plastic synthesis of frames. Engng. Opt. **16**, 91–108 (1990)
24. Tin-Loi, F.: Plastic limit analysis of plane frames and grids using GAMS. Comput. Struct. **54**, 15–25 (1995)
25. Zier, S.: Optimal design of frames under stochastic uncertainties. PAMM **7**(1), 1061805–1061806 (2007)

Reliability Analysis of Inelastic Shell Structures Under Variable Loads

T.N. Trần, P.T. Phạm, Đ.K. Vũ, and M. Staat

Abstract This paper concerns the application of a new algorithm of probabilistic limit and shakedown analysis for shell structures, in which the loading and strength of the material as well as the thickness of the shell are to be considered as random variables. The procedure involves a deterministic limit and shakedown analysis for each probabilistic iteration, which is based on the kinematical approach and the use of the re-parameterized exact Ilyushin yield surface proposed by Burgoyne and Brennan. The limit state function separating the safe and failure regions is defined directly as the difference between the obtained limit load factor and the current load factor. Different kinds of distribution of basic variables are taken into consideration and performed with First- and Second-Order Reliability Methods (FORM/SORM) for calculation of the failure probability of the structure. A non-linear optimization was implemented, which is based on the Sequential Quadratic Programming for finding the design point. Non-linear sensitivity analyses are also performed for computing the Jacobian and the Hessian of

Thanh Ngọc Trần and Phú Tình Phạm
Aachen University of Applied Sciences, Campus Jülich, Institute of Bioengineering, Ginsterweg 1, D-52428 Jülich, Germany; Hanoi Architectural University, Faculty of Civil Engineering, Km 10, Nguyen Trai Road, Thanh Xuan District, Hanoi, Vietnam, e-mail: tran@fh-aachen.de; pham@fh-aachen.de

Đức Khôi Vũ
Aachen University of Applied Sciences, Campus Jülich, Institute of Bioengineering, Ginsterweg 1, D-52428 Jülich, Germany; University of Erlangen-Nuremberg, Institute of Applied Mechanics, Egerlandstraße 5, D-91058 Erlangen, Germany, e-mail: Vu@ltm.unierlangen.de

Manfred Staat
Aachen University of Applied Sciences, Campus Jülich, Institute of Bioengineering, Ginsterweg 1, D-52428 Jülich, Germany, e-mail: m.staat@fh-aachen.de

the limit state function. This direct approach reduces considerably the necessary knowledge of uncertain technological input data, computing costs and the numerical error. Numerical examples are presented to show the validity and effectiveness of the present method.

1 Introduction

The integrity assessment of pressure vessels and piping by means of direct plasticity methods has been a problem of great interest to many designers, especially in the design of industrial and nuclear power plants. The new European pressure vessel standard EN 13445-3 is based on perfectly plastic limit and shakedown analysis (LISA) [8] thus indicating the industrial need for LISA software for safe and reliable design of such structures. Additionally, practical design codes often prescribe what kind of values to choose for safety factor of the resistance and of the loads for a given problem since all resistance and loading variables are generally random. To this case, structural reliability-based LISA can be performed to establish a rational basis for the choice of safety factors. Probabilistic limit analysis has been proposed earlier for frames using linear programming [2, 15].

The present paper concerns the application of a new upper bound algorithm of probabilistic limit and shakedown analysis for shell structures with the help of the finite element method. Both deterministic and probabilistic limit and shakedown analyses are presented. For the deterministic problem, three failure modes of structure such as plastic collapse, alternating plasticity (low cycle fatigue, LCF) and ratchetting are analyzed based on the upper bound approach. This direct method leads to convex minimum problems which results in a failure mechanism with a unique limit load or shakedown load.

Probabilistic limit and shakedown analysis deals with uncertainties originating from the loads, material strength and thickness of the shell. Based on a direct definition of the limit state function, the calculation of the failure probability may be efficiently solved by using the First- and Second-Order Reliability Methods (FORM/SORM) which are based on the computation of the most probable failure point, the so-called design point. Since the deterministic analysis is a sub-routine of the probabilistic one, even a small error in the deterministic model can lead to a big error in the reliability analysis because of the sensitivity of the failure probability. Due to this reason, a yield criterion which is exact for rigid-perfectly plastic material behaviour and is expressed in terms of stress resultants, namely the exact Ilyushin yield surface, will be applied instead of the simplified Ilyushin yield surface (linear or quadratic approximations). Along similar lines the lower bound probabilistic LISA has been developed for volume elements in a series of papers by Heitzer and Staat [11, 12, 18].

Although the deterministic LISA subproblem has a unique solution it is well known that all possible failure mechanisms contribute to the failure probability [2, 16]. The kinematic or upper bound method may give the exact failure probability only if all mechanisms are considered. In practice often few dominant mechanisms can give reasonable results. In [21] a bulge method proposed in [14] has been applied to the reliability problems of shells which constructs "barriers" around previously found (FORM/SORM) solutions, thus forcing the algorithm to seek a new solution. In this way the complete reliability problem may be solved. For the linear optimization formulation of the static or lower bound approach a different method has been suggested in [4] and extended in [1] for plane frame structures. Here we restrict the presentation to the calculation of the mechanism with the highest probability only.

2 Plastic Dissipation Function in Terms of Strain Resultants

For our purpose of dealing with the reliability problem, the loads, the yield limit σ_y and the thickness h of the shell are considered as random variables. The yield limit can be modeled as stochastic field and discretized through a vector $\mathbf{Y} = [Y_1, Y_2, \ldots, Y_m]^T$ of random variables Y_i at the ith Gaussian point so that $\tilde{\boldsymbol{\sigma}}_y = \mathbf{Y}\sigma_y$. Assuming the yield stress as a random field could render the whole procedure very burdensome. The yield stress can be modeled as a stochastic variable $\sigma_y = Y\sigma_0$ if the Y_i are fully correlated. For simplicity we restrict ourselves to this case with homogeneous material, and shells of constant thickness h. So we can always write

$$\sigma_y = Y\sigma_0, \quad h = Zh_0, \tag{1}$$

where σ_0, h_0 are constant reference values and Y, Z are random variables. Only for the simplicity of the presentation it is assumed that all parts of the shell structure are made from the same material. The software implementation has been made without this restriction.

It is convenient to define the non-dimensional "engineering" stress and strain resultant vectors as follows

$$\tilde{\boldsymbol{\sigma}} = [\boldsymbol{n}\ \boldsymbol{m}]^T, \quad \tilde{\boldsymbol{\varepsilon}} = [\bar{\boldsymbol{e}}\ \boldsymbol{k}]^T, \tag{2}$$

where

$$
\begin{aligned}
\boldsymbol{n} &= \frac{1}{N_0} [N_{11}\quad N_{22}\quad N_{12}]^T, \quad \boldsymbol{m} = \frac{1}{M_0} [M_{11}\quad M_{22}\quad M_{12}]^T, \\
\bar{\boldsymbol{e}} &= \frac{1}{\varepsilon_0} [\bar{\varepsilon}_{11}\quad \bar{\varepsilon}_{22}\quad 2\bar{\varepsilon}_{12}]^T, \quad \boldsymbol{k} = \frac{1}{\kappa_0} [\kappa_{11}\quad \kappa_{22}\quad 2\kappa_{12}]^T,
\end{aligned}
\tag{3}
$$

and $N_0 = \sigma_0 h_0$, $M_0 = \sigma_0 h_0^2/4$, $\varepsilon_0 = \sigma_0(1 - \nu^2)/E$ and $\kappa_0 = 4\varepsilon_0/h_0$ are the normalized quantities. In that way the quadratic strain intensities can be defined by

$$P_\varepsilon = \frac{3}{4} \left(\mathrm{d}\tilde{\varepsilon}^p\right)^T \mathbf{P}_1 \mathrm{d}\tilde{\varepsilon}^p \qquad (\geq 0),$$

$$P_{\varepsilon\kappa} = 3 \left(\mathrm{d}\tilde{\varepsilon}^p\right)^T \mathbf{P}_2 \mathrm{d}\tilde{\varepsilon}^p, \tag{4}$$

$$P_\kappa = 12 \left(\mathrm{d}\tilde{\varepsilon}^p\right)^T \mathbf{P}_3 \mathrm{d}\tilde{\varepsilon}^p \qquad (\geq 0).$$

where $\mathrm{d}\tilde{\varepsilon}^p$ denotes the plastic strain increment resultant vector, $\mathbf{P}$ and its inverse $\mathbf{P}^{-1}$, $\mathbf{P}_i (i = 1, 2, 3)$ are

$$\mathbf{P} = \begin{pmatrix} 1 & -1/2 & 0 \\ -1/2 & 1 & 0 \\ 0 & 0 & 3 \end{pmatrix}, \quad \mathbf{P}^{-1} = \begin{pmatrix} 4/3 & 2/3 & 0 \\ 2/3 & 4/3 & 0 \\ 0 & 0 & 1/3 \end{pmatrix},$$

$$\mathbf{P}_1 = \begin{pmatrix} \mathbf{P}^{-1} & \mathbf{0} \\ \mathbf{0} & \mathbf{0} \end{pmatrix}, \quad \mathbf{P}_2 = \begin{pmatrix} \mathbf{0} & \mathbf{P}^{-1}/2 \\ \mathbf{P}^{-1}/2 & \mathbf{0} \end{pmatrix}, \quad \mathbf{P}_3 = \begin{pmatrix} \mathbf{0} & \mathbf{0} \\ \mathbf{0} & \mathbf{P}^{-1} \end{pmatrix}. \tag{5}$$

Ilyushin [13] derived an exact form of the yield surface in terms of the stress resultant for a linear elastic-perfectly plastic isotropic material which obeys the von Mises criterion. A simpler form of this yield surface (though still exact) was proposed by Burgoyne and Brennan [3] by introducing the parameters

$$\upsilon = \frac{P_\varepsilon}{P_\kappa}, \beta = -\frac{P_{\varepsilon\kappa}}{P_\kappa} \quad \text{and} \quad \gamma = \upsilon - \beta^2, \tag{6}$$

where β and γ are proposed as two independent parameters for the description of the yield surface. With these parameters, the plastic dissipation function for a shell structure may be written in the form [20, 21]

$$D^p(\dot{\tilde{\varepsilon}}) = Y N_0 \varepsilon_0 \sqrt{\frac{P_\kappa}{3}} \left(\beta_1 \sqrt{\beta_1^2 + \gamma} + \beta_2 \sqrt{\beta_2^2 + \gamma} + \gamma K_0 \right), \tag{7}$$

where β_1, β_2 and K_0 are

$$\beta_1 = \frac{Z}{2} - \beta, \quad \beta_2 = \frac{Z}{2} + \beta, \quad K_0 = \ln \left(\frac{\sqrt{\beta_1^2 + \gamma} + \beta_1}{\sqrt{\beta_2^2 + \gamma} - \beta_2} \right). \tag{8}$$

It should be noted here, that the value of K_0 will become indefinite if both conditions $|\beta| \leq 0.5Z$ and $\gamma = 0$ are fulfilled. However, as long as γ is not exactly equal to zero, but assumes to some small positive number, a "regularized" evaluation of K_0 may be obtained [17]. Otherwise, in general, D^p is convex [5] but not everywhere differentiable as shown for continuum problems. It is only differentiable in the plastified region of the structure, i.e. $P_\kappa > 0$. In order to allow a direct non-linear, non-smooth, constrained

optimization problem, a "smooth regularization method" should be used to overcome the non-differentiability of the objective function as will be discussed in the following section.

3 Deterministic Limit and Shakedown Algorithm

Consider a convex polyhedral load domain $\mathcal{L}$ and a special loading path consisting of all load vertices $\hat{P}_k$ $(k = 1, \ldots, m)$ of $\mathcal{L}$. Let the fictitious elastic generalized stress vector be denoted by $\boldsymbol{\sigma}$. By discretizing the whole structure with the help of finite elements and the application of Koiter's theorem, the shakedown limit $\alpha_{\lim}$, which is the smaller one of the low cycle fatigue limit and the ratchetting limit, may be found by the following minimization

$$\alpha_{\lim} = \min \sum_{i=1}^{NG} \sum_{k=1}^{m} w_i Y N_0 \varepsilon_0 \sqrt{\frac{P_\kappa}{3}} \left(\beta_1 \sqrt{\beta_1^2 + \gamma} + \beta_2 \sqrt{\beta_2^2 + \gamma} + \gamma K_0 \right),$$

$$\text{s.t.} : \begin{cases} \sum_{k=1}^{m} \dot{\tilde{\varepsilon}}_{ik} = \mathbf{B}_i \dot{\boldsymbol{u}} & \forall i = 1, \ldots, NG, \\ \sum_{i=1}^{NG} \sum_{k=1}^{m} w_i N_0 \varepsilon_0 \dot{\tilde{\mathbf{e}}}_{ik}^T \tilde{\boldsymbol{\sigma}}_{ik}^E = 1, \end{cases} \tag{9}$$

in which $\dot{\boldsymbol{u}}$ denotes the velocity fields, $\mathbf{B}_i$ denotes the deformation matrix, and w_i is the weighting factor of the ith Gauss point $(i = 1, \ldots, NG)$. For the sake of simplicity some new notations are introduced

$$\dot{\mathbf{e}}_{ik} = w_i \dot{\tilde{\varepsilon}}_{ik}, \quad \mathbf{t}_{ik} = N_0 \varepsilon_0 \tilde{\boldsymbol{\sigma}}_{ik}^E, \quad \hat{\mathbf{B}}_i = w_i \mathbf{B}_i, \tag{10}$$

where $\dot{\mathbf{e}}_{ik}, \mathbf{t}_{ik}, \hat{\mathbf{B}}_i$ are the new strain rate vector, the new fictitious elastic stress vector and the new deformation matrix, respectively. By substituting (10) into (9) we obtain a simplified version for the upper bound shakedown analysis

$$\alpha_{\lim} = \min \sum_{i=1}^{NG} \sum_{k=1}^{m} Y N_0 \varepsilon_0 \sqrt{\frac{P_\kappa}{3}} \left(\beta_1 \sqrt{\beta_1^2 + \gamma} + \beta_2 \sqrt{\beta_2^2 + \gamma} + \gamma K_0 \right),$$

$$\text{s.t.} : \begin{cases} \sum_{k=1}^{m} \dot{\mathbf{e}}_{ik} = \hat{\mathbf{B}}_i \dot{\boldsymbol{u}} & \forall i = 1, \ldots, NG, \\ \sum_{i=1}^{NG} \sum_{k=1}^{m} \dot{\mathbf{e}}_{ik}^T \mathbf{t}_{ik} = 1. \end{cases} \tag{11}$$

To eliminate the first optimization constraint a penalty method is used. To this purpose, let us write the penalty function as

$$F_P = \sum_{i=1}^{NG} \left\{ \begin{array}{l} \sum_{k=1}^{m} \left(Y N_0 \varepsilon_0 \sqrt{\frac{P_\kappa}{3}} \left(\beta_1 \sqrt{\beta_1^2 + \gamma} + \beta_2 \sqrt{\beta_2^2 + \gamma} + \gamma K_0 \right) \right) \\ + \frac{c}{2} \left(\sum_{k=1}^{m} \dot{e}_{ik} - \hat{\mathbf{B}}_i \dot{\boldsymbol{u}} \right)^T \left(\sum_{k=1}^{m} \dot{e}_{ik} - \hat{\mathbf{B}}_i \dot{\boldsymbol{u}} \right) \end{array} \right\}$$

$$= \sum_{i=1}^{NG} \left\{ \sum_{k=1}^{m} (Y \eta_{ik}) + \frac{c}{2} \left(\sum_{k=1}^{m} \dot{e}_{ik} - \hat{\mathbf{B}}_i \dot{\boldsymbol{u}} \right)^T \left(\sum_{k=1}^{m} \dot{e}_{ik} - \hat{\mathbf{B}}_i \dot{\boldsymbol{u}} \right) \right\}, \tag{12}$$

where c is a penalty parameter such that $c \gg 1$. For the sake of simplicity, the same value of c is assumed at every Gauss point of the structure. The second constraint can be eliminated by using the dual Lagrange function

$$F_{PL} = F_P - \lambda \left(\sum_{i=1}^{NG} \sum_{k=1}^{m} \dot{e}_{ik}^T t_{ik} - 1 \right), \tag{13}$$

where λ is the Lagrange multiplier. The major numerical obstacle appears here due to the non-differentiability of the objective function F_{PL} and the singularity of K_0 as discussed in Sect. 2. A regularization method can be used here by replacing the original plastic dissipation function $D^p(\dot{\hat{\boldsymbol{\varepsilon}}}^p)$ by its disturbed one $D^p(\dot{\hat{\boldsymbol{\varepsilon}}}^p, \eta_0^2)$. In the new plastic dissipation function $D^p(\dot{\hat{\boldsymbol{\varepsilon}}}^p, \eta_0^2)$, η_0^2 is a small positive number which is added to γ and P_κ, i.e. $\gamma \to \gamma + \eta_0^2$ and $P_\kappa \to P_\kappa + \eta_0^2$. In this way, all elements in the structure are seen as plastified or on the plastified verge.

By applying Newton's method to solve the KKT conditions of Eq. (13) we obtain the Newton directions $d\dot{\boldsymbol{u}}$ and $d\dot{\hat{\boldsymbol{\varepsilon}}}_{ik}$, which assure that a suitable step along them will lead to a decrease of the objective function α_{lim}. If the relative improvement between two steps is smaller than a given constant, the algorithm stops and leads to the shakedown limit factor. Details of the iterative algorithm can be found in [20, 21].

4 Probabilistic Limit and Shakedown Algorithm

Denote by $\mathbf{X} = (X_1, X_1, \ldots, X_n)$ an n-dimensional random vector characterizing uncertainties in the structure and load parameters. The limit state function $g(\mathbf{x}) = 0$, which is based on the comparison of a structural resistance (threshold) and loading, defines the limit state hyper-surface ∂F which separates the failure region $F = \{ \mathbf{x} | g(\mathbf{x}) < 0 \}$ from the safe region. The failure probability P_f is the probability that $g(\mathbf{X})$ is non-positive, i.e.

$$P_f = P(g(\mathbf{X}) \le 0) = \int_F f_X(\mathbf{x}) dx, \tag{14}$$

where $f_X(\mathbf{x})$ is the n-dimensional joint probability density function. Usually, it is not possible to calculate P_f analytically since the form of the limit state surface is very complex. For the general cases, there are several approximate methods to compute the failure probability P_f. Direct Monte Carlo Simulation (MCS) becomes increasingly expensive with the increase of the structural reliability. Acceptable failure probabilities might be in the range of 10^{-4} to 10^{-6}. They are even much lower in nuclear reactor technology. For a validation that the failure probability P_f is less than an accepted limit P_c, the sample size required for direct (MCS) must be at least $100/P_c$ leading to a minimum sample size in the range of 10^6 to 10^8. Such a large number exceeds particularly for complex FE-models available resources by far. The numerical effort can be reduced considerably by variance reduction methods like Importance Sampling and by Response Surface Methods (RSM). However, the most effective analysis is based on First- and Second-Order Reliability Methods (FROM/SORM) if gradient information is available [9].

4.1 First- and Second-Order Reliability Methods

(FROM/SORM) (alternatively referred as the most likely failure point method) is used here to perform uncertainty analysis. Practical experience with (FROM/SORM)algorithms indicates that their estimates usually provide satisfactory reliability measures. Especially in the case of small failure probability (large reliability), (FROM/SORM) are extremely efficient compared with the (MCS) method regarding the requirement of computer time, such as the Central Processing Unit (CPU). In (FROM/SORM) the probability of failure is computed in three steps. Firstly the physical space $\mathbf{x}$ of uncertain parameters, $\mathbf{X}$, is transformed into a new n-dimensional space, $\mathbf{u}$, consisting of independent standard Gaussian variables $\mathbf{U}$. By this transformation, the original limit state $g(\mathbf{x}) = 0$ is mapped into the new limit state $g(\mathbf{u}) = 0$ in the $\mathbf{u}$ space. Secondly the design point or β_{HL}-point is determined by an appropriate non-linear optimization algorithm. This is the point on the limit state surface having the shortest distance to the origin in the $\mathbf{u}$ space. Due to the rotational symmetry and exponential decay of the probability density, the design point has the highest probability among all points in the failure domain. It follows that the neighbourhood of this point makes the dominant contribution to the failure probability. Details of the non-linear optimization algorithm for finding the design point which is based on the sequential quadratic programming (SQP) can be found in [20,21]. Thirdly the limit state surface $g(\mathbf{u}) = 0$ is approximated by a tangential hypersurface at the design point. This corresponds to an approximating hyperplane $g_L(\mathbf{u}) = 0$ (linear or first-order) and hyperparaboloid $g_Q(\mathbf{u}) = 0$ (quadratic or second-order), respectively (see Fig. 1). The failure probability P_f is thus approximated by $P_{f,L} = P\left(g_L\left(\mathbf{u}\right) < 0\right)$ in FORM

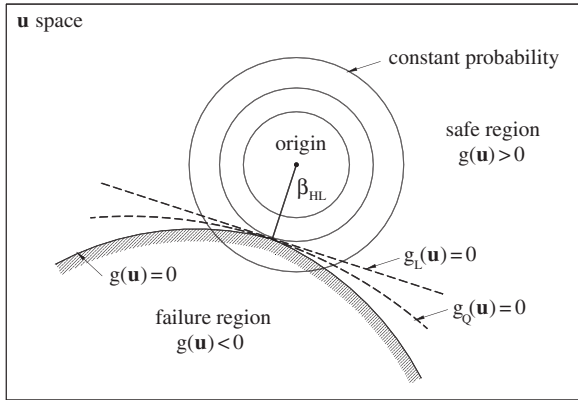**Fig. 1** Safe and failure regions based on linear and quadratic approximations in **u** space

$$P_{f,L} = \Phi(-\beta_{HL}) = \frac{1}{\sqrt{2\pi}} \int\limits_{-\infty}^{-\beta_{HL}} e^{-0.5z^2} \mathrm{d}z, \tag{15}$$

and by $P_{f,Q} = P\left(g_Q\left(\mathbf{u}\right) < 0\right)$ in SORM [10, 22]

$$P_{f,Q} = S_1 + S_2 + S_3, \tag{16}$$

with

$$S_1 = \Phi\left(-\beta_{HL}\right) \prod_{j=1}^{n-1} \left(1 - \beta_{HL}\kappa_j\right)^{-1/2},$$

$$S_2 = \left[\beta_{HL}\Phi\left(-\beta_{HL}\right) - \phi\left(\beta_{HL}\right)\right]$$

$$\left\{\prod_{j=1}^{n-1} \left(1 - \beta_{HL}\kappa_j\right)^{-1/2} - \prod_{j=1}^{n-1} \left(1 - \left(\beta_{HL} + 1\right)\kappa_j\right)^{-1/2}\right\},$$

$$S_3 = \left(\beta_{HL} + 1\right)\left[\beta_{HL}\Phi\left(-\beta_{HL}\right) - \phi\left(\beta_{HL}\right)\right] \times$$

$$\left\{\prod_{j=1}^{n-1} \left(1 - \beta_{HL}\kappa_j\right)^{-1/2} - \mathrm{Re}\left[\prod_{j=1}^{n-1} \left(1 - \left(\beta_{HL} + i\right)\kappa_j\right)^{-1/2}\right]\right\},$$

with κ_j are $n-1$ principle curvatures at the design point. The calculation of κ_j normally needs the second derivatives of the limit state function.

4.2 Definition of the Limit State Function

The shakedown load factor α_{lim} which is calculated by the constraint minimum problem (11) defines the ratio between the shakedown load P_{lim} and actual load P of the structure, i.e.

$$\alpha_{\text{lim}} = \frac{P_{\text{lim}}}{P}. \tag{17}$$

As mentioned above, the limit state function contains the parameters of structural resistance and loading. Thus it can be defined as $g = P_{\text{lim}} - P = P(\alpha_{\text{lim}} - 1)$. For the sake of simplicity, the limit state function g can be normalized with the actual load P and then becomes

$$g = \alpha_{\text{lim}} - 1. \tag{18}$$

It can be seen that the limit state function is a function of the load, the random variables yield stress and thickness. The actual load P is defined in n components by using the concept of a constant reference load P^0 as follows

$$\begin{aligned} P^0 &= P_1^0 + P_2^0 + \ldots + P_n^0, \\ P &= x_1 P_1^0 + x_2 P_2^0 + \ldots + x_n P_n^0, \end{aligned} \tag{19}$$

where x_j is the realization of the jth basic load variable X_j $(j = 1, n)$. The corresponding actual fictitious elastic stress fields $\tilde{\boldsymbol{\sigma}}^E$ can also be described in the same way

$$\tilde{\boldsymbol{\sigma}}^E = x_1 \tilde{\boldsymbol{\sigma}}_1^0 + x_2 \tilde{\boldsymbol{\sigma}}_2^0 + \ldots + x_n \tilde{\boldsymbol{\sigma}}_n^0. \tag{20}$$

From (19) and (20), the corresponding normalized fictitious elastic stress fields $\mathbf{t}$ are obtained

$$\mathbf{t} = N_0 \varepsilon_0 \tilde{\boldsymbol{\sigma}} = N_0 \varepsilon_0 \left[x_1 \tilde{\boldsymbol{\sigma}}_1^0 + x_2 \tilde{\boldsymbol{\sigma}}_2^0 + \ldots + x_n \tilde{\boldsymbol{\sigma}}_n^0 \right] = x_1 \mathbf{t}_1 + x_2 \mathbf{t}_2 + \ldots + x_n \mathbf{t}_n. \tag{21}$$

4.3 Sensitivity Analyses

The sensitivity analyses provide the Jacobian and the Hessian of the limit state function, $\partial g / \partial \mathbf{x}$ and $\partial^2 g / \partial \mathbf{x}^2$, which are needed for the SQP, FORM and SORM algorithms. They also provide a quantitative measure of the first- and second-order change in the optimal value function or show how the solution is affected by changes in the problem data. The necessary data for the

calculation of the Jacobian and the Hessian are available after the execution of the deterministic shakedown analysis since they are based on the limit load factor $\alpha_{\lim}$.

In order to get the sensitivity of the limit state function g in the physical space $\mathbf{x}$, one requirement from Eq. (18) is that the derivatives of the limit load factor $\alpha_{\lim}$ must be available. Let $(\dot{\mathbf{e}}_{ik}^*, \mathbf{u}^*, \lambda^*)$ be the solutions of the optimization problem (11). At the optimal point, the first derivative of the limit load factor $\alpha_{\lim}$ versus the jth load variable X_j and the yield stress variable Y can be calculated as follows [20, 21]

$$\frac{\partial \alpha_{\lim}}{\partial X_j} = \frac{\partial F_{PL}}{\partial X_j}\bigg|_{(\dot{\mathbf{e}}_{ik}^*, \mathbf{u}^*, \lambda^*)} = -\lambda \sum_{i=1}^{NG} \sum_{k=1}^{m} \dot{\mathbf{e}}_{ik}^T \frac{\partial \mathbf{t}_{ik}}{\partial X_j}\bigg|_{(\dot{\mathbf{e}}_{ik}^*, \lambda^*)}$$

$$= -\lambda \sum_{i=1}^{NG} \sum_{k=1}^{m} \dot{\mathbf{e}}_{ik}^T \mathbf{t}_{ik,j}\bigg|_{(\dot{\mathbf{e}}_{ik}^*, \lambda^*)}, \tag{22}$$

$$\frac{\partial \alpha_{\lim}}{\partial Y} = \frac{\partial F_{PL}}{\partial Y}\bigg|_{(\dot{\mathbf{e}}_{ik}^*, \mathbf{u}^*, \lambda^*)} = \frac{\partial}{\partial Y}\left(\sum_{i=1}^{NG} \sum_{k=1}^{m} Y \eta_{ik}\right)\bigg|_{(\dot{\mathbf{e}}_{ik}^*)}$$

$$= \sum_{i=1}^{NG} \sum_{k=1}^{m} \eta_{ik}^* = \frac{\alpha_{\lim}}{Y}. \tag{23}$$

The derivatives of the limit load factor $\alpha_{\lim}$ versus the random thickness variable Z can be determined in the same way assuming the form

$$\frac{\partial \alpha_{\lim}}{\partial Z} = \frac{\partial F_{PL}}{\partial Z}\bigg|_{(\dot{\mathbf{e}}_{ik}^*, \mathbf{u}^*, \lambda^*)}$$

$$= \frac{\partial}{\partial Z}\left(\sum_{i=1}^{NG} \sum_{k=1}^{m}\left(Y N_0 \varepsilon_0 \sqrt{\frac{P_k}{3}}\left(\beta_1 \sqrt{\beta_1^2 + \gamma} + \beta_2 \sqrt{\beta_2^2 + \gamma} + \gamma K_0\right)\right)\right)\bigg|_{\dot{\mathbf{e}}_{ik}^*}$$

$$= \sum_{i=1}^{NG} \sum_{k=1}^{m}\left(Y N_0 \varepsilon_0 \sqrt{\frac{P_k}{3}}\left(\sqrt{\beta_1^2 + \gamma} + \sqrt{\beta_2^2 + \gamma}\right)\right)\bigg|_{\dot{\mathbf{e}}_{ik}^*}. \tag{24}$$

The second partial derivatives of the limit state function versus the jth load variable X_j and the yield stress variable Y can be obtained directly from an analytical derivation of the first derivatives [20, 21]

$$\frac{\partial^2 \alpha_{\lim}}{\partial X_l X_j} = \frac{\partial}{\partial X_l} \left(-\lambda \sum_{i=1}^{NG} \sum_{k=1}^{m} \dot{\mathbf{e}}_{ik}^T \mathbf{t}_{ik,j} \right) \Bigg|_{\left(\dot{\mathbf{e}}_{ik}^*, \lambda^* \right)}$$

$$= -\frac{\partial \lambda}{\partial X_l} \sum_{i=1}^{NG} \sum_{k=1}^{m} \dot{\mathbf{e}}_{ik}^T \mathbf{t}_{ik,j} \Bigg|_{\left(\dot{\mathbf{e}}_{ik}^*, \lambda^* \right)} - \lambda \sum_{i=1}^{NG} \sum_{k=1}^{m} \mathbf{t}_{ik,j}^T \frac{\partial \dot{\mathbf{e}}_{ik}}{\partial X_l} \Bigg|_{\left(\dot{\mathbf{e}}_{ik}^*, \lambda^* \right)}, \tag{25}$$

$$\frac{\partial^2 \alpha_{\lim}}{\partial Y^2} = \frac{\partial}{\partial Y} \left(\frac{\alpha_{\lim}}{Y} \right) \Bigg|_{\dot{\mathbf{e}}_{ik}^*} = \left(\frac{1}{Y} \frac{\partial \alpha_{\lim}}{\partial Y} - \frac{\alpha_{\lim}}{Y^2} \right) \Bigg|_{\dot{\mathbf{e}}_{ik}^*} = \left(\frac{1}{Y} \frac{\alpha_{\lim}}{Y} - \frac{\alpha_{\lim}}{Y^2} \right) \Bigg|_{\dot{\mathbf{e}}_{ik}^*} = 0, \tag{26}$$

where

$$\frac{\partial \dot{\mathbf{e}}_{ik}}{\partial X_l} = \mathbf{G}_{ik}^{-1} \mathbf{t}_{ik} \frac{\partial \lambda}{\partial X_l} + \lambda \mathbf{G}_{ik}^{-1} \mathbf{t}_{ik,l}, \qquad \frac{\partial \lambda}{\partial X_l} = \frac{\dfrac{1}{\lambda} \dfrac{\partial \alpha_{\lim}}{\partial X_l} - \lambda \sum\limits_{i=1}^{NG} \sum\limits_{k=1}^{m} \mathbf{t}_{ik}^T \mathbf{G}_{ik}^{-1} \mathbf{t}_{ik,l}}{\sum\limits_{i=1}^{NG} \sum\limits_{k=1}^{m} \mathbf{t}_{ik}^T \mathbf{G}_{ik}^{-1} \mathbf{t}_{ik}}, \tag{27}$$

with $\mathbf{G}_{ik} = \partial^2 F_{PL} / \partial \dot{\mathbf{e}}_{ik}^2$. It can be seen from (26) that the limit state function is a linear function of the yield stress variable Y. In the case of a heterogeneous material, we will obtain at different Gaussian points i eventually different yield stress variables Y_i. Then the limit state function is no more a linear function of these variables.

The second derivatives of $\alpha_{\lim}$ versus the thickness variable Z are obtained by taking the derivatives of Eqs. (22), (23) and (24), versus Z, which gives

$$\frac{\partial^2 \alpha_{\lim}}{\partial X_j \partial Z} = -\frac{\partial \lambda}{\partial Z} \sum_{i=1}^{NG} \sum_{k=1}^{m} \dot{\mathbf{e}}_{ik}^T \mathbf{t}_{ik,j} \Bigg|_{\left(\dot{\mathbf{e}}_{ik}^*, \lambda^* \right)} - \lambda \sum_{i=1}^{NG} \sum_{k=1}^{m} \mathbf{t}_{ik,j}^T \frac{\partial \dot{\mathbf{e}}_{ik}}{\partial Z} \Bigg|_{\left(\dot{\mathbf{e}}_{ik}^*, \lambda^* \right)}, \tag{28}$$

$$\frac{\partial^2 \alpha_{\lim}}{\partial Y \partial Z} = \sum_{i=1}^{NG} \sum_{k=1}^{m} \left(N_0 \varepsilon_0 \sqrt{\frac{P_k}{3}} \left(\sqrt{\beta_1^2 + \gamma} + \sqrt{\beta_2^2 + \gamma} \right) \right) \Bigg|_{\dot{\mathbf{e}}_{ik}^*}, \tag{29}$$

$$\frac{\partial^2 \alpha_{\lim}}{\partial Z^2} = \left\{ \sum_{i=1}^{NG} \sum_{k=1}^{m} \frac{\sqrt{3}}{4\sqrt{P_k}} Y N_0 \varepsilon_0 \left(\frac{\partial \dot{\mathbf{e}}_{ik}}{\partial Z} \right)^T \times \left\{ \left[16 \left(\sqrt{\beta_1^2 + \gamma} + \sqrt{\beta_2^2 + \gamma} \right) \mathbf{P}_3 + 8 \left(\frac{\beta_1}{\sqrt{\beta_1^2 + \gamma}} - \frac{\beta_2}{\sqrt{\beta_2^2 + \gamma}} \right) \mathbf{A} \right. \right. \right.$$
$$\left. \left. \left. + \left(\frac{1}{\sqrt{\beta_1^2 + \gamma}} + \frac{1}{\sqrt{\beta_2^2 + \gamma}} \right) \mathbf{B} \right] \dot{\mathbf{e}}_{ik} \right\} \right\}_{\dot{\mathbf{e}}_{ik}^*} \tag{30}$$

$$+ \sum_{i=1}^{NG} \sum_{k=1}^{m} \left(Y N_0 \varepsilon_0 \sqrt{\frac{P_k}{3}} \left(\frac{\beta_1}{2\sqrt{\beta_1^2 + \gamma}} + \frac{\beta_2}{2\sqrt{\beta_2^2 + \gamma}} \right) \right) \Bigg|_{\dot{\mathbf{e}}_{ik}^*},$$

where

$$A = \mathbf{P}_2 + 4\beta\mathbf{P}_3,$$
$$B = \mathbf{P}_1 + 8\beta\mathbf{P}_2 - 16\left(\gamma - \beta^2\right)\mathbf{P}_3. \tag{31}$$

The derivatives of λ and $\dot{e}_{ik}$ versus Z are obtained in the following way. Firstly differentiate the Lagrange function F_{PL} in Eq. (13) versus $\dot{\mathbf{e}}_{ik}$, then taking derivatives of the obtained result $\partial^2 F_{PL}/\partial\dot{\mathbf{e}}_{ik}$ versus Z and using the chain rule for two variables $\dot{e}_{ik}, \lambda$. After some manipulations one has

$$\frac{\partial \dot{e}_{ik}}{\partial Z} = G_{ik}^{-1} t_{ik} \frac{\partial \lambda}{\partial Z} - \frac{1}{\sqrt{\hat{P}_\kappa}} G_{ik}^{-1} \frac{\partial H_{ik}}{\partial Z} \dot{e}_{ik}, \tag{32}$$

$$\frac{\partial \lambda}{\partial Z} = \frac{\sum\limits_{i=1}^{NG} \sum\limits_{k=1}^{m} \frac{1}{\sqrt{\hat{P}_\kappa}} t_{ik}^T G_{ik}^{-1} \frac{\partial H_{ik}}{\partial Z} \dot{e}_{ik}}{\sum\limits_{i=1}^{NG} \sum\limits_{k=1}^{m} t_{ik}^T G_{ik}^{-1} t_{ik}}, \tag{33}$$
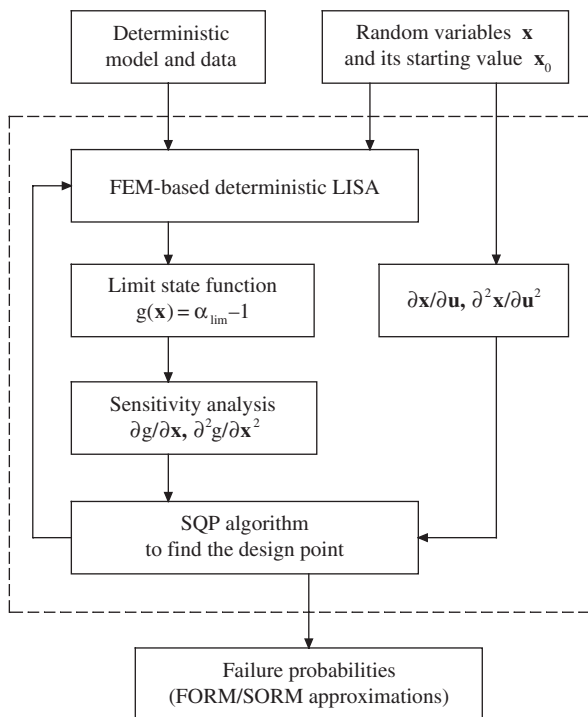

Fig. 2 Flowchart of the probabilistic limit and shakedown analysis

with

$$\frac{\partial H_{ik}}{\partial Z} = Y \tilde{N}_0 \tilde{\varepsilon}_0 \begin{pmatrix} 4\sqrt{3} \left(\sqrt{\beta_1^2 + \gamma} + \sqrt{\beta_2^2 + \gamma} \right) \mathbf{P}_3 \\ +2\sqrt{3} \left(\frac{\beta_1}{\sqrt{\beta_1^2 + \gamma}} - \frac{\beta_2}{\sqrt{\beta_2^2 + \gamma}} \right) \mathsf{A} \\ +\frac{\sqrt{3}}{4} \left(\frac{1}{\sqrt{\beta_1^2 + \gamma}} + \frac{1}{\sqrt{\beta_2^2 + \gamma}} \right) \mathsf{B} \end{pmatrix}. \tag{34}$$

The flowchart in Fig. 2 contains the logical connections of the main analysis steps as they have been implemented. In each probabilistic iteration, i.e. the iteration for finding the design point, two deterministic loops are required, the first one provides information for sensitivity analysis and the second one for the simple line search algorithm.

5 Numerical Examples

The probabilistic limit and shakedown algorithm described above is programmed and implemented in the finite element package Code_Aster 7.3 [6]. The 4-noded quadrangular isoparametric flat shell element, the DKT element, which is based on Kirchhoff's hypothesis, was applied. Higher order shell elements are not available in Code_Aster. In all numerical examples, the structures are made of elastic-perfectly plastic material. For each test case, some existing analytical and numerical solutions found in literature are briefly represented and compared. The finite element discretizations were realized by the personal pre- and post-processor GiD 7.2 [8].

Here only the most probable failure mode is calculated with FORM/SORM in all examples. Excluding failure modes one after the other by a barrier from the further search in FORM/SORM it was possible to identify the contribution of multiple failure modes of a plane frame and obtain better approximations of the failure probability [21]. In this test case taken from [16] the yield stress has only been assumed as mutually independent random variable with different log-normal distributions for the different beams in the frame. Before publication the proposed method may need further testing with more complex examples.

5.1 Pipe Bend Under In-Plane Bending Moment

The pipe bends have been a problem of great interest to many designers. They have a complex response to bending moments. When an external moment is applied to one end of the pipe bend, the annular cross section tends to deform significantly both in and out of its own plane, i.e. it is subjected to warping and ovalization. Due to their curved geometry, the pipe bends are very flexible and forced to accommodate large displacements resulting in larger stresses
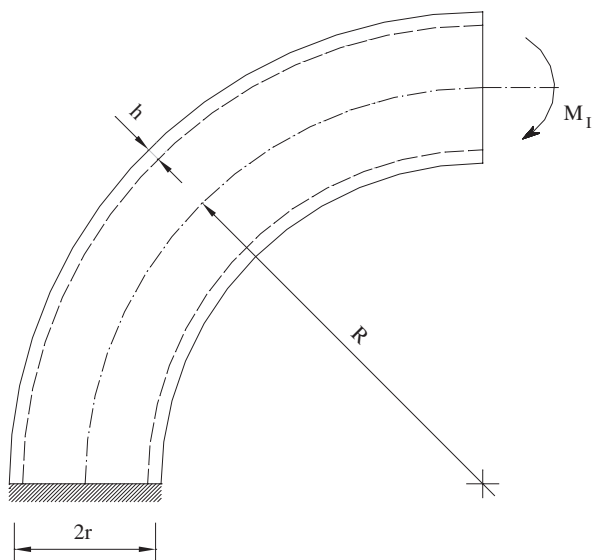
Fig. 3 Cylindrical pipe under in-plane moment loading

and strains than those present in a straight pipe of the same size and material, under the same loading conditions. For this reason pipe bends are considered as critical components of a piping system.

Consider a 90° elbow with mean radius r, bend radius of curvature R and thickness h as shown in the Fig. 3. One of its ends is assumed clamped and the other one is subjected to an in-plane closing moment M_I. The following geometrical parameters are adopted: $R = 1800\,\text{mm}$, $r = 300\,\text{mm}$, $h = 15\,\text{mm}$. In this example, only the moment M_I and the yield stress σ_y are considered as random variables with mean values μ_s, μ_r and standard deviations σ_s, σ_r respectively.

5.1.1 Limit Load Analysis

From the deterministic analysis, we got the limit moment as $0.4614 \times 4hr^2\sigma_y$. The limit state function is a linear function of basic variables X, Y and defined by

$$g(X, Y) = 0.4614 \times 4hr^2 Y - X. \tag{35}$$

Staat and Heitzer [18] introduced the analytical expressions of the reliability indices for both cases of normally and log-normally distributed random variables, respectively

$$\beta_{HL} = \frac{0.4614 \times 4hr^2 \mu_r - \mu_s}{\sqrt{(0.4614 \times 4hr^2)^2 \sigma_r^2 + \sigma_s^2}}, \tag{36}$$

$$\beta_{HL} = \frac{\log\left(0.4614 \times 4hr^2 m_r\right) - \log\left(m_s\right)}{\sqrt{\delta_r^2 + \delta_s^2}}, \tag{37}$$

where m_r, m_s and δ_r, δ_s are calculated as

$$m_{r,s} = \mu_{r,s} e^{-\delta_{r,s}^2/2} = \frac{\mu_{r,s}}{\sqrt{\left(\frac{\sigma_{r,s}^2}{\mu_{r,s}^2} + 1\right)}}, \quad \delta_{r,s} = \sqrt{\log\left(\frac{\sigma_{r,s}^2}{\mu_{r,s}^2} + 1\right)}. \tag{38}$$

5.1.2 Shakedown Load Analysis

For this case the in-plane bending moment M_I varies within the range $[-M_0, M_0]$ and only the amplitudes but not the uncertain complete load history influence the solution. Consider the case where the value M_0 is a random variable. From the deterministic analysis, we got the shakedown limit as $0.2507 \times 4hr^2 \sigma_y$. The limit state function is a linear function of basic variables X, Y and defined by

$$g(X, Y) = 0.2507 \times 4hr^2 Y - X, \tag{39}$$

and the reliability indices for both cases of normally and log-normally distributed random variables are obtained, respectively

$$\beta_{HL} = \frac{0.2507 \times 4hr^2 \mu_r - \mu_s}{\sqrt{(0.2507 \times 4hr^2)^2 \sigma_r^2 + \sigma_s^2}}, \tag{40}$$

$$\beta_{HL} = \frac{\log\left(0.2507 \times 4hr^2 m_r\right) - \log\left(m_s\right)}{\sqrt{\delta_r^2 + \delta_s^2}}. \tag{41}$$

The failure probabilities P_f are presented in Figs. 4 and 5 versus $\mu_s/4hr^2\mu_r$. Numerical solutions of the limit and shakedown analyses are compared with the analytical ones resulting from exact solutions. For each case, both random variables are normally or log-normally distributed with standard deviations $\sigma_{r,s} = 0.1\mu_{r,s}$. It is shown that our results correspond well with the analytical ones for all cases.
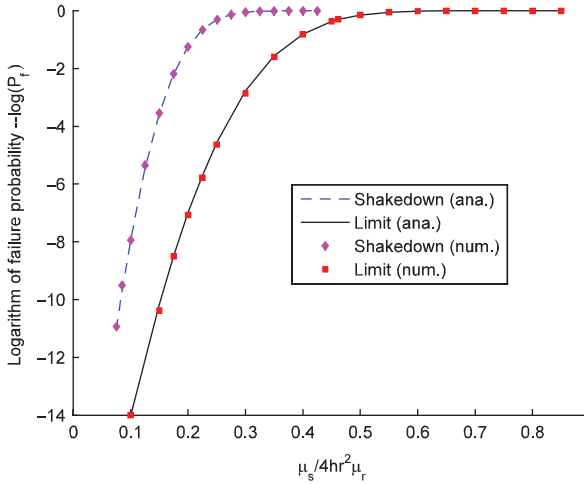
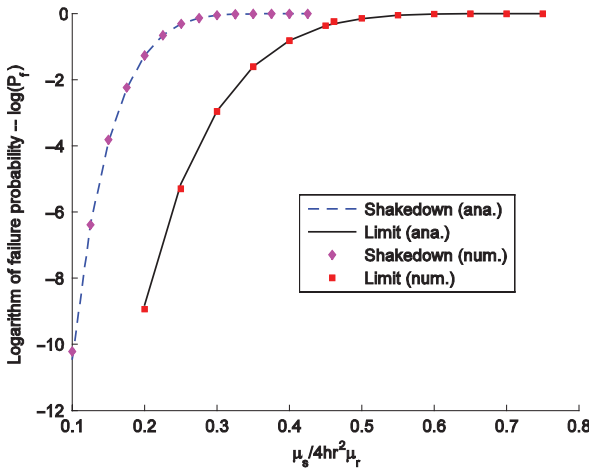**Fig. 4** Comparison of the results for normally distributed variables

Fig. 5 Comparison of the results for log-normally distributed variables

5.2 Limit Analysis of Cylindrical Pipe Under Complex Loading

Beside the loading and material strength, it is well known that the load carrying capacity of shell structures is generally influenced by their initial imperfections which occur during the manufacturing and construction stages such as variability of thickness. In this example, the effect of thickness imperfection on the limit loads of a shell structure is examined. The cylindrical
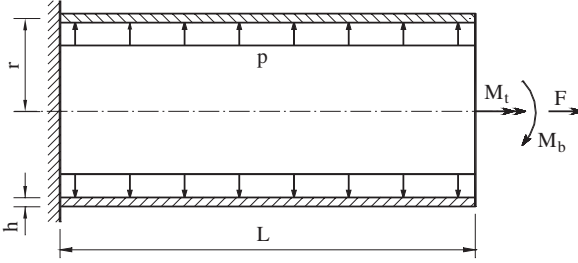
Fig. 6 Cylindrical pipe under complex loading

pipe subjected to complex loading is considered here, see Fig. 6. The following geometrical and physical parameters are adopted: $L = 2700\,\text{mm}$, $r = 300\,\text{mm}$, $\sigma_y = 120\text{MPa}$. For this purpose, only the loading and the thickness h of the pipe are modeled as random variables. Four loading cases are examined.

5.2.1 Internal Pressure

For this case, the exact plastic collapse limit pressure is given by $p_{\text{lim}} = \sigma_y h/r$. Thus, the resistance R depends linearly on the realization h of the thickness basic variable Z. The magnitude of the internal pressure is the second basic variable X. The limit state function is defined by

$$g(X, Z) = \frac{\sigma_y}{r} Z - X. \tag{42}$$

If both thickness and load random variables are supposed to be normally distributed with mean values μ_t, μ_s and standard deviations σ_t, σ_s respectively, then the limit state function $g(\mathbf{U})$ in the standard Gaussian space is a linear function. Note that σ_y is the yield stress and not a standard deviation here. The mean and standard deviation of the limit state function can be calculated as follows

$$\mu_g = \frac{\sigma_y}{r} \mu_t - \mu_s, \quad \sigma_g = \sqrt{\left(\frac{\sigma_y}{r}\right)^2 \sigma_t^2 + \sigma_s^2}, \tag{43}$$

from which, the reliability index becomes

$$\beta_{HL} = \frac{\mu_g}{\sigma_g} = \frac{\left(\frac{\sigma_y}{r}\right)\mu_t - \mu_s}{\sqrt{\left(\frac{\sigma_y}{r}\right)^2 \sigma_t^2 + \sigma_s^2}}. \tag{44}$$

The limit state function becomes nonlinear if both basic variables are lognormally distributed. Analogously to (44), we obtain the exact reliability index for FORM

$$\beta_{HL} = \frac{\log\left(\left(\frac{\sigma_y}{r}\right) m_t\right) - \log\left(m_s\right)}{\sqrt{\delta_t^2 + \delta_s^2}}, \tag{45}$$

where m_t, m_s and δ_t, δ_s are calculated as

$$m_{t,s} = \mu_{t,s} e^{-\delta_{t,s}^2/2} = \frac{\mu_{t,s}}{\sqrt{\left(\frac{\sigma_{t,s}^2}{\mu_{t,s}^2} + 1\right)}}, \quad \delta_{t,s} = \sqrt{\log\left(\frac{\sigma_{t,s}^2}{\mu_{t,s}^2} + 1\right)}. \tag{46}$$

5.2.2 Bending Moment

The exact plastic collapse limit moment is linearized by $M_b^{\text{lim}} = 4r^2 \sigma_y h$. The limit state function is a linear function of basic variables X, Z and defined by

$$g(X, Z) = 4r^2 \sigma_y Z - X. \tag{47}$$

The reliability indices for both cases of normally and log-normally distributed random variables are obtained, respectively

$$\beta_{HL} = \frac{4r^2 \sigma_y \mu_t - \mu_s}{\sqrt{\left(4r^2 \sigma_y\right)^2 \sigma_t^2 + \sigma_s^2}}, \tag{48}$$

$$\beta_{HL} = \frac{\log\left(4r^2 \sigma_y m_t\right) - \log\left(m_s\right)}{\sqrt{\delta_t^2 + \delta_s^2}}. \tag{49}$$

5.2.3 Torsion Moment

In this case the exact plastic collapse limit moment is given by $M_t^{\text{lim}} = 2\pi r^2 \sigma_y h/\sqrt{3}$. The limit state function is a linear function of basic variables X, Z and defined by

$$g(X, Z) = \frac{2}{\sqrt{3}} \pi r^2 \sigma_y Z - X. \tag{50}$$

The reliability indices for both cases of normally and log-normally distributed random variables are obtained, respectively

$$\beta_{HL} = \frac{\frac{2}{\sqrt{3}} \pi r^2 \sigma_y \mu_t - \mu_s}{\sqrt{\left(\frac{2}{\sqrt{3}} \pi r^2 \sigma_y\right)^2 \sigma_t^2 + \sigma_s^2}}, \tag{51}$$

$$\beta_{HL} = \frac{\log\left(\frac{2}{\sqrt{3}}\pi r^2 \sigma_y m_t\right) - \log(m_l)}{\sqrt{\delta_t^2 + \delta_l^2}}. \tag{52}$$

5.2.4 Axial Load

The exact plastic collapse limit load is given by $F_{\lim} = 2\pi r \sigma_y h$. The limit state function is a linear function of the basic variables X, Z and defined by

$$g(X, Z) = 2\pi r \sigma_y Z - X. \tag{53}$$

The reliability indices for both cases of normally and log-normally distributed random variables are obtained, respectively

$$\beta_{HL} = \frac{2\pi r \sigma_y \mu_t - \mu_s}{\sqrt{(2\pi r \sigma_y)^2 \sigma_t^2 + \sigma_s^2}}, \tag{54}$$

$$\beta_{HL} = \frac{\log(2\pi r \sigma_y m_t) - \log(m_s)}{\sqrt{\delta_t^2 + \delta_s^2}}. \tag{55}$$

The failure probabilities P_f are presented in Figs. 7, 8, 9 and 10 with the units kN and m of force and length, respectively. The numerical solutions of the limit analyses are compared with the analytical ones resulting from exact solutions. For each loading case, both random variables are normally or log-normally distributed with standard deviations $\sigma_{t,s} = 0.1\mu_{t,s}$. It is shown that our results compare well with the analytical ones for all cases.
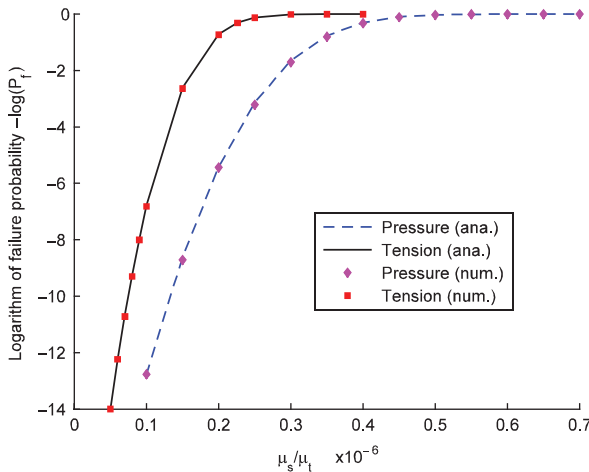

Fig. 7 Comparison of the results for normally distributed variables (kN, m)

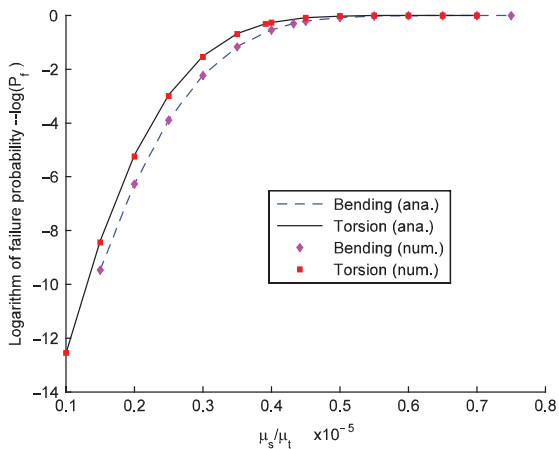**Fig. 8** Comparison of the results for normally distributed variables (kN, m)

Fig. 9 Comparison of the results for log-normally distributed variables (kN, m)
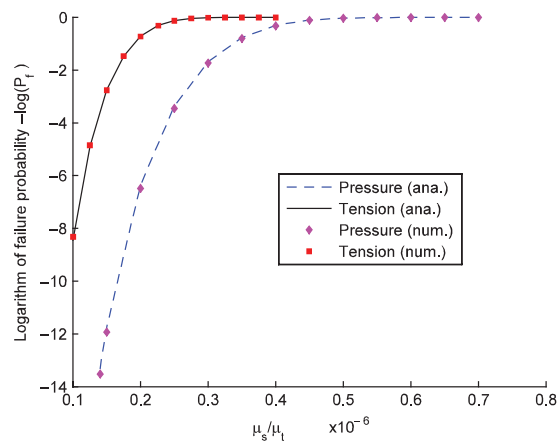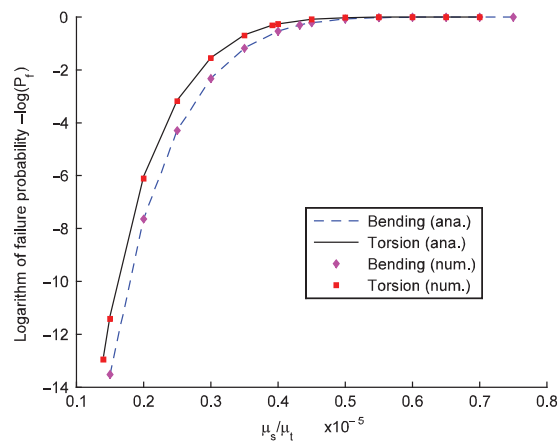

Fig. 10 Comparison of the results for log-normally distributed variables (kN, m)

6 Conclusions

A procedure for reliability analysis of inelastic shell structures under variable loads which is based on a direct plasticity method has been presented. The procedure involves a deterministic limit and shakedown analysis for each probabilistic iteration. The loading and strength of the material as well as the thickness of the shell are considered as random variables. The proposed method appears to be capable of identifying good estimates of the failure probability for the most probable failure mode, even in the case of very small probabilities. The possible extension to multiple failure modes is indicated. The proposed method makes the analysis problem of any load history time-invariant and it is applicable with incomplete data. Sensitivity analyses are obtained directly from a mathematical optimization with no extra computational cost.

References

1. Alibrandi, U., Ricciardi, G. (2008) The use of stochastic stresses in the static approach of probabilistic limit analysis. Int. J. Numer. Meth. Engng 73(6), 747–782. doi:10.1002/nme.2089
2. Augusti, G., Baratta, A., Casciati, F. (1984) Probabilistic methods in structural engineering. Chapman and Hall, London.
3. Burgoyne, C.J., Brennan, M.G. (1993) Exact Ilyushin yield surface. Int. J. Sol. Struct. 30(8), 1113–1131. doi:10.1016/0020-7683(93)90007-T
4. Caddemi, S., Ricciardi, G., Saccà, C. (2002) Limit analysis of structures with stochastic strengths by a static approach. Meccanica 37(6), 527–544. doi:10.1023/A:1020939103140
5. Capsoni, A., Corradi, L. (1997) A finite element formulation of the rigid-plastic limit analysis problem. Int. J. Num. Meth. Engng 40(11), 2063–2086. doi:10.1002/(SICI)1097-0207(19970615) 40:11<2063::AID-NME159>3.0.CO;2-%23
6. Code_Aster 7.3 (2003) User's manual. A product of EDF R&D, Clamart, France. http://www.code-aster.org
7. Der Kiureghian A., Dakessian T. (1998) Multiple design points in first and second-order reliability. Struct. Saf, 20(1), 37–49. doi:10.1016/S0167-4730(97)00026-X
8. European Standard (2005–06) Unfired pressure vessels – Part 3: Design, Annex 2: Annex B Direct route for design by analysis, CEN European Committee for Standardization, EN 13445-3:2002, Issue 14
9. GiD 7.2 (2002) User's manual. A product of the Center for Numerical Methods in Engineering (CIMNE), Barcelona. http://www.gid.cimne.upc.es
10. Gollwitzer, S., Abdo, T., Rackwitz, R. (1988) FORM Manual. RCP GmbH, München.
11. Hasofer, A.M., Lind, N.C. (1974) An exact and invariant first order reliability format. ASCE, J. Eng. Mech. Div. 100, No. EM1, 111–121

12. Heitzer, M., Staat, M. (2000) Reliability analysis of elasto-plastic structures under variable loads. In: Maier, G., Weichert, D. (eds.) Inelastic analysis of structures under variable loads: Theory and engineering Applications. Kluwer, Academic Press, Dordrecht, 269–288

13. Heitzer, M., Staat, M. (2002) Limit and shakedown analysis with uncertain data. In: Marti, K. (ed.) Stochastic optimization techniques, numerical methods and technical applications. Springer, Heidelberg, 253–267

14. Ilyushin, A.A. (1948) Plasticity. Moscow: Gostekhizdat, In Russian

15. Klingmüller, O. (1979) Anwendung der Traglastberechnung für die Beurteilung der Sicherheit von Konstruktionen. Dissertation, Universität Essen Gesamthochschule

16. Madsen, H.O., Krenk, S., Lind, N.C. (1986) Methods of structural safety. Prentice-Hall, Englewood Cliffs, NJ

17. Seitzberger, M. (2000) Contributions to an efficient numerical analysis of the plastic behaviour of thin-walled structures. Fortschritt-Berichte VDI, Reihe 18, Nr. 247, VDI-Verlag, Düsseldorf

18. Staat, M., Heitzer, M. (2003) Probabilistic limit and shakedown problems. In: Staat, M., Heitzer, M. (eds.) Numerical methods for limit and shakedown analysis. Deterministic and probabilistic problems. NIC Series Vol. 15, John von Neumann Institute for Computing, Jülich, 217–268. http://www.fz-juelich.de/nic-series/volume15/nic-series-band15.pdf

19. Trần, T.N., Kreißig, R., Vu, D.K., Staat, M. (2007) Upper bound limit and shakedown analysis of thin shells using the exact Ilyushin yield surface. Comput. Struct., 86(17–18) 1683–1695. doi:10.1016/j.compstruc.2008.02.005

20. Trần, T.N., Kreißig, R., Staat, M. (2008) Probabilistic limit and shakedown analysis of thin shells using the exact Ilyushin yield surface. Struct. Saf. doi:10.1016/j.strusafe.2007.10.003

21. Trần, T.N. (2008) Limit and shakedown analysis of plates and shells including uncertainties. Dissertation, TU Chemnitz. http://archiv.tu-chemnitz.de/pub/2008/0025

22. Tvedt, L. (1983) Two second-order approximations to the failure probability. Veritas Report RDIV/20-004-83, Det Norske Veritas, Oslo, Norway

Static Shakedown Theorem for Solids with Temperature-Dependent Elastic Modulus

A. Oueslati and G. de Saxcé

Abstract In this paper, an extension of the static shakedown theorem (Melan's theorem) for elastic-plastic materials with temperature-dependent elastic modulus is presented. Cases of the decrease of yield function and the variation of coefficient of thermal expansion with temperature are included. The proposed extension leads to the introduction of a shakedown safety coefficient. To illustrate the statements of our theorem, step-by-step finite element procedure is applied to study a three-bar problem and a plate with the central hole subjected to thermo-mechanical cyclic loadings.

1 Introduction

Since the pioneering works of Bleich [3], Melan [18] and Koiter [15] on shakedown theory, several attempts have been derived to extend shakedown theorems to complicated material behaviours, and robust algorithms have been proposed to estimate bounds of safety factors [24]. For instance, static and kinematic shakedown theorems are extended to hardening plasticity [19, 23], simultaneous actions of mechanical agencies and temperature variations [17, 21], dynamic plasticity [8], damaged and cracked bodies [2, 13], non-associated plasticity [4, 10], poroplasticity [6], gradient plasticity [20], contact with friction [1], shape memory alloy structures [12], etc.

Nevertheless, in a recent paper, Pham [19] showed that actually shakedown theorems, in Melan-Koiter path-independent spirit, have been extended successfully only for certain cases. An interesting discussion and a critical survey are presented in the same article.

Abdelbacet Oueslati and Géry de Saxé

Laboratoire de Mécanique de Lille – CNRS UMR 8107, Boulevard Paul Langevin, 59655 Villeneuve d'Ascq cedex, France, e-mail: Abdelbacet.Oueslati@univ-lille1.fr; gery.desaxce@univ-lille1.fr

Classical shakedown theorems and their extensions to various material models rest on the assumption that elastic moduli are independent of the temperature. This is reasonable for thermal loading of low amplitude. However, in many industrial domains, for instance in boilers of nuclear power plants or in airplane and automotive motors, the structural elements are subjected to thermal cycles of large amplitude in such way that the dependence of the elastic coefficients with respect to the temperature cannot be neglected. To our best knowledge, only one static shakedown theorem in this field was formulated by J.A. König in 1969 [16]. However one can show that König's theorem is not quite complete and and its proof is valid only for increasing thermal loading. It is worth noting, that some authors [5] used König theorem to provide numerical shakedown bounds.

In this paper, we propose a new consistent static shakedown theorem for elastic-plastic solids with temperature-dependent elastic modulus. The case of decrease of the yield strength with the temperature is included in the stated theorem. Illustrative examples, performed by incremental finite elements simulations, are presented.

2 Basic Relations

Consider an elastic-plastic material occupying a bounded region Ω of the space with a smooth boundary $\partial\Omega$. The elastic coefficients (Young's modulus, Poisson's ratio, coefficient of thermal expansion) and yield stress are temperature-dependent. This solid Ω is loaded by given body forces $\boldsymbol{F}_v(\boldsymbol{x}, t)$ in Ω, a prescribed displacement $\boldsymbol{u}^d(\boldsymbol{x}, t)$ on Γ_u, surface tractions $\boldsymbol{T}^d(\boldsymbol{x}, t)$ on Γ_T $\left(\Gamma_u \cup \Gamma_T = \partial\Omega,\ \Gamma_u \cap \Gamma_T = \emptyset\right)$ and a temperature variation $\theta(\boldsymbol{x}, t)$.

The data set $\left(\boldsymbol{F}_v(\boldsymbol{x}, t), \boldsymbol{T}^d(\boldsymbol{x}, t), \boldsymbol{u}^d(\boldsymbol{x}, t), \theta(\boldsymbol{x}, t)\right)$ characterizes the history of the thermo-mechanical loading at every point $\boldsymbol{x}$ and at each time $t \in [0, \infty[$.

Let $\left(\boldsymbol{\sigma}(\boldsymbol{x}, t), \boldsymbol{\varepsilon}(\boldsymbol{x}, t), \boldsymbol{u}(\boldsymbol{x}, t)\right)$ denote the quasi-static elastic-plastic response to the loading path.

Within the framework of the infinitesimal transformation, the strain field is additively split into its elastic, thermal and plastic parts

$$\boldsymbol{\varepsilon}(\boldsymbol{x}, t) = \boldsymbol{\varepsilon}^e(\boldsymbol{x}, t) + \boldsymbol{\varepsilon}^\theta(\boldsymbol{x}, t) + \boldsymbol{\varepsilon}^p(\boldsymbol{x}, t). \tag{1}$$

The elastic strains are related to the stresses through Hooke's law

$$\boldsymbol{\varepsilon}^e(\boldsymbol{x}, t) = \mathbf{S}\big(\boldsymbol{x}, \theta(\boldsymbol{x}, t)\big) : \boldsymbol{\sigma}(\boldsymbol{x}, t), \tag{2}$$

where $\mathbf{S}\big(\boldsymbol{x}, \theta(\boldsymbol{x}, t)\big)$ is the fourth order elastic compliance tensor. Its components vary with the temperature.

For isotropic materials, thermal strain is given by the following relation

$$\varepsilon^{\theta}(\boldsymbol{x}, t) = \alpha\, \theta(\boldsymbol{x}, t)\, \boldsymbol{I}\,, \tag{3}$$

where α is the coefficient of thermal expansion and $\boldsymbol{I}$ denotes the identity tensor.

The associated flow rule [10, 22] ensures that the plastic strain rate obeys to the normality law

$$\dot{\varepsilon}^{p} = \dot{\lambda}\, \frac{\partial f\big(\boldsymbol{\sigma}, \theta(\boldsymbol{x}, t)\big)}{\partial \boldsymbol{\sigma}}\,, \quad \dot{\lambda} \geq 0\,, \quad \dot{\lambda} f = 0\,, \tag{4}$$

where $f(\boldsymbol{\sigma}, \theta)$ stands for the plasticity yield function and $\dot{\lambda}$ denotes the plastic multiplier.

A stress tensor $\boldsymbol{\sigma}$ is said plastically admissible if it belongs to the closed convex set

$$K(\theta) = \{\boldsymbol{\sigma} \,|\, f(\boldsymbol{\sigma}, \theta) \leq 0\}\,, \tag{5}$$

called the elastic domain. Moreover, it is assumed further that

$$f(0, \theta) < 0 \tag{6}$$

for any value of θ, that in practice is not very restrictive. Then the origin of the stress space is inside $K(\theta)$. More precisely, there exists a positive number r and a ball of radius r and centered at the origin contained in $K(\theta)$.

Let now $(\boldsymbol{\sigma}^{E}(\boldsymbol{x}, t), \boldsymbol{\varepsilon}^{E}(\boldsymbol{x}, t), \boldsymbol{u}^{E}(\boldsymbol{x}, t))$ be the fictitious purely thermo-elastic response of the solid Ω under the same loads and temperature variations

$$\varepsilon^{E}(\boldsymbol{x}, t) = \mathbf{S}\big(\boldsymbol{x}, \theta(\boldsymbol{x}, t)\big) : \boldsymbol{\sigma}^{E}(\boldsymbol{x}, t) + \alpha\,\theta(\boldsymbol{x}, t)\,\boldsymbol{I}\,. \tag{7}$$

By definition, the residual stress tensor at the time t is given by

$$\boldsymbol{\rho}(\boldsymbol{x}, t) = \boldsymbol{\sigma}(\boldsymbol{x}, t) - \boldsymbol{\sigma}^{E}(\boldsymbol{x}, t)\,. \tag{8}$$

$\boldsymbol{\rho}(\boldsymbol{x}, t)$ is the stress field subsisting in the structure after *complete elastic unloading* of Ω at the instant t. $\boldsymbol{\rho}$ belongs to the following set

$$\boldsymbol{L} = \{\boldsymbol{\rho}(\boldsymbol{x}, t) \,|\, \mathrm{div}\boldsymbol{\rho}(\boldsymbol{x}, t) = 0 \,\text{in}\, \Omega \,\text{and}\, \boldsymbol{\rho}(\boldsymbol{x}, t) \cdot \boldsymbol{n} = 0 \,\text{on}\, \Gamma_{T}\}\,, \tag{9}$$

where $\boldsymbol{n}$ is the unit outer normal vector at any point of Γ_{T}.
It is clearly seen that $\boldsymbol{\rho}(\boldsymbol{x}, t)$ is statically admissible with zero body forces in Ω and vanishing surface traction on Γ_{T}. For this reason $\boldsymbol{\rho}(\boldsymbol{x}, t)$ is often called a self-stress field.

In the same manner, one can introduce the residual strain field as follows

$$\boldsymbol{\eta}(\boldsymbol{x}, t) = \boldsymbol{\varepsilon}(\boldsymbol{x}, t) - \boldsymbol{\varepsilon}^{E}(\boldsymbol{x}, t)\,, \tag{10}$$

which belongs to the set of residual strain (or self-strain) set

$$\boldsymbol{L}^* = \{\boldsymbol{\eta} \,|\, \exists \boldsymbol{v}(\boldsymbol{x},t) \text{ such that } \boldsymbol{\eta}(\boldsymbol{x},t) = \mathrm{grad}_s \boldsymbol{v}(\boldsymbol{x},t) \text{ in } \Omega \text{ and } \boldsymbol{v}(\boldsymbol{x},t)$$
$$= 0 \text{ on } \Gamma_u\} \,. \tag{11}$$

It is useful to notice that the following relation holds true as a consequence of Green's formula

$$\forall \boldsymbol{\rho}(\boldsymbol{x},t) \in \boldsymbol{L}, \quad \forall \boldsymbol{\eta}(\boldsymbol{x},t) \in \boldsymbol{L}^*, \quad \int_\Omega \boldsymbol{\rho}(\boldsymbol{x},t) : \boldsymbol{\eta}(\boldsymbol{x},t)\,\mathrm{d}\Omega = 0 \,. \tag{12}$$

Besides, it can be remarked that

$$\boldsymbol{\eta}(\boldsymbol{x},t) = \mathbf{S}\big(\boldsymbol{x},\theta(\boldsymbol{x},t)\big) : \Big(\boldsymbol{\sigma}(\boldsymbol{x},t) - \boldsymbol{\sigma}^E(\boldsymbol{x},t)\Big) + \boldsymbol{\varepsilon}^P(\boldsymbol{x},t)$$
$$= \mathbf{S}\big(\boldsymbol{x},\theta(\boldsymbol{x},t)\big) : \boldsymbol{\rho}(\boldsymbol{x},t) + \boldsymbol{\varepsilon}^P(\boldsymbol{x},t)$$
$$= \boldsymbol{\eta}^e(\boldsymbol{x},t) + \boldsymbol{\varepsilon}^P(\boldsymbol{x},t) \,, \tag{13}$$

where $\boldsymbol{\eta}^e(\boldsymbol{x},t)$ is called the elastic residual strain field.

In [14], it is shown that, when the elastic coefficients vary with temperature, the evolution of the residual stress field as function of time is governed by the following multivalued differential equation

$$-\frac{\mathrm{d}}{\mathrm{d}t}\Big(\mathbf{S}\big(\boldsymbol{x},\theta(\boldsymbol{x},t)\big) : \boldsymbol{\rho}(\boldsymbol{x},t)\Big) \in \partial\psi_{K(t)}\big(\boldsymbol{\rho}(\boldsymbol{x},t)\big) \,, \tag{14}$$

where $\partial\psi_{K(t)}$ is the subgradient at the point $\boldsymbol{\sigma}$ of the indicator function $\psi_{K(t)}$ of the convex set $K(t)$ of statically and plastically admissible fields at time t, with respect of the following scalar product of two second order tensor fields $\langle \mathsf{A} : \mathsf{B} \rangle = \int_\Omega \mathsf{A} : \mathsf{B}\,\mathrm{d}\Omega$.

3 New Static Shakedown Theorem

Theorem 1. *If there exists a residual stress field $\overline{\boldsymbol{\rho}}(\boldsymbol{x},t)$ and a scalar $m > 1$ such that*

- $\overline{\boldsymbol{\eta}}^e(\boldsymbol{x}) = \mathbf{S}(\boldsymbol{x},\theta(\boldsymbol{x},t)) : \overline{\boldsymbol{\rho}}(\boldsymbol{x},t)$ *is time independent and*
- $f(m\,\boldsymbol{\sigma}(\boldsymbol{x},t)) = f(m(\boldsymbol{\sigma}^E(\boldsymbol{x},t) + \overline{\boldsymbol{\rho}}(\boldsymbol{x},t))) \leq 0$

anywhere and at any time $t > 0$, then shakedown occurs.

Proof. Following [23], the proof is achieved in two steps. First, we show that the enunciated theorem implies the boundedness of the dissipated plastic energy. The second step consists in showing that $lim_{t\to\infty}\boldsymbol{\varepsilon}^P$ exists.

First Step

Suppose that all conditions of the theorem are satisfied. The actual instantaneous stress field is $\boldsymbol{\sigma}(\boldsymbol{x}, t)$ and let us consider the stress field $\overline{\boldsymbol{\sigma}}(\boldsymbol{x}, t) = m\big(\boldsymbol{\sigma}^E(\boldsymbol{x}, t) + \overline{\boldsymbol{\rho}}(\boldsymbol{x}, t)\big)$. Note that $\overline{\boldsymbol{\sigma}}$ is plastically admissible by the statement of the theorem. Moreover, these two tensors are statically admissible with the same prescribed loads and thus

$$\boldsymbol{\sigma}(\boldsymbol{x}, t) - \frac{1}{m}\overline{\boldsymbol{\sigma}}(\boldsymbol{x}, t) = \boldsymbol{\rho}(\boldsymbol{x}, t) - \overline{\boldsymbol{\rho}}(\boldsymbol{x}, t) \tag{15}$$

is a self-stress field.

On the other hand, application of Hill-Mandel maximum power principle leads to

$$\frac{1}{m}(\overline{\boldsymbol{\sigma}} - \boldsymbol{\sigma}) : \dot{\boldsymbol{\varepsilon}}^p = \left(1 - \frac{1}{m}\right)\boldsymbol{\sigma} : \dot{\boldsymbol{\varepsilon}}^p + \left(\frac{1}{m}\overline{\boldsymbol{\sigma}} - \boldsymbol{\sigma}\right) : \dot{\boldsymbol{\varepsilon}}^p \le 0, \tag{16}$$

and consequently, one has

$$\int_0^t \int_\Omega \boldsymbol{\sigma} : \dot{\boldsymbol{\varepsilon}}^p \, \mathrm{d}\Omega \, \mathrm{d}t \le \frac{m}{m-1} \int_0^t \int_\Omega \left(\boldsymbol{\sigma} - \frac{1}{m}\overline{\boldsymbol{\sigma}}\right) : \dot{\boldsymbol{\varepsilon}}^p \, \mathrm{d}\Omega \, \mathrm{d}t. \tag{17}$$

Let us now introduce the fictitious elastic energy of the stress difference

$$R = \frac{1}{2} \int_\Omega (\boldsymbol{\rho} - \overline{\boldsymbol{\rho}}) : \mathbf{S} : (\boldsymbol{\rho} - \overline{\boldsymbol{\rho}}) \, \mathrm{d}\Omega \ge 0. \tag{18}$$

The stress difference $(\boldsymbol{\rho} - \overline{\boldsymbol{\rho}})$ is associated to the strain difference $(\boldsymbol{\eta}^e - \overline{\boldsymbol{\eta}}^e)$ by Hooke's law

$$\mathbf{S} : (\boldsymbol{\rho} - \overline{\boldsymbol{\rho}}) = \boldsymbol{\eta}^e - \overline{\boldsymbol{\eta}}^e, \tag{19}$$

and because $\overline{\boldsymbol{\eta}}^e$ is time-independent, the differentiation with respect to time of the energy R reads

$$\dot{R} = \int_\Omega (\boldsymbol{\rho} - \overline{\boldsymbol{\rho}}) : (\dot{\boldsymbol{\eta}}^e - \dot{\overline{\boldsymbol{\eta}}}^e) \, \mathrm{d}\Omega = \int_\Omega (\boldsymbol{\rho} - \overline{\boldsymbol{\rho}}) : \dot{\boldsymbol{\eta}}^e \, \mathrm{d}\Omega. \tag{20}$$

Substitution of 13 leads to

$$\dot{R} = \int_\Omega (\boldsymbol{\rho} - \overline{\boldsymbol{\rho}}) : (\dot{\boldsymbol{\eta}} - \dot{\boldsymbol{\varepsilon}}^p) \mathrm{d}\Omega. \tag{21}$$

As $(\boldsymbol{\rho} - \overline{\boldsymbol{\rho}}) \in \boldsymbol{L}$ and $\dot{\boldsymbol{\eta}} \in \boldsymbol{L}^*$, because of virtual power principle and using (15), one may write

$$\dot{R} = -\int_\Omega \left(\boldsymbol{\sigma} - \frac{1}{m}\overline{\boldsymbol{\sigma}}\right) : \dot{\boldsymbol{\varepsilon}}^p \, \mathrm{d}\Omega, \tag{22}$$

and therefore

$$\dot{R} = -\int_{\Omega} \left(D(\dot{\varepsilon}^p) - \frac{1}{m}\overline{\boldsymbol{\sigma}} : \dot{\varepsilon}^p \right) d\Omega \,, \tag{23}$$

where $D(\dot{\varepsilon}^p) = \boldsymbol{\sigma} : \dot{\varepsilon}^p$. Since $\dfrac{1}{m}\overline{\boldsymbol{\sigma}}$ is plastically admissible, maximum dissipation leads to

$$\dot{R} \leq 0 \,. \tag{24}$$

Hence

$$\int_0^t \int_{\Omega} \boldsymbol{\sigma} : \dot{\varepsilon}^p \, d\Omega \, dt \leq \frac{m}{m-1} \int_0^t \int_{\Omega} (\boldsymbol{\sigma} - \frac{1}{m}\overline{\boldsymbol{\sigma}}) : \dot{\varepsilon}^p \, d\Omega \, dt = -\frac{m}{m-1} \int_0^t \dot{R} \, dt$$

$$= \frac{m}{m-1} \Big(R(0) - R(t) \Big). \tag{25}$$

Because of its definition, $R(t)$ is positive and from Eq. (24) we get

$$R(0) - R(t) \leq R(0) \,, \tag{26}$$

which conducts to

$$\forall t > 0, \qquad \int_0^t \int_{\Omega} \boldsymbol{\sigma} : \dot{\varepsilon}^p \, d\Omega \, dt \leq \frac{m}{m-1} R(0) \,. \tag{27}$$

Thus the total plastic dissipation is bounded for any initial condition.

Second Step

Following [9], one notices that there exists a ball of radius r and centered at the origin $\boldsymbol{\sigma} = 0$ contained in it. For $\dot{\varepsilon}^p \neq 0$, the stress $\boldsymbol{\sigma}^* = r\dfrac{\dot{\varepsilon}^p}{\|\dot{\varepsilon}^p\|}$ is plastically admissible. The principle of maximum plastic work gives

$$r \, \|\dot{\varepsilon}^p(\boldsymbol{x}, t)\| \leq \boldsymbol{\sigma}(\boldsymbol{x}, t) : \dot{\varepsilon}^p(\boldsymbol{x}, t) \,, \tag{28}$$

where $\|A\|$ is the norm of the second order tensor A defined by $\|A\| = \sqrt{A : A}$. If $\dot{\varepsilon}^p = 0$, (28) is trivially fulfilled; then (28) is satisfied for any $\dot{\varepsilon}^p$. Because of the triangular inequality one has

$$\|\varepsilon^p(\boldsymbol{x}, t)\| \leq \|\varepsilon^p(\boldsymbol{x}, 0)\| + \|\varepsilon^p(\boldsymbol{x}, t) - \varepsilon^p(\boldsymbol{x}, 0)\| \leq \|\varepsilon^p(\boldsymbol{x}, 0)\| + \| \int_0^t \dot{\varepsilon}^p(\boldsymbol{x}, \tau) \, d\tau \| \,, \tag{29}$$

and using (28)

$$\|\varepsilon^p(\boldsymbol{x}, t)\| \leq \|\varepsilon^p(\boldsymbol{x}, 0)\| + \frac{1}{r} \int_0^t \boldsymbol{\sigma}(\boldsymbol{x}, \tau) : \dot{\varepsilon}^p(\boldsymbol{x}, \tau) \, d\tau \tag{30}$$

is bounded for any $t \geq 0$ and almost everywhere when shakedown occurs because of the boundedness property (27) of the total plastic dissipation. Then the plastic strain field has a limit ε_∞^p in $\in L^1(\Omega)$.

Note that this convergence, ensures immediately the existence of $\lim\limits_{t \to \infty} (\varepsilon - \varepsilon^E)$:

$$\boldsymbol{\eta}(\boldsymbol{x}, t) = \boldsymbol{\varepsilon}(\boldsymbol{x}, t) - \boldsymbol{\varepsilon}^E(\boldsymbol{x}, t) = \mathbf{S}\big(\boldsymbol{x}, \theta(\boldsymbol{x}, t)\big) : \boldsymbol{\rho}(\boldsymbol{x}, t) + \boldsymbol{\varepsilon}^p(\boldsymbol{x}, t). \qquad (31)$$

In fact, $\boldsymbol{\varepsilon}^p(\boldsymbol{x}, t)$ converges to a finite limit and the shakedown theorem ensures the existence of a self-stress field $\overline{\boldsymbol{\rho}}(\boldsymbol{x}, t)$ such that $\mathbf{S}\big(\boldsymbol{x}, \theta(\boldsymbol{x}, t)\big) : \overline{\boldsymbol{\rho}}(\boldsymbol{x}, t)$ is time-independent, then $lim_{t \to \infty} \boldsymbol{\eta}$ exists and is bounded. $\square$

4 Static Shakedown Factor

Based upon the shakedown theorem one defines the static safety factor as the maximum value of the coefficient m satisfying the static shakedown theorem:

$$m^s = \max \ m$$

$$\text{s.t.} \begin{cases} f\big(m\,\boldsymbol{\sigma}(\boldsymbol{x}, t)\big) = f\Big(m\big(\boldsymbol{\sigma}^E(\boldsymbol{x}, t) + \boldsymbol{\tau}^*(\boldsymbol{x}, t)\big)\Big) \leq 0 & \forall (\boldsymbol{x}, t) \in \Omega \times [0, +\infty[\,, \\ \boldsymbol{\eta}^e(\boldsymbol{x}, t) = \mathbf{S}\big(\boldsymbol{x}, \theta(\boldsymbol{x}, t)\big) : \boldsymbol{\tau}^*(\boldsymbol{x}, t) & \text{is time-independent } \ \forall \, \boldsymbol{x} \in \Omega\,, \\ \operatorname{div} \boldsymbol{\tau}^*(\boldsymbol{x}, t) = 0 & \forall (\boldsymbol{x}, t) \in \Omega \times [0, +\infty[\,, \\ \boldsymbol{\tau}^*(\boldsymbol{x}, t) \cdot \boldsymbol{n} = 0 & \forall (\boldsymbol{x}, t) \in \Gamma_T \times [0, +\infty[\,. \end{cases}$$

It is clear that the condition $m^s > 1$ implies the occurence of shakedown. This definition leads to a standard optimization problem and numerical algorithms in view of estimation of the lower bound of safety coefficient with respect to shakedown.

5 Numerical Examples

In this section, two illustrative examples performed by step-by-step finite element procedure are presented. For each example, two numerical simulations are carried out by the software Cast3M [7] and stored separately:(i) elastic-plastic analysis under the thermo-mechanical loading path and (ii) purely elastic analysis under the same loads. The status of the response (shakedown or ratchetting or alternating plasticity) is numerically checked by following the evolution of the equivalent plastic deformation and through the evolution of the components of the plastic strain tensor $\boldsymbol{\varepsilon}^p(\boldsymbol{x}, t)$ in all the structure. Besides, the residual stress field $\boldsymbol{\rho}(\boldsymbol{x}, t)$ is simply computed

at Gauss points by the relation $\boldsymbol{\rho}(\boldsymbol{x},t) = \boldsymbol{\sigma}(\boldsymbol{x},t) - \boldsymbol{\sigma}^E(\boldsymbol{x},t)$ and the evolution of $\boldsymbol{\eta}^e(\boldsymbol{x},t) = \mathbf{S}(\boldsymbol{x},\theta) : \boldsymbol{\rho}(\boldsymbol{x},t)$ is obtained through $\boldsymbol{\eta}^e(\boldsymbol{x},t) = \boldsymbol{\varepsilon}(\boldsymbol{x},t) - \boldsymbol{\varepsilon}^E(\boldsymbol{x},t) - \boldsymbol{\varepsilon}^p(\boldsymbol{x},t)$.

5.1 Three-Bar Problem

Consider a simple mechanical system composed of three bars of equal cross-section area, fixed to a rigid substrate at their ends A, B and C, and symmetrically connected together at D, cf. Fig. 1.

The bars are made of an elastic-plastic material for which Young's modulus E and the yield stress σ_y are temperature-dependent. Their variations with respect to the temperature are the same as in [5] and are given by the following expressions:

$$E(\theta) = 196271 - 55.2765\,\theta - 0.0353701\,\theta^2 \quad \text{MPa}, \tag{32}$$

$$\sigma_y(\theta) = \begin{cases} 258.453 \text{ MPa} & \text{if } \theta < 35°C \\ 286.312 - 0.8539\,\theta + 0.0018717\,\theta^2 - 1.55146 \times 10^{-6}\,\theta^3 \text{ MPa} \\ \qquad\qquad \text{if } \theta \geq 35°C. \end{cases}$$

According to [5], these expressions are analytical fittings of the ASME III (1979) values for a 316 austenitic steel. The curves $E(\theta)$ and $\sigma_y(\theta)$ are plotted in Figs. 2 and 3 respectively.

The geometric and mechanical characteristics of the assembly are given in Table 1.

This assembly undergoes a constant force F applied at the end D and the central bar BD is subjected to a cyclic temperature variation $[\theta_0, \theta_0 + \theta_{max}]$
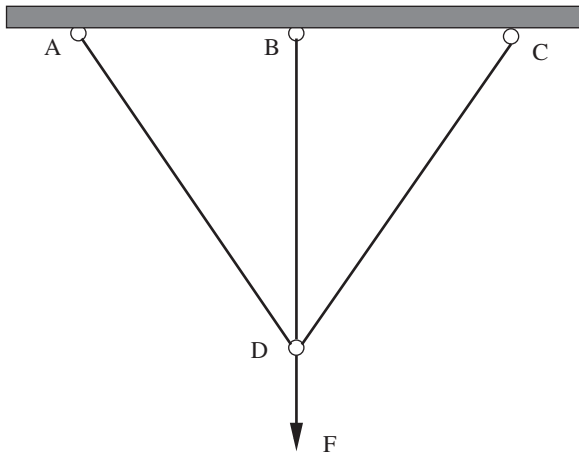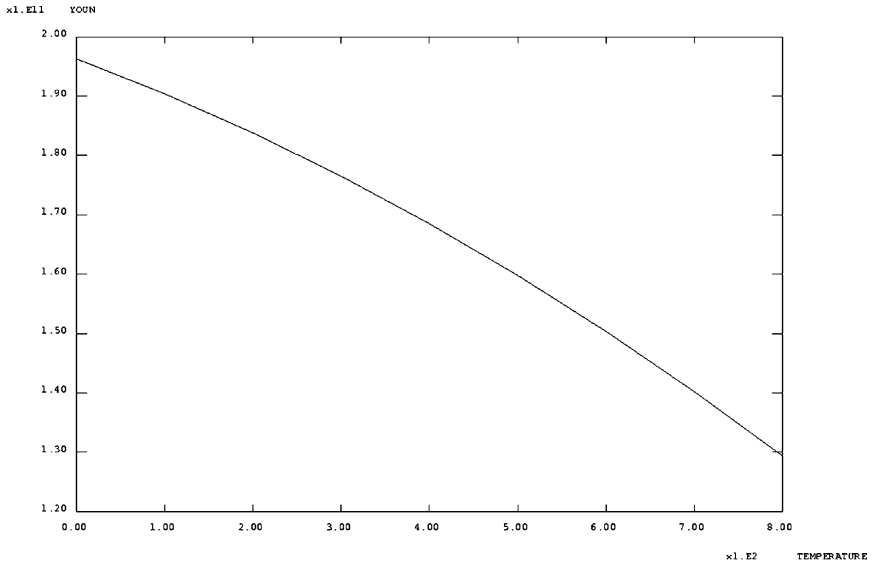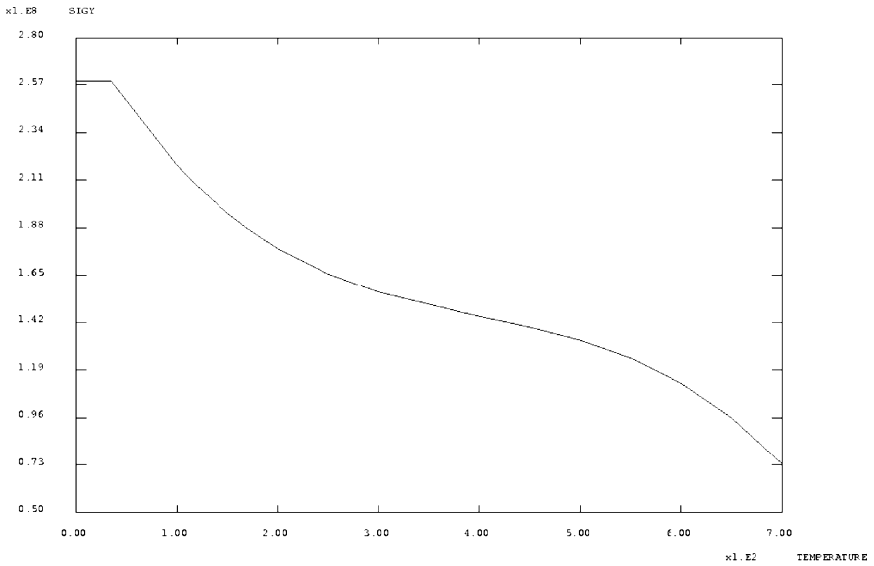

Fig. 1 The three-bar problem

Fig. 2 Young's modulus E versus temperature

Fig. 3 Variation of the yield stress σ_y with respect to the temperature

Table 1 Caracteristics of the bars

Cross-section area (m²)	1×10^{-3}
Length of the bar BD (m)	1
Length of the bars AD and CD (m)	$\sqrt{2}$
ν	0.3
$\alpha(°C^{-1})$	1.1×10^{-5}

as shown in Fig. 4. The temperature of the two remaining bars is maintained constant equal to zero.

Numerical simulations show that, for example, for (θ_{max} = 100°C, θ_0 = 200°C and F = 3000 Pa) the quasi-static response of the structure is shakedown. In this case, the incremental plastic strain becomes constant after some cycles as shown in Fig. 5 where the evolution ε^p of the node D is plotted.

In Fig. 6 we represent the variation of $\eta^e(\boldsymbol{x}, t) = \mathbf{S}(\boldsymbol{x}, \theta(\boldsymbol{x}, t)) : \boldsymbol{\rho}(\boldsymbol{x}, t)$ for the node D. As enounced in the theorem, this quantity tends to time-independent constant in the case of shakedown.

Now we present some results concerning ratchetting. This type of response is obtained for example when the input data set is (θ_{max} = 200°C, θ_0 = 200°C and F = 3000 Pa). A typical ratchetting curve of the incremental evolution of the plastic strain ε^p for the node D is displayed in Fig. 7. This
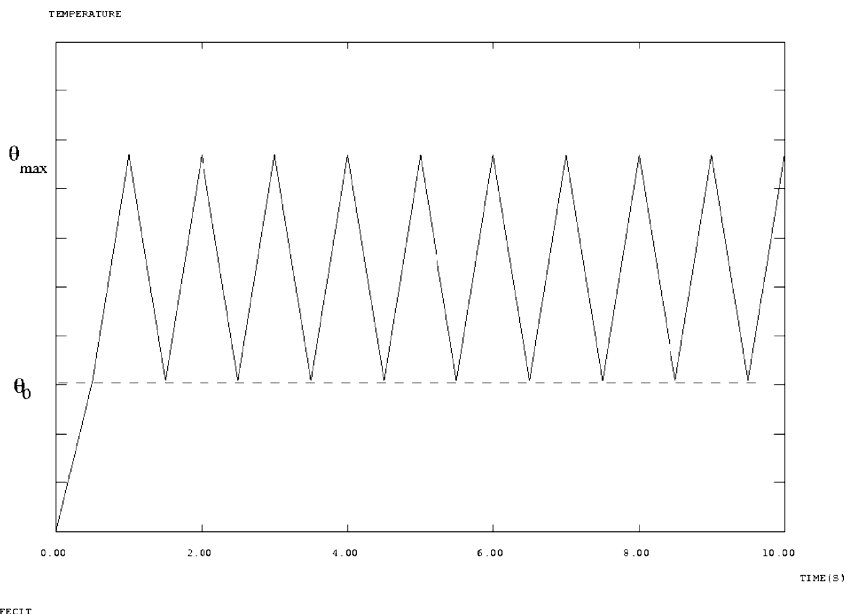

Fig. 4 Cyclic temperature variation

x1.E-4   DEF_PLAS

7.00

6.30

5.60

4.90

4.20

3.50

2.80

2.10

1.40

0.70

0.00

          0.00   2.00   4.00   6.00   8.00   10.00

                                                                    TIME(S)
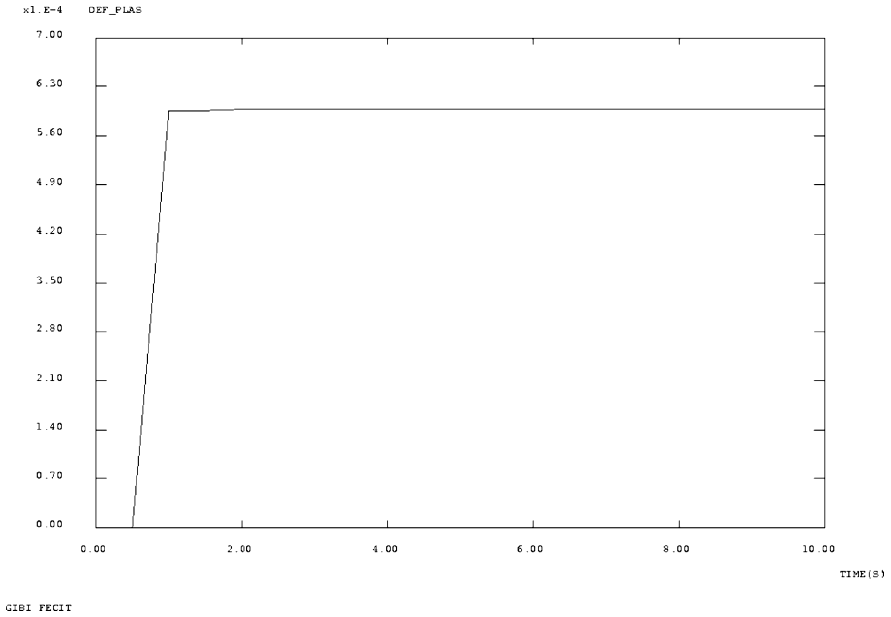
GIBI FECIT

Fig. 5 Stabilization of the plastic strain $\boldsymbol{\varepsilon}^p$ when shakedown occurs

x1.E-5   RES_STR

0.00

-0.70

-1.40

-2.10

-2.80

-3.50

-4.20

-4.90

-5.60

-6.30

-7.00

          0.00   2.00   4.00   6.00   8.00   10.00

                                                                    TIME(S)
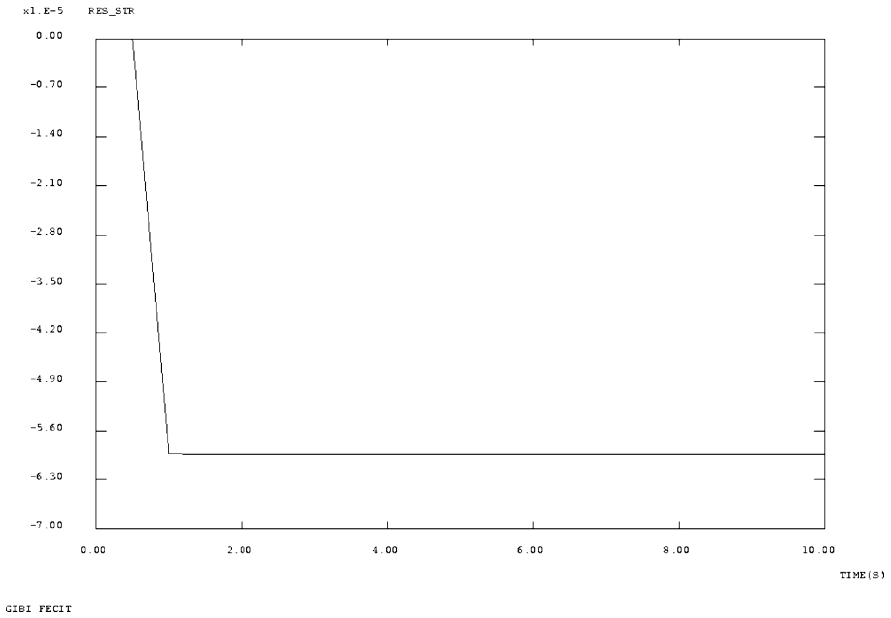
GIBI FECIT

Fig. 6 Evolution of $\boldsymbol{\eta}^e$ in the case of shakedown
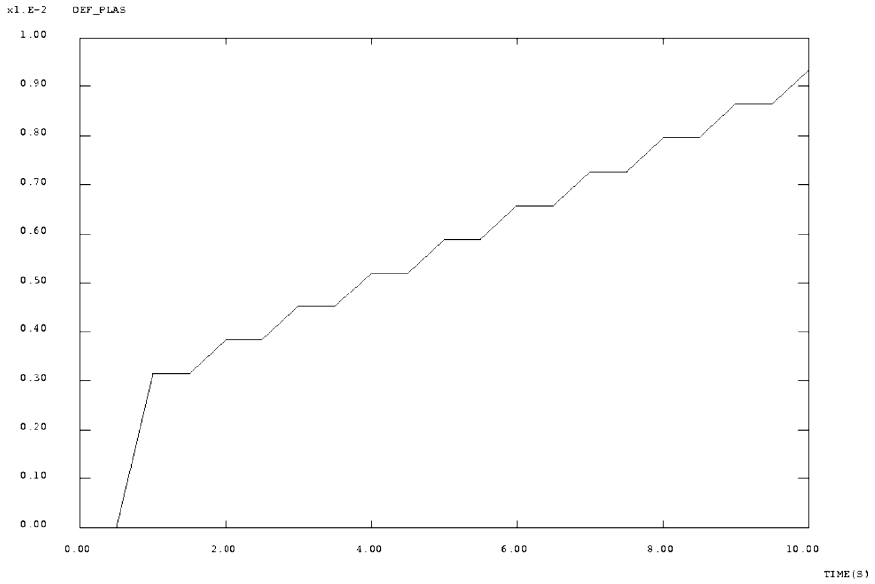
Fig. 7 Incremental increase of the plastic strain ε^p when ratchetting occurs
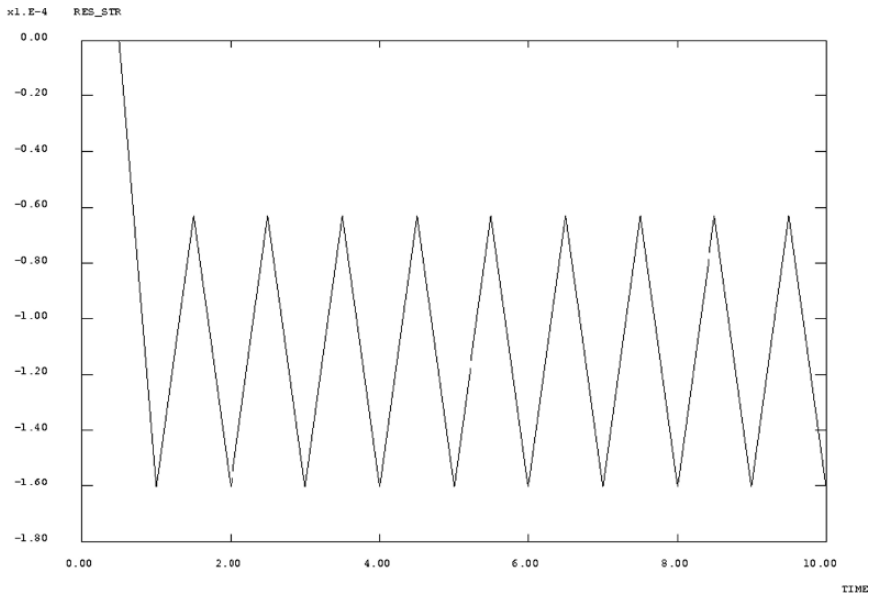
Fig. 8 Evolution of $\boldsymbol{\eta}^e$ in the case of ratchetting

figure shows that ε^p increases at each increment of time and consequently the assembly will collapse by plastic strain accumulation.

Figure 8 illustrates that $\boldsymbol{\eta}^e(\boldsymbol{x}, t) = \mathbf{S}(\boldsymbol{x}, \theta) : \boldsymbol{\rho}(\boldsymbol{x}, t)$ tends towards a periodic solution of the same period as the thermal load.

These numerical results for shakedown and ratchetting responses confirm the propositions stated in the extended static shakedown theorem. To show that this is not related to the finite dimensional character of the three-bar problem, we shall study a continuous solid in the next section.

5.2 Square Plate with a Centered Hole

The second example concerns the common benchmark test in numerical shakedown analysis [11, 24] namely the square plate with a central circular hole. The study is carried out in the framework of plane stress hypothesis.

Let the plate be made of an elastic perfectly plastic material and let us suppose that the Young's modulus E and the coefficient of thermal expansion α are temperature-dependent as shown in Figs. 9 and 10 respectively.

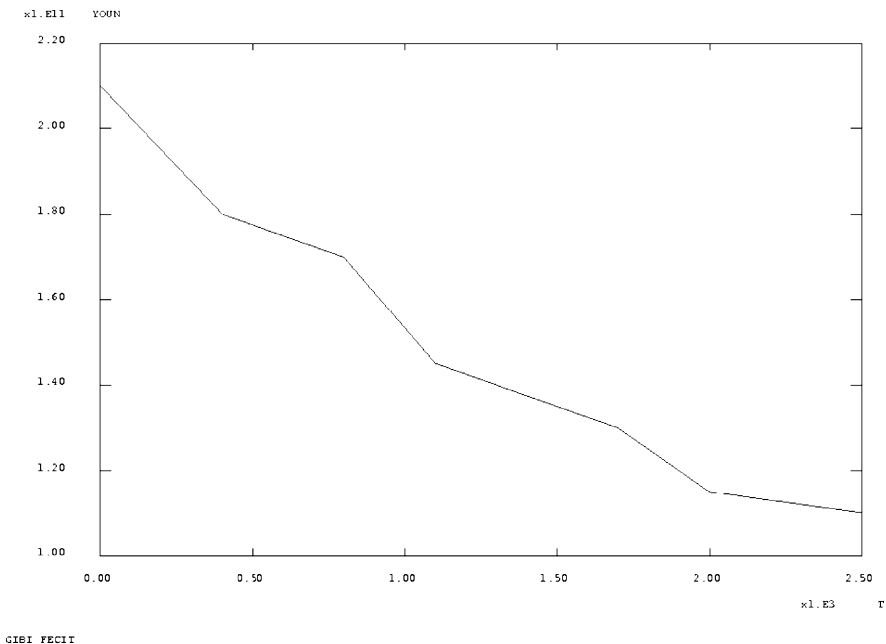The characteristics of the square plate are given in Table 2.

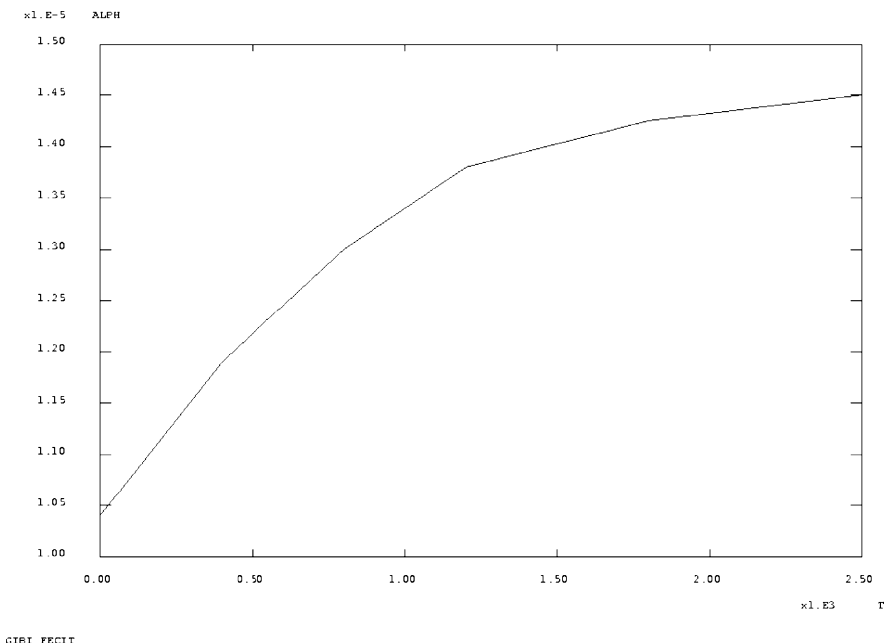**Fig. 9** Young's modulus E versus temperature

Fig. 10 Evolution of the coefficient of thermal expansion α with the temperature

Table 2 Characteristics of the square plate

L (mm)	100
Radius of the hole (mm)	10
ν	0.3
σ_y (MPa)	500

The thermo-mechanical loadings and boundary conditions are as follows. The plate is embedded on its external contour and a cyclic temperature variation θ in the range within $[\theta_0, \theta_0 + \Delta\theta]$ is uniformly distributed on the structure, cf. Fig. 11.

Due to the symmetry of the problem, numerical investigations are carried out on quarter of the plate.

The same analysis as done before for the three-bar problem is derived here again. For example, if one takes ($\theta_0 = 150°$C, $\Delta\theta = 150°$C) one obtains a shakedown regime. Figure 12 displays the iso-value map of the stabilized equivalent plastic strain field in the plate.

Now if we draw the evolution of the plastic strain extrapolated at the node $A2$ we can see that as suspected the components of this field become time-independent after some cycles. For example, Fig. 13 shows the variation of ε_{xx}^p at $A2$.
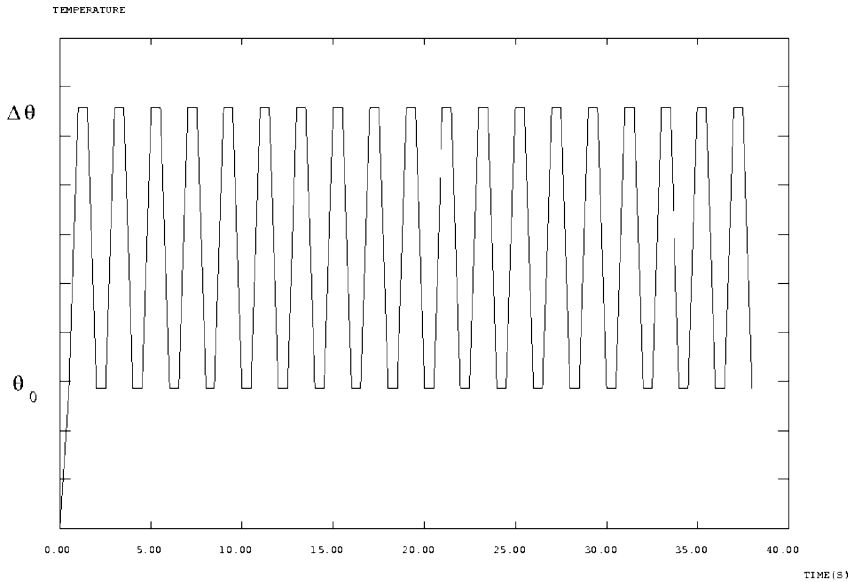
Fig. 11 Cyclic temperature variation

To check all the conditions announced in our theorem we draw the evolution of $\boldsymbol{\eta}^e(\boldsymbol{x}, t) = \mathbf{S}(\boldsymbol{x}, \theta) : \boldsymbol{\rho}(\boldsymbol{x}, t)$ according to time for $A2$ and we obtain Fig. 14 for the component η_{xx}^e. It is clear that, in the case of shakedown, this quantity tends toward a time-independent limit.

Moreover, numerical simulations show that it is possible to obtain an alternating plasticity as quasi-static response of the plate. This can be achieved for example for ($\theta_0 = 200°$C, $\Delta\theta = 200°$C). For this data input, Fig. 15 shows the evolution of ε_{yy}^p of the node $A2$. This type of curves is typical for alternating plasticity.

As done before, one can plot the variation of $\boldsymbol{\eta}^e(\boldsymbol{x}, t) = \mathbf{S}(\boldsymbol{x}, \theta) : \boldsymbol{\rho}(\boldsymbol{x}, t)$. Figure 16 shows that η_{yy}^e tends toward a periodic limit with same period as the thermal loadings.

The third and last possible regime namely the ratchetting is obtained for example when the thermal loading is ($\theta_0 = 200°$C, $\Delta\theta = 1000°$C). For the node $A2$, the increase of the incremental plastic strain is displayed in Fig. 17.

In this case, one can observe that $\boldsymbol{\eta}^e(\boldsymbol{x}, t) = \mathbf{S}(\boldsymbol{x}, \theta) : \boldsymbol{\rho}(\boldsymbol{x}, t)$ becomes cyclic with the same period of the loading as displayed in Fig. 18.

5.2.1 Remark

Numerical simulations were carried out to study the influence of the initial state of the structure on the nature of the thermo-mechanical response
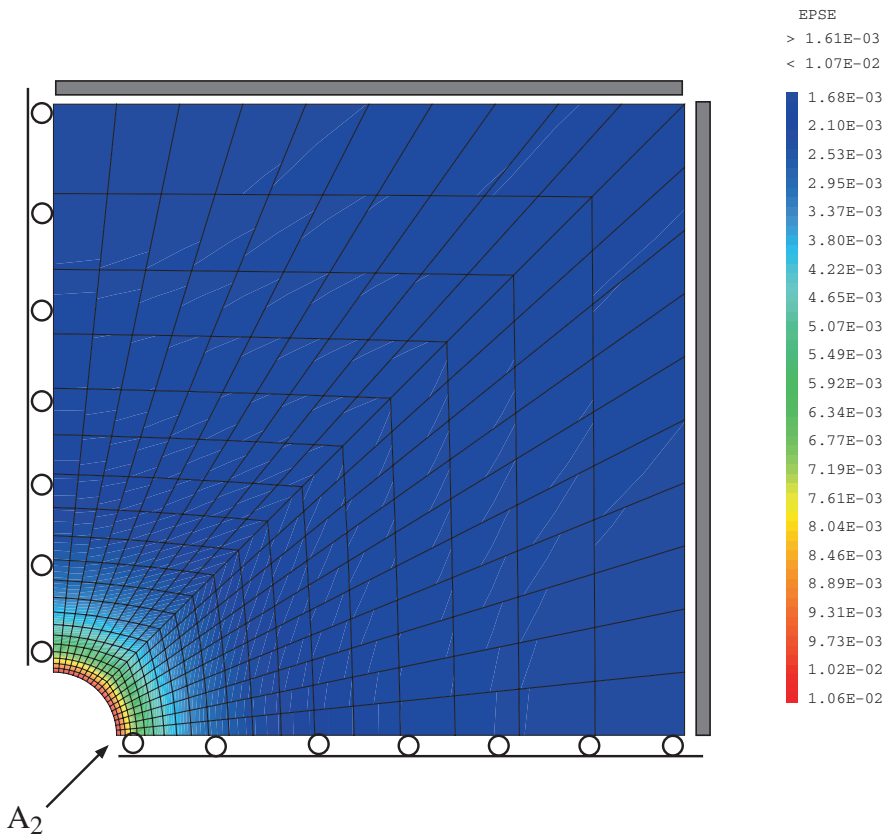
Fig. 12 Iso-value map of the stabilized equivalent plastic strain field in the case of adaptation

but are not shown here to shorten the article. It was found that the initial stress/strain state does not change the status of the limit response. It influences only the values of the numerical values of different mechanical fields.

6 Conclusion

A novel static shakedown theorem for elastic-plastic materials with temperature-dependent coefficients has been presented in this article. It concerns not only the variation of the elasticity tensor components with the temperature but also the cases of decrease of the yield stress and the variation of coefficient of thermal expansion. Compared to shakedown of materials with constant elastic modulus, it is not the residual stress tensor which is time-independent but it is the elastic residual strain field $\boldsymbol{\eta}^e$.

x1.E-3   DEF_PLAS
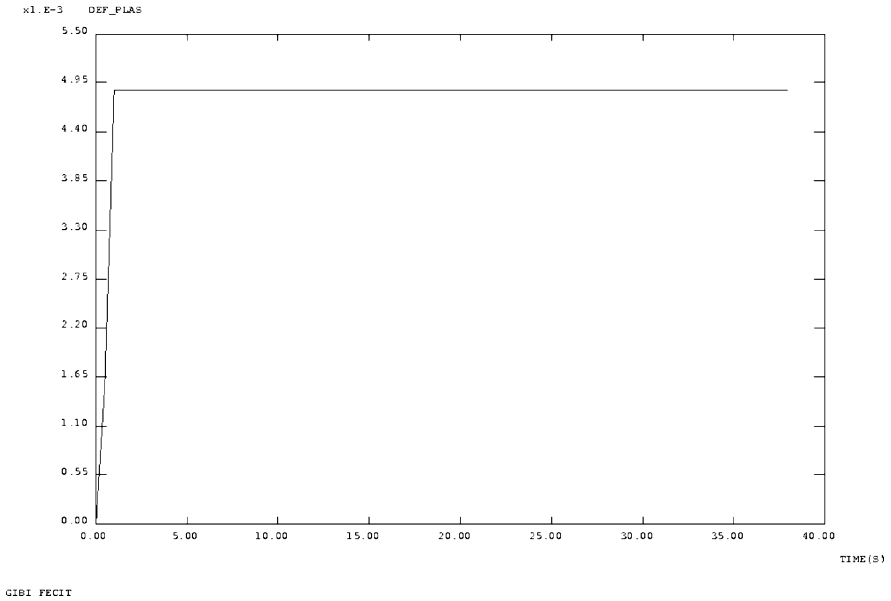
GIBI FECIT

Fig. 13 Evolution of ε_{xx}^p in case of shakedown

x1.E-3   RES_ELA
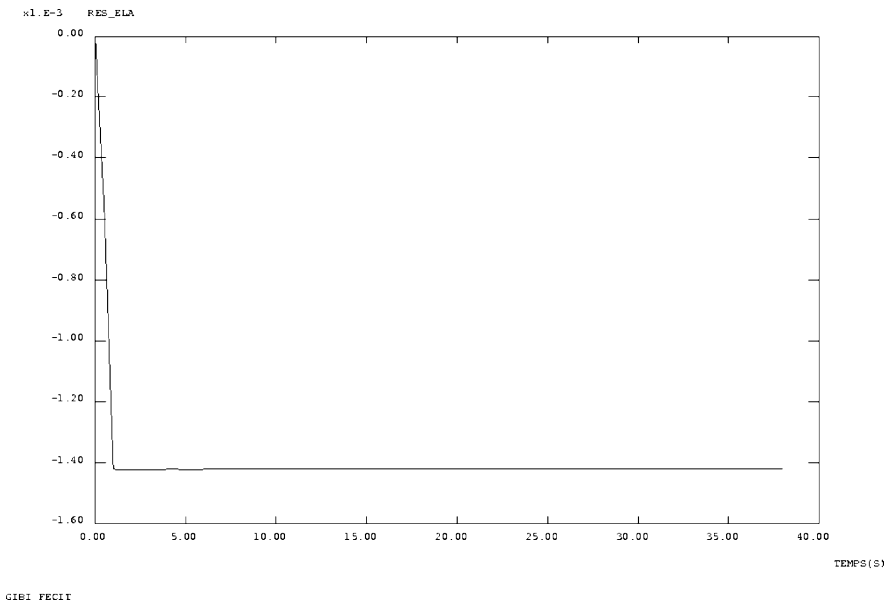
GIBI FECIT

Fig. 14 Evolution of η_{xx}^e in case of shakedown

x1.E-2 DEF_PLAS
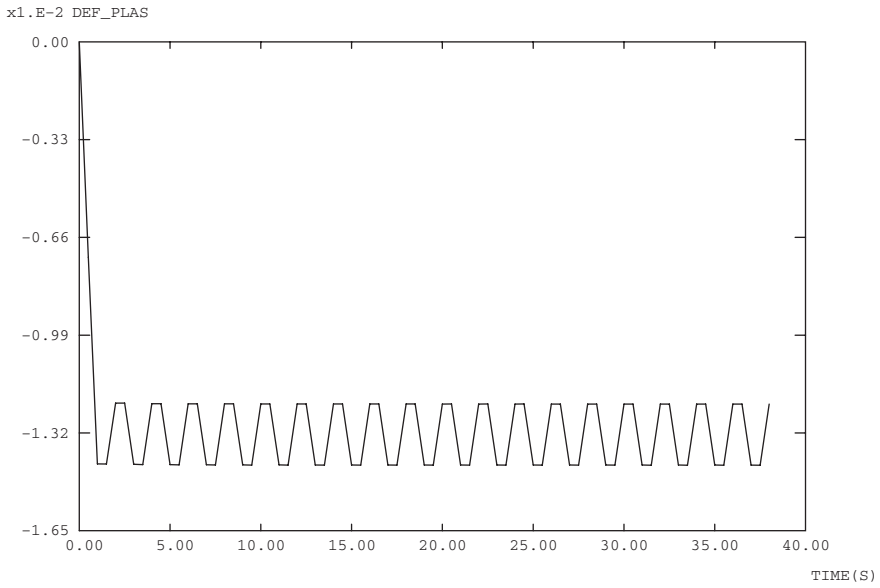
GIBI FECIT

Fig. 15 Evolution ε_{yy}^p in the case of alternating plasticity

x1.E-2 RES_ELA
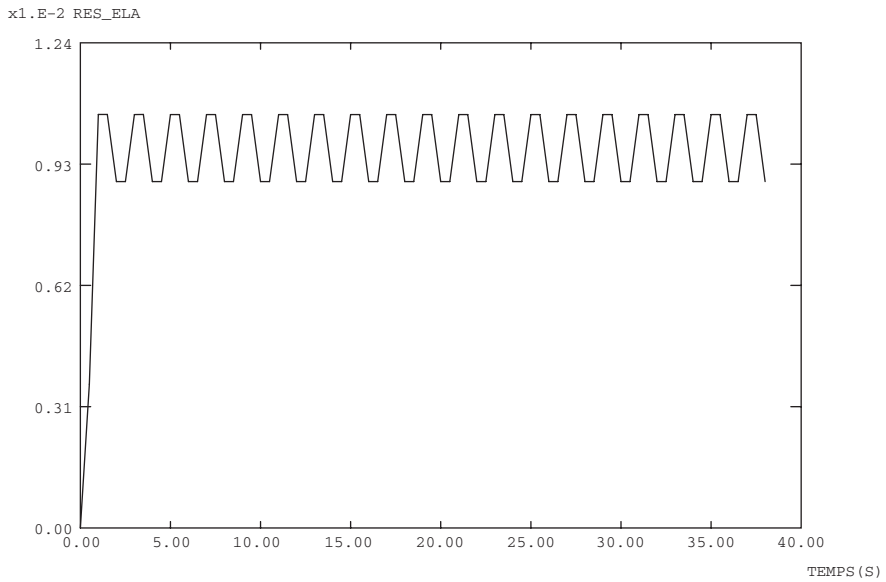
GIBI FECIT

Fig. 16 Evolution η_{yy}^e in the case of alternating plasticity

x1.E-2 DEF_PLAS

GIBI FECIT
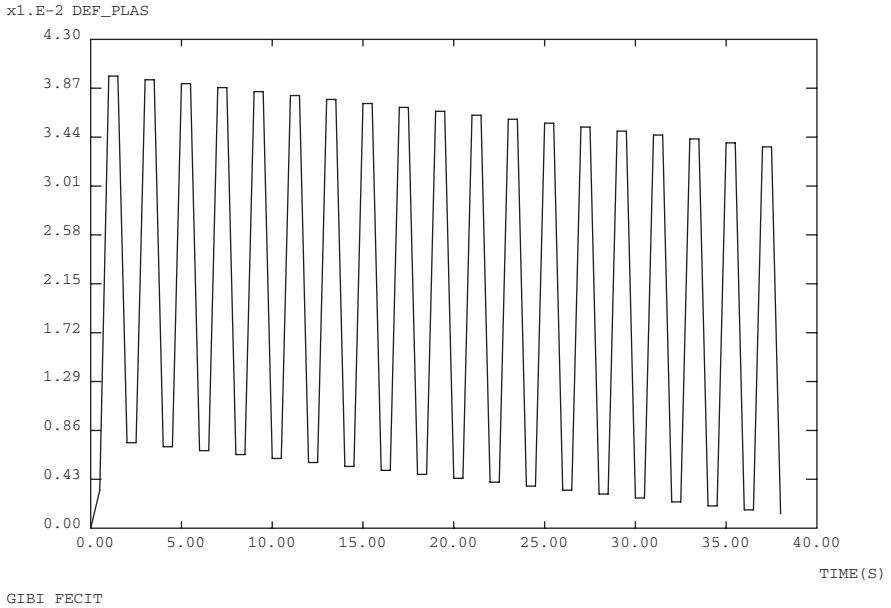
Fig. 17 Evolution of ε_{xx}^{p} in the case of ratchetting

x1.E-2 RES_ELA

GIBI FECIT
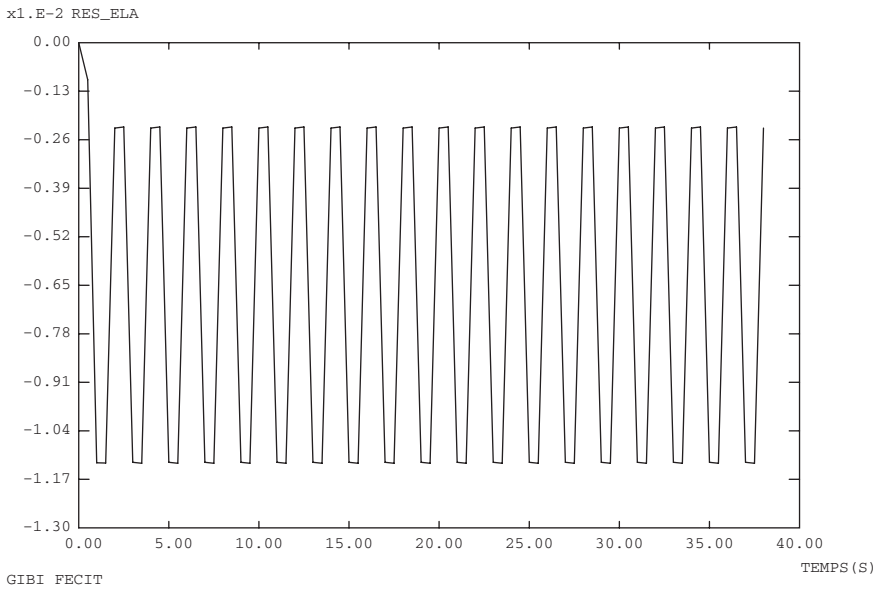
Fig. 18 Evolution of η_{xx}^{e} in the case of ratchetting

As in the classical problems of shakedown, a definition of the static shake-down safety factor is given and this can lead to algorithms for approximating of the shakedown upper bounds. This task will be addressed in a future work. Numerical simulations performed by step-by-step finite elements calculus have been addressed to verify the theorem conditions. It is found that in cases of the ratchetting and alternating plasticity, the elastic residual strain field $\boldsymbol{\eta}^e$ tends toward a cyclic time-evolution with the same period of thermal loading. It seems that this response is related to the solution of the multival-ued Eq. (14) established in [14]. A mathematical analysis of the Eq. (14) will be published by the authors in a future paper.

References

1. Barber, J., Klarbring, A., Ciavarella, M.: Shakedown in frictional contact problems for the continuum, C R Mécanique **336**, 34–41 (2008)
2. Belouchrani, M.A., Weichert, D.: An extension of the static shakedown theorem to inelastic cracked structures. Int. J. Mech. Sci. **41**, 163–177 (1999)
3. Bleich, H.: Über die Bemessung statisch unbestimmter Stahltragwerke unter Berück-sichtigung des elastisch-plastischen Verhaltens des Baustoffes. J. Bauingenieur. **19**, 261–269 (1932)
4. Bousshine, L., Chaaba, A., de Saxé, G.: A new approach to shakedown analysis for non-standard elastoplastic material by the bipotential. Int. J. Plasticity. **19**, 583–598 (2003)
5. Cazzani, G., Contro, R., Corradi, L.: On the evaluation of the shakedown boundary for temperature-dependent elastic properties. Eur. J. Mech. A/Solid. **4**, 539–550 (1992)
6. Cocchetti, G., Maier, G.: Static shakedown theorems in piecewise linearized poroplas-ticity. Arch. Appl. Mechan. **68**, 651–661 (1998)
7. Constantinescu, A.: An introduction to finite elements based on examples with Cast3M. Courses at Ecole Polytechnique (2007)
8. Corigliano, A., Maier, G., Pycko, S.: Dynamic shakedown analysis and bounds for elastoŬplastic structures with non-associated internal variable constitutive laws. Int. J. Solid. Struct. **32**, 3145–3166 (1995)
9. Débordes, O., Nayroles, B.: Sur la théorie et le calcul à l'adaptation des structures élasto-plastiques. J Mécanique **20**, 1–54 (1976)
10. de Saxé, G., Tritsch, J.B.: Shakedown with non associated flow rule. In: Weichert, D., Maier, G. (eds.) Inelastic Behaviour of Structures Under Variable Repeated Loads, CISM International Centre for Mechanical Sciences, Courses and Lectures, Springer, Wien, New York (2002)
11. di Domizio, S.: Structures élastoplastiques sous chargement cyclique: équation d'évolution de la contrainte résiduelle. Stage, Ecole Polytechnique (2005)
12. Feng, X.Q., Sun, P.R.: Shakedown analysis of shape memory alloy structures. Int. J. Plasticity **23**, 183–206 (2006)
13. Hachemi, A., Weichert, D.: An extension of the static shakedown theorem to a certain class of inelastic material with damage. Arch. Mech. **44**, 491–498 (1992)
14. Halphen, B.: Elastic perfectly plastic structures with temperature dependent elastic coefficients. C R Mécanique **333**, 617–621 (2005)
15. Koiter, J.A.: General problems for elastic-plastic solids. In: Sneddon, I.N., Hill, R. (eds.) Progress in Solid Mechanics, North-Holland, Amsterdam, pp. 165–221 (1960)
16. König, J.A.: A shakedown theorem for temperature dependent elastic moduli. Bull. Ac. Pol. Sci. Ser. Sci. Techn. **17**, 161 (1968)

17. König, J.A.: Shakedown of Elastic-Plastic Structures. General Problems for Elastic-Plastic Solids. Elsevier, Amsterdam (1987)
18. Melan, E.: Theorie statisch unbestimmter Systeme aus ideal-plastischem Baustoff. Sitzber. AKad. Wiss. Wien **145**, 195–218 (1936)
19. Pham, D.C.: On shakedown theory for elastic-plastic materials and extensions, J. Mech. Phys. Solid. **56**, 1905–1915 (2008)
20. Polizzotto, C.: Shakedown theorems for elastic plastic solids in the framework of gradient plasticity. Int. J. Plasticity **4**, 218–241 (2008)
21. Prager, W.: Shakedown in elastic plastic media subjected to cycles of load and temperature. In: La Plasticità nella Scienza delle Costruzioni, Proc Danusso Symp Zanichelli, Bologna, Italy (1956)
22. Nguyen, Q.S.: Stability and Nonlinear Mechanics. John Wiley & Sons, New York (2000)
23. Nguyen, Q.S.: On shakedown analysis in hardening plasticity. J. Mech. Phys. Solid. **51**, 101–124 (2003)
24. Heitzer, M., Staat, M.: Basis reduction technique for limit and shakedown problems. In: Staat, M., Heitzer, M. (eds.) Numerical Methods for Limit and Shakedown Analysis: Deterministic and Probabilistic Problems. NIC Series **15**, Central Institute for Applied Mathematics, Jülich (2003)

On Shakedown of Structures Under Variable Loads with a Kinematic Non-linear and Non-associated Hardening Rule

C. Bouby, G. de Saxcé, and J.-B. Tritsch

Abstract The introduction of hardening into the study of elastoplastic shakedown analysis is considered in this paper, in particular in the case of non-associated plasticity. Due to the fact that the framework of Generalized Standard Materials (GSM) is not well adapted in this last case, an alternative approach, provided by the concept of Implicit Standard Materials (ISM), is then used. In particular, we study the typical example of an homogeneous constant traction and alternating torsion state; it is analyzed by using the step-by-step computations and then within the ISM framework. The obtained results for the shakedown factor as well as the back-stresses are examined. The comparison of the incremental method predictions to the analytical solution and the mathematical programming ones, built by means of the bipotential approach, shows a very good agreement.

1 Introduction

Many engineering structures or structural elements are submitted to cyclic mechanical loads and/or temperature fields, acting simultaneously. For this kind of loading, the limit load, based on proportional loads, do not ensure the structural safety. The experimental tests show that beyond the limit load, structures subjected to cyclic loading may fail after a finite number of cycles by accumulation of plastic strains, called ratchet or incremental

Céline Bouby
LEMTA, Nancy-Université, CNRS, 2, rue Jean Lamour, Vandœuvre Les Nancy Cedex, F-54519, France, e-mail: celine.bouby@esstin.uhp-nancy.fr

Géry de Saxcé and Jean-Bernard Tritsch
Laboratoire de Mécanique de Lille, UMR CNRS 8107, Université des Sciences et Technologies de Lille, Cité Scientifique, F-59655 Villeneuve d'Ascq cedex, France, e-mail: gery.desaxce@univ-lille1.fr; jean-bernard.tritsch@polytech-lille.fr

collapse, or by periodic elastoplastic strain response, called plastic shakedown or accommodation. Nevertheless, the structure can also endure a very large number of cycles (high-cycle fatigue). In this case, called elastic shakedown, the behaviour corresponds to a stabilization of the plastic strains and the response of the structure becomes purely elastic.

In the pioneering works on shakedown theory by [9] and [15] the plastic effects covered by the theoretical development were restricted to linear elastic perfectly plastic materials, with no thermal influence and in quasi-static processes. From the engineering point of view, these assumptions were not always realistic. Consequently, extensions of the classical shakedown theorems have attracted much interest in the last years, specifically to take into account the hardening effects in the framework of generalized standard materials (see, e.g. the review in [12, 16]).

As the class of generalized standard materials is not relevant to model the non-associative constitutive laws (this is the case when the non-linear kinematic hardening rule is considered), we use the bipotential approach. Using this framework, it has been shown (see e.g. de Saxcé in [13]) that many non-standard dissipative materials are in fact governed by a normality rule, but in an implicit sense. Therefore, the main objective of the present chapter is to study non-linear kinematic hardening models in the scope of implicit standard materials. To this end, after recalling some theoretical basis of the bipotential approach and its application to shakedown analysis, we consider the example of an homogeneous constant traction and alternating torsion state and analyze it by using the step-by-step computations and then within the Implicit Standard Materials framework. The results obtained with the incremental method predictions are then compared to the analytical solution and to the mathematical programming ones, built by means of the bipotential approach.

2 Implicit Standard Materials and Shakedown

2.1 Concept of Implicit Standard Materials

Let the generalized velocities be $\dot{\boldsymbol{\kappa}} = (\dot{\boldsymbol{\varepsilon}}^p, \dot{\boldsymbol{\kappa}}') \in V$, the velocity space, including the velocities $\dot{\boldsymbol{\kappa}}'$ of additional internal variables (hardening, …), and the corresponding associated variables $\boldsymbol{\pi} = (\boldsymbol{\sigma}, \boldsymbol{\pi}') \in F$, the stress space. A bipotential is a function b from $V \times F$ into $]-\infty, \infty]$, separately convex, satisfying the fundamental inequality generalizing Legendre-Fenchel one [7]:

$$\forall (\dot{\boldsymbol{\kappa}}^*, \boldsymbol{\pi}^*) \in V \times F, \, b(\dot{\boldsymbol{\kappa}}^*, \boldsymbol{\pi}^*) \geq \dot{\boldsymbol{\kappa}}^* \cdot \boldsymbol{\pi}^* . \tag{1}$$

The couples $(\dot{\boldsymbol{\kappa}}, \boldsymbol{\pi})$, for which the variables are related by the dissipative law, are qualified as *extremal* in the sense that the equality is reached in the previous relation:

$$b(\dot{\boldsymbol{\kappa}}, \boldsymbol{\pi}) = \dot{\boldsymbol{\kappa}} \cdot \boldsymbol{\pi} \,. \tag{2}$$

Then, the extremal couples are characterized by the differential inclusions $\dot{\boldsymbol{\kappa}} \in \partial_{\boldsymbol{\pi}} b(\dot{\boldsymbol{\kappa}}, \boldsymbol{\pi})$, $\boldsymbol{\pi} \in \partial_{\dot{\boldsymbol{\kappa}}} b(\dot{\boldsymbol{\kappa}}, \boldsymbol{\pi})$ where $\partial_{\boldsymbol{\pi}}$ ($\partial_{\dot{\boldsymbol{\kappa}}}$ respectively) denotes the sub-differential when partial derivating with respect to $\boldsymbol{\pi}$ (respectively $\dot{\boldsymbol{\kappa}}$). For elastic-plastic behaviours, the set of extremal couples is equivalent to that of the material states satisfying the plastic flow rule. Physically, the bipotential stands for the plastic dissipation power, and thus, is supposed to be positive. Materials admitting a bipotential are further called implicit standard materials by analogy to the generalized standard ones.

2.2 Bipotential Approach for Shakedown Analysis

Let Ω be a solid body with an elastic-plastic material admitting a bipotential:

$$\forall (\dot{\boldsymbol{\varepsilon}}^p, \dot{\boldsymbol{\kappa}}') \in V, \, \forall (\boldsymbol{\sigma}, \boldsymbol{\pi}') \in F, \, b[(\dot{\boldsymbol{\varepsilon}}^p, \dot{\boldsymbol{\kappa}}'), (\boldsymbol{\sigma}, \boldsymbol{\pi}')] \geq \boldsymbol{\sigma} : \dot{\boldsymbol{\varepsilon}}^p + \boldsymbol{\pi}' \cdot \dot{\boldsymbol{\kappa}}', \tag{3}$$

where ":" denotes the standard double contracted tensorial product. It is subjected to variable periodic external actions varying between given limits controlled by a load factor λ. As in [3], we define admissible stress fields $(\overline{\boldsymbol{\rho}}, \overline{\boldsymbol{\pi}}')$ in the sense that:

(i) $\overline{\boldsymbol{\rho}}$ is a residual stress field;

(ii) $\overline{\boldsymbol{\rho}}$ and $\overline{\boldsymbol{\pi}}'$ are time-independent and plastically admissible when adding to $\overline{\boldsymbol{\rho}}$ the stress response $\boldsymbol{\sigma}^e = \lambda \boldsymbol{\sigma}^{e0}$ in the corresponding fictitious elastic body:

$$\forall \boldsymbol{x} \in \Omega, \, \forall t, \, (\boldsymbol{\sigma}^e(\boldsymbol{x}, t) + \overline{\boldsymbol{\rho}}(\boldsymbol{x}), \overline{\boldsymbol{\pi}}'(\boldsymbol{x})) \in K \text{ with the elastic domain } K.$$

Following [17], we define admissible generalized velocity fields $(\dot{\boldsymbol{\varepsilon}}^p, \dot{\boldsymbol{\kappa}}')$ in the sense that:

(iii) the increment of the plastic strain rate on the load cycle $\Delta \boldsymbol{\varepsilon}^p = \oint \dot{\boldsymbol{\varepsilon}}^p \mathrm{d}t$ is kinematically admissible with zero values of the corresponding displacement increments on the supports,

(iv) $\dot{\boldsymbol{\varepsilon}}^p$ is plastically admissible in the following sense:

$$\int_{\Omega} \oint \boldsymbol{\sigma}^e : \dot{\boldsymbol{\varepsilon}}^p \, \mathrm{d}t \, \mathrm{d}\Omega > 0 \,,$$

(v) the increment of kinematic internal variables on the load cycle vanishes:

$$\Delta\boldsymbol{\kappa}' = \oint \boldsymbol{\kappa}'(\boldsymbol{x},t)\,\mathrm{d}t = 0\,.$$

The reasons to introduce admissible fields $(\overline{\boldsymbol{\rho}}, \overline{\boldsymbol{\pi}}')$ characterized by (i)–(ii), and $(\dot{\boldsymbol{\varepsilon}}^p, \dot{\boldsymbol{\kappa}}')$ characterized by (iii)–(v) is that we are only interested in the asymptotic fields reached after a transient phase, which can be infinite (for further details, see [3,4]). In particular, if shakedown occurs, the plastic strain $\boldsymbol{\varepsilon}^p$ and the other internal variables $\boldsymbol{\kappa}'$ stabilize and the total dissipation is bounded. In the framework of implicit standard materials, the existence of time-independent residual fields is assumed but, up to now, has not been proved (as in Melan's famous theorem). This assumption must be considered as a reasonable generalization of the Melan's theory. Then, the admissible fields can be incorporated in a variational formulation of shakedown problems built by introducing the so-called bifunctional:

$$\beta_S(\dot{\boldsymbol{\varepsilon}}^p, \dot{\boldsymbol{\kappa}}', \overline{\boldsymbol{\rho}}, \overline{\boldsymbol{\pi}}', \lambda) = \int_\Omega \oint \left\{ b[(\dot{\boldsymbol{\varepsilon}}^p, \dot{\boldsymbol{\kappa}}'), (\overline{\boldsymbol{\rho}} + \lambda\boldsymbol{\sigma}^{e0}, \overline{\boldsymbol{\pi}}')] - \lambda\boldsymbol{\sigma}^{e0} : \dot{\boldsymbol{\varepsilon}}^p \right\}\,\mathrm{d}t\,\mathrm{d}\Omega\,. \tag{4}$$

By virtue of the principle of virtual work, a straightforward consequence of (3) is that for any admissible field the bifunctional (4) is greater or equal to zero. As λ tends to λ^a by upper values, the limit velocity field $(\dot{\boldsymbol{\varepsilon}}^p, \dot{\boldsymbol{\kappa}}')$ and the stress field $(\lambda^a\boldsymbol{\sigma}^{e0} + \overline{\boldsymbol{\rho}}, \overline{\boldsymbol{\pi}}')$ satisfy the constitutive law. According to (2), one has:

$$\beta_S(\dot{\boldsymbol{\varepsilon}}^p, \dot{\boldsymbol{\kappa}}', \overline{\boldsymbol{\rho}}, \overline{\boldsymbol{\pi}}', \lambda^a) = 0\,. \tag{5}$$

The kinematical and statical fields have to be determined together, which provides a weak form of the classical dual theorems, adapted to the class of implicit standard materials. Clearly enough, the kinematical and statical shakedown problems cannot be solved independently but are strongly "coupled". Nevertheless, one can get, as shown in [2], a formulation of kinematic bound problem:

$$\inf_{\dot{\boldsymbol{\kappa}}^k} \int_\Omega \oint \left\{ b[(\overline{\boldsymbol{\rho}} + \lambda^a\boldsymbol{\sigma}^{e0}, \overline{\boldsymbol{\pi}}'), (\dot{\boldsymbol{\varepsilon}}^{pk}, \dot{\boldsymbol{\kappa}}'^{k})] \right\}\,\mathrm{d}t\,\mathrm{d}\Omega$$
$$\text{s. t.} \begin{cases} \dot{\boldsymbol{\kappa}}^k \text{ admissible}\,, \\ \int_\Omega \oint \boldsymbol{\sigma}^{e0} : \dot{\boldsymbol{\varepsilon}}^{pk}\,\mathrm{d}t\,\mathrm{d}\Omega = 1\,. \end{cases} \tag{6}$$

Following [6], the static bound problem takes then the form:

$$\sup_{\overline{\boldsymbol{\pi}}^s, \lambda^s} \left\{ \lambda^s - \int_\Omega \oint \left\{ b[(\overline{\boldsymbol{\rho}}^s + \lambda^s\boldsymbol{\sigma}^{e0}, \overline{\boldsymbol{\pi}}'^s), (\dot{\boldsymbol{\varepsilon}}^p, \dot{\boldsymbol{\kappa}}')] \right\}\,\mathrm{d}t\,\mathrm{d}\Omega \right\} \text{ s. t. } \overline{\boldsymbol{\pi}}^s \text{ admissible}\,. \tag{7}$$

Numerical simulations show that the initial state of the back-stresses affects the delay of apparition of incipient plastic flow but does not modify the shakedown load [3].

2.3 Generalized Standard Materials by the Bipotential Approach

If the constitutive law is associated, it can be represented by a separated bipotential $b(\dot{\boldsymbol{\kappa}}, \boldsymbol{\pi}) = \varphi(\dot{\boldsymbol{\kappa}}) + \Psi_K(\boldsymbol{\pi})$, where Ψ_K is the indicator function of K, i.e. $\Psi_K(\boldsymbol{\pi}) = 0$ if $\boldsymbol{\pi} \in K$ and $\Psi_K(\boldsymbol{\pi}) = +\infty$ otherwise, while φ is the support function of K, that is the well-known dissipation function. Then the bifunctional is also separated. The bound problems (6) and (7) are then "decoupled". This gives for the kinematic bound problem:

$$\inf_{\dot{\boldsymbol{\kappa}}^k} \int_\Omega \oint \left\{ \varphi(\dot{\boldsymbol{\varepsilon}}^{pk}, \dot{\boldsymbol{\kappa}}'^k) \right\} \, \mathrm{d}t \, \mathrm{d}\Omega \quad \text{s. t.} \begin{cases} \dot{\boldsymbol{\kappa}}^k \text{ admissible} \\ \int_\Omega \oint \boldsymbol{\sigma}^{e0} : \dot{\boldsymbol{\varepsilon}}^{pk} \, \mathrm{d}t \, \mathrm{d}\Omega = 1 \,, \end{cases} \tag{8}$$

and for the static bound problem:

$$\sup_{\overline{\boldsymbol{\pi}}^s, \lambda^s} \left\{ \lambda^s - \int_\Omega \oint \left\{ \Psi_K(\overline{\boldsymbol{\rho}}^s + \lambda^s \boldsymbol{\sigma}^{e0}, \overline{\boldsymbol{\pi}}'^s) \right\} \, \mathrm{d}t \, \mathrm{d}\Omega \right\} \quad \text{s. t. } \overline{\boldsymbol{\pi}}^s \text{ admissible .} \tag{9}$$

A straightforward consequence of the bipotential-based method is the simultaneous construction of both kinematic and static bound problems.

3 Computation of Shakedown Load for a Homogeneous Constant Tension and Alternating Torsion State

In this section, we study the typical example of a homogeneous constant traction and alternating torsion state with the non-linear kinematic hardening rule. Assuming that the plastic threshold is constant and equal to σ_Y, the generalized velocity fields $\dot{\boldsymbol{\kappa}}$ are reduced to $(\dot{\boldsymbol{\varepsilon}}^p, -\dot{\boldsymbol{\alpha}})$ and the generalized stress fields $\boldsymbol{\pi}$ to $(\boldsymbol{\sigma}, \mathsf{X})$. The elastic domain K is then defined by:

$$K = \{(\boldsymbol{\sigma}, \mathsf{X}) \text{ such that } \sigma_{eq}(\boldsymbol{\sigma} - \mathsf{X}) - \sigma_Y \le 0\} \,.$$

As $\sigma_Y > 0$, the isotropic hardening rule requires that $\varepsilon_{eq}(\dot{\boldsymbol{\varepsilon}}^p) = \dot{p}$. The non-associated kinematic hardening rule introduced by Armstrong and Frederick [1] and more extensively developed by Lemaitre and Chaboche [11] and Marquis [14], can be written as:

$$\dot{\boldsymbol{\alpha}} = \dot{\boldsymbol{\varepsilon}}^p - \frac{3}{2} \frac{\mathsf{X}}{X_\infty} \varepsilon_{eq}(\dot{\boldsymbol{\varepsilon}}^p) \,. \tag{10}$$

Furthermore, the back-stresses are linearly dependent on the kinematic variables through $\mathsf{X} = \frac{2}{3} C \boldsymbol{\alpha}$ where C is a constant kinematic hardening modulus. Consider now a homogeneous constant tension and alternating torsion state

in plane strain state. For this application, stress tensor and back-stress one, reduced to its deviatoric part, read:

$$\boldsymbol{\sigma} = \begin{bmatrix} \sigma_{11} & \sigma_{12} & 0 \\ \sigma_{12} & 0 & 0 \\ 0 & 0 & \sigma_{33} \end{bmatrix}, \quad \mathsf{X} = \begin{bmatrix} X_{11} & X_{12} & 0 \\ X_{12} & -(X_{11} + X_{33}) & 0 \\ 0 & 0 & X_{33} \end{bmatrix}.$$

Accounting for von Mises criterion, σ_{eq} is given by:

$$\sigma_{eq}(\boldsymbol{\sigma} - \mathsf{X}) = (\sigma - X)^2 + (\nu\sigma - Z)^2 + (\tau - Y)^2 + 2(X + Z)^2 - (\sigma + Z)(\nu\sigma + X), \tag{11}$$

where use has been made of the following transformed variables:

$$\sigma_{11} = \sigma, \ X_{11} = X, \ \sigma_{12} = \frac{\tau}{\sqrt{3}}, \ X_{12} = \frac{Y}{\sqrt{3}}, \ \sigma_{33} = \nu\sigma, \ X_{33} = Z. \tag{12}$$

Assuming the plastic incompressibility, the plastic strains rates and kinematic internal variables rates tensors can be written as:

$$\dot{\boldsymbol{\varepsilon}}^p = \begin{bmatrix} \dot{\varepsilon}_{11}^p & \dot{\varepsilon}_{12}^p & 0 \\ \dot{\varepsilon}_{12}^p & -(\dot{\varepsilon}_{11}^p + \dot{\varepsilon}_{33}^p) & 0 \\ 0 & 0 & \dot{\varepsilon}_{33}^p \end{bmatrix}, \quad \dot{\boldsymbol{\alpha}} = \begin{bmatrix} \dot{\alpha}_{11} & \dot{\alpha}_{12} & 0 \\ \dot{\alpha}_{12} & -(\dot{\alpha}_{11} + \dot{\alpha}_{33}) & 0 \\ 0 & 0 & \dot{\alpha}_{33} \end{bmatrix}.$$

In the same spirit as previously for the stresses, let us introduce the following notations:

$$\dot{\varepsilon}_{11}^p = \dot{\varepsilon}, \ \dot{\alpha}_{11} = \dot{\alpha}, \ \dot{\varepsilon}_{12}^p = \frac{\sqrt{3}}{2}\dot{\gamma}, \ \dot{\alpha}_{12} = \frac{\sqrt{3}}{2}\dot{\beta}, \ \dot{\varepsilon}_{33}^p = \dot{\eta}, \ \dot{\alpha}_{33} = \dot{\xi}. \tag{13}$$

3.1 Step-by-Step Analysis

In this section, the purpose is to establish an incremental strain/stress relationship.

3.1.1 Stress-Strain Curve

The total strain increment $d\boldsymbol{\varepsilon}$ is assumed to be the sum of the elastic strain increment $d\boldsymbol{\varepsilon}^e$ and the plastic one $d\boldsymbol{\varepsilon}^p$:

$$d\boldsymbol{\varepsilon} = d\boldsymbol{\varepsilon}^e + d\boldsymbol{\varepsilon}^p.$$

The elastic part satisfies Hooke's law:

$$d\boldsymbol{\varepsilon} = \frac{1+\nu}{E}d\boldsymbol{\sigma} - \frac{\nu}{E}\operatorname{tr}(d\boldsymbol{\sigma})\boldsymbol{I}.$$

The plastic component is given by Prager's formulation of plastic yielding rule:

- if $f(\boldsymbol{\sigma} - \mathsf{X}) < 0$ then $\mathrm{d}\varepsilon^p = 0$

- else if $f(\boldsymbol{\sigma} - \mathsf{X}) = 0$ and $\mathrm{d}f(\boldsymbol{\sigma} - \mathsf{X}) = 0$ then $\exists \mathrm{d}\zeta \geq 0$ such that $\mathrm{d}\varepsilon^p = \mathrm{d}\zeta \frac{\partial f}{\partial \boldsymbol{\sigma}}$.

The consistency condition $\mathrm{d}f = 0$ provides an expression to compute the plastic multiplier:

$$\mathrm{d}\zeta = \frac{\frac{\partial f}{\partial \boldsymbol{\sigma}} : \mathrm{d}\boldsymbol{\sigma}}{\frac{2}{3} C \frac{\partial f}{\partial \boldsymbol{\sigma}} : \frac{\partial f}{\partial \boldsymbol{\sigma}} - \frac{C}{X_\infty} \frac{\partial f}{\partial \boldsymbol{\sigma}} : \mathsf{X} \sqrt{\frac{2}{3} \frac{\partial f}{\partial \boldsymbol{\sigma}} : \frac{\partial f}{\partial \boldsymbol{\sigma}}}} , \tag{14}$$

where C and X_∞ are materials constants. Back-stresses and plastic strains are then computed by numerical integration of the nonlinear kinematic hardening rule:

$$\mathrm{d}\mathsf{X} = \frac{2}{3} C \mathrm{d}\zeta \frac{\partial f}{\partial \boldsymbol{\sigma}} - \frac{C}{X_\infty} \mathsf{X} \mathrm{d}\zeta \sqrt{\frac{2}{3} \frac{\partial f}{\partial \boldsymbol{\sigma}} : \frac{\partial f}{\partial \boldsymbol{\sigma}}} , \tag{15}$$

and the normality law:

$$\mathrm{d}\varepsilon^p = \mathrm{d}\zeta \frac{\partial f}{\partial \boldsymbol{\sigma}} ,$$

during the two loading phases: first a tension up to σ_{max} (path OA on Fig. 1) and next, a repeated alternating torsion between τ_{max} and $-\tau_{max}$ (path ABACA on Fig. 1). Stress increments are fixed to 1 MPa for the tension
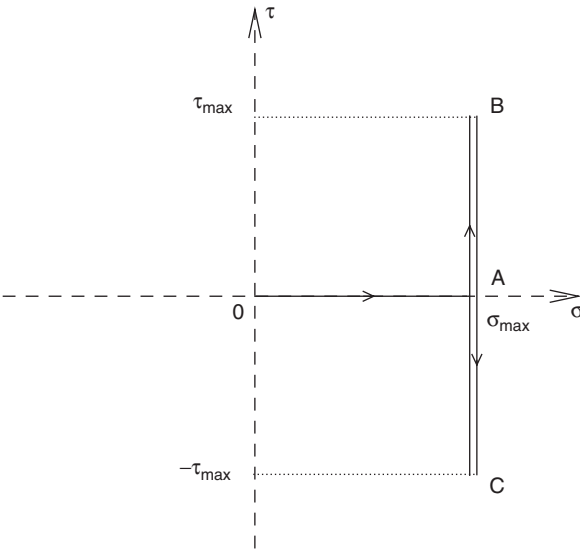

Fig. 1 Loading description

loading and to $\pm\,1\,\mathrm{MPa}$ for the alternating torsion one. Back-stresses X are initialized to $0\,\mathrm{MPa}$.

The material selected for numerical implementation is 316L steel.

First results obtained are then the strain-stress curves. For example, for a fixed tension stress $\sigma_{max} = 225\,\mathrm{MPa}$ and two different values of maximum shear stress τ_{max}, the shear strain is plotted with respect to the shear stress on Figs. 2 and 3. We observe for $\tau_{max} = 190\,\mathrm{MPa}$ that after a transient elastoplastic regime, the strain–stress curve tends to a stabilized response that shows the elastic shakedown occurs (Fig. 2), whereas for $\tau_{max} = 200\,\mathrm{MPa}$ the strain–stress curve tends to a stabilized response that shows the plastic shakedown (or accommodation) occurs (Fig. 3).
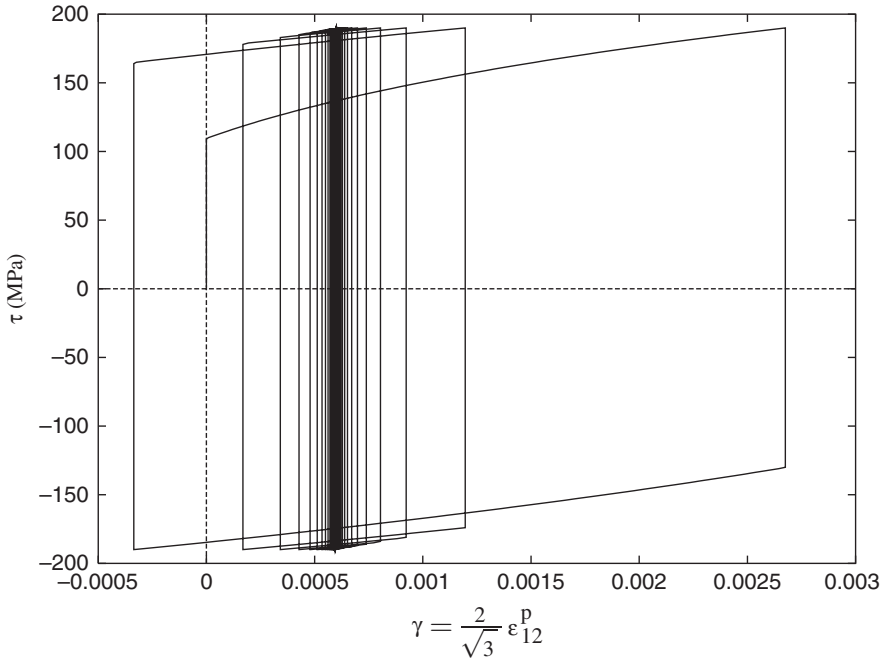
Fig. 2 Plastic shear strain in terms of shear stress for $\sigma = 225\,\mathrm{MPa}$ and $\tau_{\max} = 190\,\mathrm{MPa}$

3.1.2 Numerical Detection of Shakedown Load

In order to detect the numerical value of the shakedown load, we fix a maximum shear stress τ_{max} and we perform numerous cycles for this value. When the structure shakes down, the width of the cycle for the shear strain tends to zero, theoretically after an infinite number of cycles. In practice, the computations are stopped when the cycle width reaches a given tolerance or when the cycles number becomes greater than a given maximum. Then, the
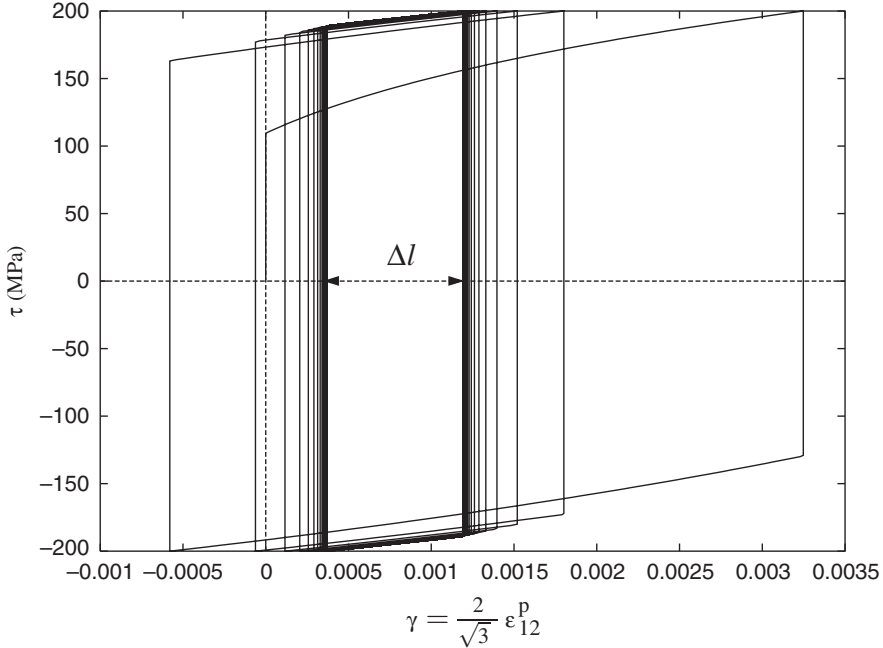
Fig. 3 Plastic shear strain in terms of shear stress for $\sigma = 225\,\text{MPa}$ and $\tau_{\max} = 200\,\text{MPa}$

corresponding maximum shear strain ε^f_{max} is considered. This procedure is performed for various values of the maximum shear stress τ_{max}.

By plotting the strain values γ^f_{max} in terms of maximal shear stress τ_{max} for a tension intensity σ_{max} of 25 MPa, we obtain the curve of Fig. 4. It seems that the sudden sloop modification observed on this curve detects the shakedown load. To confirm this idea, we have computed and plotted the curvature of this curve, by means of the second derivative, in terms of the shear stress (see Fig. 5). Effectively, we observe a significant peak of the curvature.

To confirm this result, we perform a simulation with a maximum shear stress less than 228 MPa, for example 226 MPa. We can see that the cycle width becomes less than the tolerance since the behaviour is purely elastic (see Fig. 6). When the maximum shear stress is greater than 228 MPa, for example 230 MPa, the computation stops when 1000 cycles are done. Then the cycle width never becomes less than the tolerance (see Fig. 7) and the structure does not shake down. Then the step-by-step procedure introduced here, seems to be able to detect the shakedown load. The numerical shakedown loads obtained will be compared to the ones obtained in the scope of Implicit Standard Materials in the end of the section (see Fig. 10).
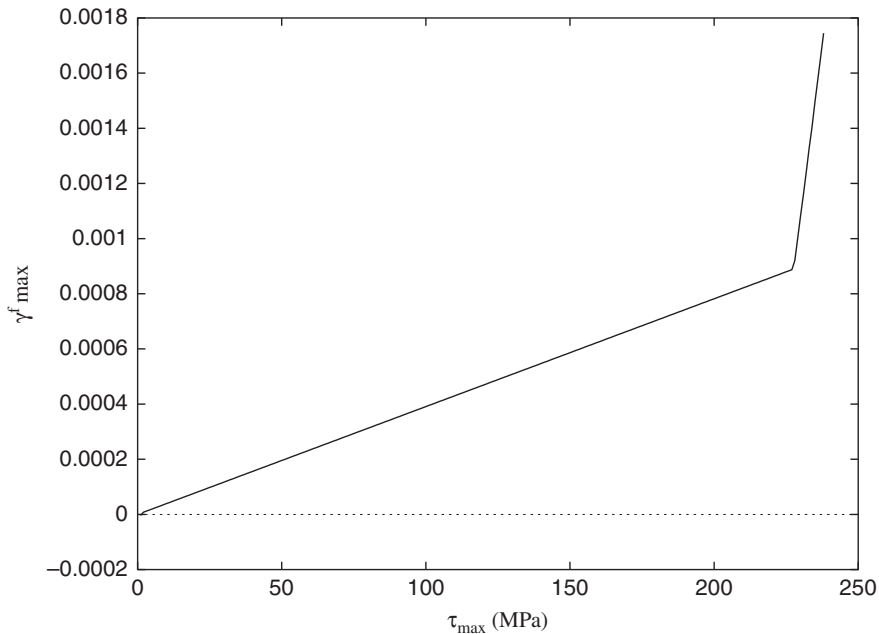
Fig. 4 Maximal final shear strain in terms of shear stress for $\sigma = 25\,\mathrm{MPa}$
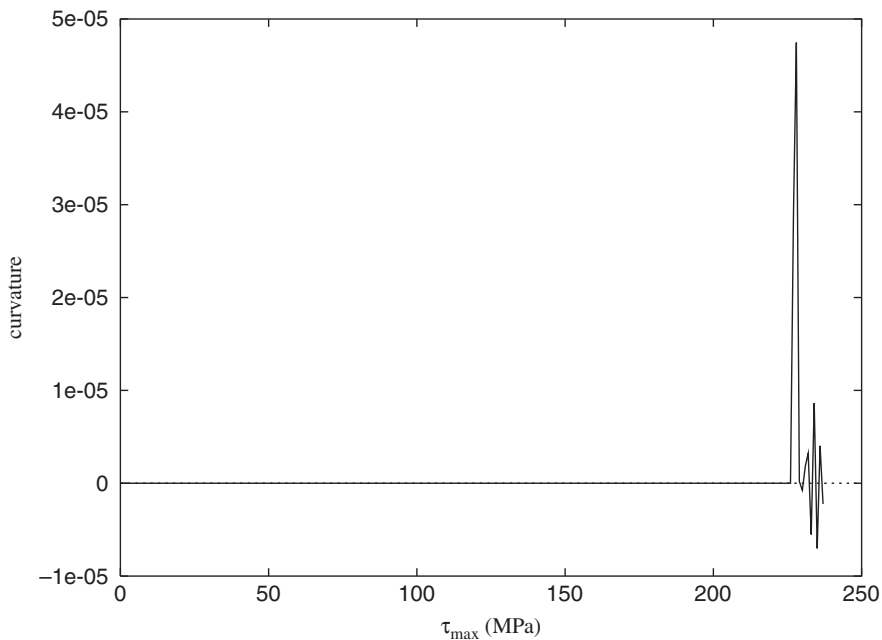
Fig. 5 Curvature of maximal final shear strain–shear stress curve in terms of shear stress for $\sigma = 25\,\mathrm{MPa}$
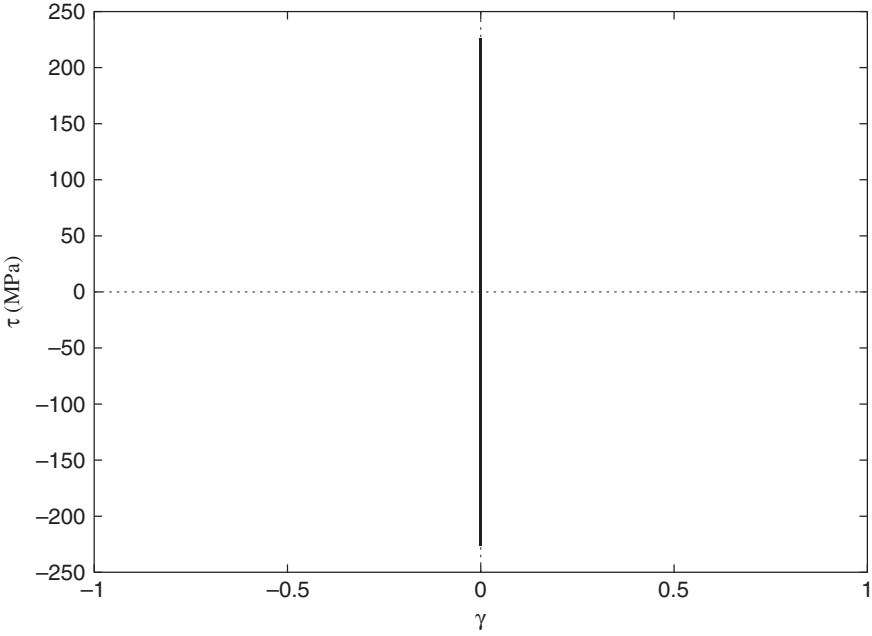
Fig. 6 Plastic shear strain in terms of shear stress for $\sigma = 25\,\mathrm{MPa}$ and $\tau_{\mathrm{max}} = 226\,\mathrm{MPa}$: **elastic cycle**
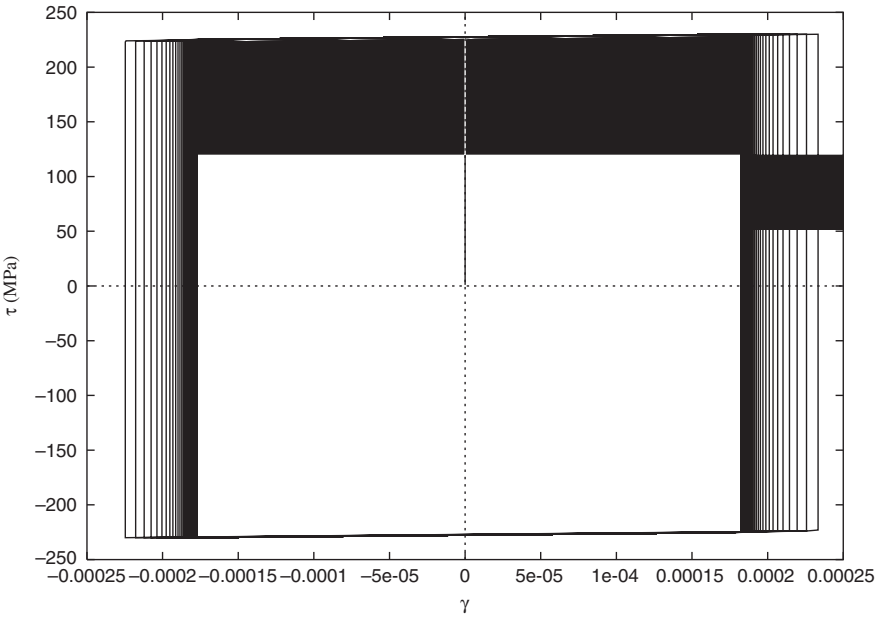
Fig. 7 Plastic shear strain in terms of shear stress for $\sigma = 25\,\mathrm{MPa}$ and $\tau_{\mathrm{max}} = 230\,\mathrm{MPa}$

3.1.3 On the Evolution of Back-Stresses

As back-stresses play an important role in shakedown analysis, it is interesting to study their evolution in terms of time and shakedown or non-shakedown of the structure. For example, for a traction stress of $\sigma_{max} = 225\,\text{MPa}$, the numerical shakedown load computed is $195\,\text{MPa}$. To compare the different cases, we plot on Fig. 8 the back-stress evolution for a maximum shear stress less than the numerical shakedown load (e.g. $\tau_{max} = 190\,\text{MPa}$), for the numerical shakedown load (in the present case $\tau_{max} = 195\,\text{MPa}$), and for a maximum shear stress greater than the numerical shakedown load (e.g. $\tau_{max} = 200\,\text{MPa}$). When the shear stress is less than the numerical shakedown load, the back-stress Y vanishes after a few cycles. In the cases of the maximum shear stress is equal or greater to the numerical shakedown load, the back-stress Y fluctuates around zero. It shows that the numerical shakedown load is probably over-estimated as the evolution of Y in this case is the same as the one when there is non-shakedown. In fact, for the exact shakedown load, the back-stress Y, as well the other components X and Z which tend to asymptotic values whenever shakedown or non-shakedwon occurs [4], should stabilize after few cycles.

Furthermore, numerical simulations show that the initial state of the back-stresses affects the delay of apparition of incipient plastic flow but does not modify the shakedown load (for further details see [3]).

Fig. 8 Evolution of back-stress Y in terms of time for $\sigma_{max} = 225\,\text{MPa}$

3.2 Implicit Standard Materials Analysis

3.2.1 Static Bound Problem

For the typical example studied in this section, the plastic yielding rule takes the form:

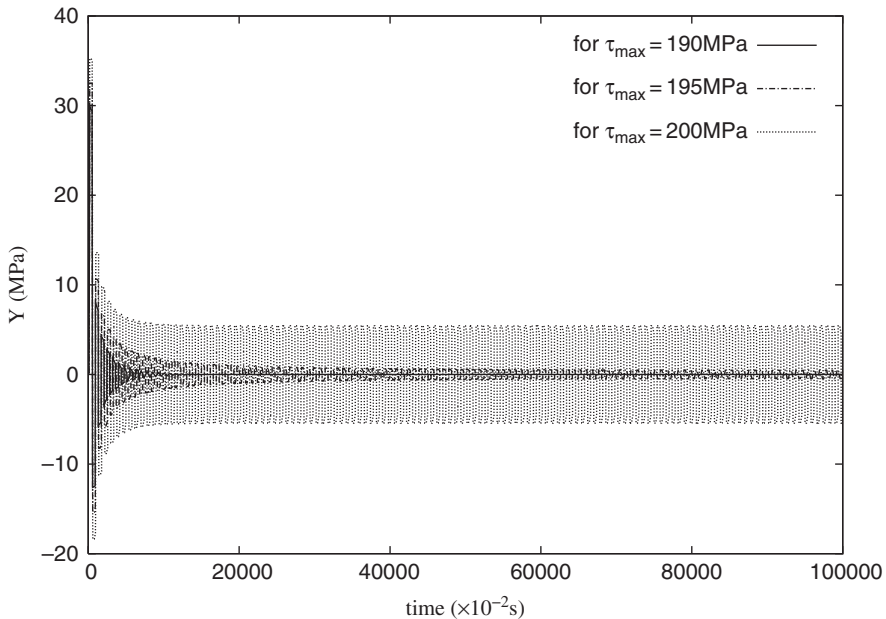$$\begin{cases} \dot{\boldsymbol{\varepsilon}}^p \in \partial \Psi_K(\boldsymbol{\sigma} - \mathsf{X})\,, \\ \dot{\boldsymbol{\alpha}} = \dot{\boldsymbol{\varepsilon}}^p - \frac{3}{2}\frac{\mathsf{X}}{X_\infty}\varepsilon_{eq}(\dot{\boldsymbol{\varepsilon}}^p)\,. \end{cases} \tag{16}$$

A bipotential associated to this plastic yielding rule (16) is then given by (see [4]):

$$b(\dot{\boldsymbol{\kappa}}, \boldsymbol{\pi}) = \Psi_K(\boldsymbol{\sigma} - \mathsf{X}) + \Psi_{\{0\}}\left(\dot{\boldsymbol{\alpha}} - \dot{\boldsymbol{\varepsilon}}^p + \frac{3}{2}\frac{\mathsf{X}}{X_\infty}\varepsilon_{eq}(\dot{\boldsymbol{\varepsilon}}^p)\right)$$
$$+ \left(\sigma_Y + \frac{3}{2}\frac{\mathsf{X}:\mathsf{X}}{X_\infty}\right)\varepsilon_{eq}(\dot{\boldsymbol{\varepsilon}}^p)\,. \tag{17}$$

Let us introduce

$$\beta((\overline{\boldsymbol{\pi}}, \lambda), \dot{\boldsymbol{\kappa}}) = \int_\Omega \oint \left\{\left(\sigma_Y + \frac{3}{2}\frac{\overline{\mathsf{X}}:\overline{\mathsf{X}}}{X_\infty}\right)\varepsilon_{eq}(\dot{\boldsymbol{\varepsilon}}^p) - \boldsymbol{\sigma}^c:\dot{\boldsymbol{\varepsilon}}^p\right\}\,\mathrm{d}t\,\mathrm{d}\Omega - \lambda, \tag{18}$$

where $\boldsymbol{\sigma}^c$ stands for the constant part of the stress tensor. Then, following the formulation (7), the static bound problem takes the form:

$$\sup_{\overline{\boldsymbol{\pi}}, \lambda} -\beta((\overline{\boldsymbol{\pi}}, \lambda), \dot{\boldsymbol{\kappa}}) \text{ s. t. } \begin{cases} \overline{\boldsymbol{\pi}} \text{ admissible}\,, \\ \dot{\boldsymbol{\alpha}} = \dot{\boldsymbol{\varepsilon}}^p + \frac{3}{2}\frac{\mathsf{X}}{X_\infty}\varepsilon_{eq}(\dot{\boldsymbol{\varepsilon}}^p)\,. \end{cases} \tag{19}$$

It can be noticed that this problem is strongly coupled. Hence the static and kinematic fields must be determined simultaneously and the problem we have to solve reads:

$$\sup_{\overline{\boldsymbol{\pi}}, \lambda, \dot{\boldsymbol{\kappa}}} -\beta((\overline{\boldsymbol{\pi}}, \lambda), \dot{\boldsymbol{\kappa}}) \text{ s. t. } \begin{cases} \overline{\boldsymbol{\pi}} \text{ admissible}\,, \\ \dot{\boldsymbol{\kappa}} \text{ admissible}\,, \\ \dot{\boldsymbol{\alpha}} = \dot{\boldsymbol{\varepsilon}}^p + \frac{3}{2}\frac{\mathsf{X}}{X_\infty}\varepsilon_{eq}(\dot{\boldsymbol{\varepsilon}}^p)\,. \end{cases} \tag{20}$$

By using convex optimization methods, in fact it is necessary to build an iterative process allowing the resolution of both static and kinematic bound problems.

As we consider a uniform distribution of stress and strain fields, the residual stress $\overline{\rho}$ must not be considered. In fact, the back-stresses $\overline{\mathsf{X}}$ play the role of the residual stresses but at a micro-scale smaller than the one of the reference elementary volume. Further, they will be considered as time-independent. For sake of simplicity, a unit volume Ω is now considered, in

order to avoid the volume integrals. Therefore, considering cyclic loading, the state will alternate between two shear stress extrema such that, for the maximum of the cycle $\tau_1 = \lambda$ and for the minimum of the cycle $\tau_2 = -\lambda$. It is then sufficient to find the maximum torsion range to obtain the shakedown load. Concerning the non-linear kinematic hardening, the static problem that we have to solve becomes

$$
\sup_{\overline{\mathsf{X}},\lambda} \left\{ \lambda - \sum_{k=1}^{2} \left[\left(\sigma_Y + \frac{3}{2} \frac{\overline{\mathsf{X}} : \overline{\mathsf{X}}}{X_\infty} \right) \varepsilon_{eq}(\dot{\boldsymbol{\varepsilon}}_k^p) - \boldsymbol{\sigma}^c : \dot{\boldsymbol{\varepsilon}}_k^p \right] \right\}
$$

$$
\text{s. t.} \begin{cases} \left[\sigma_{eq}(\lambda \boldsymbol{\sigma}_k^{e0} + \boldsymbol{\sigma}^c - \overline{\mathsf{X}}) \right]^2 - \sigma_Y^2 \leq 0,\ \forall k = 1, 2\,, \\[2mm] \dot{\boldsymbol{\alpha}}_k - \dot{\boldsymbol{\varepsilon}}_k^p + \frac{3}{2} \frac{\overline{\mathsf{X}}}{X_\infty} \varepsilon_{eq}(\dot{\boldsymbol{\varepsilon}}_k^p) = 0,\ \forall k = 1, 2\,. \end{cases}
$$

(21)

As the static bound problem has been built, the kinematic one is discretized:

$$
\sup_{\dot{\boldsymbol{\varepsilon}}_k^p} \left\{ \lambda - \sum_{k=1}^{2} \left[\left(\sigma_Y + \frac{3}{2} \frac{\overline{\boldsymbol{X}} : \overline{\boldsymbol{X}}}{X_\infty} \right) \varepsilon_{eq}(\dot{\boldsymbol{\varepsilon}}_k^p) - \boldsymbol{\sigma}^c : \dot{\boldsymbol{\varepsilon}}_k^p \right] \right\}
$$

$$
\text{s. t.} \begin{cases} \dot{\gamma}_1 - \dot{\gamma}_2 = 1\,, \\[1mm] \dot{\varepsilon}_1 + \dot{\varepsilon}_2 - \frac{3}{2} \frac{\overline{X}}{X_\infty} \left(\varepsilon_{eq}(\dot{\boldsymbol{\varepsilon}}_1^p) + \varepsilon_{eq}(\dot{\boldsymbol{\varepsilon}}_2^p) \right) = 0\,, \\[1mm] \dot{\gamma}_1 + \dot{\gamma}_2 - \frac{\overline{Y}}{X_\infty} \left(\varepsilon_{eq}(\dot{\boldsymbol{\varepsilon}}_1^p) + \varepsilon_{eq}(\dot{\boldsymbol{\varepsilon}}_2^p) \right) = 0\,, \\[1mm] \dot{\eta}_1 + \dot{\eta}_2 - \frac{3}{2} \frac{\overline{Z}}{X_\infty} \left(\varepsilon_{eq}(\dot{\boldsymbol{\varepsilon}}_1^p) + \varepsilon_{eq}(\dot{\boldsymbol{\varepsilon}}_2^p) \right) = 0\,, \end{cases}
$$

(22)

where the internal variables rates have been eliminated, using the non-linear kinematic hardening rule, to reduce the number of optimization variables. Let us remark that the presence of the term $\varepsilon_{eq}(\dot{\boldsymbol{\varepsilon}}_k^p)$ implies a regularization based on the introduction of a small parameter as in [8].

3.3 Implementation of the Bound Problems

3.3.1 First Algorithm

A first algorithm used to solve this kind of problems including coupled terms between dual variables stems from a method of successive approximation (see [5] for example). This method is based on an alternating optimization of static bound problem (21) and kinematic one (22) and leads to the construction of a bounded minimizing sequence, so that convergent. Here, due to the fact that the non-linear kinematic hardening rule is involved as a linear constraint in both kinematic and static bound problems, this method leads to a stationnarity of the sequence since the second iteration without convergence.

3.3.2 Second Algorithm

We suggest then an alternative to implement the problem (21). As the main obstacle encountered is due to the involving of the non-linear kinematic hardening rule in both static and kinematic bound problems and particularly in static problem,[1] we choose to introduce a relaxed static bound problem. For this aim, considering Karush-Kuhn-Tucker conditions of the problem (21), we notice that the non-linear kinematic hardening rule appears not only explicitly in the problem constraints, but also among the optimality conditions. This observation suggests then to introduce the following relaxed static bound problem:

$$\sup_{\overline{X},\lambda} \left\{ \lambda - \sum_{k=1}^{2} \left[\left(\sigma_Y + \frac{3}{4} \frac{\overline{X} : \overline{X}}{X_\infty} \right) \varepsilon_{eq}(\dot{\boldsymbol{\varepsilon}}_k^p) - \boldsymbol{\sigma}^c : \dot{\boldsymbol{\varepsilon}}_k^p \right] \right\}$$

$$\text{s. t. } \left[\sigma_{eq}(\lambda \boldsymbol{\sigma}_k^{e0} + \boldsymbol{\sigma}^c - \overline{X}) \right]^2 - \sigma_Y^2 \leq 0, \, \forall k = 1, 2 \,,$$

where the objective function is modified to retrieve the non-linear kinematic hardening rule through the optimality conditions. Obviously, substituting the relaxed static bound problem to the non-relaxed one does not guarantee the convergence of the sequence obtained by incremental optimization, but this one will be verified using the vanishing of the function β, defined by (18) and characterizing the exact solution, at the end of the iterative process (for further details on this subject, see [4]).

Finally, following [10], the convergence criterion used is based on a posteriori constitutive law error. Accounting for the couples $(\dot{\boldsymbol{\kappa}}, \boldsymbol{\pi})$, related by the constitutive law verifying (2), with the help of (18), a global convergence criterion E_g can be defined by:

$$E_g = \left| \frac{\beta(\dot{\boldsymbol{\kappa}}, \boldsymbol{\pi})}{\lambda} \right| \,.$$

3.3.3 On the Convergence of the Second Algorithm

As explained in the previous section, when the non-relaxed static bound problem is replaced by the relaxed one, there is no guarantee for the convergence of the sequence obtained by incremental optimization. It is then necessary to consider the convergence of the proposed algorithm. To this end, we fix a maximum tension value, for example[2] $\sigma_{max} = 375 \, \text{MPa}$, next we plot the evolution of the function $-\beta$ (18) after each kinematic bound problemoptimization, label $-\beta^c$, and after each relaxed static bound problem

---

[1] The back-stresses are only determined for non-vanishing generalized rates.

[2] This value is chosen for the significant number of iteration.
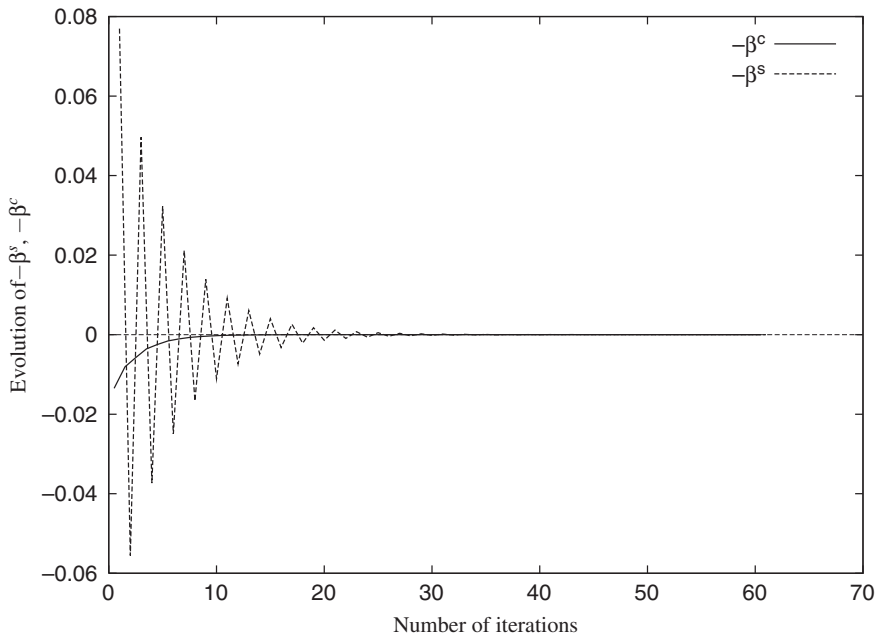
Fig. 9 Evolution of β^c and β^s in terms of iteration number

optimization, label $-\beta^s$, in terms of number of iterations. The obtained results are summarized on Fig. 9. We can then notice that both functions $-\beta^c$ and $-\beta^s$ tend to zero at the end of the iterative process that characterize the exact solution (for further details on this subject, see [4]).

3.4 Interaction Curve: Shakedown Loads Comparison

Applying the numerical method of computing the shakedown load as explained in the previous sections for various values of the fixed tension, one can compare the results obtained for the three kinds of hardening considered here (see Fig. 10). As previously forecast, the unlimited linear kinematic hardening allows only to predict alternating plasticity collapse. The limited linear hardening one [18] predicts an alternating plasticity collapse when the traction σ is less than 175 MPa and an incremental collapse beyond. Above all, the non-linear kinematic hardening model is the only one that predicts an incremental collapse for all traction values, close to the asymptotic limit of the incremental solution. The non-linear kinematic hardening shows a maximum error with the linear limited one up to 20% which is significant.
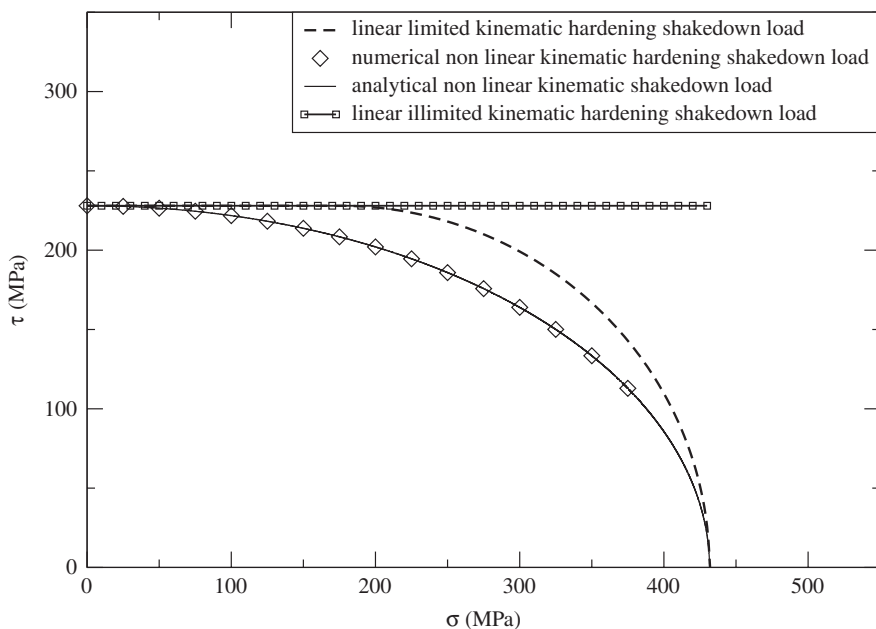
Fig. 10 Comparison between unlimited, limited linear and non-linear kinematic hardening shakedown load

Finally, despite of the use of a relaxed static problem in the case of non-linear kinematic hardening rule, a good agreement can be observed between the numerical values and analytical ones (see [4]) given by:

$$\lambda = \sigma_Y \sqrt{1 - \frac{\sigma^2}{(\sigma_Y + X_\infty)^2}(1 - \nu + \nu^2)}. \tag{23}$$

References

1. Armstrong, P.-J., Frederick, C.-O.: A mathematical representation of the multiaxial Bauschinger effect. In C.E.G.B., Report No. RD/B/N731 (1966)
2. Bodovillé, G.: A kinematic elastic nonshakedown theorem for implicit standard materials. Arch. Appl. Mech. **72**, 266–278 (2002)
3. Bouby, C., de Saxcé, G., Tritsch, J.-B.: A comparison between analytical calculations of the shakedown load by the bipotential approach and step-by-step computations for elastoplastic materials with non linear kinematic hardening. Int. J. Solid. Struct. **43**, 2670–2692 (2006)
4. Bouby, C.: Adaptation élastoplastique de structures sous chargements variables avec règle d'écrouissage cinématique non linéaire et non associée. Thèse de doctorat de l'Université des Sciences et Technologies de Lille (2006)
5. Bousshine, L., Chaaba, A., de Saxcé, G.: Plastic limit load of plane frames with frictional contact supports. Int. J. Mech. Sci. **44**, 2189–2216 (2002)

6. Bousshine, L., Chaaba, A., de Saxcé, G.: A new approach to shakedown analysis for non standard elastoplastic material by the bipotential. Int. J. Plasticity **19**, 583–598 (2003)

7. Fenchel, W.: On conjugate convex functions. Canadian J. Math. **1**, 73–77 (1949)

8. Khoi, V. D., Yan, A. M., Nguyen-Dang, H.: A dual form for discretized kinematic formulation in shakedown analysis. Int. J. Solid. Struct. **41**, 267–277 (2004)

9. Koiter, W. T.: General theorems for elastic-plastic solids. In: Sneddon, I.N., Hills, R. (eds.) Progress in Solid Mechanics. Vol. 1, North Holland, Amsterdam (1960)

10. Ladevèze, P.: Mécanique non linéaire des structures : une nouvelle approche et méthodes de calcul non incrémentales. Hermès, Paris (1996)

11. Lemaitre, J., Chaboche, J.-L.: Mechanics of Solid Materials. Cambridge University Press, Cambridge (1990)

12. Maier, G., Carvelli, V., Cocchetti, G.: On direct methods for shakedown and limit analysis. Eur. J. Mech. A-Solid, **19** (Special Issue), S79–S100 (2000)

13. Maier, G., Weichert, D.: Inelastic Behaviour of Structures under Variable Repeated Loads. CISM Courses and Lectures, No 432, Springer Wien, New-York (2002)

14. Marquis, D.: Modélisation et identification de l'écrouissage anisotrope des métaux. Thèse de 3ème cycle de l'université Pierre et Marie Curie, Paris VI (1979)

15. Melan, E.: Theorie statisch unbestimmter Systeme aus ideal-plastischem Baustoff. Sitzber. Akad. Wiss. Wien, Abt IIA, **145**, 195–218 (1936)

16. Nguyen, Q.-S.: On shakedown in hardening plasticity. J. Mech. Phys. Solid. **51**, 101–125 (2003)

17. Polizzotto, C., Borino, G., Caddemi, S., Fuschi, P.: Shakedown problems for material models with internal variables. Eur. J. Mech. A-Solid. **10**, 621–639 (1991)

18. Weichert, D., Gross-Weege, J.: Assessment of elasto-plastic sheets under variable mechanical and thermal loads using a simplified two-surface yield condition. Int. J. Mech. Sci. **30**, 757–767 (1988)

Limit Analysis of Orthotropic Laminates by Linear Matching Method

P. Fuschi, A. A. Pisano, and O. Barrera

Abstract A numerical procedure for limit analysis of orthotropic composite laminates, in plane stress conditions, is presented. The procedure can be viewed as an extension, in the context of orthotropic materials, of a method known in the relevant literature as Linear Matching Method. The structural elements here examined are composite laminates obeying, by hypothesis, to a Tsai-Wu type yield criterion. Following the kinematic approach of limit analysis theory, an upper bound to the collapse load multiplier is detected in a finite element context and in an iterative fashion. A few numerical examples are carried out to verify the effectiveness of the proposed approach and to inquire into its capability to predict experimental test results for pinned-joint composite plates.

1 Introduction

Limit analysis is an effective tool for the direct evaluation of the load bearing capacity of a structure. Such a direct method is based on two fundamental theorems due to Drucker et al. (see e.g. [15, 36]). The proof of such theorems grounds on the principle of maximum plastic dissipation and, consequently, they are strictly valid only for standard materials. The two theorems, as known, lead to two classical approaches of limit analysis, namely: the kinematic and the static one and, if the limit loads produced by the application of the two theorems are equal to each other, then they equal the collapse load. Nevertheless, the will of applying limit analysis to engineering problems even outside the realm of perfect plasticity is proved by several studies.

Paolo Fuschi, Aurora A. Pisano, and Olga Barrera
Department DASTEC University Mediterranea of Reggio Calabria, via Melissari
I-89124 Reggio Calabria, Italy, e-mail: paolo.fuschi@unirc.it; aurora.pisano@unirc.it; olga.barrera@unirc.it

The pioneeristic works [14, 18, 24, 39], or, later on, [3, 22, 30, 37], till the more recent contributions [7, 41, 46, 48], although the list is far to be exhaustive, witness for this will.

Moreover, the rapid development in the last few decades of finite element based analyses whereas on the one hand was a further essential contribution to the success of direct methods (see e.g. [4, 12, 19, 38]) on the other hand directed the researchers' interest towards the elastic-plastic evolutive analyses against the direct methods. Indeed, the evolutive analyses, able to follow the structural response in the post-elastic regime up to collapse, are often computationally more competitive than limit analysis, but this competitiveness, as well as the efficacy and trustworthiness of the obtained response, is strictly influenced by the modelling of the constitutive material behaviour.

When dealing with materials whose available constitutive laws are unable to catch the complexity of the phenomena characterizing the actual post-elastic behaviour, limit analysis comes back to being a valid and effective tool for design purposes. Stringent examples of such convincement can be found in the case of structures made of composite materials. For such materials, existing and subtle constitutive models, that take into account phenomena like interlaminar behaviour, delamination, damage evolution, etc., turn out to be effective only for solving specific case-studies. Such constitutive models are often based on material constants that are unlikely detected via laboratory tests thus resulting useless for practical engineering applications.

The interest in limit analysis approaches in the field of composite material structures is indeed testified by several contributions, see e.g. [9, 13, 16, 25, 27, 29, 31, 40] among others. The present work belongs to this research line and its main goal is to systematize and improve a procedure, recently proposed by the senior authors in [31], aimed at the evaluation of an upper bound to the collapse load multiplier for orthotropic composite laminates in plane stress conditions. The procedure can be viewed as an extension, to the orthotropic materials case, of the *Linear Matching Method* (LMM) due to Ponter and Co-workers, see e.g. [6, 7, 10, 11, 32–35]. The LMM can be interpreted as a programming technique involving an iterative FE-based procedure that allows one to define an upper bound to the collapse load multiplier. In practice, a sequence of linear analyses is performed on the structure assumed, by hypothesis, as made of a *fictitious linear viscous material* with *spatially varying* moduli. With this conjecture, at each iteration, the computed fictitious solution can be used to define a collapse mechanism for the real structure. To this aim, by rescaling the fictitious moduli and, if necessary, by adjusting other fictitious material parameters, the computed fictitious stresses are brought on the yield surface of the real material at a fixed strain rate distribution. The latter, together with the related compatible displacement rates, gives a collapse mechanism. At the end of each iteration then, the fictitious analysis produces all the quantities, namely: stress at yield, related strain and displacement rates, entering an upper bound collapse load multiplier evaluation. As noted in [32], once the convergence is assured, the computed upper bound

is the one pertaining to the class of displacement fields given by the adopted FE mesh, i.e. it depends on the richness of the kinematical model. This obvious drawback is easily overcome by using fine enough meshes in the analyses.

The present extended version of the LMM grounds on two key ideas: (i) The LMM is applied to a second order tensor polynomial form of the Tsai-Wu failure criterion [42,43], which is assumed as a Tsai-Wu type yield surface for the considered material. The above quadratic form is simple, it allows one to apply the standard rules of transformation, invariance and symmetry, it also considers interactions among the stress or strain components. The lack of associativity may be overcome following the non standard limit analysis approach of Radenkovic [26,37]. (ii) The fictitious material is defined in such a way that the number of fictitious parameters to be updated is strongly reduced. To this aim, as suggested in [31], the fictitious material is assumed linear, viscous, orthotropic and suffering a distribution of assigned initial stresses, while the whole procedure is recast in a dimensionless stress space, precisely the one adopted for the Tsai-Wu criterion formulation, see e.g. [21].

The proposed procedure is expounded in three main sections which follow this introductory one. Section 2 is devoted to the basic assumptions, the constitutive criterion and the problem position. Section 3 gives the details of the LMM, in the form here presented to deal with orthotropic materials, pointing out its peculiarities. To this aim a few geometrical sketches and a flow-chart of the main steps of the iterative scheme are also given with a twofold reason: to show the simplicity of a geometrical interpretation, at least for the studied problems; to show the simplicity of the numerical implementation. Section 4 is dedicated to the method validation. The presented numerical examples concern mechanically fastened joints in composite plates. A comparison between the predicted results and the available experimental ones is carried out to verify the effectiveness of the method. Section 5 is the closing one and is oriented to some concluding remarks, some critical comments, necessary and/or possible improvements.

Notation: Bold face symbols denote vectors or tensors. Cartesian orthogonal co-ordinates are used and subscripts denote Cartesian components. Repeated index implies summation rule. The symbol := means equality by definition. Other symbols will be defined in the text where they appear for the first time.

2 Limit Analysis for Nonstandard Orthotropic Materials

The basic assumptions to deal with a limit analysis approach for nonstandard materials are briefly summarized. The adopted constitutive criterion, obtained by a second order tensor polynomial form of the Tsai-Wu failure criterion, is then presented. The section closes with the formulae needed for evaluating an upper bound to the collapse load multiplier.

2.1 Basic Assumptions and Constitutive Criterion

A theory of limit analysis in the context of nonstandard materials was pro-
posed in the early sixties by Radenkovic [37]. The two limit analysis funda-
mental theorems where actually rephrased in the shape of "upper" and "lower
bound theorems" (see e.g. [26]). In particular, the upper bound theorem, here-
after invoked, states: "the limit loading for a body made of a nonstandard
material is bounded from above by the limit loading for a standard material
obeying the same yield criterion".

Adopting for the material in use a yield surface expressed by a second
order tensor polynomial form of the Tsai-Wu criterion [9, 42, 43], the lack
of associativity, if this latter essential requisite it is not postulated, may be
overcome by the Radenkovic's approach, i.e. searching for an upper bound
on the collapse load multiplier referred to an associative material obeying to
the adopted Tsai-Wu type yield criterion, see e.g. [26] for a deeper discussion
to this concern.

By denoting with 1 and 2 the principal directions of orthotropy in plane
stress case as well as indicating $\sigma_6 \equiv \tau_{12}$, as usual for composite laminates,
the adopted Tsai-Wu type criterion is expressed by:

$$F_{11}\,\sigma_1^2 + F_{22}\,\sigma_2^2 + F_{66}\,\sigma_6^2 + 2\,F_{12}\,\sigma_1\sigma_2 + F_1\,\sigma_1 + F_2\,\sigma_2 = 1\,, \qquad (1)$$

where:

$$F_1 := \frac{1}{X_t} + \frac{1}{X_c}\,, \qquad F_2 := \frac{1}{Y_t} + \frac{1}{Y_c}\,, \qquad F_{11} := -\frac{1}{X_t\,X_c}\,,$$

$$F_{22} := -\frac{1}{Y_t\,Y_c}\,, \qquad F_{66} := \frac{1}{S^2}\,, \qquad F_{12} := -\frac{1}{2}\,\sqrt{F_{11}\,F_{22}}\,, \qquad (2)$$

with: X_t, X_c the longitudinal tensile and compressive strengths respectively;
Y_t, Y_c the transverse tensile and compressive strengths respectively and S the
longitudinal shear strength. By inspection of (2) it is worth noting that five
of the six coefficients required for the definition of the criterion are given by
performing simple uniaxial or shear tests. The sixth, namely F_{12}, devoted to
take into account the interaction between the two normal stress components
σ_1 and σ_2 requires a biaxial test. This experimental task is not easy to perform
and simplified assumptions, as the one here adopted for F_{12}, are usually made
[5, 17]. Moreover, considering that a failure process in a laminate involves a
combination of failure mechanisms due to matrix crushing, fibre breaks, fibre
buckling, delamination, modified versions of the Tsai-Wu criterion have been
presented to remove some of its internal incoherencies [17, 23].

Despite the above remarks the Tsai-Wu type criterion, in the quadratic
form adopted, is simple; it allows to apply the standard rules of transfor-
mation, invariance and symmetry; it also contemplates interactions among
the stress or strain components analogously to the von Mises criterion for

isotropic materials. The above Tsai-Wu type criterion is used for defining an admissible stress states domain: points within the domain locate stress states pertaining to an anisotropic linear elastic behaviour of the material; points lying on the domain boundary locate stress states at which the material has exhausted its strength capabilities. After all, the Tsai-Wu type surface, in the shape of (1) locating in the stress space an ellipsoid, is here assumed as yield surface for the orthotropic material considered.

2.2 Evaluation of an Upper Bound to the Collapse Load Multiplier

Let us consider a body occupying the volume V, ∂V denoting its external surface while a Cartesian coordinate system is assumed, namely x_i, $i = 1, 2, 3$. For simplicity, only surface forces are considered, precisely $P\bar{\boldsymbol{p}}(\boldsymbol{x})$ acting on $\bar{\boldsymbol{x}} \in \partial V_t$; where P is a scalar load multiplier and $\bar{\boldsymbol{p}}(\boldsymbol{x})$ is the reference load vector collecting all the surface force components, say $\bar{p}_i$, acting on points of a portion ∂V_t of the body surface. The remaining part of ∂V, i.e. $\partial V_u = \partial V - \partial V_t$, is assumed to suffer displacements $\boldsymbol{u} = \boldsymbol{0}$. Moreover, plane stress conditions are assumed and the constituent material is, by hypothesis, orthotropic, homogeneous and with a constitutive behaviour obeying the Tsai-Wu type criterion in the form given by (1).

Following a standard formalism of the kinematic approach of limit analysis theory, in the assumed hypothesis of associated flow rule and rewriting (1) in the abridged form $f(\sigma_j) = 0$ ($j = 1, 2, 6$), the following can be stated. For a given distribution of compatible strain rates $\dot{\varepsilon}_j$, say $\dot{\varepsilon}_j^c$, i.e. such that the related displacement rates $\dot{u}_i^c$ meet the condition $\dot{u}_i^c = 0$ on ∂V_u, an upper bound to the collapse limit load multiplier is given by:

$$P_{UB} \int_{\partial V_t} \bar{p}_i \, \dot{u}_i^c \, \mathrm{d}(\partial V) = \int_V \sigma_j^y \, \dot{\varepsilon}_j^c \, \mathrm{d}V \,, \tag{3}$$

where: $\dot{\varepsilon}_j = \dot{\lambda} \, \partial f / \partial \sigma_j$ are the components of the outward normal to the yield surface $f(\sigma_j) = 0$ (with $\dot{\lambda} > 0$ scalar multiplier); P_{UB} denotes the upper bound load multiplier; σ_j^y are the stresses at yield associated to the given $\dot{\varepsilon}_j^c$; $\dot{u}_i^c$ being the related displacement rates. The set $(\dot{\varepsilon}_j^c, \dot{u}_i^c)$ defines a collapse mechanism.

3 Linear Matching for Orthotropic Materials

The Linear Matching Method, extended to the orthotropic materials case, is presented and discussed going into details with the aid of a few geometrical

sketches aimed to a better comprehension of the procedure whose geometrical interpretation is very simple and effective. The advantages of a formulation in a dimensionless stress space as well as of an appropriate choice of the initial fictitious material parameters used throughout the procedure are exploited. The section closes with an operative computational scheme expounded, in the last paragraph, in a flow-chart style.

3.1 Fundamentals

As outlined in Sect. 1, the LMM has been widely employed to perform limit analysis on structures made of von Mises materials or materials with a pressure-dependent yield condition or, also, in the context of geotechnical problems (see e.g. [6, 7, 10, 11, 32–35]). The LMM involves a sequence of FE-based analyses carried on the structure under study but assuming it as made of a material with spatially varying moduli, i.e. a *fictitious material.* At each step, the fictitious solution is used to define, at each Gauss point of the adopted FE mesh, a collapse mechanism for the real structure in terms of stress at yield, σ_j^y, plus related strain and displacement rates, namely $(\dot{\varepsilon}_j^c, \dot{u}_i^c)$. Looking at (3), this information allows one to evaluate an upper bound to the collapse load multiplier. The iterations stop when the difference between two subsequent upper bound values becomes less than a fixed tolerance.

The present LMM utilizes a *fictitious linear viscous material* which is *orthotropic* and *subjected to a distribution of imposed initial stresses.* The proposed generalization is given with reference to an orthotropic laminate, under plane stress conditions, whose material parameters, Young moduli and Poisson's ratio, have been fixed, say to values: $E_1^{(0)}$, $E_2^{(0)}$, $E_6^{(0)}$, $\nu_{12}^{(0)}$, respectively. The structure is also subjected to a given distribution of initial stresses: $\bar{\sigma}_1^{(0)}$, $\bar{\sigma}_2^{(0)}$, $\bar{\sigma}_6^{(0)}$. The notation $(\cdot)^{(0)}$ refers to an initial arbitrary choice of the quantity $(\cdot)$. For this fictitious material the *complementary dissipation rate* can be written as:

$$
\begin{aligned}
W\left(\sigma_j, E_j^{(0)}, \nu_{12}^{(0)}, \bar{\sigma}_j^{(0)}\right) = \frac{1}{2} & \left[\frac{\sigma_1^2}{E_1^{(0)}} + \frac{\sigma_2^2}{E_2^{(0)}} + \frac{\sigma_6^2}{E_6^{(0)}} - 2\,\nu_{12}^{(0)}\,\frac{\sigma_1\,\sigma_2}{E_2^{(0)}} \right. \\
& - 2\left(\frac{\bar{\sigma}_1^{(0)}}{E_1^{(0)}} - \nu_{12}^{(0)}\,\frac{\bar{\sigma}_2^{(0)}}{E_2^{(0)}} \right)\sigma_1 - 2\left(\frac{\bar{\sigma}_2^{(0)}}{E_2^{(0)}} - \nu_{12}^{(0)}\,\frac{\bar{\sigma}_1^{(0)}}{E_2^{(0)}} \right)\sigma_2 \\
& \left. - 2\,\frac{\bar{\sigma}_6^{(0)}}{E_6^{(0)}}\,\sigma_6 + \frac{\bar{\sigma}_1^{(0)2}}{E_1^{(0)}} + \frac{\bar{\sigma}_2^{(0)2}}{E_2^{(0)}} + \frac{\bar{\sigma}_6^{(0)2}}{E_6^{(0)}} - 2\,\nu_{12}^{(0)}\,\frac{\bar{\sigma}_1^{(0)}\,\bar{\sigma}_2^{(0)}}{E_2^{(0)}} \right],
\end{aligned}
\tag{4}
$$

where, by hypothesis, the moduli $E_j^{(0)}$ $(j = 1, 2, 6)$ are allowed to assume different values at different points in the structure, i.e. they are *spatially varying,* (the initial choice can assume the same values at all points). For this fictitious material and at a fixed value of the load multiplier, say $P_{UB}^{(0)}$, a

linear FE-analysis is performed on the whole structure to compute: the strain rates $\dot{\varepsilon}_j^e = \partial W(\sigma_j^e)/\partial \sigma_j^e$; the related stresses σ_j^e; the compatible displacement rates, $\dot{u}_i^e$, of the points at which surface loads act. The *fictitious kinematic solution* $(\dot{\varepsilon}_j^e, \dot{u}_i^e)$ so computed (operatively at each Gauss point of the adopted FE mesh), is then *forced to represent a collapse mechanism*, namely it is forced to identify with $(\dot{\varepsilon}_j^c, \dot{u}_i^c)$ of (3).

To this aim, referring to the sketch of Fig. 1 where, as assumed, the fixed fictitious initial values of the elastic parameters and stresses are denoted by $(\cdot)^{(0)}$, on keeping $\dot{\varepsilon}_j^e$ fixed, it is sufficient to compute the stress at yield, say σ_j^y, associated to $\dot{\varepsilon}_j^e$ – so *assumed* as a given $\dot{\varepsilon}_j^c$ – and to vary the fictitious moduli and initial stresses (values $(\cdot)^{(*)}$ in Fig. 1) so that σ_j^e coincides with σ_j^y; the fictitous $\dot{u}_i^e$ so representing the compatible displacements $\dot{u}_i^c$ associated to $\dot{\varepsilon}_j^c$. Executing such operation at all Gauss points of the discretized structure, Eq. (3) can be used to compute a $P_{UB}^{(*)}$. The above rationale, from a geometrical point of view (see again Fig. 1), merely states that the complementary dissipation rate equipotential surface of the fictitious material, $W(\sigma_j, E_j^{(*)}, \nu_{12}^{(*)}, \bar{\sigma}_j^{(*)}) = $ const., *matches* the Tsai-Wu type surface at the stress point σ_j^y.

A crucial remark has to be done at this point: the stresses at yield computed at matching, obviously do not satisfy the equilibrium conditions with the loads $P_{UB}^{(0)} \bar{\boldsymbol{p}}$ and a new fictitious analysis has to be performed on the whole structure with the updated $E_j^{(*)}$ values and loads $P_{UB}^{(*)} \bar{\boldsymbol{p}}$. Indeed, the whole procedure has to be carried out iteratively, the iterations stopping when two subsequent computed P_{UB} values become close to each other.

An essential requisite of an iterative procedure is the certainty of its convergence; to this concern, it is worth mentioning that the expounded procedure
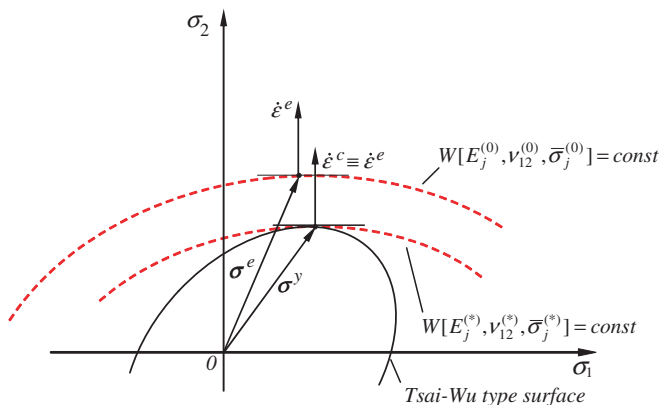

Fig. 1 Geometrical sketch of the matching procedure at the generic Gauss point in the $\sigma_6 = 0$ plane: $(\cdot)^{(0)} = $ initial arbitrary values; $(\cdot)^{(*)} = $ values at which the matching is achieved

fulfils the sufficient condition for convergence given in [34] and the final P_{UB} value is normally attained in few iterations.

It is also worth noting that the *formal analogy* existing between the linear viscous problem and the linear elastic problem allows one to compute, at each iteration, a *fictitious elastic solution,* looking at $W[\sigma_j, E_j^{(0)}, \nu_{12}^{(0)}, \bar{\sigma}_j^{(0)}]$ of (4) as at the complementary energy potential of a fictitious elastic material. The fictitious elastic analyses can then be carried out by any commercial FE-code with obvious advantages.

3.2 Dimensionless Formulation

The matching procedure can be implemented in a much simpler way if both surfaces, the Tsai-Wu type one, given by (1), and the complementary dissipation equipontential surface, expressed by (4), are rephrased in a dimensionless stress space, namely the one usually adopted for the Tsai-Wu criterion (see e.g. [21]).

To this aim, the following dimensionless parameters are set up:

$$X := \sqrt{F_{11}}\, \sigma_1\,, \qquad Y := \sqrt{F_{22}}\, \sigma_2\,, \qquad Z := \sqrt{F_{66}}\, \sigma_6\,, \qquad (5)$$

$$f_{12} := \frac{F_{12}}{\sqrt{F_{11}F_{22}}}\,, \qquad f_1 := \frac{F_1}{\sqrt{F_{11}}}\,, \qquad f_2 := \frac{F_2}{\sqrt{F_{22}}}\,. \qquad (6)$$

With the above positions Eq. (1) gives:

$$X^2 + Y^2 + Z^2 + 2\,f_{12}\,XY + f_1\,X + f_2\,Y = 1\,, \qquad (7)$$

which, in the dimensionless space (X, Y, Z), individuates an *ellipsoid* whose major axis lies on the $Z = 0$ plane and it is rotated by a counterclockwise angle of 45 degrees with respect to the X axis. Moreover, assuming that $(\cdot)_{TW}$ stands for a quantity $(\cdot)$ pertaining to the Tsai-Wu type criterion and/or surface; denoting with α_{TW}, β_{TW} and γ_{TW} the X, Y, Z coordinates of the ellipsoid centre respectively, and with a_{TW}, b_{TW} and c_{TW} the semi-axes ellipsoid dimensions (a_{TW} referring to the major axis, c_{TW} to the axis parallel to Z) it is easy to verify the following expressions hold true:

$$\alpha_{TW} = -\frac{f_1 - f_2\,f_{12}}{2\,(1 - f_{12}^2)}\,, \quad \beta_{TW} = -\frac{f_2 - f_1\,f_{12}}{2\,(1 - f_{12}^2)}\,, \quad \gamma_{TW} = 0\,, \qquad (8)$$

$$a_{TW} = \left[(1 + f_{12}) / \left(1 + \alpha_{TW}^2 + \beta_{TW}^2 + 2 f_{12} \alpha_{TW} \beta_{TW}\right)\right]^{-1/2},$$

$$b_{TW} = \left[(1 - f_{12}) / \left(1 + \alpha_{TW}^2 + \beta_{TW}^2 + 2 f_{12} \alpha_{TW} \beta_{TW}\right)\right]^{-1/2}, \qquad (9)$$

$$c_{TW} = \left[1 + \alpha_{TW}^2 + \beta_{TW}^2 + 2 f_{12} \alpha_{TW} \beta_{TW}\right]^{1/2}.$$

On the other hand, rewriting (4) in the dimensionless space (X, Y, Z), i.e. using again (5), yields:

$$W\left[X, Y, Z, E_j^{(0)}, \nu_{12}^{(0)}, \bar{X}^{(0)}, \bar{Y}^{(0)}, \bar{Z}^{(0)}\right] =$$

$$= \frac{1}{2} \left[\frac{X^2}{E_1^{(0)} F_{11}} + \frac{Y^2}{E_2^{(0)} F_{22}} + \frac{Z^2}{E_6^{(0)} F_{66}} - \frac{2\nu_{12}^{(0)}}{E_2^{(0)} \sqrt{F_{11}} \sqrt{F_{22}}} X Y \right.$$

$$- \frac{2}{\sqrt{F_{11}}} \left(\frac{\bar{X}^{(0)}}{E_1^{(0)} \sqrt{F_{11}}} - \frac{\nu_{12}^{(0)} \bar{Y}^{(0)}}{E_2^{(0)} \sqrt{F_{22}}} \right) X - \frac{2}{\sqrt{F_{22}}} \left(\frac{\bar{Y}^{(0)}}{E_2^{(0)} \sqrt{F_{22}}} - \frac{\nu_{12}^{(0)} \bar{X}^{(0)}}{E_2^{(0)} \sqrt{F_{11}}} \right) Y$$

$$\left. - \frac{2\bar{Z}^{(0)}}{E_6^{(0)} F_{66}} Z + \frac{\bar{X}^{(0)^2}}{E_1^{(0)} F_{11}} + \frac{\bar{Y}^{(0)^2}}{E_2^{(0)} F_{22}} + \frac{\bar{Z}^{(0)^2}}{E_6^{(0)} F_{66}} - \frac{2\nu_{12}^{(0)}}{E_2^{(0)} \sqrt{F_{11}} \sqrt{F_{22}}} \bar{X}^{(0)} \bar{Y}^{(0)} \right].$$

$$(10)$$

For a given initial value of the load multiplier, say $P_{UB}^{(0)}$, and for any fixed set of elastic parameters and initial stresses, namely $(E_1^{(0)}, E_2^{(0)}, E_6^{(0)}, \nu_{12}^{(0)}, \bar{X}^{(0)}, \bar{Y}^{(0)}, \bar{Z}^{(0)})$, the above expression individuates in the (X, Y, Z) space an *ellipsoid* of the form $W\left[\chi_j, E_j^{(0)}, \nu_{12}^{(0)}, \bar{\chi}_j^{(0)}\right] = \bar{W}^{(0)} \equiv$ const. The latter abridged form points out the dependence of the ellipsoid location and amplitude on the elastic parameters and initial stress values, $\bar{W}^{(0)}$ being the pertinent complementary energy equipotential value corresponding to the given loads. For brevity, χ_j for $j = 1, 2, 6$ identifies with X, Y, Z respectively.

The announced simplification of the matching is easily obtainable by taking advantage of the ellipsoidal shapes of the Tsai-Wu type surface and of the equipotential surface $W\left[\chi_j, E_j^{(0)}, \nu_{12}^{(0)}, \bar{\chi}_j^{(0)}\right] =$ const. As in facts, if the fictitious material is, from the beginning of the analysis, defined in such a way that its complementary energy equipotential surface is *homothetic* to the Tsai-Wu type surface, the two ellipsoids can be made coincident at matching. As a consequence, only one scalar parameter has to be iteratively updated, namely the *homothety ratio* between the two ellipsoids. The latter will control the axes' amplitudes of $W\left[\chi_j, E_j^{(0)}, \nu_{12}^{(0)}, \bar{\chi}_j^{(0)}\right] = \bar{W}^{(0)}$ which are directly related to the fictitious elastic moduli values $E_j^{(0)}$. To impose that $W\left[\chi_j, E_j^{(0)}, \nu_{12}^{(0)}, \bar{\chi}_j^{(0)}\right] = \bar{W}^{(0)}$ (as given by (10)) is homothetic to the Tsai-Wu type surface (given by (7)) implies that: the semi-axes ratios are equal (3 conditions); the two ellipsoids have the same centre (3 conditions) and the

main axis is rotated by a counterclokwise angle of 45 degrees with respect to the X axis (1 condition). It easy to verify that the above requirements can be satisfied with the following positions:

$$E_1^{(0)} = \frac{1}{2\,F_{11}}\,, \quad E_2^{(0)} = \frac{1}{2\,F_{22}}\,, \quad E_6^{(0)} = \frac{1}{2\,F_{66}}\,, \quad \nu_{12}^{(0)} = -f_{12}\,\frac{\sqrt{F_{11}}}{\sqrt{F_{22}}}\,, \quad (11)$$

$$\bar{X}^{(0)} = \alpha_{TW}\,, \quad \bar{Y}^{(0)} = \beta_{TW}\,, \quad \bar{Z}^{(0)} = 0\,. \tag{12}$$

By substituting Eqs.(11) and (12), Eq. (10) reduces to:

$$X^2 + Y^2 + Z^2 + 2\,f_{12}\,X\,Y - 2\,(\alpha_{TW} + f_{12}\,\beta_{TW})\,X - 2\,(\beta_{TW} + f_{12}\,\alpha_{TW})\,Y$$
$$= \bar{W}^{(0)} - \alpha_{TW}^2 - \beta_{TW}^2 - 2\,f_{12}\,\alpha_{TW}\,\beta_{TW}\,, \tag{13}$$

which is the searched (fictitious) complementary energy equipotential surface homothetic to the Tsai-Wu type surface.

Looking at the sketch of Fig. 2, dimensionless counterpart of Fig. 1, the LMM can be rephrased in the (X, Y, Z) space as follows: an elastic analysis on the structure loaded by $P_{UB}^{(0)}\bar{p}_i$ and made of a fictitious material whose complementary energy is given by (13) produces, at each GP of the FE model, an elastic solution of the form $(\chi_j^{e\,(0)}, \dot{\varepsilon}_j^{e\,(0)})$, (point A in Fig. 2), lying on the surface $W\left[\chi_j, E_j^{(0)}, \nu_{12}^{(0)}, \bar{\chi}_j^{(0)}\right] = \bar{W}^{(0)}$. Assuming $\dot{\varepsilon}_j^{e\,(0)}$ as $\dot{\varepsilon}_j^c$, the (non-dimensional) stress at yield, $\chi_j^{y\,(*)}$, associated to the (normal) $\dot{\varepsilon}_j^c$ is computed (point B in Fig. 2). The fictitious elastic solution, $\chi_j^{e\,(0)}$, is then forced to identify with the one at yield, namely $\chi_j^{e\,(*)} \equiv \chi_j^{y\,(*)}$, by rescaling the ficti-

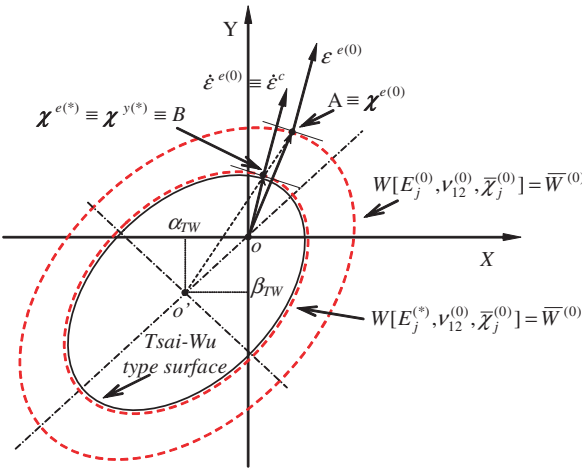**Fig. 2** Matching procedure at the generic Gauss point for $W\left[E_j^{(0)}, \nu_{12}^{(0)}, \bar{\chi}_j^{(0)}\right] = \bar{W}^{(0)}$ homothetic to the Tsai-Wu type surface: geometrical sketch in the $Z = 0$ plane

tious elastic moduli while keeping fixed the loads, namely $P_{UB}^{(0)}$, the initial stresses $\bar{\chi}_j^{(0)}$, the Poisson coefficient $\nu_{12}^{(0)}$ and $\bar{W}^{(0)}$.

The rescaling of the fictitious elastic moduli can be carried out computing first the homothety ratio between the two ellipsoids.

This is given by:

$$\Gamma^{(0)} := \frac{a_{TW}}{a_W^{(0)}} = \frac{b_{TW}}{b_W^{(0)}} = \frac{c_{TW}}{c_W^{(0)}}, \tag{14}$$

where: a_{TW}, b_{TW}, c_{TW} are the lengths of the Tsai-Wu type ellipsoid semi-axes given by (9) and $a_W^{(0)}$, $b_W^{(0)}$ and $c_W^{(0)}$ are the analogous quantities for the ellipsoid $W\left[\chi_j, E_j^{(0)}, \nu_{12}^{(0)}, \bar{\chi}_j^{(0)}\right] = \bar{W}^{(0)}$. It easy to verify that $\Gamma^{(0)}$ can be given the equivalent expression:

$$\Gamma^{(0)} = \sqrt{\frac{\Omega}{\bar{W}^{(0)}}}, \tag{15}$$

where: $\Omega := 1 + \alpha_{TW}^2 + 2 f_{12}\, \alpha_{TW} \beta_{TW} + \beta_{TW}^2 > 0$ is the known term of the Tsai-Wu type ellipsoid equation rewritten in a cartesian reference system with the origin at the ellipsoid centre and equipollent to the (X, Y, Z) system. Once $\Gamma^{(0)}$ is known, a rescaling of the fictitious elastic moduli can be carried out on setting:

$$E_j^{(*)} = E_j^{(0)} \left[\Gamma^{(0)}\right]^2, \qquad j = 1, 2, 6, \tag{16}$$

indeed, by substituting the latter expression in (10) the Tsai-Wu type ellipsoid, in the shape of (7), is obtained.

On the other hand, the stresses at yield, $\chi_j^{y\,(*)}$, can be computed (again referring to Fig. 2) with the following equations:

$$X^{y\,(*)} = \left[1 - \Gamma^{(0)}\right]\alpha_{TW} + \Gamma^{(0)}\, X^{e\,(0)},$$

$$Y^{y\,(*)} = \left[1 - \Gamma^{(0)}\right]\beta_{TW} + \Gamma^{(0)}\, Y^{e\,(0)}, \tag{17}$$

$$Z^{y\,(*)} = \Gamma^{(0)}\, Z^{e\,(0)},$$

where, for clarity, all the stress components, $\chi_j^{y\,(*)}$ for $j = 1, 2, 6$, have been explicitly reported; α_{TW} and β_{TW} being given by (8).

As noted in Sect. 3.1, the stresses at yield $\sigma_j^{y\,(*)}$, given by (17) by application of (5), will not satisfy the equilibrium conditions pertaining to the loads $P_{UB}^{(0)}\bar{p}$ but, remembering (3), they will satisfy the equilibrium requirements for loads $\bar{p}_i$ amplified by

$$P_{UB}^{(*)} = \frac{\int_V \sigma_j^{y\,(*)}\, \dot{\varepsilon}_j^c\, \mathrm{d}V}{\int_{\partial V_t} \bar{p}_i\, \dot{u}_i^c\, \mathrm{d}(\partial V)}, \tag{18}$$

that is the load multiplier value pertinent to the $E_j^{(*)}$ distribution accomplishing the matching at each GP. A new elastic analysis, performed with loads $P_{UB}^{(*)}\bar{p}$ and $E_j^{(*)}$ distribution of (16), will give at each GP a fictitious elastic solution lying on a surface $W\left[\chi_j, E_j^{(*)}, \nu_{12}^{(0)}, \bar{\chi}_j^{(0)}\right] = \bar{W}^{(*)}$, the latter obviously will not coincide with $W\left[\chi_j, E_j^{(*)}, \nu_{12}^{(0)}, \bar{\chi}_j^{(0)}\right] = \bar{W}^{(0)}$. The rationale can then be repeated in an *iterative fashion*, the starred quantities, i.e. the ones accomplishing the matching, being the values attained at convergence. The apposite recursive formulae are given in the next section where the main steps of the proposed procedure are summarized.

3.3 Iterative Scheme and Recursive Formulae

A flow-chart version of the whole procedure is hereafter depicted for clarity; the recursive formulae can be derived looking at Eqs. (16), (17), and (18).

- **Initialization**

  Knowing the strength values of the orthotropic material $(X_c; X_t; Y_c; Y_t; S)$; assign to all FEs in the mesh the initial set of fictitious elastic parameters and initial stresses such that the complementary energy equipotential surface is homothetic to the Tsai-Wu type surface, i.e.:

  $$E_1^{(0)} = 1/(2\,F_{11})\,, \qquad E_2^{(0)} = 1/(2\,F_{22})\,, \qquad E_6^{(0)} = 1/(2\,F_{66})\,,$$
  $$\bar{\sigma}_1^{(0)} = \alpha_{TW}/\sqrt{F_{11}}\,, \qquad \bar{\sigma}_2^{(0)} = \beta_{TW}/\sqrt{F_{22}}\,, \quad \bar{\sigma}_6^{(0)} = 0\,,$$
  $$\nu_{12}^{(0)} = -f_{12}\,\sqrt{F_{11}}/\sqrt{F_{22}}\,,$$

  α_{TW} and β_{TW} being the X, Y coordinates of the Tsai-Wu type ellipsoid centre. Set also $k = 1$, $P_{UB}^{(k-1)} = P_{UB}^{(0)} = 1$ (for $k = 1$, $P_{UB}^{(0)}$ can be any arbitrary value) and compute $\Omega = 1 + \alpha_{TW}^2 + 2\,f_{12}\,\alpha_{TW}\,\beta_{TW} + \beta_{TW}^2$ for later use.

- **Iteration loop**

  step # **1**: perform a fictitious elastic analysis with elastic parameters $E_j^{(k-1)}$, $\nu_{12} = \nu_{12}^{(0)}$, initial stresses $\bar{\sigma}_j = \bar{\sigma}_j^{(0)}$ and with loads $P_{UB}^{(k-1)}\bar{p}_i$, computing a fictitious elastic solution at Gauss point level, namely: $\dot{\varepsilon}_j^{e\,(k-1)}$, $\dot{u}_i^{(k-1)}$, $\sigma_j^{e\,(k-1)}$.

  step # **2**: compute the constant value of the complementary potential energy:

  $$\bar{W}^{(k-1)} = \frac{1}{2}\,\sigma_j^{e\,(k-1)}\,\varepsilon_j^{e\,(k-1)}$$

step # **3**:   compute the homothety ratio, namely

$$\Gamma^{(k-1)} = \begin{cases} \sqrt{\Omega/\bar{W}^{(0)}} & \text{for } k = 1 \\[2mm] \sqrt{\bar{W}^{(k-2)}/\bar{W}^{(k-1)}} & \text{for } k > 1 \end{cases}$$

step # **4**:   evaluate stresses at yield:

$$\sigma_1^{y\ (k-1)} = \left[1 - \Gamma^{(k-1)}\right] \frac{\alpha_{TW}}{\sqrt{F_{11}}} + \Gamma^{(k-1)} \sigma_1^{e\ (k-1)}$$

$$\sigma_2^{y\ (k-1)} = \left[1 - \Gamma^{(k-1)}\right] \frac{\beta_{TW}}{\sqrt{F_{22}}} + \Gamma^{(k-1)} \sigma_2^{e\ (k-1)}$$

$$\sigma_6^{y\ (k-1)} = \Gamma^{(k-1)} \sigma_6^{e\ (k-1)}$$

step # **5**:   set $\dot{\varepsilon}_j^{c\ (k-1)} = \dot{\varepsilon}_j^{e\ (k-1)}$, $\dot{u}_i^{c\ (k-1)} = \dot{u}_i^{e\ (k-1)}$ and evaluate the upper bound multiplier

$$P_{UB}^{\ (k)} = \frac{\int_V \sigma_j^{y\ (k-1)} \dot{\varepsilon}_j^{c\ (k-1)}\, dV}{\int_{\partial V_t} \bar{p}_i\, \dot{u}_i^{c\ (k-1)}\, d(\partial V)}$$

step # **6**:   check for convergence

$$|P_{UB}^{\ (k)} - P_{UB}^{\ (k-1)}| \le \text{TOL} \quad \begin{cases} \text{YES} \Rightarrow & \text{EXIT} \\[2mm] \text{NOT} \Rightarrow \text{CONTINUE} \end{cases}$$

step # **7**:   compute the $E_j^{(k)}$ distribution accomplishing the matching at each GP to be utilized at next iteration, namely:

$$E_j^{(k)} = E_j^{(k-1)} \left[\Gamma^{(k-1)}\right]^2 \qquad j = 1, 2, 6$$

set $k = k - 1$ and GOTO step #1.

By inspection of the above flow-chart, the LMM, also in this extended version for orthotropic materials, is easy to implement and can be carried out by any commercial FE code suitably fed, at each iteration, with the fictitious parameters accomplishing the matching at each GP.

Two remarks concern steps #4 and #7. At step #4, the given recursive formulae to compute the stresses at yield have been obtained by using (5) and (17), the latter have to be rewritten at the current iteration, i.e. the terms $(\cdot)^{(*)}$ or $(\cdot)^{(0)}$ are all in the form $(\cdot)^{(k-1)}$, following the notation above used. No use of dimensionless quantities is then necessary at operative level. At step #7, the $E_j^{(k)}$ ($j = 1, 2, 6$) values, to be utilized at next iteration, are actually evaluated at each GP of each element in the mesh. However, to avoid

accuracy problems, a unique set of $E_j^{(k)}$ is assigned within a single element, the latter being a set of averaged $E_j^{(k)}$ values within the element itself.

Finally, it is worth to note that writing (10) at the $k-$th iteration, by substituting the $E_j^{(k)}$ updated as at step #7 but rephrased, for convenience, in the equivalent form:

$$E_j^{(k)} = \frac{\Omega\, E_j^{(0)}}{W^{(k-1)}}\,,\tag{19}$$

making also use of Eqs. (11) and (12), the following expression is obtained (at the generic GP and at $k-$th iteration):

$$X^2 + Y^2 + Z^2 + 2\, f_{12}\, XY + f_1\, X + f_2\, Y = 1 + \Omega \left[\frac{\bar{W}^{(k)}}{\bar{W}^{(k-1)}} - 1\right].\tag{20}$$

The latter identifies with the Tsai-Wu type (7) when, at a certain k (namely at convergence), $\bar{W}^{(k)}$ identifies with $\bar{W}^{(k-1)}$ and the matching is accomplished. At this k it is also $\Gamma^{(k)} = 1$ and $\sigma_j^{y\ (k)} = \sigma_j^{e\ (k)}$ $(j = 1, 2, 6)$ as it has to be.

4 Validation: Numerical and Experimental Results

The proposed procedure is applied to a typical problem of composite structural elements, nowadays widely employed in many advanced engineering fields, precisely the evaluation of the strength as well as the prediction of the failure mechanism of the joints between composite plates or components.

In the present context such problem is treated in a simplified manner, i.e. in terms of evaluation of an upper bound to the collapse (failure) load multiplier, renouncing, of necessity, to a description of the intricate stress state arising within the joint. Nevertheless, the proposed analysis also allows a prediction of the failure mode. Both results are collated with experimental laboratory tests traceable in the relevant literature and this with the aim of inquiring into the effectiveness and the trustworthiness of the method.

4.1 Mechanically Fastened Joints in Composite Laminates

Joints between composite laminates are commonly made by using mechanical fasteners (like bolts, rivets, pin-connectors) and this mainly because they are easy to assemble or disassemble. On the other hand, such connections are characterized by an high stress concentration near the hole area which becomes a source of weakness; the structural joint failure usually begins at the fasteners sites. A great deal of research has therefore concentrated on this

problem with different approaches, see e.g. [2, 8, 20, 44, 47] just to quote some of the more recent contributions.

The idea of applying limit analysis on such a problem, far off the will of furnishing an exhaustive solution of the problem, has been spurred by a twofold reason. The former related to the possibility of analyzing a plane stress problem, to which the present procedure is confined, characterized by an high stress concentration. Such a circumstance, to the authors' opinion, is a good bench mark for the whole procedure. The latter is related to the chance of testing the procedure by comparison of the obtained numerical results with experimental (laboratory) ones.

The chosen mechanical problem is the one analyzed in [45], where several data and experimental results are reported for a pin-loaded plate, in plane stress conditions, as the one sketched in Fig. 3, where the geometry as well as the boundary and loading conditions are given. In particular: l indicates the distance between the hole center and the fixed plate end; e is the distance between the hole center and the free plate end; w is the plate width; t is the thickness.

The action of the pin inside the hole, of diameter d, has been assumed, following the relevant literature, as a cosine load normal distribution T_i given by:

$$T_i = -4 \frac{Q}{\pi d} n_i \cos \theta, \tag{21}$$

where: Q is the total applied load, n_i the unit vector of the outward normal to the inner hole surface and θ a clockwise angle varying in the range $[-\pi/2, \pi/2]$. The plate is made of glass-fiber/vinyl-ester composite material, fabricated by vacuum-assisted resin-transfer molding, whose mechanical characteristics, in terms of strength values and elastic moduli, are reported in Table 1.
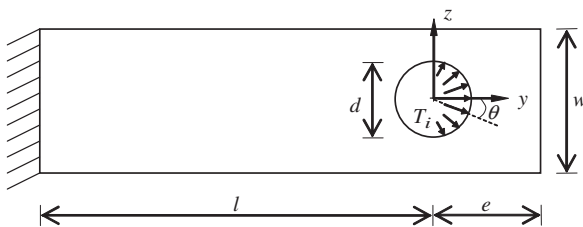

Fig. 3 Pin-loaded plate: geometry, boundary and loading conditions

Table 1 Mechanical parameters of the utilized composite material

Elastic Moduli (GPa) and Poisson ratio	E_1	E_2	G_{12}	ν_{12}
	49.8	6.9	31.9	0.3
Strengths (MPa)	$Y_t = X_t$	$Y_c = X_c$	S	
	664.3	385.1	64.6	

All the elastic analyses have been carried out using the FE code ADINA [1], while a Fortran main program has been developed to control the iterative procedure and the matching at each Gauss point as described in Sect. 3.3. Due to the symmetry of the problem with respect to the longitudinal y axis, only one half of the plate has been analyzed using the FE model shown in Fig. 4 and involving isoparametric shell elements with 16 nodes and 16 GPs per element. The utilized element allows to specify an orthogonal material axes system, the principal directions of orthotropy being $1 \equiv y$ and $2 \equiv z$. The applied reference load Q has been assumed equal to 1kN.

Many of the experimental test reported in [45] have been numerically reproduced and the obtained results are reported in Table 2 for sake of comparison. The latter is made in terms of *ultimate bearing strength*, namely σ_{BRU}, defined as the "maximum stress reached before a reduction in stress occurs for the first time". This bearing strength is given by the ratio between the load at failure, say Q_f, and the product of the hole diameter times the plate thickness: $\sigma_{BRU} := Q_f/dt$. Table 2 reports, for 16 specimens: the geometry; the experimental values of σ_{BRU} together with the experimentally observed failure mechanisms; the predicted σ_{BRU} values given by [45]; the ones given by the present analysis. The error in percentage is also listed for each specimen for the predicted numerical results. In particular, the σ_{BRU} values given by [45] are obtained by Chang's model, the ones given by the present LMM have been computed at last iteration as $\sigma_{BRU} = P_{UB}Q/dt$.

By examining the results of Table 2, it can be noted that the error in percentage of σ_{BRU} is, in several cases, very high for both predictions. To this concern, sharing the convincement of the above quoted paper, these discrepancies could be caused by a three dimensional effect which is not considered with a 2D FE formulation. Indeed, the same values of σ_{BRU} obtained for prototypes having the same w/d and e/d ratios but with different thickness are consistent with the 2D FE analysis but contradict the experimental evidences. To this concern it is to observe that a different thickness implies a different stacking sequence of the laminate layers that can strongly affect the mechanical characteristics of the laminate. Other results, about half of the run examples, are very good with a low error in percentage, but the above
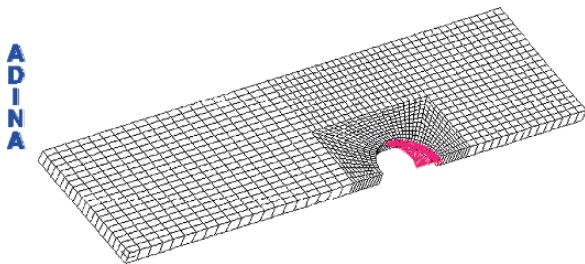
Fig. 4 Pin-loaded plate: half plate FE mesh adopted

Table 2 Pin-loaded plate of Fig. 3: experimental bearing strength values and failure modes against predicted bearing strengths

	Specimen dimensions				Experimental*		Prediction*		Prediction by LMM	
Item Number	d (mm)	w/d	e/d	t (mm)	σ_{BRU} (MPa)	Failure mode	σ_{BRU} (MPa)	Error %	σ_{BRU} (MPa)	Error %
1	6.35	4	3	1.24	329	T	533	62	386	17.3
2	6.35	4	3	2.48	537	T	533	0.7	386	28.1
3	6.35	4	3	5.63	613	T	533	13	386	37
4	6.35	8	3	1.15	421	B/S	492	16.8	387	8.1
5	6.35	8	3	2.41	499	B	492	1.4	387	22.4
6	6.35	8	3	5.62	611	B	492	19.5	387	36.6
7	6.35	4	2	2.33	460	T	459	0.2	255	44.6
8	6.35	4	4	2.31	491	B/T	538	9.6	513	4.5
9	6.35	4	6	2.32	496	T	538	8.5	520	4.8
10	6.35	8	2	2.31	458	S	414	9.6	255	44.3
11	6.35	8	4	2.27	522	B/S	520	0.4	518	0.7
12	6.35	8	6	2.28	439	B	537	22.3	532	21.2
13	12.70	4	3	1.15	281	B	276	1.8	385	37
14	12.70	4	3	2.41	376	B	276	26.6	385	2.4
15	12.70	4	3	5.63	486	B/T	276	43.2	385	20.8
16	12.70	4	3	12.71	564	T	276	51	385	31.7

*After Wu & Hahn [45].
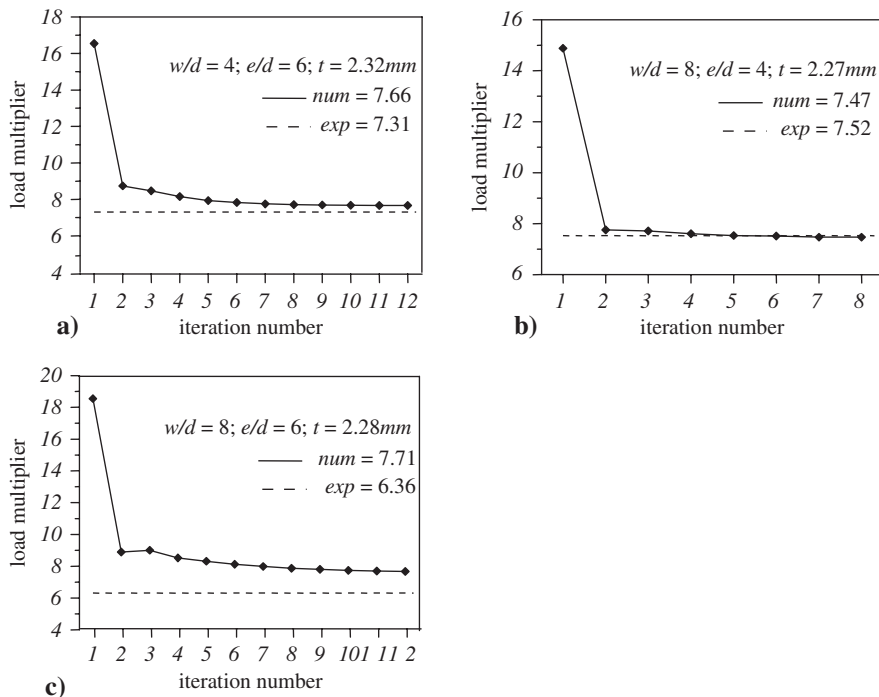
Fig. 5 Values of the upper bound to the collapse load multiplier, P_{UB}, versus iteration number; numerical results (*solid lines*) against collapse experimental threshold (*dashed lines*) for: (**a**) specimen #9; (**b**) specimen #11; (**c**) specimen #12

drawbacks need further investigations. To the authors' opinion, the noted drawbacks could be overcome by applying the LMM *layer-by-layer*, i.e. by using multilayer FEs so carrying out the matching taking into account the stacking sequence of the specimen. Another essential need is to test, for each prototype, a statistically more significant number of specimens. These are actually the objects of an ongoing research.

In all cases, the procedure has shown a very rapid convergence. For sake of brevity the upper bounds sequences obtained for specimens #9, #11 and #12, namely the ones for which good upper bound predictions have been obtained, are given in terms of upper bound values versus number of iterations in Figs. 5(a–c), respectively.

4.2 Prediction of the Collapse Mechanism

The failure of a mechanically fastened joint, as known, depends on its geometry, fiber orientation, position of the hole, thickness of the laminate, among

other factors like for example environmental conditions affecting the mechanical properties of the matrix. There are, typically, three fundamental modes of failure detected, other modes being a combination of them, precisely: net-tension (T); shear-out (S); bearing (B); see e.g. [28]. The first mode is due to high tensile stress values on the net area through the fastener hole; the second is related to the shear areas emanating from the hole edge parallel to the load and determined by the free edge distance. These two modes are usually catastrophic. The third one, is characterized by high compressive stress values within the zone surrounding the loaded inner hole surface and it is a progressive failure mode.

The prediction of the collapse mechanism for the studied problem is then a crucial goal. To this concern it is worth to note that the collapse mechanisms predicted, for all the run specimens, by the present LMM are in very good agreement with the ones observed experimentally and listed in Table 2. Once again, for specimens #9, #11 and #12, at which different failure modes have been experimentally detected, the collapse mechanisms are plotted in Figs. 6, 7 and 8, respectively. The collapse mechanisms are here individuated by the band plots, at last iteration, of the node displacement components. In particular: Fig. 6 shows a net tension failure mode, Fig. 7 a combined bearing/shear-out failure mode and Fig. 8 a bearing failure mode. The same failure modes have been observed experimentally for the three considered specimens, look again at Table 2. The results are obviously very encouraging, either for the very good agreement with the experimental findings or for the precise definition of the collapse zone.

5 Concluding Remarks and Future Developments

An extension of the Linear Matching Method for limit analysis of structures made of orthotropic materials has been presented. The extension pertains to materials obeying, by hypothesis, to a Tsai-Wu type yield condition, defined as a second order tensor polynomial form of the Tsai-Wu failure criterion for composite laminates. The proposed approach, from a wider point of view, concerns limit analysis of a class of anisotropic structures made of a material whose constitutive behaviour can be governed by a yield criterion expressed by a quadratic (strictly convex) stress function, the expounded procedure being, with no doubts, of general applicability.

The Linear Matching Method basically solves a sequence of linear analyses on the structure assumed, by hypothesis, as made of a fictitious linear viscous material with spatially varying moduli. With this conjecture, at each iteration, the computed fictitious solution can be used to define a collapse mechanism for the real structure and eventually an upper bound to the collapse load multiplier. The "matching" refers to the geometrical circumstance that, by varying (rescaling) the fictitious material parameters at each sam-
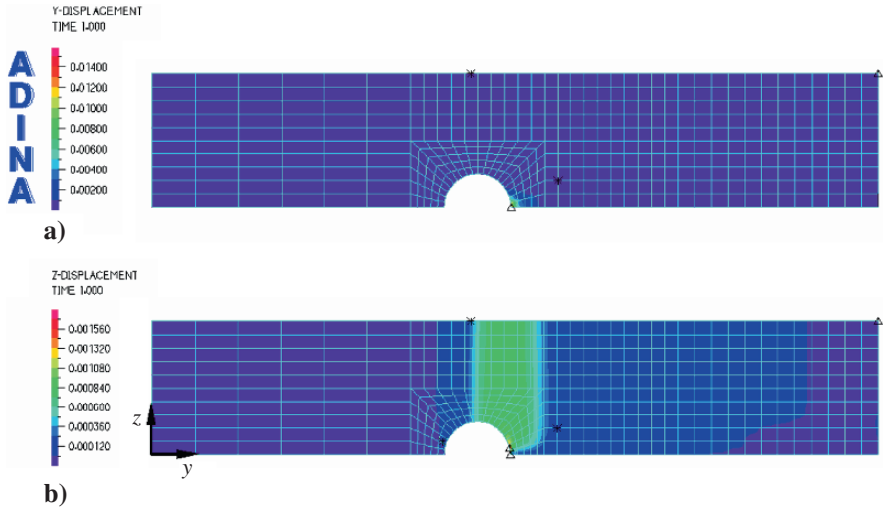
Fig. 6 Pin-loaded plate of Fig. 3, collapse mechanism of net-tension type for specimen #9: (**a**) y-displacements; (**b**) z-displacements
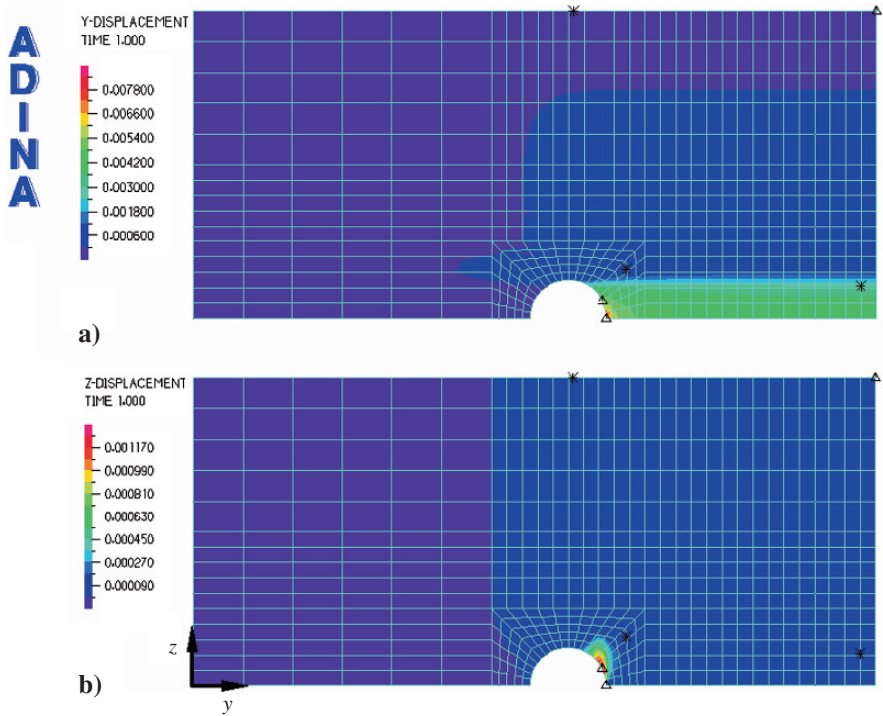

Fig. 7 Pin-loaded plate of Fig. 3, collapse mechanism of bearing/shear-out type for specimen #11: (**a**) y-displacements; (**b**) z-displacements

a)

b)
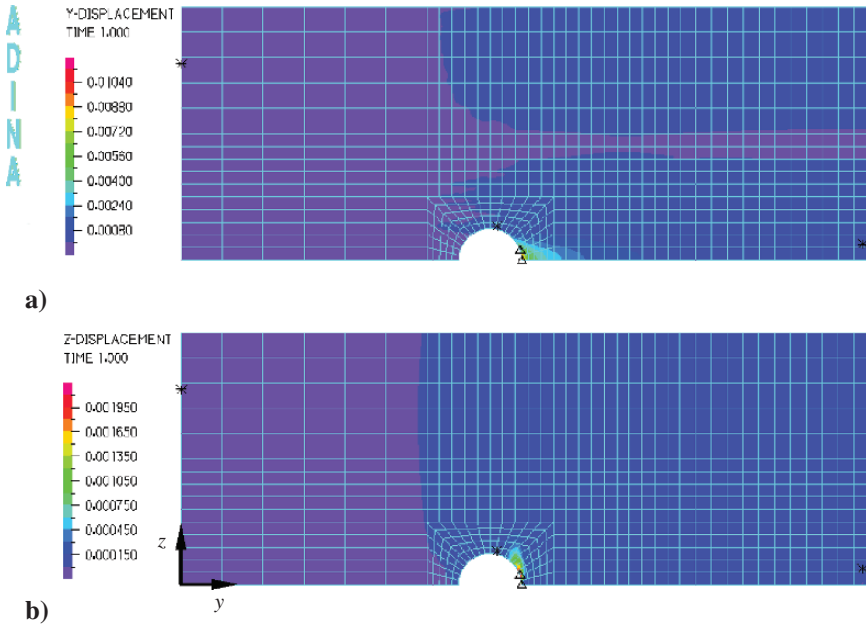
Fig. 8 Pin-loaded plate of Fig. 3, collapse mechanism of bearing type for specimen #12: (**a**) y-displacements; (**b**) z-displacements

pling point of the structure – namely at each Gauss point of the adopted FE mesh – the complementary dissipation rate equipotential surface of the fictitious material *matches* the yield function at a stress point (at yield) located by a given strain rate. The present approach proposes the use of a fictitious material which is assumed *linear, viscous, orthotropic* and suffering a distribution of *given initial stresses*. The whole method has been rephrased in a dimensionless stress space turning to an iterative procedure easy to handle, the number of fictitious material parameters to be adjusted reducing drastically to a scalar one.

The method has been tested by analyzing a typical problem of composite laminate structural elements, namely a mechanically fastened composite joint. A pin-loaded plate, under plane stress conditions, has been studied and the obtained results compared with the available experimental ones. The choice of this bench mark, whose peculiarity is the presence of an high stress concentration around the fastener area, allowed to improve and systematize the iterative scheme already employed by the senior authors for solving much simpler problems. Some numerical findings, in terms of upper bound values, show the need of further investigations to take into account three dimensional effects revealed by the experimental evidences and here disregarded by a 2D FE formulation. Other upper bound values are quite promising also showing the potentialities of the procedure. The latter exhibits, in all the run

examples, a very good convergence in agreement with a sufficient condition for convergence satisfied by this formulation. The results, obtained in terms of collapse mode prediction of the analyzed prototypes, are indeed very encouraging either for the very good agreement with the experimental findings or for the ability of the proposed procedure to locate accurately the collapse zone and the related collapse mode.

Further studies are certainly needed. To this concern a possible future step forward could be a better modeling of the composite laminate whose mechanical characteristics are strongly affected by the stacking sequence of the fiber layers. The idea is to apply the LMM layer-by-layer, i.e. by using multilayer 2D elements so performing the matching at the layer prototype level. A second crucial task is the definition of a lower bound to the collapse load multiplier. The lack of associativity, here overcome by a nonstandard limit analysis approach, will generate an unavoidable gap between the two bounds but their knowledge is essential for design purposes. A third goal is related to the definition of apposite experimental tests on prototypes suffering the same loading conditions, but having different geometry and/or fabricated with a different manufacturing technology. To the authors' opinion, the full reliability on a procedure as the one here proposed can be achieved only by comparison with a statistically meaningful number of experimental results. These are, at present, the main targets of an ongoing research work.

References

1. ADINA R & D, Inc.: Theory and Modeling Guide. Adina R & D, Watertown, MA, USA (2002)
2. Aktas, A.: Bearing strength of carbon epoxy laminates under static and dynamic loading. Composite Structures **67**, 485–489 (2005)
3. Atkinson, J.H., Potts, D.M.: Stability of a shallow circular tunnel in cohesionless soil. Géotechnique **27**, 203–215 (1977)
4. Belytschko, T., Hodge, P.G.: Plane stress limit analysis by finite elements. Journal of Engineering Mechanics Division **96**, 931–943 (1970)
5. Bolzon, G., Ghilotti, D., Maier, G.: Strength of periodic elastic-brittle composites evaluated through homogenization and parameter identification. European Journal of Mechanics A/Solids **21**, 355–378 (2002)
6. Boulbibane, M., Ponter, A.R.S.: Limit loads for multilayered half-space using the linear matching method. Computer and Geotechnics **32**, 535–544 (2005)
7. Boulbibane, M., Ponter, A.R.S.: Extension of the linear matching method to geotechnical problems. Computer Methods in Applied Mechanics and Engineering **194**, 4633–4650 (2005)
8. Camanho, P.P., Lambert, M.: A design methodology for mechanically fastened joints in laminated composite materials. Composites Science and Technology **66**, 3004–3020 (2006)

9. Capsoni, A., Corradi, L., Vena, P.: Limit analysis of anisotropic structures based on the kinematic theorem. International Journal of Plasticity **17**, 1531–1549 (2001)
10. Chen, H.F., Ponter, A.R.S.: Shakedown and limit analyses for 3-D structures using the linear matching method. International Journal of Pressure Vessels and Piping **78**, 443–451 (2001)
11. Chen, H.F., Ponter, A.R.S., Ainsworth, R.A.: The linear matching method applied to the high temperature life integrity of structures. Part 1. Assessment involving constant residual stress fields. International Journal of Pressure Vessels and Piping **83**, 123–135 (2006)
12. Chen, H.F., Shu, D.W.: A numerical method for lower bound limit analysis of 3-D structures with multi-loading systems. International Journal of Pressure Vessels and Piping **76**, 105–112 (1999)
13. Corradi, L., Vena, P.: Limit analysis of orthotropic plates. International Journal of Plasticity **19**, 1543–1566 (2003)
14. Drucker, D.C., Prager, W.: Soil mechanics and plastic analysis or limit design. Quarterly Applied Mathematics **10**, 157–165 (1952)
15. Drucker, D.C., Prager, W., Greenberg, H.J.: Extended limit design theorems for continuos media. Quarterly Applied Mathematics **9**, 381–389 (1952)
16. Francescato, P., Pastor, J.: Lower and upper numerical bounds to the off-axis strength of unidirectional fiber-reinforced composite by limit analysis method. European Journal of Mechanics A/Solids **16**, 213–234 (1997)
17. Hashin, Z.: Failure criteria for unidirectional fiber composites. Journal of Applied Mechanics **47**, 329–334 (1980)
18. Heyman, J.: The stone skeleton. International Journal of Solids and Structures **2**, 249–279 (1966)
19. Hodge, P.G., Belytschko, T.: Numerical methods for the limit analysis of plates. Trans. ASME, Journal of Applied Mechanics **35**, 796–802 (1968)
20. Içten, B.M., Karakuzu, R., Toygar, M.E.: Failure analysis of woven kevlar fiber reinforced epoxy composites pinned joints. Composite Structures **73**, 443–450 (2006)
21. Jones, R.M.: Mechanics of Composite Materials. 2nd edn., Taylor & Francis Inc., Philadelphia, PA, USA (1999)
22. Josselin de Jong, G.: Lower bound collapse theorem and lack of normality of strain rate to yield surface of soils. In: Rheology and Soil Mechanics: IUTAM Symposium, Grenoble 1964. Springer-Verlag, Berlin, Germany (1966)
23. Kolakowski, Z.: On some aspects of the modified Tsai-Wu criterion in thin-walled composite structures. Thin-Walled Structures **41**, 357–374 (2003)
24. Kooharian, A.: Limit analysis of voussoir and concrete arches. Journal of American Concrete Institute **24**, 317–328 (1952)
25. Li, H.X., Yu, H.-S.: Limit analysis of composite materials based on an ellipsoid yield criterion. International Journal of Plasticity **22**, 1962–1987 (2006)
26. Lubliner, J.: Plasticity theory. Macmillan Pub. Co., New York (1990)
27. Ma, G., Gama, B.A., Gillespie Jr., J.W.: Plastic limit analysis of cylindrically orthotropic circular plates. Composite Structures **55**, 455–466 (2002)
28. Matthews, F.L., Rawlings, R.D.: Composite Materials: Engineering and Science. Woodhead Pub. Ltd and CRC Press LLC, Cambridge, England (1999)
29. McLaughlin Jr., P.V., Batterman, S.C.: Limit behaviour of fibrous materials. International Journal of Solids and Structures **6**, 1357–1376 (1970)
30. Palmer, A.C.: A limit theorem for materials with non-associated flow laws. Journal de Mécanique **5**, 217–222 (1966)
31. Pisano, A.A., Fuschi, P.: A numerical approach for limit analysis of orthotropic composite laminates. International Journal for Numerical Methods in Engineering **70**, 71–93 (2007)
32. Ponter, A.R.S., Carter, K.F.: Limit state solutions, based upon linear elastic solutions with spatially varying elastic modulus. Computer Methods in Applied Mechanics and Engineering **140**, 237–258 (1997)

33. Ponter, A.R.S., Chen, H., Boulbibane, M., Habibullah, M.: The linear matching method for the evaluation of limit loads, shakedown limits and related problems. In: Mang, H.A., Rammerstorfer, F.G., Eberhardsteiner, J. (eds.) Proc. Fifth World Congress on Computational Mechanics. University of Technology, Wien, Austria (2002)

34. Ponter, A.R.S., Fuschi, P., Engelhardt, M.: Limit analysis for a general class of yield conditions. European Journal of Mechanics A/Solids **19**, 401–421 (2000)

35. Ponter, A.R.S., Fuschi, P., Engelhardt, M.: Limit analysis for pressure-dependent yield conditions. In: Owen, D.R.J., Oñate, E., Hinton, E. (eds.) Proc. European Congress on Computational Methods in Applied Sciences and Engineering. CIMNE, Barcelona, Spain (2000)

36. Prager, W.: An Introduction to Plasticity. Addison-Wesley, Reading, MA (1959)

37. Radenkovic, D.: Théorèmes limites pour un materiau de Coulomb à dilatation non standardisée. Comptes Rendus de l'Académie des Sciences Paris **252**, 4103–4104 (1961)

38. Save, M.: Atlas of Limit Loads of Metal Plates, Shells and Disks. Elsevier, Amsterdam (1995)

39. Shield, R.T.: On Coulomb's law of failure in soils. Journal of the Mechanics and Physics of Solids **4**, 10–16 (1955)

40. Shu, L.S., Rosen, B.W.: Strength of fiber-reinforced composites by limit analysis methods. Journal of Composite Materials **1**, 366–381 (1967)

41. Sloan, S.W., Kleeman, P.W.: Upper bound limit analysis using discontinuous velocity fields. Computer Methods in Applied Mechanics and Engineering **127**, 293–314 (1995)

42. Tsai, S.W., Hann, H.T.: Introduction to composite materials. Technomic Pub. Co., Westport, CT, USA (1980)

43. Tsai, S.W., Wu, E.M.: A general theory of strength for anisotropic materials. Journal of Composite Materials **5**, 58–80 (1971)

44. Whitworth, H.A., Aluko, O., Tomlinson, N.A.: Application of the point stress criterion to the failure of composite pinned joints. Engineering Fracture Mechanics **75**, 1829–1839 (2008)

45. Wu, T.J., Hahn, H.T.: The bearing strength of e-glass/vinyl-ester composites fabricated by VARTM. Composites Science and Technology **58**, 1519–1529 (1998)

46. Yu, H.S., Sloan, S.W.: Finite element limit analysis of reinforced soils. Computers & Structures **63**, 567–577 (1997)

47. Yýlmaz, T., Sýnmazçelik, T.: Investigation of load bearing performances of pin connected carbon/polyphenylene sulphide composites under static loading conditions. Materials & Design **28**, 520–527 (2007)

48. Zheng, X., Booker, J.R., Carter, J.P.: Limit analysis of the bearing capacity of fissured materials. International Journal of Solids and Structures **37**, 1211–1243 (2000)

Mechanical Surface Treatments and Life Improvement

G. Inglebert, I. Caron, T. Da Silva Botelho, and M. Quillien

Abstract Mechanical surface treatments such as shot-peening, hammering, cold rolling are used in order to introduce compressive residual stresses in surface layers. These stresses usually induce significant life improvement. Optimization of these treatments might be more efficient if an analytical model is used to predict the induced residual stresses and their evolution under cycling loading. Such models have been settled by L. Castex, G. Inglebert and their students between 1984 and 1992. They used the MASSI method (Simplified Analysis of Inelastic Structures Method – J. Zarka, G. Inglebert), the analytic knowledge of Hertzian contact stresses in the elastic case, and a specific behaviour law, MI2. The paper will sum up the predictive method and how it could be used for life improvement estimation using multiaxial life criteria. Accuracy of the results is strongly linked to the quality of the behaviour law; recent work of G. Inglebert, N. Point and D. Vial settled an optimization process to obtain the four material parameters for the MI2 law from a tensile test.

1 Introduction

Mechanical surface treatments such as shot-peening, hammering, cold rolling are used in order to introduce compressive residual stresses in surface layers.

These stresses usually induce significant life improvement. Optimisation of these treatments might be more efficient if an analytical model is used to predict the induced residual stresses and their evolution under cycling loading.

Geneviève Inglebert, Isabelle Caron, Tony Da Silva Botelho, and Muriel Quillien
Laboratoire d'ingénierie des Systèmes Mécaniques et des matériaux, EA2336, Institut Supérieur de Mécanique de Paris (SUPMECA) 3 rue Fernand Hainaut, F93407 Saint Ouen Cedex, France, e-mail: Genevieve.Inglebert@supmeca.fr

Such models have been settled by L. Castex, G. Inglebert and their students between 1984 and 1992. MASSI method (Simplified Analysis of Inelastic Structures Method developed by J. Zarka, G. Inglebert and colleagues), working on Standard Generalized Materials was used together with the analytic knowledge of Hertzian contact stresses in the elastic case (all these mechanical surface treatments imply contacts), and a specific behaviour law, MI2.

The final state of strains and stresses after treatment is supposed to be only a function of depth from the surface.

This work sums up the predictive method and how it could be used for life improvement estimation using multiaxial life criteria.

Accuracy of the results is strongly linked to the quality of the behaviour law; recent work of G. Inglebert, N. Point and D. Vial settled an optimisation process to obtain the four material parameters for the MI2 law from a tensile test.

2 MASSI Method

MASSI stands in French for "Méthode d'Analyse Simplifiée des Structures Inélastiques" or "Simplified Analysis for Inelastic Structures".

Using MASSI implies using specific behaviour laws from the Standard Generalized Materials class (rheological models). These classes of materials are well suited to describe kinematic hardening of the material.

Main uses of MASSI are shakedown analysis including estimation of residual stresses and plastic strains and limit analysis.

2.1 Basis

Microphysical analysis shows that the inelastic behaviour of metals is strongly linked to internal defects such as dislocations, vacancies, ... The model of Standard Generalized Materials considers the elementary volume element as an assembly of n perfectly plastic mechanisms embedded in a linear elastic matrix.

Local stresses $\boldsymbol{\sigma}^{(m)}$ on the mechanisms are linear functions of macroscopic stresses $\boldsymbol{\Sigma}$ and internal deformations $\boldsymbol{\alpha}^{(m)}$ of all the perfectly plastic mechanisms. Plastic yield conditions have to be written for each mechanism and introduce yield values $S^{(m)}$:

$$
\begin{aligned}
\left[\boldsymbol{\sigma}^{(m)}\right] &= \mathsf{A}\boldsymbol{\Sigma} - \left[\boldsymbol{y}^{(m)}\right] \quad \left\|\boldsymbol{\sigma}^{(m)}\right\| \leq S^{(m)}, \\
\left[\boldsymbol{y}^{(m)}\right] &= \mathsf{B}\left[\boldsymbol{\alpha}^{(q)}\right] \quad \text{and} \quad \boldsymbol{\varepsilon}^p = A^T\left[\boldsymbol{\alpha}^{(m)}\right].
\end{aligned}
\tag{1}
$$

A is the localisation tensor on the mechanisms proportional to the deviator tensor to account for plastic incompressibility. Matrix B is a square constant matrix defining global hardening properties of the volume element. $\boldsymbol{y}^{(m)}$ are stress like internal variables accounting for all inelastic effects at the level of the elementary mechanism (m).

Looking at this elementary volume element as part of a structure, dedicated internal variables $\mathsf{Y}^{(m)}$ are defined: They will account for all inelastic phenomena due to global equilibrium of the structure, at the level of inelastic mechanism number (m).

$$\left[\boldsymbol{\sigma}^{(m)}\right] = \mathsf{A}\boldsymbol{\Sigma}^{el} - \left[\mathsf{Y}^{(m)}\right] \quad \left\|\boldsymbol{\sigma}^{(m)}\right\| \leq S^{(m)},$$

$$\left[\mathsf{Y}^{(m)}\right] = \mathsf{B}\left[\boldsymbol{\alpha}^{(q)}\right] - \mathsf{A}\rho \quad \text{and} \quad \varepsilon^p = \mathsf{A}^T\left[\boldsymbol{\alpha}^{(m)}\right]. \tag{2}$$

$\boldsymbol{\Sigma}^{el}$ is the purely elastic stress (obtained assuming only an elastic behaviour) on the volume element which includes mechanism (m). $\boldsymbol{\rho}$ is the residual or internal stress tensor on the volume element, difference between actual stress $\boldsymbol{\Sigma}$ and $\boldsymbol{\Sigma}^{el}$.

The yield condition in equation (2) can be interpreted in the $\mathsf{Y}^{(m)}$ space in terms of "$\mathsf{Y}^{(m)}$ has to be inside the hypersphere of radius $S^{(m)}$ centred on $\mathsf{A}\boldsymbol{\Sigma}^{el}$".

2.2 Shakedown Analysis

2.2.1 Shakedown Status

Shakedown analysis first aims at estimating the stabilized state of a structure under cyclic loading: will elastic or plastic shakedown be achieved? This can be done from the purely elastic analysis $\boldsymbol{\Sigma}^{el}$ of the structure on one loading cycle.

An original algorithm SHS has been derived to answer this question: on each mechanism, the Smallest HyperSphere (SHS), surrounding the local loading path, is searched for; if, at the level of each elementary mechanism in the structure, the radius of the SHS is smaller than the local yield constant $S^{(m)}$, elastic shakedown will occur (issued from Melan's and Koiter's theorems). The successive steps are:

1. Perform one purely elastic cycle on the structure.
2. For each plastic mechanism, in each volume element extract the local loading path $\mathsf{A}\boldsymbol{\Sigma}^{el}(t)_{0 \leq t \leq T}$, find SHS radius R_{SHS} and compare it to $S^{(m)}$.
3. If all R_{SHS} are smaller than the associated $S^{(m)}$, elastic shakedown will be reached. A common part $\boldsymbol{\Omega}$ to all local elastic domains, centred on $\mathsf{A}\boldsymbol{\Sigma}^{el}$, can be defined everywhere. Else, plastic shakedown for regular B matrix or ratcheting (only possible for singular B matrix) will take place.

MASSI has been established mostly for the elastic shakedown case. Some specific cases have been solved in the plastic shakedown range, among them the prediction of residual stresses due to shot peening, cold rolling or hammering.

2.2.2 Residual Stresses Estimation (Elastic Shakedown Case)

If elastic shakedown is predicted, the constant stabilised residual stresses and plastic strains have to be estimated. They will solve the homogeneous problem on the structure: the periodic loading is taken into account through the cyclic $\mathbf{\Sigma}^{el}(t) = \mathbf{\Sigma}^{el}(t + T)$.

The $\mathsf{Y}^{(m)}$ internal variables are used to obtain the stabilised inelastic problem: $\mathsf{Y}^{(m)}$ has to be inside the convex intersection Ω of all the hyperspheres of radius $S^{(m)}$ centred on local $\mathsf{A}\mathbf{\Sigma}^{el}$.

If in some places in the structure and some mechanisms, this condition is not fulfilled, a local orthogonal projection is performed on Ω and local plastic evolution of the mechanism has occurred. An iterative process is then realised according to the following steps:

1. Perform one or one half elastoplastic cycle on the structure.
2. From the final state $\left(\mathbf{\Sigma}, \varepsilon^p, \boldsymbol{\alpha}^{(q)}\right)$ of step 1 and the previous elastic calculation, derive $\mathsf{Y}^{(m)}$ on each mechanism in each volume element:

$$\left[\mathsf{Y}^{(m)}\right] = \mathsf{B}\left[\boldsymbol{\alpha}^{(q)}\right] - \mathsf{A}\left(\mathbf{\Sigma} - \mathbf{\Sigma}^{el}\right) = \mathsf{B}\left[\boldsymbol{\alpha}^{(q)}\right] - \mathsf{A}\boldsymbol{\rho}. \tag{3}$$

3. For each mechanism in each volume element, test if $\mathsf{Y}^{(m)}$ is inside Ω or not. If not, project $\mathsf{Y}^{(m)}$ on Ω and get a new plastically admissible $\mathsf{Y}^{(m\,\mathrm{Pr})}$.
4. If no new $\mathsf{Y}^{(m\,\mathrm{Pr})}$ have been found, the stabilised solution is obtained.
5. If not, solve the global equilibrium of the residual stresses in the structure, taking into account $\mathsf{Y}^{(m\,\mathrm{Pr})}$ when it has been defined or $\boldsymbol{\alpha}^{(n)}$ elsewhere:

$$\left.\begin{array}{l} \rho_{ij} \text{ SA with 0 given body and surface forces} \\ \frac{1+\nu}{E}\rho_{ij} - \frac{\nu}{E}\rho_{kk}\delta_{ij} + \varepsilon_{ij}^p \text{ K.A. with 0 given displacements} \end{array}\right\} \tag{4}$$
$$\text{with } \begin{cases} \varepsilon^P = A^T\left[\alpha^{(m)}\right], Y^{(m)} \subset \Omega \text{ elastic part V}_\mathrm{E} \\ \varepsilon^P = A^T B^{-1} A\rho + A^T B^{-1}\left[Y^{(m)\,\mathrm{Pr}}\right] \text{ plastic part V}_\mathrm{P} \end{cases}$$

6. In $\mathrm{V_P}$, the elastic constants (E, ν) have to be replaced by (E_T, ν_T) issued from (E, ν) and $\mathsf{A}^T\mathsf{B}^{-1}\mathsf{A}$ and $\mathsf{A}^T\mathsf{B}^{-1}\left[Y^{(m)\,\mathrm{Pr}}\right]$ stands for an apparent plastic strain.
7. Solution of (4) offers new values of residual stresses $\boldsymbol{\rho}$ which will generate new values of $\mathsf{Y}^{(m)}$ in $\mathrm{V_E}$ and new values of $\boldsymbol{\alpha}^{(q)}$ and $\boldsymbol{\varepsilon}^P$ in $\mathrm{V_P}$ through (3)
8. Go back to step 3 for testing $\mathsf{Y}^{(m)}$ in $\mathrm{V_E}$.

When no more projections are needed, the associated plastic strains of the elementary mechanisms and plastic strains of the volume elements, and residual stresses give a statically, kinematically and plastically admissible constant solution.

Limit analysis solutions could also be achieved from a few elastic calculations assuming appropriate values of the structural $Y^{(m)}$ [15].

2.3 Elastic Shakedown and Polycyclic Life

Once the stabilised state of the structure has been obtained, life can be estimated through multiaxial criteria such as Dang Van coupled with a Wöhler curve. Most of these criteria imply hydrostatic pressure and some shear stress range. The effect of residual stresses is a mere translation of the whole loading path or critical point along the hydrostatic pressure axis; its intensity is the value of the hydrostatic pressure associated to the constant residual stress tensor.

Negative residual stress hydrostatic pressure will move in the security direction. Positive ones will make things less safe.

3 Prediction of Shot Peening Stresses

3.1 Shot Peening Treatment

Shot peening is an impact surface treatment. Small balls impact the surface of the part with sufficient energy to create plastic strains in the surface layers; the typical impact speeds are between 20 and 120 m/s. Peening media are small enough (0.05 up to 2.5 mm) compared to the treated part geometry (thickness, curvatures, ...).

Shot peening treatment induces isotropic roughness, strong hardening, plastic strains and residual stresses in the surface layers and these strains and stresses are homogeneous along the surface and could be taken as only function of depth.

Peening intensity is defined and controlled using Almen strips: some flat specimen of normalized dimensions, in E460 Steel. The Almen strip is fixed on a thick normalized block and peened. The strip bending after treatment gives the Almen intensity.

The part to be treated replaces the Almen strip used to settle and control the process. For proper introduction of compressive residual stresses, normal impact has to be performed.

3.2 Shot Peening Model

3.2.1 Principle

The first step of our model consists in defining for each depth some local intensity of the impact stresses. The part is considered as submitted to a cyclic loading path with two significant steps: maximum stresses along the impact axis and zero stresses far from the impact.

Elastic calculation of stresses $\mathbf{\Sigma}^{el}$ along the impact axis is given from the works of Davies [4] and Hertz [13] (Johnson [16]) using Hertz stresses in the ball on plane contact along the contact axis. Plasticity is induced by the deviatoric part of these contact stresses.

Treatment of a semi-infinite body is assumed in a first step, due to the small size of the peening media. Observed symmetry of the stresses and equilibrium equations on this semi-infinite body implies the global form of the displacements and residual stress and strain tensors:

$$[\rho_{ij}] = \begin{bmatrix} \rho(z) & 0 & 0 \\ 0 & \rho(z) & 0 \\ 0 & 0 & 0 \end{bmatrix}, [u_i] \begin{bmatrix} 0 \\ 0 \\ u_z(z) \end{bmatrix} \Rightarrow [\varepsilon_{ij}^{ine}] = \begin{bmatrix} 0 & 0 & 0 \\ 0 & 0 & 0 \\ 0 & 0 & u_{z,z} \end{bmatrix}. \quad (5)$$

So, the model can be reduced to a one dimensional problem.

Following (3), specific Y variables are introduced most often with an initial zero value. The centre of the local plastic domain in the Y space moves for each depth between zero and the maximum Hertz value.

Three cases could occur (Fig. 1):

1. A common part Ω to both main plastic domains exists and initial Y lies in Ω. A zero plastic evolution is assumed in these layers.
2. A common part Ω to both main plastic domains exists and initial Y is outside Ω and is pulled to a new value Y^{Pr}.
3. No common part Ω exists. Y is pulled to an upper value under impact and pulled back to the side of the zero domain after impact.

When all Y values have been obtained, the residual strains and stresses are calculated from (4) and (5). For complete prediction, the number of internal mechanisms and the value of yield and hardening constants have to be defined precisely.

3.2.2 Chosen Behaviour Laws

First studies on E460, ferritic alloys or titanium alloys, have been developed with a *linear kinematic hardening* law (LKH). Only one internal mechanism is used. The localisation tensor A is reduced to the deviator function, and the hardening matrix B to a single constant equal to the volume linear hardening modulus. Accurate enough results were obtained (Fig. 2).

Fig. 1 Final Y definition
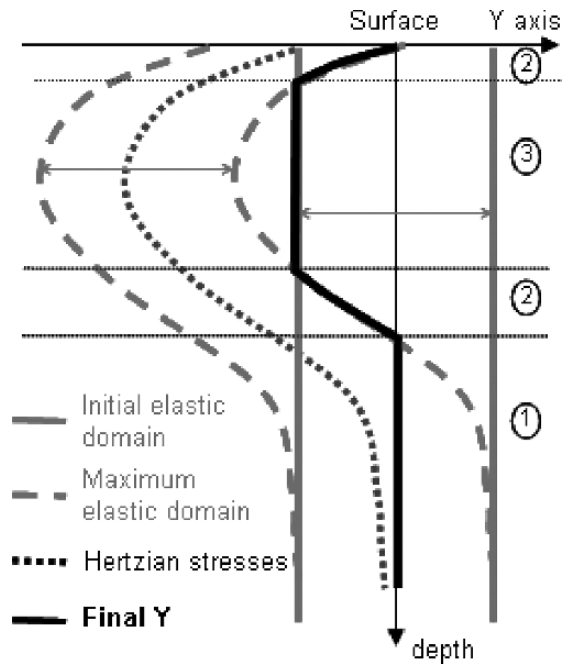
$$\sigma_{ij}^{(1)} = \Sigma_{ij}^{el} - \frac{1}{3}\Sigma_{kk}^{el}\delta_{ij} - Y_{ij}^{(1)} \quad \left\|\sigma_{ij}^{(1)}\right\| \leq \text{Re},$$

$$Y_{ij}^{(1)} = C\left[\alpha_{ij}^{(1)}\right] - \left(\rho_{ij} - \frac{\rho_{kk}}{3}\delta_{ij}\right) \quad \text{and} \quad \varepsilon_{ij}^{P} = \alpha_{ij}^{(1)}. \tag{6}$$

The same model with the same linear kinematic hardening law gave very poor results on an aluminium alloy: calculated stresses were twice the measured stresses and calculated affected depth was half the measured one. We had to introduce a better suited model for plastic behaviour (Fig. 3).

A new model MI2 with two coupled internal mechanisms provided much better results (Fig. 3). The first mechanism is the classical macroscopic plastic strain; the second has been linked to restoration phenomena:
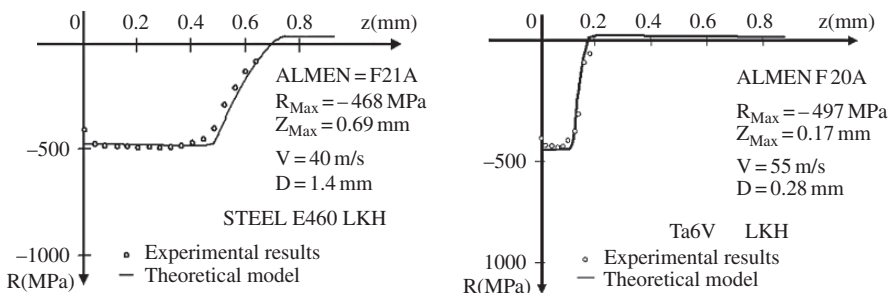

Fig. 2 Modelled and measured results with LKH for steel and titanium alloys
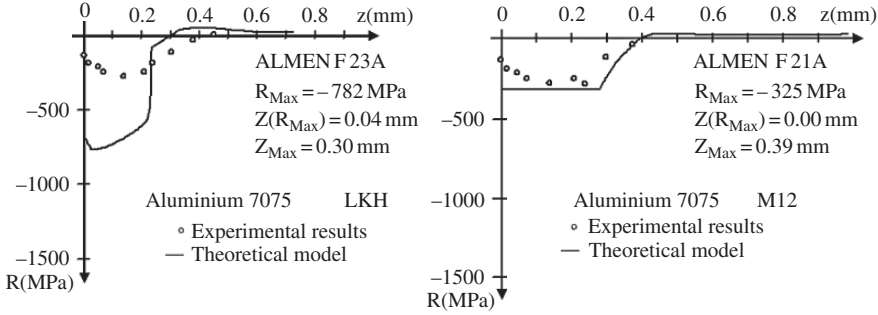
Fig. 3 Aluminium alloy modelled and measured results with LKH and MI2 laws

$$\begin{bmatrix} \sigma_{ij}^{(1)} \\ \sigma_{ij}^{(2)} \end{bmatrix} = \left(\Sigma_{ij}^{el} - \frac{\Sigma_{kk}^{el}}{3} \delta_{ij} \right) \begin{bmatrix} 1 \\ 0 \end{bmatrix} - \begin{bmatrix} Y_{ij}^{(1)} \\ Y_{ij}^{(2)} \end{bmatrix} \;, \quad \sqrt{\sigma_{ij}^{(1)} \sigma_{ij}^{(1)} + \sigma_{ij}^{(2)} \sigma_{ij}^{(2)}} \leq \mathrm{Re},$$

$$\begin{bmatrix} Y_{ij}^{(1)} \\ Y_{ij}^{(2)} \end{bmatrix} = \begin{bmatrix} B_{11} & B_{12} \\ B_{12} & B_{22} \end{bmatrix} \begin{bmatrix} \alpha_{ij}^{(1)} \\ \alpha_{ij}^{(2)} \end{bmatrix} - \left(\rho_{ij} - \frac{\rho_{kk}}{3} \delta_{ij} \right) \begin{bmatrix} 1 \\ 0 \end{bmatrix} \quad \text{and} \quad \varepsilon_{ij}^P = \alpha_{ij}^{(1)}. \quad (7)$$

The initial elastic yield stress and three hardening moduli are used to define plastic behaviour; they are identified from a monotonic or cyclic tensile test and used to predict shot peening stresses.

This MI2 law allowed us to describe numerous materials on a wide range of plastic strains with only four constants for plastic behaviour.

Inclined impact or other surface treatments such as hammering or cold rolling have been described in the same framework with the same behaviour law. We only changed the Hertz stresses to take into account friction effects or other contact geometries.

Stability of the predicted residual stresses and their influence on life of the treated parts can be investigated with MASSI when the service loading is postulated.

4 MI2 Identification Process

4.1 Tuning the Model for Tensile Test

Our main difficulty with the MI2 law was to find a reasonable identification process. A parametric definition of the stress versus plastic strain tensile curve has been obtained; allowing optimising of the material constants.

From a mathematical point of view, only four constants are needed. If the initial value and slope of the tensile stress versus plastic strain curve
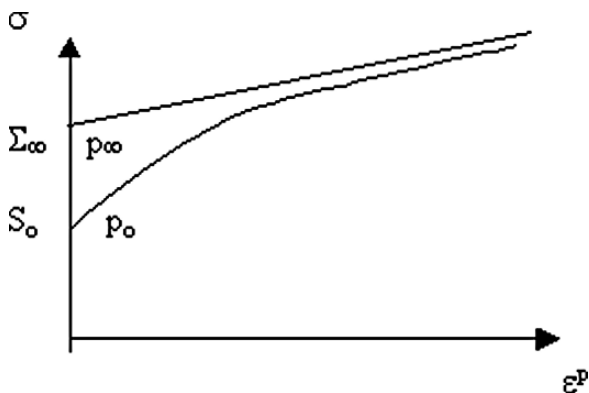
Fig. 4 Tensile stress versus plastic strain curve – initial values and asymptote

and its asymptote are known, all constants might be rather simply defined (Fig. 4).

Unfortunately, the beginning and the asymptote of this curve might be rather difficult to define properly: for the beginning, one has to detect when some non-linearity appears, and the asymptote should be searched for before emergence of significant damage. The intermediate part of the curve is much better known.

So we used the whole stress/plastic strain curve in the following non-linear mean square optimization process, which concentrates the non-linear effects on variable r. Then the physical parameters from the tensile test curve or at the level of the elementary mechanisms might be calculated.

$$r = tg\varphi_{as} = \frac{-B_{12}}{B_{22}} \quad , \quad b = B_{22} \quad , \quad p_\infty = \frac{B_{11}B_{22} - B_{12}^2}{B_{22}},$$

$$\Rightarrow \quad [\mathsf{B}] = \begin{bmatrix} p_\infty + r^2 b & -rb \\ -rb & b \end{bmatrix} \quad , \quad [\mathsf{B}]^{-1} = \frac{1}{p_\infty} \begin{bmatrix} 1 & r \\ r & r^2 + p_\infty / b \end{bmatrix}. \quad (8)$$

With these new hardening parameters, the tensile stress versus plastic strain curve can be written:

$$\sigma = p_\infty \varepsilon^p + \Sigma_\infty t, \ \varepsilon^p = \varepsilon^p_{ini} + \frac{\Sigma_\infty}{b\,(1+r^2)^2}\,(h\,(t,r) - h\,(t_{ini}, r))\,\text{and}$$

$$\text{with } h\,(t,r) = \frac{1}{2}\log\frac{1+t}{1-t} - 2r\sqrt{1-t^2} + (r^2-1)\,t\ \text{and}$$

$$t_{ini} = \frac{\sigma_{ini} - p_\infty \varepsilon^p_{ini}}{\Sigma_\infty}. \quad (9)$$

The parameter t grows from t_{ini} to one during monotonic loading. The constant r is linked to the asymptotic properties of the curve.

Fig. 5 Stresses versus total
or plastic strain for MI2 and
LKH models

Fig. 5 Stresses versus total or plastic strain for MI2 and LKH models
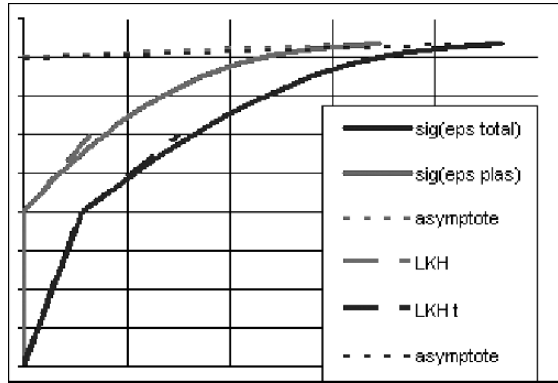
The comparison of MI2 and LKH models assuming the same initial ordinate and slope and featuring some asymptote to the tensile curve is shown on Fig. 5.

4.2 Identification Process

The identification process uses data from monotonic or cyclic tensile test [18], provided that a sufficient number of data in the plastic range have been obtained. Main steps are described in the following:

1. Check the experimental data to detect abnormal points linked to the beginning of the test or damage; n points (total strain, stress) are left.
2. Search for the beginning of plastic part with D. Gorbanzadeh [7] test: the k first points define a straight line in the mean square sense and the *(n-k)* remaining points define a parabola; a minimal principle is used and final result is an estimation of Young's modulus and initial yield stress Re or S_o.
3. Extract the elastic part and keep only the plastic one.
4. Find a first estimate of the asymptote (Fig. 3): $(p_\infty, \Sigma_\infty)$; a few candidates might be found.
5. For each of these candidates $(p_\infty, \Sigma_\infty)$ optimization of the curve is performed.

   – A first linear step gives initial values for r and b.
   – Then a non-linear mean square method (Levenberg-Marquardt or other) is used to find refined values of the four parameters.

6. The best result (showing minimum error) between all initial $(p_\infty, \Sigma_\infty)$ is selected.

4.3 Results

Results on two materials are shown on Fig. 6: on the left, stresses versus total strain, and on the right stresses versus plastic strain.
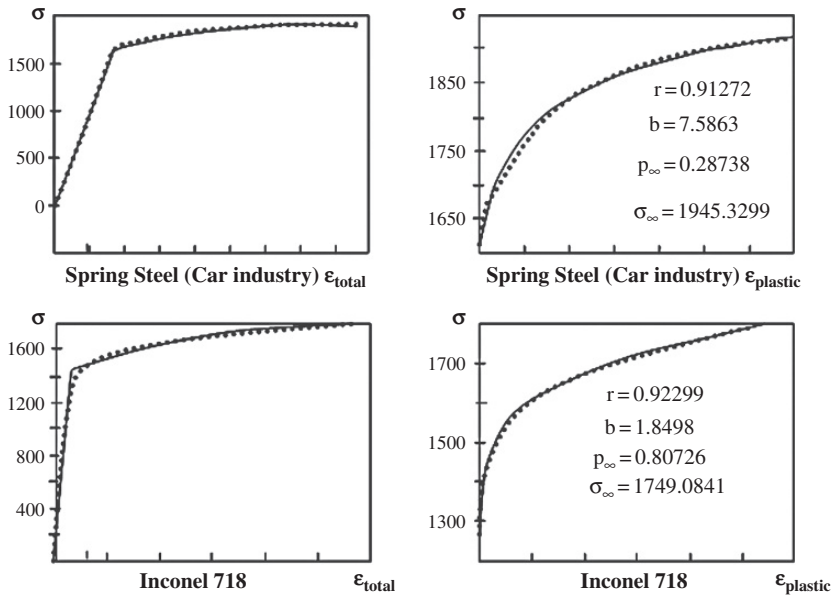

Fig. 6 Measured and modeled results with MI2 hardening law

5 Conclusion

The analytical models for surface treatments, associated to MASSI and multi-axial criteria to investigate their effects on life of the structure, gave a straight forward and quick working tool for design in the early stages.

References

1. Batista A.C., Dias A., Lebrun J.L., Le Flour J.C., Inglebert G. (2000) Contact fatigue of automotive gears: evolution and effects of residual stresses introduced by surface treatments, Fatig. Fract. Eng. Mat. Struct. vol. 23, n 3: 217–228
2. Boussinesq J. (1885) Application des potentiels à l'étude de l'équilibre et du mouvement des solides élastiques, Librairie Scientifique et Technique Albert Blanchard – Paris
3. Caron I., Inglebert G., Gras R., De Monicault J.M. (2002) Mechanical analysis of coated materials undergoing fretting fatigue in a cryogenic environment, J. Strain Anal. vol 37, n 6: 585–589
4. Davies R.M. (1949) The determination of static and dynamic yield stresses using a steel ball, Proc. Roy. Soc. A197: 416–432
5. Fatallah R., Inglebert G., Castex L. (2003) Determination of shot peening coefficient of restitution, Surf. Eng., vol 19, n 2: 109–113
6. Fathallah R., Inglebert G., Castex L. (1998) Prediction of plastic deformation and residual stresses induced in metallic parts by shot peening, Mat. Sci. Technol., vol 14: 631–639
7. Gorbanzadeh D. (1995) revue Statistique Appliquée, XLIII(2): 67–76
8. Halphen B., Nguyen Q.S. (1975) sur les matériaux standard generalizes, Journal de mécanique, vol 14, n 1:39–63
9. Hamdane N., Inglebert G., Castex L. (1991) Prediction of the residual stress field created by internal peening of Nickel based alloy tubes, Plasticity 91, 3rd Intern. Symposium on Plasticity and its current applications, 12–16 August 1991
10. Hamdane N., Inglebert G., Castex L. (1993) Martelage de surfaces par billes attachées, Mécanique Industrielle et Matériaux, vol 46, n 4: 189–191
11. Hassine T., Inglebert G. (1995) Introducing measured initial stresses in shakedown and fatigue analyses, in Aiadabi M.H. and Alessandri C. Contact Mechanics II – Computational techniques 413–420
12. Hassine T., Inglebert G., Pons M. (2000) Shakedown and damage analysis in the Ariane V program in Weichert D. et Maier G. (ed) Solid mechanics and its applications – Inelastic Analysis of structures under variable loads – Theory and Engineering Applications, Kluwer, Netherlands
13. Hertz H. (1881) Über die Berührung fester elastischer Körper, J. für die reine und angewandte Mathematik XCII156, Berlin
14. Inglebert G., Louradour G., Le Nizerhy D., Pons M. (2000) A shakedown and life prediction software integrating initial and contact stresses, European Congress on Computational Methods in Applied Sciences and Engineering, ECCOMAS 2000, Barcelona, 11–14 September
15. Inglebert G., Zarka J. (1980) On a simplified inelastic analysis of structures, Nucl Eng Des (North Holland) 57: 333–368
16. Johnson K.L. (1985) Contact mechanics, Cambridge University Press, Cambridge.
17. Khabou M.T., Castex L., Inglebert G. (1990) The effect of material behaviour law on the theoretical shot peening results, Europ. J. Mech vol A/Solids, 9, n 6: 537–549
18. Point N., Vial D. (2005) A plasticity model and hysteresis cycles in Fremond, M. & Maceri, F. (ed) Mechanical modelling and computational issue in Civil Engineering, Springer, Lecture Notes in Applied and Computational Mechanics, vol 23: 165–172
19. Vial D., Point N., Inglebert G. (1999) Modèle micromécanique à quatre paramètres pour le comportement élastoplastique, Mécanique Industrielle et Matériaux, vol. 52, n 1: 7–9
20. Zarka J., Frelat J., Inglebert G., Kasmaï-Navidi P. (1989) A new approach to inelastic analysis of structures, CADLM edition, France

Force Method – Based Procedures in the Limit Equilibrium Analysis of Framed Structures

K.V. Spiliopoulos

Abstract Within linear programming applications the force method of analysis provides the most well suited approach to handle limit equilibrium such as limit or shakedown analysis of framed structures. Nevertheless the approach using the displacement method has been used more often as it is easier to automate. The difficulty of the force method is to automatically select the basic unknowns which are the hyperstatic forces. The graph representation of a frame provides a means to solve this problem. In the present work a numerical procedure based on this representation is presented which has already been applied to the plastic design of plane frames under either monotonic or alternate loading. This procedure is herein used to find the limit and shakedown load of plane frames. It is also extended to cater for the limit load analysis of space frames, thus providing a common basis for all types of framed structures. Examples of application are included.

1 Introduction

Linear programming provides a widely used method of solution to establish the ultimate strength of structures under monotonic or alternating loading. As for any structure but especially for frames, the framework of formulation may be either the force (mesh) or the displacement (nodal) method of analysis. Depending on using either the lower bound or the upper bound theorems of structural plasticity, one may construct four different linear programs. Although recently, especially for large-scale problems, interior-point algorithms have been used for the solution of linear programs [4], it has been shown [18]

Konstantinos V. Spiliopoulos

Institute of Structural Analysis and Aseismic Research, Department of Civil Engineering, National Technical University of Athens, Zografou Campus GR 157-80, Athens, Greece, e-mail: kvspilio@central.ntua.gr

that the traditionally used simplex method is computationally superior at least for medium type problems as the ones addressed here.

With the solution performed by the simplex method it is known [15] that the force method based upper bound program (mesh unsafe) requires much smaller computation than any of the other three. Nevertheless, it is mainly the nodal unsafe program [12] that has been used more extensively since it has a better potential for automation.

Looking more closely at the nature of the force method, the stress resultant distribution in a frame due to a given loading may be split into two terms: the first one is a complementary solution formed by a maximal set of independent self-equilibrating stress system of hyperstatic forces known as a statical basis and the second term is a particular solution which satisfies equilibrium with the given loading.

The difficulty in the automation of the force method is mainly the pre-selection of the hyperstatic forces. One approach to circumvent this problem is to use an initial "hybrid" part based on algebraic procedures [8]. In this first stage, the data is set up as in a displacement method-based analysis and a Gauss type decomposition is then performed on the equilibrium matrix. From this decomposition both the above terms of the force method may be extracted. The accuracy of the approach depends largely on the degree of pivoting [2] and it tends to produce relatively dense matrices [8].

A better way followed in the present work, is to construct the two terms of the force method in a direct way. This may be accomplished using some knowledge from graph theory, since a frame may be graphically represented as a directed graph. One such important piece of knowledge is the procedure to find the minimum path between two points of a graph [14]. This is the main ingredient of an algorithm used to establish a cycle basis. If we satisfy equilibrium along each cycle, a statical basis may then be easily constructed. The shortest path technique is also used to establish equilibrium with the applied loads. The whole procedure has been used to the plastic limit [16] and the shakedown [17] design of plane frames.

Presently the above-mentioned approach is firstly applied to the plastic limit analysis of plane frames. Subsequently it is applied to the shakedown analysis of plane frames. The fact that few elements need to enter the various matrices is discussed. It is also demonstrated that the resulting flexibility matrix used to find the elastic solution has a high degree of sparseness and is constructed in skyline form. The procedure is also, in this work, extended to the limit analysis of space frames. Examples of application are also presented.

2 Construction of a Cycle Basis

A systematic way to find a self – equilibrating stress system of hyperstatic forces, called a statical basis, is based on the topological representation of a frame. According to this representation, the members (total number M) and

the nodes (total number N) of the frame coincide with the members and the nodes of a planar graph. Every planar graph has $\delta = M - N + 1$ exactly independent cycles, which constitute a cycle basis. A basis that consists of cycles of the least number of members is called minimal. The graph representation of a typical frame together with a minimal cycle basis can be seen in Fig. 1, where the ground is represented by an extra node and extra elements are used to connect this node to each foundation node. Since for any plane frame without releases each of these cycles is three times statically indeterminate, once a cycle basis is found, a statical basis can be found straight away.

The difficult task is, therefore, to construct a cycle basis in an automatic way. An algorithm has been produced in [16] which is relatively simple and amenable to easy computer implementation. The algorithm uses a shortest path technique to find the quickest way between the ends of members of the graph [14]. The difficult task of selecting independent cycles is resolved not by book-keeping methods (e.g. [9]), but merely by increasing the lengths (not in the Euclidean sense) of the members of a cycle which has already entered the cycle basis as an independent cycle.

Making a brief description of the algorithm, the algorithm starts by giving to all the members of the graph a length equal to *1*. The procedure then begins from the node that has the maximum valency (number of members incident to it), picks up one by one each of these members (called generator member) and finds the minimum path between its two ends not by going along, but around it. If the following admissibility rule is satisfied:

"The length of the found path is less than *2* (nodes along the path –1)*"
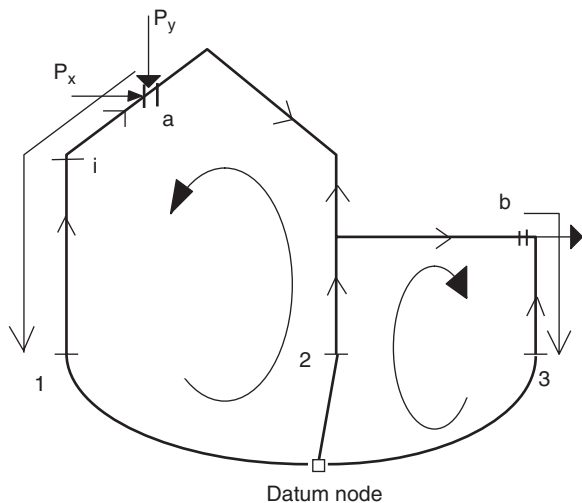
Fig. 1 Typical frame graph representation, cycle basis, shortest paths of load to the ground

then the members of this path together with the generator member form
a cycle that enters the cycle basis and the lengths of all these members are
equal to 2.

The node with the next higher valency is considered next and so on.

The effectiveness of this procedure can be better explained in Fig. 2, where
one can see a sub-graph that has been extracted from a main graph. Initially
the members have a length equal to 1 (Fig. 2(a)). Starting from node k
and selecting km as generator member, the minimum path whose length is
equal to 2 satisfies the admissibility rule and the cycle $klmk$ enters the basis.
Automatically the lengths of the members of the cycle become equal to 2
(Fig. 2(b)). This cycle can not be reselected because it will not pass the
admissibility rule. In the sequel, by picking up, for example, member kq, the
next obvious cycle enters the cycle basis (Fig. 2(c)).

A different cycle basis might form if some other member is picked up
first as a generator member (Fig. 2(d)) leading once again to a cycle basis
consisting of two cycles (Fig. 2(d)). The only difference is that this basis will
not be minimal.

A situation may arise (Fig. 3(a)), not likely to occur in common engi-
neering problems, where the cycles shown have been selected and there is no
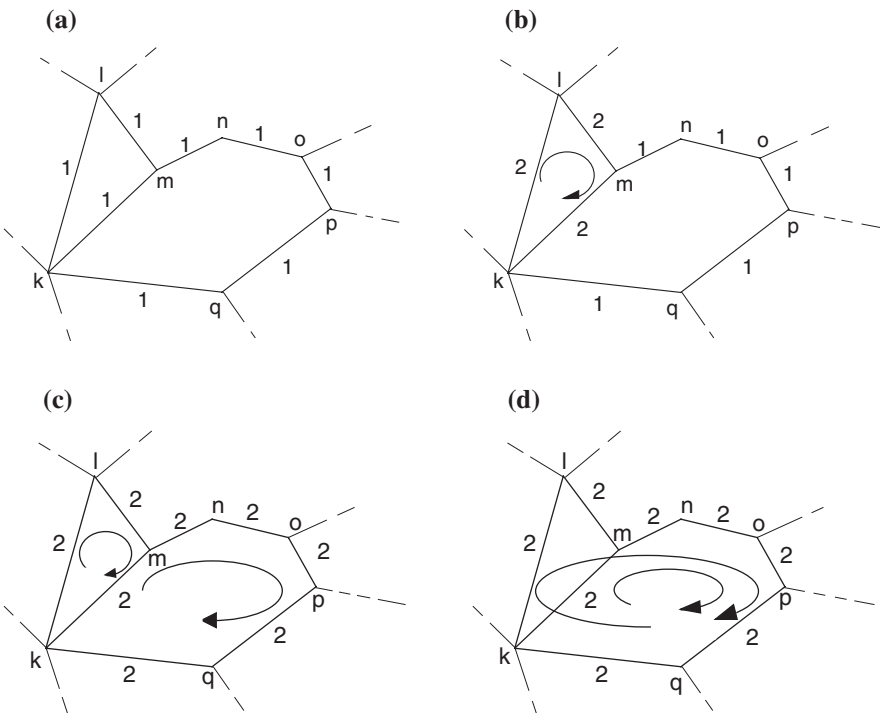
Fig. 2 (**a**)–(**c**) cycle basis formation, (**d**) different cycle basis
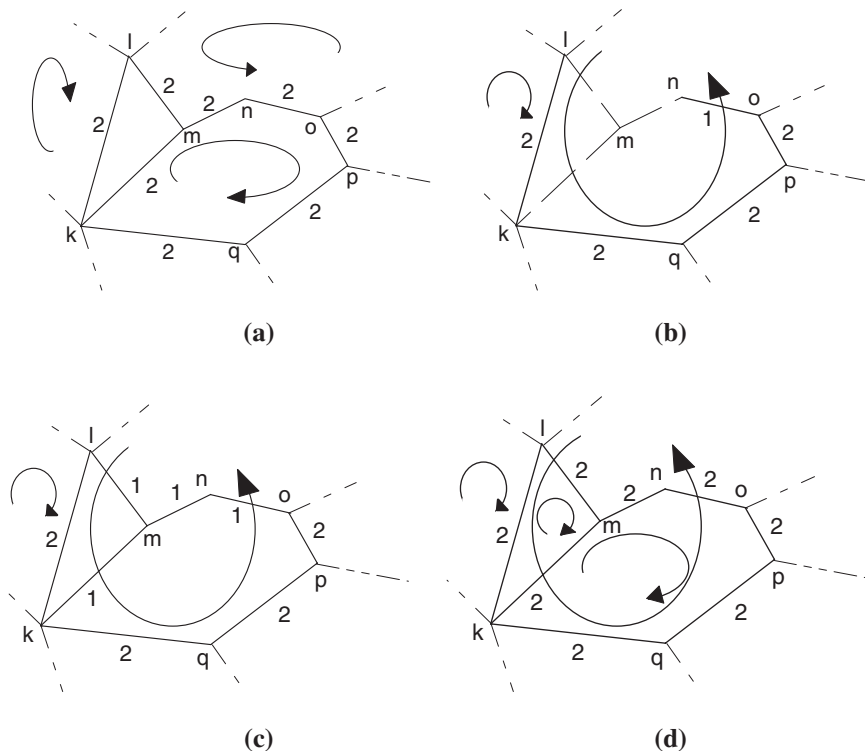
Fig. 3 Extraction of a cycle embedded in others

way for the cycle *lmkl* to enter the cycle basis. This incomplete cycle basis is easily detected since less than δ meshes will have been selected. The expansion process may then restart by excluding, for example node m and its members. We then generate, in the normal way, a cycle basis for the rest of the graph (Fig. 3(b)). Then the excluded node with its members is added back (Fig. 3(c)) and the process continues, generating a complete cycle basis (Fig. 3(d)). Full exposition and details of the algorithm may be found in the original reference [16].

3 Limit Analysis of Plane Frames

The formulation of the plastic limit analysis as a linear programming problem using the force method is briefly presented here. More details can be found elsewhere, for example [15].

Assume that a frame is subjected to point loads, varying proportionally to a load factor λ. Considering only bending deformations and denoting vectors

and matrices by bold letters we may write:

$$\boldsymbol{m} = \mathbf{B}\boldsymbol{p} + \mathbf{B}_0\lambda \quad \text{(equilibrium condition)}, \tag{1}$$

where $\boldsymbol{m}$ is the vector of bending moments at the critical sections, $\boldsymbol{p}$ is a set of independent hyperstatic forces equal to the degree of the static indeterminacy of the frame, called statical basis.

Assuming rigid plastic behaviour, the moment at every critical section i should be within the plastic limits:

$$-\mathrm{m}_{*i}^- \le \mathrm{m}_i \le \mathrm{m}_{*i}^+ \quad \text{(plastic admissibility condition)}, \tag{2}$$

where m_{*i}^- and m_{*i}^+ are the negative and positive plastic resisting moments of the cross section i.

If the above condition is put in matrix form we may get the conditions of plastic admissibility for all the critical sections of the frame:

$$\begin{bmatrix} \mathbf{B}_0 & \mathbf{B} \\ -\mathbf{B}_0 & -\mathbf{B} \end{bmatrix} \begin{Bmatrix} \lambda \\ \boldsymbol{p} \end{Bmatrix} \le \begin{Bmatrix} \mathbf{m}_*^+ \\ \mathbf{m}_*^- \end{Bmatrix}. \tag{2a}$$

At the same time if we denote by $\boldsymbol{\Theta}$ the vector of the rotations at the critical sections we may write the form of mechanism compatibility as:

$$\mathbf{B}^T\boldsymbol{\Theta} = \mathbf{0}. \tag{3}$$

Scaling of the rotations, so that they are non-zero and finite may be performed through $\mathbf{B_0}$:

$$\mathbf{B}_0^T\boldsymbol{\Theta} = 1. \tag{4}$$

To use a standard linear programming algorithm with non-negative variables, the rotation θ_i may be written as $\theta_i = \theta_i^+ - \theta_i^-$ with θ_i^+ and θ_i^- being non-negative component numbers.

Using this and grouping equations (3) and (4), the result is:

$$\begin{bmatrix} \mathbf{B}_0^T & -\mathbf{B}_0^T \\ \mathbf{B}^T & -\mathbf{B}^T \end{bmatrix} \begin{Bmatrix} \boldsymbol{\Theta}^+ \\ \boldsymbol{\Theta}^- \end{Bmatrix} = \begin{Bmatrix} 1 \\ \mathbf{0} \end{Bmatrix} \tag{5}$$

or

$$\mathbf{A}\boldsymbol{\Theta} = \boldsymbol{b} \quad \text{(kinematic admissibility)}. \tag{5a}$$

Three different possibilities may exist for a critical cross section:

1. A positive plastic hinge forms:

$$\theta_i^+ > 0, \quad \theta_i = \theta_i^+, \quad m_i = m_{*i}^+.$$

2. A negative plastic hinge forms:

$$\theta_i^- > 0, \quad \theta_i = \theta_i^-, \quad m_i = m_{*i}^-.$$

3. The cross section remains elastic or does not participate in the mechanism

$$\theta_i^+ = \theta_i^- = 0, \quad \theta_i = 0, \quad -m_{*i}^+ \leq m_i \leq m_{*i}^-.$$

All these conditions may be expressed through the complementarity condition

$$\boldsymbol{\Theta}^T \boldsymbol{\Psi} = 0 \quad \text{(complementarity)}, \tag{6}$$

where $\boldsymbol{\psi}$ are the plastic potentials indicating the remaining amount of the bending moment at the cross section from its full plastification in either sense (Fig. 4).

Complementarity when combined with the equilibrium, plastic admissibility and kinematic conditions lead to the following force-based program of plastic limit analysis:

$$\text{Minimize } \lambda = \boldsymbol{c}^T \boldsymbol{\Theta}$$
$$\text{subject to:}$$
$$\boldsymbol{A}\boldsymbol{\Theta} = \boldsymbol{b}$$
$$\boldsymbol{\Theta} \geq \boldsymbol{0}, \tag{7}$$

where $\boldsymbol{c}^T = \{\boldsymbol{m}_*^+ \ \boldsymbol{m}_*^-\}$ are the vectors of the plastic capacities of the cross section in tension or compression.

The minimum value of λ gives the collapse load factor λ_c.

This is the mesh unsafe linear program which is always in standard form for its solution by the simplex method. The computational effort in this method increases much more rapidly with the number of constraints than the number of variables. In the mesh unsafe program the number of constraints (the number of rows of the $\boldsymbol{A}$ matrix) is equal to the degree of indeterminacy of the frame +1. This is the case of the fewer constraints one can have among all four linear programs (based on either the force or the displacement methods) that can be formulated for the plastic limit analysis of frames. Thus the mesh unsafe program requires the least computation time and for this reason we

Fig. 4 Definition of the plastic potential

choose this program to solve all the cases of limit analysis presented in the present work.

The construction of a cycle basis can lead straight away to the construction of a statical basis. Since each cycle is three times statically indeterminate for any plane frame, a cut made at any point s of the cycle induces two independent forces p_s and f_s along coordinate axes x and y respectively, as well as a bending moment m_s (Fig. 5(a)). The bending moment m_i at any cross section i along the cycle with coordinates x_i and y_i is given by the relationship:

$$m_i = (\pm)[(y_s - y_i) \quad (x_i - x_s) - 1] \begin{bmatrix} p_s \\ f_s \\ m_s \end{bmatrix}, \tag{8}$$

where x_s and y_s are the coordinates of s and the positive or negative sign in the parenthesis depends on whether or not the orientation of the cycle coincides with the orientation of the member. For the shown cycle and member orientations, for example, a positive sign will hold. The convention of a positive bending moment along a member according to its orientation is shown in Fig. 5(b).

Using the above equation and filling in the appropriate places, the matrix **B**, which gives the relationship between the bending moments of the frame and its statical basis, can be constructed.

The described algorithm of the cycle basis generation produces almost minimal or nearly minimal cycle bases. This means that there will be always a small amount of non-zero entries in the matrix **B** which, in this way, appears to be quite sparse, something which is not true when using an algebraic method [8].

As far as equilibrium with external point loading is concerned, this may be established along cantilevers, as shown in Fig. 1. Each cantilever is found as the shortest path between the point of application and the foundation
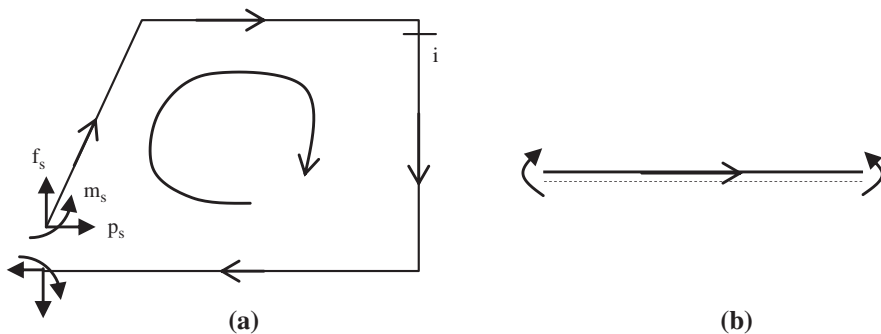

(a) **(b)**

Fig. 5 (**a**) hyperstatic force system of a mesh, (**b**) positive bending moment convention

nodes. The bending moment at any cross section i along any of these paths is given by:

$$m_i = (\pm)[(x_a - x_i) \quad (y_a - y_i)] \begin{Bmatrix} P_x \\ P_y \end{Bmatrix}, \tag{9}$$

where x_a and y_a are the coordinates of the point a. The above equation represents entries for the matrix $\mathbf{B}_0$. The term in the square bracket is multiplied by a positive or negative sign in the parenthesis according to whether the orientation of the member, that the critical cross section i belongs to, and the orientation of the cantilever coincide or not.

3.1 Example of Application

An example of application, discussed in [5] may be seen in Fig. 6(a).

The columns are of uniform cross section throughout the four storeys, and have plastic moment capacities of 355 kNm. The two upper beams have full plastic resisting moments of 531 kNm, whereas the two lower beams of 355 kNm.

In Fig. 6(b) one may see the graphical representation of the frame, as well as the numbering of its critical cross sections. The algorithm picks up the optimum cycle basis consisting of the minimum amount of members forming each cycle.

The collapse load factor is found to be $\lambda_c = 2.233$. The collapse mechanism, which coincides with the one found in [5], may be seen in Fig. 6(b).
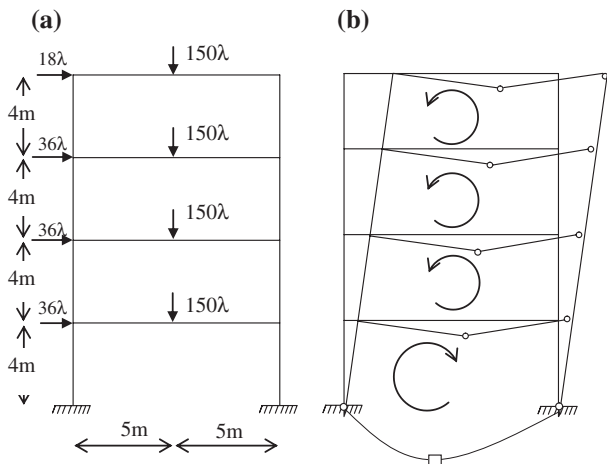

Fig. 6 (a) Frame geometry and loading, (b) Cycle basis and collapse mechanism

4 Shakedown Analysis of Plane Frames

The problem of the shakedown analysis will be briefly presented here.

Among the main assumptions are that the cross sections considered are those with a shape factor equal to unity, thus making the incremental collapse the prevailing mode of failure.

The frame, as in the limit analysis case, is subjected to point loads which are now alternating in nature. A loading mode consists of point loads that act together and vary through common load intensity μ_j. The limits of variation of the load intensities of each loading mode are known, i.e.:

$$\mu_j^- \leq \mu_j(\mathrm{t}) \leq \mu_j^+, \ j = 1, 2, \ldots, k, \tag{10}$$

where we have supposed that we have k loading modes.

A rectangular polytopic load factor domain may be constructed by the $2k$ parameters μ_j^-, μ_j^+. If a common parameter λ relates all these factors, this domain is called a single-parameter load factor domain.

The problem of shakedown analysis is to find the maximum value of λ so that, for any loading program, although some initial plastic straining may occur, we have eventually only elastic strains.

Melan's theorem states that the necessary and sufficient condition for a structure to shakedown in a prescribed loading domain is the existence of a time independent set of residual moments $\boldsymbol{m}_r$, such that when added to the moments that can be calculated assuming completely elastic behaviour, these total moments would be plastically admissible. As this condition must be satisfied for any load combination, the whole elastic moment range should be considered. Therefore the elastic moment envelope should be constructed.

The elastic moment envelope, which consists of the maximum and the minimum values of the elastic moments at every critical cross section i, can be found by the following equations [10]:

$$
\begin{aligned}
\max m_i^e &= \sum_{j=1}^k \alpha_{ji}^+ m_i^{ej}, \\
\max m_i^e &= \sum_{j=1}^k \alpha_{ji}^- m_i^{ej},
\end{aligned}
\tag{11}
$$

where:

$$\alpha_{ji}^+ = \left\{ \begin{array}{l} \mu_j^+ \text{ if } m_i^{ej} > 0 \\ \mu_j^- \text{ if } m_i^{ej} < 0 \end{array} \right\} \quad \text{and} \quad \alpha_{ji}^- = \left\{ \begin{array}{l} \mu_j^- \text{ if } m_i^{ej} > 0 \\ \mu_j^+ \text{ if } m_i^{ej} < 0 \end{array} \right\}.$$

The condition of plastic admissibility requires that the bending moment at every cross section, for the worst combination of the loading program, has

to be within the lower and upper limits of its plastic moments. This condition
is represented by the following two matrix inequalities:

$$
\begin{aligned}
- \boldsymbol{m}_*^- &\leq \mathbf{B}\boldsymbol{p}_r + \lambda \cdot \min \boldsymbol{m}_e, \\
\mathbf{B}\boldsymbol{p}_r + \lambda \cdot \max \boldsymbol{m}_e &\leq \boldsymbol{m}_*^+,
\end{aligned}
\tag{12}
$$

where the elements of $min\,\boldsymbol{m}_e$ and $max\,\boldsymbol{m}_e$ are found from (11). The term Bp_r
is the distribution of the residual bending moments $\boldsymbol{m}_r$, which was discussed
above and which can be expressed through some hyperstatic residual statical
basis $\boldsymbol{p}_r$.

This basis is in equilibrium with zero loads and its very existence safe-
guards against the possibility of an incremental collapse mechanism.

Looking at the similarities of (12) with Eq. (2a) one may write straight
away the plastic mesh unsafe program of the plastic shakedown analysis [10].

$$
\text{Minimize } \boldsymbol{\lambda} = \begin{bmatrix} \boldsymbol{m}_*^+ & \boldsymbol{m}_*^- \end{bmatrix} \begin{bmatrix} \Delta\vartheta^+ \\ \Delta\vartheta^- \end{bmatrix}
$$

subject to:

$$
\begin{bmatrix} \max \boldsymbol{m}_e^T & -\min \boldsymbol{m}_e^T \\ \mathbf{B}^T & -\mathbf{B}^T \end{bmatrix} \left\{ \begin{array}{c} \Delta\vartheta^+ \\ \Delta\vartheta^- \end{array} \right\} = \left\{ \begin{array}{c} 1 \\ 0 \end{array} \right\}
$$

$$
\Delta\vartheta^+, \Delta\vartheta^- \geq \mathbf{0}.
$$

(13)

Comparing with limit analysis here we have the increments of the rotations
that could occur in an incremental collapse mechanism.

Once this program is solved the simplex multipliers of the optimal solution
provide a distribution of residual moments.

4.1 Elastic Solution

The elastic moments may be found using once again the force method, uti-
lizing the knowledge acquired from the previous sections.

A member may belong to one or more cycles. Using Eq. (1), we thus may
write for the elastic bending moments at the two ends of an element f that
belongs to t_f meshes of the cycle basis and for the particular loading mode
j that consists of Q_j concentrated loads Pq:

$$
\boldsymbol{m}_f^{ej} = \begin{bmatrix} m_1^{ej} \\ m_2^{ej} \end{bmatrix} = \sum_d^{t_f} \mathbf{B}_f^d \boldsymbol{p}_d + \sum_{q=1}^{Q_j} \mathbf{B}_{(o)f}^q P_q,
\tag{14}
$$

where B_f^d is the 2×3 submatrix extracted from the **B** matrix for the cor-
responding member f and the mesh d that this element belongs to, with d
being an identification number and not a counter.

On the other hand, the matrix of the corresponding elastic rotations of the member's chord will be given by:

$$\boldsymbol{\Theta}_f^{ej} = \mathbf{F}_f \boldsymbol{m}_f^{ej}, \tag{15}$$

where $\mathbf{F}_f = \dfrac{\ell}{6EI} \begin{bmatrix} 2 & 1 \\ 1 & 2 \end{bmatrix}$ is the standard flexibility matrix, with E, I, ℓ the Young's modulus, moment of inertia and length of the member f.

The dual entities of the hyperstatic forces $\boldsymbol{p}_c$ of the topological mesh c are the discontinuities $\boldsymbol{\nu}_c$ which have to be equal to zero so that continuity is restored. Using the static-kinematic duality principle [11] and supposing that the cycle consists of n_c members we may write:

$$\boldsymbol{0} = \boldsymbol{\nu}_c^j = \sum_{f=1}^{n_c} (\mathbf{B}_f^c)^T \boldsymbol{\Theta}_f^{ej}. \tag{16}$$

Making substitutions in (16), using Eqs. (14) and (15), we may arrive at:

$$\left\{ \sum_{f=1}^{n_c} (\mathbf{B}_f^c)^T \mathbf{F}_f \mathbf{B}_f^c \right\} \boldsymbol{p}_c + \sum_{\substack{d=1 \\ d \neq c}}^{\delta} \left\{ \sum_{f=1}^{n_{c,d}} (\mathbf{B}_f^c)^T \mathbf{F}_f \mathbf{B}_f^d \right\} \boldsymbol{p}_d$$

$$= -\sum_{q=1}^{Q_j} \left\{ \sum_{f=1}^{n_c} (\mathbf{B}_f^c)^T \mathbf{F}_f \mathbf{B}_{(o)f}^q \right\} P_q, \tag{17}$$

with $n_{c,d}$ being the number of common members to both the topological meshes c and d, with δ being the total number of cycles in the cycle basis [17].

Looking at Eq. (17) one may realize that the left-hand side is merely the flexibility matrix $\boldsymbol{E}$ for the selected cycle basis. It may be evaluated, mesh by mesh, by implanting only 3×3 sub-matrices. The first term results to entries along the main diagonal. The second term of the left-hand side will exist if there are common members between the c and d meshes. Should such coupling exist, it represents the off-diagonal terms of the structure's flexibility matrix which is formed when we make the expansion of the above equation.

The flexibility matrix is stored as one-dimensional array in skyline form. The value of the skyline for a mesh numbered as c that has common members with other topological meshes numbered as $d_1, d_2, \ldots, d_n$, may be determined as the maximum difference $3^* \max\limits_{i=1,2,..n} |c - d_i|$. If d_m is the mesh that provides this difference, the inter-coupling of the two cycles in the flexibility matrix would look like:

$$
\mathbf{E} = \begin{bmatrix}
\cdots & \cdots & & \cdots & & \cdots \\
\cdots & \displaystyle\sum_{f=1}^{n_c} (\mathbf{B}_f^c)^{\mathrm{T}} \mathbf{F}_f \mathbf{B}_f^c & \cdots & \displaystyle\sum_{f=1}^{n_{c,d_m}} (\mathbf{B}_f^c)^{\mathrm{T}} \mathbf{F}_f \mathbf{B}_f^{d_m} & \cdots & \\
\cdots & \cdots & \cdots & \cdots & \cdots & \\
\cdots & \displaystyle\sum_{f=1}^{n_{c,d_m}} (\mathbf{B}_f^{d_m})^{\mathrm{T}} \mathbf{F}_f \mathbf{B}_f^c & \cdots & \displaystyle\sum_{f=1}^{n_{d_m}} (\mathbf{B}_f^{d_m})^{\mathrm{T}} \mathbf{F}_f \mathbf{B}_f^{d_m} & \cdots & \\
\cdots & \cdots & \cdots & \cdots & &
\end{bmatrix}
\quad \text{Skyline height}
$$

Since the flexibility is stored in a skyline form, just like the way that the stiffness matrix is stored in a displacement method of analysis, the same decomposition and back-substitution algorithms [1] may be used. Moreover the cycle selection algorithm provides a near minimal cycle basis, and it is most unlikely that for frames of common engineering interest, a renumbering scheme would ever be needed.

4.2 Examples

Two examples of shakedown analysis will be presented, a continuous beam and a frame.

4.2.1 Two-Span Beam

The beam of Fig. 7(a) that has been analyzed in [10] and [7] is studied first. The beam is subjected to two point loads applied at the middles of each span. The load on the left span varies between 0 and P, whereas the load of the right span remains constant.
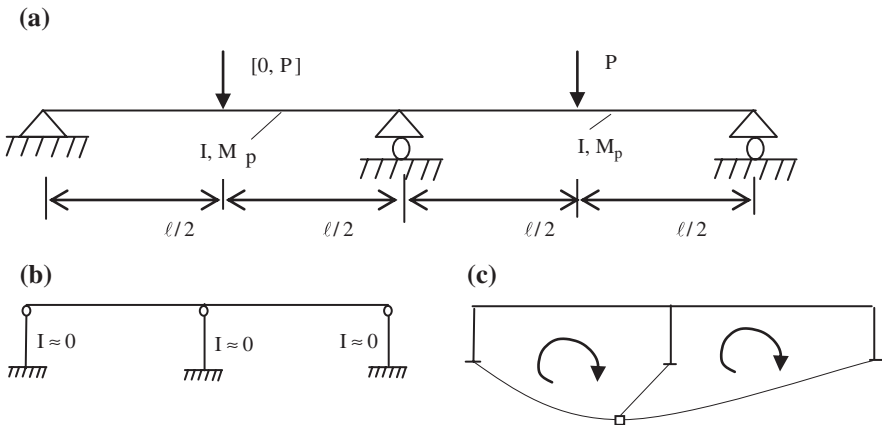
Fig. 7 (**a**) Geometry and loading of beam, (**b**) simulation of supports, (**c**) cycle basis

The hinged and the roller supports are simulated by means of small cantilevers having almost zero bending stiffness and zero plastic capacity at their ends in contact with the beam (Fig. 7(b)). The identified by the procedure cycle basis may be seen in Fig. 7(c).

The shakedown load factor λ against incremental collapse turns out to be $\lambda_{sh} = 5.054$, so that the shakedown load is $P_{sh} = 5.054 M_p/\ell$ which compares well with the value found analytically in [10] to be $5.0526 M_p/\ell$.

4.2.2 Frame Example

The frame of Fig. 8(a) is the second shakedown analysis example to be considered. This frame has been studied in [13]. Each load shown constitutes one loading mode and varies as shown in the same figure.
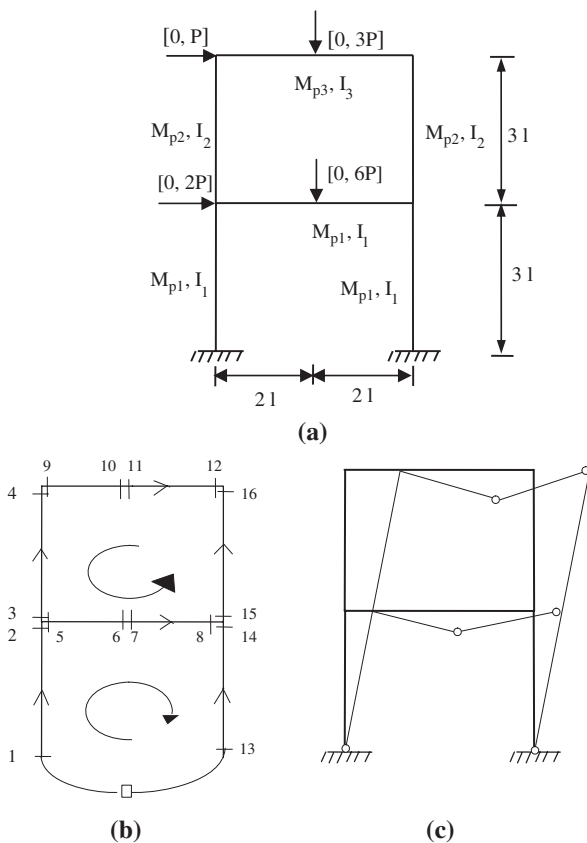
Fig. 8 (**a**) geometry and loading, (**b**) cycle basis, member orientation, numbering of critical sections, (**c**) incremental collapse mechanism

The following geometric relationships were considered among the various members: $M_{p1} = 2M_p$, $M_{p2} = M_{p3} = M_p$, $I_1 = 2.5I$, $I_2 = I_3 = I$.

In Fig. 8(b) one may see the minimal mesh basis that is identified by the numerical procedure. In the same figure one may see the orientation of the members as well as the numbering of the cross sections.

The shakedown factor turns out to be $\lambda_{sh} = 0.508$, so that the shakedown load is $P_{sh} = 0.508M_p/l$, a result that coincides with the one reported in [13].

In Table 1 one may see the elastic moment envelope at the various critical sections as well as a distribution of the residual moments generated.

Table 1 Moment distribution for the Example 4.2.2

Crit. sect.	max $m^{\mathrm{el}}/P\ell$	min $m^{\mathrm{el}}/P\ell$	$m_{\mathrm{r}}/P\ell$
1	0.881	−2.948	−50.114
2	2.032	−1.762	−7.540
3	1.102	−0.794	12.809
4	0.790	−1.170	4.519
5	2.422	−2.459	−20.350
6	3.661	−0.120	13.897
7	3.661	−0.120	13.897
8	0.000	−4.481	48.143
9	0.790	−1.170	4.519
10	1.927	−0.096	2.062
11	1.927	−0.096	2.062
12	0.000	−1.959	−0.396
13	0.160	−3.669	−13.464
14	3.474	−0.320	−56.038
15	0.084	−1.812	−7.895
16	1.959	0.000	0.396

5 Limit Analysis of Space Frames

In the case of space frames the equation of equilibrium may be written as:

$$\boldsymbol{Q}_N = \mathbf{G}\boldsymbol{p} + \boldsymbol{g_0}\lambda, \tag{18}$$

where $\boldsymbol{Q}_N$ are the independent forces of the structure. For each element k these forces are given by the vector $\boldsymbol{Q}_N^{(k)} = \{F, M_{iz'}, M_{iy'}, M_T, M_{jz'}, M_{jy'}\}^{(k)}$ and correspond, in the member's local axes, with the axial force, the bending moments at the two ends i, j of the member, as well as torsion. The independent forces may then be used to group the three forces and the three moments along the local system of axes at the two ends of each element for the whole structure using the following transformation:

$$\boldsymbol{Q} = \mathbf{T}^T \cdot \boldsymbol{Q}_N. \tag{19}$$

By combining Eqs. (18) and (19), the equation of equilibrium may be expressed in the local axes at the critical sections located at the ends of the members:

$$\boldsymbol{Q} = \mathbf{T}^T \cdot \boldsymbol{Q}_N = \mathbf{T}^T \cdot (\mathbf{G}\boldsymbol{p} + \boldsymbol{g}_0 \lambda) = \mathbf{H}\boldsymbol{p} + \boldsymbol{h}_0 \lambda. \tag{20}$$

As in Eq. (1) the first term of (18) is due to the indeterminacy of the frame, whereas the second term expresses equilibrium with applied loads with λ being once again the proportional load factor.

The graph representation of the three-dimensional framed structure with the ground node and the extra members (Fig. 9) is an admissible embedding into a two–dimensional polyhedron [3] (Fig. 10).
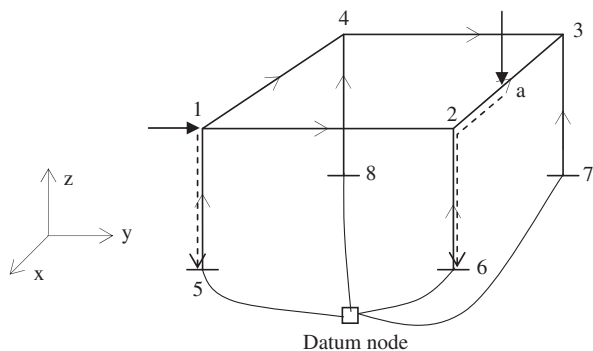

Fig. 9 Typical space frame, graph representation in 3D, global coordinate system
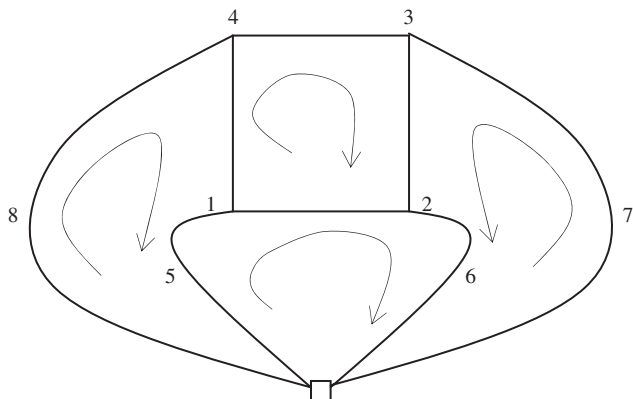

Fig. 10 Equivalent 2D representation, cycle basis
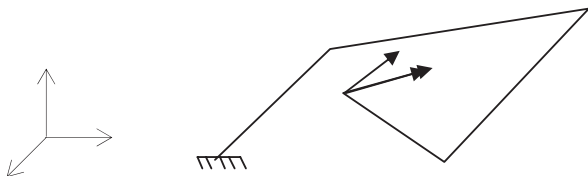
Fig. 11 Hyperstatic system of forces of a 3D mesh

Thus the algorithm that was used to find the cycle basis for two-dimensional frames may be also used for the three-dimensional case.

If we make a cut at any such cycle a pair of a force and a moment, of arbitrary direction, that appear at the cut are now the hyperstatic forces (Fig. 11).

These two vectors, if analyzed along the global axes are equivalent to three forces and three moments so that six are the hyperstatic entities for each mesh. These, following the perimeter of this cycle, create, at the ends of each member of the cycle, forces and moments in the global axes. When these, in turn, are analyzed in the local axes of each member, according to Fig. 12, we can get the elements of **G**.

The analysis may be done with the aid of Euler's angles ϑ_1 and ϑ_2 using Eq. (21). These angles may be calculated from the difference of the coordinates of the ends of the member ij which are Δx, Δy, Δz.

$$\begin{bmatrix} Q_{x'} \\ Q_{y'} \\ Q_{z'} \end{bmatrix} = \begin{bmatrix} \cos\vartheta_2\cos\vartheta_1 & \cos\vartheta_2\sin\vartheta_1 & \sin\vartheta_2 \\ -\sin\vartheta_1 & \cos\vartheta_1 & 0 \\ -\sin\vartheta_2\cos\vartheta_1 & -\sin\vartheta_2\sin\vartheta_1 & \cos\vartheta_2 \end{bmatrix} \begin{bmatrix} Q_x \\ Q_y \\ Q_z \end{bmatrix}. \qquad (21)$$

For the equilibrium with the external load that provides us with the matrix g_0, the shortest path technique is used to find the quickest way of each load to the ground, once again in the form of cantilevers, two of which may be seen in Fig. 9 (dotted lines). Equilibrium is then satisfied along this path by analyzing the resulting forces and moments at the ends of each member first in the global axes and then transforming them to the local axes.
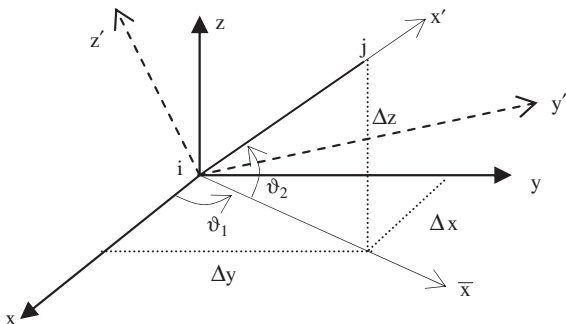
Fig. 12 Orientation of a member's local axes

Fig. 13 Yield surface,
yield planes, normal vector,
plastic capacity and
potential
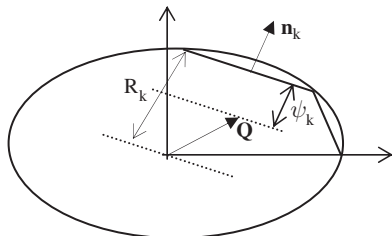
Plasticity, once again is considered concentrated at the member's end nodes. A "generalized plastic hinge" will occur whenever the combination of the above described vector touches a plastic interaction surface, which is generally non–linear. This surface may then be linearized, using planes to approximate it, with the orthogonals to these planes denoting the direction of the plastic strains (Fig. 13). The length of this vector on any such plane k is denoted by q_k.

The plastic admissibility condition requires that the combined stress is less than the plastic capacity R_k. This may be expressed through the following relation:

$$\boldsymbol{n}_{\mathrm{k}}^{\mathrm{T}} \cdot \boldsymbol{Q} + \psi_{\mathrm{k}} = \boldsymbol{R}_{\mathrm{k}}, \quad \psi_{\mathrm{k}} \geq 0, \tag{22}$$

where once again ψ_k is the plastic potential at a cross section for a specific plane k, which has to fulfill the complementarity condition with the corresponding plastic strains. $\boldsymbol{n}_k$ is the outward unit vector normal to plane k.

Once again employing (20), (22), the complementarity condition and the kinematic admissibility condition that restores the continuity at the cuts of the cycles in a completely analogous fashion as in the plane frames, that is not repeated here for brevity, the mesh unsafe program of the plastic limit analysis for space frames may be written in the following form:

$$\begin{aligned}
&\text{Minimize } \lambda = \boldsymbol{R}^T \boldsymbol{q} \\
&\text{Subject to:} \\
&\begin{bmatrix} \mathbf{h}_0^T \cdot \mathbf{N} \\ \mathbf{H}^T \cdot \mathbf{N} \end{bmatrix} q = \begin{bmatrix} 1 \\ \mathbf{0} \end{bmatrix}.
\end{aligned} \tag{23}$$
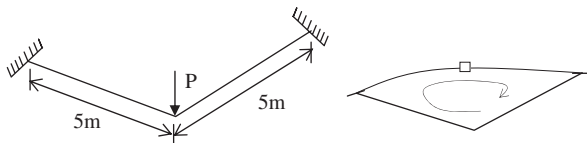
Fig. 14 Real structure and its graph representation

where the constraints of the above program are the kinematic admissibility conditions together with the normalization of the strains, so that they are finite. The matrix N groups the direction cosines of the unit normal to the planes the yield surface has been divided into, for all the critical sections; R and q are the vectors of the corresponding plastic resistances and plastic strain lengths.

5.1 Grillage Example

This example (Fig. 14) which is a grillage type frame has been considered in [6]. The two members have equal length $\ell = 5m$. The whole frame lies in a horizontal plane and at its right-angle bent carries a vertical load P.

The loading will induce a bending moment M and a moment of twist M_T which both lie on the horizontal plane.

If the value of the full plastic bending moment in the absence of twisting moment is M_p, and of the full plastic twisting moment in the absence of bending is M_{T_p}, for many practical reasons a common yield surface may be the simple doubly symmetric one given by the following equation:

$$(M/M_p)^2 + \left(M_T/M_{T_p}\right)^2 = 1. \tag{24}$$

This surface is approximated by eight planes preserving the double symmetry. Assuming $M_p = M_{T_p}$, the limit load factor turns out to be $0.5657M_p$ that coincides with the one evaluated analytically in [6], as $2/\ell(\sqrt{2})M_p$.

A different situation arises when the load is placed in the middle of one of the members (Fig. 15).

In this non-symmetric case the same over-complete mechanism of [6] is predicted, with the limit load factor found $0.9478M_p$, which is near the analytic solution of $1.012M_p$ (once again under the assumption that $M_p = M_{T_p}$).

Other more complicated examples of space framed structures are currently tested with various and different yield surfaces. At the time of writing the present paper, these results are not available but will be reported in the near future.

Fig. 15 (a) Non-symmetric case, (b) collapse mechanism

6 Concluding Remarks

In this work, a robust procedure for the limit or shakedown analysis of framed structures, using the force method, is presented. It is based on employing the shortest path technique from graph theory to pre-select the hyperstatic forces and to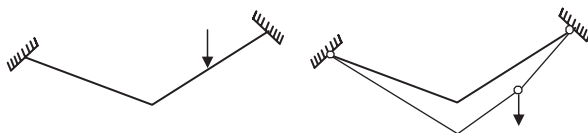 satisfy equilibrium with the external load. It is shown that although originally applied to plane frames, it may also be applied with little modifications to space frames. The simplicity of the presented approach makes it amenable to easy computer implementation. Due to the high degree of sparseness of the matrices involved, the procedure is also computationally efficient.

References

1. Bathe K-J (1996) Finite element procedures. Prentice-Hall, New Jersey
2. Damkilde L and Høyer O (1993) An efficient implementation of limit state calculations based on lower-bound solutions. Comput Struct 49: 953–962
3. de Henderson JC, Bickley WG (1955) Statical indeterminacy of a structure. Aircr Eng 27: 400–402
4. Gilbert M and Tyas A (2003) Layout optimization of large-scale pin-jointed frames. Eng Comput 20: 1044–1064
5. Heyman J (1971) Plastic design of frames – applications, II. Cambridge University Press, Cambridge
6. Heyman J (1996) Elements of the theory of structures. Cambridge University Press, Cambridge
7. Horne MR (1971) Plastic theory of structures. W. Clowes & Sons Ltd., London
8. Kaneko I, Lawo M and Thiearauf G (1982) On computational procedures for the force method. Int J Numer Methods Eng 18:1469–1495
9. Kaveh A (1992) Structural Mechanics: graph and matrix methods. Wiley, New York
10. König JA (1987) Shakedown of elastic – plastic structures. Elsevier, New York
11. Munro J (1979) The stress analysis and topology of skeletal structures. Report CSTR 14, Imperial College, London
12. Nguyen DH (1984) CEPAO – An automatic program for rigid – plastic and elastic – plastic analysis and optimization of frame structures. Eng Struct 6: 33–51
13. Nguyen DH and Morelle P (1990) Optimal plastic design and the development of practical software. In Smith DL (ed.) CISM Courses No.299 on Mathematic programming methods in structural plasticity, Springer-Verlag, Wien-New York
14. Nicholson TAJ (1966) Finding the shortest route between two points in a network. Comput J 26: 275–280
15. Smith DL (1990) Plastic limit analysis. In Smith DL (ed) CISM Courses No.299 on Mathematic programming methods in structural plasticity, Springer-Verlag, Wien-New York
16. Spiliopoulos KV (1997) On the automation of the force method in the optimal plastic design of frames. Comput Methods Appl Mech Eng 141: 141–156
17. Spiliopoulos KV (1999) A fully automatic force method for the optimal shakedown design of frames. Comput Mech 23: 299–307
18. Vanderbei RJ (1998) Linear Programming: foundations and extensions. Kluwer Academic Publishers, Boston

Shakedown Analysis of Composite Materials Based on Non-linear Mathematical Programming

H.X. Li and H.S. Yu

Abstract Using a *Representative Volume Element* (RVE) to represent the microstructure of periodic composite materials, a non-linear numerical technique is developed to calculate the macroscopic shakedown domains of composites subjected to cyclic loads. With the aid of homogenization theory, the classical kinematic shakedown theorem is generalized to incorporate the microstructure of composites. Using an associated flow rule, the plastic dissipation power for an ellipsoid yield criterion is expressed in terms of the kinematically admissible velocity. By means of non-linear mathematical programming techniques, a finite element formulation of kinematic shakedown analysis is then developed leading to a non-linear mathematical programming problem subject to only a small number of equality constraints. An effective, direct iterative algorithm is proposed to solve the non-linear programming problem. This can serve as a useful numerical tool for developing engineering design methods involving composite materials.

1 Introduction

Shakedown analysis is a direct method of assessing the stability condition and bearing capacity of an elastoplastic structure subjected to repeated or cyclic loads. When the load is larger than the elastic limit but is less than a critical limit, plastic deformation takes place in some part of the structure. However, after a number of cycles, the plastic deformation will cease to develop further

Hua-Xiang Li
Department of Engineering Science, University of Oxford, Oxford OX1 3PJ, UK,
e-mail: huaxiang.li@eng.ox.ac.uk

Hai-Sui Yu
School of Civil Engineering, University of Nottingham, Nottingham NG7 2RD, UK,
e-mail: hai-sui.yu@nottingham.ac.uk

and the structure will respond purely elastically to the remaining load cycles. If this happens, then the structure is said to have shakedown. The critical load limit below which shakedown can occur is known as the 'shakedown limit'. Shakedown analysis is based on two fundamental shakedown theorems, the static or lower bound theorem [21] and the kinematic or upper bound theorem [15]. The early research works were mainly focused on the theoretical analysis for simple structures. Over the last two decades, the numerical methods of shakedown analysis have been developed rapidly [2, 5, 20, 23, 25, 29, 35, 38, 39].

In recent years, the study of composites became more important as the modern industry such as aerospace and automobile is increasingly making use of composite materials. By means of shakedown analysis, the strength properties of composites can be studied. The previous research work on the strength of composites was mainly on the macroscopic descriptions, which required empirical data to capture the basic features of the fatigue failure. Tarn [33] pioneered a theoretical investigation on two-dimensional shakedown analysis of unidirectional metal matrix composites under cyclic loading. The effect of working temperature on the shakedown loads of composites has attracted many researchers [3, 4, 13, 14, 24, 26, 42]. Some valuable experimental and theoretical results were presented. Tirosh [34] obtained lower and upper approximate solutions to two-dimensional shakedown problems of unidirectional fiber-reinforced composites. Based on the static theorem of shakedown analysis, Weichert et al. [36, 37] developed a two-dimensional finite element technique to calculate the shakedown limit of composites under cyclic loading and a lower bound to the shakedown limit can be obtained.

By introducing micromechanics theories into classical continuous mechanics theorems, the mechanical mechanism of composites and the effects of microstructures on the macroscopic properties can be understood more clearly. Suquet [30] introduced homogenization theory of micromechanics into the study of the effects of microstructures on macroscopic behaviors of composites, which provided a powerful tool for both theoretical analysis and engineering design of composites. In recent years, the homogenization technique has been successfully used in the study of composites [6, 22, 31, 32]. Based on the homogenization technique and the kinematic shakedown theorem, Carvelli [1] presented a plane strain finite element model to calculate the shakedown domain of unidirectional composites, where only von Mises' criterion was considered. Using homogenization theory and finite element method, Li et al. [18] developed a non-linear mathematical programming method to perform kinematic limit analysis of composites with von Mises' constituents. The calculation is based purely on kinematic velocity fields. The stress field does not need to be calculated and the limit state of a composite can be obtained.

The purpose of this work is to generalize the recently developed non-linear technique for microscopic limit analysis of Li et al. [18] to microscopic shakedown analysis. Furthermore, a more general yield criterion to model the plastic behaviour of the constituents of composite materials is used. First, us-

ing the homogenization theory, the classical shakedown theorems (which are usually used to calculate the shakedown limit of a macrostructure under repeated or cyclic loading) is extended to explain the shakedown behaviour of a microstructure. Using an associated flow rule, a more general, ellipsoid yield criterion is directly introduced into the kinematic shakedown theorem and a non-linear shakedown formulation is then obtained. The yield surface does not need to be linearized, which significantly reduces the number of constraints and the computational effort. König's technique [16, 17] is used to overcome the difficulty in solving the time integration along a deformation path. Finally, the finite element model of shakedown analysis for a microstructure is formulated as a non-linear mathematical programming problem subject to a small number of equality constraints. An effective, direct iteration algorithm is then proposed to solve the resulting non-linear programming problem.

2 Kinematic Shakedown Analysis of a Macrostructure

In shakedown analysis, it is assumed that the deformation is small at incipient collapse and the material can be modelled with sufficient accuracy using the theory of elastic-perfectly plastic materials. In order to use the finite element method, we adopt column vectors to represent strains and stresses. For example, in a 3D model, $\boldsymbol{\varepsilon} = [\varepsilon_{11}, \varepsilon_{22}, \varepsilon_{33}, 2\varepsilon_{12}, 2\varepsilon_{23}, 2\varepsilon_{31}]^{\mathrm{T}}$ and $\boldsymbol{\sigma} = [\sigma_{11}, \sigma_{22}, \sigma_{33}, \sigma_{12}, \sigma_{23}, \sigma_{31}]^{\mathrm{T}}$.

2.1 An Ellipsoid Yield Criterion

Many widely used yield criteria, especially for metal materials, can be expressed by an ellipsoid equation defined by:

$$\phi(\boldsymbol{\sigma}) = \boldsymbol{\sigma}^{\mathrm{T}} \boldsymbol{P} \boldsymbol{\sigma} - 1 = 0, \tag{1}$$

where $\phi(\boldsymbol{\sigma})$ defines a yield function in terms of strength parameters and $\boldsymbol{P}$ is a coefficient matrix which is related to the strength properties of materials.

Equation (1) is valid for most frequently used yield criteria. For example, Hill's yield criterion [8] is often used for anisotropic materials and expressed as:

$$\begin{aligned}
\phi(\sigma_{ij}) =& F\left(\sigma_{22} - \sigma_{33}\right)^2 + G\left(\sigma_{33} - \sigma_{11}\right)^2 + H\left(\sigma_{11} - \sigma_{22}\right)^2 \\
& + 2L\sigma_{23}^2 + 2M\sigma_{31}^2 + 2N\sigma_{12}^2 = 1,
\end{aligned} \tag{2}$$

where F, G, H, L, M and N are material constants defined by

$$\begin{cases} 2H = \dfrac{1}{X^2} + \dfrac{1}{Y^2} - \dfrac{1}{Z^2}, \ 2G = \dfrac{1}{Z^2} + \dfrac{1}{X^2} - \dfrac{1}{Y^2}, \\[2mm] 2F = \dfrac{1}{Y^2} + \dfrac{1}{Z^2} - \dfrac{1}{X^2}, \\[2mm] 2L = \dfrac{1}{S_1^2}, \ 2M = \dfrac{1}{S_2^2}, \ 2N = \dfrac{1}{S_3^2} \end{cases} \qquad (3\text{a,b,c,d,e,f})$$

where X, Y, Z, resp, denotes the uniaxial strength of the material in the principal anisotropic directions, and S_1, S_2, S_3, resp., denotes the corresponding shear strength. With the following coefficient definition, the ellipsoid Eq. (1) can become Hill's criterion:

$$\boldsymbol{P} = \begin{bmatrix} G+H & -H & -G & 0 & 0 & 0 \\ -H & H+F & -F & 0 & 0 & 0 \\ -G & -F & F+G & 0 & 0 & 0 \\ 0 & 0 & 0 & 2N & 0 & 0 \\ 0 & 0 & 0 & 0 & 2L & 0 \\ 0 & 0 & 0 & 0 & 0 & 2M \end{bmatrix}. \qquad (4)$$

2.2 Kinematic Theorem of Shakedown Analysis

An upper bound to shakedown limit can be obtained by the kinematic shakedown theorem [15]. The kinematic theorem states: 'shakedown can not occur for a structure under cyclic loads when the rate of plastic dissipation power is less than the work rate done by the applied tractions and body forces for at least one admissible cycle of plastic strain'. It can be formulated as follows:

$$\lambda_{sd} \int_0^T \left(\int_{\Gamma_t} t_i \dot{u}_i^* \mathrm{d}\Gamma + \int_V f_i \dot{u}_i^* \mathrm{d}v \right) \mathrm{d}t \le \int_0^T \int_V D\left(\dot{\varepsilon}_{ij}^{p^*}\right) \mathrm{d}v\mathrm{d}t, \qquad (5)$$

where λ_{sd} is the shakedown load multiplier, t_i is the basic surface load, f_i is the basic body force, $\dot{u}_i$ is the displacement velocity, $\dot{\varepsilon}_{ij}^p$ is the plastic strain rate, '$D(\dot{\varepsilon}_{ij}^{p^*})$' denotes a function for rate of plastic dissipation work, the superscript '$*$' stands for a parameter corresponding to kinematically admissible strain, Γ_t is the traction boundary, and V represents the space domain of the structure. The basic loads t_i and f_i are cyclic over a time interval $[0, T]$, amplified by the load multiplier λ_{sd} to form a load domain Ω.

Based on the mathematical programming theory, if the body force is omitted, the kinematic shakedown formulation (5) can be re-expressed as the following non-linear programming problem:

$$
\begin{cases}
\lambda_{sd} = \min_{\dot{\varepsilon}_{ij}^{p^*}, \Delta u_i} \int_0^T \int_V D\left(\dot{\varepsilon}_{ij}^{p^*}\right) \mathrm{d}v \mathrm{d}t \\[2mm]
\text{s.t.} \quad \int_0^T \int_V \sigma_{ij}^e \dot{\varepsilon}_{ij}^{p^*} \mathrm{d}v \mathrm{d}t = 1, \\[2mm]
\Delta \varepsilon_{ij}^p = \int_0^T \dot{\varepsilon}_{ij}^{p^*} \mathrm{d}t = \dfrac{1}{2}(\Delta u_{i,j} + \Delta u_{j,i}) \quad \text{in } V, \\[2mm]
\Delta u_i = \int_0^T \dot{u}_i \mathrm{d}t \qquad\qquad\qquad\quad \text{in } V, \\[2mm]
\Delta u_i = 0 \qquad\qquad\qquad\qquad\qquad \text{on } \Gamma_u,
\end{cases}
\tag{6}
$$

where σ_{ij}^e is the linear elastic stress response to the current external traction t_i, $\Delta \varepsilon_{ij}^p$ and Δu_i are the cumulative plastic strain and displacement fields at the end of one loading cycle, and Γ_u denotes the displacement boundary.

More details about the application of the non-linear programming method to limit/shakedown analysis can be found in the literature [18]. Finally the kinematic shakedown analysis is formulated as the calculation of shakedown multiplier λ_{sd}, with $\lambda_{sd}\, t_i$ being the shakedown limit of the structure.

2.3 Plastic Dissipation Power for an Ellipsoid Yield Criterion

Since that the kinematic shakedown analysis is based on displacement modes, the stress terms need to be expressed in terms of the strain terms, which can be obtained by using the yield criterion of a material and a plastic flow rule. In the theory of shakedown analysis, the plastic flow rule is assumed to be associated as $\dot{\varepsilon}_{ij}^p = \dot{\mu} \cdot \partial \phi(\sigma_{ij})/\partial \sigma_{ij}$, where $\dot{\mu}$ is a non-negative plastic proportionality factor. Therefore, the plastic strain rate can be determined by

$$
\dot{\boldsymbol{\varepsilon}}^p = 2\dot{\mu}\boldsymbol{P}\boldsymbol{\sigma}.
\tag{7}
$$

By applying Eq. (7) to the yield condition (1), one can obtain

$$
\dot{\mu} = \frac{1}{2}\sqrt{(\dot{\boldsymbol{\varepsilon}}^p)^{\mathrm{T}} \boldsymbol{P}^{-1} \dot{\boldsymbol{\varepsilon}}^p} \ .
\tag{8}
$$

Equation (8) implies the matrix $\boldsymbol{P}$ is invertible. However, for some material yield criteria, the matrix $\boldsymbol{P}$ is singular. For these materials, we can use $(\boldsymbol{P} + \gamma \boldsymbol{I})^{-1}$ as an approximation for $\boldsymbol{P}^{-1}$, where $\boldsymbol{I}$ is the identity matrix of the same order with the matrix $\boldsymbol{P}$ and γ is a very small real number. Then, the plastic dissipation power for the general yield criterion (1) can be expressed as follows:

$$D\left(\dot{\varepsilon}_{ij}^{p}\right) = \sigma_{ij}\dot{\varepsilon}_{ij}^{p} = \boldsymbol{\sigma}^{T}\dot{\boldsymbol{\varepsilon}}^{p} = \left(\frac{1}{2\dot{\mu}}\boldsymbol{P}^{-1}\dot{\boldsymbol{\varepsilon}}^{p}\right)^{T}\dot{\boldsymbol{\varepsilon}}^{p}$$

$$= \frac{1}{2\dot{\mu}}(\dot{\boldsymbol{\varepsilon}}^{p})^{T}\boldsymbol{P}^{-1}\dot{\boldsymbol{\varepsilon}}^{p} = \sqrt{(\dot{\boldsymbol{\varepsilon}}^{p})^{T}\boldsymbol{P}^{-1}\dot{\boldsymbol{\varepsilon}}^{p}}$$

(9)

As a result, the kinematic shakedown analysis for a macrostructure modelled by the ellipsoid yield criterion can be formulated as the following nonlinear mathematical programming problem:

$$
\begin{cases}
\lambda_{sd} = \min\limits_{\dot{\varepsilon}_{ij}^{p},\Delta u_i} \int_0^T \int_V \sqrt{(\dot{\boldsymbol{\varepsilon}}^{p})^{\mathrm{T}}\boldsymbol{P}^{-1}\dot{\boldsymbol{\varepsilon}}^{p}}\ \mathrm{d}v\mathrm{d}t \\[2mm]
\text{s.t.} \quad \int_0^T \int_V \sigma_{ij}^e \dot{\varepsilon}_{ij}^p \mathrm{d}v\mathrm{d}t = 1, \\[2mm]
\quad \Delta\varepsilon_{ij}^p = \int_0^T \dot{\varepsilon}_{ij}^p \mathrm{d}t = \frac{1}{2}(\Delta u_{i,j} + \Delta u_{j,i}) \quad \text{in } V, \\[2mm]
\quad \Delta u_i = \int_0^T \dot{u}_i \mathrm{d}t \qquad\qquad\qquad\qquad \text{in } V, \\[2mm]
\quad \Delta u_i = 0 \qquad\qquad\qquad\qquad\qquad\quad \text{on } \Gamma_u.
\end{cases}
$$

(10a,b,c,d,e)

By solving the above non-linear programming problem, the objective variable $\dot{\varepsilon}_{ij}^{p}$ can be found from the kinematically admissible plastic strain rate $\dot{\varepsilon}_{ij}^{p*}$ and the shakedown limit of the structure can be determined.

2.4 Approximation of the Time Integration

In order to apply the mathematical programming formulation (10) to a structure, the time integration will be approximately estimated because it would be difficult to calculate the integration along a deformation path. To overcome this potential difficulty, König's technique [16, 17] is used.

Considering that the loading is repeated or cyclic, the load domain Ω can be thought of as a load space which can be defined by a convex linear combination of load vertices $\boldsymbol{P}_k(k = 1, 2, \ldots, l)$. It is first under the vertex loads that plastic deformation occurs in a structure. Therefore, it can be assumed that if a structure reaches a state of shakedown under any sequence of vertex loads within the set of vertices $\boldsymbol{P}_k$, then it will shakedown under the whole load domain Ω defined by those vertices. The cyclic loading remains constant over a time interval $\tau_k(\sum\limits_{k=1}^{l}\tau_k = T)$ on each vertex, and the admissible plastic strain cycles on these vertices can generate a plastic strain increment:

$$\varepsilon_k^p = \int_{\tau_k} \dot{\varepsilon}^p \mathrm{d}t \qquad (k = 1, 2, \dots, l). \tag{11}$$

Then the cumulative plastic strain at the end of one loading cycle over the time interval $[0, T]$ can be obtained as follows

$$\Delta\varepsilon^p = \sum_{k=1}^{l} \varepsilon_k^p. \tag{12}$$

Finally, the kinematic shakedown analysis for a macrostructure subjected to repeated or cyclic loads can be expressed as the following non-linear mathematical programming problem:

$$
\begin{cases}
\lambda_{sd} = \min_{\varepsilon_k^p, \Delta u} \sum_{k=1}^{l} \int_{V} \sqrt{(\varepsilon_k^p)^{\mathrm{T}} \, \boldsymbol{P}^{-1} \varepsilon_k^p} \mathrm{d}v \\[2mm]
\text{s.t.} \quad \sum_{k=1}^{l} \int_{V} (\boldsymbol{\sigma}_k^e)^{\mathrm{T}} \varepsilon_k^p \mathrm{d}v = 1, \\[2mm]
\Delta\varepsilon^p = \sum_{k=1}^{l} \varepsilon_k^p = \Re(\Delta\boldsymbol{u}) \qquad \text{m } V, \\[2mm]
\Delta\boldsymbol{u} = 0 \qquad\qquad\qquad\qquad \text{on } \Gamma_u,
\end{cases}
\tag{13a,b,c,d}
$$

where $\Re$ is a linear compatibility differential operator which is defined by Eq. (10c).

3 Kinematic Shakedown Analysis of a Microstructure

In order to apply the kinematic shakedown analysis (13) to a microstructure from composites, the homogenization technique will be used.

3.1 Homogenization Theory

As an innovative micromechanics technique, homogenization theory [30] was developed in the 1980's and has been widely exploited in recent years. The homogenization technique is mostly performed upon a periodic composite material. First, a RVE is chosen from a composite material with periodic microstructures, as shown in Fig. 1, to account for the effect of microstructures on macroscopic behaviours. Then, the mechanical fields in a RVE are described by means of microscopic fluctuation variables as follows:
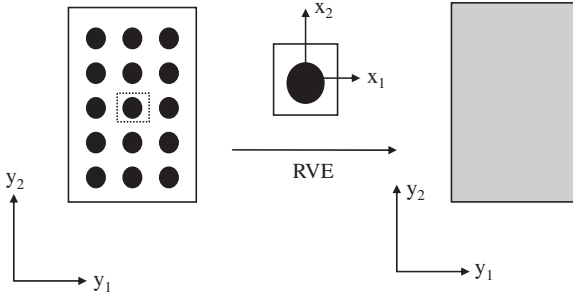
Fig. 1 Periodic microstructures and a RVE of a composite

$$\boldsymbol{u} = \boldsymbol{E} \cdot \boldsymbol{x} + \tilde{\boldsymbol{u}}, \tag{14}$$

$$\boldsymbol{\varepsilon} = \boldsymbol{E} + \tilde{\boldsymbol{\varepsilon}}, \tag{15}$$

$$\boldsymbol{\sigma} = \boldsymbol{\Sigma} + \tilde{\boldsymbol{\sigma}}, \tag{16}$$

where $\boldsymbol{x}$ denotes the macroscopic position of the RVE in the structure, $\boldsymbol{u}, \boldsymbol{\varepsilon}$ and $\boldsymbol{\sigma}$ denote the local displacement, strain and stress terms, $\boldsymbol{E}$ and $\boldsymbol{\Sigma}$ are the average strain and stress terms over the RVE, and $\tilde{\boldsymbol{u}}$, $\tilde{\boldsymbol{\varepsilon}}$ and $\tilde{\boldsymbol{\sigma}}$ are their fluctuation terms, respectively. We therefore have

$$\boldsymbol{E} = \langle \boldsymbol{\varepsilon} \rangle, \quad \boldsymbol{\Sigma} = \langle \boldsymbol{\sigma} \rangle, \tag{17a,b}$$

$$\langle \tilde{\boldsymbol{\varepsilon}} \rangle = \boldsymbol{0}, \quad \langle \tilde{\boldsymbol{\sigma}} \rangle = \boldsymbol{0}, \tag{18a,b}$$

where the operator $\langle \cdot \rangle$ stands for the volume average over the RVE. The fluctuation terms $\tilde{\boldsymbol{u}}$ and $\tilde{\boldsymbol{\sigma}} \cdot \boldsymbol{n}$ are periodic and anti-periodic, resp., on the boundary of the RVE, whereas $\boldsymbol{n}$ is the outer normal to the boundary. Instead of giving boundary values, the periodic feature of the fluctuation terms on the boundary of the RVE must be imposed. This is a big difference between the homogenization technique and other micromechanics approaches [7, 9, 10]. More details above the homogenization technique can be found in the literature [30].

3.2 Shakedown Analysis Based on Homogenization Theory

Corresponding to a macroscopic cyclic load on a macrostructure, a microscopic cyclic load on a RVE can be described as $\boldsymbol{\Sigma}$.

$$\boldsymbol{\Sigma} = [\mu_1 \Sigma_{11}, \mu_2 \Sigma_{22}, \mu_3 \Sigma_{33}, \mu_4 \Sigma_{12}, \mu_5 \Sigma_{23}, \mu_6 \Sigma_{31}]^{\mathrm{T}}, \tag{19a}$$

$$\mu_i^- \leq \mu_i \leq \mu_i^+ \qquad (i = 1, 2, \ldots, 6), \tag{19b}$$

where $\mu_i(i = 1, 2, \ldots, 6)$ is an amplifying multiplier and each varies independently.

By using the homogenization technique, the objective function (13a) of the non-linear programming problem can be re-written as

$$
\sum_{k=1}^{l} \int_V \sqrt{(\tilde{\varepsilon}_k^p)^{\mathrm{T}} \boldsymbol{P}^{-1} \tilde{\varepsilon}_k^p} \, \mathrm{d}v = \sum_{k=1}^{l} \int_V \sqrt{\left(\tilde{\varepsilon}_k^p + \boldsymbol{E}_k^p\right)^{\mathrm{T}} \boldsymbol{P}^{-1} \left(\tilde{\varepsilon}_k^p + \boldsymbol{E}_k^p\right)} \, \mathrm{d}v
$$
$$
= \sum_{k=1}^{l} \int_V \sqrt{(\tilde{\varepsilon}_k^p)^{\mathrm{T}} \boldsymbol{P}^{-1} \tilde{\varepsilon}_k^p + 2 \left(\boldsymbol{E}_k^p\right)^{\mathrm{T}} \boldsymbol{P}^{-1} \tilde{\varepsilon}_k^p + \left(\boldsymbol{E}_k^p\right)^{\mathrm{T}} \boldsymbol{P}^{-1} \boldsymbol{E}_k^p} \, \mathrm{d}v, \tag{20}
$$

where $\boldsymbol{E}_k^p$ and $\tilde{\varepsilon}_k^p$ are the macroscopic average plastic strain over the RVE and the microscopic fluctuation plastic strain on loading vertex $k(k = 1, 2, \ldots l)$.

Meanwhile, the normalization condition (13b) can be re-expressed as

$$
\sum_{k=1}^{l} \int_V (\boldsymbol{\Sigma}_k)^{\mathrm{T}} \boldsymbol{E}_k^p \mathrm{d}v = V_0 \sum_{k=1}^{l} (\boldsymbol{\Sigma}_k)^{\mathrm{T}} \boldsymbol{E}_k^p = 1. \tag{21}
$$

It is worth noting that because the cyclic loading on a RVE is a macroscopic average stress field $\boldsymbol{\Sigma}$, the linear elastic stress $\boldsymbol{\Sigma}^e$ response to the current loading $\boldsymbol{\Sigma}$ is satisfied with the equation

$$
\boldsymbol{\Sigma}^e = \boldsymbol{\Sigma}. \tag{22}
$$

Then, the kinematic shakedown analysis based on homogenization theory for a microstructure RVE can be obtained as follows:

$$
\begin{cases}
\lambda_{sd} = \min_{\tilde{\varepsilon}_k^p, \boldsymbol{E}_k^p, \Delta\tilde{\boldsymbol{u}}} \sum_{k=1}^{l} \int_V \\
\quad \sqrt{(\tilde{\varepsilon}_k^p)^{\mathrm{T}} \boldsymbol{P}^{-1} \tilde{\varepsilon}_k^p + 2(\boldsymbol{E}_k^p)^{\mathrm{T}} \boldsymbol{P}^{-1} \tilde{\varepsilon}_k^p + (\boldsymbol{E}_k^p)^{\mathrm{T}} \boldsymbol{P}^{-1} \boldsymbol{E}_k^p} \, \mathrm{d}v \\
\\
\text{s.t.} \qquad V_0 \sum_{k=1}^{l} (\boldsymbol{\Sigma}_k)^{\mathrm{T}} \boldsymbol{E}_k^p = 1, \\
\\
\quad \Delta\tilde{\varepsilon}^p = \sum_{k=1}^{l} \tilde{\varepsilon}_k^p = \Re(\Delta\tilde{\boldsymbol{u}}) \qquad \text{in } V, \\
\\
\quad \Delta\tilde{\boldsymbol{u}} \quad periodic \qquad\qquad \text{on } \Gamma,
\end{cases} \tag{23}
$$

where $\Delta\tilde{\boldsymbol{u}}$ is the cumulative microscopic fluctuation displacement over a loading cycle and periodic on the boundary of the RVE, and V_0 is the volume of the RVE.

Thus, the kinematic shakedown analysis of a microstructure is formulated as a non-linear programming problem subject to equality constraints. An upper bound to the shakedown limit multiplier λ_{sd} can be calculated, with $\lambda_{sd}\boldsymbol{\Sigma}$ denoting the shakedown limit of a composite under cyclic loading.

3.3 Finite Element Modelling

According to the finite element technique, the body V of the RVE is discretized
into finite elements, i.e. $V = \bigcup\limits_{e=1}^{N} V_e$. Then, the microscopic fluctuation fields
can be interpolated as

$$\Delta\tilde{\boldsymbol{u}}_e(\boldsymbol{x}) = \boldsymbol{N}_e(\boldsymbol{x})\Delta\tilde{\boldsymbol{\delta}}_e \tag{24}$$

$$\Delta\tilde{\boldsymbol{\varepsilon}}_e(\boldsymbol{x}) = \boldsymbol{B}_e(\boldsymbol{x})\Delta\tilde{\boldsymbol{\delta}}_e \tag{25}$$

where, with reference to the $\boldsymbol{e}$-th finite element, $\Delta\tilde{\boldsymbol{\delta}}_e$ is the nodal cumulative
fluctuation displacement vector over a loading cycle, $\boldsymbol{N}_e(\boldsymbol{x})$ is the interpola-
tion function matrix and $\boldsymbol{B}_e(\boldsymbol{x})$ is the strain matrix.

By means of the Gaussian integration technique, the objective function in
the kinematic shakedown analysis defined by Eq. (23) can be discretized as

$$\sum_{k=1}^{l} \int_V \sqrt{(\tilde{\boldsymbol{\varepsilon}}_k^p)^{\mathrm{T}}\boldsymbol{P}^{-1}\tilde{\boldsymbol{\varepsilon}}_k^p + 2(\boldsymbol{E}_k^p)^{\mathrm{T}}\boldsymbol{P}^{-1}\tilde{\boldsymbol{\varepsilon}}_k^p + (\boldsymbol{E}_k^p)^{\mathrm{T}}\boldsymbol{P}^{-1}\boldsymbol{E}_k^p}\; \mathrm{d}v$$

$$= \sum_{k=1}^{l}\sum_{e=1}^{N} \int_{V_e} \sqrt{(\tilde{\boldsymbol{\varepsilon}}_{ek}^p)^{\mathrm{T}}\boldsymbol{P}^{-1}\tilde{\boldsymbol{\varepsilon}}_{ek}^p + 2(\boldsymbol{E}_k^p)^{\mathrm{T}}\boldsymbol{P}^{-1}\tilde{\boldsymbol{\varepsilon}}_{ek}^p + (\boldsymbol{E}_k^p)^{\mathrm{T}}\boldsymbol{P}^{-1}\boldsymbol{E}_k^p}\; \mathrm{d}v \tag{26}$$

$$= \sum_{k=1}^{l}\sum_{r=1}^{n} \rho_r|\boldsymbol{J}|_r \sqrt{(\tilde{\boldsymbol{\varepsilon}}_{kr}^p)^{\mathrm{T}}\boldsymbol{P}^{-1}\tilde{\boldsymbol{\varepsilon}}_{kr}^p + 2(\boldsymbol{E}_k^p)^{\mathrm{T}}\boldsymbol{P}^{-1}\tilde{\boldsymbol{\varepsilon}}_{kr}^p + (\boldsymbol{E}_k^p)^{\mathrm{T}}\boldsymbol{P}^{-1}\boldsymbol{E}_k^p},$$

where ρ_r is the integral weight at the r-th Gaussian integral point, $|\boldsymbol{J}|_r$ is the
determinant of the Jacobian matrix at the r-th Gaussian integral point, and
n is the number of Gaussian integral points of the whole RVE.

The geometric compatibility of cumulative plastic strains in Eq. (23) can
be rewritten as

$$\Delta\tilde{\boldsymbol{\varepsilon}}_r^p = \sum_{k=1}^{l} \tilde{\boldsymbol{\varepsilon}}_{kr}^p = \boldsymbol{B}_r\Delta\tilde{\boldsymbol{\delta}} \qquad (r = 1, 2, \cdots, n), \tag{27}$$

where $\Delta\tilde{\boldsymbol{\delta}}$ is a global nodal cumulative fluctuation displacement vector of the
discretized RVE over a loading cycle and $\boldsymbol{B}_r$ is the strain matrix at the r–th
Gaussian integral point and has $\boldsymbol{B}_r = \boldsymbol{B}_e \cdot \boldsymbol{C}_e$, and $\boldsymbol{C}_e$ is the transformation
matrix which assembles the element matrix into the global matrix.

Based on the above analyses, the finite element formulation of the shake-
down analysis based on homogenization theory can be expressed by

$$
\begin{cases}
\lambda_{sd} = \min\limits_{\tilde{\boldsymbol{\varepsilon}}^p_{kr},\boldsymbol{E}^p,\Delta\tilde{\delta}} \sum\limits_{k=1}^{l} \sum\limits_{r=1}^{n} \rho_r |J|_r \\[2mm]
\quad \sqrt{(\tilde{\boldsymbol{\varepsilon}}^p_{kr})^{\mathrm{T}}\boldsymbol{P}^{-1}\tilde{\boldsymbol{\varepsilon}}^p_{kr} + 2(\boldsymbol{E}^p_k)^{\mathrm{T}}\boldsymbol{P}^{-1}\tilde{\boldsymbol{\varepsilon}}^p_{kr} + (\boldsymbol{E}^p_k)^{\mathrm{T}}\boldsymbol{P}^{-1}\boldsymbol{E}^p_k} \\[2mm]
\text{s.t.}\quad V_0 \sum\limits_{k=1}^{l} (\boldsymbol{\Sigma}_k)^{\mathrm{T}}\boldsymbol{E}^p_k = 1, \\[2mm]
\qquad \Delta\tilde{\boldsymbol{\varepsilon}}^p_r = \sum\limits_{k=1}^{l} \tilde{\boldsymbol{\varepsilon}}^p_{kr} = \boldsymbol{B}_r \Delta\tilde{\boldsymbol{\delta}} \qquad (r = 1, 2, \cdots, n).
\end{cases}
\tag{28a,b,c}
$$

It is noted that the periodic feature of the nodal cumulative fluctuation displacement $\boldsymbol{\Delta\tilde{\delta}}$ on the boundary of the RVE must be enforced when the finite element technique is performed. The shakedown limit multiplier λ_{sd} can be obtained by solving the above minimum optimization problem.

4 Iterative Solution Algorithm

The kinematic shakedown analysis (28) is a programming problem subject to equality constraints. For a continuous and differentiable quadratic programming problem under the Kuhn-Tucker's conditions, several effective methods [11] can be used to solve it. However, for the programming problem (28), there is a calculation of square root which makes the objective function unsmooth and non-differentiable. If the objective function is finite and continuous in a feasible set, it is not necessary to be differentiable everywhere and an optimal solution can be obtained [27]. The non-linear objective function was shown to be non-differentiable for limit/shakedown analyses using von Mises' criterion [18, 19, 43]. The difficulty was overcome by an iterative algorithm [43]. This technique is similar to the procedure used by Huh and Yang [12] and is used in this study to solve the non-linear programming problem (28).

4.1 Minimum Optimization Strategy

According to the mathematical programming theory, equality constraints (the normalization condition (28b) and the geometric compatibility (28c)) can be introduced into an optimization problem by means of the Lagrangean method [11]. For the yield criterion such as von Mises' or Hill's criterion, however, the plastic incompressibility as a constitutive feature should also be satisfied:

$$
\boldsymbol{D}^{\mathrm{T}}_{\mathrm{v}}(\tilde{\boldsymbol{\varepsilon}}^p_{kr} + \boldsymbol{E}^p_k) = 0 \quad (r = 1, 2, \cdots, n; \quad k = 1, 2, \cdots, l),
\tag{29}
$$

where $\boldsymbol{D}_{\mathrm{v}} = [1, 1, 1, 0, 0, 0]^{\mathrm{T}}$. This condition can be regarded as an extra constraint and introduced into the mathematical programming problem by means of the penalization function method. As a result, an unconstrained minimum optimization problem can be obtained as follows

$$L(\tilde{\varepsilon}_{kr}^p, \boldsymbol{E}_k^p, \Delta\tilde{\boldsymbol{\delta}}, \lambda, \boldsymbol{L}_r) = \sum_{k=1}^{l}\sum_{r=1}^{n} \rho_r |J|_r$$

$$\sqrt{(\tilde{\varepsilon}_{kr}^p)^{\mathrm{T}} \boldsymbol{P}^{-1} \tilde{\varepsilon}_{kr}^p + 2(\boldsymbol{E}_k^p)^{\mathrm{T}} \boldsymbol{P}^{-1} \tilde{\varepsilon}_{kr}^p + (\boldsymbol{E}_k^p)^{\mathrm{T}} \boldsymbol{P}^{-1} \boldsymbol{E}_k^p}$$

$$+ \lambda \left(1 - V_0 \sum_{k=1}^{l} (\boldsymbol{\Sigma}_k)^{\mathrm{T}} \boldsymbol{E}_k^p\right) + \sum_{r=1}^{n} \boldsymbol{L}_r^{\mathrm{T}} \left(\sum_{k=1}^{l} \tilde{\varepsilon}_{kr}^p - \boldsymbol{B}_r \Delta\tilde{\boldsymbol{\delta}}\right) + \frac{1}{2}\alpha \sum_{k=1}^{l}\sum_{r=1}^{n}$$

$$\rho_r |J|_r ((\tilde{\varepsilon}_{kr}^p)^{\mathrm{T}} \boldsymbol{D}_{\mathrm{w}} \tilde{\varepsilon}_{kr}^p + 2(\boldsymbol{E}_k^p)^{\mathrm{T}} \boldsymbol{D}_{\mathrm{w}} \tilde{\varepsilon}_{kr}^p + (\boldsymbol{E}_k^p)^{\mathrm{T}} \boldsymbol{D}_{\mathrm{w}} \boldsymbol{E}_k^p)$$

$$(30)$$

where λ and $\boldsymbol{L}_r$ are the Lagrangean multipliers, and α is the penalization factor, $\boldsymbol{D}_{\mathrm{w}}$ is a coefficient matrix and $\boldsymbol{D}_{\mathrm{w}} = \boldsymbol{D}_{\mathrm{v}} \cdot \boldsymbol{D}_{\mathrm{v}}^{\mathrm{T}}$. Based on the Kuhn-Tucker stationarity conditions [11], the following formulation can be obtained:

$$\begin{cases} \boldsymbol{H}_{kr} \tilde{\varepsilon}_{kr}^p + \boldsymbol{H}_{kr} \boldsymbol{E}_k^p + (\rho_r |J|_r)^{-1} \boldsymbol{L}_r = 0, \\[2mm] \sum_{r=1}^{n} (\rho_r |J|_r \boldsymbol{H}_{kr} \tilde{\varepsilon}_{kr}^p) + \\[2mm] \sum_{r=1}^{n} (\rho_r |J|_r \boldsymbol{H}_{kr}) \boldsymbol{E}_k^p - \lambda V_0 (\boldsymbol{\Sigma}_k)^{\mathrm{T}} = 0, \\[2mm] \sum_{r=1}^{n} (\boldsymbol{B}_r^{\mathrm{T}} \boldsymbol{L}_r) = \boldsymbol{0}, \; V_0 \sum_{k=1}^{l} (\boldsymbol{\Sigma}_k)^{\mathrm{T}} \boldsymbol{E}_k^p = 1, \\[2mm] \sum_{k=1}^{l} \tilde{\varepsilon}_{kr}^p - \boldsymbol{B}_r \Delta\tilde{\boldsymbol{\delta}} = \boldsymbol{0} \quad (k = 1, 2, \cdots, l; r = 1, 2, \cdots, n), \end{cases} \quad (31\mathrm{a,b,c,d,e})$$

where $\boldsymbol{H}_{kr}$ is the coefficient matrix with $\boldsymbol{H}_{kr} = \boldsymbol{P}^{-1}(\boldsymbol{z}_{kr})_{ICP}^{-1} + \alpha \boldsymbol{D}_{\mathrm{w}}$ and $\boldsymbol{z}_{kr} = \sqrt{(\tilde{\varepsilon}_{kr}^p)^{\mathrm{T}} \boldsymbol{P}^{-1} \tilde{\varepsilon}_{kr}^p + 2(\boldsymbol{E}_k^p)^{\mathrm{T}} \boldsymbol{P}^{-1} \tilde{\varepsilon}_{kr}^p + (\boldsymbol{E}_k^p)^{\mathrm{T}} \boldsymbol{P}^{-1} \boldsymbol{E}_k^p}$, where the subscript 'ICP' indicates that $\boldsymbol{z}_{kr}$ is an *Iteration Control Parameter*. By solving Eq. (31), $\tilde{\varepsilon}_{kr}^p$, $\Delta\tilde{\boldsymbol{\delta}}$ and $\boldsymbol{E}_k^p$ are calculated and the shakedown multiplier can be determined as

$$\lambda_{sd} = \sum_{k=1}^{l}\sum_{r=1}^{n} \rho_r |J|_r$$

$$\sqrt{(\tilde{\varepsilon}_{kr}^p)^{\mathrm{T}} \boldsymbol{P}^{-1} \tilde{\varepsilon}_{kr}^p + 2(\boldsymbol{E}_k^p)^{\mathrm{T}} \boldsymbol{P}^{-1} \tilde{\varepsilon}_{kr}^p + (\boldsymbol{E}_k^p)^{\mathrm{T}} \boldsymbol{P}^{-1} \boldsymbol{E}_k^p}. \qquad (32)$$

4.2 Iterative Strategy

Although the unknown fields can be determined by solving the set of Eqs. (31), it is quite difficult to directly solve it because the equations are non-linear and not smooth. To overcome this difficulty, the non-plastic areas should be distinguished where the objective function is not differentiable. The non-plastic areas are unknown at the beginning of the calculation and they can be identified by a step-by-step iteration.

Step 0: initializing the non-linear objective function

As shown in Huh and Yang [12] and Liu et al. [19], the selection of the initial nodal velocity field does not affect the convergence of iteration. For simplicity, we follow their strategies and start iteration by defining an iteration seed

$$(\boldsymbol{z}_{kr})_0 = 1 \; (k = 1, 2, \cdots, l; r = 1, 2, \cdots, n), \tag{33}$$

where the subscript '0' denotes that the variable is determined at step 0. Then, one can obtain

$$(\boldsymbol{H}_{kr})_0 = \boldsymbol{P}^{-1} + \alpha \boldsymbol{D}_{\mathrm{w}}. \tag{34}$$

Accordingly, the set of Eqs. (31) becomes linear and the objective variables $(\tilde{\varepsilon}^p_{kr})_0$, $\left(\Delta\tilde{\boldsymbol{\delta}}\right)_0$ and $(\boldsymbol{E}^p_k)_0$ can be calculated at this step. Then, the initial shakedown load multiplier $(\lambda_{sd})_0$ can be determined by (32).

Step $h + 1 (h = 0, 1, 2, \ldots)$: distinguishing the non-plastic areas to revise the objective function

Based on the computational results at the iteration step h, the value of $\boldsymbol{z}_{kr}(\boldsymbol{z}_{kr} = \sqrt{(\tilde{\varepsilon}^p_{kr})^{\mathrm{T}}\boldsymbol{P}^{-1}\tilde{\varepsilon}^p_{kr} + 2(\boldsymbol{E}^p_k)^{\mathrm{T}}\boldsymbol{P}^{-1}\tilde{\varepsilon}^p_{kr} + (\boldsymbol{E}^p_k)^{\mathrm{T}}\boldsymbol{P}^{-1}\boldsymbol{E}^p_k})$ needs to be calculated at every Gaussian integral point to check whether it is in the non-plastic or plastic area. Then the Gaussian integral point set I will be subdivided into two subsets, a subset $(I_E)_{h+1}$ where the plastic dissipation work is equal to zero and a subset $(I_P)_{h+1}$ where the plastic dissipation work occurs.

$$I = (I_{\mathrm{E}})_{h+1} \cup (I_{\mathrm{P}})_{h+1} \tag{35a}$$

$$(I_{\mathrm{E}})_{h+1} = \{r \in I, (\boldsymbol{z}_{kr})_h = 0\} \tag{35b}$$

$$(I_{\mathrm{P}})_{h+1} = \{r \in I, (\boldsymbol{z}_{kr})_h \neq 0\} \tag{35c}$$

However, considering that there is a limitation of storage for a computer and that any attempt to evaluate the gradient of a square root near a zero argument would cause computational overflow, a small real number $\zeta(\zeta \to 0)$ is needed in a computer program to distinguish the non-plastic/plastic regions. In other words, a region with $\boldsymbol{z}_{kr} < \zeta$ can be regarded as non-plastic. From a theoretical point of view, the smaller ζ is, the more precise the

numerical calculation would be. In practice, however, the value ζ adopted in a computer program may vary from 10^{-8} to 10^{-12}. The numerical calculations suggest that when ζ is less than 10^{-8}, it has very little effect on the results. A similar smoothing parameter was also adopted by Huh and Yang [12] to remove the same numerical difficulty in their limit analysis formulation.

Then the coefficient matrix $\boldsymbol{H}_{kr}$ at this iteration step will be determined by

$$(\boldsymbol{H}_{kr})_{h+1} = \begin{cases} \alpha \boldsymbol{D}_{\mathrm{w}} + \beta \boldsymbol{P}^{-1} & r \in (I_E)_{h+1}, \\ \alpha \boldsymbol{D}_{\mathrm{w}} + \boldsymbol{P}^{-1}(\boldsymbol{z}_{kr})_h^{-1} & r \in (I_P)_{h+1}, \end{cases} \tag{36}$$

where β is the penalization factor which is used to introduce the non-plastic area as a constraint into the programming problem.

By solving the linearizied set of Eqs. (31), the objective variables $(\tilde{\boldsymbol{\varepsilon}}_{kr}^p)_{h+1}$, $\left(\Delta \tilde{\boldsymbol{\delta}}\right)_{h+1}$ and $(\boldsymbol{E}_k^p)_{h+1}$ can be calculated. Then the shakedown load multiplier $(\lambda_{sd})_{h+1}$ can be determined by Eq. (32).

The above iteration is repeated until the convergence criteria are satisfied as $|(\lambda_{sd})_{h+1} - (\lambda_{sd})_h| / |(\lambda_{sd})_{h+1}| \le \eta_1$, $\left\|\Delta \tilde{\boldsymbol{\delta}}_{h+1} - \Delta \tilde{\boldsymbol{\delta}}_h\right\| / \left\|\Delta \tilde{\boldsymbol{\delta}}_{h+1}\right\| \le \eta_2$ and $\|(\boldsymbol{E}_k^p)_{h+1} - (\boldsymbol{E}_k^p)_h\| / \|(\boldsymbol{E}_k^p)_{h+1}\| \le \eta_3$, where η_1, η_2 and η_3 are computational error tolerances. The iterative process leads to the shakedown load multiplier λ_{sd} through a monotonically decreasing convergence sequence and a minimum optimal upper bound to the shakedown multiplier can be obtained.

5 Applications

The proposed numerical method is now applied to conduct shakedown analysis of composites under cyclic loads and both von Mises' and Hill's criteria are used to model the plastic behaviour of constituents. Finite elements with a reduced Gaussian integration strategy are used, which may be helpful to overcome the 'locking' in the numerical analysis of incompressible materials, as discussed in detail by Zienkiewicz et al. [44], Sloan and Randolph [28], Yu et al. [40], Yu and Netherton [41] among others.

5.1 Fiber-Reinforced Composites – A Plane Strain Case

The first numerical example, for comparison with other works, is for shakedown analysis of unidirectional fiber-reinforced composites in the plane strain model and von Mises' yield criterion is used. The fiber has a circular cross section and its volume fraction is 0.5 and its mechanical features are: $E = 370\,\mathrm{GPa}$, $\nu = 0.3$ and $\sigma_{\mathrm{s}} = 2000\,\mathrm{MPa}$. The mechanical features of the matrix are: $E = 70\,\mathrm{GPa}$, $\nu = 0.3$ and $\sigma_{\mathrm{s}} = 80\,\mathrm{MPa}$. A unit hexagonal RVE is chosen to model the microstructure of composites. Biaxial cyclic loads
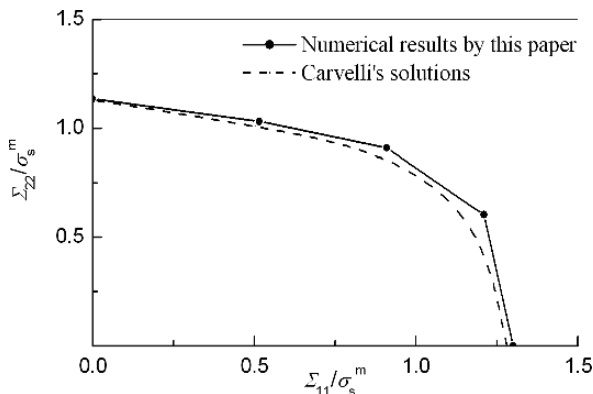
Fig. 2 The macroscopic shakedown domain of the composite

are investigated which are defined by $\boldsymbol{\Sigma} = [\mu_1 \Sigma_{11}, \mu_2 \Sigma_{22}]^{\mathrm{T}} (0 \leq \mu_1 \leq 1; 0 \leq \mu_2 \leq 1)$. The numerical shakedown domain is calculated as shown in Fig. 2, where σ_s^m denotes the yield stress of the matrix, and agrees well with those obtained by Carvelli [1] using a different approach only valid for von Mises' constituents.

5.2 Hill's Matrix Composites – A Plane Stress Case

In this section, the effect of anisotropic constituents on the macroscopic shakedown domain of composites is studied by the proposed numerical method. Unidirectional fiber-reinforced composites subjected to biaxial cyclic loads acting transverse to the fibers and a plane stress model is adopted. The fiber has a circular cross section and its volume fraction is 0.5. The mechanical parameters of fiber are $E = 350\,\mathrm{GPa}$, $\nu = 0.3$ and $\sigma_s = 1600\,\mathrm{MPa}$, and it is modelled by von Mises' criterion. The parameters of the anisotropic matrix are $E = 70\,\mathrm{GPa}$, $\nu = 0.3$, $X = 80\,\mathrm{MPa}$, $Y = 20\,\mathrm{MPa}$, $Z = 120\,\mathrm{MPa}$, and it is modeled by Hill's criterion. A unit hexagonal RVE is chosen from the composite and eight-node quadrilateral elements are used in the finite element analysis. The shakedown limit (which corresponds to repeated/cyclic loading and whose loading mode is $0 \leq \mu_1 \leq 1; 0 \leq \mu_2 \leq 1$) and plastic collapse limit (which corresponds to static loading and whose loading mode is $\mu_1 = \mu_2 = 1$) are calculated respectively. The numerical shakedown and collapse limit domains are shown in Fig. 3, where σ_s^m denotes the yield stress of the matrix. From the numerical results, it can be concluded that under a plane stress model, the shakedown limit and plastic limit of a composite are mainly determined by its weak phase.
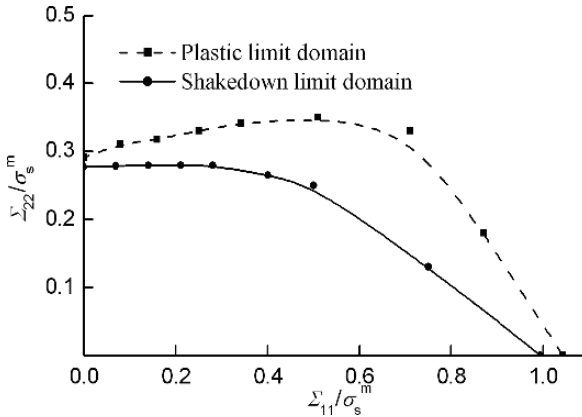
Fig. 3 The macroscopic shakedown domain of the composite

6 Conclusions

A non-linear numerical technique has been developed to perform the shakedown analysis on a microstructure by introducing the homogenization theory into the kinematic theorem of shakedown analysis. By using the homogenization technique, the classical shakedown theory for a macrostructure can be extended to explain the plastic behavior of a microstructure and the effect of the microstructure on the macroscopic properties of composites can be studied in detail. An ellipsoid yield criterion is assumed for the constituents of composites and a general method for deriving the dissipation power of the microstructure is provided. The finite element model of kinematic shakedown analysis for a microstructure is formulated as a non-linear programming problem subject to a small number of equality constraints. An upper bound to the shakedown domain of a periodic composite can then be calculated. As an extension of the classical shakedown analysis for a macrostructure to a microstructure, the proposed method gives a mechanical interpretation and quantitative prediction for the macroscopic strength of a periodic composite. The proposed numerical approach can, therefore, provide a powerful tool for designing the periodic composites against plastic failure under cyclic loads.

References

1. Carvelli V. Shakedown analysis of unidirectional fiber reinforced metal matrix composites. *Comput. Mater. Sci.* 2004; **31:** 24–32.
2. Chen HF., Ponter ARS. Shakedown and limit analyses for 3-D structures using the linear matching method. *Int. J. Pres. Ves. Pip.* 2001; **78:** 443–451.
3. Cocks ACF., Jansson S., Leckie FA. Effect of cyclic thermal loading on the properties of metal matrix composites. *J. Therm. Stress* 1992; **15:** 175–184.

4. Daehn GS., Anderson PM., Zhang HY. Temperature change induced plasticity in metal matrix composites. *Scripta Metallurgica et Materialia* 1991; **25:** 2279–2284.

5. Feng XQ., Liu XS. On shakedown of three-dimensional elastoplastic strain-hardening structures. *Int. J. Plasticity* 1997; **12:** 1241–1256.

6. Francescato P., Pastor J. Lower and upper numerical bounds to the off-axis strength of unidirectional fiber-reinforced composite by limit analysis methods. *Eur. J. Mech. A Solids* 1997; **16:** 213–234.

7. Gurson AL. Continuum theory of ductile rupture by void nucleation and growth: Part I – yield criteria and flow rules for porous ductile media. *J. Eng. Mat. Tech.* 1977; **99:** 2–15.

8. Hill R. A theory of the yielding and plastic flow of anisotropic metals. *Proc. Roy. Soc. London* 1948; **193:** 282–287.

9. Hill R. A self-consistent mechanics of composite materials. *J. Mech. Phys. Solids*, 1965; **13:** 213–222.

10. Hill R. Continuum micromechanics of elastoplastic polycristals. *J. Mech. Phys. Solids* 1965; **13:** 89–101.

11. Himmelblau DM. Applied Non-linear Programming. McGraw-Hill Book Company: New York, 1972.

12. Huh H., Yang WH. A general algorithm for limit solutions of plane stress problems. *Int. J. Solid. Struct.* 1991; 28: 727–738.

13. Jansson S., Leckie FA. Transverse tensile and inplane shear strength of weakly bonded fiber reinforced MMC's subjected to cyclic thermal loading. *Mech. Mater.* 1994; **18:** 205–212.

14. Jansson S., Leckie FA. Effect of cyclic thermal loading on the inplane shear strength of fiber reinforced MMC's. *Eur. J. Mech. A Solids* 1997; **16:** 561–572.

15. Koiter WT. General theorems for elastic-plastic bodies. In: Sneddon IN, Hill R (eds).*Progress in Solid Mechanics*, North-Holland: Amsterdam, 1960; 165–221.

16. König JA. On upper bounds to shakedown loads. *ZAMM* 1979; **59:** 349–354.

17. König JA. Shakedown of Elastic-Plastic Structure. Elsevier: Amsterdam, 1987.

18. Li HX., Liu YH., Feng XQ., Cen ZZ. Limit analysis of ductile composites based on homogenization theory. *Proc. Roy. Soc. London A* 2003; **459:** 659–675.

19. Liu YH., Cen ZZ., Xu BY. A numerical method for plastic limit analysis of 3-D structures. *Int. J. Solid. Struct.* 1995; **32:** 1645–1658.

20. Maier G. Shakedown theory in perfect elastoplasticity with associated and nonassociated flow-laws: a finite element linear programming approach. *Meccanica* 1969; **4:** 250–260.

21. Melan E. Theorie Statisch Unbestimmter Tragwerke aus idealplastischem Baustoff. *Sitzungsbericht der Akademie der Wissenschaften (Wien) Abt. IIA* 1938; **195:** 145–195.

22. Michel JC., Moulinec H., Suquet P. Effective properties of composite materials with periodic microstructure: a computational approach. *Comp. Methods Appl. Mech. Engrg.* 1999; **172:** 109–143.

23. Morelle P. Numerical shakedown analysis of axisymmetric sandwich shells: an upper bound formulation. *Int. J. Num. Meth. Eng.* 1986; **23:** 2071–2088.

24. Ponter ARS., Carter KF., Duggan JM. Shakedown limits for a metal matrix composite. *J. Comp. Tech. Res.* 2001; **23**: 197–204.

25. Ponter ARS., Engelhardt M. Shakedown limits for a general yield condition: implementation and application for a von Mises yield condition. *Eur. J. Mech. A/Solids* 2000; **19:** 423–445.

26. Ponter ARS., Leckie FA. Bounding properties of metal-matrix composites subjected to cyclic thermal loading. *J. Mech. Phys. Solids* 1998; **46:** 697–717.

27. Shapiro JF. Mathematical Programming: Structures and Algorithms. A Wiley-Interscience Publication: New York, 1979.

28. Sloan SW., Randolph MF. Numerical prediction of collapse loads using finite element methods. Int. J. Numer. Anal. Meth. Eng. Geomech. 1982; 6: 47–76.

29. Stein E., Zhang G., Huang Y. Modeling and computation of shakedown problems for non-linear hardening materials. *Comput. Meth. Appl. Mech. Eng.*, 1993; **103:** 247–272.
30. Suquet P. Homogenization Techniques for Composite Media. Lecture Notes in Physics 272, Springer: New York, 1987.
31. Taliercio A. Lower and upper bounds to the macroscopic strength domain of a fiber-reinforced composite material. *Int. J. Plasticity* 1992; **8:** 741–762.
32. Taliercio A., Sagramoso P. Uniaxial strength of polymeric-matrix fibrous composites predicted through a homogenization approach. *Int. J. Solid. Struct.* 1995; **14:** 2095–2123.
33. Tarn JQ., Dvorak GJ., Rao MSM. Shakedown of unidirectional composites. *Int. J. Solid. Struct.* 1975; **11:** 751–764.
34. Tirosh J. The dual shakedown conditions for dilute fibrous composites. *J. Mech. Phys. Solids* 1998; **46:** 167–185.
35. Weichert D., Groß-Weege J. On the influence of geometrical non-linearities on the shakedown of elastic-plastic structures. *Int. J. Plasticity* 1986; **2:** 135–148.
36. Weichert D., Hachemi A., Schwabe F. Application of shakedown analysis to the plastic design of composites. *Arch. Appl. Mech.* 1999; **69:** 623–633.
37. Weichert D., Hachemi A., Schwabe F. Shakedown analysis of composites. *Mech. Res. Commun.* 1999; **26:** 309–318.
38. Xue MD., Wang XF., Williams FW., Xu BY. Lower-bound shakedown analysis of axisymmetric structures subjected to variable mechanical and thermal loads. *Int. J. Mech. Sci.* 1997; **39:** 965–976.
39. Yu HS., Hossain MZ. Lower bound shakedown analysis of layered pavements using discontinuous stress field. *Comput. Meth. Appl. Mech. Eng.* 1998; **167:** 209–222.
40. Yu HS., Houlsby GT., Burd HJ. A novel isoparametric finite element formulation for axisymmetric analysis of nearly incompressible materials. *Int. J. Num. Meth. Eng.* 1993; 36: 2453–2472.
41. Yu HS., Netherton MD. Performance of displacement finite elements for modeling incompressible materials. *Int. J. Numer. Anal. Meth. Eng. Geomech.* 2000; **24:** 627–653.
42. Zhang HY., Daehn G.S., Wagoner RH. Simulation of the plastic response of whisker reinforced metal matrix composites under thermal cycling conditions. *Scripta Metallurgica et Materialia* 1991; **25:** 2285–2290.
43. Zhang PX., Lu MW., Hwang K. A mathematical programming algorithm for limit analysis. *Acta Mech. Sinica* 1991; **7:** 267–274.
44. Zienkiewicz OC., Taylor RL., Too TM. Reduced integration technique in general analysis of plates and shells. Int. J. Num. Meth Eng. 1971; 3: 275–290.

A Non-linear Programming Approach to Shakedown Analysis for a General Yield Condition

H.S. Yu and H.X. Li

Abstract A non-linear programming approach combined with the finite element method is developed to directly calculate the shakedown load of structures. The analysis is based on a general yield condition, which can be used for both isotropic materials (e.g. von Mises' and Mohr-Coulomb's criteria) and anisotropic materials (e.g. Hill's criterion). By means of the associated flow rule, a general, non-linear yield criterion can be directly introduced into the kinematic shakedown theorem without linearization and a non-linear, purely kinematic formulation is obtained. The corresponding finite element formulation is developed as a non-linear mathematical programming problem subject to only a small number of equality constraints. So, the computational effort is very modest. A direct iterative algorithm is proposed to solve the resulting non-linear programming problem, which is validated by numerical simulations.

1 Introduction

Shakedown analysis is a direct method to calculate the bearing capacity and the stability condition of an elastoplastic structure subjected to variable loads. This can provide a powerful tool for the engineering design and safety estimation of structures. When a variable load is applied to a structure, three conditions may occur: purely elastic (the applied load magnitude is lower than the elastic limit); shakedown (the load is larger than the elastic

Hai-Sui Yu

School of Civil Engineering, University of Nottingham, Nottingham NG7 2RD, UK,
e-mail: hai-sui.yu@nottingham.ac.uk.

Hua-Xiang Li

Department of Engineering Science, University of Oxford, Oxford OX1 3PJ, UK,
e-mail: huaxiang.li@eng.ox.ac.uk

limit but is less than a critical limit), and non-shakedown (the applied load is higher than the shakedown limit, a non-restricted plastic flow will occur). If the non-shakedown condition happens, the structure may undergo the failure mode of either incremental collapse (ratchetting) or alternating plasticity (low cycle fatigue).

Shakedown analysis is based on two fundamental shakedown theorems, the static or lower bound theorem [24] and the kinematic or upper bound theorem [15]. The early research works were mainly focused on the theoretical analysis for simple structures. Due to the complexity of engineering problems, numerical techniques are required for shakedown analysis. Over the last two decades, with the rapid development of computational techniques, the numerical methods of shakedown analysis have been developed rapidly (e.g. [3, 4, 7–9, 14, 22, 23, 25, 26, 32–38, 42–44]). However, these works are mostly for von Mises' yield criterion.

For the stability problem of soil structure under repeated/cycle loads, there are some works based on shakedown analysis, which applied the Mohr-Coulomb or Drucker-Prager criteria in static or kinematic shakedown theorems [2, 5, 6, 10, 27–29, 31, 39, 40].

Recently, Li and Yu [19] developed a novel non-linear numerical approach to perform limit analysis for a general yield criterion by means of a non-linear mathematical programming technique and the finite element method. Kinematic limit analysis was finally constructed as a non-linear mathematical programming problem and an upper bound to the limit load of a structure subjected to static loads can be calculated. The proposed method is based entirely on kinematically admissible velocities without calculation of stress fields and only a single equality constraint is introduced into the non-linear programming problem. Therefore, the computational effort is very modest. Moreover, the proposed method is based on a general yield criterion, which covers most of current yield criteria.

The purpose of this work is to extend the non-linear technique of Li and Yu [19] for limit analysis to shakedown analysis. A general yield criterion defined by a second-order polynomial is used, which makes the developed method suitable for most of frequently-used yield criteria. Non-linear yield surfaces are not linearized and are directly introduced into the kinematic shakedown analysis. This can significantly reduce the number of constraints and the computational error. The finite element model of shakedown analysis is formulated as a non-linear programming problem subject to a small number of equality constraints, which can be solved by a direct iterative algorithm. The objective function corresponding to plastic dissipation power is to be minimized and then an upper bound to shakedown limit is calculated. The purely kinematic formulation for shakedown analysis has the advantage that the shakedown limit can be solved without calculation of stress fields.

2 Shakedown Analysis Based on a General Yield Criterion

In shakedown analysis, the material is assumed to be elastic-perfectly plastic. The problem consists of a body V with boundary Γ, which experiences a cyclic load on Γ_t. On the remainder of Γ, namely Γ_u, the displacement rate is fixed to zero. In order to use the finite element method, the responses of the body to the load, true stress $\boldsymbol{\sigma}$ and true strain $\boldsymbol{\varepsilon}$, are represented as column vectors, e.g., in a 2D model, $\boldsymbol{\varepsilon} = [\varepsilon_{11}, \varepsilon_{22}, 2\varepsilon_{12}]^\mathrm{T}$, and $\boldsymbol{\sigma} = [\sigma_{11}, \sigma_{22}, \sigma_{12}]^\mathrm{T}$, and in a 3D model, $\boldsymbol{\varepsilon} = [\varepsilon_{11}, \varepsilon_{22}, \varepsilon_{33}, 2\varepsilon_{12}, 2\varepsilon_{23}, 2\varepsilon_{31}]^\mathrm{T}$, and $\boldsymbol{\sigma} = [\sigma_{11}, \sigma_{22}, \sigma_{33}, \sigma_{12}, \sigma_{23}, \sigma_{31}]^\mathrm{T}$.

2.1 A General Yield Criterion

Many widely used yield criteria for materials can be expressed in a general form as follows:

$$F(\boldsymbol{\sigma}) = \boldsymbol{\sigma}^\mathrm{T} \boldsymbol{P} \boldsymbol{\sigma} + \boldsymbol{\sigma}^\mathrm{T} \boldsymbol{Q} - 1 = 0 , \tag{1}$$

where $F(\boldsymbol{\sigma})$ defines a yield function in terms of strength parameters, and $\boldsymbol{P}$ and $\boldsymbol{Q}$ are coefficient matrices and related to the strength properties of the material.

The expression (1) can be regarded as a general yield criterion for frictional materials. For example, the Mohr-Coulomb criterion in the plane strain model can be expressed as

$$\begin{aligned} F(\sigma_{ij}) = {} & (\sigma_{xx} - \sigma_{yy})^2 + (2\sigma_{xy})^2 \\ & - (2c \cos \varphi - (\sigma_{xx} + \sigma_{yy}) \sin \varphi)^2 = 0 , \end{aligned} \tag{2}$$

where c and φ are the cohesion and internal friction angle of the material respectively.

If the following relations are adopted, the Mohr-Coulomb criterion (2) can be expressed in the form of Eq. (1):

$$\boldsymbol{P} = \begin{bmatrix} \dfrac{1}{4c^2} & \dfrac{-1 - \sin^2 \varphi}{4c^2 \cos^2 \varphi} & 0 \\[3mm] \dfrac{-1 - \sin^2 \varphi}{4c^2 \cos^2 \varphi} & \dfrac{1}{4c^2} & 0 \\[3mm] 0 & 0 & \dfrac{1}{c^2 \cos^2 \varphi} \end{bmatrix} , \tag{3}$$

$$\boldsymbol{Q} = \begin{bmatrix} \dfrac{\sin \varphi}{c \cos \varphi} & \dfrac{\sin \varphi}{c \cos \varphi} & 0 \end{bmatrix}^\mathrm{T} . \tag{4}$$

2.2 Kinematic Theorem of Shakedown Analysis

An upper bound to the shakedown limit of a structure can be obtained using the kinematic theorem of shakedown analysis [15]: "Shakedown can not occur for a structure subject to repeated or cyclic loads when the rate of plastic dissipation power is less than the work rate done by the applied tractions and body forces for at least one admissible cycle of plastic strain". In other words, shakedown occurs if the rate of plastic dissipation power exceeds the work rate due to external forces for any admissible cycle of plastic strain.

Since the kinematic shakedown theorem is based on kinematically admissible plastic strain rates, it can be formulated as follows:

$$\lambda_{sd} \int_0^T \left(\int_{\Gamma_t} t_i \dot{u}_i^* d\Gamma + \int_V f_i \dot{u}_i^* dv \right) dt \leq \int_0^T \int_V D(\dot{\varepsilon}_{ij}^{p^*}) dv \, dt \,, \qquad (5)$$

where λ_{sd} is the shakedown load multiplier, t_i is the basic load of surface tractions, f_i is the basic load of body force, t_i and f_i are cyclic over a time interval $[0, T]$, $\dot{u}_i$ is the displacement velocity, $\dot{\varepsilon}_{ij}^p$ is the plastic strain rate, "$D(\dot{\varepsilon}_{ij}^{p^*})$" denotes a function for the rate of plastic dissipation power in terms of the admissible strain rate $\dot{\varepsilon}_{ij}^{p^*}$, and the superscript "*" stands for a parameter corresponding to the kinematically admissible strain field.

By applying the principle of virtual work to the first term of the left-hand side of Eq. (5), one can obtain

$$\int_0^T \int_{\Gamma_t} t_i \dot{u}_i^* d\Gamma dt = \int_0^T \int_V \sigma_{ij}^e (\dot{\varepsilon}_{ij}^{p^*} + C_{ijkl} \dot{\rho}_{kl}^{s^*}) dv \, dt$$
$$= \int_0^T \int_V \sigma_{ij}^e \dot{\varepsilon}_{ij}^{p^*} dv \, dt \,, \qquad (6)$$

where σ_{ij}^e is the linear elastic stress response to the current external traction t_i, C_{ijkl} is the elastic compliance tensor, and $\dot{\rho}_{kl}^{s^*}$ is the self-equilibrated, residual stress rate associated with $\dot{\varepsilon}_{ij}^{p^*}$.

Based on the mathematical programming theory and applying (6) to (5), the kinematic shakedown theorem can be re-expressed as the following programming problem, if the body force is omitted:

$$\begin{cases} \lambda_{sd} = \min_{\dot{\varepsilon}_{ij}^{p^*}, \Delta u_i} \int_0^T \int_V D(\dot{\varepsilon}_{ij}^{p^*}) dv dt \\[2mm] \text{s.t.} \quad \int_0^T \int_V \sigma_{ij}^e \dot{\varepsilon}_{ij}^{p^*} dv dt = 1 \,, \\[2mm] \Delta \varepsilon_{ij}^p = \int_0^T \dot{\varepsilon}_{ij}^{p^*} dt = \frac{1}{2}(\Delta u_{i,j} + \Delta u_{j,i}) \quad \text{in} V \,, \\[2mm] \Delta u_i = \int_0^T \dot{u}_i dt \qquad\qquad\qquad\qquad \text{in} V \,, \\[2mm] \Delta u_i = 0 \qquad\qquad\qquad\qquad\qquad\quad \text{on } \Gamma_u, \end{cases} \qquad (7)$$

where $\Delta\varepsilon_{ij}^p$ and Δu_i are the cumulative plastic strain and displacement fields at the end of one loading cycle over the time interval $[0,\ T]$ respectively.

Finally shakedown analysis is formulated as calculation of shakedown multiplier λ_{sd}, with $\lambda_{sd}t_i$ being shakedown limit.

2.3 Plastic Dissipation Power for a General Yield Criterion

Since the kinematic shakedown analysis is based on displacement modes, the stress terms need to be expressed in terms of the strain terms (i.e. the plastic dissipation power per unit volume in Eq. (7) should be expressed in terms of strain fields, which can be obtained by using the yield criterion and a plastic flow rule). The plastic flow rule determines the direction of the plastic strain rate with the following normality relation:

$$\dot{\varepsilon}_{ij}^p = \dot{\mu}\frac{\partial\psi(\sigma_{ij})}{\partial\sigma_{ij}}\ ,\tag{8}$$

where $\psi(\sigma_{ij})$ denotes a plastic potential function that resembles the yield function and $\dot{\mu}$ is a non-negative plastic proportionality factor. If the flow rule is assumed to be associated, i.e. $\psi(\sigma_{ij}) = F(\sigma_{ij})$, the plastic strain rate can be expressed as

$$\dot{\boldsymbol{\varepsilon}}^p = 2\dot{\mu}\boldsymbol{P}\boldsymbol{\sigma} + \dot{\mu}\boldsymbol{Q}\ .\tag{9}$$

By introducing Eq. (9) into the yield criterion (1), the plastic proportionality factor $\dot{\mu}$ can be determined by:

$$\dot{\mu} = \sqrt{\frac{(\dot{\boldsymbol{\varepsilon}}^p)^{\mathrm{T}}\boldsymbol{P}^{-1}\dot{\boldsymbol{\varepsilon}}^p}{4 + \boldsymbol{Q}^{\mathrm{T}}\boldsymbol{P}^{-1}\boldsymbol{Q}}}\ .\tag{10}$$

Then, the plastic dissipation power for the general criterion (1) is expressed as:

$$\begin{aligned}
\mathrm{D}(\dot{\varepsilon}_{ij}^p) = \sigma_{ij}\dot{\varepsilon}_{ij}^p = \boldsymbol{\sigma}^{\mathrm{T}}\dot{\boldsymbol{\varepsilon}}^p &= \left(\frac{1}{2\dot{\mu}}\boldsymbol{P}^{-1}\dot{\boldsymbol{\varepsilon}}^p - \frac{1}{2}\boldsymbol{P}^{-1}\boldsymbol{Q}\right)^{\mathrm{T}}\dot{\boldsymbol{\varepsilon}}^p \\
&= \frac{1}{2\dot{\mu}}(\dot{\boldsymbol{\varepsilon}}^p)^{\mathrm{T}}\boldsymbol{P}^{-1}\dot{\boldsymbol{\varepsilon}}^p - \frac{1}{2}(\dot{\boldsymbol{\varepsilon}}^p)^{\mathrm{T}}\boldsymbol{P}^{-1}\boldsymbol{Q} \\
&= \frac{1}{2}\sqrt{\left((\dot{\boldsymbol{\varepsilon}}^p)^{\mathrm{T}}\boldsymbol{P}^{-1}\dot{\boldsymbol{\varepsilon}}^p\right)\cdot(4 + \boldsymbol{Q}^{\mathrm{T}}\boldsymbol{P}^{-1}\boldsymbol{Q})} - \frac{1}{2}(\dot{\boldsymbol{\varepsilon}}^p)^{\mathrm{T}}\boldsymbol{P}^{-1}\boldsymbol{Q}.
\end{aligned}\tag{11}$$

As a result, the kinematic shakedown analysis can be formulated as

$$
\begin{cases}
\lambda_{sd} = \min\limits_{\dot\varepsilon^p_{ij},\Delta u_i} \int_0^T \int_V \left(\dfrac{1}{2}\sqrt{\left((\dot{\boldsymbol\varepsilon}^p)^{\mathrm T}\boldsymbol{P}^{-1}\dot{\boldsymbol\varepsilon}^p\right)\cdot(4+\mathbf{Q}^{\mathrm T}\boldsymbol{P}^{-1}\boldsymbol{Q})-}{\dfrac{1}{2}(\dot{\boldsymbol\varepsilon}^p)^{\mathrm T}\boldsymbol{P}^{-1}\boldsymbol{Q}} \right) \mathrm{d}v\mathrm{d}t \\[4pt]
\text{s.t.} \quad \int_0^T \int_V \sigma^e_{ij}\dot\varepsilon^p_{ij}\mathrm{d}v\mathrm{d}t = 1, \\[4pt]
\Delta\varepsilon^p_{ij} = \int_0^T \dot\varepsilon^p_{ij}\mathrm{d}t = \dfrac{1}{2}(\Delta u_{i,j}+\Delta u_{j,i}) \qquad\qquad \text{in } V, \\[4pt]
\Delta u_i = \int_0^T \dot u_i\mathrm{d}t \text{ in } V, \quad \Delta u_i = 0 \qquad\qquad\qquad \text{on}\, \varGamma_u.
\end{cases}
$$

$$(12a,b,c,d)$$

2.4 Removal of the Time Integration

To apply the mathematical programming formulation (12) to a structure, the time integration must be removed because it is difficult to calculate integration along a deformation path. The potential difficulty can be overcome by König's technique [16, 17].

Due to cyclic loading, the load domain $\varOmega$ can be thought of as a load space, the shape of which is a hyper polyhedron defined by a convex linear combination of load vertices $\boldsymbol{P}_k(k = 1, 2, \ldots, l)$. It is assumed that if a structure reaches a state of shakedown under any load vertices, then it will shakedown under the whole load domain $\varOmega$. The cyclic loading remains constant over a time interval $\tau_k(\sum\limits_{k=1}^{l}\tau_k = T)$ on each vertex, and the admissible plastic strain cycles on these vertices can generate a plastic strain increment:

$$
\varepsilon^p_k = \int_{\tau_k} \dot{\boldsymbol\varepsilon}^p\mathrm{d}t \qquad (k = 1, 2, \ldots, l). \tag{13}
$$

Then the cumulative plastic strain at the end of one loading cycle over the time interval $[0, T]$ can be obtained as follows

$$
\Delta\varepsilon^p = \sum_{k=1}^{l} \varepsilon^p_k. \tag{14}
$$

Finally, the kinematic shakedown analysis of a structure subject to repeated or cyclic loads can be expressed as the following non-linear mathematical programming problem:

$$
\begin{cases}
\lambda_{sd} = \min_{\boldsymbol{\varepsilon}_k^p, \Delta \boldsymbol{u}} \sum_{k=1}^{l} \int_V \left(\begin{array}{l} \dfrac{1}{2}\sqrt{((\boldsymbol{\varepsilon}_k^p)^{\mathrm{T}} \boldsymbol{P}^{-1} \boldsymbol{\varepsilon}_k^p) \cdot (4 + \boldsymbol{Q}^{\mathrm{T}} \boldsymbol{P}^{-1} \boldsymbol{Q})} \\ -\dfrac{1}{2}(\boldsymbol{\varepsilon}_k^p)^{\mathrm{T}} \boldsymbol{P}^{-1} \boldsymbol{Q} \end{array} \right) \mathrm{d}v \\[4mm]
\text{s.t.} \quad \sum_{k=1}^{l} \int_V (\boldsymbol{\sigma}_k^e)^{\mathrm{T}} \boldsymbol{\varepsilon}_k^p \mathrm{d}v = 1, \\[3mm]
\qquad \Delta \boldsymbol{\varepsilon}^p = \sum_{k=1}^{l} \boldsymbol{\varepsilon}_k^p = \Psi(\Delta \boldsymbol{u}) & \text{in } V, \\[3mm]
\qquad \Delta \boldsymbol{u} = 0 & \text{on } \Gamma_u,
\end{cases}
\tag{15}
$$

where Ψ is a linear compatibility differential operator which is defined by Eq. (12c).

3 Finite Element Modelling

The traditional displacement-based finite element method is used in this paper to perform the numerical calculation for the kinematic limit analysis (15). The structure is discretized into finite elements $V_e(V = \overset{N}{\underset{e=1}{\mathrm{U}}} V_e)$. Then, the displacement velocity and strain rate fields can be interpolated in terms of an unknown nodal displacement velocity vector:

$$
\Delta \boldsymbol{u}_e(\boldsymbol{x}) = \boldsymbol{N}_e(\boldsymbol{x}) \Delta \boldsymbol{\delta}_e \tag{16}
$$

$$
\Delta \boldsymbol{\varepsilon}_e(\boldsymbol{x}) = \boldsymbol{B}_e(\boldsymbol{x}) \Delta \boldsymbol{\delta}_e \tag{17}
$$

where, with reference to the $\boldsymbol{e}$-th finite element, $\Delta \boldsymbol{\delta}_e$ is the nodal cumulative displacement column vector over a loading cycle, $\boldsymbol{N}_e$ is the interpolation function, and $\boldsymbol{B}_e$ is the strain function.

By applying the Gaussian integration technique to the objective function and normalization condition in Eq. (15), finally, the finite element modelling of kinematic shakedown analysis can be expressed as the following non-linear programming problem:

$$
\begin{cases}
\lambda_{sd} = \min_{\boldsymbol{\varepsilon}_{kr}^p, \Delta \boldsymbol{\delta}} \sum_{k=1}^{l} \sum_{r=1}^{n} \rho_r |J|_r \cdot \\[3mm]
\left(\dfrac{1}{2}\sqrt{((\boldsymbol{\varepsilon}_{kr}^p)^{\mathrm{T}} \boldsymbol{P}^{-1} \boldsymbol{\varepsilon}_{kr}^p) \cdot (4 + \boldsymbol{Q}^{\mathrm{T}} \boldsymbol{P}^{-1} \boldsymbol{Q})} - \dfrac{1}{2}(\boldsymbol{\varepsilon}_{kr}^p)^{\mathrm{T}} \boldsymbol{P}^{-1} \boldsymbol{Q} \right) \\[4mm]
\text{s.t.} \quad \sum_{k=1}^{l} \sum_{r=1}^{n} \rho_r |J|_r (\boldsymbol{\sigma}_{kr}^e)^{\mathrm{T}} \boldsymbol{\varepsilon}_{kr}^p = 1, \\[3mm]
\qquad \Delta \boldsymbol{\varepsilon}_r^p = \sum_{k=1}^{l} \boldsymbol{\varepsilon}_{kr}^p = \boldsymbol{B}_r \Delta \boldsymbol{\delta} \quad (r = 1, 2, \cdots, n),
\end{cases}
\tag{18a,b,c}
$$

where, with reference to the r-th Gaussian integral point, ρ_r is the integral weight, $|J|_r$ is the determinant of the Jacobian matrix, n is the number of Gaussian integral points of FE-discretized structure, $\Delta\boldsymbol{\delta}$ is a global nodal cumulative displacement vector over a loading cycle, $\boldsymbol{B}_r$ is the strain matrix at the r-th Gaussian integral point, $\boldsymbol{B}_r = \boldsymbol{B}_e \cdot \boldsymbol{C}_e$, and $\boldsymbol{C}_e$ is the transformation matrix which assembles element matrix into global matrix.

Then, a minimum optimized upper bound λ_{sd} to shakedown limit multiplier can be obtained by solving the above mathematical programming problem and the shakedown limit is given by $\lambda_{sd}\boldsymbol{F}$.

4 Iterative Solution Algorithm

The kinematic shakedown analysis (18) is a mathematical programming problem subject to equality constraints. The objective function is non-linear, continuous, but may be nondifferentiable, which results from the calculation of square root. A linear nondifferentiable programming problem, if the objective function is finite and continuous in a feasible set, it is not necessary to be differentiable everywhere and an optimal solution can be obtained [30]. For a non-linear programming problem similar to Eq. (18), which was constructed to perform limit and shakedown analyses for von Mises criterion [18, 20, 41], was overcome by means of an iterative algorithm [41], where a technique based on distinguishing rigid/plastic areas was developed. Li and Yu [19] developed a general iterative algorithm to solve the non-linear problem for limit analysis. It can be extended to solve the non-linear programming problem (18).

4.1 Minimum Optimization Strategy

According to the mathematical programming theory, an equality constraint is often introduced into an optimization problem by means of the Lagrangean method [1, 11, 12, 21], which is also used here to remove the equality constraints (the normalization condition (18b), and the geometric compatibility (18c)). As a result, an unconstrained minimum optimization problem is obtained as

$$
L(\boldsymbol{\varepsilon}_{kr}^p, \Delta\boldsymbol{\delta}, \lambda, \boldsymbol{L}_r)
$$

$$
= \sum_{k=1}^{l}\sum_{r=1}^{n} \rho_r |J|_r \left(\frac{1}{2}\sqrt{((\boldsymbol{\varepsilon}_{kr}^p)^{\mathrm{T}}\boldsymbol{P}^{-1}\boldsymbol{\varepsilon}_{kr}^p)\cdot(4 + \boldsymbol{Q}^{\mathrm{T}}\boldsymbol{P}^{-1}\boldsymbol{Q})} - \frac{1}{2}(\boldsymbol{\varepsilon}_{kr}^p)^{\mathrm{T}}\boldsymbol{P}^{-1}\boldsymbol{Q} \right)
$$

$$
+ \lambda\left(1 - \sum_{k=1}^{l}\sum_{r=1}^{n}\rho_r|J|_r(\boldsymbol{\sigma}_{kr}^e)^{\mathrm{T}}\boldsymbol{\varepsilon}_{kr}^p \right) + \sum_{r=1}^{n}\boldsymbol{L}_r^{\mathrm{T}}\left(\sum_{k=1}^{l}\boldsymbol{\varepsilon}_{kr}^p - \boldsymbol{B}_r\Delta\boldsymbol{\delta} \right) \quad (19)
$$

where λ and $\boldsymbol{L}_r$ are Lagrangean multipliers.

According to the Kuhn-Tucker stationary condition, the following formulation can be obtained for solving the kinematic shakedown analysis problem (18) by applying $\dfrac{\partial L}{\partial \varepsilon_{kr}^p} = \boldsymbol{0}, \ \dfrac{\partial L}{\partial \Delta \boldsymbol{\delta}} = \boldsymbol{0}, \ \dfrac{\partial L}{\partial \lambda} = 0, \ \dfrac{\partial L}{\partial \boldsymbol{L}_r} = \boldsymbol{0}$ to Eq. (19):

$$
\begin{cases}
\dfrac{\boldsymbol{P}^{-1}\left(4+\boldsymbol{Q}^{\mathrm{T}}\boldsymbol{P}^{-1}\boldsymbol{Q}\right)}{2\sqrt{\left((\varepsilon_{kr}^p)^{\mathrm{T}}\boldsymbol{P}^{-1}\varepsilon_{kr}^p\right)\cdot(4+\boldsymbol{Q}^{\mathrm{T}}\boldsymbol{P}^{-1}\boldsymbol{Q})}}\varepsilon_{kr}^p - \lambda\boldsymbol{\sigma}_{kr}^e + (\rho_r|J|_r)^{-1}\boldsymbol{L}_r \\[4pt]
\quad -\dfrac{1}{2}\boldsymbol{P}^{-1}\boldsymbol{Q} = 0, \qquad (k=1,2,\cdots,l; r=1,2,\cdots,n) \\[4pt]
\displaystyle\sum_{r=1}^{n}\left(\boldsymbol{B}_r^{\mathrm{T}}\boldsymbol{L}_r\right) = 0, \\[4pt]
\displaystyle\sum_{k=1}^{l}\sum_{r=1}^{n}\rho_r|J|_r(\boldsymbol{\sigma}_{kr}^e)^{\mathrm{T}}\varepsilon_{kr}^p = 1, \\[4pt]
\displaystyle\sum_{k=1}^{l}\varepsilon_{kr}^p - \boldsymbol{B}_r\Delta\boldsymbol{\delta} = 0 \quad (r=1,2,\cdots,n).
\end{cases}
$$

$$(20\text{a,b,c,d})$$

It is quite difficult to directly solve the optimization problem (20) because it is non-linear and nondifferentiable. So, a set of solving formulations based on an iteration technique for the problem (20) can be obtained as:

$$
\begin{cases}
(\boldsymbol{H}_{kr})_{ICP}\varepsilon_{kr}^p - \lambda\boldsymbol{\sigma}_{kr}^e + (\rho_r|J|_r)^{-1}\boldsymbol{L}_r - \dfrac{1}{2}\boldsymbol{P}^{-1}\boldsymbol{Q} = \boldsymbol{0} \\[4pt]
\qquad (k=1,2,\cdots,l; r=1,2,\cdots,n) \\[4pt]
\displaystyle\sum_{r=1}^{n}\left(\boldsymbol{B}_r^{\mathrm{T}}\boldsymbol{L}_r\right) = 0 \\[4pt]
\displaystyle\sum_{k=1}^{l}\sum_{r=1}^{n}\rho_r|J|_r(\boldsymbol{\sigma}_{kr}^e)^{\mathrm{T}}\varepsilon_{\boldsymbol{kr}}^{\boldsymbol{p}} = 1 \\[4pt]
\displaystyle\sum_{k=1}^{l}\varepsilon_{kr}^p - \boldsymbol{B}_r\Delta\boldsymbol{\delta} = 0 \quad (r=1,2,\cdots,n)
\end{cases}
$$

$$(21\text{a,b,c,d})$$

where $\boldsymbol{H}_{kr}$ is the coefficient matrix, which is defined by

$$
(\boldsymbol{H}_{kr})_{ICP} = \frac{1}{2}\boldsymbol{P}^{-1}\left(4+\boldsymbol{Q}^{\mathrm{T}}\boldsymbol{P}^{-1}\boldsymbol{Q}\right)(z_{kr})_{ICP}^{-1} \tag{22}
$$

and the subscript "ICP" indicates that the variable is an *Iteration Control Parameter*. The parameter z_{kr} is defined by

$$
z_{kr} = \sqrt{\left((\varepsilon_{kr}^p)^{\mathrm{T}}\boldsymbol{P}^{-1}\varepsilon_{kr}^p\right)\cdot(4+\boldsymbol{Q}^{\mathrm{T}}\boldsymbol{P}^{-1}\boldsymbol{Q})} \tag{23}
$$

By solving the set of linearized equations (21), the variable ε_{kr}^p can be calculated and then the shakedown load multiplier is determined as

$$
\lambda_{sd} = \sum_{k=1}^{l} \sum_{r=1}^{n} \rho_r |J|_r
$$
$$
\cdot \left(\frac{1}{2} \sqrt{ \left((\varepsilon_{kr}^p)^{\mathrm{T}} \boldsymbol{P}^{-1} \varepsilon_{kr}^p \right) \cdot (4 + \boldsymbol{Q}^{\mathrm{T}} \boldsymbol{P}^{-1} \boldsymbol{Q}) } - \frac{1}{2} (\varepsilon_{kr}^p)^{\mathrm{T}} \boldsymbol{P}^{-1} \boldsymbol{Q} \right). \qquad (24)
$$

4.2 Iterative Strategy

In order to overcome the numerical difficulty of non-linearity and unsmoothness in Eq. (19), all of non-differentiable areas need to be identified where
$z_{kr} = \sqrt{ \left((\varepsilon_{kr}^p)^{\mathrm{T}} \boldsymbol{P}^{-1} \varepsilon_{kr}^p \right) \cdot (4 + \boldsymbol{Q}^{\mathrm{T}} \boldsymbol{P}^{-1} \boldsymbol{Q}) } = 0$ by an iterative technique.
The iteration starts with the hypothesis that there is no non-differentiable area in the whole structure but all non-differentiable areas will be found by a step-by-step iterative technique.

Step 0: initializing the non-linear objective function

The iteration starts with the plastic strain rate being non-zero everywhere in the structure, which can guarantee the iterative process will monotonically decrease towards the exact solution [13, 19]. The iteration seed can be chosen as:
$$
(z_{kr})_0 = 1 (k = 1, 2, \cdots, l; r = 1, 2, \cdots, n) \qquad (25)
$$

Accordingly, the set of Eq. (21) becomes linear and the objective variable $(\varepsilon_{kr}^p)_0$ can be calculated at this iterative step. Then, the initial shakedown load multiplier $(\lambda_{sd})_0$ can be determined by means of Eq. (24).

Step $h+1 (h = 0, 1, 2, \ldots)$: distinguishing the non-differentiable areas to revise the objective function

Based on the computational results at the iteration step h, the value of
$z_{kr} \left(z_{kr} = \sqrt{ \left((\varepsilon_{kr}^p)^{\mathrm{T}} \boldsymbol{P}^{-1} \varepsilon_{kr}^p \right) \cdot (4 + \boldsymbol{Q}^{\mathrm{T}} \boldsymbol{P}^{-1} \boldsymbol{Q}) } \right)$ needs to be updated at
every Gaussian integral point to check whether it is in a non-differentiable area. Then the Gaussian integral point set I will be subdivided into two subsets: a subset $(I_E)_{h+1}$ where the objective function is not differentiable, and a subset $(I_P)_{h+1}$ where the objective function is differentiable. Then, the coefficient matrix $\boldsymbol{H}_{kr}$ will be updated as

$$
(\boldsymbol{H}_{kr})_{h+1} = \begin{cases} \beta \boldsymbol{P}^{-1} & r \in (I_E)_{h+1}, \\ \frac{1}{2} \boldsymbol{P}^{-1} \left(4 + \boldsymbol{Q}^{\mathrm{T}} \boldsymbol{P}^{-1} \boldsymbol{Q} \right) (z_{kr})_{ICP}^{-1} & r \in (I_P)_{h+1}, \end{cases} \qquad (26)
$$

where β is the penalization factor, which is used to introduce the non-differentiable area as a constraint into the programming problem. In practice, the typical value of β is from 10^6 to 10^{12}.

By solving the set of linearized equations (21), the objective variables $(\varepsilon^p_{kr})_{h+1}$ can then be calculated and the shakedown load multiplier $(\lambda_{sd})_{h+1}$ can be determined by means of Eq. (24).

The above iteration is repeated until the following convergence criteria are satisfied

$$\left\{\frac{|(\lambda_{sd})_{h+1} - (\lambda_{sd})_h|}{|(\lambda_{sd})_{h+1}|} \leq \eta_1, \quad \frac{\|\Delta\boldsymbol{\delta}_{h+1} - \Delta\boldsymbol{\delta}_h\|}{\|\Delta\boldsymbol{\delta}_{h+1}\|} \leq \eta_2,\right. \tag{27a,b}$$

where η_1 and η_2 are computational error tolerances. Through a monotonically decreasing convergence sequence the above iterative process leads to the shakedown load multiplier λ_{sd} and a minimum optimal upper bound to the shakedown multiplier can be obtained.

4.3 Solution of Linearized Equations

By means of the preceding iteration technique, the set of Eq. (21) is linearized at each step of iteration and then solved. However, the linearized set of equations can not be directly solved to obtain the values of all variables because it is involved in solving a set of implicit equations. Additional manipulations are needed to eliminate the difficulty from the implicit feature. Based on the linearization by means of the proposed iterative algorithm, the set of Eq. (21) can be solved by the following strategy:

(a) Subtract the equation sets (21a) corresponding to a vertex, say m, from all the other Eq. (21a) to obtain

$$\varepsilon^p_{kr} = (\mathbf{H}_{kr})^{-1}_{ICP} \{\lambda\boldsymbol{\sigma}^e_{kr} - \lambda\boldsymbol{\sigma}^e_{mr} + (\mathbf{H}_{mr})_{ICP}\varepsilon^p_{mr}\} \tag{28}$$

(b) Substitute (28) into (21d), then the latter becomes

$$\varepsilon^p_{mr} = (\boldsymbol{H}_{mr})^{-1}_{ICP} \left(\sum_{k=1}^l (\boldsymbol{H}_{kr})^{-1}_{ICP}\right)^{-1}$$

$$\left\{\boldsymbol{B}_r\Delta\boldsymbol{\delta} + \lambda\sum_{k=1}^l (\boldsymbol{H}_{kr})^{-1}_{ICP}(\boldsymbol{\sigma}^e_{mr} - \boldsymbol{\sigma}^e_{kr})\right\} \tag{29}$$

(c) Substitute (29) into (21a) first and subsequently, this into (21b) to obtain

$$\left\{ \sum_{r=1}^{n} \rho_r |J|_r \boldsymbol{B}_r^{\mathrm{T}} \left(\sum_{k=1}^{l} (\boldsymbol{H}_{kr})_{ICP}^{-1} \right)^{-1} \boldsymbol{B}_r \right\} \boldsymbol{\Delta\delta} - \frac{1}{2} \sum_{r=1}^{n} \rho_r |J|_r \boldsymbol{B}_r^{\mathrm{T}} \boldsymbol{P}^{-1} \boldsymbol{Q}$$

$$= \lambda \sum_{r=1}^{n} \rho_r |J|_r \boldsymbol{B}_r^{\mathrm{T}} \left(\sum_{k=1}^{l} (\boldsymbol{H}_{kr})_{ICP}^{-1} \right)^{-1} \sum_{k=1}^{l} (\boldsymbol{H}_{kr})_{ICP}^{-1} \boldsymbol{\sigma}_{kr}^{e}$$

$$\tag{30}$$

(d) Substitute (29) into (21c) which thus becomes

$$\sum_{k=1}^{l} \sum_{r=1}^{n} \rho_r |J|_r (\boldsymbol{\sigma}_{kr}^{e})^{\mathrm{T}} (\boldsymbol{H}_{kr})_{ICP}^{-1} \left(\sum_{m=1}^{l} (\boldsymbol{H}_{mr})_{ICP}^{-1} \right)^{-1}$$

$$\tag{31}$$

$$\cdot \left\{ \boldsymbol{B}_r \boldsymbol{\Delta\delta} + \lambda \sum_{m=1}^{l} (\boldsymbol{H}_{mr})_{ICP}^{-1} (\boldsymbol{\sigma}_{kr}^{e} - \boldsymbol{\sigma}_{mr}^{e}) \right\} = 1$$

Finally, by solving the linear equation set of Eqs. (30) and (31), the variables $\boldsymbol{\Delta\delta}$ and λ can be calculated. Then, the remaining unknown variable ε_{kr}^{p} in Eq. (29) can be calculated and the shakedown load multiplier can be determined.

5 Applications

Pavements are civil engineering structures built for the purpose of allowing wheeled vehicles to operate safely and economically. The vehicles include cars and trucks on highway pavements, aircraft on airport runways and taxiways, mobile cranes on port and container terminal pavements together with locomotives and rolling stock on railways. By means of shakedown analysis, the effect of moving loads on the pavements can be revealed and the shakedown condition can be effectively determined.

In this section, a plane strain model is assumed for a pavement under moving loads, as shown in Fig. 1, where $p(0 \leq p \leq p^{\max})$ is normal load with trapezoidal load distribution applied to the pavement from a repeated loading, $p_0(0 \leq p \leq p_0^{\max})$ is the peak value of p, and q is shear force due to the friction between moving wheel and the pavement. Therefore, the relation between p and q is defined as:

$$q = \mu\, p, \tag{32}$$

where μ is the friction coefficient.

The size of the simulated region is determined as: $L = 10\mathrm{m}$, $H = 4\mathrm{m}$, $B = 1.0\mathrm{m}$, and $a = 0.5\mathrm{m}$, where L and H denote the length and height of
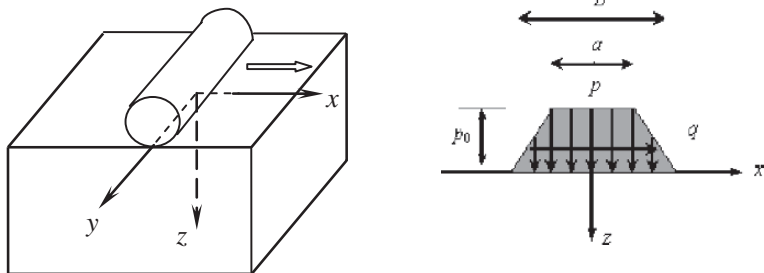
Fig. 1 2D model for a pavement under moving loads

the simulated region respectively, and B and a are the size of trapezoidally loading area. The selected body is discretized with 1750 eight-node quadrilateral finite elements, and the convergence tolerances adopted in the numerical simulation are $\eta_1 = \eta_2 = 10^{-3}$. The Mohr-Coulomb yield criterion is assumed to model the plastic behaviour of material with the Young's modulus $E = 100$MPa and the Poisson's ratio $\nu = 0.3$. In order to simulate the moving of loads on a pavement, it is assumed that the failure mode varies only along the depth.

First, in order to verify the validity of the proposed numerical method, a pavement without surface friction is considered, i.e. the coefficient of surface friction is equal to zero ($\mu = 0$). Therefore, there is only the normal loading p applied to the pavement and no shear force ($q = 0$). The numerical results of the dimensionless shakedown limits $\lambda_{sd}(\lambda_{sd} = p_0^{max}/c)$ with the variation of soil friction angle are presented in Fig. 2, where c and φ are the friction angle
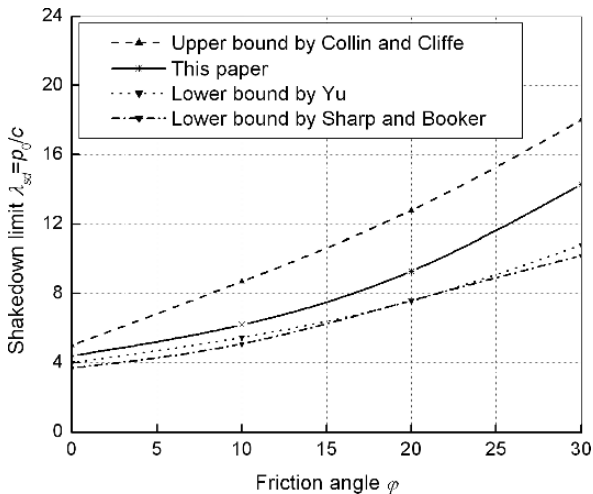

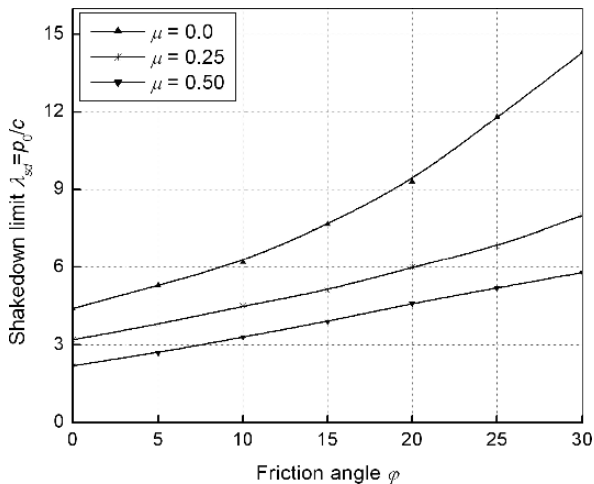**Fig. 2** Effect of friction angle on shakedown limits

Fig. 3 Shakedown limits with friction angles

and cohesion of material respectively. It can be concluded that the shakedown
limits obtained by the proposed method are closer to those upper bounds by
Collins and Cliffe [5], and a little larger than those lower bounds by Sharp
and Booker [29], and Yu [40].

The interactive effects of the internal friction angle and the friction coeffi-
cient of a pavement surface on the shakedown limits are shown in Figs. 3 and
4. It can be concluded that for a pavement under moving loads, both the fric-
tion angle of materials and the surface friction coefficient of a pavement have
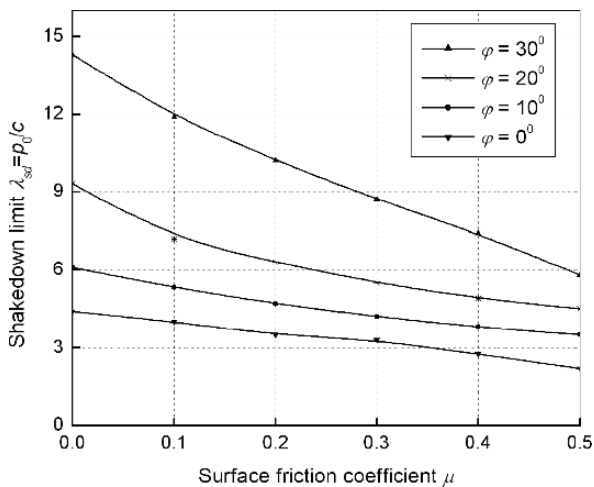a significant effect on its shakedown condition. For a pavement subjected to

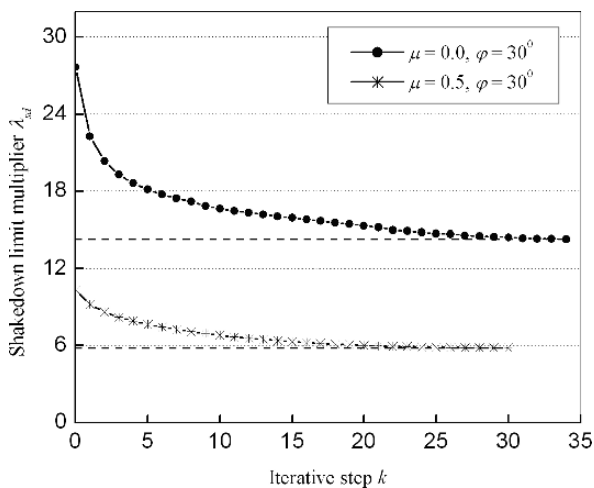**Fig. 4** Shakedown limits with surface friction coefficient

Fig. 5 The convergence sequence λ_{sd} with iterative steps

compressive forces, the shakedown limits increase significantly with the rising of the friction angle of materials, while they decrease rapidly with the rising of the surface friction coefficient.

The relation between the iterative convergence sequences λ_{sd} and the iterative step k is shown in Fig. 5 (for the cases $\mu = 0$, $\varphi = 30°$ and $\mu = 0.5$, $\varphi = 30°$). The numerical results show that the efficiency and numerical stability of the proposed algorithm are fairly high and that the amount of computational effort is very small.

6 Conclusions

A novel general numerical method has been developed to perform the kinematic shakedown analysis for a general yield condition by means of a non-linear programming technique in conjunction with the displacement-based finite element method. The proposed method is the extension of the non-linear programming technique applied to the numerical limit analysis [19]. By using an associated flow rule, the dissipation work based on a general yield criterion is explicitly expressed in terms of the kinematically admissible velocity. The yield surface does not need to be linearized, which can reduce the number of constraints and therefore computational costs. Based on the mathematical programming theory, the finite element model of the kinematic shakedown analysis is proposed as a non-linear programming problem subject to a small number of equality constraints. The numerical examples show that the proposed iterative algorithm has the advantages of high computational accuracy and good numerical stability.

References

1. Bazaraa, M.S., Sherali, H.D., Shetty, C.M. Non-linear Programming: Theory and Algorithms. Wiley, New York (2006)
2. Boulbibane, M., Weichert, D. Application of shakedown theory to soils with non associated flow rules. Mech. Res. Commun., 24, 513–519 (1997)
3. Carvelli, V., Cen, Z.Z., Liu. Y.H., Maier, G. Shakedown analysis of defective pressure vessels by a kinematic approach. Arch. Appl. Mech., 69, 751–764 (1999)
4. Chen, H.F., Ponter, A.R.S. Shakedown and limit analyses for 3-D structures using the linear matching method. Int. J. Pres. Vess. Pip., 78, 443–451 (2001)
5. Collins, I.F., Cliffe, P.F. Shakedown in frictional materials under moving surface loads. Int. J. Num. Analy. Meth. Geom., 11, 409–420 (1987)
6. Collins, I.F., Boulbibane, M. Geomechanical analysis of unbound pavements based on shakedown theory. J. Geot. Geoen. Eng., *ASCE*, 126, 50–59 (2000)
7. Feng, X.Q., Liu, X.S. On shakedown of three-dimensional elastoplastic strain-hardening structures. Int. J. Plasticity, 12, 1241–1256 (1997)
8. Genna, F. A non-linear inequality, finite element approach to the direct computation of shakedown load safety factors. Int. J. Mech. Sci., 30, 769–789 (1988)
9. Hachemi, A., Weichert, D. Numerical shakedown analysis of damaged structures. Comput. Meth. Appl. Mech. Eng., 160, 57–70 (1998)
10. Hamadouche, M.A., Weichert, D. Application of shakedown theory to soil dynamics. Mech. Res. Commun., 26, 565–574 (1999)
11. Hartley, R. Linear and Non-linear Programming: An Introduction to Linear Methods in Mathematical Programming. Prentice Hall, New York (1985)
12. Himmelblau, D.M. Applied Non-linear Programming. McGraw-Hill Book Company, New York (1972)
13. Huh, H., Yang, W.H. A general algorithm for limit solutions of plane stress problems. Int. J. Solid. Struct., 28, 727–738 (1991)
14. Khoi, V.D., Yan, A.M., Huang, N.D. A dual form for discretized kinematic formulation in shakedown analysis. Int. J. Solid. Struct., 41, 267–277 (2004)
15. Koiter, W.T. General theorems for elastic-plastic bodies. In: Sneddon IN, Hill R (eds). Progress in Solid Mechanics, North-Holland, Amsterdam, 165–221 (1960)
16. König, J.A. On upper bounds to shakedown loads. ZAMM, 59, 349–354 (1979)
17. König, J.A. Shakedown of Elastic-Plastic Structure. Elsevier, Amsterdam (1987)
18. Li, H.X., Liu, Y.H., Feng, X.Q., Cen, Z.Z. Limit analysis of ductile composites based on homogenization theory. Proc. Roy. Soc. London A 459, 659–675 (2003)
19. Li, H.X., Yu, H.S. Kinematic limit analysis of frictional materials using non-linear programming. Int. J. Solid. Struct. 42, 4058–4076 (2005)
20. Liu, Y.H., Cen, Z.Z., Xu, B.Y. A numerical method for plastic limit analysis of 3-D structures. Int. J. Solid. Struct. 32, 1645–1658 (1995)
21. Luenberger, D.G., Ye, Y. Linear and Non-linear Programming. Springer, New York (2007)
22. Maier, G. Shakedown theory in perfect elastoplasticity with associated and nonassociated flow-laws: a finite element linear programming approach. Meccanica, 4, 250–260 (1969)
23. Maier, G., Carvelli, G., Cocchetti, G. On direct methods of shakedown and limit analysis. Plenary Lecture, 4th Euromech Solid Mechanics Conference, Metz, June (2000)
24. Melan, E. Theorie Statisch Unbestimmter Tragwerke aus idealplastischem Baustoff. Sitzungsbericht der Akademie der Wissenschaften (Wien) Abt. IIA 195, 145–195 (1938)
25. Morelle, P. Numerical shakedown analysis of axisymmetric sandwich shells: an upper bound formulation. Int. J. Num. Meth. Eng., 23, 2071–2088 (1986)
26. Ponter, A.R.S., Engelhardt, M. Shakedown limits for a general yield condition: implementation and application for a von Mises yield condition. Eur. J. Mech. A/Solids, 19, 423–445 (2000)

27. Raad, L., Weichert, D., Najm, W. Stability of multilayer systems under repeated loads, Transp. Res. Record, 1207, 181–186 (1988)
28. Radovsky, B.S., Murashina, N.V. Shakedown of subgrade soil under repeated loading. Transp. Res. Record, 1547, 82–88 (1996)
29. Sharp, R.W., Booker J.R. Shakedown of pavements under moving surface loads. J. Transp. Eng., ASCE, 110, 1–14 (1984)
30. Shapiro, J.F. Mathematical Programming: Structures and Algorithms. A Wiley-Interscience Publication, New York (1979)
31. Shiau, S.H., Yu, H.S. Load and displacement prediction for shakedown analysis of layered pavements. Transp. Res. Record, 1730, 117–124 (2000)
32. Stein, E., Zhang, G., Konig, J.A. Shakedown with non-linear strain-hardening including structural computation using finite element method. Int. J. Plasticity, 8, 1–31 (1992)
33. Stein, E., Zhang, G., Huang, Y. Modeling and computation of shakedown problems for non-linear hardening materials. Comput. Meth. Appl. Mech. Eng., 103, 247–272 (1993)
34. Weichert, D. Shakedown at finite displacement: a note on Melan's theorem. Mech. Res. Commun., 11, 121–127 (1984)
35. Weichert, D., Groß-Weege, J. On the influence of geometrical non-linearities on the shakedown of elastic-plastic structures. Int. J. Plasticity, 2, 135–148 (1986)
36. Weichert, D., Hachemi, A., Schwabe, F. Shakedown analysis of composites. Mech. Res. Commun., 26, 309–318 (1999)
37. Weichert, D., Hachemi, A., Schwabe, F. Application of shakedown analysis to the plastic design of composites. Arch. Appl. Mech., 69, 623–633 (1999)
38. Xue, M.D., Wang, X.F., Williams, F.W., Xu, B.Y. Lower-bound shakedown analysis of axisymmetric structures subjected to variable mechanical and thermal loads. Int. J. Mech. Sci., 39, 965–976 (1997)
39. Yu, H.S., Hossain, M.Z. Lower bound shakedown analysis of layered pavements using discontinuous stress field. Comput. Meth. Appl. Mech. Eng., 167, 209–222 (1998)
40. Yu, H.S. Three-dimensional analytical solutions for shakedown of cohesive-frictional materials under moving surface loads. Proc. Roy. Soc. London A, 461, 1951–1964 (2005)
41. Zhang, P.X., Lu, M.W., Hwang, K. A mathematical programming algorithm for limit analysis. Acta Mechan. Sinica, 7, 267–274 (1991)
42. Zhang, Y.G. An iteration algorithm for kinematic shakedown analysis. Comput. Meth. Appl. Mech. Eng., 127, 217–226 (1995)
43. Zhang, Y.G., Lu, M.W. An algorithm for plastic limit analysis. Comp. Meth. Appl. Mech. Engrg. 126, 333–341 (1995)
44. Zouain, N., Borges, L., Silveira, J.L. An algorithm for shakedown analysis with non-linear yield functions. Comput. Meth. Appl. Mech. Eng., 191, 2463–2481 (2002)

Application of Shakedown Analysis to Large-Scale Problems with Selective Algorithm

A. Hachemi, S. Mouhtamid, A.D. Nguyen and D. Weichert

Abstract Recent results obtained by using the lower-bound theorem of shakedown analysis are presented in this paper together with a new method for solving large-scale problems by using a selective algorithm. Industrially important examples from mechanical and pavement engineering are presented.

1 Introduction

Direct Methods, comprising Limit Analysis (LA) and Shakedown Analysis (SDA) are powerful tools to predict whether or not structural failure may occur under monotonous or variable thermo-mechanical loads. Characteristic features are that this information is obtained directly, without solving an evolution problem and that in case of SDA, the loading path is not to be

A. Hachemi
RWTH Aachen, Institut für Allgemeine Mechanik, Templergraben 64, 52062 Aachen, Germany, e-mail: hachemi@iam.rwth-aachen.de

S. Mouhtamid
RWTH Aachen, Institut für Allgemeine Mechanik, Templergraben 64, 52062 Aachen, Germany, e-mail: mouhtami@iam.rwth-aachen.de

A.D. Nguyen
RWTH Aachen, Institut für Allgemeine Mechanik, Templergraben 64, 52062 Aachen, Germany, e-mail: andanh@iam.rwth-aachen.de

D. Weichert
RWTH Aachen, Institut für Allgemeine Mechanik, Templergraben 64, 52062 Aachen, Germany, e-mail: weichert@iam.rwth-aachen.de

known in detail, except for its bounding envelope. Readers interested in the foundations of "Direct Methods" are referred to [11, 12, 14–16, 23].

From practical point of view, lower-bound theorems are of special interest, because they provide in principle conservative bounds to the loading space. Nevertheless, their practical use has been for long time handicapped as they involve genuinely optimization procedures, which are in general non-linear and numerical solutions in case of large numbers of degrees of freedom suffered from time consuming calculations.

Over the last years, considerable progress has been made in developing problem-tailored numerical algorithms to overcome this problem. In particular the so called Interior Point Methods have proven highly efficient [13, 25]. In this paper focus is laid on the use of the IPDCA algorithm (Interior Point Difference of Convex functions Algorithm) developed by the authors in cooperation with others [2] and a new selective algorithm, reducing the number of optimization variables to the plastically active set located in the plastic process zone.

2 Lower-Bound Shakedown Theorem

Focusing on the numerical aspects of the methodology, we confine the discussion to the classical, linear-elastic, perfectly plastic material behavior. Extensions of SDA to more advanced material models can be found in modern literature (for references, see e.g. [14, 23]) and easily be implemented in the presented numerical schemes.

Then, the starting point is the well known static shakedown-theorem [16]: An elastic-perfectly plastic body $\mathcal{B}$ shakes down if there exist a real number $\alpha > 1$ and a time- independent field of self-equilibrated stresses $\bar{\boldsymbol{\rho}}$ with

$$\text{Div } \bar{\boldsymbol{\rho}} = 0 \qquad \text{in } V \tag{1}$$

$$\boldsymbol{n} \cdot \bar{\boldsymbol{\rho}} = 0 \qquad \text{on } S_{\text{p}} \tag{2}$$

such that the superposition of the elastic stresses $\boldsymbol{\sigma}^{\text{E}}$ with $\bar{\boldsymbol{\rho}}$ constitutes a safe state of stresses

$$\alpha \boldsymbol{\sigma}^{\text{E}} + \bar{\boldsymbol{\rho}} \subset \mathcal{C}. \tag{3}$$

Here, $\boldsymbol{\sigma}^{\text{E}}$ is the solution of a reference problem, differing from the original one only by the fact, that the material behaves purely elastically, $\mathcal{C}$ denotes the elastic domain, usually defined by the yield criterion, $\mathbf{n}$ denotes the outer normal vector on the surface of $\mathcal{B}$, V and S_{p} stand, respectively, for the volume of $\mathcal{B}$ and the part of the surface with prescribed tractions. The discrete formulation of the lower bound shakedown theorem for the determination of the shakedown loading factor is then given by

$$\alpha_{\text{SD}} = \max_{\bar{\boldsymbol{\rho}}} \alpha \tag{4}$$

with the subsidiary conditions

$$[\mathbf{C}]\{\bar{\boldsymbol{\rho}}\} = \{\mathbf{0}\} \tag{5}$$

$$F(\alpha\,\boldsymbol{\sigma}_{\mathrm{i}}^{\mathrm{E}}(P_{\mathrm{j}}) + \bar{\boldsymbol{\rho}}_{\mathrm{i}}) \leq 0 \tag{6}$$

$$\forall i \in [1, NG] \text{ and } \forall j \in [1, NV].$$

Here, $[\mathbf{C}]$ is a constant equilibrium matrix, uniquely defined by the chosen discretisation and the boundary conditions and $\{\bar{\boldsymbol{\rho}}\}$ is the global residual stress vector of the discretised reference body. The yield criterion F has to be fulfilled at all Gaussian points $i \in [1, NG]$ and each load vertex $j \in [1, NV]$. The number of unknowns of the optimization problem (4)–(6) is $N = 1 + NG \times NS$ corresponding to α and $\{\bar{\boldsymbol{\rho}}\}$. The number of constraints is $NV \times NG + NK$, where NS is the dimension of the stress vector at each Gaussian point and NK denotes the number of degrees of freedom of displacements of the discretised body. This problem can not be solved efficiently by classical algorithms of optimization because in technical design applications the number of unknowns is in general very high. Therefore, special software has been developed for solving large-scale non-linear optimization problems. It has turned out, that interior-point or barrier methods provide an attractive possibility to handle such problems and constitute to the authors' opinion a major breakthrough for numerical shakedown analysis (for more details see [2, 3, 17]).

3 Selective Algorithm

To further enhance the calculation, a new selective algorithm has been developed (Fig. 1), taking care that only the plastically active zones of the considered structure are involved in the optimization procedure. Among several ad-hoc criteria for the selection of the active Gaussian points the following has turned out to be the most efficient one: A Gaussian point is identified as active, if in the considered iteration step of the optimization procedure its equivalent eigenstress in the von Mises sense is superior to the maximum value of equivalent eigenstress detected in the entire structure, divided by a weighting factor β

$$F(\bar{\boldsymbol{\rho}}) \geq (F(\bar{\boldsymbol{\rho}}))_{\mathrm{max}}/\beta \tag{7}$$

Because the active zones change during the process, the selective algorithm is disabled at several levels of calculation in order to guarantee that the calculations do not collapse in a subspace.
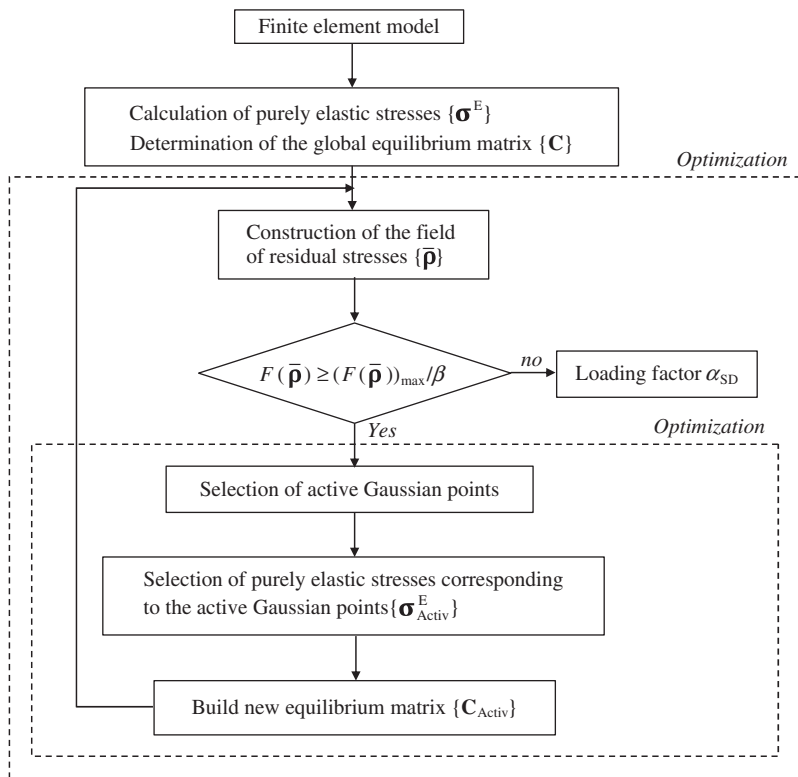
Fig. 1 Flow-chart of the selective algorithm

4 Industrially Relevant Examples

To show the efficiency and robustness of the method, several numerical results are presented. The input data for the optimization procedure have been obtained with the commercial code ANSYS [4], where the lower bound direct method has been implemented as post-processor (see [3, 17]).

4.1 Pavement with Rolling and Sliding Line Contact

The shakedown load factor of a repeated rolling/sliding line contact as presented in Fig. 2 is determined and compared with the analytical solution by Johnson [9, 10]. With Johnson's assumption of plane deformation and equilibrium with a traction free surface, the residual stress field has the following form:
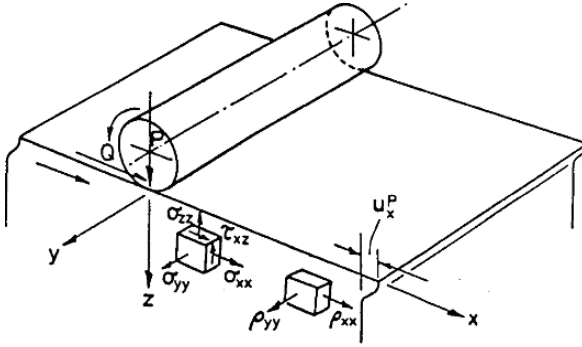
Fig. 2 Repeated rolling/sliding contact of a cylinder with an elastic-plastic half-space [10]

$$\begin{cases} \bar{\rho}_x = f_1(z), \bar{\rho}_y = f_2(z) \\ \bar{\rho}_z = \bar{\rho}_{xy} = \bar{\rho}_{yz} = \bar{\rho}_{zx} = 0 \end{cases} \qquad (8)$$

where $f_1(z)$ and $f_2(z)$ are certain arbitrary functions. Obviously the residual stresses are independent of the coordinates x, y and the components $\bar{\rho}_{yz}$ and $\bar{\rho}_{xy}$ vanish. The identities $\bar{\rho}_{zx} = 0$ and $\bar{\rho}_y = 0$ follow from the plane problem equilibrium [8, 10].

A two-dimensional model with 646 finite elements is used to model the pavement over which a cylinder moves repeatedly (Fig. 3). A semi-cylindrical pressure distribution for both vertical and horizontal loading over the surface is assumed. The vertical contact pressure is represented by a Hertzian pressure distribution:
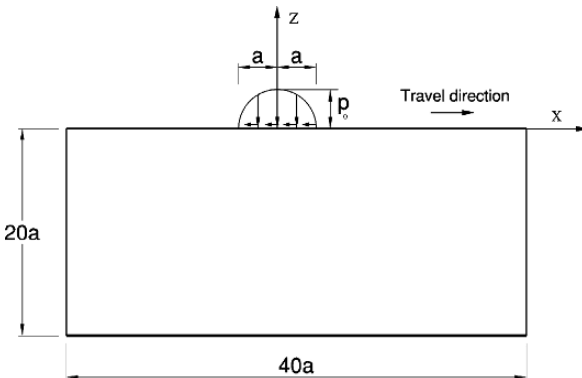
$$p(x, y) = p_0 \sqrt{1 - \frac{x^2}{a^2}} \qquad (9)$$

Fig. 3 Two-dimensional repeated rolling/sliding line contact

When surface friction is considered, additional shear traction acts in the x-direction on the same area:

$$q(x, y) = \mu_f \, p_0 \sqrt{1 - \frac{x^2}{a^2}} \tag{10}$$

where μ_f is the coefficient of friction and $p_0 = 2P/a$. Regarding the condition (8) and using the Tresca criterion the shakedown problem can be formulated as follows:

Find

$$\alpha_{\mathrm{SD}} = \max_{\bar{\rho}} \alpha \tag{11}$$

with the subsidiary conditions

$$[\mathbf{C}]\{\bar{\rho}\} = \{\mathbf{0}\} \tag{12}$$

$\bar{\rho}_x$ coupled

$$\frac{1}{4} \, (\alpha \, \sigma_x^{\mathrm{E}} + \rho_x - \alpha \, \sigma_z^{\mathrm{E}})^2 + (\alpha \, \sigma_{zx}^{\mathrm{E}})^2 \le k^2 \tag{13}$$

The shakedown loading factor as function of the angle of friction is given in Fig. 4. It is observed that the presented shakedown domain is very close to Johnson's solution [10]. The shakedown factor α_{SD} determined
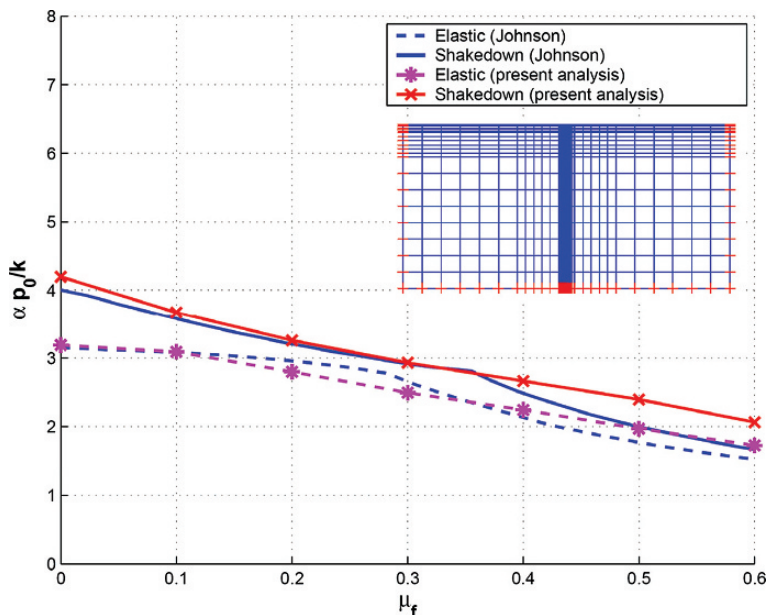

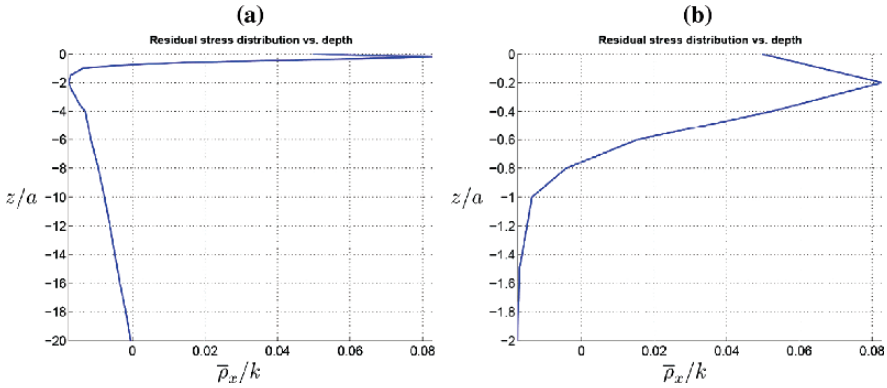**Fig. 4** Shakedown load factor versus angle of friction

Fig. 5 Distribution of residual stress $\bar{\rho}_x$ with depth z/a

by the optimization process may be represented by a dimensionless shake-down factor $||\alpha_{\mathrm{SD}}|| = \alpha \mathrm{p}_0/k$, where $k = \sigma_y/2$ [3, 19]. The distribution of the residual stress $\bar{\rho}_x$ in the case of $\mu_f = 0$ ($p = 1$ and $q = 0$), which is extrapolated from values at Gaussian points to those at nodes, is given in Fig. 5 with a zoom on the upper part in Fig. 5(b). It is observed that the maximum residual stress $\bar{\rho}_x$ does not occur at the surface but it is found, as expected, at a depth ratio of 0.2. The residual stress $\bar{\rho}_x$ changes the sign at a depth ratio of 0.76 and decreases to zero value at a depth ratio of 20.

4.2 Pavement with Locally Stationary Line Contact

The line contact problem with frictional material solved by Sharp and Booker [20] is considered. As yield condition of pressure-sensitive material, the rounded Mohr-Coulomb criterion proposed by Aboudi and Sloan [1] which can be generalized to a family of Mohr-Coulomb yield criteria in order to eliminate the singularity at the tip as well as at the edge intersections of the yield surface is used (Fig. 6). The hyperbolic Mohr-Coulomb which is both continuous and differentiable is summarised below.

Hyperbolic Mohr-Coulomb Yield Criterion:

$$F_{\mathrm{hyp}} = \sigma_{\mathrm{m}} \sin \varphi + \sqrt{\bar{\sigma}^2 K^2(\theta) + a^2 \sin^2 \varphi} - c \cos \varphi \leq 0 \qquad (14)$$

Mohr-Coulomb Yield Criterion:

$$F_{\mathrm{MC}} = \sigma_{\mathrm{m}} \sin \varphi + \bar{\sigma} K - c \cos \varphi \leq 0 \qquad (15)$$
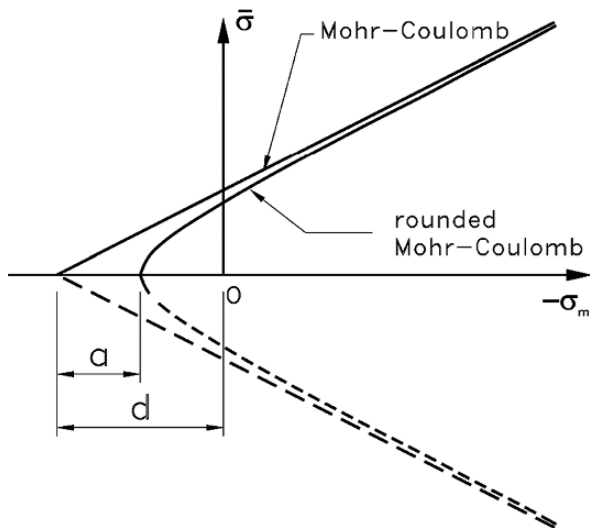
Fig. 6 Hyperbolic approximation to Mohr-Coulomb meridional section

To avoid calculating the principal stresses explicitly, the following stress invariants, proposed by Nayak and Zienkiewicz [18], are used:

$$\sigma_{\mathrm{m}} = \frac{1}{3} \left(\sigma_{11} + \sigma_{22} + \sigma_{33} \right) \tag{16}$$

$$\bar{\sigma} = \sqrt{\frac{1}{2} \left(s_{11}^2 + s_{22}^2 + s_{33}^2 \right) + \sigma_{12}^2 + \sigma_{23}^2 + \sigma_{13}^2} \tag{17}$$

$$\theta = \frac{1}{3} \sin^{-1} \left(-\frac{3\sqrt{3}}{2} \frac{J_3}{\bar{\sigma}^3} \right) \tag{18}$$

where

$$s_{11} = \sigma_{11} - \sigma_{\mathrm{m}}; \quad s_{22} = \sigma_{22} - \sigma_{\mathrm{m}}; \quad s_{33} = \sigma_{33} - \sigma_{\mathrm{m}} \tag{19}$$

$$J_3 = s_{11}s_{22}s_{33} + 2\sigma_{12}\sigma_{23}\sigma_{13} - s_{11}\sigma_{23}^2 - s_{22}\sigma_{13}^2 - s_{33}\sigma_{12}^2 \tag{20}$$

$$K(\theta) = \begin{cases} A - B \ \sin(3\theta) & \text{if } |\theta| > \theta_{\mathrm{T}} \\ \left(\cos \theta - \dfrac{1}{\sqrt{3}} \sin \varphi \ \sin \theta \right) & \text{if } |\theta| \leq \theta_{\mathrm{T}} \end{cases} \tag{21}$$

with

$$A = \frac{1}{3} \ \cos \theta_{\mathrm{T}} \left[3 + \tan \theta_{\mathrm{T}} \ \tan(3\theta_{\mathrm{T}}) + \frac{1}{\sqrt{3}} \ \text{sign}(\theta)(\tan(3\theta_{\mathrm{T}}) - 3 \tan \theta_{\mathrm{T}}) \sin \varphi \right] \tag{22}$$
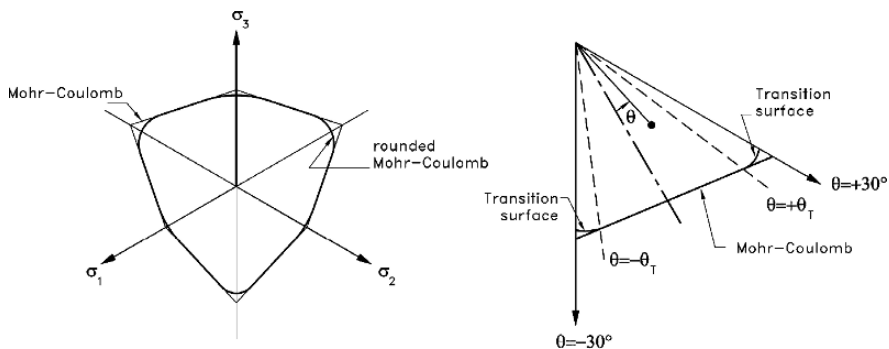
Fig. 7 Rounded Mohr-Coulomb surface in the $\pi-$ plane

Table 1 Mechanical characteristics of pavement

Young's modulus E (MPa)	468
Poisson's ratio ν	0.4
Cohesion c (KPa)	17.4

$$B = \frac{1}{3\cos(3\theta_T)}\left[\text{sign}(\theta)\sin\theta_T + \frac{1}{\sqrt{3}}\sin\varphi\cos\theta_T\right] \tag{23}$$

$$\text{sign}(\theta) = \begin{cases} +1 & \text{for } \theta \geq 0; \\ -1 & \text{for } \theta < 0 \end{cases} \tag{24}$$

$$d = c\cot\varphi \tag{25}$$

To avoid the singularities at the vertices of Mohr-Coulomb surface, a different type of yield surface is assumed whenever θ approaches $\pm 30°$. In practice, the rounded Mohr-Coulomb criterion is used for $|\theta| \geq \theta_T$ (cf. Fig. 7), where θ_T is a specified transition angle. Here we choose $a = 0.05c\cot\varphi$ and $\theta_T = 25°$ so that the hyperbolic surface closely represents the Mohr-Coulomb surface.

Instead of a trapezoid distribution of contact pressure as in Sharp and Booker [20], a semi-cylindrical pressure distribution for both vertical and horizontal loading over the surface is assumed (Eq. (9) and (10)). The material properties used in the presented analysis are given in Table 1. Figure 8 depicts the variation of the shakedown load factor versus angle of friction μ_f in comparison with those of Sharp and Booker [20] for different values of frictional angle $\varphi = 15°$, $30°$ and $45°$ [19].

4.3 Pipe-Junction Under Internal Pressure

A pipe-junction under internal pressure is considered where the corresponding geometrical and mechanical characteristics are given in Tables 2 and 3,
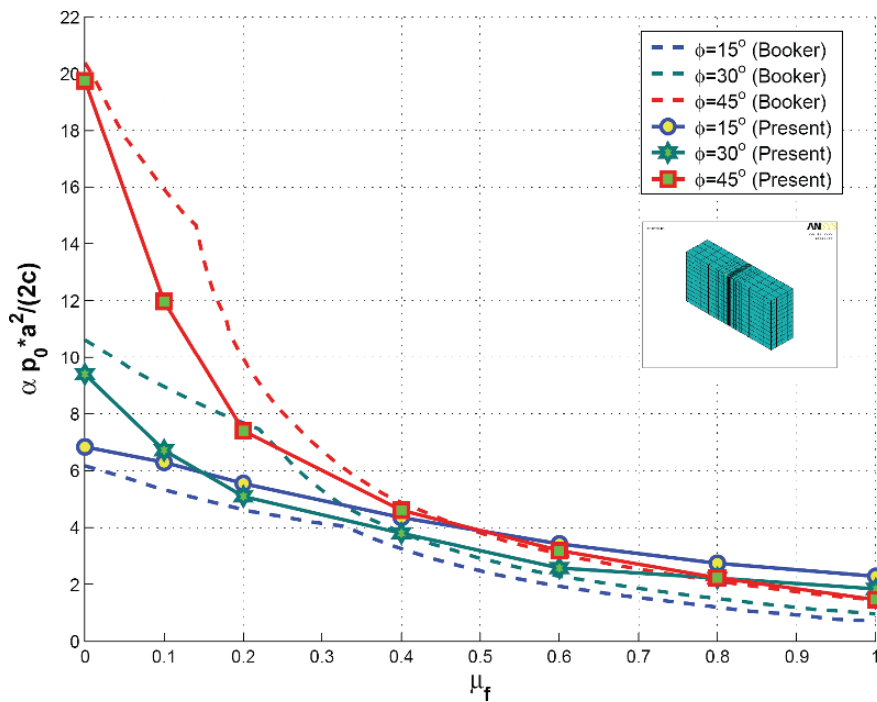
Fig. 8 Shakedown load factor versus angle of friction

respectively [17]. The pipe is discretised by 8544 elements and 10874 nodes where the FE-mesh and the essential dimensions are represented in Figs. 9 and 10.

Table 2 Geometrical characteristics of pipe-junction

	Pipe	Nozzle
Length (mm)	600	100
Internal radius (mm)	53.55	18.6
Thickness (mm)	3.6	2.6

Table 3 Mechanical characteristics of pipe-junction

Young's modulus E (MPa)	$2.1 \times 10^{+5}$
Poisson's ratio ν	0.3
Yield stress σ_Y (MPa)	300

The result for the case of limit analysis, which can be considered as particular case of shakedown analysis, is compared with those obtained by the

Fig. 9 Finite element mesh
of pipe-junction
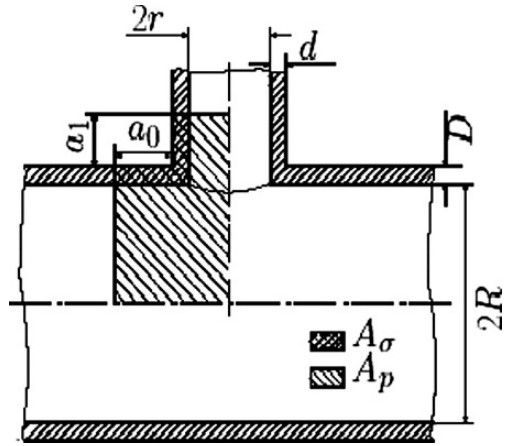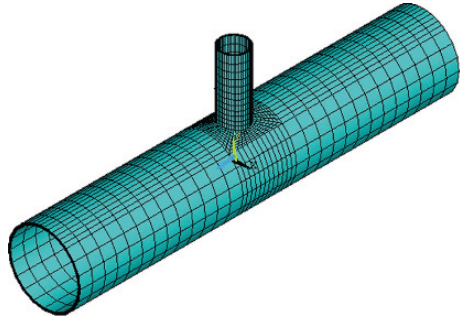
Fig. 10 Dimensions of the
pipe-junction

German design rules AD-Merkblatt [22], Cloud and Rodabaugh [5] and the incremental method [4] (Table 4). The expressions by [22] and [5] of the limit pressure are given as follows:

Limit pressure by AD-Merkblatt [22]:

$$p_{lim} = \frac{D\nu_A}{R+D}\, \sigma_Y \qquad (26)$$

where

$$\nu_A = \frac{a_0 + a_1\dfrac{d}{D} + d}{a_0 + d + r + \dfrac{r}{R}(a_1 + D)} \qquad (27)$$

with

$$a_0 = \sqrt{(2R+D)D} \text{ and } a_1 = 1.25\sqrt{(2r+d)d} \qquad (28)$$

Table 4 Limit pressure of pipe-junction

AD-Merkblatt	Cloud-Rodabaugh	Increment. Meth.	Present
0.0427 σ_Y	0.0511 σ_Y	0.0456 σ_Y	0.0450 σ_Y

Limit pressure by Cloud and Rodabaugh [5]:

$$p_{\lim} = \frac{1.5\dfrac{d^2}{\bar{r}^2} + \dfrac{D^2}{2\bar{r}^2}\left(1 + \dfrac{2}{f\sqrt{g}}\right) + \dfrac{38d}{9g\bar{r}} + \dfrac{D}{\bar{r}}\left(\dfrac{26}{9fg} + \dfrac{47}{54f^2\sqrt{g^3}}\right)}{\dfrac{38}{9g} + \dfrac{38}{9f^2g} + \dfrac{76}{27f^3\sqrt{g^3}} + \dfrac{2}{f\sqrt{g}}}\sigma_Y \quad (29)$$

where

$$f = \frac{\bar{r}}{\bar{R}} \text{ and } g = \frac{2\bar{R}}{D} \quad (30)$$

with

$$\bar{R} = R + \frac{D}{2}, \bar{r} = r + \frac{d}{2} \text{ and } \frac{\bar{r}}{\bar{R}} \quad (31)$$

4.4 Pipe-Junction Under Internal Pressure, Torsion and Bending Moments

The pipe-junction considered in Sect. 4.3 is investigated under internal pressure p, torsion M_y and bending moments M_x and M_z where the corresponding geometrical and mechanical characteristics are given in Tables 5 and 6, respectively. The pipe is discretised by 9264 elements and 11124 nodes where the FE-mesh is represented in Fig. 11.

Table 5 Geometrical characteristics of pipe-junction

	Pipe	Nozzle
Length (mm)	620	300
Internal radius (mm)	160	41
Thickness (mm)	65	23

Table 6 Mechanical characteristics of pipe-junction

Young's modulus E (MPa)	$2.0 \times 10^{+5}$
Poisson's ratio ν	0.3
Yield stress σ_Y (MPa)	205

Fig. 11 Loading and finite element mesh of pipe-junction
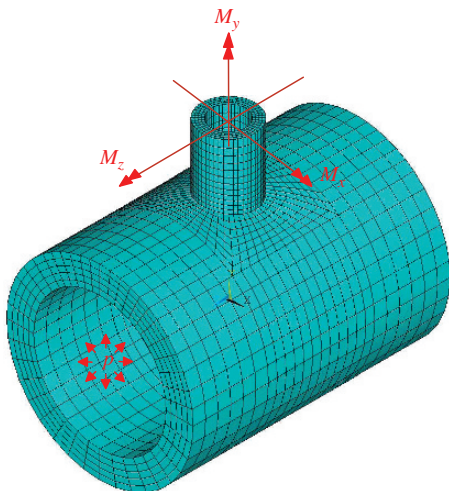
The results for the case of limit analysis are compared with the results obtained by incremental analyses by using Ansys and analytical expressions (Table 7). The expression of the limit pressure, limit torsion and bending moments p, M_y, M_x and M_z respectively are given as follows:

Limit pressure [24]:

$$p_{lim} = \frac{2}{\sqrt{3}} \, \sigma_Y \ln \left(\frac{R+D}{R} \right) \tag{32}$$

Limit torsion moment [21]:

$$M_{y(lim)} = \frac{2}{\sqrt{3}} \, \sigma_Y \left(\frac{\pi a^2}{4} \right) d \tag{33}$$

Limit bending moments [7]:

$$M_{x(lim)} = M_{z(lim)} = \frac{4}{3} \, \sigma_Y \, (r_a^3 - r^3) \tag{34}$$

with

Table 7 Limit loads of pipe-junction

	p (MPa)	M_x (KN·m)	M_y (KN·m)	M_z (KN·m)
Analytical approximation	80.95	52.812	47.143	52.812
Incremental results	61.354	52.749	47.309	52.736
Present results	62.363	52.343	48.060	52.343

$$a = 2r + d \tag{35}$$

$$r_{\mathrm{a}} = r + d \tag{36}$$

where R and D are respectively, the internal radius and the thickness of the pipe and r and d are the internal radius and the thickness of the nozzle.

4.5 Application of Selective Algorithm

The advantage of the previously mentioned selective algorithm is demonstrated by the two following illustrative examples. First, a flanged-pipe under internal pressure p and longitudinal force is considered. The pipe is discretised by 265 elements and 678 nodes where the FE-mesh and the essential dimensions are represented in Fig. 12. Length and internal diameter are respectively $L = 386.93 \,\mathrm{mm}$ and $d_i = 120 \,\mathrm{mm}$. The external diameters d_e of the parts A, B and C and the mechanical characteristics are given in Tables 8 and 9, respectively.

Table 10 gives an indication for the shakedown factor α_{SD} obtained by this method for differing values of β and different numbers of iterations. By
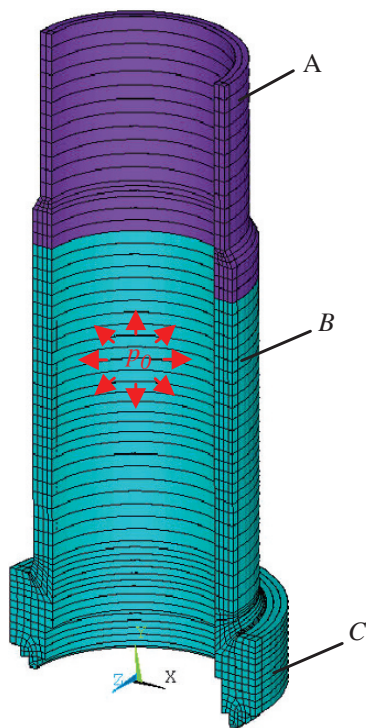
Fig. 12 Flanged-pipe

Table 8 External diameters of flanged-pipe

	A	B	C
External diameter (mm)	136.10	155.66	181

Table 9 Mechanical characteristics of flanged-pipe

Young's modulus E (MPa)	$2.0 \times 10^{+5}$
Poisson's ratio ν	0.3
Yield stress σ_Y (MPa)	200.63

Table 10 Shakedown factor of flanged-pipe with selective algorithm

β	Iterations	Nb. of active Gaussian points	α_{SD}	CPU(s)
	20	1440	2.9005	1150
	25	1470	2.9006	1140
100	35	1490	2.9010	1160
	40	1520	2.9010	1200
	20	1260	2.9006	880
	25	1285	2.9010	1080
80	35	1310	2.9010	720
	40	1330	2.9009	650
	20	1150	2.9010	1100
	25	1180	2.9010	900
70	35	1215	2.9008	810
	40	1235	2.9010	700

disabling the selective algorithm, the loading factor $\alpha_{SD} = 2.9005$ had been obtained for 2120 Gaussian points with the CPU-time of 100200 s by using the code Lancelot [6]. This time is roughly divided by the factor 100 when using the selective algorithm.

The pipe-junction considered in Sect. 4.4 is investigated under internal pressure p. The pipe is discretised by 3684 elements and 4830 nodes. By disabling the selective algorithm, the loading factor $\alpha_{SD} = 6.1450$ had been obtained for 29 472 Gaussian points with the CPU-time of 18 000 s by using IPDCA [2]. The obtained shakedown factor with the selective algorithm is given in Table 11 for differing values of β and for different numbers of iterations.

Table 11 Shakedown factor of pipe-junction with selective algorithm

β	Iterations	Nb. of active Gaussian points	α_{SD}	CPU(s)
	20	12 720	5.915	5300
150	35	12 140	5.850	5190
	45	11 600	5.856	4950
	20	11 000	5.858	5100
120	35	10354	5.900	5050
	45	10050	5.890	4850
	20	9985	5.850	5300
100	35	9750	5.995	5030
	45	9230	6.020	4200

5 Conclusions

Compared to high-standard general codes for non-linear optimization, a combination of IPDCA [14, 25] and Selective Optimization allowed to reduce drastically the necessary CPU time for lower bound Shakedown- and Limit Analysis. The presented solutions of complex problems from different technical areas demonstrate the wide range of applicability of the method and its high potential for industrial design purposes, in particular as a post-processing method for conventional finite-element analyses.

References

1. Aboudi, A.J., Sloan, S.W.: A smooth hyperbolic approximation to the Mohr-Coulomb yield criterion. Computers and Structures 54, 427–441 (1995).
2. Akoa, F., Hachemi, A., Le Thi Hoai An, Mouhtamid, S., Pham Dinh Tao: Application of lower bound direct method to engineering structures. J. Global Optim. 37, 609–630 (2007).
3. An Danh Nguyen: Lower-bound shakedown analysis of pavements by using the interior point method. Doctor thesis, RWTH Aachen (2007).
4. Ansys Release 8.0: Ansys, Inc. Southpointe 275 Technology Drive Canonsburg, PA 15317.
5. Cloud, R.L., Rodabaugh, E.C.: Approximate analysis of the plastic limit pressures of nozzles in cylindrical shells. Trans. ASME, J. Engrg. Power 4, 171–176 (1968).
6. Conn, A.R., Gould, N.I.M., Toint, Ph.L.: LANCELOT: A Fortran Package for Large-Scale Nonlinear Optimization (Release A). Berlin, Springer-Verlag (1992).
7. Feige, A.: Das Traglast-Berechnungsverfahren, 2. Aufl.; Verlag Stahleisen, Düsseldorf (1980).
8. Gokhfeld, D.A., Cherniavsky, O.F.: Limit analysis of structures at thermal cycling. Sijthoff and Noordhoff (1980).
9. Johnson, K.L.: Contact Mechanics. Cambridge University Press, Cambridge (1985).
10. Johnson, K.L.: The application of shakedown principles in rolling and sliding contact. Eur. J. Mech. A/Solids 11, 155–172 (1992).

11. Koiter, W.T.: General theorems for elastic-plastic solids. In: Sneddon, I.N., Hill, R. (eds.), Progress in Solid Mechanics. North-Holland, Amsterdam, pp. 165–221 (1960).
12. König, J.A.: Shakedown of elastic-plastic structures. Elsevier, Amsterdam (1987).
13. Le Thi Haoi An, Pham Dinh Tao: The DC (difference of convex functions) Programming and DCA revisited with DC models of real world nonconvex optimization problems. Ann. Oper. Res. 133, 23–46 (2005).
14. Maier, G., Pastor, J., Ponter, A.R.S., Weichert, D.: Direct Methods of Limit and Shakedown Analysis. In: De Borst, R.; Mang, H. A. (eds.), Numerical and computational methods, Chapter 12, Vol. 3. In: Milne, I., Ritchie, R. O.; Karihaloo, B. (eds.), Comprehensive Structural Integrity. Elsevier-Pergamon, Amsterdam (2003).
15. Martin, G.B.: Plasticity: Fundamentals and General Results. MIT Press, Cambridge, MA (1975).
16. Melan, E.: Zur Plastizität des räumlichen Kontinuums. Ing. Arch. 9, 116–126 (1938).
17. Mouhtamid, S.: Anwendung direkter Methoden zur industriellen Berechnung von Grenzlasten mechanischer Komponenten. Doctor thesis, RWTH Aachen (2007).
18. Nayak G.C., Zienkiewicz O.C.: Conventional form of stress invariants for plasticity. J. Struct. Div., Proc. American Society Civil Engineers 98, 949–954 (1972).
19. Nguyen An Danh, Hachemi, A., Weichert, D.: Application of the interior-point method to shakedown analysis of pavements. Int. J. Numer. Meth. Engng. 75, 414–439 (2008).
20. Sharp, R.W., Booker, J.R.: Shakedown of pavements under moving surface loads. J. Transp. Enrg. 110, 1–14 (1984).
21. Vu, D.K.: Dual limit and shakedown analysis of structures. Doctor thesis, University of Liege Faculty of Applied Sciences (2001).
22. Wagner, W.: Festigkeitsberechnungen im Apparate- und Rohrleitungsbau. Vogel Buchverlag, Würzburg (1991).
23. Weichert, D., Maier, G.: Inelastic Behaviour of Structures under Variable Repeated Loads: Direct Analysis methods. CISM Courses and Lectures No. 432, International Centre for Mechanical Sciences, Springer Wien-New York (2002).
24. Wellinger, K, Dietmann, H.: Festigkeitsberechnung. Alfred Kröner Verlag, Stuttgart (1969).
25. Wächter, A., Biegler, L.T.: On the Implementation of a Primal-Dual Interior Point Filter Line Search Algorithm for Large-Scale Non-linear Programming. IBM Research Report RC 23149 IBM T. J. Watson Research Center March, Yorktown Heights, NY. USA, pp. 1–28 (2004).